Complexity

Behavior Analysis, Complexity and Control of Networked Dynamical Systems 2022

Lead Guest Editor: Hou-Sheng Su
Guest Editors: Zhiwei Gao, Xiao Ling Wang, Yue Song, and Miaomiao Wang

Behavior Analysis, Complexity and Control of Networked Dynamical Systems 2022

Complexity

Behavior Analysis, Complexity and Control of Networked Dynamical Systems 2022

Lead Guest Editor: Hou-Sheng Su
Guest Editors: Zhiwei Gao, Xiao Ling Wang, Yue Song, and Miaomiao Wang

Contents

Hindawi
Complexity
Volume 2023, Article ID 3635342, 8 pages
https://doi.org/10.1155/2023/3635342

Research Article

Local Fractional Strong Metric Dimension of Certain Complex Networks

Faiza Jamil,[1] **Agha Kashif**,[1] **Sohail Zafar**,[1] **and Michael Onyango Ojiema**[2]

[1]*University of Management and Technology (UMT), Lahore, Pakistan*
[2]*Masinde Muliro University of Science and Technology, Kakamega, Kenya*

Correspondence should be addressed to Michael Onyango Ojiema; mojiema@mmust.ac.ke

Received 30 March 2022; Revised 14 July 2022; Accepted 10 April 2023; Published 5 May 2023

Academic Editor: Miaomiao Wang

Fractional variants of distance-based parameters have application in the fields of sensor networking, robot navigation, and integer programming problems. Complex networks are exceptional networks which exhibit significant topological features and have become quintessential research area in the field of computer science, biology, and mathematics. Owing to the possibility that many real-world systems can be intelligently modeled and represented as complex networks to examine, administer and comprehend the useful information from these real-world networks. In this paper, local fractional strong metric dimension of certain complex networks is computed. Building blocks of complex networks are considered as the symmetric networks such as cyclic networks C_n, circulant networks $C_n(1,2)$, mobious ladder networks M_{2n}, and generalized prism networks G_m^n. In this regard, it is shown that LSFMD of $C_n\,(n \geq 3)$ and $G_m^n\,(n \geq 6)$ is 1 when n is even and $n/n-1$ when n is odd, whereas LSFMD of M_{2n} is 1 when n is odd and $n/n-1$ when n is even. Also, LSFMD of $C_n(1,2)$ is $n/2\,(\lceil m+1/2 \rceil)$ where $n \geq 6$ and $m = \lceil n-5/4 \rceil$.

1. Introduction

Distance-based parameters for networks play a vital role in pharmaceutical chemistry [1], network discovery [2], robot navigation, and optimizations [3]. Many real-life large-scale systems having substantial topological features can be modeled as complex networks such as social networks, information networks, technological networks, and biological networks. This representation has innovative impacts to information processing and co-ordination of these large-scale networks. Management of large-scale networks such as Internet with their tremendous growth and heterogeneity is a challenging mathematical problem which have profound implications for the efficient design of future communication networks. Complex networks are composed of building blocks, and if the building blocks are considered as symmetric networks, then complexity of these networks can be reduced for better analysis and interpretation. A few important building blocks are cycles, circulant networks, mobious ladder networks, and generalized prism networks, which are discussed in this article.

Over the past few decades, circulant and mobious ladder networks have been comprehensively explored by many researchers due to their vast application and importance in telecommunication networks [4], computer science (see [5, 6]), chemistry [7], discrete mathematics, and very large-scale integration (VLSI) design. Complex large-scale interconnection networks used in the design of local area networks, distributed computer systems, and telecommunication networks have been constructed based on VLSI circuit technology. In telecommunication networks, many stations are placed at short distances (less than 5 km) to share data at a very high speed, and the main objective is to optimize the exchange of data with an efficient network topology.

In a finite network N of order n, $V(N)$ and $E(N)$ represent the collection of vertices and edges of the network N, respectively. The collection of all the vertices of the network N that are adjacent to the vertex v is known as the open neighbourhood of any vertex v in N. The distance between the vertices v_1 and v_2 of N denoted by $d(v_1, v_2)$ is the length of shortest path (geodesic) between these vertices. A pair of vertices v_1 and v_2 of N is said to be mutually

maximally distant if v_1 is maximally distant from v_2 and v_2 is maximally distant from v_1 where the vertex v_1 is maximally distant from v_2 if $d(v_1, v_2) \geq d(v, v_2)$ for all v in the open neighbourhood of v_1. A vertex w of N is said to resolve two vertices v_1 and v_2 of N if v_1 and v_2 are at unequal distance from the vertex w. A set S of vertices of the network N is a resolving set for N if every two distinct vertices of N are resolved by some vertex of S. Metric basis is the resolving set having minimum cardinality, and this cardinality is said to be the metric dimension (MD) of N, denoted by $\dim(N)$. In 1975, the notion of MD was initiated by Slater [8], motivated by the problem of uniquely determining the location of an intruder in a network and later studied independently by Harary and Melter in [9]. MD has been heavily studied, and the advancements in this field can be seen in [10]. Some bounds for MD in terms of diameter of network are given in [1]. Chartrand et al. [1] formulated MD as integer programming problem. The problem of finding MD of a graph is NP-hard (see [11]). The MD of trees and Cayley diagraphs are studied in [1, 12], respectively. A pair of vertices v_1 and v_2 in N is said to be strongly resolved by a vertex v, if there exist either a shortest path from v_1 to v containing v_2 or a shortest path from v_2 to v containing v_1. Strong resolving set S of N is a collection of vertices such that each distinct pair of vertices in N is strongly resolved by some vertex in S. Strong metric basis of N is the strong resolving set having smallest cardinality, and this cardinality is labelled as strong metric dimension (SMD) of N, denoted by $\text{sdim}(N)$. In 2004, SMD of a network was discovered by Sebő and Tannier [13] and later in 2007, and computation of SMD was declared as NP-hard problem by Oellermann and Peters-Fransen [14]. The resolving neighbourhood (RN) denoted by $R\{v_1, v_2\}$ for a pair of vertices v_1 and v_2 in N is composed of all vertices at varying distances from v_1 and v_2. If $\eta: V(N) \longrightarrow [0, 1]$ is a real valued function that assigns a number between 0 and 1 to each vertex of N and $U \subseteq V(N)$, then the function η applied on the set U is given by $\eta(U) = \sum_{v \in U} \eta(v)$. If the weight of $R\{v_1, v_2\}$ is greater than or equal to 1 for any two vertices $v_1 \neq v_2$ in N, then the function η is called resolving function of N. The fractional metric dimension (FMD) of N expressed as $\dim_f(N)$ is given by the least possible weight of a resolving function of N. In 2001, Currie and Oellermann [10] initiated the concept of FMD by formulating the linear programming problem using the integer programming problem that was presented for MD given in [1]. This relaxation technique transforms an NP-hard integer programming into a related problem that is solvable in polynomial time. In 2012, Arumugam and Mathew [15] defined FMD using the concept of resolving neighbourhoods. In [16], FMD of Generalized Jahangir graph was calculated. In [17], FMD of tree and unicyclic graphs was computed. FMD of hierarchical product, corona product, and lexicographic product graphs were calculated in [18, 19]. The problem of computing the FMD for all the connected networks is an NP-hard problem. Strong resolving neighbourhood (SRN) denoted by $S\{v_1, v_2\}$ for the pair of vertices v_1 and v_2 in N is the set of all vertices $w \in V(N)$ such that either v_1 lies on $w - v_2$ geodesic or v_2 lies on $w - v_1$ geodesic. If the weight $\eta(S\{v_1, v_2\})$ is greater than or equal to 1, then the real-valued function that assigns a number between 0 and 1 to each vertex of N given by $\eta: V(N) \longrightarrow [0, 1]$ is known as a strong resolving function of N for each distinct pair of vertices in $V(N)$. The fractional strong metric dimension (FSMD) of N expressed as $\text{sdim}_f(N)$ is given by the least possible weight of a strong resolving function of N. In 2013, Kang and Yi [20] gave the notion of FSMD, studied it for various significant finite connected graph classes and mentioned that FSMD problem can be interpreted as linear programming problem with the same strategy as in [12]. In 2010, Okamoto et al. [21] gave the concept of local metric dimension (LMD) by considering the adjacent vertices of graph only. A set of vertices W in a connected network N is a local metric set of N if every two adjacent vertices of N are distinguished by some vertex of W. Local metric basis is the local metric set having smallest cardinality, and this cardinality is said to be the LMD of N, denoted by $\text{ldi m}(N)$. In [22, 23], LMD of corona product graphs and circulant graphs has been discussed, respectively. LMD of some families of graphs was given in [24, 25]. The local resolving neighbourhood (LRN) denoted by $L\{v_1, v_2\}$ for a pair of adjacent vertices v_1 and v_2 in N is composed of all vertices which are resolved by $L\{v_1, v_2\}$. The concept of local resolving neighbourhood and local resolving function arises similar to resolving neighbourhood and resolving function in case of dealing with only the pair of adjacent vertices. In [26], authors set forth a localized variant of FMD known as local fractional metric dimension (LFMD) and studied it for strong and cartesian products of graphs. LFMD of the network N denoted by $\text{ldi m}_f(N)$ is the least possible weight of local resolving function of N. LFMD of rotationally symmetric planar graphs arisen from planar chorded cycles was computed in [27]. In [28, 29], LFMD of rotationally symmetric and planer networks and corona products graphs were computed, respectively. Local strong resolving neighbourhood (LSRN) $L_S\{v_1, v_2\}$ for the pair of adjacent vertices v_1 and v_2 in N is the set of all vertices $w \in V(N)$ such that either v_1 lies on $w - v_2$ geodesic or v_2 lies on $w - v_1$ geodesic. If for each adjacent pair of vertices in $V(N)$, the weight $\alpha(L_S\{u_1, u_2\})$ is greater or equal to 1, then the mapping $\alpha: V(N) \longrightarrow [0, 1]$ is called a local strong resolving function of N, where $\alpha(L_S(x, y)) = \sum_{x \in L_S(x,y)} \alpha(x)$. The local fractional strong metric dimension (LFSMD) of the network N denoted by $\text{lsdim}_f(N)$ is defined as the least possible weight of a local strong resolving function of N. In [30], the notion of LFSMD was introduced, and the authors devised a combinatorial technique to compute LFSMD of a general network and was further applied to compute LFSMD for rotationally symmetric and planer networks. In [30], the notion of LFSMD was initiated. The combinatorial criteria to calculate LFSMD of a general network was devised and further applied to compute LFSMD for rotationally symmetric and planer networks. This criteria is given in Lemma 1. This motivated us to compute LFSMD of certain complex networks with symmetric networks as their building blocks. The symmetric networks considered in this article are cyclic networks C_n, circulant networks $C_n(1, 2)$, mobious ladder networks M_{2n}, and generalized prism networks G_m^n. The collection of LSRNs of a network N with

least cardinality and its compliment is represented by the notations $\mathscr{L}(N)$ and $\overline{\mathscr{L}}(N)$, respectively. Here, $\mathscr{L}(N) = \{LS(N) \mid LS(N)$ is th
e LSRN with the condition $|LS(N)| = \gamma(N)\}$, where $\gamma(N)$ is the cardinality of smallest SRNs of N. Moreover, $\overline{\mathscr{L}}(N) = \{\widetilde{L} \mid \widetilde{L}$ is the LSRN of N not in $\mathscr{L}(N)\}$.

Lemma 1 (see [30]). *Let $\mu(N) = \mathscr{L}(N) \cup \overline{\mathscr{L}}(N)$ be a set consisting of all LSRNs of network N in such a manner that for every adjacent pair of vertices x and y in the vertex set of N, if the condition $|S\{x, y\} \cap [\cup LS(N)]| \geq \gamma(N)$ holds. Then,* $\mathrm{lsdim}_f(N) = \sum_{s=1}^{\beta(N)} (1/\gamma(N))$, where $\beta(N) = |[\cup LS(N)]|$.

1.1. Main Results. The research conducted in this article leads to the following results:

Theorem 1

(1) For $n \geq 3$, $\mathrm{lsdim}_f(C_n) = \begin{cases} 1 & \text{if } n \equiv 0 \pmod 2; \\ n/n-1 & \text{if } n \equiv 1 \pmod 2 \end{cases}$

(2) For $n \geq 6$,

(a) $\mathrm{lsdim}_f(C_n(1,2)) = n/2(\lceil m + 1/2 \rceil)$

(b) $\mathrm{lsdim}_f(M_{2n}) = \begin{cases} 1 & \text{if } n \equiv 1 \pmod 2; \\ n/n-1 & \text{if } n \equiv 0 \pmod 2 \end{cases}$

(c) $\mathrm{lsdim}_f(G_m^n) = \begin{cases} 1 & \text{if } n \equiv 0 \pmod 2; \\ n/n-1 & \text{if } n \equiv 1 \pmod 2. \end{cases}$

The remaining part of the article is structured in the following manner. Sections 2 and 3 are devoted for LSRNs and LFSMD of certain complex networks with symmetric building blocks.

2. Local Strong Resolving Neighbourhoods of Certain Complex Networks

In this section, we compute LSRNs of certain complex networks. These complex networks are composed of building blocks to unravel the dynamics of these networks, and symmetric building blocks play a vital role. The symmetric networks considered in this section are cyclic networks C_n, circulant networks $C_n(1,2)$, mobious ladder networks M_{2n}, and generalized prism networks G_m^n.

2.1. Cyclic Networks. One of the most important building blocks of complex networks is cyclic network. The vertex and edge set of a cyclic network C_n are given by $V(C_n) = \{a_i \mid 1 \leq i \leq n\}$ and $E(C_n) = \{a_i a_{i+1} \mid 1 \leq i \leq n\}$, respectively, with indices taken mod n. The network C_n is shown in Figure 1. In this section, LSRNs of cyclic network C_n are considered.

Lemma 2. *Let $a_i \in V(C_n)$, where $n \geq 3$ and $1 \leq r \leq n$. Then,*

(1) $|S\{a_r, a_{r+1}\}| = \begin{cases} n & \text{if } n \equiv 0 \pmod 2; \\ n-1 & \text{if } n \equiv 1 \pmod 2 \end{cases}$

(2) $S\{x, y\} \in \mathscr{L}(C_n)$ if and only if $x = a_r$, $y = a_{r+1}$

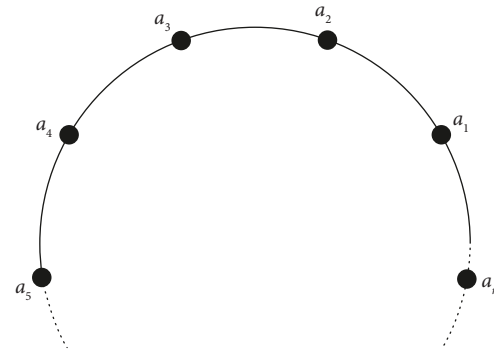

Figure 1: Cyclic network C_n.

(3) $|\cup[\mathscr{L}(C_n)]| = n$ *where* $\cup[\mathscr{L}(C_n)] = \cup_{LS(C_n) \in \mathscr{L}(C_n)} LS(C_n)$

(4) $|S\{x, y\} \cap [\cup \mathscr{L}(C_n)]| \geq \gamma(C_n)$ *for each distinct* $x, y \in V(C_n)$.

Proof. In order to prove this lemma, we proceed as follows:

(1) For $n \equiv 0 \pmod 2$, $S\{a_r, a_{r+1}\} = V(C_n)$ where as for $n \equiv 1 \pmod 2$, $S\{a_r, a_{r+1}\} = V(C_n) - \{a_{r+\lceil n/2 \rceil}\}$. Hence, $|S\{a_r, a_{r+1}\}| = n$ or $n-1$, respectively.

(2) It is clear that $S\{a_r, a_{r+1}\}$ are the only LSRNs of C_n and hence, we conclude $S\{x, y\} \in \mathscr{L}(C_n)$ if and only if $x = a_r$, $y = a_{r+1}$.

(3) From the proof of (1) and (2), we have $|\cup[\mathscr{L}(C_n)]| = n$ where $\cup[\mathscr{L}(C_n)] = \cup_{LS(C_n) \in \mathscr{L}(C_n)} LS(C_n)$.

(4) Indeed, the only pair of adjacent vertices in C_n are a_r, a_{r+1} so we have $|S\{x, y\} \cap [\cup \mathscr{L}(C_n)]| \geq \gamma(C_n)$ for each distinct $x, y \in V(C_n)$. □

2.2. Circulant Networks. The circulant network $C_n(s_1, s_2, s_3, \ldots, s_k)$ is formed by arranging the n vertices labelled a_i with the indices taken mod n cyclically and connecting each vertex a_i with k immediately following and k preceeding vertices, where $k \leq \lfloor n/2 \rfloor$. If $= \lfloor n/2 \rfloor$, then the circulant network represented by a complete graph. $C_n(1,2)$ is a circulant network with vertex set $V(C_n(1,2)) = \{a_i; 1 \leq i \leq n\}$ and edge set $E(C_n(1,2)) = \{a_i a_{i+1}, a_i a_{i+2}, a_i a_{i-1}, a_i a_{i-2}; 1 \leq i \leq n\}$. The network $C_n(1,2)$ is shown in Figure 2.

Lemma 3. *Let $a_i \in V(C_n(1,2))$, where $n \geq 6$ and $1 \leq r \leq n$. Then,*

(1) $|S\{a_r, a_{r+1}\}| = |S\{a_r, a_{r-1}\}| = 2(\lceil m + 1/2 \rceil)$, *where* $m = \lceil n - 5/4 \rceil$

(2) $S\{x, y\} \in \mathscr{L}(C_n(1,2))$ if and only if either $x = a_r$, $y = a_{r-1}$ or $x = a_r$, $y = a_{r+1}$

(3) $|\cup \mathscr{L}(C_n(1,2))| = n$ *where* $\cup \mathscr{L}(C_n(1,2)) = \cup_{LS(C_n(1,2)) \in \mathscr{L}(C_n(1,2))} LS(C_n(1,2))$

(4) $|S\{x, y\} \cap [\cup \mathscr{L}(C_n(1,2))]| \geq \gamma(C_n(1,2))$ *for each distinct* $x, y \in V(C_n(1,2))$

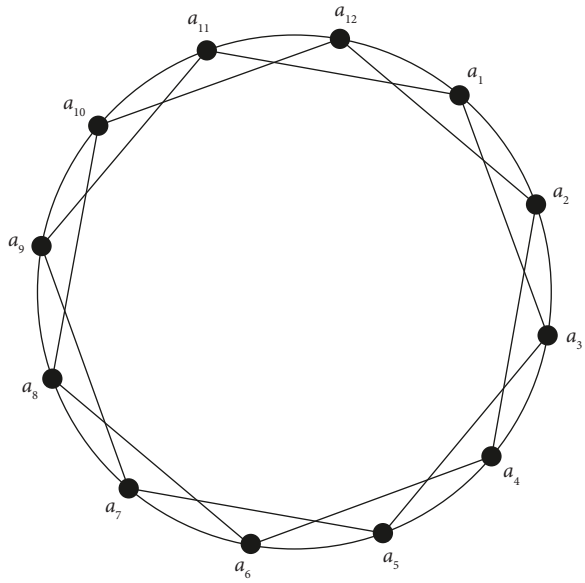

FIGURE 2: The circulant network $C_{12}(1,2)$.

Proof. The proof of this lemma is as follows:

(1) We consider the LSRNs of the vertex pair $a_r a_{r+1}$ which are $S\{a_r, a_{r+1}\} = \{a_r, a_{r+1}, \ldots, a_{r+k}, a_r, a_{r-2}, \ldots, a_{r-m}\}$ where $m = 2\lceil n - 5/4\rceil$ and $k = 2\lceil n - 5/4\rceil + 1$. Hence, due to symmetry of $C_n(1,2)$, $|S\{a_r, a_{r-1}\}| = |S\{a_r, a_{r+1}\}| = 2(\lceil m + 1/2\rceil)$.

(2) To prove this claim, we consider the LSRNs for $a_r a_{r+2}$ and $a_r a_{r-2}$. Here, following cases arise:

Case 1 $(n \equiv 0 \pmod 2)$
It is easy to see that the LSRNs in this case are given by $S\{a_r, a_{r+2}\} = \{a_{r+1}, a_{r+n/2+1}\}^c$. Hence, due to symmetry, $|S\{a_r, a_{r+2}\}| = |S\{a_r, a_{r-2}\}| = n - 2$.
Case 2 $(n \equiv 1 \pmod 2)$
This case is further subdivided into following cases:

Case 2.1 (when $n = 7 + 4k$ where $k \in Z$)
Here, we have $S\{a_r, a_{r+2}\} = \{a_{r+1}\}^c$. Hence, due to symmetry, $|S\{a_r, a_{r+2}\}| = |S\{a_r, a_{r-2}\}| = n - 1$
Case 2.2 (when $n = 9 + 4k$ where $k \in Z$)
The LSRNs in this case are given by $S\{a_r, a_{r+2}\} = \{a_{r+\lceil n/2\rceil}, a_{r+\lceil n/2\rceil+1}, a_{r+1}\}^c$. Hence, due to symmetry, $|S\{a_r, a_{r+2}\}| = |S\{a_r, a_{r-2}\}| = n - 3$.
Hence from above, we conclude $S\{x, y\} \in \mathscr{L}(C_n(1,2))$ if and only if either $x = a_r$, $y = a_{r-1}$ or $x = a_r$, $y = a_{r+1}$. Also, $|LS(C_n(1,2))| \le |S\{a_r, a_{r+2}\}|$ and $|LS(C_n(1,2))| \le |S\{a_r, a_{r-2}\}|$.

(3) From the proof of (1) and (2), we have $|(\cup_{r=1}^{n} S\{a_r, a_{r-1}\}) \cup (\cup_{r=1}^{n} Sa_r, a_{r+1})| = |\{a_i \mid 1 \le i \le n\}| = n$. Hence, $|\cup \mathscr{L}(C_n(1,2))| = n$ where $\cup \mathscr{L}(C_n(1,2)) = \cup_{LS(C_n(1,2)) \in \mathscr{L}(C_n(1,2))} LS(C_n(1,2))$.

(4) It can be concluded from the proof of (1) and (2) that $|S\{x, y\} \cap [\cup \mathscr{L}(C_n(1,2))]| \ge \gamma(C_n(1,2))$ for each distinct $x, y \in V(C_n(1,2))$. □

2.3. Mobious Ladder Network. The network obtained by introducing a twist in a prism network of order n is known as the mobious ladder network denoted by M_{2n}. It is formed by arranging its $2n$ vertices labelled a_i and b_i with the indices taken mod n cyclically and connecting each vertex a_i with b_i similar to a prism with two edges crossed. The collection of vertices and edges of mobious ladder M_{2n} is represented by $V(M_{2n}) = \{a_i, b_i; 1 \le i \le n\}$ and $E(M_{2n}) = \{a_i a_{i+1}, b_i b_{i+1}, a_j b_j, a_1 b_n, a_n b_1; 1 \le i \le n - 1, 1 \le j \le n\}$, respectively. The network M_{2n} is shown in Figure 3.

Lemma 4. *Let $a_i, b_i \in V(M_{2n})$, where $n \ge 6$, $1 \le r \le n - 1$ and $1 \le q \le n$. Then,*

(1) $|S\{a_r, b_{r+1}\}| = |S\{a_q, b_q\}| = |S\{a_n, b_1\}| = |S\{a_1, b_n\}| = |S\{b_r, b_{r+1}\}| = \begin{cases} 2(n-1) & \text{if } n \equiv 0 \pmod 2; \\ 2n & \text{if } n \equiv 1 \pmod 2 \end{cases}$

(2) $S\{x, y\} \in \mathscr{L}(M_{2n})$ *if and only if* $S\{x, y\} \in \{S\{a_r, b_{r+1}\}, S\{a_q, b_q\}, S\{b_r, b_{r+1}\}, S\{a_n, b_1\}, S\{a_1, b_n\}\}$

(3) $|\cup [\mathscr{L}(M_{2n})]| = 2n$ *where* $\cup [\mathscr{L}(M_{2n})] = \cup_{LS(M_{2n}) \in \mathscr{L}(M_{2n})} LS(M_{2n})$

(4) $|S\{x, y\} \cap [\cup \mathscr{L}(M_{2n})]| \ge \gamma(M_{2n})$ *for each distinct* $x, y \in V(M_{2n})$.

Proof. To prove this lemma, we proceed as follows:

(1) In order to prove this claim, we consider the following cases:

Case 1 In this specific case, when $n \equiv 0 \pmod 2$, the LSRNs of the vertex pairs $a_r a_{r+1}$ and $b_r b_{r+1}$ are given by $S\{a_r, a_{r+1}\} = \{a_{r+n/2+1}, b_{r+n/2}\}^c$ and $S\{b_r, b_{r+1}\} = \{a_{r+n/2}, b_{r+n/2+1}\}^c$. For the vertex pair $a_q b_q$, the LSRN is given by $S\{a_q, b_q\} = \{a_{q+n/2}, b_{q+n/2}\}^c$ where $1 \le r \le n - 1$ and $1 \le q \le n$. Also, $S\{a_1, b_n\} = \{a_{n/2+1}, b_{n/2}\}^c$ and $S\{a_n, b_1\} = \{a_{n/2}, b_{n/2+1}\}^c$. Hence, we have $|S\{a_r, b_{r+1}\}| = |S\{a_q, b_q\}| = |S\{a_n, b_1\}| = |S\{a_1, b_n\}| = |S\{b_r, b_{r+1}\}| = 2(n-1)$.
Case 2 It can be seen when $n \equiv 1 \pmod 2$, all the LSRNs of M_{2n} are given by $S\{x, y\} = V(M_{2n})$ where $xy \in E(M_{2n})$. Hence, we have $|S\{a_q, b_q\}| = |S\{a_r, a_{r+1}\}| = |S\{b_r, b_{r+1}\}| = |S\{a_1, b_n\}| = |S\{a_n, b_1\}| = |V(M_{2n})|$.

(2) The only LSRNs of M_{2n} are $S\{a_r, b_{r+1}\}, S\{a_q, b_q\}, S\{b_r, b_{r+1}\}, S\{a_n, b_1\}, S\{a_1, b_n\}$, and hence, we conclude $S\{x, y\} \in \mathscr{L}(C_n)$ if and only if $S\{x, y\} \in \{S\{a_r, b_{r+1}\}, S\{a_q, b_q\}, S\{b_r, b_{r+1}\}, S\{a_n, b_1\}, S\{a_1, b_n\}\}$.

(3) From the proof of (1) and (2), we have $|\cup [\mathscr{L}(M_{2n})]| = 2n$ where $\cup [\mathscr{L}(M_{2n})] = \cup_{LS(M_{2n}) \in \mathscr{L}(M_{2n})} LS(M_{2n})$.

(4) As the only LSRNs of the pairs of adjacent vertices in M_{2n} are $\{S\{a_r, b_{r+1}\}, S\{a_q, b_q\}, S\{b_r, b_{r+1}\}, S\{a_n, b_1\}, S\{a_1, b_n\}\}$. Hence, we have $|S\{x, y\} \cap [\cup \mathscr{L}(M_{2n})]| \ge \gamma(M_{2n})$ for each distinct $x, y \in V(M_{2n})$. □

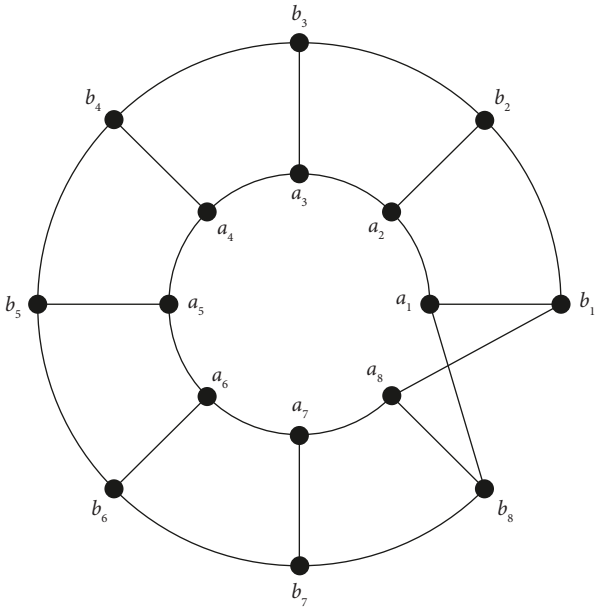

Figure 3: Mobious ladder network M_{16}.

2.4. Generalized Prism Network $P_m \times C_n$. Generalized prism network G_m^n is formed by the box product of networks P_m and C_n. The vertex set of G_m^n is given by $V(G_m^n) = \{a_{ij}: 1 \le i \le m, 1 \le j \le n\}$, and edge set is represented as $E(G_m^n) = \{\{a_{ik}a_{i(k+1)}; 1 \le i \le m, 1 \le k \le n\} \cup \{a_{st}a_{(s+1)t}; 1 \le s \le m-1, 1 \le t \le n\}\}$, respectively, where for the vertices, the first indices are taken mod m, and the second indices are taken mod n. G_m^n is shown in the Figure 4. LSRNs of generalized prism network G_m^n will be calculated in this section.

Lemma 5. *Let $a_{ij} \in V(G_m^n)$, where $n \ge 6$, $1 \le i \le m$ and $1 \le j \le n$. Then,*

(1) $|S\{a_{ij}, a_{(i+1)j}\}| = mn$ *and* $|S\{a_{ij}, a_{i(j+1)}\}| = \begin{cases} mn & \text{if } n \equiv 0 \pmod 2; \\ m(n-1) & \text{if } n \equiv 1 \pmod 2 \end{cases}$

(2) $S\{x, y\} \in \mathscr{L}(G_m^n)$ *if and only if* $x = a_{ij}$, $y = a_{i(j+1)}$ *when* $n \equiv 1 \pmod 2$ *and* $S\{x, y\} \in \mathscr{L}(G_m^n)$ *if and only if* $x = a_{ij}$, $y = a_{i(j+1)}$ *or* $x = a_{ij}$, $y = a_{(i+1)j}$ *when* $n \equiv 0 \pmod 2$

(3) $|\cup [\mathscr{L}(G_m^n)]| = mn$ *where* $\cup [\mathscr{L}(G_m^n)] = \cup_{LS(G_m^n) \in \mathscr{L}(G_m^n)} LS(G_m^n)$

(4) $|S\{x, y\} \cap [\cup \mathscr{L}(G_m^n)]| \ge \gamma(G_m^n)$ *for each distinct* $x, y \in V(G_m^n)$.

Proof. To prove this lemma, we proceed in the following way:

(1) It can be seen in this case when $n \equiv 0 \pmod 2$ that all the LSRNs of G_m^n are given by $S\{x, y\} = V(G_m^n)$ where $xy \in E(G_m^n)$. On the account of n being an odd number for generalized prism network G_m^n, the cardinality of LSRNs of the vertex pairs $a_{ij}a_{i(j+1)}$ is given by $|S\{a_{ij}, a_{i(j+1)}\}| = |\{a_{i(j+\lceil n/2 \rceil + 1)} | 1 \le i \le m, 1 \le j \le n\}^c| = m(n-1)$. The cardinality of the LSRNs of $a_{ij}a_{(i+1)j}$ is given by $|S\{a_{ij}, a_{(i+1)j}\}| = |V(G_m^n)| = mn$.

(2) From the proof of (1), we have $S\{x, y\} \in \mathscr{L}(G_m^n)$ if and only if $x = a_{ij}$, $y = a_{i(j+1)}$ when $n \equiv 1 \pmod 2$ and $S\{x, y\} \in \mathscr{L}(G_m^n)$ if and only if $x = a_{ij}$, $y = a_{i(j+1)}$ or $x = a_{ij}$, $y = a_{(i+1)j}$ when $n \equiv 0 \pmod 2$.

(3) From (1) and (2), we note that $|\cup [\mathscr{L}(G_m^n)]| = mn$ where $\cup [\mathscr{L}(G_m^n)] = \cup_{LS(G_m^n) \in \mathscr{L}(G_m^n)} LS(G_m^n)$.

(4) From above, we conclude that

$$|S\{x, y\} \cap [\cup \mathscr{L}(G_m^n)]| \ge \gamma(G_m^n), \tag{1}$$

for each distinct $x, y \in V(G_m^n)$. □

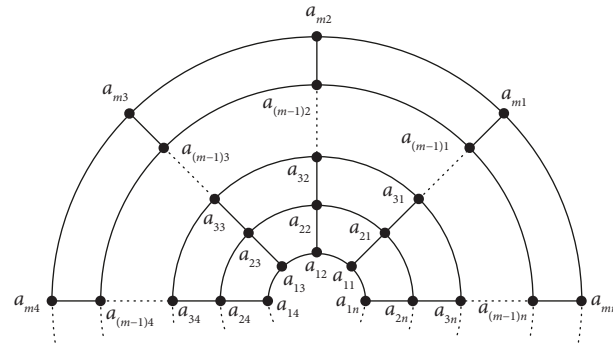

Figure 4: Generalized prism network $G_{m,n}$.

3. Local Fractional Strong Metric Dimension of Certain Complex Networks

In this section, LFSMD of certain complex networks is computed.

Theorem 2. *For $n \ge 3$,*

$$\text{lsdim}_f(C_n) = \begin{cases} 1, & \text{if } n \equiv 0 \pmod 2; \\ \dfrac{n}{n-1}, & \text{if } n \equiv 1 \pmod 2. \end{cases} \tag{2}$$

Proof. To prove the above claim, we consider the following cases:

Case 1 ($n \equiv 0 \pmod 2$)

We take note of Lemma 2, $\gamma(C_n) = |V(C_n)| = n$ and $\beta(C_n) = |\cup \mathscr{L}(C_n)| = |V(C_n)| = n$. Hence, from Lemma 1, we conclude

$$\text{lsdim}_f(C_n) = \sum_{s=1}^{\beta(C_n)} \frac{1}{\gamma(C_n)} = 1. \tag{3}$$

Case 2 ($n \equiv 1 \pmod 2$)

Here, from Lemma 2, $\gamma(C_n) = (n-1)$ and $\beta(C_n) = |\cup \mathscr{L}(C_n)| = n$. By using the Lemma 1, we have

$$\mathrm{lsdim}_f(C_n) = \sum_{s=1}^{\beta(C_n)} \frac{1}{\gamma(C_n)} = \frac{n}{n-1}. \quad (4)$$

□

Theorem 3. *For $n \geq 6$, $\mathrm{lsdim}_f(C_n(1,2)) = n/2(\lceil m + 1/2 \rceil)$.*

Proof. On account of Lemma 3, $\gamma(C_n(1,2)) = |S\{a_r, a_{r+1}\}| = |S\{a_r, a_{r-1}\}| = 2(\lceil m + 1/2 \rceil)$ where $1 \leq r \leq n$ and $m = \lceil n - 5/4 \rceil$. Moreover, $\beta(C_n(1,2)) = |\cup \mathscr{L}(C_n(1,2))| = n$. Therefore, from Lemma 1, we have

$$\mathrm{lsdim}_f(C_n(1,2)) = \sum_{s=1}^{\beta(C_n(1,2))} \frac{1}{\gamma(C_n(1,2))} = \frac{n}{2(\lceil m + 1/2 \rceil)}. \quad (5)$$

□

Theorem 4. *For $n \geq 6$,*

$$\mathrm{lsdim}_f(M_{2n}) = \begin{cases} 1, & \text{if } n \equiv 1 \pmod 2; \\ \dfrac{n}{n-1}, & \text{if } n \equiv 0 \pmod 2. \end{cases} \quad (6)$$

Proof. The proof of this theorem is subdivided into the following two cases:

Case 1 ($n \equiv 1 \pmod 2$)

Taking Lemma 4 into consideration, we have $\gamma(M_{2n}) = |V(M_{2n})| = 2n$ and $\beta(M_{2n}) = |\cup \mathscr{L}(M_{2n})| = |V(M_{2n})| = 2n$. Hence, from Lemma 1, the following can be concluded:

$$\mathrm{lsdim}_f(M_{2n}) = \sum_{s=1}^{\beta(M_{2n})} \frac{1}{\gamma(M_{2n})} = 1. \quad (7)$$

Case 2 ($n \equiv 0 \pmod 2$)

In this case by considering Lemma 4, $\gamma(M_{2n}) = 2(n-1)$ and $\beta(M_{2n}) = |\cup \mathscr{L}(M_{2n})| = 2n$. Hence, from Lemma 1 we have

$$\mathrm{lsdim}_f(M_{2n}) = \sum_{s=1}^{\beta(M_{2n})} \frac{1}{\gamma(M_{2n})} = \frac{n}{n-1}. \quad (8)$$

□

Theorem 5. *For $n \geq 6$,*

$$\mathrm{lsdim}_f(G_m^n) = \begin{cases} 1, & \text{if } n \equiv 0 \pmod 2; \\ \dfrac{n}{n-1}, & \text{if } n \equiv 1 \pmod 2. \end{cases} \quad (9)$$

Proof. The proof can be segregated into the following two cases:

Case 1 ($n \equiv 1 \pmod 2$)

In view of Lemma 5, $\gamma(G_m^n) = m(n-1)$ and $\beta(G_m^n) = |\cup \mathscr{L}(G_m^n)| = |V(G_m^n)| = mn$. By using Lemma 1, we have

$$\mathrm{lsdim}_f(G_m^n) = \sum_{t=1}^{\beta(G_m^n)} \frac{1}{\gamma(G_m^n)} = \frac{n}{n-1}. \quad (10)$$

Case 2 ($n \equiv 0 \pmod 2$)

In this case using Lemma 5, $\gamma(G_m^n) = mn$ and $\beta(G_m^n) = |\cup \mathscr{L}(G_m^n)| = mn$. Hence, from Lemma 1, we conclude that

$$\mathrm{lsdim}_f(G_m^n) = \sum_{s=1}^{\beta(G_m^n)} \frac{1}{\gamma(G_m^n)} = 1. \quad (11)$$

□

4. Application

In this section, an application of LFSMD is considered in the information processing and co-ordination of large-scale interconnection networks. Complex large-scale interconnection networks used in the design of local area networks, distributed computer systems, and telecommunication networks have been constructed based on VLSI circuit technology. In telecommunication networks, many stations are placed at short distances to share data at a very high speed, and the main objective is to optimize the exchange of data with an efficient network topology. For an illustrative case, consider a telecommunication network consisting of different stations placed at nodes of a network $C_6(1,2)$ as shown in Figure 5. In order to maintain connectivity, certain stations are required to maintain their working capacity at an optimal level. These stations are required to be at a uniform distance from all stations in order to achieve optimal connectivity. The nodes of the network $C_6(1,2)$ are $x_1, x_2, x_3, x_4, x_5, x_6$. The LSRNs of $C_6(1,2)$ are given as follows: $S\{x_1, x_2\} = S\{x_2, x_4\} = S\{x_4, x_5\} = S\{x_1, x_5\} = \{x_1, x_2, x_4, x_5\}$, $S\{x_1, x_3\} = S\{x_3, x_4\} = S\{x_4, x_6\} = S\{x_1, x_6\} = \{x_1, x_3, x_4, x_6\}$, $S\{x_2, x_3\} = S\{x_3, x_5\} = S\{x_5, x_6\} = S\{x_2, x_6\} = \{x_2, x_3, x_5, x_6\}$. For any given network, LSRN is the collection of nodes that are at unequal distances from a pair of adjacent nodes, and therefore, by assigning minimum weights to the nodes from LSRNs of the network, there will be minimum reliance on these nodes, and an optimal exchange of data is achieved in certain complex large-scale networks. In a network, stations are placed in such a way that the distance of every node of the network to the station is minimum which aids in the sharing of data at a very high speed. Taking Lemma 1 into consideration, if weight of 1/4 is assigned to all the nodes in the union of all LSRNs with minimum cardinality and zero to the remaining vertices of $C_6(1,2)$, then optimal exchange of data is achieved.

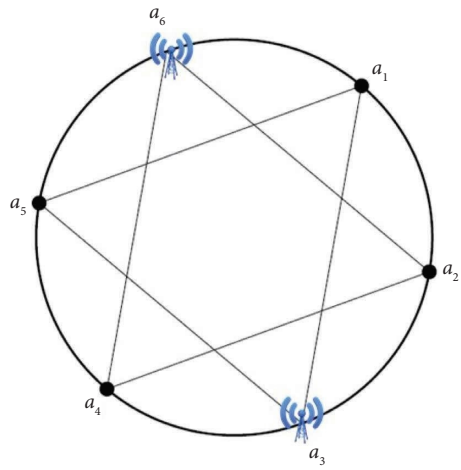

FIGURE 5: Telecommunication network using circulant network $C_6(1,2)$.

5. Conclusion

In this paper, LFSMD of complex networks is computed with the building blocks of complex networks considered as the symmetric networks such as cyclic networks C_n, circulant networks $C_n(1,2)$, mobious ladder networks M_{2n}, and generalized prism networks G_m^n.

Problem 1. Compute the LFSMD of some general classes of convex polytopes.

Data Availability

All the data used to support the findings of this study are included within this article and are available from corresponding author upon request.

Conflicts of Interest

The authors declare that they have no conflicts of interest.

References

[1] G. Chartrand, L. Eroh, M. A. Johnson, and O. R. Oellermann, "Resolvability in graphs and the metric dimension of a graph," *Discrete Applied Mathematics*, vol. 105, no. 1-3, pp. 99–113, 2000.

[2] Z. Beerliova, F. Eberhard, T. Erlebach et al., "Network discovery and verification," *IEEE Journal on Selected Areas in Communications*, vol. 24, no. 12, pp. 2168–2181, 2006.

[3] S. Khuller, B. Raghavachari, and A. Rosenfeld, "Landmarks in graphs," *Discrete Applied Mathematics*, vol. 70, no. 3, pp. 217–229, 1996.

[4] J. C. Bermond, F. Comellas, and D. F. Hsu, "Distributed loop computer-networks: a survey," *Journal of Parallel and Distributed Computing*, vol. 24, no. 1, pp. 2–10, 1995.

[5] F. T. Boesch and J. F. Wang, "Reliable circulant networks with minimum transmission delay," *IEEE Transactions on Circuits and Systems*, vol. 32, no. 12, pp. 1286–1291, 1985.

[6] G. Bolotashvili, M. Kovalev, and E. Girlich, "New facets of the linear ordering polytope," *SIAM Journal on Discrete Mathematics*, vol. 12, no. 3, pp. 326–336, 1999.

[7] D. M. Walba, R. M. Richards, and R. C. Haltiwanger, "Total synthesis of the first molecular Moebius strip," *Journal of the American Chemical Society*, vol. 104, no. 11, pp. 3219–3221, 1982.

[8] P. J. Slater, "Leaves of trees," *Congressus Numerantium*, vol. 14, pp. 549–559, 1975.

[9] F. Harary and R. A. Melter, "On the metric dimension of a graph," *Ars Combinatoria*, vol. 2, pp. 191–195, 1976.

[10] J. Currie and O. R. Oellermann, "The metric dimension and metric independence of a graph," *Journal of Combinatorial Mathematics and Combinatorial Computing*, vol. 39, pp. 157–167, 2001.

[11] M. R. Garey and D. S. Johnson, *Computers And Ineractability: A Guide To The Theory Of Np-Completenesss*, Freeman, New York, NY, USA, 1969.

[12] M. Fehr, S. Gosselin, and O. R. Oellermann, "The metric dimension of Cayley digraphs," *Discrete Mathematics*, vol. 306, no. 1, pp. 31–41, 2006.

[13] A. Sebő and E. Tannier, "On metric generators of graphs," *Mathematics of Operations Research*, vol. 29, no. 2, pp. 383–393, 2004.

[14] O. R. Oellermann and J. Peters-Fransen, "The strong metric dimension of graphs and digraphs," *Discrete Applied Mathematics*, vol. 155, no. 3, pp. 356–364, 2007.

[15] S. Arumugam and V. Mathew, "The fractional metric dimension of graphs," *Discrete Mathematics*, vol. 312, no. 9, pp. 1584–1590, 2012.

[16] J. B. Liu, A. Kashif, T. Rashid, and M. Javaid, "Fractional metric dimension of generalized Jahangir graph," *Mathematics*, vol. 7, pp. 100–110, 2019.

[17] D. A. Krismanto and S. W. Saputro, "Fractional metric dimension of tree and unicyclic graph," *Procedia Computer Science*, vol. 74, pp. 47–52, 2015.

[18] M. Feng and K. Wang, "On the metric dimension and fractional metric dimension for hierarchical product of graphs," *Applicable Analysis and Discrete Mathematics*, vol. 7, no. 2, pp. 302–313, 2013.

[19] M. Feng and K. Wang, "On the fractional metric dimension of corona product graphs and lexicographic product graphs," 1906, https://arxiv.org/abs/1206.1906.

[20] C. X. Kang and E. Yi, "The fractional strong metric dimension of graphs," in *Proceedings of the COCOA 2013, Lecture Notes in Computer Science*, vol. 8287, Chengdu, China, October 2013.

[21] F. Okamoto, B. Phinezy, P. Zhang, and P. Zhang, "The local metric dimension of a graph," *Mathematica Bohemica*, vol. 135, no. 3, pp. 239–255, 2010.

[22] J. A. Rodríguez-Velázquez, G. A. Barragán-Ramírez, and C. García Gómez, "On the local metric dimension of corona product graphs," *Bulletin of the Malaysian Mathematical Sciences Society*, vol. 39, no. S1, pp. 157–173, 2016.

[23] R. Rimadhany, "Local metric dimension of circulant graph circ (n: 1, 2, . . ., n + 1 2)," in *Proceedings of the AIP Conference prceedings*, vol. 1867, pp. 1–4, Surabaya, Indonesia, November 2017.

[24] G. A. Barragán-Ramírez, A. Estrada-Moreno, Y. Ramírez-Cruz, and J. A. Rodríguez-Velázquez, "The local metric dimension of the lexicographic product of graphs," *Bulletin of the Malaysian Mathematical Sciences Society*, vol. 42, no. 5, pp. 2481–2496, 2019.

[25] A. N. Cahyabudi and T. A. Kusmayadi, "On the local metric dimension of a lollipop graph, a web graph, and a friendship graph," *Journal of Physics: Conference Series*, vol. 909, Article ID 012039, 2017.

[26] H. Benish, M. Murtaza, and I. Javaid, "The fractional local metric dimension of graphs," 2018, https://arxiv.org/abs/1810.02882.

[27] S. Ali, R. M. Falcon, and M. K. Mehmood, "Local fractional metric dimension of rotationally symmetric planar graphs arisen from planar chorded cycles," 2021, https://arxiv.org/abs/2105.07808.

[28] S. Aisyah, M. I. Utoyo, and L. Susilowati, "On the local fractional metric dimension of corona product graphs," in *Proceedings of the IOP Conference Series: Earth and Environmental Science*, vol. 243, Indonesia, August 2019.

[29] J. B. Liu, M. K. Aslam, and M. Javaid, "Local fractional metric dimensions of rotationally symmetric and planar Networks," *IEEE Access*, vol. 8, pp. 82404–82420, 2020.

[30] F. Jamil, A. Kashif, S. Zafar, Z. Bassfar, and A. M. Alanazi, "Local fractional strong metric dimension of certain rotationally symmetric planer networks," *IEEE Access*, vol. 9, pp. 159326–159333, 2021.

Hindawi
Complexity
Volume 2022, Article ID 7413588, 17 pages
https://doi.org/10.1155/2022/7413588

Research Article

Improved Double-Layer Structure Multilabel Classification Model via Optimal Sequence and Attention Mechanism

Geqiao Liu [1,2] **and Mingjie Tan** [1,2]

[1] *College of Engineering and Technology, The Open University of Sichuan, Chengdu 610073, China*
[2] *Research Center for Educational Information Management and Information Systems, The Open University of China, Beijing 100039, China*

Correspondence should be addressed to Geqiao Liu; liugq@scrtvu.net

Received 1 April 2022; Revised 29 July 2022; Accepted 14 September 2022; Published 22 November 2022

Academic Editor: Xiao Ling Wang

Multilabel classification is a key research topic in the machine learning field. In this study, the author put forward a two/two-layer chain classification algorithm with optimal sequence based on the attention mechanism. This algorithm is a classification model with a two-layer structure. By introducing an attention mechanism, this study analyzes the key attributes to achieve the goal of classification. To solve the problem of algorithm accuracy degradation caused by the order of classifiers, we adopt the OSS (optimal sequence selection) algorithm to find the optimal sequence of tags. The test results based on the actual dataset show that the ATDCC-OS algorithm has good performance on all performance evaluation metrics. The average accuracy of this algorithm is over 80%. The microaverage AUC performance reaches 0.96. In terms of coverage performance, its coverage performance is below 10%. The comprehensive result of single error performance is the best. The loss performance is about 0.03. The purpose of the ATDCC-OS algorithm proposed in the study is to help improve the accuracy of multilabel classification so as to obtain more effective data information.

1. Introduction

Multilabel classification, a commonly used method in big data analysis, aims to associate multiple labels to a sample at the same time. The ubiquity of multilabel data in real-life scenarios makes multilabel classification methods a popular research topic. However, in real-life applications, the integrity of the labels is usually not guaranteed. Due to poor data collection and the high cost of labeling and other reasons, only part of the labels in those samples is marked. There are many ambiguous examples in the real world. Sample instances are of a certain probability to be calibrated to different attributes. Many multilabel classification algorithms come into being. Usually, it is very challenging to extend the theory of single-label classification to multilabel classification. With the development of machine learning, multilabel classification algorithms can be applied to imaging, recommendation systems, medical diagnosis, information retrieval, and many other fields [1–8]. In recent years, an ocean of research works accepted by top conferences (e.g., ACL, AAAI, COLING, KDD, NIPS, ICDM, CIKM, INTERSPEECH, ICML, and IJCAI) proposed technologies and solutions for multilabel classification. The multilabel classification theory is a heated topic in data mining, which has attracted wide attention in the machine learning community.

There are two commonly used methods to construct a multilabel classification model: algorithm adaptation and problem transformation. The algorithm adaptation method is to adjust the existing algorithms (e.g., AdaBoost and decision trees) to solve multilabel classification issues. The performance of the algorithm adaptation method often remains poor. The problem transformation method splits a multilabel classification task into several single-label classification tasks. Then, the classical single-label classification theory is utilized to solve the problem, which brings the

trained single-label classifiers together as a super-classifier through linear combination. In this study, we investigate the multilabel classification theory algorithm based on problem transformation.

There are many existing problem transformation methods, such as the BR method [9], the CC theory [10], the MBR model [11], and the DLMC-OS algorithm [12]. However, these methods usually ignore the correlation among labels, the randomness of label sequences, and the redundant interactive label information, which reduces the accuracy of classification. The problem transformation method uses extended attributes to dig out the correlation between labels, but for different classification tasks, the importance of feature attributes is usually ignored during the process, which decreases the sensitivity of the classifiers. Therefore, we try to introduce an attention mechanism into the methods. Such attention mechanism method [13] is a bionic process based on how the human brain works. It is widely used in machine learning in areas such as speech recognition, image recognition, natural language processing, and so on. The attention mechanism usually calculates the probability mapping from an input to different outputs. The result with the largest probability will be chosen as the output, which has a great impact on considering the correlation between multiple attributes and labels. Then, we propose an attention mechanism-based multilabel classification algorithm, based on the double-layer chain structure.

In the proposed algorithm (algorithm of two/double-layer chain classification with optimal sequence based on attention mechanism, ATDCC-OS), we integrate three multilabel classification frameworks (including BR, MBR, and CC) and an attention mechanism into a chain structure with two layers. This structure exploits a binary association classification framework. In layer one, it carries out the initial classification. In layer two, the chain-based classifier utilizes an updating process to complete the final classification, which interacts with the label information coming from the output of layer one. In particular, we put an attention mechanism in layer two and use the output of layer one to calculate the probability of final classification results. Thus, this can find important information between different attributes and can improve the final classifier accuracy for different tasks. However, there is a random chain order problem in ATDCC-OS. We leverage the optimal sequence selection (OSS) algorithm to solve this issue. OSS integrates several variables and methods (including the hierarchical traversal algorithm, PageRank, Kruskal's algorithm, and mutual information) to decide labels' priority. Then, the priority rank is used to help ATDCC-OS to assign classifiers and construct the chain classification model.

In this study, the main contributions are as follows: (1) A double-layer structure multilabel classification model is constructed to fully integrate the advantages of three classical classification models. At the same time, an attention mechanism is introduced to further analyze the influence of key attributes on classification results to optimize traditional classification. (2) The OSS algorithm is proposed to solve the problem of low classification accuracy due to the existence of random chain order in the chain classification model. It is applied to improve the second layer of the chained classification model. This classification model does not depend on any classification algorithm separately. Experiments on benchmark datasets validate the effectiveness of the proposed approach by comparing it with the state-of-the-art methods in terms of predictive performance.

The rest of this study includes the following: Section 2 deals with related work. Section 3 displays the proposed ATDCC-OS method. Then, we introduce the datasets used in the experiments and perform some simulations to verify the proposed method and discuss the experimental results in Section 4. We conclude our work in Section 5.

2. Related Work

2.1. Multilabel Classification Method. The multilabel classification approach has received much attention and is widely used in various fields, including text classification, scene and video classification, and bioinformatics. The multilabel classification includes two common methods: problem transformation process and algorithm adaptation process. The former changes a multilabel problem into one or several single-label issues [11] and uses basic classification algorithms, such as Naive Bayesian, supporting vector machine [14], k-nearest neighbor algorithm, and so on to solve them. The latter transforms the existing algorithms so that they can solve the multiclassification problem, e.g., ML-RBF method [15, 16], ML-kNN approach [17, 18], rank-SVM classification [9], and associated classification algorithm [19, 20].

BR (binary relevance) [9] is a common method of problem transformation, which transforms the multilabel classification issue into several binary relevance problems where it trains a binary classification model one by one for all labels. However, BR is often overlooked because it cannot effectively use the correlation between labels. The MBR based on BR was proposed [11], which was constructed as a two-layer model. Layer one in MBR is taken as the input of layer two as a sample attribute to consider label correlation. However, the problem of the label value redundancy is ignored in the training process of layer two.

The CC method was proposed by the authors in [10], where the chain is exploited to build the correlation among all labels. It converts all classifiers into the linear stochastic data chain and adds previous classifiers' output to the data sample attribute set and takes it as the input to the next classifier. However, there are many disadvantages to the random chain. First, in the CC training process, the classifier output is input as a new attribute together with the original attribute into the next classifier. So, the former classifiers in the chain have a greater impact on classification than the latter classifiers. The order of classifiers in the chain affects the classification result. Second, CC considers the correlation of attributes, but two linked classifiers can use the correlation between adjacent attributes, and the other correlation between attributes cannot be used. Finally, the order of classifiers in the chain is randomly assigned, so the CC model is not unique, which makes the model have strong randomness and ruins the stability of the algorithm [21, 22].

The two-layer classification model, DLMC-OS, is proposed to solve the classification problem [12]. In this model, the output of the first-level classifier is forwarded to the second-level classifier as an extended feature. Each classifier in the second layer of the model passes the latest classification results backward through a chain to consider the correlation between labels. This approach suppresses the classifier chain randomness, but it cannot obtain the unique classifier sequence in the chain.

2.2. Attention Mechanism. The attention mechanism method [23–25] is derived from the study of human vision, which simulates the perspective interest of human vision when observing. When the human eye scans the global image, the part of the information that assists the judgment is tracked dynamically in the image, and irrelevant information is ignored. This process can effectively decrease or reduce the amount of information processing when the eyes recognize images by paying more attention to part information. The modern attention mechanism is adopted for machine translation, and it greatly improves the performance of the model [26]. In 2014, Google Brain published an article on the attention mechanism [27]. The article pointed out that when viewing an image, people do not first look at the image pixels but pay more attention to the image's specific parts based on their requirements. In addition, as humans, we will focus on the required attention locations in the future based on previous observations of images. The authors designed a new architecture named transformer. In a transformer, the self-attention mechanisms are extensively utilized to perform text representations [28], which break away from the traditional RNN/CNN. In recent years, transformer-style models achieved many good results in various tasks. Subsequently, attention mechanisms have become more common and are widely used in classification tasks, such as sentiment classification [29], musical instrument recognition [30], visual recommender systems [31], multilabel text classification [32], and multiple protein subcellular location prediction [33].

3. ATDCC-OS

3.1. Preliminaries. We set $\chi \in \Re^d$ and $Y \in R^L$ as the input domain and output domain, respectively. There are d-dimensional attributes in the input domain and L-dimensional labels in the output domain. Instance x belongs to a subset of attributes. We use the set Lvector $x_i \in \chi$ to represent that x is the input and y is the output. If the label j is related to x, then $y_j = 1$, or $y_j = 0$. The set $D = \{(x_i, Y_i)|1 \le i \le m\}$represents the trained multilabel classification model, where $x_i \in \chi$ is an attribute vector $(x_{i1}, x_{i2}, \cdots, x_{\mathrm{id}})^T$ with d dimensions and $Y_i \subset \gamma$ indicates a label set corresponding to x_i. To construct a multilabel classifier, we let H: $\chi \longrightarrow 2^{\gamma}$. $H^f = (H_1^f, H_2^f, \cdots, H_L^f)$ and $H^s = (H_1^s, H_2^s, \cdots, H_L^s)$ as the first and second layers of the multilabel classifier, respectively. $c^f = (y_1^f, y_2^f, \cdots, y_L^f)$ and $c^S = (y_1^S, y_2^S, \cdots, y_L^S)$ are the outputs of the first and second layers.

3.2. The ATDCC Framework. By referring to algorithm DLMC-OS, we construct the double-layer chain classification based on the attention mechanism (ATDCC). ATDCC converts the multilabel classification issue into a series of binary classification issues, each one of which is independent of others. In layer one, ATDCC performs binary transformation on labels and constructs some classifiers between attributes and labels. After training, the classifiers of each binary classification model can be obtained [12]. ATDCC completes the binary classification of instances in layer one and then makes the classification results as the extended attributes transfer to layer two. In layer two, ATDCC constructs a classification method with a chain structure by realizing the updating process of dynamic feedback. It exploits the classifier chain to transfer and change the labels. It realizes the interaction among labels and optimizes the classification result. ATDCC utilizes correlation among all labels for multilabel classification through label information interaction within layers and labels information transfer between layers.

3.2.1. ATDCC$^{First\text{-}Layer}$. ATDCC$^{\text{First-layer}}$ follows the idea of a binary correlation classification model. It constructs a classifier with a binary structure for all labels. These binary classifiers are combined as classification one, as shown in Figure 1.

In step one, assume there is an annotated dataset with a size being L. ATDCC$^{\text{First-layer}}$ constructs an attribute set for all labels by using the following equation:

$$D_{y_k}^f = \{(x_i, y_k)|1 \le i \le m\},$$
$$\text{where} y_k = \begin{cases} 1, & \text{if } y_k \in Y_k, \\ 0, & \text{otherwise.} \end{cases} \quad (1)$$

In step two, some binary algorithms B (such as SMO) are utilized to create the binary classifier of the training instance: $H_{y_k}^f \leftarrow B(D_{y_k}^f)$.

In step three, we use the obtained binary classifier to classify and predict the unseen instance X.

$$H_{y_k}^f : X \times \{0,1\}^{L-1} \longrightarrow \{0,1\},$$
$$y_k^f = \left\{H_{y_k}^f(X)|X \in X \times (0,1)^{k-1}, \quad 1 \le k \le L\right\}. \quad (2)$$

Finally, the prediction result of each classifier (i.e., $c^f = (y_1^f, y_2^f, \ldots, y_L^f)$, as shown in Figure 1(b)) is the output of the unseen instance in the first layer of ATDCC, integrating these output c^f with the attribute set of samples to build a new attribute set $x' = \{(x_i, c^f)|1 \le i \le m\}$. Let x' be the input of layer two in ATDCC.

3.2.2. ATDCC$^{AT\text{-}Layer}$. The attention mechanism is usually exploited in sequence-to-sequence learning paradigms. For different multilabel classification tasks, the attribute mapping weights between the two layers of ATDCC are different. The attention mechanism method can capture the weight value of all attributes in samples according to requirements. It can improve the final accuracy of classification results.

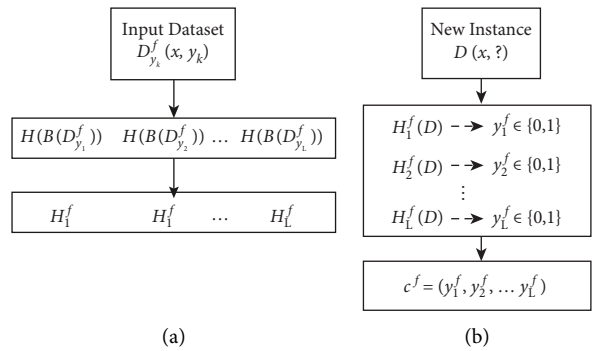

Figure 1: The first layer of ATDCC: (a) the training procedure of ATDCC $^{\text{First-layer}}$ and (b) the test procedure of ATDCC $^{\text{First-layer}}$.

ATDCC$^{\text{AT-layer}}$ uses the attention mechanism mentioned above to dynamically compute the extended attributes' weights. The layer two model can adapt to the requirement of the current classification task by adjusting the weight value of the transfer attributes between the two layers in ATDCC.

In step one, according to the original sample attributes' dimension of the first layer to define weight matrix W, the tanh function is exploited to train ATDCC$^{\text{AT-layer}}$ to capture correlations between input attributes and label i. The trained model can be expressed as

$$e_{ij} = \tanh\left(W_{ij}x'_{ij} + b\right), \quad (1 \le i \le m), \tag{3}$$

where W and b, respectively, denote the weight matrix and the model's bias.

In step two, ATDCC$^{\text{AT-layer}}$ uses a softmax function to transform the output of equation (3) to a probability value and then obtains the weight value of the attention scores.

$$W'_{ij} = \text{softmax}\left(e_{ij}\right) = \frac{\exp\left(e_{ij}\right)}{\sum_m^{j=1} \exp\left(e_{ij}\right)}. \tag{4}$$

Finally, the extended attribute set is weighted based on the attention weights obtained from equation (4):

$$x'' = \sum_m^{i=1} x'_{ij}w'_{ij}. \tag{5}$$

The parameters in our model are optimized by carrying out the minimization of the feedback result of the loss function. The cross-entropy loss in equation (6) is used as the loss function. The following equation calculates the accumulated loss derived from actual and predicted labels for each instance:

$$J(\theta) = -\frac{1}{l}\sum_{l}^{k=1} \log p\left(y_k | y'_k\right). \tag{6}$$

3.2.3. ATDCC$^{\text{Second-Layer}}$. ATDCC$^{\text{Second-layer}}$ is the second layer of the ATDCC model (Figure 2), which uses the classification structure with a chain and exploits an updating process to classify instances in the second time. The attribute set of each binary model expands the correlation of the classification labels before the instance to create the chain structure of classifiers. The attribute set of all binary models is augmented via the 0/1 label estimation value obtained in layer one as well as the whole prior binary correlation estimations from layer two. In the second layer, the correlations between each label are fully applied. Given the attribute set, each classifier in the chain will learn and predict the binary association of labels.

In step one, ATDCC$^{\text{Second-layer}}$ creates the extended attribute vector $D^s_{yk}(1 \le k \le L)$ for each class label as shown in the following equation.

$$D^s_{y_k} = \left\{\left(\left[w_i x_i, w_{i+1}y^f_1, \cdots, w_{i+k-1}y^f_{k-1}, w_{i+k+1}y^f_{k+1}, \cdots, w_{i+L}y^f_L\right], y^f_k\right) | 1 \le i \le m\right\}, \tag{7}$$

where W represents the set of attributes' weight value.

In step two, we use binary approach B (such as SM) to learn the constructed extended attribute vector (O) to create the binary classifier, $H^s_{yk} \leftarrow B(D^s_{yk})$.

In the third step, use the constructed binary classifier to classify and predict the unseen instance X.

$$D^s_{y_k} = \left\{\left(\left[w_i x_i, w_{i+1}y^f_1, \cdots, w_{i+k-1}y^f_{k-1}, w_{i+k+1}y^f_{k+1} \cdots, w_{i+L}y^f_L\right], y^f_k\right) | 1 \le i \le m\right\}. \tag{8}$$

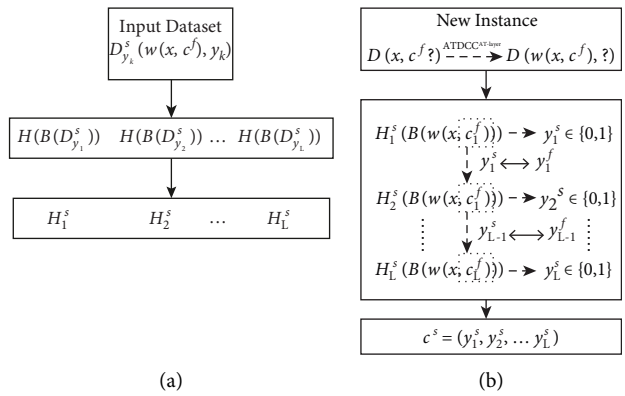

Figure 2: The second layer of ATDCC: (a) the training procedure of ATDCC$^{\text{Second-layer}}$ and (b) the testing procedure of ATDCC$^{\text{Second-layer}}$.

In the model training process, we use the latest predicted label value to change each sample attribute set's label value. For example, for the third classifier $H^S_{y_3}$ in a chain, the next sample's attribute variable is $[x, y^s_1 y^s_2, y^f_3, y^f_4, \ldots, y^f_L]$ instead of $[x, y^f_1, y^f_2, y^f_3, y^f_4, \ldots, y^f_L]$.

Finally, ATDCC evaluates the classification prediction result $c^s = (y^s_1, y^s_{2'}, \ldots, y^s_L)$ of each classifier as the final classification for the unseen instance.

3.3. OSS Method. In the MBR model, the sequence of the classifiers in the chain is randomly arranged. If the classification accuracy of the classifier at the core of this chain is very low, an error will be propagated via a backward way along this classifier chain, decreasing the classifier's accuracy. This further leads to lower classification correctness and accuracy for the whole chain. As the number of labels increases, the randomness of the OSS classifier chain also increases rapidly. The algorithm DLMC-OS can reduce the classifier chain's randomness, but the optimal label recognition sequence cannot be determined due to the nonuniqueness of the root node. The most effective method is to sort the sequence of the chain. The sequence of the classifier needs to be ranked according to attributes and the characteristics of the chain classification model. For this reason, the following constraints are proposed to search for the optimal chain sequence:

(A) The label list is ordered according to a sequence which contains all label information

(B) The label sequence satisfies the greatest correlation of labels

(C) The label list sequence is optimal under current conditions

Under these design rules, we propose OSS in the model, which integrates mutual information and PageRank with the Kruskal algorithm and the hierarchical traversal method to find an optimal label sequence. The chain classification model uses sequences as the rules to assign the order of each classifier, and the second layer will optimize the ATDCC with the OSS algorithm.

3.3.1. Subalgorithm Related with OSS

(1) *Mutual Information (MI) Theory*. In the information theory and probability theory, mutual information (MI) is used to evaluate the interdependence between two random variables, so we can obtain the "information amount" of a stochastic variable by observing the other random variables. Equation (9) shows the MI of the two variables. In current information technologies, the probability theory and information theory have been widely used. The MI theory is widely exploited in research works. In the machine learning field, MI can be utilized to select the features [34, 35]. The search engine often uses MI among phrases and contexts to find discover semantic clusters [36]. In statistical mechanics, MI is usually used to solve mechanical problems together with Loschmidt's paradox [37, 38].

Based on the MI application, we evaluate the correlation between labels by capturing MI among labels. Then, we exploit it as edges' weight in the fully connected graph.

(2) *PageRank.* PageRank (PR) is used to overcome the page ranking issue in the detailed link analysis process, which was proposed in reference [39]. The key idea of this algorithm includes that the page's importance is related to the number as well as the detailed quality of another page that points to this page. This algorithm is applied in Google's search engine [40]. The importance of a Webpage can be quantified by the number of links in the link structure, rather than relying on specific search requests. Twitter uses a personalized PageRank to show users' another account [41]. In this study, we use PageRank and priority search to build the customized PageRank algorithm to decide a very important label to act as the chain's first node. This can overcome the issue of nonuniqueness of the chain head.

(3) *Edge Weight-Based Graph Algorithm.* Usually, the connection between different entities can be

formulated as a graph with edge weights [42]. The weight of an edge may represent cost, length, or capacity, depending on the current problem to be solved [43–46]. In the model, we exploit this weighted graph method to create the graph with a fully connected relationship related to the labels in Algorithm 1.

(4) *Detailed Kruskal's Algorithm Idea.* In this study, the referred Kruskal's algorithm is utilized to seek a tree with minimum spanning [47]. We use Kruskal's method to seek a tree with the largest label spanning. This can provide a basis to create a sequence in which the association with labels is the largest. The designed algorithm is shown in Algorithm 2.

(5) *Breadth-First Based Search Method.* In this study, the breadth-first based search (BFS) is an algorithm used for seeking the available paths of the graph, which traverses or searches the tree or graph data structures. Then, we use PageRank to find the starting point and use BFS to traverse the spanning tree with the maximum label to construct the resulting label order, as shown in Algorithm 3.

3.3.2. The OSS's Detailed Design Framework. The detailed design steps for the OSS algorithm in this study are shown in Figure 3.

Step 1. Calculate the MI of the correlation between labels. Assuming that there are N labels $y_1, y_2, \ldots, y_n$, we use formula (9) to calculate the MI on any two labels y_i and y_j, and the MI must be nonnegative.

Definition 1. The formula of MI calculation is

$$I(y_i, y_j) = \sum_{y_i y_j} p(y_i, y_j) \log\left(\frac{p(y_i, y_j)}{p(y_i)p(y_j)}\right). \tag{9}$$

Step 2. Construct a fully connected graph G via labels, where the labels are the graph's vertices, and MI volume among labels acts as edges' weights. Utilize the Kruskal algorithm to build the label tree with the maximum weight. Then, invert the mutual information value to obtain the maximum weight spanning tree.

Step 3. Use the PageRank algorithm to sort each label in the dataset by "voting" and decide on the label node whose PR value is the highest. This node acts as the root node that belongs to a tree with the maximum weight. It is also selected to act as the first node of the traversal algorithm that is hierarchical. This can overcome the issue of not unique head label in the chain.

Step 4. Use Kruskal's algorithm to generate a minimum weight label tree (MWT) used for the fully connected graph G. The label tree includes the whole labels and the entire edges. These edges connect the label nodes. The weighted sum is the largest.

Step 5. Traverse the MWT with the label nodes obtained by BFS and PageRank to obtain the label sequence. Use this sequence as a guide for constructing the sequence of each classifier in a chain to overcome the uncertainty issue for the classification, as shown in Algorithm 4.

3.4. The ATDCC-OS Framework. The ATDCC-OS design framework is plotted in Figure 4. Figure 4 shows that the $\text{ATDCC}^{\text{First-layer}}$ and $\text{ATDCC}^{\text{Second-layer}}$ are the first and second layers. We utilize the OSS approach to optimize the chain structure in the ATDCC-OS framework. Then, we can seek an optimal sequence of labels. According to the best and optimal serials, we train each classifier in our model. We utilize this attention mechanism layer between layer one and layer two to find important attributes and features from the current task. In such a case, we can build a better classifier in layer two, as shown in Algorithms 5 and 6.

4. Experiments

To validate the method, we perform some simulations and use the experimental results to analyze the performance of the proposed algorithm. In the simulation, we analyze the algorithm (ATDCC-OS) presented in this study with other algorithms of multilabel classification (including DLMC-OS and BR and CC and MBR) via five metrics. We then take seven datasets as the multilabel benchmark.

4.1. Test Datasets. We utilize the standard datasets provided on the Mulan [48] platform as the multilabel benchmark. Table 1 describes each dataset and related statistical data in the simulation. N, F, and L represent instances' numbers, attributes' numbers contained in each instance, and labels' numbers in the dataset, respectively. The notation label cardinality (LCard) represents the normal measure as shown in [49]. LCard denotes the average label number associated with an instance.

4.2. Evaluation Methods. The evaluation indicator is a measure that directs the indication of the algorithm's performance. To better evaluate the method, we used mean accuracy, coverage rate, single error, ranking loss rate, and microaverage AUC to analyze the performance of ATDCC-OS.

(1) Average precision: average precision [12] is an accurate metric, which associates recall with precision to sort search results. It reviews a mean score of labels with a higher rank than a specific tag. The larger the value of the average precision is, the better the classifier will be. The average precision can be expressed as

Input label values to construct a label map with weights:
Input $Y = \{y_1, y_2, \ldots, y_L\}$
Output: G
(1) $G \leftarrow \{\}$
(2) $G.V \leftarrow Y$
(3) For each (u, v) in $G.V$
(4) Calculate the mutual information of MI (u, v) according to Definition 1.
(5) $G.E \leftarrow$ MI (u, v)
(6) $G \leftarrow G(V, E)$
(7) Return G

Algorithm 1

Constructing the minimum spanning tree of labels based on Algorithm 1:
Input: $G(V, E)$
Output: MWT
(1) MWT $\leftarrow \{\}$
(2) For $v \in G$, then V is:
(3) Make the set (v)
(4) For (u, v) in G. E is ordered according to weight (u, v) via an increasing way:
(5) If set$(u) \neq$ set(v):
(6) MST = MST $\cup$ $\{(u, v)\}$
(7) Let it Union (u, v)
(8) Return MWT $\leftarrow$ MST

Algorithm 2

Hierarchical traversal to get the label sequence:
Input: MWT (V, E)
Output: OS
(1) Queue $Q \leftarrow \{\}$
(2) For each $v \in$ MWT.V:
(3) $Q \leftarrow Q \cup (v)$
(4) while$(Q! = \varnothing)$
(5) $v \leftarrow$Q.head, $w \leftarrow$Q.next
(6) while$(w! = \varnothing)$
(7) $Q \leftarrow Q \cup (w)$
(8) end while
(9) end while
(10) end for
(11) OS$\leftarrow Q$
(12) Return OS

Algorithm 3

$$\text{avgprec}_D(H) = \frac{1}{P}\sum_{i=1}^{P}\frac{1}{|Y_i|}\sum_{y\in Y_i}\frac{\left|\left\{y' | \text{rank}_C(x, y') \leq \text{rank}_C(x_i, y), y' \in Y_i\right\}\right|}{\text{rank}_C(x_i, y)}, \tag{10}$$

Where rank(.) is a sort function.

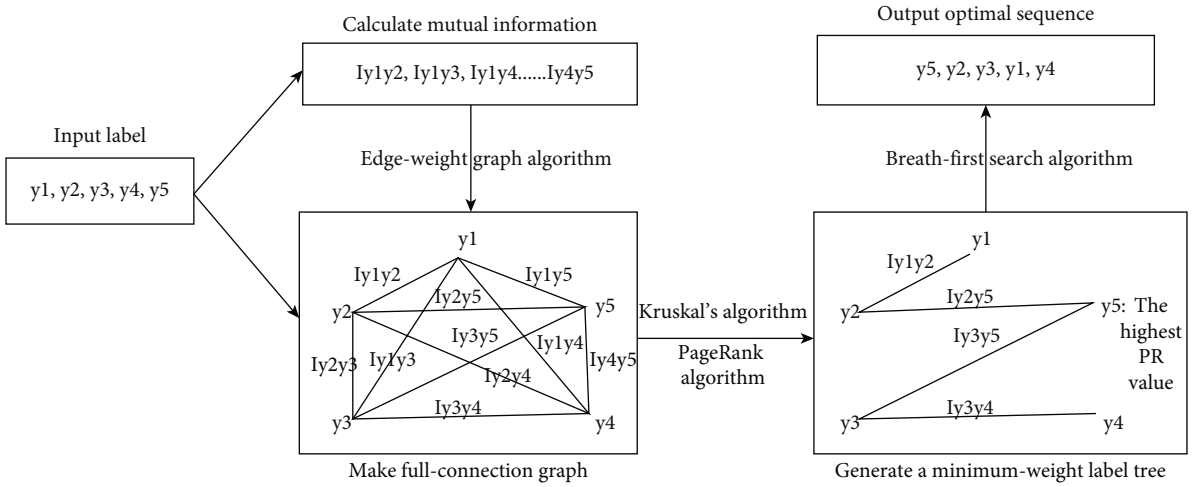

Figure 3: The OS computation process.

Find labels' optimized chain order:
Input: Variable $D = (x_1, x_2, \cdots, x_n | y_1, y_2, \cdots, y_L)$
Output: OS$(y_1, y_2, \ldots, y_L)$
(1) ▷Calculate mutual information according to Definition 1
(2) for$i = 1, 2 \ldots, L$
(3) for$j = i + 1, 2, \ldots, L$
(4) $I_{ij} \leftarrow$MI(y_i, y_j)
(5) Array$A \leftarrow I_{ij}$
(6) End for
(7) End for
(8) ▷Make a fully connected graph
(9) $G \leftarrow$Edge – weightedgraph(L, A)
(10) ▷Determine the root node by PageRank
(11) $V \leftarrow$PageRank(D)
(12) ▷Get the maximum weight label Tree
(13) $T \leftarrow$Kruskal(G, V)
(14) ▷Get the optimal sequence
(15) OS$(y_1, y_2, \ldots, y_L) \leftarrow$Breadth – firstsearch$(T)$
(16) Return OS

Algorithm 4

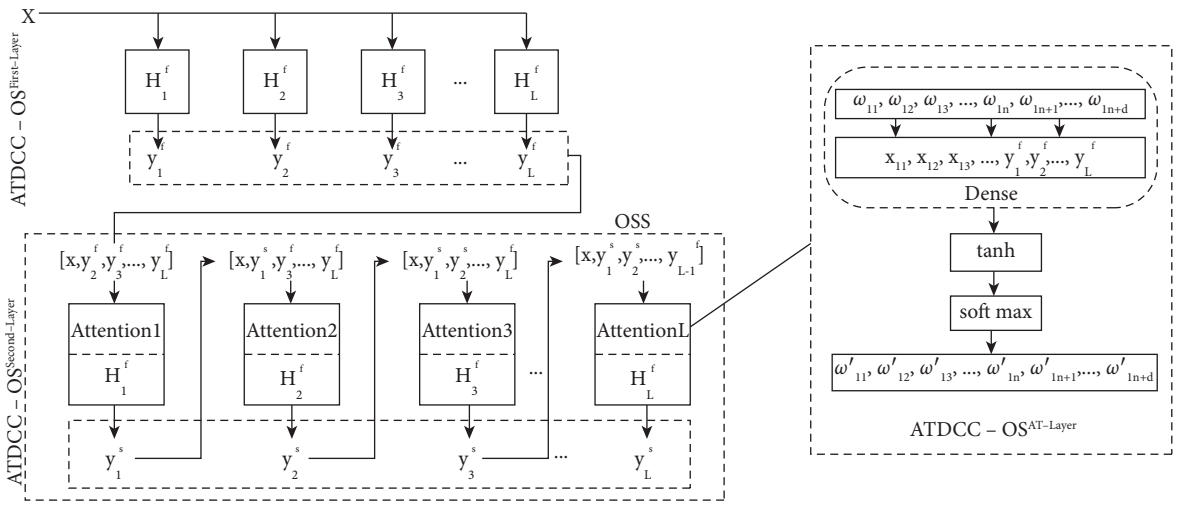

Figure 4: The DCC-OS model's design framework.

D is the training set, L is the labels' number
TRAINING $D = \{(x_i, Y_i) | i = 1, 2, \ldots, m\}$
(1) ▷Train the first-layer classifier
(2) for $j = 1, 2, \ldots, L$
(3) $D_{y_j}^f \leftarrow$
(4) do $x \leftarrow [x_{i1}, x_{i2}, \ldots, x_{im}]$
(5) $D_{y_j}^f \leftarrow x \cup y_j$
(6) $H_j^f \leftarrow \mathrm{B}(D_{y_j}^f)$
(7) end for
(8) ▷Use the OSS algorithm to obtain the label priority order to guide the training of the second-layer classifier
(9) for $j = \mathrm{sort}1, 2, \ldots, L\mathrm{byOSS}(D)$
(10) $D_{y_j}^s \leftarrow$
(11) do $x \leftarrow [x_{i1}, x_{i2}, \ldots, x_{im}, y_1, \ldots, y_{j-1}, y_{j+1}, \ldots, y_L]$
(12) ▷Compute attribute value weights using the attention mechanism
(13) $W \leftarrow \{W_{i1}, W_{i2}, \ldots, W_{im+L}\}$
(14) $W \leftarrow \mathrm{attention}(x)$
(15) $x' \leftarrow x \times W$
(16) $D_{y_j}^s \leftarrow x' \cup y_j$
(17) $H_j^s \leftarrow \mathrm{B}(D_{y_j}^s)$
(18) $y_j = H_j^s(x')$
(19) End for

Algorithm 5

Classify(x): classify new instance X
(1) Global $c^f = (y_1^f, y_2^f, \cdots, y_L^f) c^s = (y_1^s, y_2^s, \cdots, y_L^s)$
(2) ▷Classify x for the first time using the first-layer classifier
(3) for $j = 1, 2, \ldots, L$
(4) do $x \leftarrow [x_{i1}, x_{i2}, \ldots, x_{im}]$
(5) $y_j^f \leftarrow H_{y_j}^f(x)$
(6) End for
(7) ▷Classify x for the first time using the second-layer classifier
(8) $x' \leftarrow [x, y_1^f, y_2^f, \ldots, y_L^f]$
(9) for $j = \mathrm{sort}1, 2, \ldots, L\mathrm{byOSS}(D)$
(10) do $x'' \leftarrow x' \times W_j'$
(11) $y_j^s \leftarrow H_j^s(x'')$
(12) End for
(13) ▷Get the final classification result
(14) $c^s \leftarrow (y_1^s, y_2^s, \ldots, y_L^s)$
(15) Return c^s

Algorithm 6

(2) Coverage [12]: coverage indicates that the algorithm can cover all possible labels. This metric describes how far or how deep we are to go in the tag list on average to include possible labels related to the document. At the perfect recall level, coverage is loosely related to accuracy. The smaller the value of coverage is, the better the algorithm will be. The coverage can be calculated as

$$\mathrm{coverage}_D(H) = \frac{1}{P} \sum_{i=1}^{P} \max \mathrm{rank}_f(x_i, y) - 1, \tag{11}$$

Where notation rank(.) denotes a sort and ranking function related to the classifier $H(.)$.

(3) One-error metric [50]: one-error metric is used to indicate the proportion of examples where the top label does not fall into the selected label set. The bigger this metric is, the worse the algorithm will be. The one-error metric can be expressed as

$$\mathrm{one} - \mathrm{error}_D(H) = \frac{1}{P} \sum_{i=1}^{P} \left\| \left[\mathrm{argmax}_{y \in \gamma} f(x_i, y) \notin Y_i \right] \right\|, \tag{12}$$

Table 1: Datasets with multiple labels.

Dataset	N	F	L	LCard	Type
Flags	194	19	7	3.392	Images
Emotion	593	72	6	1.87	Music
Birds	654	300	21	1.104	Audio
Medical	978	1449	45	1.245	Text
Enron	1702	1001	53	3.38	Text
Yeast	2417	103	14	4.24	Biology
BibTeX	7395	1836	159	2.40	Text

Where $f(.)$ stands for a function associated with a classifier $H(.)$ with multiple labels.

(4) Ranking loss metric [12]: the ranking loss metric is related to those situations in which the classed labels of samples are not sorted in order, that is, in the label serials, the classified labels (that are not related to the researched instance) fall into the previous related labels. The bigger this indicator is, the better the algorithm performance will be. The ranking loss metric can be expressed as

$$\text{rloss}_D(H) = \frac{1}{P}\sum_{i=1}^{P}\frac{1}{|Y_i||\overline{Y_i}| \times |\{(y', y'') | f(x_i, y') \le f(x_i, y''), (y', y'') \in Y_i \times \overline{Y_i}\}|}. \tag{13}$$

(5) Microaveraged AUC [50]: this metric shows the area covered by a ROC curve graph. Its value is from 0.1 to 1. This metric is directly exploited to review the classifier's performance. The smaller this metric is, the worse this algorithm will be. The microaveraged AUC metric is

$\text{AUC}_{\text{micro}} = |\{(x', x'', y', y'') | f(x', y') \ge f(x'', y''), (x', y') \in S^+, (x'', y'') \in S^-\}|/|S^+||S^-|$, where $f(.)$ is a real-valued function [51] and the following equations can be obtained:

$$S^+ = \{(x_i, y) | y \in Y_i, 1 \le i \le p\}. \tag{14}$$

$$S^- = \{(x_i, y) | y \notin Y_i, 1 \le i \le p\}, \tag{15}$$

where they denote label pairs' sets which are related or unrelated.

4.3. Experimental Setting. We use the dataset provided by the Mulan platform to evaluate all algorithms. The Mulan [48] is an open-source dataset used for classification with multiple labels, which is based on Weka. In this study, we use SMO as a basis for classification algorithms. Four different classifiers are utilized to carry out comparisons, including the DLMC-OS algorithm, the MBR algorithm, the CC algorithm, and the BR algorithm. We select 80% of instances from every dataset to act as training datasets, while we choose the rest to act as testing datasets. We adopt Adam [52] as the optimizer during the training process. We list the default parameters of Adam's hyperparameters as follows: let alpha be 0.001, set beta1 to be 0.9, let beta2 be 0.999, and set epsilon to be 10^{-8}. Our simulation platform includes the Intel(R) Xeon(R) E5-2630 CPU, 128 GB RAM, as well as the operating system Centos 7.6. We design and implement the algorithms in the Java (JDK 1.8) running environment.

4.4. Results and Discussion. Figures 5–10 show the performance comparison among ATDCC-OS, DLMC, MBR, CC, and BR algorithms, using mean accuracy, coverage metric, single error metric, ranking loss metric, and microaverage AUC metric. We use the metric of the mean ranking (Ave. rank) parameter to review different classification results of the algorithms [53]. In these figures, each color represents an algorithm and the name of the algorithm has been listed in the upper left corner of the graph. The number on the top of each bar is the performance rank of the algorithms in the dataset. In Figures 5–9, the ordinate y-axis denotes the results of the evaluation, while the abscissa x-axis stands for the names of the dataset. In Figure 10, x-axis denotes the name of the algorithm, while y-axis shows the average rank of algorithms in all datasets.

Figure 5 shows the accuracy of each algorithm in each dataset. The ATDCC-OS method proposed in the study has the best performance in the dataset. Compared with other methods, except for the lowest accuracy in the yeast dataset, the accuracy in other datasets is the highest. Among them, the accuracy in the datasets of flags, emotions, and the medical dataset is over 80%.

In Figure 6, we can see the comparison of the microaverage AUC performance of the algorithms. The ATDCC-OS algorithm is also the most excellent and stable in terms of microaverage AUC performance. The performance of this algorithm is the best except for that in the birds dataset, and the performance in the medical dataset is 0.96.

Figure 7 shows the comparison of the coverage performance of each algorithm. The lower the coverage, the

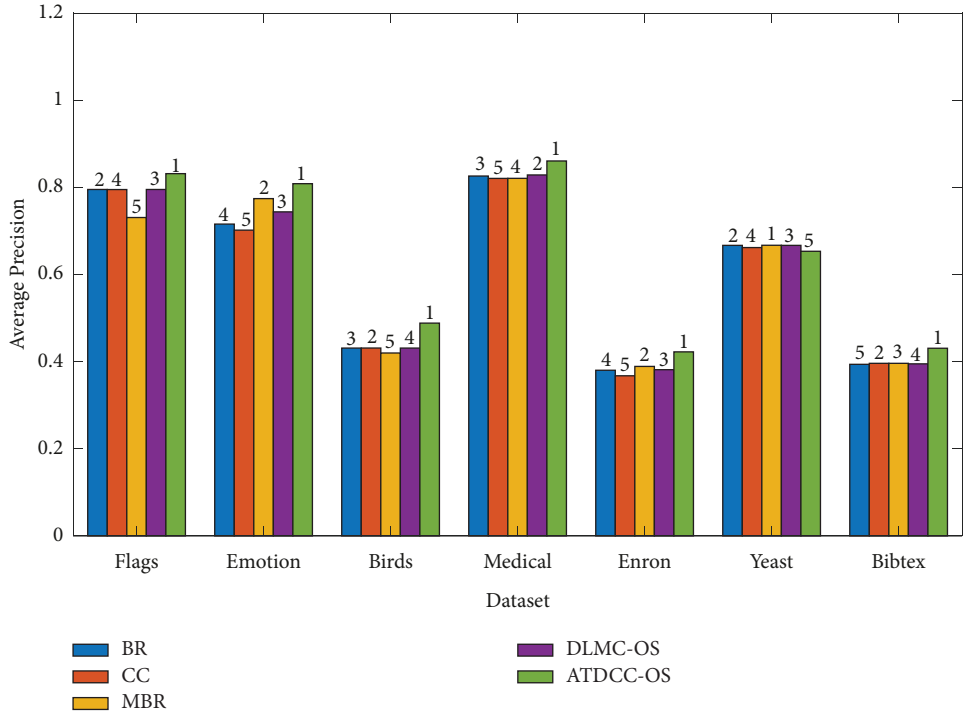

Figure 5: The average precision of algorithms.

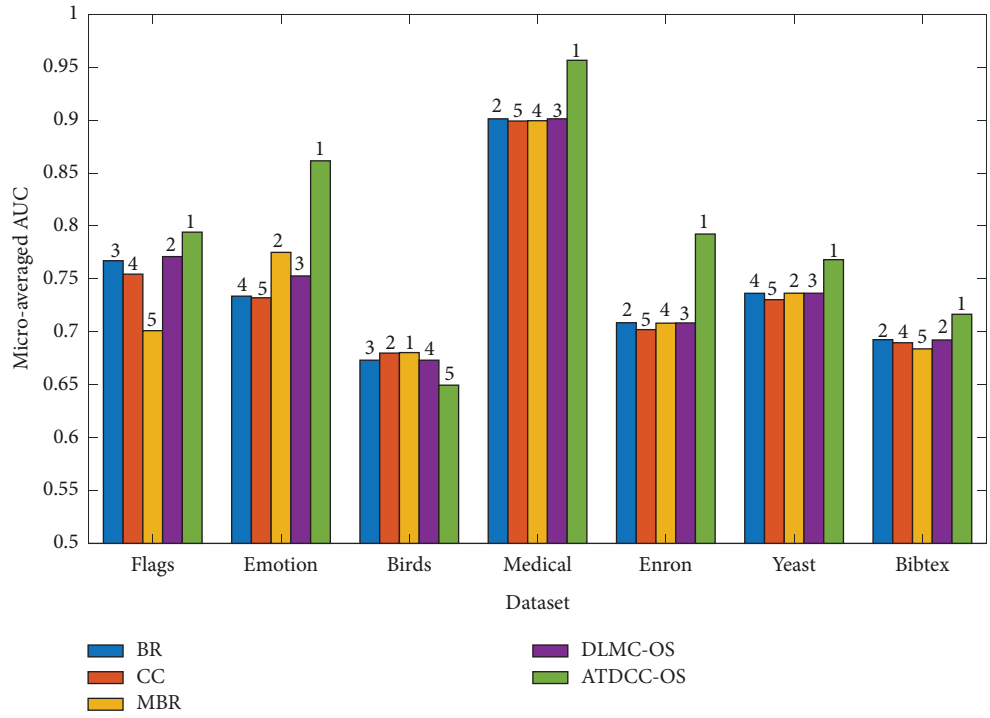

Figure 6: The microaveraged AUC performance of algorithms.

better the performance of the algorithm. The coverage performance of the ATDCC-OS algorithm proposed in the study is optimal in all datasets, and its coverage performance is less than 10% in flags, emotions, birds, medical datasets, and yeast datasets.

The single error performance of each algorithm is shown in Figure 8. The performance of the proposed ATDCC-OS algorithm in this graph is relatively unstable compared with other algorithms. However, from a comprehensive perspective, the performance of this algorithm is still good, and

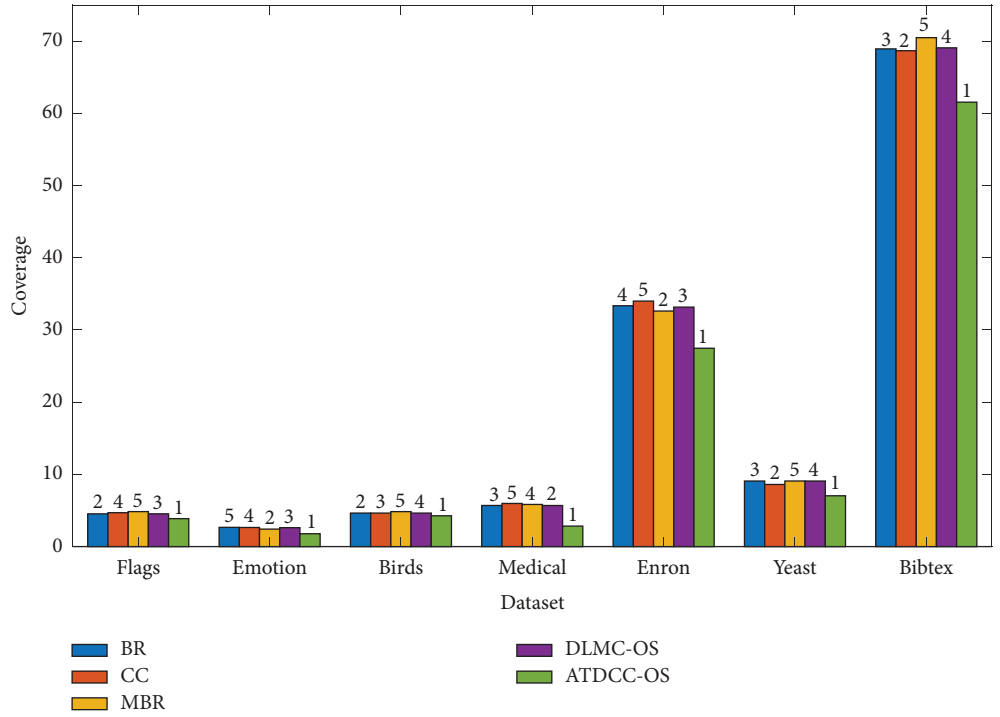

Figure 7: The coverage performance of algorithms.

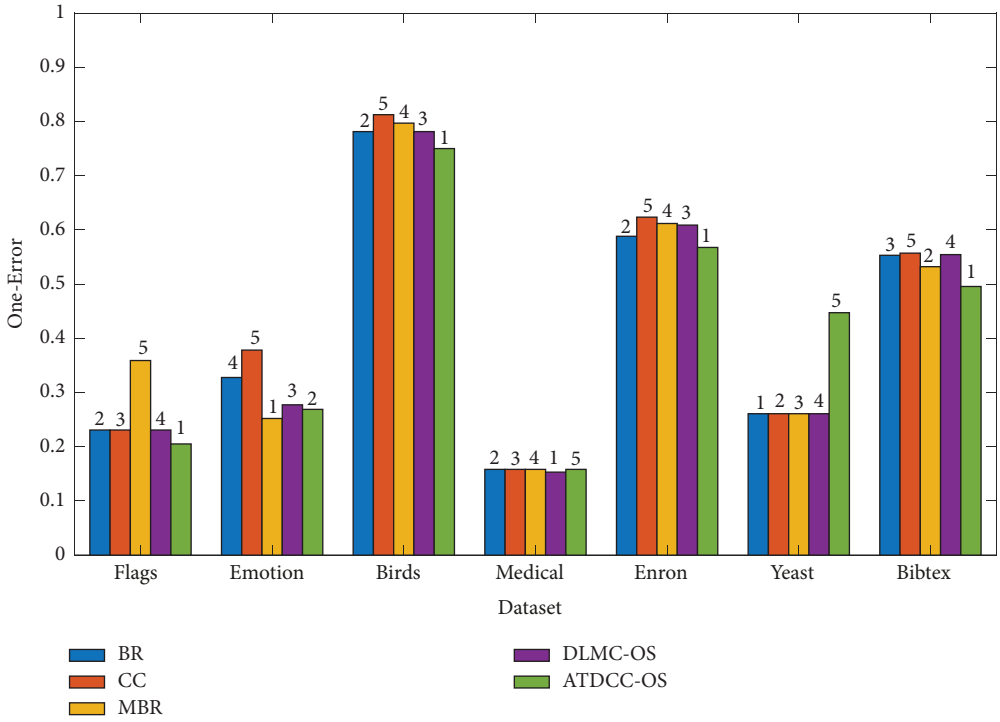

Figure 8: The one-error performance of algorithms.

the performance in the flags, birds, Enron, and BibTeX datasets is the best. In the emotion dataset, the performance of this algorithm is second only to that of the MBR algorithm.

From Figures 5–9, we can see that ATDCC-OS shows the optimal classification performance, while algorithm DLMC-OS presents better performance. However, other methods indicate worse performance. For all reviewing metrics, the

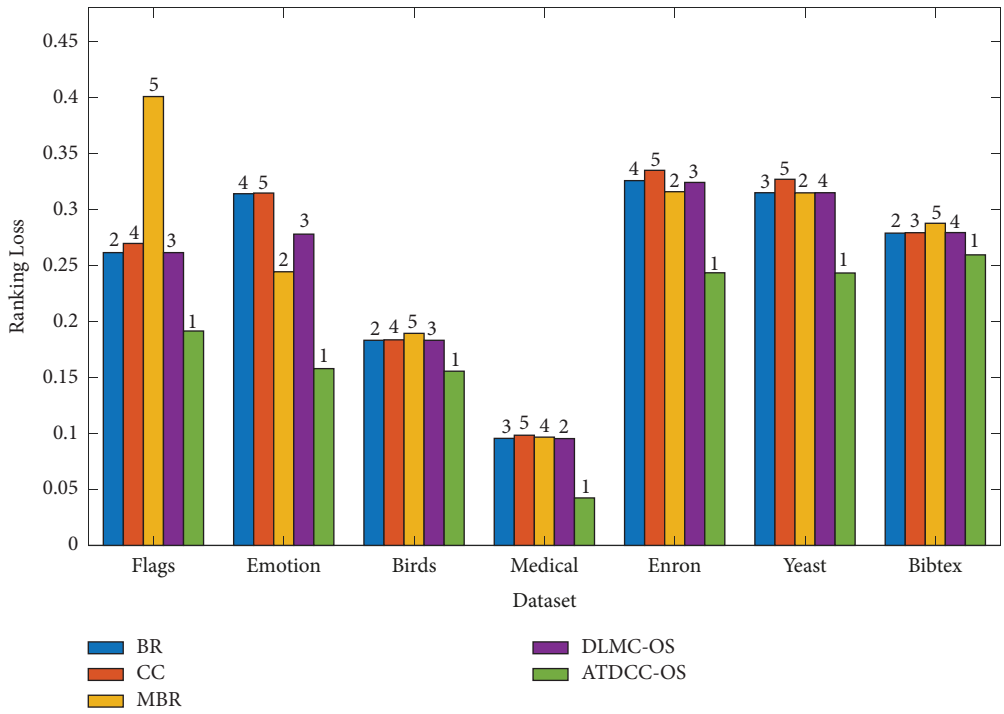

Figure 9: The ranking loss performance of algorithms.

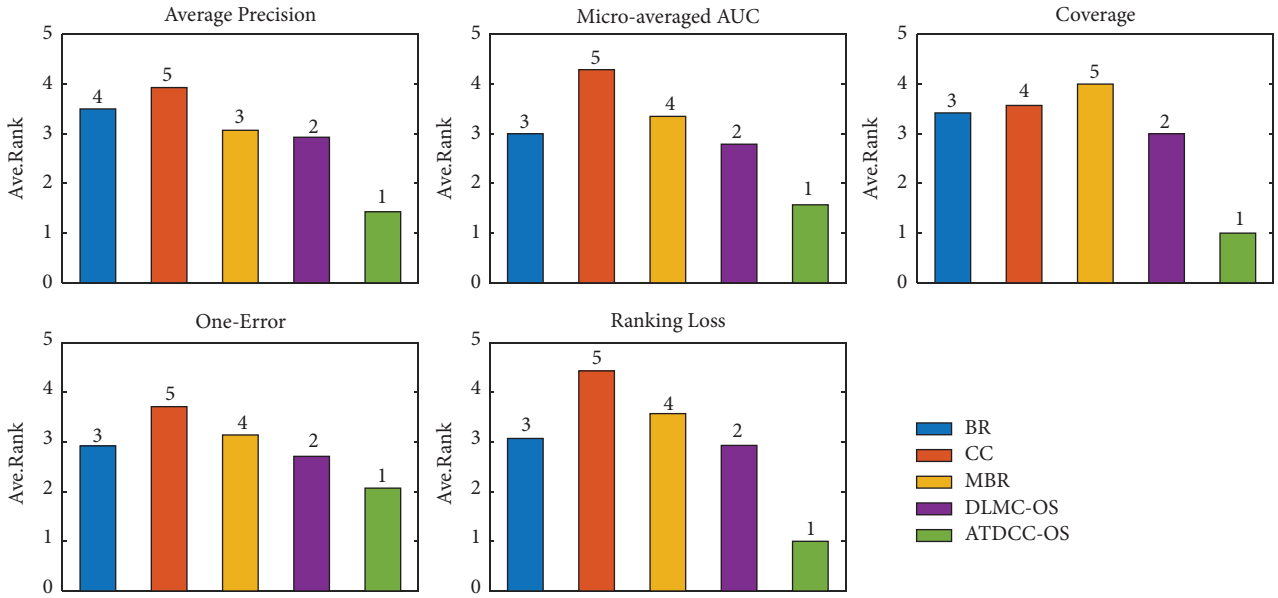

Figure 10: The average rank of five classifiers for different metrics.

mean precision metric and microaveraged AUC metric directly indicate the performance of the classifiers. The larger the values, the better the performance of the algorithms. According to Figures 5 and 6, we can see that the algorithm ATDCC-OS proposed in this study and the method DLMC-OS demonstrate much better performance compared with other algorithms. This is because they utilize a two-layer classification structure and the label information interaction to create detailed classifiers. This design structure takes into consideration the interrelationship between labels. At the same time, the algorithm ATDCC-OS also exploits the classical attention mechanism theory to improve the sensibility of classifiers and adapt them to a variety of tasks. Three indicators, namely, coverage, ranking loss, and the one-error metric are often exploited to decide and find irrelevant labels in classification results. As shown in

Figures 7–9, we find that the algorithm ATDCC-OS and the previous algorithm DLMC-OS also demonstrate better performance compared with the rest of the algorithms, while the BR approach presents a medium performance. The MBR method and the CC approach are the worst in this metric. This is because the algorithm ATDCC-OS and the previous approach DLMC-OS utilize optimization algorithms to train all classifiers in order. The randomness of serials in the CC method and the MBR approach directly leads to poorer performance. On the contrary, the BR method does not take into account the sequence of the labels, while it shows better performance.

The loss performance of each algorithm is shown in Figure 9. Among them, the ATDCC-OS algorithm is the most excellent in terms of loss performance. In all datasets, the performance of this algorithm is one level better than other algorithms. In the medical dataset, the loss performance is about 0.03.

From Figure 10, we can see the comprehensive performance ranking of the comparison algorithms in various indicators. Among all the indexes, the ATDCC-OS algorithm has the best performance. The comprehensive performance of the DLMC-OS algorithm is second only to that of the ATDCC-OS algorithm, and the subsequent performance is different in different algorithms.

Figure 10 shows the mean ranking performance metrics of the five classifiers for mean accuracy, coverage metric, single error metric, ranking loss metric, and microaverage AUC metric.

From our simulations, we can find that our algorithm ATDCC-OS outperforms the rest of the algorithms for most of the datasets, while it performs poorly in yeast and birds. As we all know, this algorithm cannot obtain the best performance for all types of different test datasets [10]. The algorithm performance is related not only to the detailed structure of the algorithm but also to the dataset's detailed type and size, as well as labels' balance in our test dataset.

Figures 11 and 12 show the plots of the percentage of training data versus average precision and ranking loss. These two figures illustrate how the percentage change of training data affects the enhancement of performance. In this experiment, we take the emotions dataset as an example for both comparisons.

Figure 11 shows the change curve for average precision under the two pairs of classifiers scale with respect to the percentage of training data. From Figure 11, we observe that the average precision is elevated for the four classifiers when the percentage of training data increases. When the percentage of training data is between 10% and 30%, the accuracy of all algorithms floats up and down. When the percentage of training data is over 30%, the average precision of the ATDCC-OS and DLMC-OS rises steadily, while MBR needs to reach 40%, and CC and BR need to reach 60%. Overall, as the training data increase, ATDCC-OS shows better performance than DLMC-OS, followed by MBR and BR, while CC is the worst.

From Figure 12, we can see the results of the comparison in terms of ranking loss. In this figure, as the percentage of training data increases, the ranking loss of ATDCC-OS and

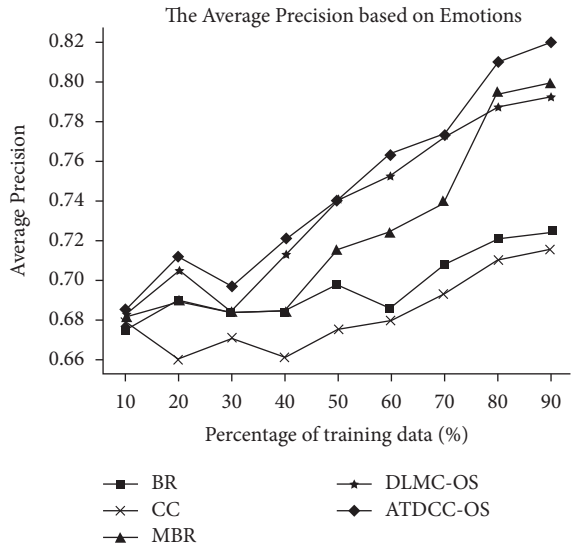

Figure 11: Average precision with different percentages of training data.

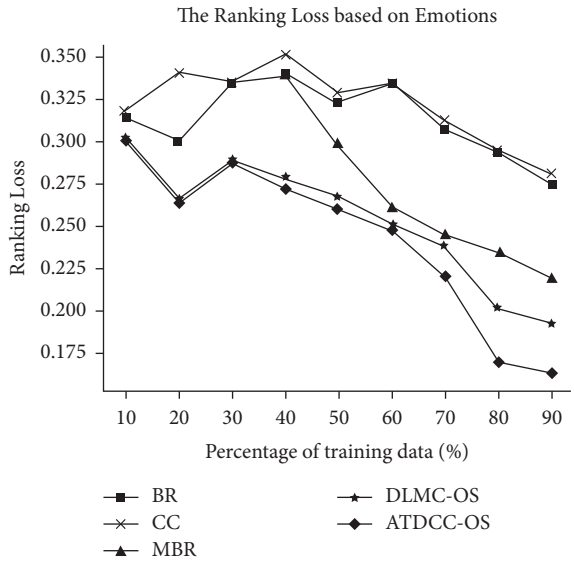

Figure 12: Ranking loss with different percentages of training data.

DLMC-OS tend to decrease steadily, compared to MBR, CC, and BR. When the training data is between 10% and 40%, the ranking loss of each algorithm is unstable, among which the MBR fluctuates the most, followed by CC and BR, while ATDCC-OS and DLMC-OS perform better. When the dataset is larger than 40%, the ranking loss curves of all algorithms show a downward trend. ATDCC-OS still presents the lowest loss in such a scenario.

5. Conclusion

In this study, we propose a simple and effective multilabel classification model (ATDCC-OS) that integrates the multilabel classification framework of three classic problem-

conversion types. It fully explores all kinds of advantages of every method to resolve these issues without considering the correlation among labels when performing classifications. In order to further improve the performance of classification, the algorithm solves the problem of nonreal-time label information interaction in the second-layer chained classification model by introducing the idea of "update replacement." At the same time, the algorithm dynamically calculates the weight values of all feature attributes through an attention mechanism in order to add more important attribute features to the current classification target for each classifier. It is helpful to add the classification sensibility of classifiers, which greatly improves the preciseness of classification. Five different metrics are utilized to describe different algorithms on seven different datasets. The results of the experiments show that the proposed method obtains high predictive performance compared with the state-of-the-art multilabel classification methods in most cases. In terms of average accuracy, the average accuracy of the ATDCC-OS algorithm is basically the highest in all datasets, and the accuracy in flags, emotions, and the medical dataset is more than 80%. In the microaverage AUC performance, the performance of the ATDCC-OS algorithm in all datasets is the best except for that in the bird's dataset, and the performance in the medical dataset is 0.96. In terms of coverage performance, the ATDCC-OS algorithm has the best coverage performance in all datasets, and its coverage performance is less than 10% in some datasets. In single error performance, this algorithm has the best comprehensive performance. In the loss performance, the algorithm has a loss performance of about 0.03 in the medical dataset. Based on the above results, it is concluded that the performance of the proposed ATDCC-OS algorithm is the best. This is only the preliminary result of this study. In the future, we will further optimize the algorithm to solve the problem of time complexity caused by the model structure, and we will also try to apply the algorithm to solve classification problems in everyday work and life. Finally, we hope that the research work in this study can provide some reference and assistance to researchers or scholars in the field of multilabel classification of problem transformation types.

Data Availability

The data used and/or analyzed during the current study are available from the corresponding author upon request.

Conflicts of Interest

The authors declare that they have no conflicts of interest.

Acknowledgments

This research was supported by the Key Research Project of Education Department of Sichuan Province of China (18ZA319).

References

[1] R. Wang, R. Ridley, X. Su, W. Qu, and X. Dai, "A novel reasoning mechanism for multi-label text classification," *Information Processing & Management*, vol. 58, no. 2, Article ID 102441, 2021.

[2] J. Cai, W. Sun, J. Guan, and I. You, "Multi-ECGNet for ECG arrythmia multi-label classification," *IEEE Access*, vol. 8, pp. 110848–110858, 2020.

[3] H. Chougrad, H. Zouaki, and O. Alheyane, "Multi-label transfer learning for the early diagnosis of breast cancer," *Neurocomputing*, vol. 392, pp. 168–180, 2020.

[4] J. Saha, C. Chowdhury, and S. Biswas, *Review of Machine Learning and Deep Learning Based Recommender Systems for Health informaticsDeep Learning Techniques for Biomedical and Health Informatics*, pp. 101–126, Springer, Cham, 2020.

[5] J. Wu, V. S. Sheng, J. Zhang et al., "Multi-label active learning algorithms for image classification: overview and future promise," *ACM Computing Surveys*, vol. 53, no. 2, pp. 1–35, 2021.

[6] M. Bogaert, J. Lootens, D. Van den Poel, and M. Ballings, "Evaluating multi-label classifiers and recommender systems in the financial service sector," *European Journal of Operational Research*, vol. 279, no. 2, pp. 620–634, 2019.

[7] G. N. Karagoz, A. Yazici, T. Dokeroglu, and A. Cosar, "A new framework of multi-objective evolutionary algorithms for feature selection and multi-label classification of video data," *International Journal of Machine Learning and Cybernetics*, vol. 12, no. 1, pp. 53–71, 2021.

[8] Z. M. Chen, X. S. Wei, and P. Wang, "Multi-label image recognition with graph convolutional networks," *CVPR*, vol. 27, 2019.

[9] G. Wu, R. Zheng, Y. Tian, and D. Liu, "Joint ranking SVM and binary relevance with robust low-rank learning for multi-label classification," *Neural Networks*, vol. 122, pp. 24–39, 2020.

[10] J. Read, B. Pfahringer, G. Holmes, and E. Frank, "Classifier chains: a review and perspectives," *Journal of Artificial Intelligence Research*, vol. 70, pp. 683–718, 2021.

[11] K. Feng, C. Li, M. Zhang, and X. Liu, "Simulation and computational study of CFD on tube MBR membrane assembly," *Discrete Dynamics in Nature and Society*, vol. 2021, no. 7-8, pp. 1–8, 2021.

[12] J. Li, P. Wei, S. Yang, J. Wu, P. Liu, and X. He, "Crystal-KMC: parallel software for lattice dynamics Monte Carlo simulation of metal materials," *Tsinghua Science and Technology*, vol. 23, no. 4, pp. 501–510, 2018.

[13] C. Pan, J. Tan, D. Feng, and Y. Li, "Very short-term solar generation forecasting based on LSTM with temporal attention mechanism," in *2019 IEEE 5th International Conference on Computer and Communications (ICCC)*, Chengdu, China, December 2019.

[14] Q. Ai, Y. Kang, A. Wang, X. Li, and F. Li, "An effective semi-supervised multi-label least squares twin support vector machine," *IEEE Access*, vol. 8, pp. 213460–213472, 2020.

[15] X. Xu, D. Shan, S. Li, T. Sun, P. Xiao, and J. Fan, "Multi-label learning method based on ML-RBF and laplacian ELM," *Neurocomputing*, vol. 331, pp. 213–219, 2019.

[16] F. Javed, J. Ahmed, and M. Hayat, "ML-RBF: predict protein subcellular locations in a multi-label system using evolutionary features," *Chemometrics and Intelligent Laboratory Systems*, vol. 203, Article ID 104055, 2020.

[17] X. Zhu, C. Ying, J. Wang, J. Li, X. Lai, and G. Wang, "Ensemble of ML-KNN for classification algorithm recommendation," *Knowledge-Based Systems*, vol. 221, Article ID 106933, 2021.

[18] D. Zhu, H. Zhu, X. Liu et al., "CREDO: efficient and privacy-preserving multi-level medical pre-diagnosis based on ML-kNN," *Information Sciences*, vol. 514, pp. 244–262, 2020.

[19] D. Jiaman, Z. Shujie, L. Runxin, F. Xiaodong, and J. Lianyin, "Association rules-based classifier chains method," *IEEE Access*, vol. 10, pp. 18210–18221, 2022.

[20] E. Hüllermeier, J. Fürnkranz, and M. E. Loza, "Rule-based multi-label classification: challenges and opportunities," in *Proceedings of the International Joint Conference on Rules and Reasoning*, Oslo, Norway, July 2020.

[21] P. Teisseyre, "Classifier chains for positive unlabelled multi-label learning," *Knowledge-Based Systems*, vol. 213, Article ID 106709, 2021.

[22] N. K. Mishra and P. K. Singh, "Linear ordering problem based classifier chain using genetic algorithm for multi-label classification," *Applied Soft Computing*, vol. 117, Article ID 108395, 2022.

[23] Z. Niu, G. Zhong, and H. Yu, "A review on the attention mechanism of deep learning," *Neurocomputing*, vol. 452, pp. 48–62, 2021.

[24] E. Lieskovská, M. Jakubec, R. Jarina, and M. Chmulik, "A review on speech emotion recognition using deep learning and attention mechanism," *Electronics*, vol. 10, no. 10, p. 1163, 2021.

[25] S. He, H. R. Tavakoli, A. Borji, and N. Pugeault, "Human attention in image captioning: dataset and analysis," in *Proceedings of the 2019 IEEE/CVF International Conference on Computer Vision (ICCV)*, pp. 8528–8537, Seoul, Korea (South), October 2019.

[26] Z. Wu, D. Pi, J. Chen, M. Xie, and J. Cao, "Rumor detection based on propagation graph neural network with attention mechanism," *Expert Systems with Applications*, vol. 158, Article ID 113595, 2020.

[27] Y. Bazi, L. Bashmal, M. M. A. Rahhal, R. A. Dayil, and N. A. Ajlan, "Vision transformers for remote sensing image classification," *Remote Sensing*, vol. 13, no. 3, p. 516, 2021.

[28] Y. Zhou, L. Pan, C. Bai, S. Luo, and Z. Wu, "Self-selective attention using correlation between instances for distant supervision relation extraction," *Neural Networks*, vol. 142, pp. 213–220, 2021.

[29] Q. Xu, L. Zhu, T. Dai, and C. Yan, "Aspect-based sentiment classification with multi-attention network," *Neurocomputing*, vol. 388, pp. 135–143, 2020.

[30] J. Gan, "Music feature classification based on recurrent neural networks with channel attention mechanism," *Mobile Information Systems*, vol. 202110 pages, 2021.

[31] A. V. Savchenko, K. V. Demochkin, and L. V. Savchenko, "Neural attention mechanism and linear squeezing of descriptors in image classification for visual recommender systems," *Optical Memory & Neural Networks*, vol. 29, no. 4, pp. 297–304, 2020.

[32] Y. Xiao, Y. Li, J. Yuan, S. Guo, Y. Xiao, and Z. Li, "History-based attention in Seq2Seq model for multi-label text classification," *Knowledge-Based Systems*, vol. 224, Article ID 107094, 2021.

[33] D. Wang, Z. Zhang, Y. Jiang et al., "DM3Loc: multi-label mRNA subcellular localization prediction and analysis based on multi-head self-attention mechanism," *Nucleic Acids Research*, vol. 49, no. 8, p. e46, 2021.

[34] A. Hashemi, M. B. Dowlatshahi, and H. Nezamabadi-Pour, "A bipartite matching-based feature selection for multi-label learning," *International Journal of Machine Learning and Cybernetics*, vol. 12, no. 2, pp. 459–475, 2021.

[35] P. Zhang, W. Gao, J. Hu, and Y. Li, "Multi-label feature selection based on high-order label correlation assumption," *Entropy*, vol. 22, no. 7, p. 797, 2020.

[36] R. Xia, Y. Chen, and B. Ren, "Improved Anti-occlusion Object Tracking Algorithm Using Unscented Rauch-Tung-Striebel Smoother and Kernel Correlation Filter," *Journal of King Saud University-Computer and Information Sciences*, vol. 34, 2022.

[37] J. Kudler-Flam, L. Nie, and S. Ryu, "Conformal field theory and the web of quantum chaos diagnostics," *Journal of High Energy Physics*, vol. 2020, no. 1, pp. 175–233, 2020.

[38] O. B. Ericok and J. K. Mason, "Foundations of a Finite Non-equilibrium Statistical Thermodynamics: Extrinsic Quantities," 2022, https://arxiv.org/abs/2201.02777.

[39] C. Wen, Q. Y. Hu, B. Y. Pu, and Y. Y. Huang, "Acceleration of an adaptive generalized Arnoldi method for computing PageRank," *AIMS Mathematics*, vol. 6, no. 1, pp. 893–907, 2021.

[40] Y. Gao, X. Yu, and H. Zhang, "Overlapping community detection by constrained personalized PageRank," *Expert Systems with Applications*, vol. 173, no. 1, p. 114682, 2021.

[41] X. Zhang, J. You, H. Xue, and J. Wang, "A decentralized PageRank based content dissemination model at the edge of network," *International Journal of Web Services Research*, vol. 17, no. 1, pp. 1–16, 2020.

[42] U. S. Premarathne, "Preference biased edge weight assignment for connectivity-based resilience computation in telecommunication networks," *IT Professional*, vol. 22, no. 6, pp. 26–32, 2020.

[43] J. Zhang, W. Feng, T. Yuan, J. Wang, and A. K. Sangaiah, "SCSTCF: spatial-channel selection and temporal regularized correlation filters for visual tracking," *Applied Soft Computing*, vol. 118, Article ID 108485, 2022.

[44] D. Di Caprio, A. Ebrahimnejad, H. Alrezaamiri, and F. J. Santos-Arteaga, "A novel ant colony algorithm for solving shortest path problems with fuzzy arc weights," *Alexandria Engineering Journal*, vol. 61, no. 5, pp. 3403–3415, 2022.

[45] J. Dutta, P. S. Barma, S. Kar, and T. De, "A Modified Kruskal's algorithm to improve genetic search for open vehicle routing problem," *International Journal of Business Analytics*, vol. 6, no. 1, pp. 55–76, 2019.

[46] Y. Chen, V. Phonevilay, J. Tao et al., "The face image super-resolution algorithm based on combined representation learning," *Multimedia Tools and Applications*, vol. 80, no. 20, pp. 30839–30861, 2021.

[47] J. P. Zhou, L. Chen, T. Wang, and M. Liu, "iATC-FRAKEL: a simple multi-label web server for recognizing anatomical therapeutic chemical classes of drugs with their fingerprints only," *Bioinformatics*, vol. 36, no. 11, pp. 3568-3569, 2020.

[48] J. Yang, S. Hu, Q. Wang, and S. Fong, "Discriminable multi-label attribute selection for pre-course student performance prediction," *Entropy*, vol. 23, no. 10, p. 1252, 2021.

[49] A. Sinha Roy, R. Biswas, and A. S. Dhar, "On fast and exact computation of error metrics in approximate LSB adders," *IEEE Transactions on Very Large Scale Integration Systems*, vol. 28, no. 4, pp. 876–889, 2020.

[50] M. C. Pinto, A. Rodriguez-Ruiz, K. Pedersen et al., "Impact of artificial intelligence decision support using deep learning on breast cancer screening interpretation with single-view wide-angle digital breast tomosynthesis," *Radiology*, vol. 300, no. 3, pp. 529–536, 2021.

[51] M. L. Welch, C. Mcintosh, A. Traverso et al., "External validation and transfer learning of convolutional neural networks for computed tomography dental artifact classification," *Physics in Medicine and Biology*, vol. 65, no. 3, p. 035017, 2020.

[52] M. Feurer and F. Hutter, *Hyperparameter optimization// Automated Machine Learning*, pp. 3–33, Springer, New York, 2019.

[53] A. Zeng, H. Yu, Q. Da, Y. Zan, and C. Miao, "Accelerating ranking in E-Commerce search engines through contextual factor selection," *Proceedings of the AAAI Conference on Artificial Intelligence*, vol. 34, no. 08, pp. 13212–13219, 2020.

Hindawi
Complexity
Volume 2022, Article ID 8742772, 10 pages
https://doi.org/10.1155/2022/8742772

WILEY | Hindawi

Research Article

Multiple Quasisynchronization of Uncertain Fractional-Order Delayed Neural Networks by Impulsive Control Mechanism

Biwen Li and Lin Xu

College of Mathematics and Statistics, Hubei Normal University, Huangshi 435002, China

Correspondence should be addressed to Biwen Li; lbw20200320@163.com

Received 26 March 2022; Revised 14 September 2022; Accepted 30 September 2022; Published 17 October 2022

Academic Editor: Xiao Ling Wang

We study the dynamical behavior of multiple quasi-synchronization of a type of fractional-order coupled neural networks (FCNNs) with delay and uncertain parameters. By utilizing the pinned pulse control strategy technique, we establish a new pulse controller, which realizes the multiple quasisynchronization of the system. Furthermore, we derive some new criteria of multiple quasisynchronization by using the comparison principle and mathematical analysis. Eventually, simulations are carried out with two examples to explicate the effectiveness of the conclusions.

1. Introduction

Fractional-order calculus is related to model memory, complexity, and heritability, so it has advantages over integer calculus (see [1, 2]). In many actual questions, we generally first consider the fractional dynamic system because it can better descript the actual problem than the integral order dynamic system. There have been many reports on fractional-order system dynamics. It plays an extremely significant effect in the modeling of engineering system, power system, and physical system (see [3, 4]). In Reference [3], Bao and Cao combined Caputo derivatives and fractional calculus inequalities and sufficiency condition for projection synchronization of fractional memristor-based neural networks (FMNNs) was theoretically derived. Xu et al. in Reference [5] studied a new fractional Hopfield neural network chaotic system and its application in image encryption. Li et al. in Reference [4] studied the application of neural network fractional-order PID in the control of piezoelectric stacks.

Parameter uncertainty is caused by incomplete understanding of some knowledge of mathematical model, such as constitutive law and empirical quantity (see [6]). In various engineering discipline systems, the model parameters studied are often uncertain, so the parameter uncertainty needs to be considered when facing the actual system. Fortunately, in recent years, many scholars have considered the parameter uncertainty in the model. In Reference [7], the author designs an appropriate event triggering mechanism and controller to ensure the stability of randomly nonlinearity system of time lag with uncertain parameters. However, with the continuous maturity of technology, the task of designing a good controller for an uncertain fractional-order neural network so that the network can achieve the desired effect is still very arduous, and many problems need to be further studied.

Synchronization is an extremely important dynamic behavior in complex dynamic networks, which has a wide range of applications in many fields. Therefore, many researchers have studied it (see [8]). Moreover, the synchronization behavior of fractional-order coupled neural networks (FCNNs) is also discussed. For example, Xu et al. designed a suitable controller in Reference [9], so that FCNNs with time-variable delays could realize the synchronization behavior in a finite time. Chen et al. [10] investigated the synchronization of FMNNs with time lag. It is a well-known fact that time delay often exists in plenty of complex networks; hence, it is very significant to premeditate time delay when studying FCNNs.

In general, the coupled neural network is not synchronized without external force interference, so it is

necessary to develop a controller to make it synchronize. Some scholars also use various control technologies, for example, impulse control, adaptive control, pinning control, and feedback control to achieve synchronization. However, if there are too many nodes in the network, the cost of applying controller to each node is too high and difficult to implement. Therefore, it is possible to try to control the network by only controlling the fixed part of the time and some nodes, so as to arrive the purpose of reducing the control cost. But, few authors have applied the pinning impulse control project to NNs (see Reference [11]). In Reference [11], Wang et al. theoretically derived a few sufficient conditions for pinning synchronization and robust synchronization of FCNNs through the pinning control strategy. Also, some networks can only achieve quasi-synchronization due to external and internal interference, and there are few studies on quasisynchronization of NNs with couple (see [12, 13]). In Reference [12], Feng et al., based on the matrix-related knowledge theory and Lyapunov functional method, derived several simple sufficient optimality conditions for quasisynchronization of coupled memristor NNs theoretically, and a suitable controller is constructed to ensure the quasisynchronization of such networks. In Reference [13], Lv et al. introduced a type of activation function and a few sufficient conditions to guarantee that each subnetwork in the time-delay coupled neural network has multiple equilibrium states and made the network achieve dynamic and static multisynchronization by constructing an appropriate impulse controller and Lyapunov function. Based on the abovementioned phenomenon, this paper will research the multiple quasi-synchronization issue of FCNNs with uncertain parameters and delay by pinning pulse control method.

For as much as the above discussion, the major dedications of this article involve the following: (1) The multiple quasisynchronization problem of FCNNs with uncertain parameters and time delays is studied. (2) The concept of multiple quasisynchronization is proposed. (3) Aiming at the problem of multiple quasisynchronization, a new method combining pinning and pulse control is proposed.

The rest of the main content of this article is as follows: Section 2 mainly describes the prerequisites and models required in this article. The primary contribution is in Section 3. Section 4 gives two examples that demonstrate the validity of the conclusion. Finally, Section 5 gives the main conclusions of this article.

2. Preliminary Knowledge and Model Description

2.1. Fraction-Order Calculus. Firstly, existing definitions of fraction-order calculus are given, which can be seen in Reference [14], that are needed later.

Define the Gamma function $\Gamma(\cdot)$ as below:

$$\Gamma(p) = \int_{t_0}^{+\infty} t^{p-1} \exp\{-t\}\mathrm{d}t, \tag{1}$$

where $p > 0$.

Define the Caputo fractional derivative ${}^{c}D_{t_0,t}^{p} g(\cdot)$ of the function $g(t)$ as below:

$${}^{c}D_{t_0,t}^{p} g(t) = \frac{1}{\Gamma(n-p)} \int_{t_0}^{t} \frac{g^{(n)}(s)}{(t-s)^{p-n+1}}\mathrm{d}s, \tag{2}$$

where t_0 is the initial time, $t \geq t_0$, p is the order, $n-1 < p < n, n \in Z^+$.

Define the fractional integral $I_{t_0,t}^{p} g(\cdot)$ of the function $g(t)$ as below:

$$I_{t_0,t}^{p} g(t) = \frac{1}{\Gamma(p)} \int_{t_0}^{t} (t-s)^{p-1} g(s)\mathrm{d}s, \tag{3}$$

where t_0 is the initial time, $t \geq t_0$.

Define the Mittag-Leffler function with single parameter $E_p(\cdot)$ as below:

$$E_p(s) = \sum_{k=0}^{+\infty} \frac{s^k}{\Gamma(kp+1)}, \tag{4}$$

where $p > 0, s$ is a complex number.

Define the Mittag-Leffler function with double parameters $E_{p,\overline{p}}(\cdot)$ as below:

$$E_{p,\overline{p}}(s) = \sum_{k=0}^{+\infty} \frac{s^k}{\Gamma(kp+\overline{q})}, \tag{5}$$

where $p > 0, \overline{p} > 0, s$ is a complex number.

2.2. Model Description. A collection that makes Z^+ a positive integer. The superscript T represents the transpose, and $\#\mathfrak{I}$ is an element in the finite collection $\mathfrak{I}$. Denote R^n is the set of n-dimensional real-valued vectors. R^+ is the group of fixed non-negative numbers. For an arbitrary vector $a \in R^n$ and the existence of a constant $\sigma_0 > 0$, we record $\mathscr{M}(a, \sigma_0) = \{x \| x - a \| < \sigma_0\}$ as a set of vectors, where the distance between x and a is less than σ_0. The set of $n \times n$ real matrices is written as $R^{n\times n}$. If a real matrix $X > 0$, then X is a positive definite matrix. $A \otimes B$ represents the Kronecker product of matrices A and B. For any matrix A, $\lambda_{\min}(A), \lambda_{\max}(A)$ denotes its minimum eigenvalue and maximum eigenvalue, respectively, and the norm of A is defined as $\|A\| = (\lambda_{\max}(A^T A))^{(1/2)}$. In this article, we regard the following FCNNs with N same nodes, uncertainties, and time delays.

$$\begin{aligned} {}^{c}D_{t_0,t}^{\alpha} x_i(t) = &-(\widehat{P} + \Delta\mathscr{P}(t))x_i(t) + (\widehat{Q} + \Delta\mathscr{Q}(t))f_i(x_i(t)) \\ &+ (\widehat{R} + \Delta\mathscr{R}(t))f_i(x_i(t-\tau)) \\ &+ \sum_{j=1}^{N} \widehat{G}_{ij}\Gamma x_j(t) + J, \end{aligned} \tag{6}$$

where $i = 1, 2, \ldots, N$, and $N \geq 2$ represents the quantity of subnetworks; τ represents the time delay in transmission; $x_i(t) = (x_{i1}(t), x_{i2}(t), \ldots, x_{in}(t))^T$ is the state vector of i-th neuron; $\Delta\mathscr{P}(t), \Delta\mathscr{Q}(t), \Delta\mathscr{R}(t)$ are the norm-bounded parametric uncertainties; $\widehat{P}$ is a diagonal matrix that

expresses the self-feedback item of the j-th network, in which the diagonal elements are $p_1, p_2, \ldots, p_n, p_i > 0$. $\widehat{Q} = (Q_{ij})_{n\times n}$ is the connection weight matrices and $\widehat{R} = (r_{ij})_{n\times n}$ is the time lag join matrices, where $i, j = 1, 2, \ldots, n$. $f_i(x_i(t))$ is the activation function; $\widehat{G} = (\widehat{G}_{ij})_{N\times N}$ is the coupled matrix, when there exists a connection among the i-th node with the j-th node, $i \neq j, \widehat{G}_{ij} \neq 0$, if not, $\widehat{G}_{ij} = 0$, in which the diagonal elements are defined by $\widehat{G}_{ii} = -\sum_{j=1, j\neq i}^{N} \widehat{G}_{ij}$; $\Gamma = \mathrm{diag}\{\gamma_1, \gamma_2, \ldots, \gamma_n\}$ is the internal coupling matrix; $J = (J_1, J_2, \ldots, J_N)$ is the input vector.

Next, we give several basic assumptions.

(A1) The activation function $f_i(\cdot)$ is continuous, for any vector x, y, exists $\mathscr{L}_i > 0$, and the following formula holds:

$$\left|f_i(x) - f_i(y)\right| \leq \mathscr{L}_i |x - y|. \tag{7}$$

(A2)

$$\% \ \Delta\mathscr{P} = \widehat{\mathscr{A}}_1 \widehat{\mathscr{C}}_1(t) \widehat{\mathscr{B}}_1, \Delta\mathscr{Q} = \widehat{\mathscr{A}}_2 \widehat{\mathscr{C}}_2(t) \widehat{\mathscr{B}}_2, \Delta\mathscr{R} = \widehat{\mathscr{A}}_3 \widehat{\mathscr{C}}_3(t) \widehat{\mathscr{B}}_3, \tag{8}$$

where $\widehat{\mathscr{A}}_i, \widehat{\mathscr{B}}_i (i = 1, 2, 3)$ are constant matrices with the corresponding matching dimensions and $\widehat{\mathscr{C}}_i(t) (i = 1, 2, 3)$ is an indeterminate matrix, where $\widehat{\mathscr{C}}_i^T(t)\widehat{\mathscr{C}}_i(t) \leq I$ (I is the unity matrix with the corresponding matching dimensions).

Remark 1. $\#D_k = \kappa_k$ means that the group D_k has κ_k nodes and $\kappa_k \neq 0$.

For any initial state $x(t) = (x_1^T(t), x_2^T(t), \ldots, x_N^T(t))^T$ where $x_i(t) \in C([-\tau, 0], R), i = 1, 2, \ldots, N$, for any given initial value condition, there is a solution $s(t)$, if all the node trajectories in the network satisfy the formula $\lim_{t\longrightarrow\infty} \|x_i(t) - s(t)\| = 0, i = 1, 2, \ldots, N$, then this network is called complete synchronization. Furthermore, if the margin of error $\sigma > 0$, exists $T > 0$, for all $x(t)$ and $\forall t > T$, $\|x_i(t) - s(t)\| < \sigma$ holds, then this network is called uniformly quasisynchronized.

Definition 1 (see [15]). For an arbitrary complex network with N nodes, $\{D_1, D_2, \ldots, D_m\}$ is a set of disjoint nodes, that is, $\sum_{k=1}^{m} D_k = \{1, 2, \ldots, N\}$, $D_k = \{l_{k1}, l_{k2}, \ldots\}$, $D_k \cap D_u = \varnothing$ for $k \neq u$. The network is called multiple quasisynchronization with the error vector $\delta = \{\delta_1, \delta_2, \ldots, \delta_m\}^T > 0$ under any initial value conditions, if there exist a series of reference solutions $\{s_1(t), s_2(t), \ldots, s_m(t)\}$ and for any constant $\kappa > 0$ small enough, T exists, for $\forall t > T$, the nodes $x_i(t) \in \mathscr{M}(s_k(t), \sigma_k), i \in D_k$ holds, in which $\mathscr{M}(s_k(t), \sigma_k) \neq \mathscr{M}(s_u(t), \overline{\sigma}_u), u \neq k$.

Remark 2. It can be seen from Definition 1 that $s_k(t)$ is the reference trajectory for all nodes in set $\#D_k$.

The target trajectory $s_{\bar{i}}(t)$ satisfies the following formula:

$$\begin{aligned} {}^{c}D_{t_0,t}^{\alpha} s_{\bar{i}}(t) = &-(\widehat{P} + \Delta\mathscr{P}(t)) s_{\bar{i}}(t) + (\widehat{Q} + \Delta\mathscr{Q}(t)) f_{\bar{i}}\left(s_{\bar{i}}(t)\right) \\ &+ (\widehat{R} + \Delta\mathscr{R}(t)) f_{\bar{i}}\left(s_{\bar{i}}(t - \tau)\right) + J, \end{aligned} \tag{9}$$

where if $x_i(t) \in \mathscr{M}(s_k(t), \sigma_k)$, then $s_{\bar{i}}(t) = s_k(t)$, $i = 1, 2, \ldots, N, k = 1, 2, \ldots, m$.

Now let's note $\overline{\varepsilon}_i(t) = x_i(t) - s_{\bar{i}}(t)$ is the error signal, where $i = 1, 2, \ldots, N$, and devise a new pinned pulse controller as shown below:

$$u_i(t) = \begin{cases} \sum_{h=1}^{+\infty} \theta_k \overline{\varepsilon}_i(t) \delta(t - t_h), & i \in \mathfrak{T}_k(t_h), \ \#\mathfrak{T}_k(t_h) = \omega_k, \\ 0, & i \notin \mathfrak{T}_k(t_h), \end{cases} \tag{10}$$

where $\delta(\cdot)$ and θ_k represents the Dirac impulsive function and impulsive gain, respectively, and $t_h (h = 0, 1, 2, \ldots)$ indicates the instant of the pulse that satisfies $0 = t_1 < t_2 < \cdots < t_h < \cdots, \lim_{t_h \longrightarrow +\infty} t_h = +\infty$. The node set on $t = t_h$ is represented by $\sum_{k=1}^{m} \mathfrak{T}_k(t_h) = \{\mathfrak{T}_1(t_h), \mathfrak{T}_2(t_h), \ldots, \mathfrak{T}_m(t_h)\} \subset \{D_1, D_2, \ldots, D_m\} \subset \{1, 2, \ldots, N\}$, and make $0 < \omega_k \leq \kappa_k, k = 1, 2, \ldots, m$, namely, $\mathfrak{T}_k(t_h)$ is a subset of D_k, and $\mathfrak{T}_k(t_h)$ represents the set of pinned nodes at $t = t_h$. Assume the error vector $\overline{\varepsilon}_{i1} \geq \overline{\varepsilon}_{i2} \geq \cdots \geq \overline{\varepsilon}_{in}$. Under the pulse controller (10), the system of errors can be described:

$$\begin{cases} {}^{c}D_{t_0,t}^{\alpha} \overline{\varepsilon}_i(t) = -(\widehat{P} + \Delta\mathscr{P}(t)) \overline{\varepsilon}_i(t) + (\widehat{Q} + \Delta\mathscr{Q}(t)) \widetilde{f}_i\left(\overline{\varepsilon}_i(t)\right) \\ +(\widehat{R} + \Delta\mathscr{R}(t)) \widetilde{f}_i\left(\overline{\varepsilon}_i(t - \tau)\right) + \sum_{j=1}^{N} \widehat{G}_{ij} \Gamma \overline{\varepsilon}_i(t), t \neq t_h \\ \overline{\varepsilon}_i\left(t_h^+\right) = (1 + \theta_k) \overline{\varepsilon}_i\left(t_h^-\right), i \in \sum_{k=1}^{m} \mathfrak{T}_k(t_h), \\ \overline{\varepsilon}_i\left(t_h^+\right) = \overline{\varepsilon}_i\left(t_h^-\right), i \notin \sum_{k=1}^{m} \mathfrak{T}_k(t_h), \end{cases} \tag{11}$$

where $h = 0, 1, 2, \ldots, \bar{\varepsilon}_i(t_h^+) = \lim_{t \longrightarrow t_h^+} \bar{\varepsilon}_i(t), \bar{\varepsilon}_i(t_h^-) = \lim_{t \longrightarrow t_h^-} \bar{\varepsilon}_i(t_h), \widetilde{f}_i(\bar{\varepsilon}_i(t)) = f_i(x_i(t)) - f_{\tilde{i}}(s_{\tilde{i}}(t)), \widetilde{f}_i(\bar{\varepsilon}_i(t-\tau)) = f_i(x_i(t-\tau)) - f_{\tilde{i}}(s_{\tilde{i}}(t-\tau))$, and $\widetilde{f}_i(0) = 0$.

The initial value condition of the above error system (11) is as follows:

$$\bar{\varepsilon}_i(s) = \phi_i(s), s \in [-\tau, 0], \tag{12}$$

where $\phi_i(s) \in C([-\tau, 0], R^n)$ and $i = 1, 2, \ldots, N$.

Lemma 1 (see [16]). *If $x(t) \in R^n$ is a vector-valued function that is differentiable and continuous for t, next for any $\alpha \in (0, 1)$ and $t \geq t_0$, we have the following relationship:*

$$^cD_{t_0,t}^{\alpha}\left(x^T(t)Px(t)\right) \leq 2x^T(t)P^cD_{t_0,t}^{\alpha}x(t), \tag{13}$$

where $P \in R^{n \times n}$ is a constant matrix that is symmetric and positive definite.

Lemma 2 (see [17]). *Let $\widehat{\mathscr{R}}, \widehat{\mathscr{W}}$, and $\widehat{\mathscr{S}}(t)$ be the real matrices corresponding matching dimensions, then if there is $\widehat{\mathscr{S}}^T(t)\widehat{\mathscr{S}}(t) \leq I$, then there is the following equation:*

$$\widehat{\mathscr{R}}^T\widehat{\mathscr{S}}^T(t)\widehat{\mathscr{W}}^T + \widehat{\mathscr{W}}\widehat{\mathscr{S}}(t)\widehat{\mathscr{R}} \leq \frac{1}{\xi}\widehat{\mathscr{R}}^T\widehat{\mathscr{R}} + \xi\widehat{\mathscr{W}}\widehat{\mathscr{W}}^T, \tag{14}$$

where $\xi > 0$ is the constant.

Lemma 3 (see [17]). *Let $\widehat{\mathscr{R}}$ and $\widehat{\mathscr{W}}$ be the real matrices corresponding matching dimensions, then*

$$\widehat{\mathscr{R}}^T\widehat{\mathscr{W}} + \widehat{\mathscr{W}}^T\hat{R} \leq \xi\widehat{\mathscr{R}}^T\widehat{\mathscr{R}} + \frac{1}{\xi}\widehat{\mathscr{W}}^T\widehat{\mathscr{W}}, \tag{15}$$

where $\xi > 0$ is the constant.

Lemma 4 (see [18]). *For arbitrary vector $x_1, x_2 \in R^n$ and $Q \in R^{n \times n}$ which is a positive definite matrix, we have the below inequalities hold:*

$$2x_1^Tx_2 \leq x_1^TQ^{-1}x_1 + x_2^TQx_2. \tag{16}$$

Lemma 5 (see [19]). *For positive definite matrix R, vector x_i with proper dimensionality and symmetric matrix W, then we have the following:*

$$\lambda_{\min}\left(R^{-1}W\right)x_i^TRx_i \leq x_i^TWx_i \leq \lambda_{\max}\left(R^{-1}W\right)x_i^TRx_i, \tag{17}$$

where $\lambda_{\max}(\cdot), \lambda_{\min}(\cdot)$ denote the maximum and minimum eigenvalues, respectively, and R^{-1} stands for the inverse of a matrix R.

Definition 2. The definition of the pinning rate η_k at $t = t_h$ is as follows:

$$\frac{\sum_{i \in \Im_k(t_h)}\bar{\varepsilon}_i^T(t_h^-)\bar{\varepsilon}_i(t_h^-)}{\sum_{i \in D_k}\bar{\varepsilon}_i^T(t_h^-)\bar{\varepsilon}_i(t_h^-)} = \eta_k, \tag{18}$$

here the pinning rate η_k is related to time and impulse instants, and we can also determine the lower bound of the pinning rate η_k.

Lemma 6 (see [20]). *Consider the following system, where the system has a time delay:*

$$\begin{cases} ^cD_{t_0,t}^{\alpha}V_k(t) \leq -K_1V_k(t) + K_2V_k(t-\tau), & t > 0, i \in D_k, \\ V_k(s) = \Phi_k(s), & s \in [-\tau, 0], \end{cases} \tag{19}$$

and the linear fractional-order delay differential system is as follows:

$$\begin{cases} ^cD_{t_0,t}^{\alpha}W_k(t) = -K_1W_k(t) + K_2W_k(t-\tau), & t > 0, i \in D_k, \\ W_k(t) = \Phi_k(s), & s \in [-\tau, 0], \end{cases} \tag{20}$$

where except for the point $t_k, k = 1, 2, \ldots, V_k(t), W_k(t) \in R^n$ is continuous everywhere, and $\Phi_k(s) \geq 0$ is continuous in $[-\tau, 0]$. If $K_1 > 0, K_2 > 0$, then $V_k(t) \leq W_k(t), t \in [0, +\infty]$.

3. Main Result

We will derive several synchronization standards in this section. Under the action of the pinning impulsive controller, D_k, $i \in D_k, D_k \in \{D_1, D_2, \ldots, D_m\}$, system (7) and reference trajectory $s_k(t) \in \{s_1(t), s_2(t), \ldots, s_m(t)\}$ to achieve multiple quasisynchronization.

Theorem 1. *Let $\xi_i > 0 (i = 1, 2, 3)$. For any $i \in D_k, k = 1, 2, \ldots, m$, under the pinning impulsive control (10), system (7) can achieve multiple quasisynchronization if Assumptions (A1) and (A2) hold, there exist symmetric matrices $M_i \in R^{n \times n} > 0 (i = 1, 2)$ and positive definite matrix $P \in R^{n \times n}$ and such that*

$$\begin{pmatrix} \widehat{G} & 0 \\ 0 & P\Gamma \end{pmatrix} < 0, \tag{21}$$

$$\omega_1 = \begin{pmatrix} P\hat{P} + \hat{P}^TP + \xi_1P\widehat{\mathscr{A}}_1\widehat{\mathscr{A}}_1^TP + \frac{1}{\xi_1}\widehat{\mathscr{B}}_1^T\widehat{\mathscr{B}}_1 - P\hat{Q}M_1^{-1}\hat{Q}^TP - \mathscr{L}_i^TM_1\mathscr{L}_i \\ -\xi_2P\widehat{\mathscr{A}}_2\widehat{\mathscr{A}}_2^TP - \frac{1}{\xi_2}\mathscr{L}_i^T\widehat{\mathscr{B}}_2^T\widehat{\mathscr{B}}_2\mathscr{L}_i - P\hat{R}M_2^{-1}\hat{R}^TP - \xi_3P\widehat{\mathscr{A}}_3\widehat{\mathscr{A}}_3^TP \end{pmatrix} \geq K_1P > 0, \tag{22}$$

$$\omega_2 = \mathscr{L}_i^T M_2 \mathscr{L}_i + \frac{1}{\xi_3}\mathscr{L}_i^T \widehat{\mathscr{B}}_3^T \widehat{\mathscr{B}}_3 \mathscr{L}_i \le K_2 P, \tag{23}$$

$$\omega_3 = (1+\theta_k)^2 \eta_k \frac{\lambda_{\max}(P)}{\lambda_{\min}(P)} + (1-\eta_k)\frac{\lambda_{\max}(P)}{\lambda_{\min}(P)} \le \rho_k \in (0,1), \tag{24}$$

where $K_1>0, K_2>0, K_1>\sqrt{2}K_2$ *and* $\sqrt{(\lambda_{\max}(P)\kappa/\lambda_{\min}(P))} < \sigma_k$. *Define the Lyapunov function as follows:*

$$V_k(t) = \sum_{i\in D_k} \overline{\varepsilon}_i^T(t) P \overline{\varepsilon}_i(t). \tag{25}$$

For $t \in [t_{h-1}, t_h), h = 0, 1, 2, \ldots$, from Lemma 1 we obtained the following:

$$\begin{aligned}
{}^{c}D_{t_0,t}^{\alpha} V_k(t) &\le \sum_{i\in D_k} \overline{2}\varepsilon_i^T(t) P {}^{c}D_{t_0,t}^{\alpha} \overline{\varepsilon}_i(t) \\
&= \sum_{i\in D_k} \overline{2}\varepsilon_i^T(t) P \left(-(\hat{P}+\Delta\mathscr{P}(t))\overline{\varepsilon}_i(t) + (\hat{Q}+\Delta\mathscr{Q}(t))\widetilde{f}_i(\overline{\varepsilon}_i(t))\right. \\
&\quad \left. + (\hat{R}+\Delta\mathscr{R}(t))\widetilde{f}_i(\overline{\varepsilon}_i(t-\tau)) + \sum_{j\in D_k} \hat{G}_{ij}\Gamma\overline{\varepsilon}_j(t)\right) \\
&= 2\sum_{i\in D_k} \overline{\varepsilon}_i^T(t) P\Big(-(\hat{P}+\Delta\mathscr{P}(t))\Big)\overline{\varepsilon}_i(t) + 2\sum_{i\in D_k} \overline{\varepsilon}_i^T(t) P(\hat{Q}+\Delta\mathscr{Q}(t))\widetilde{f}_i(\overline{\varepsilon}_i(t)) \\
&\quad + 2\sum_{i\in D_k} \overline{\varepsilon}_i^T(t) P(\hat{R}+\Delta\mathscr{R}(t))\widetilde{f}_i(\overline{\varepsilon}_i(t-\tau)) + 2\sum_{i\in D_k} \overline{\varepsilon}_i^T(t) P \sum_{j\in D_k} \hat{G}_{ij}\Gamma\overline{\varepsilon}_j(t).
\end{aligned} \tag{26}$$

By Assumptions (A1) and (A2) and Lemmas 1-4, we obtain the following:

$$\begin{aligned}
&\sum_{i\in D_k} 2\overline{\varepsilon}_i^T(t) P\Big(-(\hat{P}+\Delta\mathscr{P}(t))\Big)\overline{\varepsilon}_i(t) \\
&\le \sum_{i\in D_k} \overline{\varepsilon}_i^T(t)\left(-\left(P\hat{P}+\hat{P}^T P + P\widehat{\mathscr{A}}_1\widehat{\mathscr{C}}_1(t)\widehat{\mathscr{B}}_1 + \widehat{\mathscr{B}}_1^T\widehat{\mathscr{C}}_1^T(t)\widehat{\mathscr{A}}_1^T P\right)\right)\overline{\varepsilon}_i(t) \\
&\le \sum_{i\in D_k} \overline{\varepsilon}_i^T(t)\left(-\left(P\hat{P}+\hat{P}^T P + \xi_1 P\widehat{\mathscr{A}}_1\widehat{\mathscr{A}}_1^T P + \frac{1}{\xi_1}\widehat{\mathscr{B}}_1^T\widehat{\mathscr{B}}_1\right)\right)\overline{\varepsilon}_i(t),
\end{aligned} \tag{27}$$

$$\begin{aligned}
&\sum_{i\in D_k} 2\overline{\varepsilon}_i^T(t) P(\hat{Q}+\Delta\mathscr{Q}(t))\widetilde{f}_i(\overline{\varepsilon}_i(t)) \\
&\le \sum_{i\in D_k} 2\overline{\varepsilon}_i^T(t) P\hat{Q}\widetilde{f}_i(\overline{\varepsilon}_i(t)) + \sum_{i\in D_k} 2\overline{\varepsilon}_i^T(t) P\widehat{\mathscr{A}}_2\widehat{\mathscr{C}}_2(t)\widehat{\mathscr{B}}_2\widetilde{f}_i(\overline{\varepsilon}_i(t)) \\
&\le \sum_{i\in D_k} \overline{\varepsilon}_i^T(t) P\hat{Q}M_1^{-1}\hat{Q}^T P\overline{\varepsilon}_i(t) + \sum_{i\in D_k} \widetilde{f}_i^T(\overline{\varepsilon}_i(t)) M_1 \widetilde{f}_i(\overline{\varepsilon}_i(t)) \\
&\quad + \sum_{i\in D_k} \overline{\varepsilon}_i^T(t) P\widehat{\mathscr{A}}_2\widehat{\mathscr{C}}_2(t)\widehat{\mathscr{B}}_2\widetilde{f}_i(\overline{\varepsilon}_i(t)) + \sum_{i\in D_k} \widetilde{f}_i^T(\overline{\varepsilon}_i(t))\widehat{\mathscr{B}}_2^T\widehat{\mathscr{C}}_2^T(t)\widehat{\mathscr{A}}_2^T P\overline{\varepsilon}_i(t) \\
&\le \sum_{i\in D_k} \overline{\varepsilon}_i^T(t) P\hat{Q}M_1^{-1}\hat{Q}^T P\overline{\varepsilon}_i(t) + \sum_{i\in D_k} \overline{\varepsilon}_i^T(t)\mathscr{L}_i^T M_1 \mathscr{L}_i\overline{\varepsilon}_i(t) \\
&\quad + \sum_{i\in D_k} \frac{1}{\xi_2}\overline{\varepsilon}_i^T(t)\mathscr{L}_i^T\widehat{\mathscr{B}}_2^T\widehat{\mathscr{B}}_2\mathscr{L}_i\overline{\varepsilon}_i(t) + \sum_{i\in D_k} \xi_2\overline{\varepsilon}_i^T(t) P\widehat{\mathscr{A}}_2\widehat{\mathscr{A}}_2^T P\overline{\varepsilon}_i(t) \\
&= \sum_{i\in D_k} e_i^T(t)\left(P\hat{Q}M_1^{-1}\hat{Q}^T P + L_i^T M_1 L_i + \frac{1}{\xi_2}L_i^T\hat{B}_2^T\hat{B}_2 L_i + \xi_2 P\hat{A}_2\hat{A}_2^T P\right)e_i(t),
\end{aligned} \tag{28}$$

$$\begin{aligned}
&\sum_{i\in D_k} 2\overline{\varepsilon}_i^T(t)P(\hat{R}+\Delta\mathscr{R}(t))\widetilde{f}_i(\overline{\varepsilon}_i(t-\tau))\\
&\le \sum_{i\in D_k} 2\overline{\varepsilon}_i^T(t)P\hat{R}\widetilde{f}_i(\overline{\varepsilon}_i(t)) + \sum_{i\in D_k} 2\overline{\varepsilon}_i^T(t)P\widehat{\mathscr{A}}_3\widehat{\mathscr{C}}_3(t)\widehat{\mathscr{B}}_3\widetilde{f}_i(\overline{\varepsilon}_i(t-\tau))\\
&\le \sum_{i\in D_k} \overline{\varepsilon}_i^T(t)P\hat{R}M_2^{-1}\hat{R}^TP\overline{\varepsilon}_i(t) + \sum_{i\in D_k} \widetilde{f}_i^T(\overline{\varepsilon}_i(t-\tau))M_2\widetilde{f}_i(\overline{\varepsilon}_i(t-\tau))\\
&\quad + \sum_{i\in D_k} \overline{\varepsilon}_i^T(t)P\widehat{\mathscr{A}}_3\widehat{\mathscr{C}}_3(t)\widehat{\mathscr{B}}_3\widetilde{f}_i(\overline{\varepsilon}_i(t-\tau)) + \sum_{i\in D_k} \widetilde{f}_i^T(\overline{\varepsilon}_i(t-\tau))\widehat{\mathscr{B}}_3^T\widehat{\mathscr{C}}_3^T(t)\widehat{\mathscr{A}}_3^TP\overline{\varepsilon}_i(t)\\
&\le \sum_{i\in D_k} \overline{\varepsilon}_i^T(t)P\hat{R}M_2^{-1}\hat{R}^TP\overline{\varepsilon}_i(t) + \sum_{i\in D_k} \overline{\varepsilon}_i^T(t-\tau)\mathscr{L}_i^TM_2\mathscr{L}_i\overline{\varepsilon}_i(t-\tau)\\
&\quad + \sum_{i\in D_k} \frac{1}{\xi_3}\overline{\varepsilon}_i^T(t-\tau)\mathscr{L}_i^T\widehat{\mathscr{B}}_3^T\widehat{\mathscr{B}}_3\mathscr{L}_i\overline{\varepsilon}_i(t-\tau) + \sum_{i\in D_k} \xi_3\overline{\varepsilon}_i^T(t)P\widehat{\mathscr{A}}_3\widehat{\mathscr{A}}_3^TP\overline{\varepsilon}_i(t)\\
&= \sum_{i\in D_k} \overline{\varepsilon}_i^T(t)\left(P\hat{R}M_2^{-1}\hat{R}^TP + \xi_3P\widehat{\mathscr{A}}_3\widehat{\mathscr{A}}_3^TP\right)\overline{\varepsilon}_i(t) + \sum_{i\in D_k} \overline{\varepsilon}_i^T(t-\tau)\left(\mathscr{L}_i^TM_2\mathscr{L}_i + \frac{1}{\xi_3}\mathscr{L}_i^T\widehat{\mathscr{B}}_3^T\widehat{\mathscr{B}}_3\mathscr{L}_i\right)\overline{\varepsilon}_i(t-\tau).
\end{aligned} \tag{29}$$

Form (21), we have the following:

$$\sum_{i\in D_k} 2\overline{\varepsilon}_i^T(t)P\sum_{j\in D_k}\widehat{G}_{ij}\Gamma\overline{\varepsilon}_j(t) = 2\overline{\varepsilon}^T(t)(\widehat{G}\otimes P\Gamma)\overline{\varepsilon}(t)\le 0. \tag{30}$$

Substituting (27)-(30) into (27282930) yields the following equation:

$$\begin{aligned}
{}^cD_{t_0,t}^{\alpha}V_k(t) &\le \sum_{i\in D_k} -\overline{\varepsilon}_i^T(t)\omega_1\overline{\varepsilon}_i(t) + \sum_{i\in D_k}\overline{\varepsilon}_i^T(t-\tau)\omega_2\overline{\varepsilon}_i(t-\tau)\\
&\quad + 2\overline{\varepsilon}^T(t)(\widehat{G}\otimes P\Gamma)\overline{\varepsilon}(t).
\end{aligned} \tag{31}$$

From (21)-(24), we have the following equation:

$$\begin{aligned}
{}^cD_{t_0,t}^{\alpha}V_k(t) &\le \sum_{i\in D_k} -\overline{\varepsilon}_i^T(t)K_1P\overline{\varepsilon}_i(t) + \overline{\varepsilon}_i^T(t-\tau)K_2P\overline{\varepsilon}_i(t-\tau)\\
&\le -K_1V_k(t) + K_2V_k(t-\tau).
\end{aligned} \tag{32}$$

When $t = t_h$, from (11) and (24), Lemma 5, and Definition 2, we obtain the following:

$$\begin{aligned}
V_k(t_h^+) &= \sum_{i\in D_k}\overline{\varepsilon}_i^T(t_h^+)P\overline{\varepsilon}_i(t_h^+)\\
&= \sum_{i\in\Im_k(t_h)}\overline{\varepsilon}_i^T(t_h^+)P\overline{\varepsilon}_i(t_h^+) + \sum_{i\notin\Im_k(t_h)}\overline{\varepsilon}_i^T(t_h^+)P\overline{\varepsilon}_i(t_h^+)\\
&= \sum_{i\in\Im_k(t_h)}(1+\theta_k)^2\overline{\varepsilon}_i^T(t_h^-)P\overline{\varepsilon}_i(t_h^-) + \sum_{i\notin\Im_k(t_h)}\overline{\varepsilon}_i^T(t_h^-)P\overline{\varepsilon}_i(t_h^-)\\
&\le (1+\theta_k)^2\lambda_{\max}(P)\sum_{i\in\Im_k(t_h)}\overline{\varepsilon}_i^T(t_h^-)\overline{\varepsilon}_i(t_h^-) + \lambda_{\max}(P)\sum_{i\notin\Im_k(t_h)}\overline{\varepsilon}_i^T(t_h^-)\overline{\varepsilon}_i(t_h^-)\\
&\le (1+\theta_k)^2\lambda_{\max}(P)\sum_{i\in D_k}\overline{\varepsilon}_i^T(t_h)\overline{\varepsilon}_i(t_h) + (1-\eta_k)\lambda_{\max}(P)\sum_{i\in D_k}2\,\overline{\varepsilon}_i^T(t_h)\overline{\varepsilon}_i(t_h)\\
&\le \omega_3V_k(t_h)\\
&\le \rho_kV_k(t_h).
\end{aligned} \tag{33}$$

Now, consider the following system with time lag:

$$\begin{cases}
{}^cD_{t_0,t}^{\alpha}W_k(t) = -K_1W_k(t) + K_2W_k(t-\tau), & t>0,\\
W_k(t) = \Phi_k(s), & s\in[-\tau,0].
\end{cases} \tag{34}$$

If $\lim_{t\longrightarrow\infty}W_k(t) = 0, \Phi_k(s)\ge 0$, afterward through Lemma 6, we can have $\lim_{t\longrightarrow\infty}V_k(t) = 0, \Phi_k(s)\ge 0$.

Next, we will prove that when $K_1 > \sqrt{2}K_2$ ($K_1>0$, $K_2>0$), there is $\lim_{t\longrightarrow\infty}W_k(t) = 0, \Phi_k(s)\ge 0$.

In order to distinguish the subsystem subscript in this article from the original imaginary unit, here, we change the original inherent imaginary unit $\widetilde{i}$. The characteristic (34) can be changed to the following form according to Corollary 3 in Reference [21].

$$\overline{v}_k^{\alpha} + K_1 - K_2 e^{-\overline{v}_k \tau} = 0, \tag{35}$$

If $K_1 > \sqrt{2}K_2$ and (35) has no pure imaginary roots, so the zero solution of equation (34) is globally Lyapunov asymptotically stable, namely, $\lim_{t\longrightarrow\infty} W_k(t) = 0, \Phi_k(s) \geq 0$.

Next, we will use contradiction analysis to show that (35) does not have pure imaginary roots. Then, suppose (35) has pure imaginary roots $\overline{v}_k$, and $\overline{v}_k = \nu_k \widetilde{i} = |\nu_k|(\cos(\pi/2) + \widetilde{i}\sin(\pi/2))$, where ν_k is a real number. If $\nu_k \leq 0$, then $\overline{v}_k = \nu_k \widetilde{i} = |\nu_k|(\cos(\pi/2) - \widetilde{i}\sin(\pi/2))$, and if $\nu_k > 0$, then $\overline{v}_k = \nu_k \widetilde{i} = |\nu_k|(\cos(\pi/2) + \widetilde{i}\sin(\pi/2))$.

By substituting $\overline{v}_k = \nu_k \widetilde{i}$ into (35), we can obtain the following:

$$\left|(\nu_k \widetilde{i})^{\alpha} + K_1\right|^2 = \left|K_2 e^{-\tau \nu_k \widetilde{i}}\right|^2, \tag{36}$$

that is,

$$\begin{aligned} &|\nu_k|^{2\alpha} + 2K_1 \cos\left(\frac{\alpha\pi}{2}\right)|\nu_k|^{\alpha} + K_1^2 = \left|K_2 \cos(\tau\nu_k)\right|^2 \\ &\quad + \left|K_2 \sin(\tau\nu_k)\right|^2 \leq 2(K_2)^2. \end{aligned} \tag{37}$$

Let

$$\begin{aligned} h_k(x_k) &= x_k^2 + 2K_1 \cos\left(\frac{\alpha\pi}{2}\right)x_k + K_1^2 \\ &\quad - \left((K_2 \cos(\tau\nu_k))^2 + (K_2 \sin(\tau\nu_k))^2\right). \end{aligned} \tag{38}$$

So,

$$h_k(0) = K_1^2 - \left((K_2 \cos(\tau\nu_k))^2 + (K_2 \sin(\tau\nu_k))^2\right) \geq K_1^2 - 2(K_2)^2. \tag{39}$$

Because $K_1 > \sqrt{2}K_2 (K_1 > 0, K_2 > 0)$, so $h_k(0) > 0$. We know that h_k is a second-order polynomial, so we have $h_k(|\nu_k|^{\alpha}) > 0$, which contradicts (37). That is, (37) has no solution, which means that (35) has no pure imaginary roots, namely, $\lim_{t\longrightarrow\infty} V_k(t) = 0$.

Therefore, there exists T_k, and for arbitrary $\kappa > 0$ and for all $t > T_k$, we have the following equation:

$$V_k(t) < \lambda_{\max}(P)\kappa, \quad t > T_k, \tag{40}$$

where $V_k(t) = \sum_{i\in D_k} \overline{\varepsilon}_i^T(t) P \overline{\varepsilon}_i(t)$, so we have the following equation:

$$\lambda_{\min}(P)\left\|\overline{\varepsilon}_i(t)\right\|^2 < \lambda_{\max}(P)\kappa, \quad t > T_k, \tag{41}$$

that is,

$$\left\|\overline{\varepsilon}_i(t)\right\| \leq \sqrt{\frac{\lambda_{\max}(P)\kappa}{\lambda_{\min}(P)}} < \sigma_k, \tag{42}$$

where $i \in D_k$ and $\sum_{k=1}^{m} T_k = \{T_1, T_2, \ldots, T_N\}$. So there exits $T = \max\{T_1, T_2, \ldots, T_N\}$, for $\forall t > T$ and any small positive number $\sigma_k > 0$, such that $0 < \|x_i(t) - s_k(t)\| < \sigma_k, k = 1, 2, \ldots, m$.

If $\Delta\mathscr{P}(t) = 0, \Delta\mathscr{Q}(t) = 0, \Delta\mathscr{R}(t) = 0$, (2.1) will degrade into

$$\begin{aligned} {}^{c}D_{t_0,t}^{\alpha} x_i(t) &= -\widehat{P}x_i(t) + \widehat{Q}f_i(x_i(t)) + \widehat{R}f_i(x_i(t-\tau)) \\ &\quad + \sum_{j=1}^{N} \widehat{G}_{ij}\Gamma x_j(t) + J. \end{aligned} \tag{43}$$

Corollary 1. *For any $i \in D_k, k = 1, 2, \ldots, m$, under the pinning impulsive control (10), system (43) can achieve multiple quasisynchronization if Assumptions (A1) and (A2) hold, there exist symmetric matrices $M_i \in R^{n\times n} > 0 (i = 1, 2)$, and positive definite matrix $P \in R^{n\times n}$ such that*

$$\begin{aligned} &\begin{pmatrix} \widehat{G} & 0 \\ 0 & P\Gamma \end{pmatrix} < 0, \\ &\omega_1 = \left(P\widehat{P} + \widehat{P}^T P - P\widehat{Q}M_1^{-1}\widehat{Q}^T P - \mathscr{L}_i^T M_1 \mathscr{L}_i - P\widehat{R}M_2^{-1}\widehat{R}^T P\right) \geq K_1 P > 0, \\ &\omega_2 = \mathscr{L}_i^T M_2 \mathscr{L}_i \leq K_2 P, \\ &\omega_3 = (1+\theta_k)^2 \eta_k \frac{\lambda_{\max}(P)}{\lambda_{\min}(P)} + (1-\eta_k)\frac{\lambda_{\max}(P)}{\lambda_{\min}(P)} \leq \rho_k \in (0,1), \end{aligned} \tag{44}$$

where $K_1 > 0$, $K_2 > 0$, $K_1 > \sqrt{2}K_2$, and $\sqrt{(\lambda_{\max}(P)\kappa/\lambda_{\min}(P))} < \sigma_k$.

Remark 3. We give general theoretical results for multiple quasisynchronization of FCNNs with uncertain terms and delays in Theorem 1 Among existing references, the quasisynchronization problem of FCNNs with uncertainty is rarely discussed. Moreover, unlike the analytical method of Reference [22], the model (7) in this article is a fractional-order system instead of the integer-order model in Reference [22]. The analysis and processing method of fractional-order system is unlike that of integer-order system, so it cannot be applied directly.

Remark 4. Multiple quasisynchronization is the extension of quasisynchronization. When $m = 1$ in reference trajectory

indicates that there is only one reference track, next, the multiple quasisynchronization is reduced to quasisynchronization.

Remark 5. Corollary 1 gives the sufficient conditions for multiple quasisynchronization of DFCNN when the uncertainty term is zero.

Remark 6. In Reference [23], the author solved the synchronization problem through adaptive control method. In this article to reduce the control cost and realize the pinned pulse control, only some nodes need to be controlled to be in the bounded field where they share the reference trajectory.

Remark 7. Compared with Reference [20], the difference of this article is that we consider parameter uncertainty satisfying bounded conditions in the model, and the advantage is that the model considered in this article is more practical in practical systems and applications. In particular, our model is fractional-order, and parameter uncertainties and coupling terms are taken into account in the model.

4. Examples

In this section, we give two numerical simulation examples to illustrate the abovementioned theoretical values.

Example 1. We design the FCNNs with uncertain terms and delays (7), where $f_i(x_i(t)) = \tanh(x_i(t))$, $i = 1, 2$, $m = 1, 2$, time-delay $\tau = 1$, and $\alpha = 0.96$, and the parameter matrix of the network is as follows:

$$\begin{aligned}
&\widehat{P} = \begin{pmatrix} 5.2 & 0 \\ 0 & 5.2 \end{pmatrix}, \widehat{Q} = \begin{pmatrix} 4.8 & -2 \\ -3 & 2.5 \end{pmatrix}, \widehat{R} = \begin{pmatrix} 0.25 & 0 \\ 0 & 1.5 \end{pmatrix}, \\
&\Delta\mathscr{P} = \cos(t)\begin{pmatrix} 1 & 1 \\ 1 & 1 \end{pmatrix}, \Delta\mathscr{Q} = \sin(t)\begin{pmatrix} 1 & 1 \\ 1 & 1 \end{pmatrix}, \Delta\mathscr{R} = \cos(t)\begin{pmatrix} 1 & 1 \\ 1 & 1 \end{pmatrix}, \\
&\widehat{G} = \begin{pmatrix} -5 & 0.2 \\ 0.4 & -1 \end{pmatrix}, J = \begin{pmatrix} 0 \\ 0 \end{pmatrix}.
\end{aligned} \tag{45}$$

Two corresponding reference trajectories (9), where $k = 1, 2$, $\alpha = 0.96$, $\tau = 1$, $f_{\bar{i}}(s_{\bar{i}}(t)) = \tanh(s_{\bar{i}}(t))$.

We select $\Gamma = \mathrm{diag}(1, 1)$, pulse gain $\theta_1 = -0.2$, $\theta_2 = -0.6$, $\eta_1 = 0.7$, $\eta_2 = 0.4$, $\rho_1 = 0.84$, and $\rho_2 = 0.74$. It can be proved that the conditions (21)-(24) in Theorem 1 are established and can be obtained by the following calculation:

$$P = \begin{pmatrix} 1.0017 & 0.0022 \\ 0.0022 & 1.0945 \end{pmatrix}, \tag{46}$$

at the same time, $(\lambda_{\max}(P)/\lambda_{\min}(P)) = 10/9$, $\sigma_1 = 0.08$, and $\sigma_2 = 0.12$, after that we can get $\omega_1 = \begin{pmatrix} 173.0088 & -0.0003 \\ -0.0003 & 21.0120 \end{pmatrix}$, $\omega_2 = \begin{pmatrix} 2.4908 & 0 \\ 0 & 4.4362 \end{pmatrix}$, $\omega_3 = \begin{pmatrix} 0.8311 \\ 0.3271 \end{pmatrix}$ through the abovementioned formulas (22)-(24). Then, the uncertain fractional-order neural network can realize multiple quasisynchronization, and the convergence of its error signals $e_{1m}(t)$, $e_{2m}(t)$, and $m = 1, 2$, under the fixed pulse controller is shown in Figure 1.

Example 2. We design the FCNNs with uncertain terms and delays (6), where $f_i(x_i(t)) = \tanh(x_i(t))$, $i = 1, 2$, $m = 1, 2$, time delay $\tau = 1$, and $\alpha = 0.98$, and the parameter matrix of the network is as follows:

$$\begin{aligned}
&\widehat{P} = \begin{pmatrix} 6 & 0 \\ 0 & 6 \end{pmatrix}, \widehat{Q} = \begin{pmatrix} 5 & -5 \\ -5 & 3.8 \end{pmatrix}, \widehat{R} = \begin{pmatrix} 0.25 & 0 \\ 0 & 1.5 \end{pmatrix}, \\
&\Delta\mathscr{P} = \sin(t)\begin{pmatrix} 1 & 1 \\ 1 & 1 \end{pmatrix}, \Delta\mathscr{Q} = \cos(t)\begin{pmatrix} 1 & 1 \\ 1 & 1 \end{pmatrix}, \Delta\mathscr{R} = \sin(t)\begin{pmatrix} 1 & 1 \\ 1 & 1 \end{pmatrix}, \\
&\widehat{G} = \begin{pmatrix} -5 & 0.2 \\ 0.4 & -1 \end{pmatrix}, J = \begin{pmatrix} 0 \\ 0 \end{pmatrix}.
\end{aligned} \tag{47}$$

Two corresponding reference trajectories (9), where $k = 1, 2$, $\alpha = 0.98$, $\tau = 1$, $f_{\bar{i}}(s_{\bar{i}}(t)) = \tanh(s_{\bar{i}}(t))$.

We select $\Gamma = \mathrm{diag}(1, 1)$, pulse gain $\theta_1 = -0.3$, $\theta_2 = -0.7$, $\eta_1 = 0.5$, $\eta_2 = 0.6$, $\rho_1 = 0.83$, and $\rho_2 = 0.51$. It can be proved that conditions (21)-(24) in Theorem 1 are established and can be obtained by the following calculation:

$$P = \begin{pmatrix} 1.0017 & 0.0022 \\ 0.0022 & 1.0945 \end{pmatrix}, \tag{48}$$

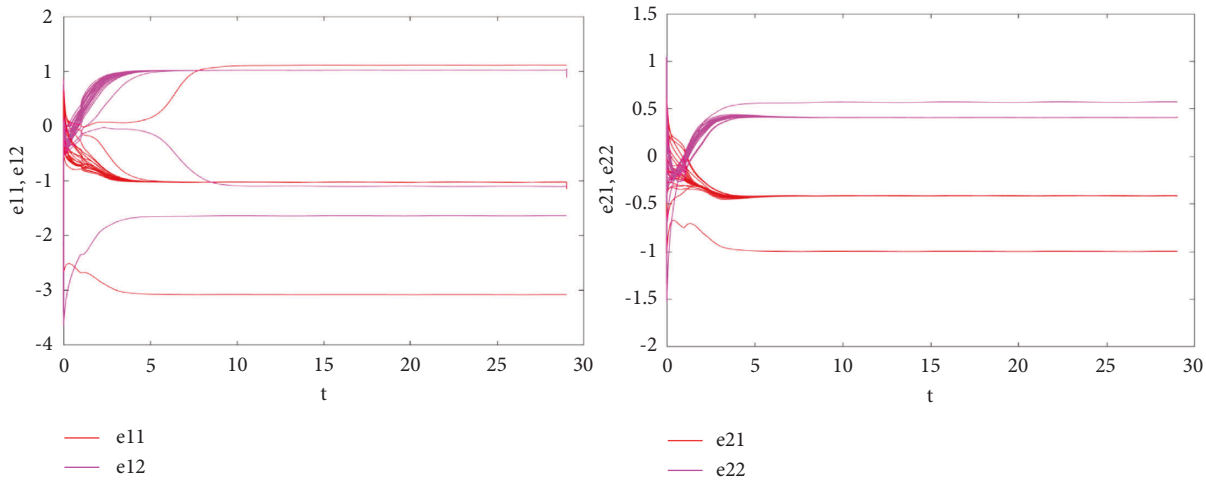

Figure 1: Trajectory of e_{11}, e_{12}, e_{21}, and e_{22} of the system in Example 1 under the impulsive controller.

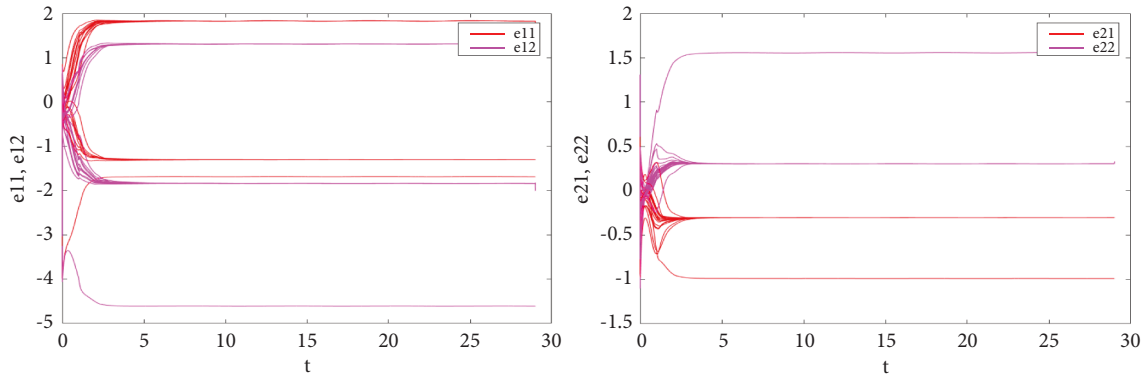

Figure 2: Trajectory of e_{11}, e_{12}, e_{21}, and e_{22} of the system in Example 2 under the impulsive controller.

at the same time, $(\lambda_{\max}(P)/\lambda_{\min}(P)) = (10/9)$, $\sigma_1 = 0.06$, and $\sigma_2 = 0.18$. After that we can get $\omega_1 = \begin{pmatrix} 135.2047 & -0.0012 \\ -0.0012 & 74.7350 \end{pmatrix}$, $\omega_2 = \begin{pmatrix} 3.0918 & 0 \\ 0 & 1.1362 \end{pmatrix}$, $\omega_3 = \begin{pmatrix} 0.8278 \\ 0.5044 \end{pmatrix}$ through the abovementioned formulas (22)-(24). Then, the uncertain fractional-order neural network can realize multiple quasisynchronization, and the convergence of its error signals $e_{1m}(t)$, $e_{2m}(t)$, $m = 1, 2$, and under the fixed pulse controller is shown in Figure 2.

5. Conclusion

In this article, the multiple quasisynchronization problem of FCNNs with uncertainty and time-delay is studied. Firstly, our main theoretical method is to construct an impulse controller to control some nodes and then divide the nodes into several disjoint subsets, so as to make the system achieve multiple quasisynchronization. Secondly, using the relevant knowledge of the comparison principle and the method of constructing the Lyapunov function, we obtain the sufficient conditions for the system to realize multiple quasisynchronization. Finally, two examples are given to carry out simulation operations to demonstrate the validity of the theoretical results in this article.

Data Availability

No data were used to support this study.

Conflicts of Interest

The authors declare that they have no conflicts of interest.

Acknowledgments

This work is supported by the Natural Science Foundation of China under Grants 62072164 and 11704109.

References

[1] P. Schirmer and I. Mporas, "Energy disaggregation using fractional calculus," in *Proceedings of the 2020 IEEE International Conference on Acoustics, Speech and Signal Processing (ICASSP)*, pp. 3257–3261, Barcelona, Spain, May 2020.

[2] A. Bendaoud and F. Hachouf, "Fractional calculus for improving edge-based active contour models," in *Proceedings of the 2021 International Conference on Recent Advances in*

Mathematics and Informatics (ICRAMI), pp. 1–5, Tebessa, Algeria, September 2021.

[3] H. B. Bao and J. D. Cao, "Projective synchronization of fractional-order memristor-based neural networks," *Neural Networks*, vol. 63, pp. 1–9, 2015.

[4] 李. Li Xin-bo, 付. Fu Yun-bo, 姜. Jiang Liang-xu, 石 DuShi Yao-wu, and 杨 Yang Zhi-gang, "Application of neural network fractional order PIDto piezoelectric stack control," *Optics and Precision Engineering*, vol. 23, no. 12, pp. 3439–3445, 2015.

[5] S. Xu, X. Wang, and X. Ye, "A new fractional-order chaos system of Hopfield neural network and its application in image encryption," *Chaos, Solitons & Fractals*, vol. 157, p. 111889, 2022.

[6] W. Du, Q. Y. Miao, L. Tong, and Y. Tang, "Identification of fractional-order systems with unknown initial values and structure," *Physics Letters A*, vol. 381, no. 23, pp. 1943–1949, 2017.

[7] H. Liu and J. Zhang, "Stabilization of Uncertain Stochastic Nonlinear Delay Systems Subject to Event-Triggered Mechanism," in *Proceedings of the 2019 IEEE Symposium Series on Computational Intelligence (SSCI)*, pp. 1263–1270, Xiamen, China, December 2019.

[8] S. Wang, X. Wang, and Y. Zhou, "A memristor-based complex lorenz system and its modified projective synchronization," *Entropy*, vol. 17, no. 12, pp. 7628–7644, 2015.

[9] M. Xu, Y. Li, P. Liu, P. Yu, S. Li, and J. Sun, "On synchronization of coupled fractional-order neural networks in finite-time sense," in *Proceedings of the 2021 International Conference on Neuromorphic Computing (ICNC)*, pp. 41–46, Wuhan, China, October 2021.

[10] C. Chen, Z. Ding, S. Li, and L. Wang, "Synchronization of Fractional-Order Memristive Neural Networks with Time Delays," in *Proceedings of the 2019 Chinese Automation Congress (CAC)*, pp. 2754–2759, Hangzhou, China, November 2019.

[11] S. Wang, Y. Huang, and S. Ren, "Synchronization and robust synchronization for fractional-order coupled neural networks," *IEEE Access*, vol. 5, pp. 12439–12448, 2017.

[12] J. Feng, S. Chen, J. Wang, and Y. Zhao, "Quasi-Synchronization of coupled nonlinear memristive neural networks with time delays by pinning control," *IEEE Access*, vol. 6, pp. 26271–26282, 2018.

[13] X. Lv, X. Li, J. Cao, and M. Perc, "Dynamical and static multisynchronization of coupled multistable neural networks via impulsive control," *IEEE Transactions on Neural Networks and Learning Systems*, vol. 29, no. 12, pp. 6062–6072, 2018.

[14] C. P. Li and F. R. Zhang, "A survey on the stability of fractional differential equations," *The European Physical Journal - Special Topics*, vol. 193, no. 1, pp. 27–47, 2011.

[15] D. X. He, G. Ling, Z. H. Guan, B. Hu, and R. Q. Liao, "Multisynchronization of coupled heterogeneous genetic oscillator networks via partial impulsive control," *IEEE Transactions on Neural Networks and Learning Systems*, vol. 29, no. 2, pp. 335–342, 2018.

[16] M. A. Duarte-Mermoud, N. Aguila-Camacho, J. A. Gallegos, and R. Castro-Linares, "Using general quadratic Lyapunov functions to prove Lyapunov uniform stability for fractional order systems," *Communications in Nonlinear Science and Numerical Simulation*, vol. 22, no. 1-3, pp. 650–659, 2015.

[17] Y. L. Wang and C. E. de Souza, "Robust control of a class of uncertain nonlinear systems," *Systems & Control Letters*, vol. 19, no. 2, pp. 139–149, 1992.

[18] L. Pan and J. Cao, "Stochastic quasi-synchronization for delayed dynamical networks via intermittent control," *Communications in Nonlinear Science and Numerical Simulation*, vol. 17, no. 3, pp. 1332–1343, 2012.

[19] L. Huang, *Linear Algebria in Systems and Control Theory*, Science Press, Beijing, China, 1984.

[20] X. Ruan and A. Wu, "Multi-quasi-synchronization of coupled fractional-order neural networks with delays via pinning impulsive control," *Advances in Difference Equations*, no. 1, p. 359, 2017.

[21] W. Deng, C. Li, and J. Lü, "Stability analysis of linear fractional differential system with multiple time delays," *Nonlinear Dynamics*, vol. 48, no. 4, pp. 409–416, 2006.

[22] W. He, F. Qian, and J. Cao, "Pinning-controlled synchronization of delayed neural networks with distributed-delay coupling via impulsive control," *Neural Networks*, vol. 85, pp. 1–9, 2017.

[23] A. Jajarmi, M. Hajipour, and D. Baleanu, "New aspects of the adaptive synchronization and hyperchaos suppression of a financial model," *Chaos, Solitons & Fractals*, vol. 99, pp. 285–296, 2017.

Hindawi
Complexity
Volume 2022, Article ID 4634326, 9 pages
https://doi.org/10.1155/2022/4634326

Research Article

Distance-Based Topological Descriptors on Ternary Hypertree Networks

Yun Yu,[1] D. Antony Xavier,[2] Eddith Sarah Varghese,[2] Deepa Mathew,[3] Muhammad Kamran Siddiqui,[4] and Samuel Asefa Fufa[5]

[1]*School of Big Data and Artificial Intelligence, Anhui Xinhua University, 230088 Hefei, China*
[2]*Department of Mathematics, Loyola College (Affliated to University of Madras), Chennai, India*
[3]*Department of Mathematics, St. Joseph's College, Bangalore, India*
[4]*Department of Mathematics, COMSATS University Islamabad, Lahore Campus, Pakistan*
[5]*Department of Mathematics, Addis Ababa University, Addis Ababa, Ethiopia*

Correspondence should be addressed to Samuel Asefa Fufa; samuel.asefa@aau.edu.et

Received 27 February 2022; Revised 18 July 2022; Accepted 27 August 2022; Published 27 September 2022

Academic Editor: Yue Song

Topological indices are numeric parameters which portray the topology of a subatomic structure. In QSAR/QSPR analysis, topological descriptors play a vital role to examine the topology of a network. An interconnection network is a structure whose components are connected physically according to some pattern. In this paper, an interconnection network, ternary hypertree, which is a structural combination of complete ternary tree and hypertree, is introduced. We have evaluated the topological descriptors grounded on the distances for the ternary hypertree. The analytical expressions for Wiener, different types of Szeged, and Mostar indices are determined.

1. Introduction

A connected graph having order n and size $n-1$ is termed as a tree that contains no cycle. In computer science, trees are designed as data structures. Trees are helpful to store data information in a hierarchical manner and provide insertion and deletion of data. They are also useful in manipulating hierarchical data, making it easy to search information and aid in multistage decision making. One of the basic tree structures which have many applications in the field of computer science is the rooted tree [1, 2]. Rooted tree is a tree that has a root node from where the children arise. The root node is called the parent node [3, 4]. A binary tree is a rooted tree in which every vertex has at the most two children and each child of a vertex is assigned as its left child or right child [5]. A complete binary tree is a rooted tree in which every node has two children-a right child and a left child. Ternary tree which has at the most three children $3x-1, 3x, 3x+1$, where $x \in \mathbb{Z}$ is a root node, is a rooted tree. Ternary tree is introduced by Barning, a Dutch mathematician in Reference [6]. It is a tool for the ternary search tree which can be used in spell check and as a database when indexing several nonkey fields. In a complete ternary tree, every node has exactly three children.

Hypertree of dimension n is a basic skeleton of complete binary tree, i.e., the vertex x has exactly two children $2x$ and $2x+1$, where $x \in 2^{n-1}-1$, and the vertices on the same level are connected by a horizontal edge with a label difference of $2^{i-2}; 2 \le i \le n$. The hypertree is an interconnection network which has minimum average distance which results in an efficient multicomputer system [7]. It has an excellent combination of characteristics of the hypercube and the binary tree. Recursive hypertrees are modelled as biological networks such as dendrimers [8–10]. The branching of biological networks is not restricted to two branches. With this motivation, we introduce the concept of ternary hypertree. Ternary hypertrees can be modelled as biological networks for protein interactions and to analyze the spread of diseases.

The structure of the ternary hypertree is a combination of a complete ternary tree and hypertree. It is a spanning

subgraph of the complete ternary tree. We denote ternary hypertree with dimension n as THT(n).

The level of root node is 1. The root node gives rise to three children, which is at level 2. We label the root node as 1 and their children as 2, 3, 4. Likewise, if the node is labelled as x; then, the children are labelled as $3x-1, 3x, 3x+1$ where $x \in [3^{n-1} - 1/2]$. At each level i; $1 \le i \le n$ of the ternary hypertree of dimension n has 3^{i-1} nodes. For a ternary hypertree of dimension n, the network has n levels. There are horizontal edges in the level i, $2 \le i \le n$ connecting the nodes with a label difference of 3^{i-2} along the complete ternary tree structure. See Figure 1.

Ternary hypertree consists of $(3^n - 1/2)$ nodes and $(3^n - 3)$ edges. The vertex connectivity is 4 and edge connectivity is 3. Ternary hypertree of dimension n has a diameter of $2n-3$. Also, it is not a regular network. THT(n); $n \ge 3$ is nonplanar, i.e., it cannot be embedded in a plane and non-Hamiltonian where every vertex can be visited more than once.

Real-life problems can be converted to graphical representations using mathematical modelling, especially in the field of biology [11–14]. Networks helps in analysing various health problems by modelling the spread of diseases [15–17]. Topological indices are numeric invariants showing a correlation between the subatomic structure and its physical (as well as chemical) properties [18, 19]. Thus, it characterises the topology of a graph [20, 21]. Topological indices analyse the physical, chemical, and biological characteristics of a synthetic framework [22, 23]. Topological indices are essential in the field of chemistry and pharmacology, notably in nanomedicine. It helps in the study of the properties of networks. These descriptors are used in measuring irregularity, connectivity, centrality, and peripherality in networks [24]. Topological indices for various networks have been studied in recent years [25–28].

Computing the topological indices helps in anatomising the properties of the biological network. In the next section, we have discussed some terminologies and two types of topological descriptors (distance-based and degree-based descriptors) of the ternary hypertree are derived and are graphically represented. Section 3 concludes the paper with discussion on the possible applications of ternary hypertree.

2. Topological Indices

The graph Ω considered in the paper is a simple connected graph. $d(\mathfrak{x}, \mathfrak{y})$ is used to represent the distance between $\mathfrak{x}$ and $\mathfrak{y}$ and is the length of the shortest path connecting the vertices, $\mathfrak{x}$ and $\mathfrak{y}$. For $1 \le i \le n$, we represent $i = [n]$. The cardinality of collection of adjacent vertices of $\mathfrak{x}$ is termed as the degree of a vertex $\mathfrak{x}$, it is denoted by $d_{\mathfrak{x}}$ [29, 30]. Neighbourhood of a vertex, $\mathfrak{x}$ is represented by $N(\mathfrak{x})$ and is defined as follows:

$$N_{\mathfrak{x}}(\mathfrak{x}\mathfrak{y}|\Omega) = \{\tau \in V_\Omega : d(\mathfrak{x}, \tau) < d(\mathfrak{y}, \tau)\}, \tag{1}$$

and

$$M_{\mathfrak{x}}(\mathfrak{x}\mathfrak{y}|\Omega) = \{e \in E(\Omega) : d(\mathfrak{x}, e) < d(\mathfrak{y}, e)\}, \tag{2}$$

We denote the cardinality of $N_{\mathfrak{x}}(\mathfrak{x}\mathfrak{y}|\Omega)$ and $M_{\mathfrak{x}}(\mathfrak{x}\mathfrak{y}|\Omega)$ as $n_{\mathfrak{x}}(\mathfrak{x}\mathfrak{y}|\Omega)$ and $m_{\mathfrak{x}}(\mathfrak{x}\mathfrak{y}|\Omega)$, respectively.

Let $(\mathfrak{w}_v, \mathfrak{s}_v)$ be the vertex weight and vertex strength and let $(e_{\mathfrak{w}}, \mathfrak{s}_e)$ be the edge weight and edge strength. The notion of strength-weighted graph $\Omega_{sw} = (\Omega, V_{sw}, E_{sw})$, where $V_{\mathfrak{s}\mathfrak{w}} = (\mathfrak{w}_v, \mathfrak{s}_v), E_{\mathfrak{s}\mathfrak{w}} = (e_{\mathfrak{w}}, \mathfrak{s}_e)$, was introduced in Reference [31]. For strength-weighted graph $\Omega_{\mathfrak{s}\mathfrak{w}} = (\Omega, (\mathfrak{w}_v, \mathfrak{s}_v), \mathfrak{s}_e)$, the degree of any vertex $v \in V_{\Omega_{\mathfrak{s}\mathfrak{w}}}$ is $d_{\Omega_{\mathfrak{s}\mathfrak{w}}}(\mathfrak{x}) = 2\mathfrak{s}_v(\mathfrak{x}) + \sum_{p \in N_{\Omega_{\mathfrak{s}\mathfrak{w}}}(\mathfrak{x})} \mathfrak{s}_e(\mathfrak{x}p)$. For $\mathfrak{x}\mathfrak{y} \in E_{\Omega_{\mathfrak{s}\mathfrak{w}}}$, we define

$$\begin{aligned} n_{\mathfrak{x}}(e|\Omega_{\mathfrak{s}\mathfrak{w}}) &= \sum_{p \in n_{\mathfrak{x}}(e|\Omega_{\mathfrak{s}\mathfrak{w}})} \mathfrak{w}_v(p), \\ m_{\mathfrak{x}}(e|\Omega_{\mathfrak{s}\mathfrak{w}}) &= \sum_{p \in n_{\mathfrak{x}}(e|\Omega_{\mathfrak{s}\mathfrak{w}})} \mathfrak{s}_v(p) + \sum_{f \in m_{\mathfrak{x}}(e|\Omega_{\mathfrak{s}\mathfrak{w}})} \mathfrak{s}_e(f). \end{aligned} \tag{3}$$

We refer to References [32–34] for the distance-based topological indices. The formulas of these indices for strength-weighted graph $\Omega_{\mathfrak{s}\mathfrak{w}}$ are given in Table 1 and the degree-based formulas of topological indices of graph Ω are illustrated in Table 2.

In this paper, we consider $\mathfrak{w}_v = e_{\mathfrak{w}} = \mathfrak{s}_e = 1; \mathfrak{s}_v = 0$.

If the distance of any two vertices in $\mathscr{H}$, a subgraph of a graph of Ω, lies in the same subgraph, then the subgraph $\mathscr{H}$ is called convex. For Ω, Djoković-Winkler's relation Θ on $E(\Omega)$, References [41, 42] can be expressed as follows: if $d(\mathfrak{x}, \mathfrak{w}) + d(\mathfrak{y}, \mathfrak{z}) \ne d(\mathfrak{x}, \mathfrak{z}) + d(\mathfrak{y}, \mathfrak{w})$, then $\mathfrak{x}\mathfrak{y} \in E(\Omega)$ is Θ related with $\mathfrak{w}\mathfrak{z} \in E(\Omega)$. Θ is an equivalence relation in case of partial cubes. Θ partitioned $E(\Omega)$ into convex cuts. Θ^* (a transitive closure) is an equivalence relation. The edges partition into Θ^* classes and let $\{F_i; 1 \le i \le k\}$ is the Θ^* partition set of $E(\Omega)$. Using Θ^* relation, we can find the topological indices of any graph [31, 40, 43–45]. For any $i \in [k]$, the quotient Ω/F_i graph in which vertex set belongs to the components of $\Omega - F_i$ and $\mathfrak{x}, \mathfrak{y} \in \Omega/F_i$ are adjacent in Ω/F_i if $\mathfrak{x}\mathfrak{y} \in E(\Omega)$, where $\mathfrak{x} \in C_1$, $\mathfrak{y} \in C_2$ and where C_1, C_2 are components. A partition $X = \{X_1, X_2, \ldots, X_r\}$ of $E(\Omega)$ is coarser than $Y = \{Y_1, Y_2, \ldots, Y_s\}$ if X_i is the union of one or more sets in Y. To study about the Wiener index, see References [46–48]. We have used Theorem 2.1 and the technique in Reference [48], reduction of original graph Ω into quotient graphs and further into reduced graphs, to compute the Wiener index of ternary hypertree. To compute other distance-based topological indices of ternary hypertree, we use Theorem 1.

Theorem 1 *References [49, 50]. "For a connected strength-weighted graph $G_{sw} = (G, (w_v, s_v), s_e)$, let $E = E_1, E_2, \ldots, E_k$ be a partition of $E(G)$ coarser than F. Let $X = W$, $Sz_v, Sz_e, Sz_{ev}, Mo, Mo_e, Mo_t, PI$. Then,*

$$X(G_{sw}) = \sum_{i=1}^{k} X\left(\frac{G}{E_i}, \left(w_v^i, s_v^i\right), s_e^i\right), \tag{4}$$

where

$w_v^i : V(G/E_i) \longrightarrow \mathbb{R}^+$ *is defined by* $w_v^i(C) = \sum_{x \in C} w_v(x), \quad \forall C \in G/E_i,$

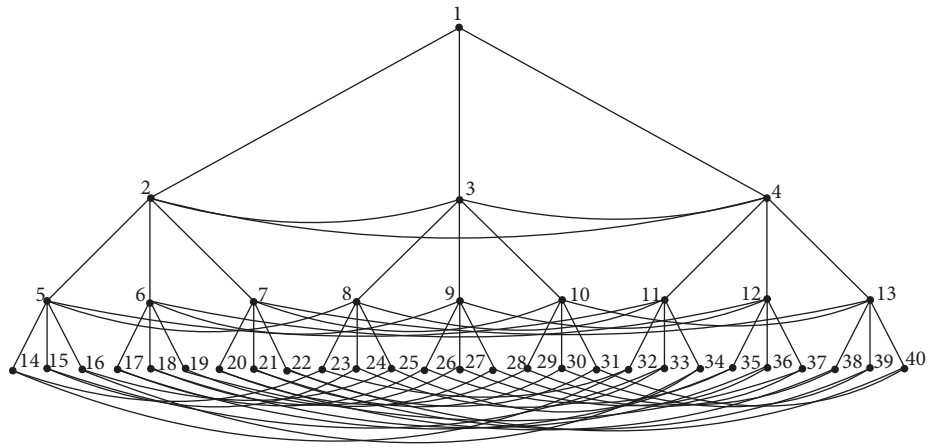

Figure 1: Ternary hypertree of dimension 4.

Table 1: Distance-based topological indices.

Topological indices	Mathematical expressions
Wiener [31]	$W(\Omega) = \sum_{\{\mathfrak{x},\mathfrak{y}\}\subseteq V_\Omega} \mathfrak{w}_v(\mathfrak{x})\mathfrak{w}_v(\mathfrak{y}) d(\mathfrak{x},\mathfrak{y})$
Szeged [31]	$Sz(\Omega) = \sum_{\mathfrak{x}\mathfrak{y}\in E(\Omega)} \mathfrak{s}_e(e) n_{\mathfrak{x}}(e\|\Omega_{\mathfrak{s}\mathfrak{w}}) n_{\mathfrak{y}}(e\|\Omega_{\mathfrak{s}\mathfrak{w}})$
Edge Szeged [31]	$Sz(\Omega) = \sum_{\mathfrak{x}\mathfrak{y}\in E(\Omega)} \mathfrak{s}_e(e) m_{\mathfrak{x}}(e\|\Omega_{\mathfrak{s}\mathfrak{w}}) m_{\mathfrak{y}}(e\|\Omega_{\mathfrak{s}\mathfrak{w}})$
Edge vertex Szeged [31]	$Sz_{ev}(\Omega) = \frac{1}{2}\sum_{\mathfrak{x}\mathfrak{y}\in E(\Omega)} \mathfrak{s}_e(e)[n_{\mathfrak{x}}(e\|\Omega_{\mathfrak{s}\mathfrak{w}}) m_{\mathfrak{y}}(e\|\Omega_{\mathfrak{s}\mathfrak{w}}) + n_{\mathfrak{x}}(e\|\Omega_{\mathfrak{s}\mathfrak{w}}) m_{\mathfrak{y}}(e\|\Omega_{\mathfrak{s}\mathfrak{w}})]$
Mostar [40]	$Mo(\Omega) = \sum_{\mathfrak{x}\mathfrak{y}\in E(\Omega)} \mathfrak{s}_e(e) \lvert n_{\mathfrak{x}}(e\|\Omega_{\mathfrak{s}\mathfrak{w}}) - n_{\mathfrak{y}}(e\|\Omega_{\mathfrak{s}\mathfrak{w}})\rvert$
Edge Mostar [40]	$Mo(\Omega) = \sum_{\mathfrak{x}\mathfrak{y}\in E(\Omega)} \mathfrak{s}_e(e) \lvert m_{\mathfrak{x}}(e\|\Omega_{\mathfrak{s}\mathfrak{w}}) - m_{\mathfrak{y}}(e\|\Omega_{\mathfrak{s}\mathfrak{w}})\rvert$
Total Mostar [40]	$Mo(\Omega) = \sum_{\mathfrak{x}\mathfrak{y}\in E(\Omega)} \mathfrak{s}_e(e) \lvert \mathfrak{t}_{\mathfrak{x}}(e\|\Omega_{\mathfrak{s}\mathfrak{w}}) - \mathfrak{t}_{\mathfrak{y}}(e\|\Omega_{\mathfrak{s}\mathfrak{w}})\rvert$
Padmakar Ivan [31]	$PI(\Omega) = \sum_{\mathfrak{x}\mathfrak{y}\in E(\Omega)} \mathfrak{s}_e(e)[n_{\mathfrak{x}}(e\|\Omega_{\mathfrak{s}\mathfrak{w}}) + n_{\mathfrak{y}}(e\|\Omega_{\mathfrak{s}\mathfrak{w}})]$

Table 2: Degree-based topological indices.

Topological indices	Mathematical expressions
First Zagreb [35]	$\sum_{\mathfrak{x}\mathfrak{y}\in E(\Omega)} (d_{\mathfrak{x}} + d_{\mathfrak{y}})$
Second Zagreb [35]	$\sum_{\mathfrak{x}\mathfrak{y}\in E(\Omega)} d_{\mathfrak{x}} d_{\mathfrak{y}}$
Randic [36]	$\sum_{\mathfrak{x}\mathfrak{y}\in E(\Omega)} 1/\sqrt{d_{\mathfrak{x}} d_{\mathfrak{y}}}$
Atom bond connectivity [37]	$\sum_{\mathfrak{x}\mathfrak{y}\in E(\Omega)} \sqrt{d_{\mathfrak{x}} + d_{\mathfrak{y}} - 2/d_{\mathfrak{x}} d_{\mathfrak{y}}}$
Sum connectivity [38]	$\sum_{\mathfrak{x}\mathfrak{y}\in E(\Omega)} 1/\sqrt{d_{\mathfrak{x}} + d_{\mathfrak{y}}}$
Geometric arithmetic [39]	$\sum_{\mathfrak{x}\mathfrak{y}\in E(\Omega)} 2\sqrt{d_{\mathfrak{x}} d_{\mathfrak{y}}}/d_{\mathfrak{x}} + d_{\mathfrak{y}}$

s_v^i: $E(G/E_i) \longrightarrow \mathbb{R}^+$ *is defined by* $s_v^i(C) = \sum_{xy\in C} s_e(xy) + \sum_{x\in C} s_v(x)$, $\forall C \in G/E_i$,

s_e^i: $E(G/E_i) \longrightarrow \mathbb{R}^+$ *is defined as the number of edges in* E_i *such that one end in* C *and the other end in* D, *for any two connected components* C *and* D *of* (G/E_i).

Theorem 2. *If* $n \geq 2$, *then*

(1) $W(THT(n)) = 3^{2n}/4 + 5 \times 3^n(n-2)/4 - (3^{2n} - 3^{n+2})/8 + (9 - 3^n)/4 + (3^{2+n} - 3^{2n})/8 + (3^n - 3)/2 + 3(-1 + 3^{n-1})^2/4$

(2) $Sz(THT(n)) = (3^{3n-2} - 19 \times 3^{2n} + 30 \times 3^n n - 5 \times 3^n + 6 \times 3^{2n} n + 39/8)$

(3) $Sz_e(THT(n)) = 3^{3n}/18 - 11 \times 3^{2n} + 18 \times 3^n n + 9 \times 3^n + 3^{2n+1} n - 33/2$

(4) $Sz_{ev}(THT(n)) = 3^{3n}/36 - 41 \times 3^{2n}/8 + 33 \times 3^n n/4 + 7 \times 3^n/8 + 3^{2n+1} n/2 + 15/2$

(5) $PI(THT(n)) = 5 \times 3^{2n}/12 - 3 \times 3^n + 21/4$

(6) $Mo(THT(n)) = 3^{2n}/4 - 3^{n+1} n + 11 \times 3^n/2 - 63/4$

(7) $Mo_e(THT(n)) = 3^{2n}/2 - 6 \times 3^n n + 12 \times 3^n - 81/2$

(8) $Mo_t(THT(n)) = 3 \times 3^{2n}/4 - 9 \times 3^n n + 35 \times 3^n/2 - 225/4$

Proof. For a ternary hypertree of dimension n, there are $(3^{n-1} - 1/2 + 1)\Theta^*$ classes. The Θ classes are as follows:

(1) For $2 \leq i \leq n-1$, $j = [3^{-1+i}], k = [3]$, let S_i^j be the Θ^*- classes containing the edges $(3^{i-1} - 1/2 + \lceil j/3 \rceil + (k-1)3^{i-2}, 3^i - 1/2 + j + (k-1)3^{i-1})$.

(2) Let $S = S_1 \bigcup S_2$ be the Θ^*- classes, which consist of the horizontal edges and the edges connecting the first and second level. It comprises of $S_1 = \{(1,2), (1,4), ((3^{i-1} - 1/2) + j, (j + 3^{i-1} - 1/2) + 3^{-2+i}), ((3^{i-1}/2) + j, (j + 3^{i-1} - 1/2) + 2 \times 3^{-2+i}), ((j + 3^{i-1} - 1/2) + 3^{-2+i}, j + 3^{i-1} - 1/2 + 2 \times 3^{-2+i})$: $i = [n-1]$, $j = \{1,3\}\}$ and $S_2 = \{((3\ \ i - 1 - 1/2) + j, (3^{i-1} - 1/2) + j + 3^{i-2}), ((3^{i-1}/2) + j, (j + 3^{i-1} - 1/2) + 3^{i-2} \times 2), ((3\ \ i - 1 - 1/2) + j + 3\ \ i - 2, (j + 3^{i-1} - 1/2) + 3^{-2+i} \times 2)$: $i = [n-1]$, $j = 2\}$.

Let $F_i, i = [n-1]$ be the partition which is coarser than the Θ^* classes. Define $F_1 = S$ and $F_i, 2 \leq i \leq n-1$ be the edges joining the levels i and $i+1$, i.e., $F_i = \cup_j S_i^j$.

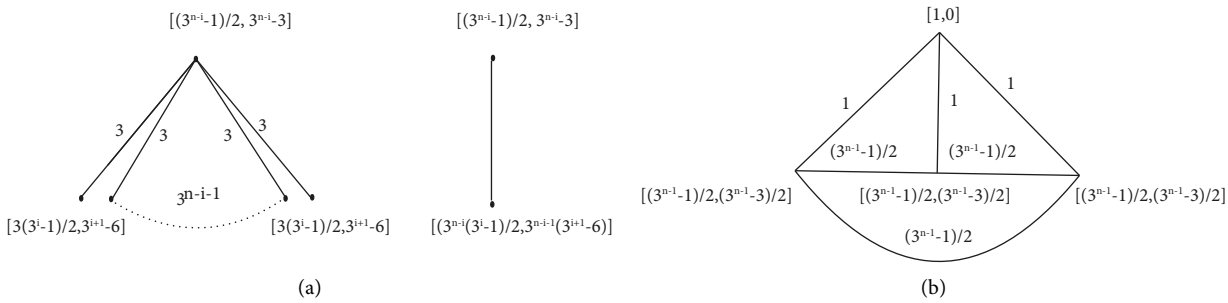

FIGURE 2: General case of quotient graph and reduced graph. (a) $THT(n)/F_i$, $1 \le i \le n-2$,. (b) $THT(n)/F_{n-1}$.

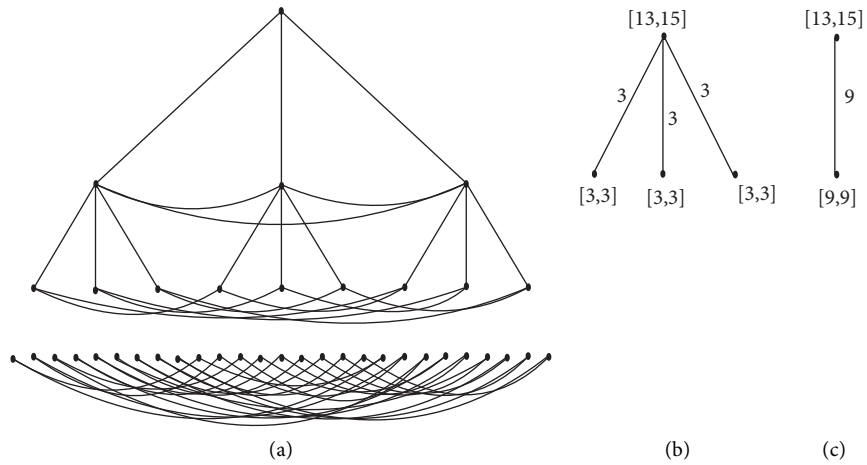

FIGURE 3: (a) $THT(4)/F_1$. (b) Quotient graph THT$(4)/F_1$. (c) Reduced graph.

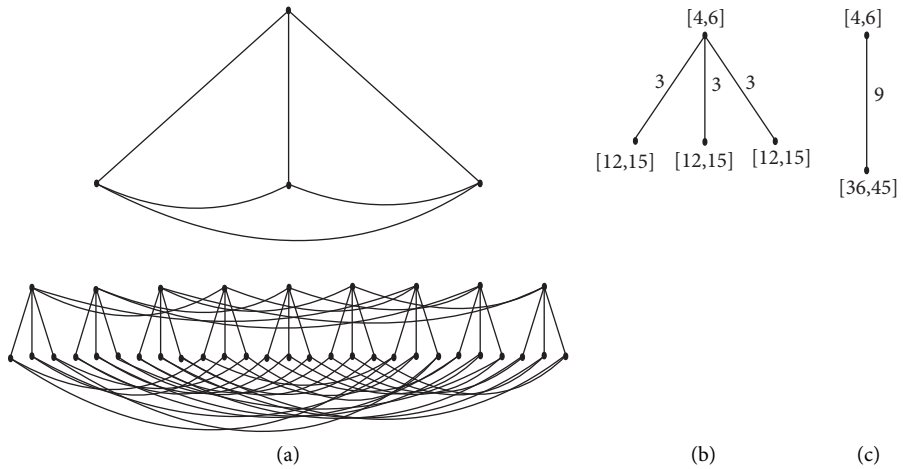

FIGURE 4: (a) $THT(4)/F_2$. (b) Quotient graph THT$(4)/F_2$. (c) Reduced graph.

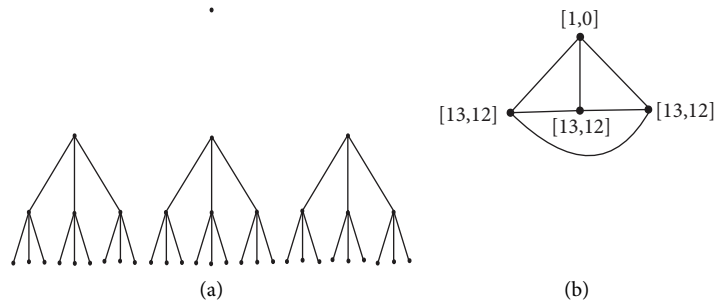

FIGURE 5: (a) $THT(4)/F_3$. (b) Quotient graph THT$(4)/F_3$.

In general, $THT(n)/F_i$ is isomorphic to $K_{1,3^{-(i+1)+n}}$, $i \in \{1, 2, \ldots, n-2\}$. In $K_{1,3^{-(i+1)+n}}$, $i \in \{1, 2, \ldots, n-2\}$, one vertex is of weight $(3^{n-i} - 1/2)$ and edge weight $3^{n-i} - 3$ and other 3^{n-i-1} vertices with vertex and edge weight $(3(3^i - 1)/2)$ and $3^{i+1} - 6$, respectively. We can see that $\mathrm{GHT}(n)/F_{n-1}$ and K_4 are isomorphic, with vertex and edge weights 1 and 0 for one vertex and $(3^{n-1} - 1/2)$ and $(3^{n-1} - 1/2)$ for the remaining adjacent vertices as shown in Figure 2. Figures 3, 4, and 5 give an example for the quotient graph.

Now, $W(\mathrm{THT}(n))$ is calculated as follows:

$$\begin{aligned}
\sum_{i=1}^{-2+n} W\left(\frac{\mathrm{THT}(n)}{F_i}\right) &= \frac{3^{2n}}{4} + \frac{3^n \times 5(-2+n)}{4} + \frac{\left(3^{2n} - 3^{n+2}\right)}{8} + \frac{\left(9 - 3^n\right)}{4} + \frac{3^{2n}\left(3^{2-n} - 1\right)}{8}, \\
W\left(\frac{\mathrm{THT}(n)}{F_{n-1}}\right) &= \frac{\left(3^n - 3\right)}{2} + \frac{3\left(-1 + 3^{n-1}\right)^2}{4}, \\
W(\mathrm{THT}(n)) &= \frac{3^{2n}}{4} + \frac{3^n \times 5(-2+n)}{4} - \frac{\left(3^{2n} - 3^{n+2}\right)}{8} + \frac{3^n\left(3^{2-n} - 1\right)}{4} + \frac{3^{2n}\left(3^{2-n} - 1\right)}{8} + \frac{3\left(3^{n-1} - 1\right)}{2} + \frac{3\left(3^{n-1} - 1\right)^2}{4},
\end{aligned} \tag{5}$$

$Sz(\mathrm{THT}(n))$ is calculated as follows:

$$\begin{aligned}
Sz\left(\frac{\mathrm{THT}(n)}{F_i}\right) &= \frac{\left(3^{n+1} - 3^{(n-i+1)}\left(2 + 3^n - 3^i \times 3\right)\right)}{4}, \\
\sum_{i=1}^{n-2} Sz\left(\frac{\mathrm{THT}(n)}{F_i}\right) &= \frac{15 \times 3^n n}{4} - \frac{3^{2n+2}}{4} - \frac{3^{n+1}}{2} + \frac{3^{2n+1} n}{4} + \frac{27}{4}, \\
Sz\left(\frac{\mathrm{THT}(n)}{F_{n-1}}\right) &= \left(\frac{\left(3^{n-1} - 1\right)^2}{4} + 1\right)\left(\frac{3^n - 3}{2}\right), \\
Sz(\mathrm{THT}(n)) &= \frac{3^{3n-2} - 19 \times 3^{2n} + 30 \times 3^n n - 5 \times 3^n + 6 \times 3^{2n} n + 39}{8}.
\end{aligned} \tag{6}$$

The edge-Szeged index of ternary hypertree of dimension n is as follows:

$$\begin{aligned}
Sz_e\left(\frac{\mathrm{THT}(n)}{F_i}\right) &= 3^{n-i}\left(3^{i+1} - 6\right)\left(3^n - 3^{i+1}\right), \\
\sum_{i=1}^{n-2} Sz_e\left(\frac{\mathrm{THT}(n)}{F_i}\right) &= 3^n\left(18n + 3^{n+1} n - \frac{21 \times 3^n}{2} + \frac{9}{2}\right), \\
Sz_e\left(\frac{\mathrm{THT}(n)}{F_{n-1}}\right) &= -15 + 3^{n+1} + \frac{\left(3^n - 3\right)}{2} \times \left(3^{n-1} - 1\right)^2, \\
Sz_e(\mathrm{THT}(n)) &= \frac{3^{3n}}{18} - 11 \times 3^{2n} + 18 \times 3^n n + 9 \times 3^n + 3^{2n+1} n - \frac{33}{2}.
\end{aligned} \tag{7}$$

The edge-vertex Szeged index is as follows:

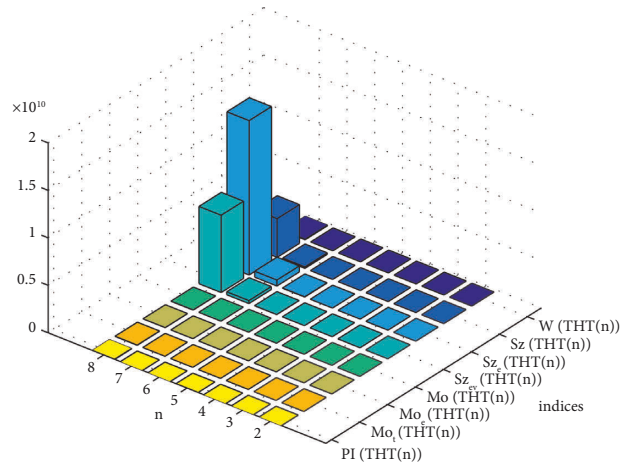

Figure 6: Graphical comparison of numerical values of distance-based indices of $THT(n)$.

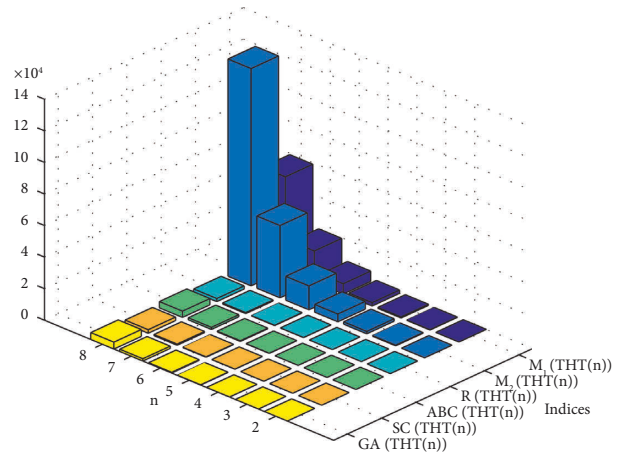

Figure 7: Graphical representation of numerical values of degree-based indices.

Table 3: Partition of edges of ternary hypertree of dimension n grounded on the degree vertices.

$(d_{\mathfrak{x}}, d_{\mathfrak{y}}); \mathfrak{x}\mathfrak{y} \in E(\Omega)$	No: Of edges
(3, 3)	3^{n-1}
(6, 3)	$3^{n-1}+3$
(6, 6)	$3^{n-1}-6$

$$
\begin{aligned}
Sz_{ev}\left(\frac{\mathrm{THT}(n)}{F_i}\right) &= 3^{n-i}\left(\frac{33\times 3^i - 18\times 3^{2i}}{4} - \frac{9\times 3^n}{4} + \frac{3\times 3^i \times 3^n}{2} - 3\right),\\
\sum_{i=1}^{n-2} Sz_{ev}\left(\frac{\mathrm{THT}(n)}{F_i}\right) &= \frac{66\times 3^n n - 39\times 3^{2n} - 9\times 3^n + 12\times 3^{2n} n + 108}{8},\\
Sz_{ev}\left(\frac{\mathrm{THT}(n)}{F_{n-1}}\right) &= \frac{15\times 3^{n-1} - 21 + ((3\times(3^n/3)) - 3)\left(3^{n-1}-1\right)^2}{4},\\
Sz_{ev}(\mathrm{THT}(n)) &= \frac{3^{3n}}{36} - \frac{41\times 3^{2n}}{8} + \frac{33\times 3^n n}{4} + \frac{7\times 3^n}{8} + \frac{3^{2n+1} n}{2} + \frac{15}{2}.
\end{aligned}
\tag{8}
$$

The Padmakar Ivan index is as follows:

$$
\begin{aligned}
PI\left(\frac{\mathrm{THT}(n)}{F_i}\right) &= \frac{3^{n-i}\left(3^n-1\right)}{2},\\
\sum_{i=1}^{n-2} PI\left(\frac{\mathrm{THT}(n)}{F_i}\right) &= \frac{\left(3^n-1\right)\left(3^n-9\right)}{4},\\
PI\left(\frac{\mathrm{THT}(n)}{F_{n-1}}\right) &= \frac{3^{2n} - 3^{n+1} + 18}{6},\\
PI(\mathrm{THT}(n)) &= \frac{5\times 3^{2n}}{12} - 3\times 3^n + \frac{21}{4}.
\end{aligned}
\tag{9}
$$

The Mostar index of ternary hypertree is as follows:

$$
\begin{aligned}
Mo\left(\frac{\mathrm{THT}(n)}{F_i}\right) &= \frac{3^{n-i}-1}{2} + \frac{\left(3^i-1\right)}{2} \times\left(3^{n-i}-3\right) - \frac{\left(3^i-1\right)}{2}\times 3\Bigg)\times 3^{n-i},\\
\sum_{i=1}^{n-2} Mo\left(\frac{\mathrm{THT}(n)}{F_i}\right) &= \frac{3^{2n}}{4} - 3^{n+1} n + 5\times 3^n - \frac{45}{4},\\
Mo\left(\frac{\mathrm{THT}(n)}{F_{n-1}}\right) &= \frac{3^n-9}{2},\\
Mo(\mathrm{THT}(n)) &= \frac{3^{2n}}{4} - 3^{n+1} n + \frac{11\times 3^n}{2} - \frac{63}{4},\\
Mo_e\left(\frac{\mathrm{THT}(n)}{F_i}\right) &= 3^{n-i}\left(3^n - 6\times 3^i + 6\right),\\
\sum_{i=1}^{n-2} Mo_e\left(\frac{\mathrm{THT}(n)}{F_i}\right) &= \frac{3^{2n}}{2} - 6\times 3^n n + \frac{21\times 3^n}{2} - 27,\\
Mo_e\left(\frac{\mathrm{THT}(n)}{F_{n-1}}\right) &= \frac{3^{n+1}-27}{2},\\
Mo_e(\mathrm{THT}(n)) &= \frac{3^{2n}}{2} - 6\times 3^n n + 12\times 3^n - \frac{81}{2}.
\end{aligned}
\tag{10}
$$

$$
\begin{aligned}
Mo_t\left(\frac{\mathrm{THT}(n)}{F_i}\right) &= 3^{n-i}\left(\frac{3^{n+1}}{2} - 9\times 3^i + \frac{17}{2}\right),\\
\sum_{i=1}^{n-2} Mo_t\left(\frac{\mathrm{THT}(n)}{F_i}\right) &= \frac{3\times 3^{2n}}{4} - 9\times 3^n n + \frac{31\times 3^n}{2} - \frac{153}{4},\\
Mo_t\left(\frac{\mathrm{THT}(n)}{F_{n-1}}\right) &= 6\times 3^{n-1} - 18,\\
Mo_t(\mathrm{THT}(n)) &= \frac{3\times 3^{2n}}{4} - 9\times 3^n n + \frac{35\times 3^n}{2} - \frac{225}{4}.
\end{aligned}
\tag{11}
$$

The graphical comparison of numerical values of distance-based indices of THT(n) is given in Figure 6. □

Theorem 3. *For* $n \geq 2$,

(1) $M_1(THT(n)) = 3^{n+2} - 45$

(2) $M_2(THT(n)) = 7 \times 3^{n+1} - 162$

(3) $R(THT(n)) = 0.2357(3^{n-1} + 3) + 2 \times 3^{n-2} - 2$

(4) $ABC(THT(n)) = 0.6236(3^{n-1} + 3) + 0.6667 \times 3^{n-1} + 0.5270 \times (3^{n-1} - 6)$

(5) $SC(THT(n)) = 1 + 3^{n-2} + 0.4082 \times 3^{n-1} + 0.2887(3^{n-1} - 6)$

(6) $GA(THT(n)) = 2.828 + 2 \times 3^{n-1} - 6$

Proof. Ternary hypertree has $(3^n - 3)$ edges. We divide the edges according to its degrees on either vertex, which is given in Table 1. We denote F_{mn} as the set of edges $\mathfrak{xy}$ such that $d_{\mathfrak{x}} = m$ and $d_{\mathfrak{y}} = n$.

$M_1(\mathrm{THT}(n))$ is calculated as follows:

$$M_1(\mathrm{THT}(n)) = \sum_{\mathfrak{xy} \in F_{33}} (3+3) + \sum_{\mathfrak{xy} \in F_{63}} (6+3) + \sum_{\mathfrak{xy} \in F_{66}} (6+6) = 3^{n-1} \times 6 + \left(3^{n-1} + 3\right) \times 9 + \left(3^{n-1} - 6\right) \times 12 = 9 \times 3^n - 45, \tag{12}$$

$M_2(\mathrm{THT}(n))$ is calculated as follows:

$$M_2(\mathrm{THT}(n)) = \sum_{\mathfrak{xy} \in F_{33}} 3 \times 3 + \sum_{\mathfrak{xy} \in F_{63}} 6 \times 3 + \sum_{\mathfrak{xy} \in F_{66}} 6 \times 6 = 3^{n+1} + \left(3^{n-1} + 3\right) \times 18 + \left(2 \times 3^{n+1} - 6\right) \times 36 = 21 \times 3^n - 162. \tag{13}$$

Randic index of THT(n) is calculated as follows:

$$R(\mathrm{THT}(n)) = \sum_{\mathfrak{xy} \in F_{33}} \frac{1}{3} + \sum_{\mathfrak{xy} \in F_{63}} \frac{1}{\sqrt{18}} + \sum_{\mathfrak{xy} \in F_{66}} \frac{1}{6} = \frac{3^n}{9} \times \frac{1}{3} + \left(3^{n-1} + 3\right) \times \frac{1}{\sqrt{18}} + \left(3^{n-1} - 6\right) \times \frac{1}{6} = 0.2357 \times \left(3^{n-1} + 3\right) + 2 \times 3^{n-2} - 2, \tag{14}$$

$\mathrm{ABC}(\mathrm{THT}(n))$ is calculated as follows:

$$\mathrm{ABC}(\mathrm{THT}(n)) = \sum_{\mathfrak{xy} \in F_{33}} \frac{1}{6} + \sum_{\mathfrak{xy} \in F_{63}} \frac{1}{9} + \sum_{\mathfrak{xy} \in F_{66}} \frac{1}{12} = \frac{3^{n-1} + 3}{9} + \frac{3^{n-1}}{6} + \frac{3^{n-1} - 6}{12} = 0.1111\left(3^{n-1} + 3\right) + 0.1667 \times 3^{n-1} + 0.0833\left(3^{n-1} - 6\right), \tag{15}$$

$SC(\mathrm{THT}(n))$ is calculated as follows:

$$SC(\mathrm{THT}(n)) = \sum_{\mathfrak{xy} \in F_{33}} \frac{1}{\sqrt{6}} + \sum_{\mathfrak{xy} \in F_{63}} \frac{1}{\sqrt{9}} + \sum_{\mathfrak{xy} \in F_{66}} \frac{1}{\sqrt{12}} = \frac{3^{n-1}}{\sqrt{6}} + \frac{3^{n-1} + 3}{\sqrt{9}} + \left(-6 + 3^{n-1}\right) \times \frac{1}{\sqrt{12}} = 1 + 3^{n-2} + 0.4082 \times 3^{n-1} + 0.2887\left(3^{n-1} - 6\right). \tag{16}$$

The geometric arithmetic index of THT(n) is as follows:

$$GA(\mathrm{THT}(n)) = \sum_{\mathfrak{xy} \in F_{33}} \frac{\sqrt{9}}{6} + \sum_{\mathfrak{xy} \in F_{63}} \frac{\sqrt{18}}{9} + \sum_{\mathfrak{xy} \in F_{66}} \frac{\sqrt{36}}{12} = 3^{n-1} \times \frac{\sqrt{9}}{6} + \left(3^{n-1} + 3\right) \times \frac{\sqrt{18}}{9} + \left(3^{n-1} - 6\right) \times \frac{\sqrt{36}}{12} = 2.828\left(1 + 3^{n-2}\right) + 2 \times 3^{n-1} - 6. \tag{17}$$

The graphical comparison of numerical comparison of degree-based indices is given in Figure 7. □

3. Conclusion

Hypertree has many chemical applications such as in recursive molecular networks, for example, dendrimers [51]. Also, the topological indices for hypertree are used in the prognosis of physical (as well as chemical) properties of the complex network of molecular and material systems when there are substantial atoms [10, 52–54]. In this article, we have introduced a ternary hypertree, an interconnection network, and evaluated some distance-based and degree-based topological indices of the ternary hypertree. The topological indices of the ternary hypertree may help in determining the chemical properties of complex molecular networks. It can be used to obtain irregularity measures, connectivity measures, centrality measures, and peripherality measures of the ternary hypertree. The degree-based topological indices can help in the study of bioactivity of the ternary hypertree. In future, we can model networks by considering the spread of different viruses and can study their properties. We can also determine the entropy of ternary hypertree in order to analyse data complexity and transmission of information. Also, eccentricity-based topological indices, which help in analysing the toxicological properties, and various topological indices based on different constraints can also be computed. [55].

Data Availability

The data used to support the study are cited within the text as references.

Conflicts of Interest

The authors declare that they have no conflicts of interest.

Authors' Contributions

All authors contributed equally to this work.

Acknowledgments

This research work was supported by 1 Anhui Teaching Demonstration Course: Data Structure (NO. 2020SJJXSFK1291). 2 Quality Engineering in Anhui Province: Exploration of Data Structure Curriculum Reform Towards Engineering Education Certification under the Background of New Engineering (NO. 2020jyxm0793). 3 Research Team of Anhui Xinhua University: Machine Learning and Image Processing Research Team (NO. kytd201902).

References

[1] X. Zhang, X. Wu, S. Akhter, M. K. Jamil, J. B. Liu, and M. R. Farahani, "Edge-version atom-bond connectivity and geometric arithmetic indices of generalized bridge molecular graphs," *Symmetry*, vol. 10, no. 12, pp. 751–786, 2018.

[2] X. Zhang, H. M. Awais, M. Javaid, and M. K. Siddiqui, "Multiplicative Zagreb indices of molecular graphs," *Journal of Chemistry*, vol. 2019, pp. 1–19, 2019.

[3] X. Zhang, A. Rauf, M. Ishtiaq, M. K. Siddiqui, and M. H. Muhammad, "On degree based topological properties of two carbon nanotubes," *Polycyclic Aromatic Compounds*, vol. 42, no. 3, pp. 866–884, 2020.

[4] X. Zhang, H. Jiang, J. B. Liu, and Z. Shao, "The cartesian product and join graphs on edge-version atom-bond connectivity and geometric arithmetic indices," *Molecules*, vol. 23, no. 7, pp. 1731–1817, 2018.

[5] D. B. West, *Introduction to graph theory*, Vol. 2, Prenticehall Upper, , Saddle River, USA, 2001.

[6] F. J. M. Barning, "On Pythagorean and quasi-Pythagorean triangles and a generation process with the help of unimodular matrices," *Math. Centrum Amsterdam Afd. Zuivere Wisk. ZW-001*, 1963.

[7] J. R. Goodman and C. H. Sequin, "Hypertree: a multiprocessor interconnection topology," *IEEE Transactions on Computers*, vol. C-30, no. 12, pp. 923–933, 1981.

[8] M. Imran, M. K. Siddiqui, A. Q. Baig, and H. Shaker, "Molecular topological description of bacterial hypertrees," *Journal of Intelligent and Fuzzy Systems*, vol. 38, no. 4, pp. 5095–5105, 2020.

[9] W. Gao, H. Wu, M. K. Siddiqui, and A. Q. Baig, "Study of biological networks using graph theory," *Saudi Journal of Biological Sciences*, vol. 25, no. 6, pp. 1212–1219, 2018.

[10] R. S. Rajan, K. J. Kumar, A. A. Shantrinal, T. M. Rajalaxmi, I. Rajasingh, and K. Balasubramanian, "Biochemical and phylogenetic networks-I: hypertrees and corona products," *Journal of Mathematical Chemistry*, vol. 59, no. 3, pp. 676–698, 2021.

[11] P. Barton, P. Jobanputra, J. Wilson, S. Bryan, and A. Burls, "The use of modelling to evaluate new drugs for patients with a chronic condition: the case of antibodies against tumour necrosis factor in rheumatoid arthritis," *Health Technology Assessment*, vol. 8, no. 11, 1 page, 2004.

[12] P. Harjule, V. Tiwari, and A. Kumar, "Mathematical models to predict COVID-19 outbreak: an interim review," *Journal of Interdisciplinary Mathematics*, vol. 24, no. 2, pp. 259–284, 2021.

[13] B. Ivorra and A. M. Ramos, "Application of the be-codis mathematical model to forecast the international spread of the 2019–20 wuhan coronavirus outbreak," *ResearchGate Preprint*, vol. 9, pp. 1–13, 2020.

[14] G. A. Pavlopoulos, P. I. Kontou, A. Pavlopoulou, C. Bouyioukos, E. Markou, and P. G. Bagos, "Bipartite graphs in systems biology and medicine: a survey of methods and applications," *GigaScience*, vol. 7, no. 4, pp. 1–31, 2018.

[15] S. Kanwal, M. K. Siddiqui, E. Bonyah, K. Sarwar, T. S. Shaikh, and N. Ahmed, "Analysis of the epidemic biological model of tuberculosis (TB) via numerical schemes," *Complexity*, vol. 2022, pp. 1–13, Article ID 5147951, 2022.

[16] O. Mason and M. Verwoerd, "Graph theory and networks in biology," *IET Systems Biology*, vol. 1, no. 2, pp. 89–119, 2007.

[17] G. A. Pavlopoulos, M. Secrier, C. N. Moschopoulos et al., "Using graph theory to analyze biological networks," *BioData Mining*, vol. 4, no. 1, pp. 10–27, 2011.

[18] X. Zhang, M. Naeem, A. Q. Baig, and M. A. Zahid, "Study of hardness of superhard crystals by topological indices," *Journal of Chemistry*, vol. 2021, Article ID 9604106, 10 pages, 2021.

[19] X. Zhang, M. K. Siddiqui, S. Javed, L. Sherin, F. Kausar, and M. H. Muhammad, "Physical analysis of heat for formation and entropy of Ceria Oxide using topological indices," *Combinatorial Chemistry & High Throughput Screening*, vol. 25, no. 3, pp. 441–450, 2022.

[20] M. Javaid, F. Farid, J. B. Liu, and A. M. Alanazi, "Exact formulae for degree distance indices of sum graphs," *Journal of Mathematics*, vol. 2022, Article ID 6193727, 16 pages, 2022.

[21] I. Rajasingh, P. Manuel, N. Parthiban, D. Azubha Jemilet, and R. Sundara Rajan, "Transmission in butterfly networks," *The Computer Journal*, vol. 59, no. 8, pp. 1174–1179, 2016.

[22] A. Hussain, M. Numan, N. Naz, S. I. Butt, A. Aslam, and A. Fahad, "On topological indices for new classes of benes network," *Journal of Mathematics*, vol. 2021, Article ID 6690053, 7 pages, 2021.

[23] M. Imran, S. Hayat, and M. Y. H. Mailk, "On topological indices of certain interconnection networks," *Applied Mathematics and Computation*, vol. 244, pp. 936–951, 2014.

[24] N. Tratnik, *Computing the Mostar index in Networks with Applications to Molecular Graphs*, arXiv preprint arXiv: 1904.04131, 2019.

[25] S. Hayat and M. Imran, "Computation of topological indices of certain networks," *Applied Mathematics and Computation*, vol. 240, pp. 213–228, 2014.

[26] G. Ma, M. Ibrahim, G. Abbas, M. K. Siddiqui, and S. A. Fufa, "On degree-based topological indices of thermodynamic cuboctahedral Bi-metallic structure," *Journal of Mathematics*, vol. 2022, Article ID 6484704, 10 pages, 2022.

[27] R. Huang, M. H. Muhammad, M. K. Siddiqui, S. Khalid, S. Manzoor, and E. Bashier, "Analysis of topological aspects for metal-insulator transition superlattice network," *Complexity*, vol. 2022, Article ID 8344699, 11 pages, 2022.

[28] A. Sattar, M. Javaid, and M. N. Alam, "On the studies of dendrimers via connection-based molecular descriptors," *Mathematical Problems in Engineering*, vol. 2022, pp. 1–13, Article ID 1053484, 2022.

[29] I. Gutman and A. R. Ashrafi, "The edge version of the Szeged index," *Croatica Chemica Acta*, vol. 81, no. 2, pp. 263–266, 2008.

[30] I. Gutman, "A formula for the Wiener number of trees and its extension to graphs containing cycles," *Graph Theory Notes NY*, vol. 27, no. 9, pp. 9–15, 1994.

[31] M. Arockiaraj, J. Clement, and K. Balasubramanian, "Topological indices and their applications to circumcised donut

benzenoid systems, kekulenes and drugs," *Polycyclic Aromatic Compounds*, vol. 40, no. 2, pp. 280–303, 2020.

[32] P. V. Khadikar, S. Karmarkar, and V. K. Agrawal, "A novel PI index and its applications to QSPR/QSAR studies," *Journal of Chemical Information and Computer Sciences*, vol. 41, no. 4, pp. 934–949, 2001.

[33] A. Mahmiani, O. Khormali, A. Iranmanesh, and M. Yousefidaz, "The new version of Szeged index," *Optoelectronics and Advanced Materials-Rapid Communications*, vol. 4, pp. 2182–2184, 2010.

[34] H. Wiener, "Structural determination of paraffin boiling points," *Journal of the American Chemical Society*, vol. 69, no. 1, pp. 17–20, 1947.

[35] I. Gutman and N. Trinajstić, "Graph theory and molecular orbitals. Total π-electron energy of alternant hydrocarbons," *Chemical Physics Letters*, vol. 17, no. 4, pp. 535–538, 1972.

[36] M. Randic, "Characterization of molecular branching," *Journal of the American Chemical Society*, vol. 97, no. 23, pp. 6609–6615, 1975.

[37] E. Estrada, L. Torres, L. Rodriguez, and I. Gutman, "An atom-bond connectivity index: modelling the enthalpy of formation of alkanes," *Indian journal of chemistry. Sect. A: Inorganic, physical, theoretical & analytical*, vol. 37, pp. 849–855, 1998.

[38] B. Zhou and N. Trinajstić, "On a novel connectivity index," *Journal of Mathematical Chemistry*, vol. 46, no. 4, pp. 1252–1270, 2009.

[39] D. Vukičević and B. Furtula, "Topological index based on the ratios of geometrical and arithmetical means of end-vertex degrees of edges," *Journal of Mathematical Chemistry*, vol. 46, no. 4, pp. 1369–1376, 2009.

[40] M. Arockiaraj, J. Clement, and N. Tratnik, "Mostar indices of carbon nanostructures and circumscribed donut benzenoid systems," *International Journal of Quantum Chemistry*, vol. 119, no. 24, pp. 1–15, 2019.

[41] D. Z. Djoković, "Distance-preserving subgraphs of hypercubes," *Journal of Combinatorial Theory - Series B*, vol. 14, no. 3, pp. 263–267, 1973.

[42] P. M. Winkler, "Isometric embedding in products of complete graphs," *Discrete Applied Mathematics*, vol. 7, no. 2, pp. 221–225, 1984.

[43] S. Mushtaq, M. Arockiaraj, S. Klavžar, J. C. Fiona, and K. Balasubramanian, "Comment on Mostar indices of SiO_2 nanostructures and melem chain nanostructures," *International Journal of Quantum Chemistry*, vol. 122, no. 11, Article ID e26894, 2022.

[44] D. A. Xavier, E. S. Varghese, and D. Mathew, "Glued hypertree: comparative analysis and distance-based topological descriptors," *Indian Journal of Science and Technology*, vol. 15, no. 15, pp. 658–667, 2022.

[45] D. A. Xavier, E. S. Varghese, A. Baby, D. Mathew, and M. K. Kaabar, "Distance based topological descriptors of zinc porphyrin dendrimer," *Journal of Molecular Structure*, vol. 1268, Article ID 133614, 2022.

[46] S. Klavžar and I. Gutman, "Wiener number of vertex-weighted graphs and a chemical application," *Discrete Applied Mathematics*, vol. 80, no. 1, pp. 73–81, 1997.

[47] S. Klavžar and M. J. Nadjafi-Arani, "Wiener index in weighted graphs via unification of$\Theta*$-classes," *European Journal of Combinatorics*, vol. 36, pp. 71–76, 2014.

[48] S. Klavžar, P. Manuel, M. J. Nadjafi-Arani, R. S. Rajan, C. Grigorious, and S. Stephen, "Average distance in interconnection networks via reduction theorems for vertex-weighted graphs," *The Computer Journal*, vol. 59, no. 12, pp. 1900–1910, 2016.

[49] M. Arockiaraj, S. Klavžar, J. Clement, S. Mushtaq, and K. Balasubramanian, "Edge distance-based topological indices of strength-weighted graphs and their application to coronoid systems, carbon nanocones and SiO2 nanostructures," *Molecular Informatics*, vol. 38, no. 11-12, 205 pages, Article ID 1900039, 2019.

[50] J. B. Liu, M. Arockiaraj, M. Arulperumjothi, and S. Prabhu, "Distance based and bond additive topological indices of certain repurposed antiviral drug compounds tested for treating COVID-19," *International Journal of Quantum Chemistry*, vol. 121, no. 10, pp. e26617–18, Article ID e26617, 2021.

[51] K. Balasubramanian, "Nested wreath groups and their applications to phylogeny in biology and Cayley trees in chemistry and physics," *Journal of Mathematical Chemistry*, vol. 55, no. 1, pp. 195–222, 2017.

[52] K. Balasubramanian, "Ten low-lying electronic states of Pd3," *The Journal of Chemical Physics*, vol. 91, no. 1, pp. 307–313, 1989.

[53] K. Balasubramanian and P. Y. Feng, "Potential energy surfaces for $Pt2 + H$ and $Pt + H$ interactions," *The Journal of Chemical Physics*, vol. 92, no. 1, pp. 541–550, 1990.

[54] W. C. Ermler, *Relativistic Effects in Chemistry Part A: Theory and Techniques by Krishnan Balasubramanian (Arizona State University)*, p. 145, Wiley-Interscience, New York, 1998.

[55] J. B. Liu, J. Zhao, H. He, and Z. Shao, "Valency-based topological descriptors and structural property of the generalized sierpiński networks," *Journal of Statistical Physics*, vol. 177, no. 6, pp. 1131–1147, 2019.

Hindawi
Complexity
Volume 2022, Article ID 4038598, 15 pages
https://doi.org/10.1155/2022/4038598

Research Article

Observer-Based Synchronization and Quasi-Synchronization for Multiple Neural Networks with Time-Varying Delays

Biwen Li, Donglun Wang, and Jingjing Huang

College of Mathematics and Statistics, Hubei Normal University, Huangshi 435002, China

Correspondence should be addressed to Biwen Li; lbw20200320@163.com

Received 28 March 2022; Revised 18 May 2022; Accepted 24 June 2022; Published 9 September 2022

Academic Editor: Miaomiao Wang

In this paper, we study the synchronization of a class of multiple neural networks (MNNs) with delay and directed disconnected switching topology based on state observer via impulsive coupling control. The coupling topology is connected sequentially, and the controller adjusts the state value through event-triggering strategies. Different from the related works on MNNs, its state in this paper is assumed to be unmeasurable, and the time delay is also unmeasurable. Therefore, the observer does not contain the time-delay term. The impulsive switching controller and observer controller adjust the system through the observed value. By constructing the corresponding augmented matrix, the system can finally achieve quasi-synchronization (synchronization). Through derivation, we give the sufficient conditions ensuring quasi-synchronization (synchronization) via the event-triggered impulse control mechanism. In addition, numerical simulation examples are given to test our results of the theorem.

1. Introduction

There has been rapid development of multi-agent systems (MASs). In practical application, the application of MAS mainly includes power engineering [1], bioengineering [2], robot formation control [3], vehicle formation control [4], and some other fields. Theoretically, the dynamic behavior of MAS, such as stability [5], robustness [6], synchronization [7], and so on, has become the basis of various theories and greatly promoted the development of MAS. So far, a number of achievements have been made in the study of MAS.

In addition, as a complex network, the topology of MAS plays an important role in the dynamic behavior. For example, in [8], second-order leaderless and leader-following consensus algorithms with communication and input delays in directed network topology are studied. In addition, this paper involves three different situations: leaderless consumption, consumption regulation, and consumption tracking. On the other hand, the network topology plays an important role in the asymptotical stability scheme. In the leader-following problem of multi-agent network, it is assumed that the network topology switches arbitrarily between limited topology sets and there is a time-varying delay in the coupling of agents [9]. Different from the general topology, the switching topology in this paper is of great significance to the sudden change or failure of the environment, so switching topology widely exists in MAS.

In recent years, MNNs have been widely used, especially in automatic control [10], signal processing [11], optimization [12], and so on. Such complex systems are extremely dependent on the synchronization and stability of MNNs. Therefore, synchronization problem is receiving more and more attention and has always been a very important research direction [13–16]. Especially, Chen et al. [16] considered synchronization for nonlinear neural complex networks by a switching topology. On the other hand, different from synchronous, quasi-synchronous is a special form of dynamical behavior, where all of the control systems in networks are almost synchronized with a given synchronization error, which could not tend to zero with time. Chen et al. [17] discussed the quasi-synchronization problem through a coupled memristor neural network with time-varying delay. The quasi-synchronization problem in fractional-order multi-layer networks with fractional mismatch is studied in [18].

With the development of industrial demand and information technology, some traditional control strategies have been replaced by other control schemes. The feasibility and advantages of event-triggered control (ETC) have been proposed for the first time since 1999. Different from traditional control scheme, ETC can ensure system performance while effectively reducing the execution of control tasks. In recent years, ETC has become a popular research subject [19–22]. Because we only need to adjust the state of the controller at the event-trigger instants via setting an appropriate event-trigger mechanism. Different from continuous control and ETC, controller status is updated only at the moment of event trigger, it is adjusted to meet the needs of the system. At present, existing work of ETC in the multiagent field (see [23, 24]). Especially, [25] the recurrent neural network triggered by finite-time event-triggered strategy is studied, and the stability of finite-time systems is proved by novel inequality methods such as, LyapunovCKrasovskii functional and Wirtinger single and double integral inequality. Compared with static trigger conditions, dynamic trigger conditions have more advantages. For example, a new fuzzy filter error system model under dynamic event-triggered control strategy is considered. In addition, there are different triggered thresholds for different fuzzy rules, which can save communication resources more effectively in [26].

In order to realize the synchronization of MNNs, we often add appropriate controllers to the system. According to Tang et al. [27], the leader following consistency problem for a class of nonlinear multiagent systems with mixed impulses and time-varying bounded delays is studied. The time-varying impulses in this paper is not only composed of synchronization impulses and desynchronization impulses but also placed in some nodes of the system. Based on Riemann Liouville derivative, Lyapunov functional method and comparison theorem, we can get the global synchronization problem of time-varying delay neural networks with impulsive fractional complex memristor [10]. The impulse controller is one of the most widely used controllers in recent years. Different from the traditional continuous control strategy, impulse control mechanism has the advantage of short action time, which makes it possible to use the impulse controller to occupy less communication resources for a system with a very large amount of information transmission (see [28, 29]). In order to reduce communication bandwidth and save communication costs, a new control strategy based on event-trigger impulse is given. For example, Yi et al. [30] proposed an impulsive control mechanism based on ETC. Except for above control strategy, the impulse coupling protocol is also studied. The coupling between neural networks only occurs at some discrete-time instants, that is, impulse instants. Consequently, the impulse coupling scheme is naturally proposed.

Observer-based output feedback control is one of the traditional hot topics. It can be divided into two categories according to whether the variables are measurable or not. For the former, a relaxed stability condition based on state observer is proposed [31], and for the latter, a scheme based on fuzzy controller for a class of nonlinear systems is presented [32]. More recently, it is usually presumed that MAS state is measurable. Due to the limitations of measurement methods, many states cannot be measured. On the other hand, system states are unavailable for the state feedback control or too expensive to measure. Thus, it is imperative to research the observer for the system state is not measurable.

In general, we design an observer to estimate the value of different MNNs and then use the information to establish an observer based on feedback controller. However, the measured value is usually collected in discrete time. Therefore, an impulse observer is promoted. It was first proposed by Raf and Allgower in [33]. The observer is updated in the form of impulsive; hence, the measured output is discrete. So, use the impulse observer to estimate the error. Apart from this, designing a suitable control scheme based on impulsive observer is still a challenging problem.

Motivated by the previous research, this paper studies synchronization problem of MNNs with observer via an ETC mechanism. The main contributions of this paper are as follows:

(1) An impulsive switching controller is designed via the event-triggered strategy of MNNs with disconnection switching topology. Considering the practical needs, the actual state may be unpredictable in reality. Thus, the system state in this paper is assumed to be unmeasurable.

(2) A particular observer is constructed. Considering the unknown time delay in practical application, the observer does not exhibit time delay. Through the observation value of synchronization error and the tracking error of synchronization error, an augmented system is formed. The synchronization (quasi-synchronization) of the augmented system is also of the MNN system.

(3) The MNNs with a switching topology is studied and the topology is disconnect. At the same time, impulse control, event-triggered strategies, and observers are used to study synchronization (quasisynchronization) issues. In the real system, the sufficient conditions of the synchronization (quasi-synchronization) are proved. We discuss this kind of question and give the relevant theorems. The Zeno behavior can be ruled out.

The remainder of this article is organized as follows. Section 2 describes problem formulation and some necessary preliminaries. In Section 3, a number of results are presented. In Section 4, a numerical simulation is presented to test the obtained theoretical analysis. Some conclusions are drawn in Section 5.

2. Preparation and Modeling

Notations. Throughout this study, sign( ) is the standard sign function. $\mathbb{Z}$ and $\mathbb{Z}_+$ represent a set of integer and positive integer. $\mathbb{R}^n$ represents n-dimensional Euclid space. $\|\cdot\|$

represents 1-norm. $\mathrm{sign}(x) = (\mathrm{sign}(x_1), \mathrm{sign}(x_2), \ldots, \mathrm{sign}(x_n))^T$, and thus $\|x\| = \mathrm{sign}(x)^T x$ where $x \in \mathbb{R}^n$, and I is an identity matrix. Let $\mathcal{G} = (\mathcal{F}, \mathcal{S})$ denote a graph. $\mathcal{F}$ is the set of nodes. $\mathcal{S} \subseteq \mathcal{F} \times \mathcal{F}$ is the set of edges. An arbitrary matrix $A = (a_{ij})_{N\times N} \in R^{N\times N}$ is given, corresponding to A, and thus from $\mathcal{G}(A) = (\mathcal{F}, \mathcal{S})$, the graph is indicated, where $(i, j) \in \mathcal{S}$ if and only if $a_{ij} > 0$.

Also, a subset $\mathcal{K} \subseteq \mathcal{F}$ and a graph $\mathcal{G} = (\mathcal{F}, \mathcal{S})$ are given. Define the neighborhood of $\partial(\mathcal{K}, \mathcal{G})\{k \in \mathcal{F}/\mathcal{K} | \exists i \in \mathcal{K}$, such that $(i, k) \in \mathcal{S}\}$. If $\mathcal{K}$ is a singleton set, $\partial(\mathcal{K}, \mathcal{G})$ represents the neighborhood of one single point.

When $(j, i) = (i, j)$, the graph $\mathcal{G}$ is undirected. $\mathcal{G} = (\mathcal{F}, \mathcal{S})$ has a directed path from node i to j if there is a sequence of edges in the form (i, i_1), $(i, i_2), \cdots, (i, i_k)$ and the $i_p \in N$, where $p = 1, 2, \ldots, k$, $\mathcal{G}$ is called connected if there exists a directed path between each pair of nodes. The node $\hat{r}$ is called a root of $\mathcal{G}$ if has a directed path from $\hat{r}$ to every other node $\mathcal{G}$ contains a directed spanning tree if there exists at least one root.

For the graphs $\mathcal{G}_1 = (\mathcal{F}, \mathcal{S}_1)$ and $\mathcal{G}_2 = (\mathcal{F}, \mathcal{S}_2)$, $\mathcal{G}_1 \cup \mathcal{G}_2 = (\mathcal{F}, \mathcal{S}_1 \cup \mathcal{S}_2)$ is the union of $\mathcal{G}_1, \mathcal{G}_2$. A sequence of graphs with common nodes $(\mathcal{G}_i)_{i=1}^m$ is jointly connected if $\cup_{i=1}^m \mathcal{G}_i$ contains a spanning tree. A sequence of graphs with common nodes $(\mathcal{G}_i)_{i=1}^m$ is sequentially connected if there exist $m+1$node sets $\mathcal{F}_0, \mathcal{F}_1, \ldots, \mathcal{F}_m$such that $\mathcal{F}_{k+1} \subseteq \partial(\mathcal{G}_{k+1}, \Omega_k)$ and $\Omega_k = \cup_{l=0}^k \mathcal{F}_l$, $\Omega_0 = \mathcal{F}_0$is a set of Singleton, $\Omega_m = \mathcal{F}$.

Then, by the following dynamics:

$$\frac{\mathrm{d}x_i}{\mathrm{d}t} = Ax_i(t) + Bx_i(t - \tau(t)) + u_i(t) + I(t), \tag{1}$$

where $t \geqslant t_0$, $i \in \mathcal{F} = \{1, 2, \ldots, N\}$, $x_i(t) = (x_{i1}(t), x_{i2}(t), \ldots, x_{in}(t))^T$, $A = (a_{ij})_{n\times n}$ and $B = (b_{ij})_{n\times n}$ are weight matrices; $\tau(t)$ is transmission delay and satisfies $\tau \geqslant \tau(t) \geqslant 0$; $u_i(t)$ is a controller; and $I(t) \in \mathbb{R}^n$ indicates external input.

In the actual situation, considering that the system state value cannot be measured, we give the observer of the corresponding ith node as follows:

$$\frac{\mathrm{d}\hat{x}_i(t)}{\mathrm{d}t} = A\hat{x}_i(t) + v_i(t) + I(t). \tag{2}$$

$\hat{x}_i(t) = (\hat{x}_{i1}(t), \hat{x}_{i2}(t), \ldots, \hat{x}_{in}(t))^T$ is the estimated value of the corresponding ith node. $v_i(t) \in \mathbb{R}^n$ is the controller of the observer. Under (2), we can see that the observer does not contain time-delay term. Considering the fact that the time delay is unknown in practical application, observer (2) does not contain time delay.

Let $S \subset \mathbb{Z}_+$ be a limited set of index and $\{\mathcal{G}_s : s \in S\}$ be a directed graph set. $\sigma(t)$: $[t_0, +\infty) \longrightarrow S$ represent function of switching in $\{\mathcal{G}_s : s \in S\}$, and $\{t_p = qh, q \in \mathbb{Z}_+\}$ (where $h > 0$) represent instants of switching impulsive time. Let $\mathcal{G}_{\sigma(t)}$ indicate the graph of directed at t, where $t \geqslant t_0$. Thus, obviously $t = t_q$ is the switch time unchanged for $t \in (t_q, t_{q+1})$. We use $(\varpi_{ij}^{\sigma(t)})_{N\times N}$ to express $\mathcal{G}_{\sigma(t)}$ of adjacent matrix, where $\varpi_{ij}^{\sigma(t)} = 1$ when the system sends information from node j to node i and $\varpi_{ij}^{\sigma(t)} = 0$ otherwise. In addition, we give $\varpi_{ii}^{\sigma(t)} = 0$, namely, there is no self-loop in $\mathcal{G}_{\sigma(t)}$ where $t \geqslant t_0$. In order to convenient calculation, we assume that $\varpi_i^{\sigma(t)} = \sum_{j=1}^N \varpi_{ij}^{\sigma(t)}$ and $\varpi = \sup_{t\geqslant t_0} \max_{i\in\mathcal{F}} \varpi_i^{\sigma(t)}$

Consider the following assumptions:

(A1) The set of discrete graphs $\{\mathcal{G}_{\sigma(t)} : t_{mT} \leqslant t < t_{(m+1)T}\}$ is sequentially connected, if there exists a positive integer $T \in \mathbb{Z}_+$, where $m \in \mathbb{Z}_+$.

(A2) The set of discrete graphs $\{\mathcal{G}_{\sigma(t)} : t_{mT_0} \leqslant t < t_{(m+1)T_0}\}$ is jointly connected, if there exists a positive integer $T_0 \in \mathbb{Z}_+$, where $m \in \mathbb{Z}_+$.

$\{t_q^i\}_{q=1}^{+\infty}$ denotes a sequence of triggering time. Hence, we will give the event-trigger protocol (ETP). In order to make the system achieve synchronization (quasi-synchronization), we design the impulsive switching controller with ETP and the controller of the corresponding observer. In order to make the system achieve synchronization (quasi-synchronization), we design the impulsive switching controller and the corresponding observer controller of the ith node as follows:

$$u_i(t) = \gamma \sum_{q=1}^{+\infty} \delta(t - t_k) \sum_{j=1}^N \varpi_{ij}^{\sigma(t)} \left(\hat{x}_j\left(t_q^i\right) - \hat{x}_i\left(t_q^i\right)\right), \tag{3}$$

$$v_i(t) = \eta \sum_{q=1}^{+\infty} \delta(t - t_k) \sum_{j=1}^N \varpi_{ij}^{\sigma(t)} \left(\hat{x}_j\left(t_q^i\right) - \hat{x}_i\left(t_q^i\right)\right), \tag{4}$$

where $\gamma > 0, \eta > 0$.

The state is not measurable.

Therefore, (3) and (4) are only related to the observed values. For$i \in \mathcal{V}$, the measurement error is defined as follows:

$$\Lambda_i(t) = \sum_{j=1}^N \varpi_{ij}^{\sigma(t)} \left(\hat{x}_j\left(t_q^i\right) - \hat{x}_i\left(t_q^i\right)\right) - \sum_{j=1}^N \varpi_{ij}^{\sigma(t)} \left(\hat{x}_j(t) - \hat{x}_i(t)\right). \tag{5}$$

Meanwhile, by Figure 1, we can get the block diagram for ETC and the ETP:

$$t_{q+1}^i = \inf\left\{t > t_q^i, \left\|\Lambda_i(t)\right\| > \beta e^{-\varsigma\left(t - t_0\right)} + \alpha\right\}, \tag{6}$$

where $\varsigma > 0$, $\alpha^2 + \beta^2 \neq 0$; moreover, $\alpha \geqslant 0$ and $\beta \geqslant 0$. They are both threshold parameters.

From (1)–(4), we have

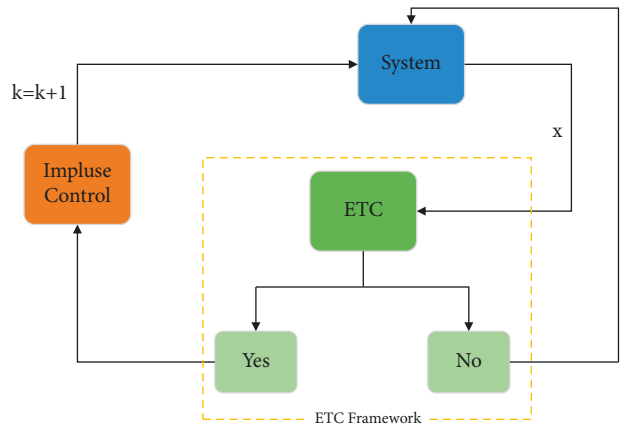

Figure 1: The block diagram for ETC.

$$\begin{cases} \dfrac{\mathrm{d}x_i}{\mathrm{d}t} = Ax_i(t) + Be_{ij}(t-\tau(t)) + I, & t \neq t_k, \\ \hat{x}_i(t_k^+) = x_i(t_k) + \gamma \sum_{j=1}^{N} \omega_{ij}^{\sigma(t)} \left(\hat{x}_j\left(t_q^i\right) - \hat{x}_i\left(t_q^i\right)\right), & t = t_k, \end{cases} \tag{7}$$

$$\begin{cases} \dfrac{\mathrm{d}\hat{x}_i(t)}{\mathrm{d}t} = A\hat{x}_i(t) + I, & t \neq t_k, \\ x_i(t_k^+) = x_i(t_k) + \eta \sum_{j=1}^{N} \omega_{ij}^{\sigma(t)} \left(\hat{x}_j\left(t_q^i\right) - \hat{x}_i\left(t_q^i\right)\right), & t = t_k, \end{cases} \tag{8}$$

where $k \geqslant 1$, $i \in \mathscr{F}$, $t_q^i \leqslant t_k < t_{q+1}^i$, $x_i(t_k^+) = \lim_{t \longrightarrow t_k + 0} x_i(t)$, and $x_i(t_k^-) = x_i(t_k)$.

Let C_τ be a Banach space and $C_\tau = C([-\tau, 0], \mathbb{R}^n)$. Let φ: $[-\tau, 0] \longrightarrow \mathbb{R}^n$ represent all continuity functions, and thus the initial value of (7) and (8) can be given:

$$\begin{aligned} x_i(t_0 + \theta) &= \varphi_i(\theta), \ \theta \in [-\tau, 0], \\ \hat{x}_i(t_0) &= \hat{\varphi}_i(t_0), \quad i = 1, \ldots, N, \end{aligned} \tag{9}$$

for $\varphi_i \in C_\tau$ and $\hat{\varphi}_i(t_0) \in \mathbb{R}^n$. Let $e_{ij}(t) = x_i(t) - x_j(t)$ denote the synchronization error for $i, j \in \mathscr{F}$, where $t \geqslant t_0$ and $\hat{e}_{ij}(t) = \hat{x}_i(t) - \hat{x}_j(t)$ denotes the observed value of $e_{ij}(t)$.

Then,

$$\begin{cases} \dfrac{\mathrm{d}e_{ij}(t)}{\mathrm{d}t} = Ae_{ij}(t) + Be_{ij}(t-\tau(t)), \quad t \neq t_k, \\ e_{ij}(t_k^+) = e_{ij}(t_k) + \gamma \left(\sum_{v=1}^{N} \omega_{iv}^{\sigma(t)} \left(\hat{x}_v\left(t_q^i\right) - \hat{x}_i\left(t_q^i\right)\right) - \sum_{v=1}^{N} \omega_{jv}^{\sigma(t)} \left(\hat{x}_v\left(t_q^j\right) - \hat{x}_j\left(t_q^j\right)\right) \right) \\ = e_{ij}(t_k) + \gamma \left(\sum_{v=1}^{N} \omega_{iv}^{\sigma(t)} \left(\hat{e}_{vj}(t_k) - \hat{e}_{ij}(t_k)\right) + \sum_{v=1}^{N} \omega_{jv}^{\sigma(t)} \left(\hat{e}_{iv}(t_k) - \hat{e}_{ij}(t_k)\right) \right) + \gamma\left(\Lambda_i(t_k) - \Lambda_j(t_k)\right), \quad t = t_k, \end{cases} \tag{10}$$

$$\begin{cases} \dfrac{\mathrm{d}\hat{e}_{ij}(t)}{\mathrm{d}t} = A\hat{e}_{ij}(t), \quad t \neq t_k, \\ \hat{e}_{ij}(t_k^+) = \hat{e}_{ij}(t_k) + \eta \left(\sum_{v=1}^{N} \omega_{iv}^{\sigma(t)} \left(\hat{x}_v\left(t_q^i\right) - \hat{x}_i\left(t_q^i\right)\right) - \sum_{v=1}^{N} \omega_{jv}^{\sigma(t)} \left(\hat{x}_v\left(t_q^j\right) - \hat{x}_j\left(t_q^j\right)\right) \right) \\ = \hat{e}_{ij}(t_k) + \eta \left(\sum_{v=1}^{N} \omega_{iv}^{\sigma(t)} \left(\hat{e}_{vj}(t_k) - \hat{e}_{ij}(t_k)\right) + \sum_{v=1}^{N} \omega_{jv}^{\sigma(t)} \left(\hat{e}_{iv}(t_k) - \hat{e}_{ij}(t_k)\right) \right) + \eta\left(\Lambda_i(t_k) - \Lambda_j(t_k)\right), \quad t = t_k. \end{cases} \tag{11}$$

Let $\xi_{ij}(t) = e_{ij}(t) - \widehat{e}_{ij}(t)$ denote tracking error of synchronization error of ith node and jth node. Then,

$$\% \begin{cases} \dfrac{\mathrm{d}\xi_{ij}(t)}{\mathrm{d}t} = A\xi_{ij}(t) + Be_{ij}(t-\tau(t)), & t \neq t_k, \\ \xi_{ij}(t_k^+) = \xi_{ij}(t_k) + (\gamma-\eta)\left(\sum\limits_{v=1}^{N} \omega_{iv}^{\sigma(t)}\left(\widehat{e}_{vj}(t_k) - \widehat{e}_{ij}(t_k)\right) + \sum\limits_{v=1}^{N} \omega_{jv}^{\sigma(t)}\left(\widehat{e}_{iv}(t_k) - \widehat{e}_{ij}(t_k)\right)\right) + (\gamma-\eta)\left(\Lambda_i(t_k) - \Lambda_j(t_k)\right), & t = t_k. \end{cases} \tag{12}$$

Let $W_{ij}(t) = \begin{pmatrix} \widehat{e}_{ij}(t) \\ \xi_{ij}(t) \end{pmatrix}$; from (10) and (11), there are the following augmentation systems:

$$\begin{cases} \dfrac{\mathrm{d}W_{ij}(t)}{\mathrm{d}t} = \begin{bmatrix} A & 0 \\ 0 & A \end{bmatrix}\begin{pmatrix} \widehat{e}_{ij}(t) \\ \xi_{ij}(t) \end{pmatrix} + \begin{bmatrix} 0 & 0 \\ B & B \end{bmatrix}\begin{pmatrix} \widehat{e}_{ij}(t-\tau(t)) \\ \xi_{ij}(t-\tau(t)) \end{pmatrix}, & t \neq t_k, \\ W_{ij}(t_k^+) = \begin{bmatrix} I & 0 \\ 0 & I \end{bmatrix}\begin{pmatrix} \widehat{e}_{ij}(t_k) \\ \xi_{ij}(t_k) \end{pmatrix} + \begin{bmatrix} I\eta & 0 \\ I(\gamma-\eta) & 0 \end{bmatrix}\sum\limits_{v=1}^{N} \omega_{iv}^{\sigma(t)}\left(\begin{pmatrix} \widehat{e}_{vj}(t_k) \\ \xi_{vj}(t_k) \end{pmatrix} - \begin{pmatrix} \widehat{e}_{ij}(t_k) \\ \xi_{ij}(t_k) \end{pmatrix}\right) \\ + \begin{bmatrix} I\eta & 0 \\ I(\gamma-\eta) & 0 \end{bmatrix}\sum\limits_{v=1}^{N} \omega_{jv}^{\sigma(t)}\left(\begin{pmatrix} \widehat{e}_{iv}(t_k) \\ \xi_{iv}(t_k) \end{pmatrix} - \begin{pmatrix} \widehat{e}_{ij}(t_k) \\ \xi_{ij}(t_k) \end{pmatrix}\right) + \begin{bmatrix} I\eta & 0 \\ I(\gamma-\eta) & 0 \end{bmatrix}\begin{pmatrix} \Lambda_i(t_k) - \Lambda_j(t_k) \\ \Lambda_i(t_k) - \Lambda_j(t_k) \end{pmatrix}, & t = t_k. \end{cases} \tag{13}$$

In addition, assume that $C_1 = \begin{bmatrix} A & 0 \\ 0 & A \end{bmatrix}$, $C_2 = \begin{bmatrix} 0 & 0 \\ B & B \end{bmatrix}$, $C_3 = \begin{bmatrix} I\eta & 0 \\ I(\gamma-\eta) & 0 \end{bmatrix}$ and $\nabla_i(t) = \begin{pmatrix} \Lambda_i(t) \\ \Lambda_i(t) \end{pmatrix}$ where $i \in \mathscr{F}$ and $t \geqslant t_0$.

Thus, from (13), it follows that

$$\begin{cases} \dfrac{\mathrm{d}W_{ij}(t)}{\mathrm{d}t} = C_1W_{ij}(t) + C_2W_{ij}(t-\tau(t)), & t \neq t_k, \\ W_{ij}(t_k^+) = W_{ij}(t_k) + C_3\left(\sum\limits_{v=1}^{N} \omega_{iv}^{\sigma(t)}\left(W_{vj}(t_k) - W_{ij}(t_k)\right) + \sum\limits_{v=1}^{N} \omega_{jv}^{\sigma(t)}\left(W_{iv}(t_k) - W_{ij}(t_k)\right)\right) + C_3\left(\nabla_i(t_k) - \nabla_j(t_k)\right), & t = t_k. \end{cases} \tag{14}$$

Definition 1. (14) is called to achieve final synchronization, if $\lim_{t\longrightarrow\infty}\|W_{ij}(t)\| = 0$.

Definition 2. (14) is called to achieve final quasi-synchronization, if $\lim_{t\longrightarrow\infty}\|W_{ij}(t)\| \leqslant a$, where $a > 0$.

Remark 1. From augmented matrix (14), we can find that there are $\lim_{t\longrightarrow\infty}\|e_{ij}(t)\| = 0\,(\lim_{t\longrightarrow\infty}\|e_{ij}(t)\| \leqslant a)$ if $\lim_{t\longrightarrow\infty}\|W_{ij}(t)\| = 0\,(\lim_{t\longrightarrow\infty}\|W_{ij}(t)\| \leqslant a)$ for any $i, j \in \mathscr{F}$. The synchronization (quasi-synchronization) of augmented system (13) is also of (1). Moreover, $\lim_{t\longrightarrow\infty}\|e_{ij}(t)\| = 0$ by observer of error systems $\widehat{e}_{ij}(t)$ and $\xi_{ij}(t)$ of tracking error of error system. We do not directly quote the state of the error system, and thus it has certain significance for the system. Its state is not measurable in

practical application. For notational convenience, we denote $\omega_{ij}^{\sigma(t_k)} = d_{ij}(t_k)$ at any time instant t_k for $i, j \in \mathcal{F}$, and $\mathcal{G}_k$ denotes $\mathcal{G}_{\sigma(t_k)}$.

3. Main Results

where $\widetilde{W}(t) = \sup_{-\tau \leqslant \theta \leqslant 0} W(t+\theta)$.where $0 < \zeta \leqslant \min\{2\|C_3\|, 1 - 4\|C_3\|\omega\}$.

Lemma 1. *A sequence of graphs $\{\mathcal{G}_j\}_{j=1}^{T_0}$ is jointly connected if a sequence of graphs $\{\mathcal{G}_j\}_{j=1}^{T}$ is sequentially connected.*

Lemma 2. *There exists $l > 0$ such that*

$$l + \|C_2\|e^{l\tau} + d_1 \leqslant 0, \tag{15}$$

for any $i, j \in \mathcal{F}$ and $t \in (t_k, t_{k+1}]$ where d_1 denotes the largest eigenvalue of C_1, and we obtain that

$$\|W_{ij}(t)\| \leqslant \|\widetilde{W}_{ij}(t)\| \leqslant \|\widetilde{W}_{ij}(t_k^+)\|e^{-l(t-t_k)}. \tag{16}$$

Proof. Let $V(t) = \|W_{ij}(t)\|e^{l(t-t_k)}$ for $t \in (t_k, t_{k+1})$. From (14), we can deduce

$$\begin{aligned}\frac{\mathrm{d}V(t)}{\mathrm{d}t} &= \operatorname{sign}\big(W_{ij}(t)\big)^T \frac{dW_{ij}(t)}{dt} e^{l(t-t_k)} + lV(t) \\ &= \operatorname{sign}\big(W_{ij}(t)\big)^T C_1 W_{ij}(t) e^{l(t-t_k)} + \operatorname{sign}\big(W_{ij}(t)\big)^T C_2 W_{ij}(t-\tau(t)) e^{l(t-t_k)} + lV(t) \\ &\leqslant d_1 V(t) + \|C_2\| V(t-\tau(t)) e^{l\tau} + lV(t).\end{aligned} \tag{17}$$

Here let $\widetilde{V}(t) = \sup_{-\tau \leqslant \theta \leqslant 0} V(t+\theta)$.

We have

$$\frac{\mathrm{d}V(t)}{\mathrm{d}t} \leqslant \big(d_1 + \|C_2\|e^{l\tau} + l\big)\widetilde{V}(t) \leqslant 0. \tag{18}$$

Then, one has $\mathrm{d}\widetilde{V}(t)/\mathrm{d}t \leqslant 0$, and so $\|W_{ij}(t)\|e^{l(t-t_k)} = V(t) \leqslant V(t_k^+) \leqslant \widetilde{V}(t_k^+) = \|\widetilde{W}_{ij}(t_k^+)\|$, i.e., $\|W_{ij}(t)\| \leqslant \|\widetilde{W}_{ij}(t_k^+)\|e^{-l(t-t_k)}$. The proof is completed.

From Assumption (A2), there exists a sequence of graphs $\{\mathcal{G}_j\}_{j=mT+1}^{(m+1)T}$ which is sequentially connected where $m \in \mathbb{Z}_+$. Hereafter, $\mathcal{G}_r^m$ represents $\mathcal{G}_{mT+r}$. A sequence of graphs $\{\mathcal{G}_r^m\}_{r=1}^{T}$ is sequentially connected for any $m \in \mathbb{Z}_+$; meanwhile, $\Omega_T^m = \mathcal{F}$ and Ω_0^m is a set of singleton.

Let

$$\begin{aligned}\mathcal{H}(t) &= \max_{i,j \in \mathcal{F}} \|W_{ij}(t)\|, \\ \widetilde{\mathcal{H}}(t) &= \sup_{\theta \in [-\tau, 0]} \mathcal{H}(t+\theta), \\ \mathcal{H}_r^m &= \mathcal{H}(t_{mT+r}), \\ \mathcal{H}_r^{m+} &= \mathcal{H}(t_{mT+r}^+), \\ \mathcal{H}_r^m(t) &= \max_{i,j \in \Omega_r^m} \|W_{ij}(t)\|, \\ \widetilde{\mathcal{H}}_r^m(t) &= \sup_{\theta \in [-\tau, 0]} \mathcal{H}_r^m(t+\theta), \\ \mathcal{H}_r^m &= \mathcal{H}(t_{mT+r}), \\ \mathcal{H}_r^{m+} &= \mathcal{H}_{r+1}(t_{mT+r}^+),\end{aligned} \tag{19}$$

where $0 \leqslant r \leqslant T-1$ and $m \in \mathbb{Z}_+$. □

Lemma 3. *By Assumption (A2), if $0 < \|C_3\| < 1/2\omega$, then*

$$\|W_{ij}(t_k^+)\| \leqslant \zeta \mathcal{H}_r^m(t_k) + (1-\zeta)\mathcal{H}(t_k) + 4\|C_3\|\big(\beta e^{-\varsigma(mT+r)h} + \alpha\big), \tag{20}$$

where $m \in \mathbb{Z}_+, 0 \leqslant r \leqslant T-1, t_q^i \leqslant t_{mT+r} < t_{q+1}^i, q \in \mathbb{Z}_+$, and $0 < \zeta \leqslant \min\{\|C_3\|, 1 - 2\omega\|C_3\|\}$.

Proof. First, we review the state equation of (14) at the impulse instant.

$$W_{ij}(t_k^+) = W_{ij}(t_k) + C_3\left(\sum_{v=1}^{N} \omega_{iv}^{\sigma(t)}\big(W_{vj}(t_k) - W_{ij}(t_k)\big) + \sum_{v=1}^{N} \omega_{jv}^{\sigma(t)}\big(W_{iv}(t_k) - W_{ij}(t_k)\big)\right) + C_3\big(\nabla_i(t_k) - \nabla_j(t_k)\big), \tag{21}$$

for $t_q^i \leqslant t_k < t_{q+1}^i$ and $q \in \mathbb{Z}_+$.

Considering $i, j \in \Omega_{r+1}^m$ and $t_k = mT + r$, where $\Omega_{r+1}^m = \Omega_r^m \cup \mathscr{F}_{r+1}^m$, we give the following three cases. □

Case 1. For $i, j \in \Omega_r^m$, under (21), we get

$$\left\|W_{ij}(t_k^+)\right\| \leqslant \operatorname{sign}\left(W_{ij}(t_k^+)\right)^T W_{ij}(t_k) + 2\|C_3\|\varpi\left(\mathscr{H}(t_k) - \operatorname{sign} W_{ij}(t_k^+)^T W_{ij}(t_k)\right) + \|C_3\|\left[\left\|\nabla_i(t_k)\right\| + \left\|\nabla_j(t_k)\right\|\right]. \tag{22}$$

From (6), ETP, and ∇_i, we deduce

$$\|\nabla_i\| \leqslant 2\left(\beta e^{-\varsigma(t-t_0)} + \alpha\right), \tag{23}$$

for $t \in [t_q^i, t_{q+1}^i)$. Hence, due to (22), we have

$$\begin{aligned}\left\|W_{ij}(t_k^+)\right\| \leqslant{}& \left(1 - 2\|C_3\|\varpi\right)\left\|W_{ij}(t_k)\right\| + 2\|C_3\|\varpi\mathscr{H}(t_k)\\ &+ 4\|C_3\|\left(\beta e^{-\varsigma(t_k-t_0)} + \alpha\right).\end{aligned} \tag{24}$$

From $0 < \zeta \leqslant \min\{\|C_3\|, 1 - 2\varpi\|C_3\|\}$ and $\mathscr{H}_r^m(t_k) \leqslant \mathscr{H}(t_k)$, we can deduce

$$\begin{aligned}\left\|W_{ij}(t_k^+)\right\| \leqslant{}& \zeta\mathscr{H}_r^m(t_k) + (1-\zeta)\mathscr{H}(t_k)\\ &+ 4\|C_3\|\left(\beta e^{-\varsigma(t_k-t_0)} + \alpha\right).\end{aligned} \tag{25}$$

Therefore, (20) is established.

Case 2. Let $i \in \mathscr{F}_{r+1}^m$, $j \in \Omega_r^m$, and $d_{is}(t_k) = 1$ if a, $s \in \Omega_r^m$.

Under (21), one has

$$\begin{aligned}W_{ij}(t_k^+) = {}& W_{ij}(t_k) + C_3\left(W_{sj}(t_k) - W_{ij}(t_k)\right) + C_3\left(\sum_{v=1, v\neq s}^{N} \varpi_{iv}^{\sigma(t)}\left(W_{vj}(t_k) - W_{ij}(t_k)\right) + \sum_{v=1}^{N} \varpi_{jv}^{\sigma(t)}\left(W_{iv}(t_k) - W_{ij}(t_k)\right)\right)\\ &+ C_3\left(\nabla_i(t_k) - \nabla_j(t_k)\right).\end{aligned} \tag{26}$$

From (26), we can deduce

$$\begin{aligned}\left\|W_{ij}(t_k^+)\right\| &= \left(1 - \|C_3\|\right)\operatorname{sign}\left(W_{ij}(t_k^+)\right)^T W_{ij}(t_k) + \|C_3\|\mathscr{H}_r^m(t_k)\\ &\quad + \|C_3\|(2\varpi - 1)\left(\mathscr{H}(t_k) - \operatorname{sign}\left(W_{ij}(t_k^+)\right)^T W_{ij}(t_k)\right) + \|C_3\|\left(\left\|\nabla_i(t_k)\right\| + \left\|\nabla_j(t_k)\right\|\right)\\ &\leqslant \zeta\mathscr{H}_r^m(t_k) + (1-\zeta)\mathscr{H}(t_k) + 4\|C_3\|\left(\beta e^{-\varsigma(t_k-t_0)} + \alpha\right).\end{aligned} \tag{27}$$

Hence, (20) is established.

Case 3. $i, j \in \mathscr{F}_{r+1}^m$, $d_{is}(t_k) = 1$, and $d_{jq}(t_k) = 1$ if $s, q \in \Omega_r^m$.

Because

$$W_{sj}(t_k) + W_{iq}(t_k) = W_{sq}(t_k) + W_{ij}(t_k), \tag{28}$$

from (21), we have

$$\begin{aligned}W_{ij}(t_k^+) = {}& W_{ij}(t_k) + C_3\left(W_{sj}(t_k) - W_{ij}(t_k)\right) + C_3\left(W_{iq}(t_k) - W_{ij}(t_k)\right)\\ &+ C_3\left(\sum_{v=1, v\neq s}^{N} \varpi_{iv}^{\sigma(t)}\left(W_{vj}(t_k) - W_{ij}(t_k)\right) + \sum_{v=1, v\neq q}^{N} \varpi_{jv}^{\sigma(t)}\left(W_{iv}(t_k) - W_{ij}(t_k)\right)\right) + C_3\left(\nabla_i(t_k) - \nabla_j(t_k)\right)\\ ={}& W_{ij}(t_k) + C_3\left(W_{sq}(t_k) - W_{ij}(t_k)\right) + C_3\left(\sum_{v=1, v\neq s}^{N} \varpi_{iv}^{\sigma(t)}\left(W_{vj}(t_k) - W_{ij}(t_k)\right) + \sum_{v=1, v\neq q}^{N} \varpi_{jv}^{\sigma(t)}\left(W_{iv}(t_k) - W_{ij}(t_k)\right)\right)\\ &+ C_3\left(\nabla_i(t_k) - \nabla_j(t_k)\right).\end{aligned} \tag{29}$$

By (29),

$$\begin{aligned}\left\|W_{ij}(t_k^+)\right\| &\le \left(1-\|C_3\|\right)\operatorname{sign}\left(W_{ij}(t_k^+)\right)^T W_{ij}(t_k)+\|C_3\|\mathscr{H}_r^m(t_k)\\ &\quad+\|C_3\|(2\varpi-2)\left(\mathscr{H}(t_k)-\operatorname{sign}\left(W_{ij}(t_k^+)\right)^T W_{ij}(t_k)\right)+\|C_3\|\left(\|\nabla_i(t_k)\|+\|\nabla_j(t_k)\|\right)\\ &\le \|C_3\|\mathscr{H}_r^m(t_k)+\left(1-2\|C_3\|\varpi+\|C_3\|\right)\|W_{ij}(t_k)\|+\|C_3\|(2\varpi-2)\mathscr{H}(t_k)+4\|C_3\|\left(\beta e^{-\varsigma(t_k-t_0)}+\alpha\right)\\ &\le \zeta\mathscr{H}_r^m(t_k)+(1-\zeta)\mathscr{H}(t_k)+4\|C_3\|\left(\beta e^{-\varsigma(t_k-t_0)}+\alpha\right).\end{aligned} \tag{30}$$

Obviously, (20) holds. Now the proof is completed.

It is always important to assure that Zeno behavior can not be occurred under ETC (3) and (4) in order to prove the synchronization or quasi-synchronization that can be reached by (14).

For error observation (11), it follows that

$$\begin{aligned}\mathscr{G}(t) &= \max_{i,j\in\mathscr{F}}\left\|\widehat{e}_{ij}(t)\right\|,\\ \widetilde{\mathscr{G}}(t) &= \sup_{\theta\in[-\tau,0]}\mathscr{G}(t+\theta),\\ \mathscr{G}_r^m &= \mathscr{G}\left(t_{mT+r}\right),\\ \mathscr{G}_r^{m+} &= \mathscr{G}\left(t_{mT+r}^+\right),\\ \mathscr{Q}_r^m(t) &= \max_{i,j\in\Omega_r^m}\left\|\widehat{e}_{ij}(t)\right\|,\\ \widetilde{\mathscr{Q}}_r^m(t) &= \sup_{\theta\in[-\tau,0]}\mathscr{Q}_r^m(t+\theta),\\ \mathscr{Q}_r^m &= \mathscr{Q}\left(t_{mT+r}\right),\\ \mathscr{Q}_r^{m+} &= \mathscr{Q}\left(t_{mT+r}^+\right).\end{aligned} \tag{31}$$

Theorem 1. *Assume that all the conditions of Lemma 2, hold, and satisfy following conditions:*

C1: $l_2>0$ *and* $l_2+c_1\le 0$

C2: $0<\eta<(1/2\varpi)$

where c_1 *is the maximum eigenvalue of matrix* A*, and thus (14) does not exhibit Zeno behavior. Event-triggered time sequence* $\{t_q^i\}$ *is generated under event-triggered strategy (6), which satisfies* $q\longrightarrow+\infty$ *when* $t_q^i\longrightarrow+\infty$.

Proof. Let $\{t_q^i\}$ be a bounded set and $\{\mathscr{G}(t_q^i)\}$ also be a bounded set. It is assumed that $\mathscr{G}(t_q^i)<D_2$.

For any $i\in\mathscr{F}$, $t\in[t_q^i,t_{q+1}^i)$, there are

$$\begin{aligned}\|\Lambda_i(t)\| &= \left\|\sum_{v=1}^N \varpi_{iv}^{\sigma(t)}\widehat{e}_{vi}\left(t_q^i\right)-\sum_{v=1}^N\varpi_{iv}^{\sigma(t)}\widehat{e}_{vi}(t)\right\|\\ &= \left\|\sum_{v=1}^N\left(\varpi_{iv}^{\sigma(t)}\widehat{e}_{vi}\left(t_q^i\right)-\varpi_{iv}^{\sigma(t)}\widehat{e}_{vi}(t)\right)\right\|\\ &\le \sum_{v=1}^N\varpi_{iv}^{\sigma(t)}\int_{t_q^i}^t\left\|\dot{\widehat{e}}_{vi}(t)\right\|\mathrm{d}t.\end{aligned} \tag{32}$$

Let $m\in\mathbb{Z}_+$ such that $[t_q^i,t_{q+1}^i)\subset[t_{mT},t_{(m+1)T})$. By (11), $\|\dot{\widehat{e}}_{vi}(s)\|\le D_1\widetilde{\mathscr{G}}(s)$ where $D_1=\|A\|$.

Similar to Lemma 2, there is $l_2+c_1\le 0$, where $l_2>0$ and c_1 is maximum eigenvalue of A. Thus, we can deduce $\widetilde{\mathscr{G}}(s)\le\widetilde{\mathscr{G}}(t_q^{i+})e^{|l_2|(s-t_q^i)}$, where $s\in[t_q^i,t]$ and $\widetilde{\mathscr{G}}(t_q^{i+})=\lim_{s\longrightarrow t_q^i+0}\widetilde{\mathscr{G}}(s)$.

Then, we have

$$\left\|\dot{\widehat{e}}_{vi}(s)\right\|\le D_1\widetilde{\mathscr{G}}\left(t_q^{i+}\right)e^{l_2\left(s-t_q^i\right)}, \tag{33}$$

where $s\in[t_q^i,t]$. Obviously, there are $\widetilde{\mathscr{G}}(t_q^{i+})=\widetilde{\mathscr{G}}(t_q^i)\le D_2$ for $t_q^i\in(t_{mT},t_{(m+1)T})$.

Similar to Lemma 3, at impulse instants, (11) has

$$\mathscr{Q}_r^m(t_k^+)=\psi\mathscr{Q}_r^m(t_k)+(1-\psi)\mathscr{G}_r^m(t_k)+2\eta\left(\beta e^{-\varsigma(mT+r)h}+\alpha\right), \tag{34}$$

if exists $0<\eta<21\varpi$, where $0<\psi\le\min\{\eta,1-2\varpi\eta\}$, if $t_q^i=t_{mT}$, $\widetilde{\mathscr{Q}}_0^m(t_{mT})=\widetilde{\mathscr{G}}_0^m(t_{mT})$ thus

$$\begin{aligned}\widetilde{\mathscr{G}}\left(t_q^{i+}\right) &= \widetilde{\mathscr{G}}_0^{m+}\\ &\le \widetilde{\mathscr{G}}_0^m+2\eta\left[\beta e^{-\varsigma mTh}+\alpha\right]\\ &\le D_2+2\eta\left[\beta e^{-\varsigma mTh}+\alpha\right].\end{aligned} \tag{35}$$

Let $D_2+2\eta[\beta e^{-\varsigma mTh}+\alpha]=\Pi$. Combine (32)–(35), and we have

$$\begin{aligned}\left\|\Lambda_i(t)\right\| &\leqslant D_1\Pi\omega\int_{t_q^i}^{t} e^{l_2\left(s-t_q^i\right)}\mathrm{d}s\\ &= \frac{D_1\Pi\omega}{l_2}\left[e^{l_2\left(t-t_q^i\right)}-1\right].\end{aligned} \tag{36}$$

From (6), event-triggered strategy is triggered to update the controller when $\|\Lambda_i(t)\| = \beta e^{-\varsigma(t-t_0)} + \alpha$; in other words, $t_q^i \longrightarrow t_{q+1}^i$. Hence, from (36), we obtain that

$$\begin{aligned}\left\|\Lambda_i\left(t_{q+1}^i\right)\right\| &= \beta e^{-\varsigma\left(t_{q+1}^i-t_0\right)}+\alpha\\ &\leqslant \frac{D_1\Pi\omega}{l_2}\left[e^{l_2\left(t_{q+1}^i-t_q^i\right)}-1\right],\end{aligned} \tag{37}$$

which means

$$\frac{\left(\beta e^{-\varsigma\left(t_{q+1}^i-t_0\right)}+\alpha\right)l_2}{D_1\Pi\omega}+1\leqslant e^{l_2\left(t_{q+1}^i-t_q^i\right)}, \tag{38}$$

and then

$$t_{q+1}^i-t_q^i\geqslant \frac{\ln\left(\left(\left(\beta e^{-\varsigma\left(t_{q+1}^i-t_0\right)}+\alpha\right)l_2/D_1\Pi\omega\right)+1\right)}{l_2}, \tag{39}$$

such that the event-triggered sequence $\left\{t_q^i\right\}$ has time interval. This is contrary to the assumption that the sequence $\left\{t_q^i\right\}$ is bounded. This ends the proof. □

Theorem 2. *By Assumption (A1), ifTheorem 1,Lemma 2, andLemma 3hold, then the quasi-synchronization of (7) can be obtained based on observer if$l \neq 0$satisfies (15) besides*

$$e^{-lTh}\left(1-\zeta^T\right)<1, \tag{40}$$

where$0<\zeta\leqslant \min\{2\|C_3\|, 1-4\|C_3\|\omega\}$.

Proof. According to Lemma 2, we can see that

$$\mathscr{H}_{r+1}^m \leqslant \widetilde{\mathscr{H}}_{r+1}^m \leqslant \widetilde{\mathscr{H}}_r^{m+} e^{-lh}, \tag{41}$$

$$\mathscr{H}_{r+1}^m \leqslant \widetilde{\mathscr{H}}_{r+1}^m \leqslant \widetilde{\mathscr{H}}_r^{m+} e^{-lh}, \tag{42}$$

where $m\in\mathbb{Z}_+, 0\leq r\leq T-1$. By Theorem 1, we can know that Zeno behavior cannot occur.

Meanwhile, according to Lemma 3, it follows that

$$\begin{aligned}\widetilde{\mathscr{H}}_r^{m+} &\leqslant \zeta\widetilde{\mathscr{H}}_r^m+(r-\zeta)\widetilde{\mathscr{H}}_r^m+4\|C_3\|\left(\beta e^{-\varsigma(mT+r)h}+\alpha\right),\\ \widetilde{\mathscr{H}}_r^{m+} &\leqslant \widetilde{\mathscr{H}}_r^m+4\|C_3\|\left(\beta e^{-\varsigma(mT+r)h}+\alpha\right).\end{aligned} \tag{43}$$

Combining (41) and (43), we can obtain that

$$\widetilde{\mathscr{H}}_{r+1}^m \leqslant e^{-lh}\left[\widetilde{\mathscr{H}}_r^m+4\|C_3\|\left(\beta e^{-\varsigma(mT+r)h}+\alpha\right)\right]. \tag{44}$$

Then, from (41)–(44), through the iterative method, we can obtain that

$$\begin{aligned}\widetilde{\mathscr{H}}_r^{m+} &\leqslant e^{-lh}\left[\zeta\widetilde{\mathscr{H}}_{r-1}^{m+}+(1-\zeta)\widetilde{\mathscr{H}}_{r-1}^m\right]+\beta_1 e^{-\varsigma(mT+r-1)h}+\alpha_1\\ &\leqslant e^{-2lh}\left[\zeta^2\widetilde{\mathscr{H}}_{r-2}^{m+}+\left(1-\zeta^2\right)\widetilde{\mathscr{H}}_{r-2}^m\right]+\beta_2 e^{-\varsigma(mT+r-2)h}+\alpha_2\\ &\cdots\\ &\leqslant e^{-lvh}\left[\zeta^v\widetilde{\mathscr{H}}_{r-v}^{m+}+\left(1-\zeta^v\right)\widetilde{\mathscr{H}}_{r-v}^m\right]+\beta_v e^{-\varsigma(mT+r-v)h}+\alpha_v,\end{aligned} \tag{45}$$

and

$$\begin{aligned}\alpha_1 &= 4\|C_3\|\alpha\left[(1-\zeta)e^{-lh}+1\right],\\ \alpha_2 &= \left[e^{-2lh}\zeta^2+1\right]\alpha_1+4\|C_3\|(1-\zeta)e^{-2lh}\alpha,\\ &\cdots\\ \alpha_v &= \left[e^{-vlh}\zeta^v+1\right]\alpha_v+4\|C_3\|\left(1-\zeta^{v-1}\right)e^{-vlh}\alpha,\\ \beta_1 &= 4\|C_3\|\left[(1-\zeta)e^{-lh}+e^{-\varsigma h}\right]\beta,\\ \beta_2 &= \left[e^{-2lh}\zeta^2+e^{-2\varsigma h}\right]\beta_1+4\|C_3\|(1-\zeta)e^{-2lh}\beta,\\ &\cdots\\ \beta_v &= \left[e^{-vlh}\zeta^v+e^{-v\varsigma h}\right]\beta_{v-1}+4\|C_3\|\left(1-\zeta^{v-1}\right)e^{-vlh}\beta,\end{aligned} \tag{46}$$

and thus

$$\begin{aligned}\widetilde{\mathscr{H}}_T^m &\leqslant e^{-lh}\widetilde{\mathscr{H}}_{T-1}^{m+}\\ &\leqslant e^{-lTh}\left[\zeta^{T-1}\widetilde{\mathscr{H}}_0^{m+}+\left(1-\zeta^{T-1}\right)\widetilde{\mathscr{H}}_0^m\right]+e^{-lh}\beta_{T-1}e^{-\varsigma mTh}\\ &\quad+e^{-lh}\alpha_{T-1}.\end{aligned} \tag{47}$$

From the introduction of the previous preparation part, we have $\Omega_{T-1}=\mathscr{F}$ and $\widetilde{\mathscr{H}}_T^m=\widetilde{\mathscr{H}}_T^m=\widetilde{\mathscr{H}}_0^{m+1}$. Meanwhile, from Ω_0 which is a single point, we can obtain $\widetilde{\mathscr{H}}_0^m=0$. By using (47), one has

$$\begin{aligned}\widetilde{\mathscr{H}}_0^{m+} &\leqslant \zeta\widetilde{\mathscr{H}}_0^m+(1-\zeta)\widetilde{\mathscr{H}}_0^m+4\|C_3\|\left[\beta e^{-\varsigma mTh}+\alpha\right]\\ &\leqslant (1-\zeta)\widetilde{\mathscr{H}}_0^m+4\|C_3\|\left[\beta e^{-\varsigma mTh}+\alpha\right].\end{aligned} \tag{48}$$

By applying (47) and (48), we can prove the following result:

$$\widetilde{\mathscr{H}}_0^{m+1}\leqslant \varepsilon\widetilde{\mathscr{H}}_0^m+\overline{\alpha}+\overline{\beta}e^{-m\varsigma Th}, \tag{49}$$

where $0<\varepsilon=e^{-lTh}(1-\zeta^T)<1, \overline{\alpha}=4\|C_3\|\alpha e^{-lTh}+e^{-lh}\alpha_{T-1}+$, and $\overline{\beta}=e^{-lh}\beta_{T-1}+4\|C_3\|\beta e^{-lTh}$. From (43), it follows that

$$\begin{aligned}\widetilde{\mathscr{H}}_0^{m+1} &\leqslant \varepsilon\widetilde{\mathscr{H}}_0^{m} + \overline{\beta}e^{-m\varsigma Th} + \overline{\alpha}\\ &\leqslant \varepsilon^2\widetilde{\mathscr{H}}_0^{m-1} + \overline{\beta}\varepsilon e^{-(m-1)\varsigma Th} + \overline{\beta}e^{-m\varsigma Th} + \varepsilon\overline{\alpha} + \overline{\alpha}\\ &\cdots\\ &\leqslant \varepsilon^{m-1}\widetilde{\mathscr{H}}_0^{2} + \overline{\beta}\varepsilon^{m-2}e^{-2\varsigma Th} + \cdots + \overline{\beta}\varepsilon e^{-(m-1)\varsigma Th} + \overline{\beta}e^{-m\varsigma Th} + \left(\varepsilon^{m-1} + \cdots + \varepsilon + 1\right)\overline{\alpha}\\ &\leqslant \varepsilon^{m}\widetilde{\mathscr{H}}_0^{1} + \frac{e^{-m\varsigma Th} - \varepsilon^{m}}{1 - \varepsilon e^{\varsigma Th}}\overline{\beta} + \frac{1 - \varepsilon^{m+1}}{1 - \varepsilon}\overline{\alpha}.\end{aligned} \tag{50}$$

Therefore, we can obtain

$$\lim_{m\longrightarrow\infty}\sup\widetilde{\mathscr{H}}_0^{m} \leqslant \overline{\alpha}. \tag{51}$$

(14) can achieve quasi-synchronization. In other words, (7) can also quasi-synchronization-based observer.

In addition, $\lim_{m\longrightarrow\infty}\sup\widetilde{\mathscr{H}}_0^{m} = 0$ if $\overline{\alpha} = 0$. From Theorem 2, (7) can reach synchronization-based observer if the sufficient conditions are satisfied. □

Remark 2. Under all the conditions of Theorem 2, (14) can be quasi-synchronized. According to the definition of (14), we can find that the system is composed of an observation error system $\widehat{e}_{ij}(t)$ and a tracking error system $\xi_{ij}(t)$. Therefore, when (14) can be quasi-synchronized by means of $\widehat{e}_{ij}(t) and \xi_{ij}(t)$, we can have the quasi-synchronization of (1). In this process, we do not directly use the state value of the original system (1). It is consistent with the situation that the state value of the system is unknown in practical application.

Theorem 3. *Under Assumption (A3), usingLemma 2,Lemma 3, andTheorem 1, system (7) can obtain quasi-synchronization-based observer if*

$$e^{-l(N-1)^2T_0h}\left(1 - \zeta^{(N-1)^2T_0}\right) < 1. \tag{52}$$

Proof. From Lemma 1, when the sequence of graphs $\left\{\mathscr{G}_j\right\}_{j=1}^{T_0}$ satisfies $e^{-l(N-1)^2T_0h}(1 - \zeta^{(N-1)^2T_0}) < 1$, the sequence of graphs $\left\{\mathscr{G}_j\right\}_{j=1}^{T}$ satisfies $e^{-lTh}(1 - \zeta^{T}) < 1$. Therefore, under Lemma 2, system (7) can have quasi-synchronization-based observer and can have synchronization if $\alpha = 0$. □

4. Numerical Simulations

In this section, a numerical example is given to verify the validity of theory analyses.

Review original system (7) with controller and observer system (8):

$$\begin{cases}\dfrac{\mathrm{d}x_i(t)}{\mathrm{d}t} = Ax_i(t) + Bx_i(t - \tau(t)) + I, & t \neq t_k,\\ x_i(t_k^+) = x_i(t_k) + \gamma\displaystyle\sum_{j=1}^{N}\varpi_{ij}^{\sigma(t)}\left(\widehat{x}_j\left(t_q^i\right) - \widehat{x}_i\left(t_q^i\right)\right), & t = t_k,\end{cases}$$

$$\begin{cases}\dfrac{\mathrm{d}\widehat{x}_i(t)}{\mathrm{d}t} = A\widehat{x}_i(t) + I, & t \neq t_k,\\ \widehat{x}_i(t_k^+) = \widehat{x}_i(t_k) + \eta\displaystyle\sum_{j=1}^{N}\varpi_{ij}^{\sigma(t)}\left(\widehat{x}_j\left(t_q^i\right) - \widehat{x}_i\left(t_q^i\right)\right), & t = t_k.\end{cases} \tag{53}$$

Let $i \in \mathscr{F} = \{1, 2, 3, 4, 5, 6, 7, 8\}$, and the parameters in the system are designed as follows: $\gamma = 0.12$ and $\eta = 0.05$, and the weight matrix is designed as

$$A = \begin{pmatrix} -4 & 1\\ 2 & -3\end{pmatrix},\qquad B = \begin{pmatrix} 1 & -0.5\\ -0.5 & 0.8\end{pmatrix}. \tag{54}$$

Meanwhile, the initial function is given as follows: $\varphi_1 = [0.8, -0.3]^T$, $\varphi_2 = [-0.7, 0.4]^T$, $\varphi_3 = [1.2, -0.5]^T$, $\varphi_4 = [1.3, -0.2]^T$, $\varphi_5 = [0.3, -0.3]^T$, $\varphi_6 = [0.78, -0.5]^T$, $\varphi_7 = [0.42, -0.32]^T$, $\varphi_8 = [-0.4, -0.6]^T$, $\widehat{\varphi}_1 = [1.1, -0.8]^T$, $\widehat{\varphi}_2 = [0.7, -0.78]^T$, $\widehat{\varphi}_3 = [0.45, -1]^T$, $\widehat{\varphi}_4 = [-0.63, 0.9]^T$, $\widehat{\varphi}_5 = [-0.43, -0.56]^T$, $\widehat{\varphi}_6 = [0.7, -1.3]^T$, $\widehat{\varphi}_7 = [0.3, -0.4]^T$, $\widehat{\varphi}_8 = [0.86, -0.3]^T$, and $\tau(t) = |\sin(t)|$, and we set $t_k = 0.5k$, $k\epsilon_+$. Figures 2 and 3 show the switching topology.

From Figure 2 ($\mathscr{G}_{2m}$) and Figure 3 ($\mathscr{G}_{2m+1}$), we can find that $\left\{\mathscr{G}_{2m}, \mathscr{G}_{2m+1}\right\}$ is sequential connection. In the switching period $T = 2$, it is also a joint connection and $T_0 = 2$. The change of node set is as follows: $\Omega_0 = \{1\}$, $\Omega_1 = \{1, 4, 5, 8\}$, and $\Omega_2 = \{1, 2, 3, 4, 5, 6, 7, 8\} = \mathscr{V}$. Satisfy Assumptions (A1) and (A2), and the coupling matrix is as follows:

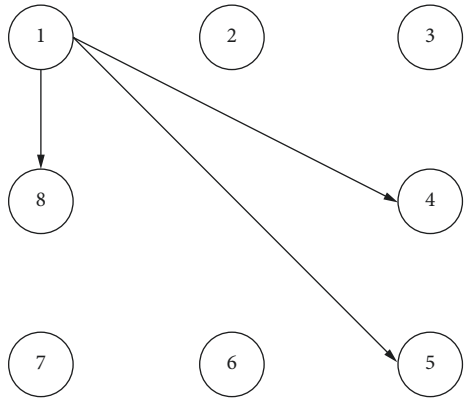

Figure 2: $\mathcal{G}_{2m}$.

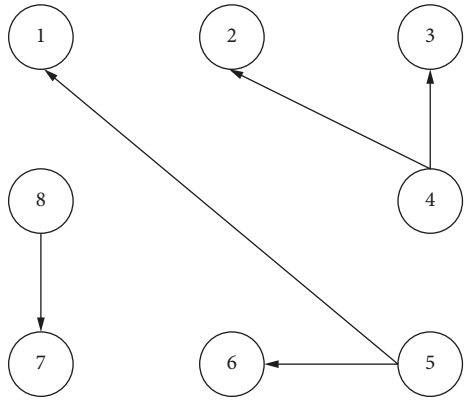

Figure 3: $\mathcal{G}_{2m+1}$.

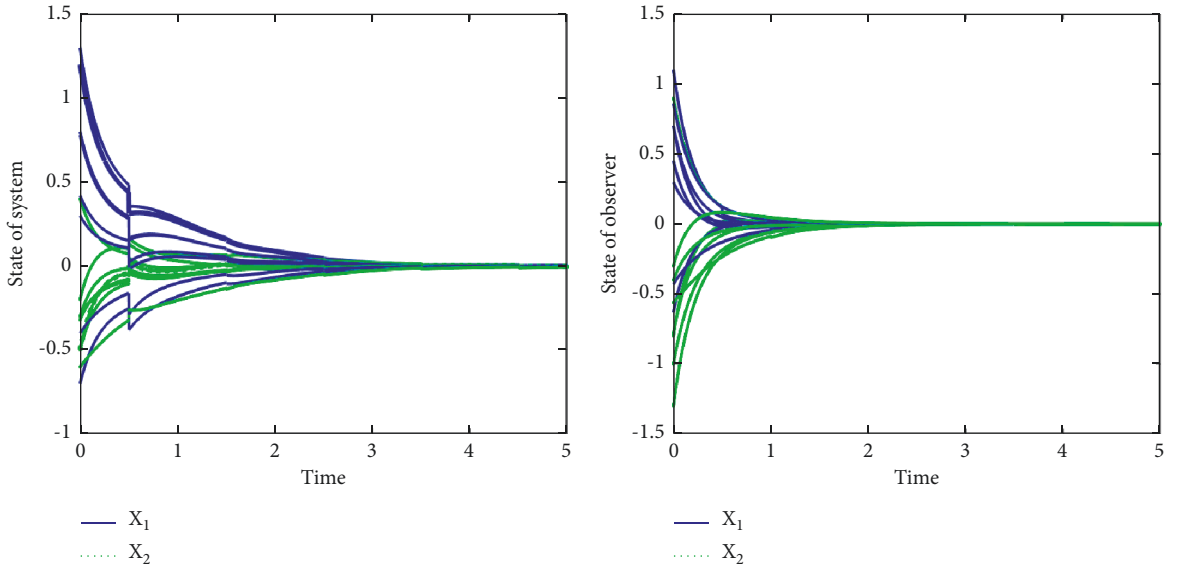

Figure 4: The quasi-synchronization. State diagram of 8 nodes of observation system (1) and system (2), when $\alpha = 0.2$.

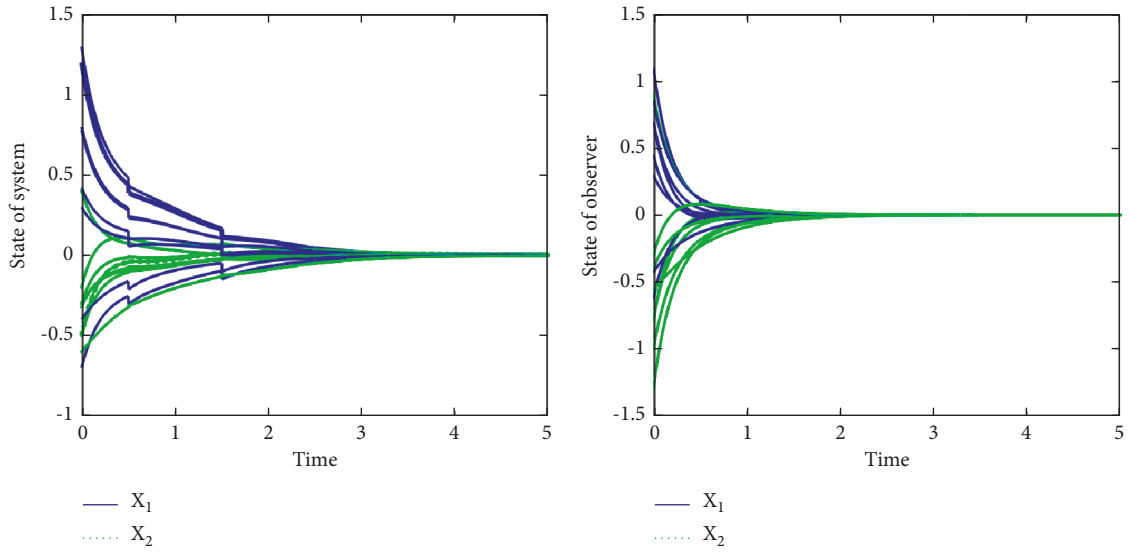

Figure 5: The quasi-synchronization. State diagram of 8 nodes of observation system (1) and system (2), when $\alpha = 0$.

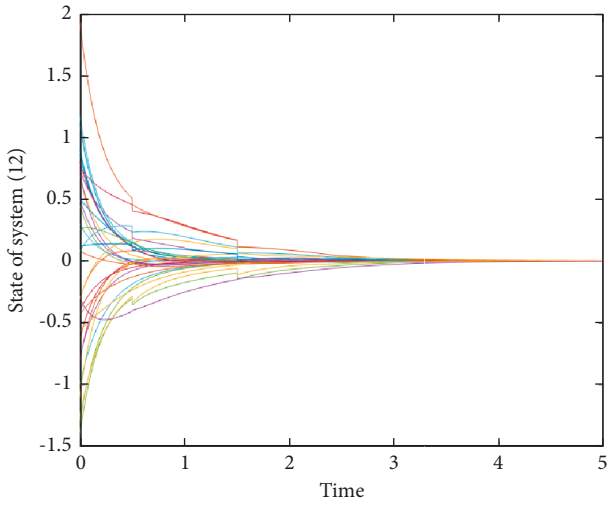

Figure 6: The state diagram of 8 nodes of system (14) when $\alpha = 0.2$.

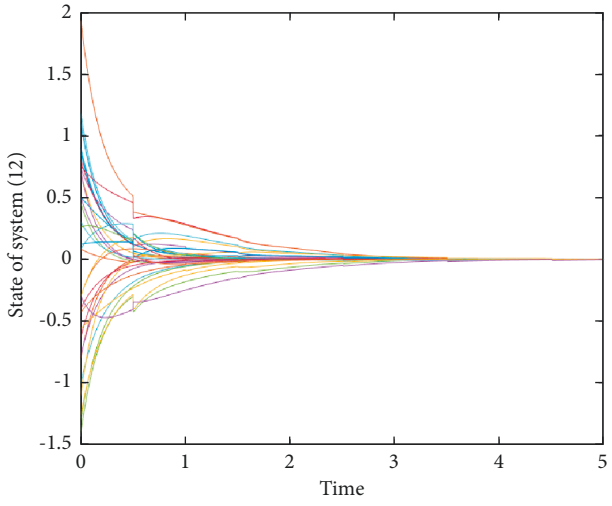

Figure 7: The state diagram of 8 nodes of system (14) when $\alpha = 0$.

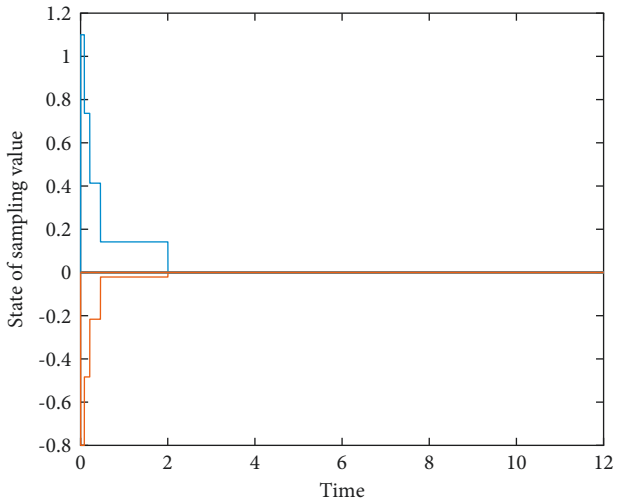

Figure 8: The state of sampling value is given when $\alpha = 0.2$.

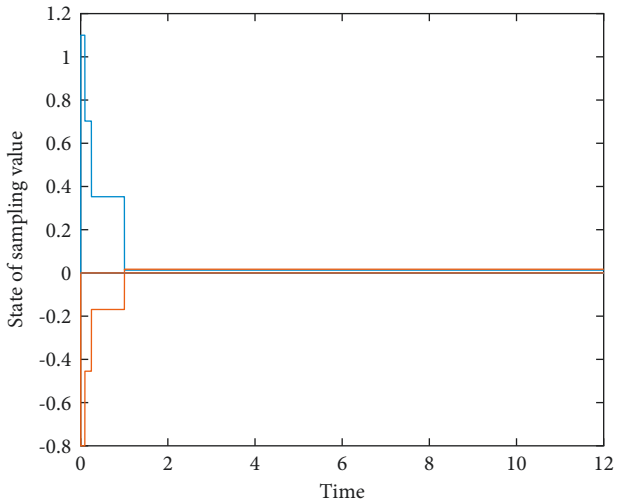

Figure 9: The state of sampling value is given when $\alpha = 0$.

$$\mathcal{G}_{2m} = \begin{pmatrix} 0 & 0 & 0 & 1 & 1 & 0 & 0 & 1 \\ 0 & 0 & 0 & 0 & 0 & 0 & 0 & 0 \\ 0 & 0 & 0 & 0 & 0 & 0 & 0 & 0 \\ 0 & 0 & 0 & 0 & 0 & 0 & 0 & 0 \\ 0 & 0 & 0 & 0 & 0 & 0 & 0 & 0 \\ 0 & 0 & 0 & 0 & 0 & 0 & 0 & 0 \\ 0 & 0 & 0 & 0 & 0 & 0 & 0 & 0 \\ 0 & 0 & 0 & 0 & 0 & 0 & 0 & 0 \end{pmatrix},$$

$$\mathcal{G}_{2m+1} = \begin{pmatrix} 0 & 0 & 0 & 0 & 0 & 0 & 0 & 0 \\ 0 & 0 & 0 & 0 & 0 & 0 & 0 & 0 \\ 0 & 0 & 0 & 0 & 0 & 0 & 0 & 0 \\ 0 & 1 & 1 & 0 & 0 & 0 & 0 & 0 \\ 1 & 0 & 0 & 0 & 0 & 1 & 0 & 0 \\ 0 & 0 & 0 & 0 & 0 & 0 & 0 & 0 \\ 0 & 0 & 0 & 0 & 0 & 0 & 0 & 0 \\ 0 & 0 & 0 & 0 & 0 & 0 & 1 & 0 \end{pmatrix}. \tag{55}$$

Thus, we know $\omega = 3$, $T = 2$.

From the above data, augmented matrix (14), we have

$$C_1 = \begin{bmatrix} A & 0 \\ 0 & A \end{bmatrix} = \begin{pmatrix} -4 & 1 & 0 & 0 \\ 2 & -3 & 0 & 0 \\ 0 & 0 & -4 & 1 \\ 0 & 0 & 2 & -3 \end{pmatrix},$$

$$C_2 = \begin{bmatrix} 0 & 0 \\ B & B \end{bmatrix} = \begin{pmatrix} 0 & 0 & 0 & 0 \\ 0 & 0 & 0 & 0 \\ 1 & -0.5 & 1 & -0.5 \\ -0.5 & 0.8 & -0.5 & 0.8 \end{pmatrix}, \tag{56}$$

$$C_3 = \begin{bmatrix} I\eta & 0 \\ I(\gamma - \eta) & 0 \end{bmatrix} = \begin{pmatrix} 0.05 & 0 & 0 & 0 \\ 0 & 0.05 & 0 & 0 \\ 0.07 & 0 & 0 & 0 \\ 0 & 0.07 & 0 & 0 \end{pmatrix}.$$

For Lemma 2, $l + \|C_2\|e^{l\tau} + d_1 = l + 1.5e^r - 2 \le 0$ by solution of the integral equation reach $l < = 0.188$. Let $l = 0.15$, and the condition of Lemma 2 can be satisfied.

For Lemma 3, we can obtain $\|C_3\| = 0.12 \le (1/2\omega) = (1/6)$, and Lemma 3 is also satisfied. According to the conditions in Theorem 1, we have $l_2 + c_1 \le 0$ and $l_2 \le 2$. Let $l_2 = 0.15$ and satisfy the condition of Theorem 1. For C2, we have $\eta = 0.05 < (1/2\varpi) = (1/6)$. Thus, according to Theorem 1, there is no Zeno behavior.

For Theorem 2, $0 < \zeta \le \min\{2\|C_3\|, 1 - 4\|C_3\|\varpi\}$ obtain $\zeta = 0.3$. According to $e^{-lTh}(1 - \zeta^T) = e^{-0.15\times2\times0.0025}(1 - 0.3^2) < 1$, the condition of Theorem 2 is also established where $h = 0.0025$. Then, (14) can reach the quasi-synchronization, namely, (1) achieves quasi-synchronization based on observers.

Take $\alpha > 0$, $\beta = 2$, and $\varsigma = 0.8$.

Under quasi-synchronization, the state diagram of 8 nodes of (1) and (2) when $\alpha = 0.2$ is shown in Figure 4. Under synchronization, the state diagram of 8 nodes of (1) and (2) when $\alpha = 0$ is shown in Figure 5.

Figure 6 shows the state diagram of 8 nodes of system (14) when $\alpha = 0.2$.

Figure 7 shows the state diagram of 8 nodes of system (14) when $\alpha = 0$.

In Figure 8, the state of sampling value is given when $\alpha = 0.2$. In Figure 9, the state of sampling value is given when $\alpha = 0$. When the system meets the conditions given in this paper, all nodes reach synchronization. Thus, we can find that the theorem given in this article is valid.

5. Conclusion

The question of quasi-synchronization (synchronization) in MNNs with observers in impulsive coupling controller via event-trigger strategy is discussed. An event-triggering mechanism is designed by using the combination measurement method. The real system state in this paper is assumed to be unmeasurable, and the system time delay is also unmeasurable. The state of (1) is measured by observer. The time delay is unknown, so the observer does not have time delay too. The augmented system is composed of the observer and the tracking error system of the error system. In the real system, the sufficient conditions of the quasi-synchronization and synchronization are proved. Compared with existing works, this paper considers the real state and unmeasurable time delay, and the controller used in this paper is a impulsive controller with event-triggered mechanism, so it plays a significant role in saving communication resources. In addition, we consider trying to spread it to the more general system and more complex systems.

Data Availability

No data were used to support this study.

Conflicts of Interest

The authors declare that there are no conflicts of interest regarding the publication of this paper.

Acknowledgments

This study was supported by the Natural Science Foundation of China (62072164 and 11704109).

References

[1] M. Pipattanasomporn, H. Feroze, and S. Rahman, "Multi-agent systems in a distributed smart grid: design and implementation," in *Proceedings of the 2009 IEEE/PES Power Systems Conference and Exposition*, pp. 1–8, IEEE, Seattle, WA, USA, 15-18 March 2009.

[2] H. Li, A. Mynett, E. Penning, and H. Qi, "Revealing spatial pattern dynamics in aquatic ecosystem modelling with Multi-Agent Systems in Lake Veluwe," *Ecological Informatics*, vol. 5, no. 2, pp. 97–107, 2010.

[3] W. Ren and N. Sorensen, "Distributed coordination architecture for multi-robot formation control," *Robotics and Autonomous Systems*, vol. 56, no. 4, pp. 324–333, 2008.

[4] J. A. Fax and R. M. Murray, "Information flow and cooperative control of vehicle formations," *IEEE Transactions on Automatic Control*, vol. 49, no. 9, pp. 1465–1476, 2004.

[5] M. S. Ali and P. Balasubramaniam, "Exponential stability of uncertain stochastic fuzzy BAM neural networks with time-varying delays," *Neurocomputing*, vol. 72, no. 4-6, pp. 1347–1354, 2009.

[6] M. S. Ali and R. Saravanakumar, "Improved delay-dependent robust H_∞ control of an uncertain stochastic system with interval time-varying and distributed delays," *Chinese Physics B*, vol. 23, no. 12, p. 120201, 2014.

[7] K. Hengster-Movric, K. You, F. L. Lewis, and L. Xie, "Synchronization of discrete-time multi-agent systems on graphs using Riccati design," *Automatica*, vol. 49, no. 2, pp. 414–423, 2013.

[8] Q. Jia, W. K. S. Tang, and W. A. Halang, "Leader following of nonlinear agents with switching connective network and coupling delay," *IEEE Transactions on Circuits and Systems I: Regular Papers*, vol. 58, no. 10, pp. 2508–2519, 2011.

[9] Z. Meng, W. Ren, Y. Cao, and Z. You, "Leaderless and leader-following consensus with communication and input delays under a directed network topology," *IEEE Transactions on Systems, Man, and Cybernetics, Part B (Cybernetics)*, vol. 41, no. 1, pp. 75–88, 2011.

[10] M. S. Ali, M. Hymavathi, and S. Senan, "Global asymptotic synchronization of impulsive fractional-order complex-valued memristor-based neural networks with time varying delays," *Communications in Nonlinear Science and Numerical Simulation*, vol. 78, p. 104869, 2019.

[11] S. Kiranyaz, T. Ince, and O. Abdeljaber, "1-d convolutional neural networks for signal processing applications," in *Proceedings of the ICASSP 2019-2019 IEEE International Conference on Acoustics, Speech and Signal Processing (ICASSP)*, pp. 8360–8364, IEEE, Brighton, UK, 12-17 May 2019.

[12] F. Cus and U. Zuperl, "Approach to optimization of cutting conditions by using artificial neural networks," *Journal of Materials Processing Technology*, vol. 173, no. 3, pp. 281–290, 2006.

[13] H. Zhang, Y. Sheng, and Z. Zeng, "Synchronization of coupled reaction-diffusion neural networks with directed topology via an adaptive approach," *IEEE Transactions on Neural Networks and Learning Systems*, pp. 1–12, 2017.

[14] C. Chen, F. L. Lewis, K. Xie, S. Xie, and Y. Liu, "Off-policy learning for adaptive optimal output synchronization of heterogeneous multi-agent systems," *Automatica*, vol. 119, p. 109081, 2020.

[15] P. Liu, Z. Zeng, and J. Wang, "Global synchronization of coupled fractional-order recurrent neural networks," *IEEE Transactions on Neural Networks and Learning Systems*, vol. 30, no. 8, pp. 2358–2368, 2019.

[16] Y. Chen, W. Yu, S. Tan, and H. Zhu, "Synchronizing nonlinear complex networks via switching disconnected topology," *Automatica*, vol. 70, pp. 189–194, 2016.

[17] J. Chen, B. Chen, and Z. Zeng, "Exponential quasi-synchronization of coupled delayed memristive neural networks via intermittent event-triggered control," *Neural Networks*, vol. 141, pp. 98–106, 2021.

[18] Y. Xu, J. Liu, and W. Li, "Quasi-synchronization of fractional-order multi-layer networks with mismatched parameters via delay-dependent impulsive feedback control," *Neural Networks*, vol. 150, pp. 43–57, 2022.

[19] J. Chen, B. Chen, and Z. Zeng, "Event-based synchronization for multiple neural networks with time delay and switching

disconnected topology," *IEEE Transactions on Cybernetics*, vol. 99, pp. 1–11, 2020.

[20] D. A. Hao, B. Jj, and Y. B. Li, "Event-triggered exponential synchronization of complex dynamical networks with cooperatively directed spanning tree topology," *Neurocomputing*, vol. 330, pp. 355–368, 2019.

[21] E. Arslan, R. Vadivel, M. Syed Ali, and S. Arik, "Event-triggeredH∞filtering for delayed neural networks via sampled-data," *Neural Networks*, vol. 91, pp. 11–21, 2017.

[22] R. Vadivel and Y. H. Joo, "Robust event-triggered TCS fuzzy system with successive time-delay signals and its application," *IET Control Theory & Applications*, vol. 14, no. 20, pp. 3697–3712, 2020.

[23] S. Wen, G. Guo, and B. Chen, "Event-triggered cooperative control of vehicle platoons in vehicular ad hoc networks," *Information ences*, pp. 341–353, 2018.

[24] J. Qiang and W. Tang, "Event-triggered protocol for the consensus of multi-agent systems with state-dependent nonlinear coupling[J]," *IEEE Transactions on Circuits and Systems I: Regular Papers*, vol. 65, no. 99, pp. 723–732, 2017.

[25] R. Vadivel, R. Suresh, P. Hammachukiattikul, B. Unyong, and N. Gunasekaran, "Event-triggered L_2–L_∞ filtering for network-based neutral systems with time-varying delays via T-S fuzzy approach," *IEEE Access*, vol. 9, pp. 145133–145147, 2021.

[26] R. Vadivel, P. Hammachukiattikul, G. Rajchakit, M. Syed Ali, and B. Unyong, "Finite-time event-triggered approach for recurrent neural networks with leakage term and its application," *Mathematics and Computers in Simulation*, vol. 182, pp. 765–790, 2021.

[27] Y. Tang, H. Gao, W. Zhang, and J. Kurths, "Leader-following consensus of a class of stochastic delayed multi-agent systems with partial mixed impulses," *Automatica*, vol. 53, pp. 346–354, 2015.

[28] L. Li, C. Li, and H. Li, "An analysis and design for time-varying structures dynamical networks via state constraint impulsive control," *International Journal of Control*, pp. 1–23, 2018.

[29] Y. Meng, Y. W. Wang, and J. W. Xiao, "Robust synchronization of impulsively-coupled complex switched networks with parametric uncertainties and time-varying delays," *Nonlinear Analysis: Real World Applications*, vol. 11, no. 4, pp. 3008–3020, 2010.

[30] C. Yi, C. Xu, J. Feng, J. Wang, and Y. Zhao, "Leading-following consensus for multi-agent systems with event-triggered delayed impulsive control," *IEEE Access*, vol. 7, pp. 136419–136427, 2019.

[31] W. Chen, W. Yang, and X. Lu, "Impulsive observer-based stabilisation of uncertain linear systems," *IET Control Theory & Applications*, vol. 8, no. 3, pp. 149–159, 2014.

[32] T. M. Guerra, H. Kerkeni, J. Lauber, and L. Vermeiren, "An e function for discrete T–S models: observer design," *IEEE Transactions on Fuzzy Systems*, vol. 20, no. 1, pp. 187–192, 2012.

[33] T. Raff and F. Allgower, "Observers with impulsive dynamical behavior for linear and nonlinear continuous-time systems," in *Proceedings of the 2007 46th IEEE conference on decision and control*, pp. 4287–4292, IEEE, New Orleans, LA, USA, 12-14 December 2007.

Hindawi
Complexity
Volume 2022, Article ID 6288054, 20 pages
https://doi.org/10.1155/2022/6288054

Research Article

Computation of the Complexity of Networks under Generalized Operations

Hafiz Usman Afzal,[1] **Muhammad Javaid**,[1] **Ali Ovais**,[2] **and Md Nur Alam**[3]

[1]*Department of Mathematics, School of Science, University of Management and Technology, Lahore 54770, Pakistan*
[2]*Department of Mathematics, University of Engineering and Technology, Lahore, Pakistan*
[3]*Department of Mathematics, Pabna University of Science and Technology, Pabna 6600, Bangladesh*

Correspondence should be addressed to Md Nur Alam; nuralam23@pust.ac.bd

Received 28 April 2022; Accepted 21 July 2022; Published 8 September 2022

Academic Editor: Miaomiao Wang

The connected and acyclic components contained in a network are identified by the computation of its complexity, where complexity of a network refers to the total number of spanning trees present within. The article in hand deals with the enumeration of the complexity of various networks' operations such as sum ($K_{2,n} + W_3$, $K_{2,n} + nK_1$, $K_n + S_n$), product ($K_{2,n} \boxtimes K_2$, $K_{2,n} \ltimes K_2$, $K_n \times K_2$, $K_n \boxtimes K_2$), difference ($K_{2,n} \ominus K_2$), and the conjunction of S_n with K_2. All our computations have been concluded by implementation of the methods of linear algebra and matrix theory. Our derivations will also be highlighted with the assistance of 3D plots at the end of this article.

1. Introduction

Only simple network $\mathbb{G} = (V(\mathbb{G}), E(\mathbb{G}))$ shall be dealt with throughout the paper. One of the most useful algebraic invariants is the complexity, i.e., number of spanning trees in a network admitting roots in combinatorics, algebraic graph theory, and networking. It is prominently linked with network engineering and particular branches of computer sciences that deal in the security designs specifically. Realistically, concreteness and precision in a network are based on the number of spanning trees it possesses. This indicates that complexity is an identifier for the quality of a network. Certain applications of complexity in different fields of mathematics and physics can be observed in [1–4]. For instance, we are living in an era of networking. The tools similar to complexity ensure the robustness and accuracy in a network so that one can obtain interruption free signals, since the complexity is an identifier of the number of connected and acyclic pathways present in a network, where every such pathway contains all junctions or vertices present in a network. So, this invariant helps in the enhancement of robustness of wireless sensor networks (WSNs) and other similar mobile networks by relating the total number of spanning trees present within. Another application of complexity can be observed in the security design of a sensitive area of a building. Say there are several secured chambers, and there are legitimate passages only to reach to those chambers. One legitimate passage can be identified by a unique pathway. That is, no cyclic pathway is allowed from one chamber to another. A programming-based software application will ensure if a visitor follows a legitimate passage or not through acyclic pathway mechanism, whereas such unique acyclic pathway is termed as complexity of the network.

1.1. Definitions and Preliminaries. The following lemma is a direct derivation of Temperley's equation mentioned previously.

Lemma 1 (see [5]). *Let $\mathbb{G}$ be ϱ order network; then,*

$$\tau(\mathbb{G}) = \frac{1}{\varrho^2} \det\left(\varrho I - D(\overline{\mathbb{G}}) + A(\overline{\mathbb{G}})\right), \tag{1}$$

where $\overline{\mathbb{G}} \cong \mathbb{G}$.

The above expression is more useful as it represents the complexity of $\mathbb{G}$ as the determinant of a particular matrix, rather than involving its eigenvalues. The eigenvalues based process is relatively difficult and complex.

The solution of the following iterative expression defines the first kind of Chebyshev polynomials.

$$\mathbb{T}_{\varrho+1}(x) - 2x\mathbb{T}_{\varrho}(x) + \mathbb{T}_{\varrho-1}(x) = 0; \mathbb{T}_0(x) = 1, \mathbb{T}_1(x) = x. \tag{2}$$

The standard solution of (2) gives

$$\mathbb{T}_{\varrho}(x) = \frac{1}{2}\left[\left(x + \sqrt{x^2-1}\right)^{\varrho} + \left(x - \sqrt{x^2-1}\right)^{\varrho}\right]; \varrho \geq 1. \tag{3}$$

The solution of the following iterative expression defines the second kind of Chebyshev polynomials.

$$\mathbb{U}_{\varrho+1}(x) - 2x\mathbb{U}_{\varrho}(x) + \mathbb{U}_{\varrho-1}(x) = 0; \mathbb{U}_0(x) = 1, \mathbb{U}_1(x) = x. \tag{4}$$

The standard solution of (4) gives

$$\mathbb{U}_m(z) = \frac{1}{2\sqrt{z^2-1}}\left[\left(z + \sqrt{z^2-1}\right)^{\varrho+1} - \left(z - \sqrt{z^2-1}\right)^{\varrho+1}\right]; \varrho \geq 1. \tag{5}$$

Identity (4) is valid $\forall z \in \mathbb{C}$ excluding $z = \pm 1$ [6]. The determinants are closely related to both 1^{st} and $2^{n\,d}$ kind Chebyshev Polynomials.where H_1 and H_2 are non-singular matrices.

Lemma 2 (see [7, 8]).

(i) $\forall \phi \geq 3$, $det[\mathbb{A}_m(\phi)] = 2[\mathbb{T}_m(\phi/2) - 1]$, *where*

$$\mathbb{A}_m(\phi) = \begin{pmatrix} \phi & -1 & 0 & 0 & \dots & 0 & 0 & 0 & -1 \\ -1 & \phi & -1 & 0 & \dots & 0 & 0 & 0 & 0 \\ 0 & -1 & \phi & -1 & \dots & 0 & 0 & 0 & 0 \\ 0 & 0 & -1 & \phi & \dots & 0 & 0 & 0 & 0 \\ \vdots & \vdots & \vdots & \vdots & \ddots & \vdots & \vdots & \vdots & \vdots \\ 0 & 0 & 0 & 0 & \dots & \phi & -1 & 0 & 0 \\ 0 & 0 & 0 & 0 & \dots & -1 & \phi & -1 & 0 \\ 0 & 0 & 0 & 0 & \dots & 0 & -1 & \phi & -1 \\ -1 & 0 & 0 & 0 & \dots & 0 & 0 & -1 & \phi \end{pmatrix}. \tag{6}$$

(i) $\forall \phi \geq 4$, $m \geq 3$, $det[\mathbb{B}_m(\phi)] = 2(\phi + m - 3)/\phi - 3[\mathbb{T}_m(\phi - 1/2) - 1]$, *where*

$$\mathbb{B}_m(\phi) = \begin{pmatrix} \phi & 0 & 1 & 1 & \dots & 1 & 1 & 1 & 0 \\ 0 & \phi & 0 & 1 & \dots & 1 & 1 & 1 & 1 \\ 1 & 0 & \phi & 0 & \dots & 1 & 1 & 1 & 1 \\ 1 & 1 & 0 & \phi & \dots & 1 & 1 & 1 & 1 \\ \vdots & \vdots & \vdots & \vdots & \ddots & \vdots & \vdots & \vdots & \vdots \\ 1 & 1 & 1 & 1 & \dots & \phi & 0 & 1 & 1 \\ 1 & 1 & 1 & 1 & \dots & 0 & \phi & 0 & 1 \\ 1 & 1 & 1 & 1 & \dots & 1 & 0 & \phi & 0 \\ 0 & 1 & 1 & 1 & \dots & 1 & 1 & 0 & \phi \end{pmatrix}. \tag{7}$$

(i) $\forall m, \phi$, $det[\mathbb{C}_m(\phi)] = (\phi - 1)\mathbb{U}_{m-1}(\phi + 1/2)$, *where*

$$\mathbb{C}_m(\phi) = \begin{pmatrix} \phi & -1 & 0 & 0 & \dots & 0 & 0 & 0 & 0 \\ -1 & \phi+1 & -1 & 0 & \dots & 0 & 0 & 0 & 0 \\ 0 & -1 & \phi+1 & -1 & \dots & 0 & 0 & 0 & 0 \\ 0 & 0 & -1 & \phi+1 & \dots & 0 & 0 & 0 & 0 \\ \vdots & \vdots & \vdots & \vdots & \ddots & \vdots & \vdots & \vdots & \vdots \\ 0 & 0 & 0 & 0 & \dots & \phi+1 & -1 & 0 & 0 \\ 0 & 0 & 0 & 0 & \dots & -1 & \phi+1 & -1 & 0 \\ 0 & 0 & 0 & 0 & \dots & 0 & -1 & \phi+1 & -1 \\ 0 & 0 & 0 & 0 & \dots & 0 & 0 & -1 & \phi \end{pmatrix}. \tag{8}$$

(i) $\forall \phi \geq 2$, $m \geq 3$, $det[\mathbb{D}_m(\phi)] = (m + \phi - 2)U_{m-1}(\phi/2)$, *where*

$$\mathbb{D}_m(\phi) = \begin{pmatrix} \phi & 0 & 1 & 1 & \dots & 1 & 1 & 1 & 1 \\ 0 & \phi+1 & 0 & 1 & \dots & 1 & 1 & 1 & 1 \\ 1 & 0 & \phi+1 & 0 & \dots & 1 & 1 & 1 & 1 \\ 1 & 1 & 0 & \phi+1 & \dots & 1 & 1 & 1 & 1 \\ \vdots & \vdots & \vdots & \vdots & \ddots & \vdots & \vdots & \vdots & \vdots \\ 1 & 1 & 1 & 1 & \dots & \phi+1 & 0 & 1 & 1 \\ 1 & 1 & 1 & 1 & \dots & 0 & \phi+1 & 0 & 1 \\ 1 & 1 & 1 & 1 & \dots & 1 & 0 & \phi+1 & 0 \\ 1 & 1 & 1 & 1 & \dots & 1 & 1 & 0 & \phi \end{pmatrix}. \tag{9}$$

Lemma 3 (see [9]). $\forall \phi$ *and* m, $det[\mathbb{W}_m(\phi)] = (\phi + m - 1)(\phi - 1)^{m-1}$, *where*$\mathbb{W}_m(\phi)$*is an*$m \times m$*circulant matrix given as*

$$\mathbb{W}_m(\phi) = \begin{pmatrix} \phi & 1 & 1 & 1 & \ldots & 1 & 1 & 1 & 1 \\ 1 & \phi & 1 & 1 & \ldots & 1 & 1 & 1 & 1 \\ 1 & 1 & \phi & 1 & \ldots & 1 & 1 & 1 & 1 \\ 1 & 1 & 1 & \phi & \ldots & 1 & 1 & 1 & 1 \\ \vdots & \vdots & \vdots & \vdots & \ddots & \vdots & \vdots & \vdots & \vdots \\ 1 & 1 & 1 & 1 & \ldots & \phi & 1 & 1 & 1 \\ 1 & 1 & 1 & 1 & \ldots & 1 & \phi & 1 & 1 \\ 1 & 1 & 1 & 1 & \ldots & 1 & 1 & \phi & 1 \\ 1 & 1 & 1 & 1 & \ldots & 1 & 1 & 1 & \phi \end{pmatrix}. \tag{10}$$

Lemma 4 (see [10]). *Let H_1, H_2, H_3, andH_4be the block matrices of orders$\theta \times \theta$, $\theta \times \vartheta$, $\vartheta \times \theta$, and$\vartheta \times \vartheta$, respectively. Then,*

$$\begin{aligned} \det\begin{pmatrix} H_1 & H_2 \\ H_3 & H_4 \end{pmatrix} &= \det\left(H_4 - H_3 H_1^{-1} H_2\right) \times \det\left(H_1\right) \\ &= \det\left(H_1 - H_2 H_4^{-1} H_3\right) \times \det\left(H_4\right), \end{aligned} \tag{11}$$

Lemma 5 (see [11]). *For $\phi \geq 5$, let us consider a circulant matrix given as*

$$E_\phi = \begin{pmatrix} \zeta & \eta & 1 & 0 & \ldots & 0 & 0 & 1 & \eta \\ \eta & \zeta & \eta & 1 & \ldots & 0 & 0 & 0 & 1 \\ 1 & \eta & \zeta & \eta & \ldots & 0 & 0 & 0 & 0 \\ 0 & 1 & \eta & \zeta & \ldots & 0 & 0 & 0 & 0 \\ \vdots & \vdots & \vdots & \vdots & \ddots & \vdots & \vdots & \vdots & \vdots \\ 0 & 0 & 0 & 0 & \ldots & \zeta & \eta & 1 & 0 \\ 0 & 0 & 0 & 0 & \ldots & \eta & \zeta & \eta & 1 \\ 1 & 0 & 0 & 0 & \ldots & 1 & \eta & \zeta & \eta \\ \eta & 1 & 0 & 0 & \ldots & 0 & 1 & \eta & \zeta \end{pmatrix}_{\phi \times \phi}, \tag{12}$$

$$\tau\left(E_\phi\right) = \begin{cases} \left[\zeta^2 + 4\left(\zeta - \eta^2 + 1\right)\right] \prod_{i=1}^{\frac{\phi}{2}-1} \left[\zeta + 2\eta \cos\left(\frac{2\pi i}{\phi}\right) + 2 \cos\left(\frac{4\pi i}{\phi}\right)\right]^2 : & \text{for even } \phi; \\ \left[\zeta + 2\left(\eta + 1\right)\right] \prod_{i=1}^{\lfloor \frac{\phi}{2} \rfloor} \left[\zeta + 2\eta \cos\left(\frac{2\pi i}{\phi}\right) + 2 \cos\left(\frac{4\pi i}{\phi}\right)\right]^2 : & \text{for odd } \phi. \end{cases} \tag{13}$$

We shall also provide a few definitions [12, 13] in Section 3 before a certain result, where necessary. Throughout the article, $\overline{G}$ represents the complement of the network G.

1.2. Main Contributions. In the present article, we will mainly compute the closed formulae for the complexity of various generalized operations on graphs such as sum ($K_{2,n} + W_3$, $K_{2,n} + nK_1$, $K_n + S_n$), product ($K_{2,n} \boxtimes K_2$, $K_{2,n} \ltimes K_2$, $K_n \times K_2$, $K_n \boxtimes K_2$), difference ($K_{2,n} \ominus K_2$), and the conjunction of S_n with K_2. Furthermore, all our computations have been concluded by implementation of the methods of linear algebra and matrix theory.

1.3. Main Structure. The main structure of this article is as follows:

1. Section 1 comprises the introduction and preliminaries of our main work.
2. Section 2 contains the salient work related to our derivations.
3. Section 3 consists of the main derivations we have obtained in the form of the complexities of various networks' operations.
4. Section 4 contains a brief summary and graphical illustrations of our work.
5. Section 5 gives the conclusion and also tells about the future work related to this paper.

2. Related Work

If we talk about the closed formulae for the complexity of an infinite family of networks, we shall not be able to locate any such generalized result. Although it is still possible to derive the new closed formulae of the complexity of classes of networks having order m, where m is sufficiently large, it is

useful to obtain this invariant for the networks of finite order for the values as we increase the order of a network. If we look into the historical development of this concept, the calculation of the complexity of the complete network as $\tau(K_\beta) = \beta^{\beta-2}$ is the foremost concept that appeared in [14]. The second prominent result in this regard is the complexity of the complete bipartite network which is again derived by Cayley [14] as $\tau(K_{\mu,\nu}) = \mu^{\nu-1}\nu^{\mu-1}$. In [15], the closed formula for the complexity of Mobius ladder has been obtained as $\tau(M_\chi) = \chi/2[(2+\sqrt{3})^\chi + (2-\sqrt{\chi})^\chi + 2]$ for $\chi \geq 2$ in [15].

The determination of the total spanning trees of a network has recently reappeared as an active topic. Kirchhoff's matrix tree theorem [16] is a prominent result in this regard. It represents the complexity of a network as the determinant of a random cofactor of its Kirchhoff's matrix, where, say for a network $\mathbb{G}$, $K(\mathbb{G})$ = degree matrix of $\mathbb{G}$ – adjacency matrix of $\mathbb{G}$ indicates its Kirchhoff's matrix.

A combinatorial method for computing the complexity of a network is with the use of contraction-deletion theorem. As an iterative process for an edge $uv \in E(\mathbb{G})$, the complexity of $\mathbb{G}$ is the sum of $\tau(\mathbb{G}|uv)$ and $\tau(\mathbb{G} - uv)$. Here, $\mathbb{G}|uv$ is the network derived as the result of contraction of uv in $\mathbb{G}$ repeatedly until the end points u and v coincide [17].

In [18], the self-adapted task scheduling strategies in the wireless sensor networks have been designed and analyzed. Wang et al. [19] discussed the ant colony optimization-based location-aware routing for wireless sensor networks. In [20], a pedestrian detection method has been designed and examined based on the genetic algorithm for optimizing XGBoost training parameters. For wireless sensor networks, Wan and Xiong designed and assessed an energy-efficient sleep scheduling mechanism with similarity measure [21]. Lu et al. in [22] explored a finger vein-based personal authentication mechanism for Internet-related security. Furthermore, in [23, 24], some latest work on the enumeration of the complexity of networks can be observed.

3. Main Results

In networking, the characteristic of developing new structures from the existing ones through network operations and studying their various properties always remains active. The present section addresses our main derivations consisting of the closed formulae of the complexity of various networks obtained as the result of network operations.

Theorem 1. *For all n, the complexity of the network $K_{2,n} + W_3$ is given by*

$$\tau\left(K_{2,n} + W_3\right) = 6^{n-1}(n+4)(n+6)^4. \tag{14}$$

Proof. Consider the network $K_{2,n} + W_3$ with $|V(K_{2,n} + W_3)| = n + 6$ and $|E(K_{2,n} + W_3)| = 6n + 14$ (see the general formation in Figure 1).

Applying Lemma 1, we have

$$\tau\left(K_{2,n} + W_3\right) = \frac{1}{(n+6)^2}\det\left[(n+6)I - \overline{D} + \overline{A}\right]$$

$$= \frac{1}{(n+6)^2}\det\begin{pmatrix}
n+6 & 0 & 0 & 0 & 0 & 0 & 0 & 0 & 0 & 0 & \dots & 0 & 0 & 0 & 0 \\
0 & n+6 & 0 & 0 & 0 & 0 & 0 & 0 & 0 & 0 & \dots & 0 & 0 & 0 & 0 \\
0 & 0 & n+6 & 0 & 0 & 0 & 0 & 0 & 0 & 0 & \dots & 0 & 0 & 0 & 0 \\
0 & 0 & 0 & n+6 & 0 & 0 & 0 & 0 & 0 & 0 & \dots & 0 & 0 & 0 & 0 \\
0 & 0 & 0 & 0 & n+5 & 1 & 0 & 0 & 0 & 0 & \dots & 0 & 0 & 0 & 0 \\
0 & 0 & 0 & 0 & 1 & n+5 & 0 & 0 & 0 & 0 & \dots & 0 & 0 & 0 & 0 \\
0 & 0 & 0 & 0 & 0 & 0 & 7 & 1 & 1 & 1 & \dots & 1 & 1 & 1 & 1 \\
0 & 0 & 0 & 0 & 0 & 0 & 1 & 7 & 1 & 1 & \dots & 1 & 1 & 1 & 1 \\
0 & 0 & 0 & 0 & 0 & 0 & 1 & 1 & 7 & 1 & \dots & 1 & 1 & 1 & 1 \\
0 & 0 & 0 & 0 & 0 & 0 & 1 & 1 & 1 & 7 & \dots & 1 & 1 & 1 & 1 \\
\vdots & \vdots & \vdots & \vdots & \vdots & \vdots & \vdots & \vdots & \vdots & \vdots & \ddots & \vdots & \vdots & \vdots & \vdots \\
0 & 0 & 0 & 0 & 0 & 0 & 1 & 1 & 1 & 1 & \dots & 7 & 1 & 1 & 1 \\
0 & 0 & 0 & 0 & 0 & 0 & 1 & 1 & 1 & 1 & \dots & 1 & 7 & 1 & 1 \\
0 & 0 & 0 & 0 & 0 & 0 & 1 & 1 & 1 & 1 & \dots & 1 & 1 & 7 & 1 \\
0 & 0 & 0 & 0 & 0 & 0 & 1 & 1 & 1 & 1 & \dots & 1 & 1 & 1 & 7
\end{pmatrix}_{(n+6)\times(n+6)}. \tag{15}$$

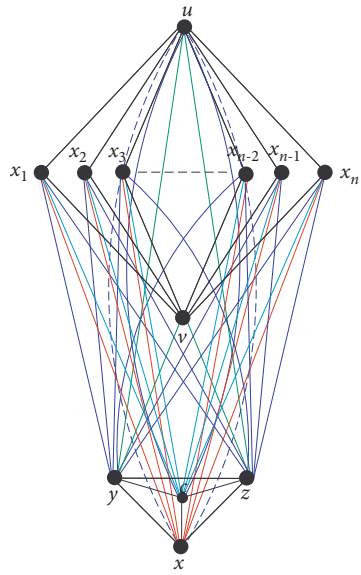

Figure 1: The network $K_{2,n} + W_3$.

Now on the above determinant, we perform the following operations simultaneously:

(i) Adding all columns to C_1.

(ii) From C1, we take the number n+5 as common.

(iii) Subtracting C_1 from all columns.

(iv) Expanding along R_1.

This yields

$$= \det \begin{pmatrix} n+5 & -1 & -1 & -1 & -1 & -1 & -1 & -1 & -1 & \ldots & -1 & -1 & -1 & -1 \\ -1 & n+5 & -1 & -1 & -1 & -1 & -1 & -1 & -1 & \ldots & -1 & -1 & -1 & -1 \\ -1 & -1 & n+5 & -1 & -1 & -1 & -1 & -1 & -1 & \ldots & -1 & -1 & -1 & -1 \\ -1 & -1 & -1 & n+4 & 0 & -1 & -1 & -1 & -1 & \ldots & -1 & -1 & -1 & -1 \\ -1 & -1 & -1 & 0 & n+4 & -1 & -1 & -1 & -1 & \ldots & -1 & -1 & -1 & -1 \\ -1 & -1 & -1 & -1 & -1 & 6 & 0 & 0 & 0 & \ldots & 0 & 0 & 0 & 0 \\ -1 & -1 & -1 & -1 & -1 & 0 & 6 & 0 & 0 & \ldots & 0 & 0 & 0 & 0 \\ -1 & -1 & -1 & -1 & -1 & 0 & 0 & 6 & 0 & \ldots & 0 & 0 & 0 & 0 \\ -1 & -1 & -1 & -1 & -1 & 0 & 0 & 0 & 6 & \ldots & 0 & 0 & 0 & 0 \\ \vdots & \vdots & \vdots & \vdots & \vdots & \vdots & \vdots & \vdots & \vdots & \ddots & \vdots & \vdots & \vdots & \vdots \\ -1 & -1 & -1 & -1 & -1 & 0 & 0 & 0 & 0 & \ldots & 6 & 0 & 0 & 0 \\ -1 & -1 & -1 & -1 & -1 & 0 & 0 & 0 & 0 & \ldots & 0 & 6 & 0 & 0 \\ -1 & -1 & -1 & -1 & -1 & 0 & 0 & 0 & 0 & \ldots & 0 & 0 & 6 & 0 \\ -1 & -1 & -1 & -1 & -1 & 0 & 0 & 0 & 0 & \ldots & 0 & 0 & 0 & 6 \end{pmatrix}_{(n+5)\times(n+5)}, \tag{16}$$

$$\Rightarrow \tau\left(K_{2,n} + W_3\right) = \det \begin{pmatrix} P_{5\times 5} & Q_{5\times n} \\ R_{n\times 5} & S_{n\times n} \end{pmatrix}_{(n+5)\times(n+5)}.$$

By using Lemma 4, we get

$$\tau\left(K_{2,n}+W_3\right)=\det(S).\det\left(P-QS^{-1}R\right)$$

$$=6^n\left(\frac{1}{6}\right)^5(-1)^5\det\begin{pmatrix}-5n-30 & n+6 & n+6 & n+6 & n+6\\ n+6 & -5n-30 & n+6 & n+6 & n+6\\ n+6 & n+6 & -5n-30 & n+6 & n+6\\ n+6 & n+6 & n+6 & -5n-24 & n\\ n+6 & n+6 & n+6 & n & -5n-24\end{pmatrix}. \tag{17}$$

Evaluating and simplifying, we obtain $\tau(K_{2,n}+W_3)=6^{n-1}(n+4)(n+6)^4$. □

Theorem 2. *For all n, the complexity of the strong product $K_{2,n}\boxtimes K_2$ is given by*

$$\tau\left(K_{2,n}\boxtimes K_2\right)=(24)^n\left(2\left(n^3+2n^2+n\right)\right). \tag{18}$$

Proof. Consider the network $K_{2,n})K_2$ with $|V(K_{2,n})K_2)|=2n+4$ and $|E(K_{2,n})K_2)|=9n+2$ (see the general formation in Figure 2).

Applying Lemma 1, we have

$$\tau\left(K_{2,n}\boxtimes K_2\right)=\frac{1}{(2n+4)^2}\det\left[(2n+4)I-\overline{D}+\overline{A}\right]$$

$$=\frac{1}{(n+6)^2}\det\begin{pmatrix}
n+6 & 0 & 0 & 0 & 0 & 0 & 0 & 0 & 0 & 0 & \dots & 0 & 0 & 0 & 0\\
0 & n+6 & 0 & 0 & 0 & 0 & 0 & 0 & 0 & 0 & \dots & 0 & 0 & 0 & 0\\
0 & 0 & n+6 & 0 & 0 & 0 & 0 & 0 & 0 & 0 & \dots & 0 & 0 & 0 & 0\\
0 & 0 & 0 & n+6 & 0 & 0 & 0 & 0 & 0 & 0 & \dots & 0 & 0 & 0 & 0\\
0 & 0 & 0 & 0 & n+5 & 1 & 0 & 0 & 0 & 0 & \dots & 0 & 0 & 0 & 0\\
0 & 0 & 0 & 0 & 1 & n+5 & 0 & 0 & 0 & 0 & \dots & 0 & 0 & 0 & 0\\
0 & 0 & 0 & 0 & 0 & 0 & 7 & 1 & 1 & 1 & \dots & 1 & 1 & 1 & 1\\
0 & 0 & 0 & 0 & 0 & 0 & 1 & 7 & 1 & 1 & \dots & 1 & 1 & 1 & 1\\
0 & 0 & 0 & 0 & 0 & 0 & 1 & 1 & 7 & 1 & \dots & 1 & 1 & 1 & 1\\
0 & 0 & 0 & 0 & 0 & 0 & 1 & 1 & 1 & 7 & \dots & 1 & 1 & 1 & 1\\
\vdots & \vdots & \vdots & \vdots & \vdots & \vdots & \vdots & \vdots & \vdots & \vdots & \ddots & \vdots & \vdots & \vdots & \vdots\\
0 & 0 & 0 & 0 & 0 & 0 & 1 & 1 & 1 & 1 & \dots & 7 & 1 & 1 & 1\\
0 & 0 & 0 & 0 & 0 & 0 & 1 & 1 & 1 & 1 & \dots & 1 & 7 & 1 & 1\\
0 & 0 & 0 & 0 & 0 & 0 & 1 & 1 & 1 & 1 & \dots & 1 & 1 & 7 & 1\\
0 & 0 & 0 & 0 & 0 & 0 & 1 & 1 & 1 & 1 & \dots & 1 & 1 & 1 & 7
\end{pmatrix}_{(n+6)\times(n+6)}$$

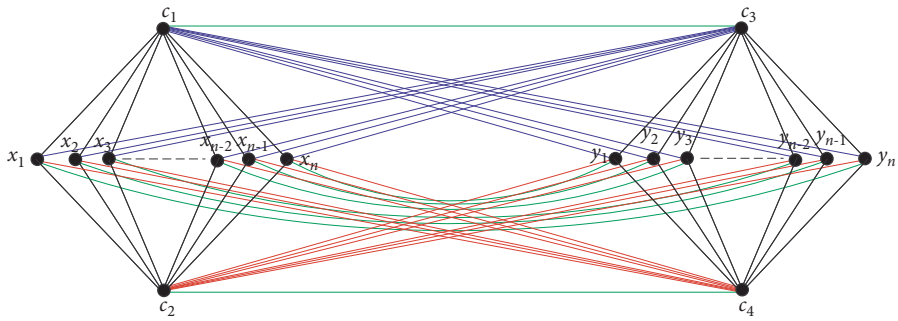

Figure 2: The strong product $K_{2,n}\boxtimes K_2$.

$$= \det \begin{pmatrix} n+5 & -1 & -1 & -1 & -1 & -1 & -1 & -1 & -1 & \dots & -1 & -1 & -1 & -1 \\ -1 & n+5 & -1 & -1 & -1 & -1 & -1 & -1 & -1 & \dots & -1 & -1 & -1 & -1 \\ -1 & -1 & n+5 & -1 & -1 & -1 & -1 & -1 & -1 & \dots & -1 & -1 & -1 & -1 \\ -1 & -1 & -1 & n+4 & 0 & -1 & -1 & -1 & -1 & \dots & -1 & -1 & -1 & -1 \\ -1 & -1 & -1 & 0 & n+4 & -1 & -1 & -1 & -1 & \dots & -1 & -1 & -1 & -1 \\ -1 & -1 & -1 & -1 & -1 & 6 & 0 & 0 & 0 & \dots & 0 & 0 & 0 & 0 \\ -1 & -1 & -1 & -1 & -1 & 0 & 6 & 0 & 0 & \dots & 0 & 0 & 0 & 0 \\ -1 & -1 & -1 & -1 & -1 & 0 & 0 & 6 & 0 & \dots & 0 & 0 & 0 & 0 \\ -1 & -1 & -1 & -1 & -1 & 0 & 0 & 0 & 6 & \dots & 0 & 0 & 0 & 0 \\ \vdots & \vdots & \vdots & \vdots & \vdots & \vdots & \vdots & \vdots & \vdots & \ddots & \vdots & \vdots & \vdots & \vdots \\ -1 & -1 & -1 & -1 & -1 & 0 & 0 & 0 & 0 & \dots & 6 & 0 & 0 & 0 \\ -1 & -1 & -1 & -1 & -1 & 0 & 0 & 0 & 0 & \dots & 0 & 6 & 0 & 0 \\ -1 & -1 & -1 & -1 & -1 & 0 & 0 & 0 & 0 & \dots & 0 & 0 & 6 & 0 \\ -1 & -1 & -1 & -1 & -1 & 0 & 0 & 0 & 0 & \dots & 0 & 0 & 0 & 6 \end{pmatrix}_{(n+5)\times(n+5)},$$

$$\Rightarrow \tau\left(K_{2,n}\boxtimes K_2\right) = \det \begin{pmatrix} P_{3\times 3} & Q_{3\times 2n} \\ R_{2n\times 3} & S_{2n\times 2n} \end{pmatrix}_{(2n+3)\times(2n+3)}. \tag{19}$$

By using Lemma 4, we get

$$\tau\left(K_{2,n}\boxtimes K_2\right) = \det(S).\det\left(P - QS^{-1}R\right)$$

$$= 5^n\left(\frac{24}{5}\right)^n \det \begin{pmatrix} \frac{3n+2}{2} & \frac{-n}{2} & \frac{-n-2}{2} \\ \frac{-n}{2} & \frac{3n+2}{2} & \frac{-n}{2} \\ \frac{-n-2}{2} & \frac{-n}{2} & \frac{3n+2}{2} \end{pmatrix}. \tag{20}$$

Evaluating the above determinant, we obtain finally $\Rightarrow \tau(K_{2,n}\boxtimes K_2) = (24)^n(2(n^3 + 2n^2 + n))$. □

Theorem 3. *For all n , the complexity of the homomorphic product $K_{2,n}\ltimes K_2 \cong K_{2,n} \times K_2$ is given by*

$$\tau\left(K_{2,n}\ltimes K_2\right) = 8^{n-1}\left(n^3 + 6n^2 + 8n\right). \tag{21}$$

Proof. Consider the network $K_{2,n}\ltimes K_2$ with $|V(K_{2,n}\ltimes K_2)| = 2n + 4$ and $|E(K_{2,n}\ltimes K_2)| = 5n + 2$ (see the general formation in Figure 3).

Applying Lemma 1, we have

$$\tau\left(K_{2,n}\ltimes K_2\right)=\frac{1}{(2n+4)^2}\det\left[(2n+4)I-\overline{D}+\overline{A}\right]$$

$$=\det\begin{pmatrix}
n+5 & -1 & -1 & -1 & -1 & -1 & -1 & -1 & -1 & \ldots & -1 & -1 & -1 & -1\\
-1 & n+5 & -1 & -1 & -1 & -1 & -1 & -1 & -1 & \ldots & -1 & -1 & -1 & -1\\
-1 & -1 & n+5 & -1 & -1 & -1 & -1 & -1 & -1 & \ldots & -1 & -1 & -1 & -1\\
-1 & -1 & -1 & n+4 & 0 & -1 & -1 & -1 & -1 & \ldots & -1 & -1 & -1 & -1\\
-1 & -1 & -1 & 0 & n+4 & -1 & -1 & -1 & -1 & \ldots & -1 & -1 & -1 & -1\\
-1 & -1 & -1 & -1 & -1 & 6 & 0 & 0 & 0 & \ldots & 0 & 0 & 0 & 0\\
-1 & -1 & -1 & -1 & -1 & 0 & 6 & 0 & 0 & \ldots & 0 & 0 & 0 & 0\\
-1 & -1 & -1 & -1 & -1 & 0 & 0 & 6 & 0 & \ldots & 0 & 0 & 0 & 0\\
-1 & -1 & -1 & -1 & -1 & 0 & 0 & 0 & 6 & \ldots & 0 & 0 & 0 & 0\\
\vdots & \vdots & \vdots & \vdots & \vdots & \vdots & \vdots & \vdots & \vdots & \ddots & \vdots & \vdots & \vdots & \vdots\\
-1 & -1 & -1 & -1 & -1 & 0 & 0 & 0 & 0 & \ldots & 6 & 0 & 0 & 0\\
-1 & -1 & -1 & -1 & -1 & 0 & 0 & 0 & 0 & \ldots & 0 & 6 & 0 & 0\\
-1 & -1 & -1 & -1 & -1 & 0 & 0 & 0 & 0 & \ldots & 0 & 0 & 6 & 0\\
-1 & -1 & -1 & -1 & -1 & 0 & 0 & 0 & 0 & \ldots & 0 & 0 & 0 & 6
\end{pmatrix}_{(n+5)\times(n+5)} \tag{22}$$

$$=6^n\left(\frac{1}{6}\right)^5(-1)^5\det\begin{pmatrix}
-5n-30 & n+6 & n+6 & n+6 & n+6\\
n+6 & -5n-30 & n+6 & n+6 & n+6\\
n+6 & n+6 & -5n-30 & n+6 & n+6\\
n+6 & n+6 & n+6 & -5n-24 & n\\
n+6 & n+6 & n+6 & n & -5n-24
\end{pmatrix},$$

$$\Rightarrow\tau\left(K_{2,n}<\text{imes}K_2\right)=\det\begin{pmatrix}P_{3\times3} & Q_{3\times2n}\\ R_{2n\times3} & S_{2n\times2n}\end{pmatrix}_{(2n+3)\times(2n+3)}.$$

By using Lemma 4, we get

$$\tau\left(K_{2,n}\ltimes K_2\right)=\det(S).\det\left(P-QS^{-1}R\right)$$

$$=8^n\left(\frac{1}{8}\right)^3\det\begin{pmatrix}5n+8 & -n & -n-8\\ -n & 5n+8 & -3n\\ -n-8 & -3n & 5n+8\end{pmatrix}. \tag{23}$$

Evaluating the above determinant and simplifying, we obtain finally $\Rightarrow\tau(K_{2,n}\ltimes K_2)=8^{n-1}(n^3+6n^2+8n)$. □

Theorem 4. *For all n, the complexity of the mirror network $K_{2,n}+nK_1$ is given as*

$$\tau\left(K_{2,n}+nK_1\right)=4n(n+1)(n+2)^{2n-2}. \tag{24}$$

Proof. Consider the network $K_{2,n}+nK_1$ with $|V(K_{2,n}+nK_1)|=2n+2$ and $|E(K_{2,n}+nK_1)|=n^2+4n$ (see Figure 4).

Applying Lemma 1, we have

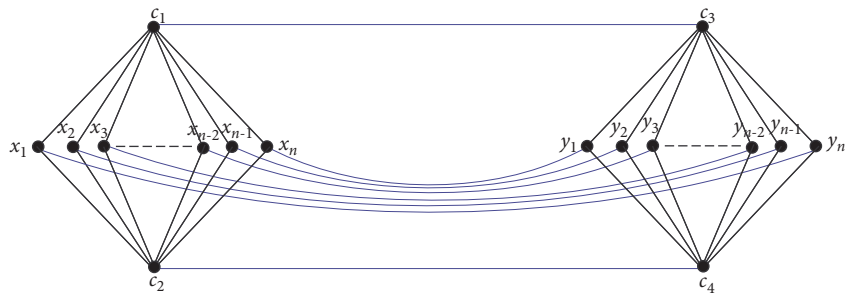

Figure 3: The homomorphic product $K_{2,n} \ltimes K_2$.

$$\tau\left(K_{2,n} + nK_1\right) = \frac{1}{(2n+2)^2}\det\left[(2n+2)I - \overline{D} + \overline{A}\right]$$

$$= \frac{1}{(2n+2)^2}$$

$$\det\begin{pmatrix}
2n+1 & 1 & 0 & 0 & 0 & \dots & 0 & 0 & 0 & 0 & 0 & 0 & \dots & 0 & 0 & 0 \\
1 & 2n+1 & 0 & 0 & 0 & \dots & 0 & 0 & 0 & 0 & 0 & 0 & \dots & 0 & 0 & 0 \\
0 & 0 & n+3 & 1 & 1 & \dots & 1 & 1 & 1 & 0 & 0 & 0 & \dots & 0 & 0 & 0 \\
0 & 0 & 1 & n+3 & 1 & \dots & 1 & 1 & 1 & 0 & 0 & 0 & \dots & 0 & 0 & 0 \\
0 & 0 & 1 & 1 & n+3 & \dots & 1 & 1 & 1 & 0 & 0 & 0 & \dots & 0 & 0 & 0 \\
\vdots & \vdots & \vdots & \vdots & \vdots & \ddots & \vdots & \vdots & \vdots & \vdots & \vdots & \vdots & \ddots & \vdots & \vdots & \vdots \\
0 & 0 & 1 & 1 & 1 & \dots & n+3 & 1 & 1 & 0 & 0 & 0 & \dots & 0 & 0 & 0 \\
0 & 0 & 1 & 1 & 1 & \dots & 1 & n+3 & 1 & 0 & 0 & 0 & \dots & 0 & 0 & 0 \\
0 & 0 & 1 & 1 & 1 & \dots & 1 & 1 & n+3 & 0 & 0 & 0 & \dots & 0 & 0 & 0 \\
0 & 0 & 0 & 0 & 0 & \dots & 0 & 0 & 0 & n+3 & 1 & 1 & \dots & 1 & 1 & 1 \\
0 & 0 & 0 & 0 & 0 & \dots & 0 & 0 & 0 & 1 & n+3 & 1 & \dots & 1 & 1 & 1 \\
0 & 0 & 0 & 0 & 0 & \dots & 0 & 0 & 0 & 1 & 1 & n+3 & \dots & 1 & 1 & 1 \\
\vdots & \vdots & \vdots & \vdots & \vdots & \ddots & \vdots & \vdots & \vdots & \vdots & \vdots & \vdots & \ddots & \vdots & \vdots & \vdots \\
0 & 0 & 0 & 0 & 0 & \dots & 0 & 0 & 0 & 1 & 1 & 1 & \dots & n+3 & 1 & 1 \\
0 & 0 & 0 & 0 & 0 & \dots & 0 & 0 & 0 & 1 & 1 & 1 & \dots & 1 & n+3 & 1 \\
0 & 0 & 0 & 0 & 0 & \dots & 0 & 0 & 0 & 1 & 1 & 1 & \dots & 1 & 1 & n+3
\end{pmatrix}$$

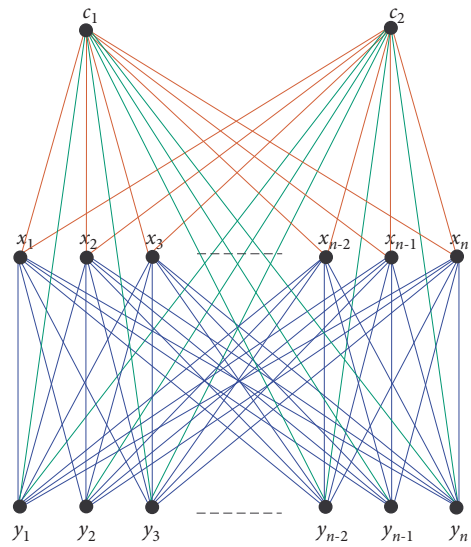

FIGURE 4: The network $K_{2,n} + nK_1$.

$$= \det \begin{pmatrix} 2n & -1 & -1 & -1 & \cdots & -1 & -1 & -1 & -1 & -1 & -1 & \cdots & -1 & -1 & -1 \\ -1 & n+2 & 0 & 0 & \cdots & 0 & 0 & 0 & -1 & -1 & -1 & \cdots & -1 & -1 & -1 \\ -1 & 0 & n+2 & 0 & \cdots & 0 & 0 & 0 & -1 & -1 & -1 & \cdots & -1 & -1 & -1 \\ -1 & 0 & 0 & n+2 & \cdots & 0 & 0 & 0 & -1 & -1 & -1 & \cdots & -1 & -1 & -1 \\ \vdots & \vdots & \vdots & \vdots & \ddots & \vdots & \vdots & \vdots & \vdots & \vdots & \vdots & \ddots & \vdots & \vdots & \vdots \\ -1 & 0 & 0 & 0 & \cdots & n+2 & 0 & 0 & -1 & -1 & -1 & \cdots & -1 & -1 & -1 \\ -1 & 0 & 0 & 0 & \cdots & 0 & n+2 & 0 & -1 & -1 & -1 & \cdots & -1 & -1 & -1 \\ -1 & 0 & 0 & 0 & \cdots & 0 & 0 & n+2 & -1 & -1 & -1 & \cdots & -1 & -1 & -1 \\ -1 & -1 & -1 & -1 & \cdots & -1 & -1 & -1 & n+2 & 0 & 0 & \cdots & 0 & 0 & 0 \\ -1 & -1 & -1 & -1 & \cdots & -1 & -1 & -1 & 0 & n+2 & 0 & \cdots & 0 & 0 & 0 \\ -1 & -1 & -1 & -1 & \cdots & -1 & -1 & -1 & 0 & 0 & n+2 & \cdots & 0 & 0 & 0 \\ \vdots & \vdots & \vdots & \vdots & \ddots & \vdots & \vdots & \vdots & \vdots & \vdots & \vdots & \ddots & \vdots & \vdots & \vdots \\ -1 & -1 & -1 & -1 & \cdots & -1 & -1 & -1 & 0 & 0 & 0 & \cdots & n+2 & 0 & 0 \\ -1 & -1 & -1 & -1 & \cdots & -1 & -1 & -1 & 0 & 0 & 0 & \cdots & 0 & n+2 & 0 \\ -1 & -1 & -1 & -1 & \cdots & -1 & -1 & -1 & 0 & 0 & 0 & \cdots & 0 & 0 & n+2 \end{pmatrix}_{(2n+1)\times(2n+1)},$$

$$\Rightarrow \tau\left(K_{2,n} + nK_1\right) = \det \begin{pmatrix} P_{1\times 1} & Q_{1\times 2n} \\ R_{2n\times 1} & S_{2n\times 2n} \end{pmatrix}_{(2n+1)\times(2n+1)}. \tag{25}$$

By using Lemma 4, we have

$$\tau\left(K_{2,n}+nK_1\right)=\det(S).\det\left(P-QS^{-1}R\right)$$
$$=3^n\times\det\begin{bmatrix}\frac{2n+3}{3} & \frac{-n}{3}\\ \frac{-n}{3} & \frac{2n+3}{3}\end{bmatrix}. \quad (26)$$

Simplification finally gives $\tau(K_{2,n}+nK_1)=4n(n+1)(n+2)^{2n-2}$. □

Theorem 5. *For all n, the complexity of the cartesian product $K_n\times K_2$ is given as*

$$\tau\left(K_n\times K_2\right)=n^{n-2}(n+2)^{n-1}. \quad (27)$$

Proof. Consider thenetwork $K_n\times K_2$ with $|V(K_n\times K_2)|=2n$ and $|E(K_n\times K_2)|=n^2$ (see Figure 5).

Applying Lemma 1, we have

$$\tau\left(K_n\times K_2\right)=\frac{1}{(2n)^2}\det\left[(2n)I-\overline{D}+\overline{A}\right]$$
$$=\frac{1}{(2n)^2}\det\begin{pmatrix}
n+1 & 0 & 0 & \dots & 0 & 0 & 0 & 0 & 1 & 1 & \dots & 1 & 1 & 1\\
0 & n+1 & 0 & \dots & 0 & 0 & 0 & 1 & 0 & 1 & \dots & 1 & 1 & 1\\
0 & 0 & n+1 & \dots & 0 & 0 & 0 & 1 & 1 & 0 & \dots & 1 & 1 & 1\\
\vdots & \vdots & \vdots & \ddots & \vdots & \vdots & \vdots & \vdots & \vdots & \vdots & \ddots & \vdots & \vdots & \vdots\\
0 & 0 & 0 & \dots & n+1 & 0 & 0 & 1 & 1 & 1 & \dots & 0 & 1 & 1\\
0 & 0 & 0 & \dots & 0 & n+1 & 0 & 1 & 1 & 1 & \dots & 1 & 0 & 1\\
0 & 0 & 0 & \dots & 0 & 0 & n+1 & 1 & 1 & 1 & \dots & 1 & 1 & 0\\
0 & 1 & 1 & \dots & 1 & 1 & 1 & n+1 & 0 & 0 & \dots & 0 & 0 & 0\\
1 & 0 & 1 & \dots & 1 & 1 & 1 & 0 & n+1 & 0 & \dots & 0 & 0 & 0\\
1 & 1 & 0 & \dots & 1 & 1 & 1 & 0 & 0 & n+1 & \dots & 0 & 0 & 0\\
\vdots & \vdots & \vdots & \ddots & \vdots & \vdots & \vdots & \vdots & \vdots & \vdots & \ddots & \vdots & \vdots & \vdots\\
1 & 1 & 1 & \dots & 0 & 1 & 1 & 0 & 0 & 0 & \dots & n+1 & 0 & 0\\
1 & 1 & 1 & \dots & 1 & 0 & 1 & 0 & 0 & 0 & \dots & 0 & n+1 & 0\\
1 & 1 & 1 & \dots & 1 & 1 & 0 & 0 & 0 & 0 & \dots & 0 & 0 & n+1
\end{pmatrix}_{2n\times 2n}, \quad (28)$$

$$\Rightarrow\tau\left(K_n\times K_2\right)=\frac{1}{(2n)^2}\det\begin{pmatrix}P_{n\times n} & Q_{n\times n}\\ R_{n\times n} & S_{n\times n}\end{pmatrix}_{2n\times 2n}.$$

By using Lemma 4, we have

$$\tau(K_n \times K_2) = \frac{1}{(2n)^2}\det(S).\det\left(P - QS^{-1}R\right)$$

$$= \frac{1}{(2n)^2} \times \det\begin{pmatrix} \frac{n^2+n+2}{2-n} & 1 & 1 \\ 1 & \frac{n^2+n+2}{2-n} & 1 \\ 1 & 1 & \frac{n^2+n+2}{2-n} \end{pmatrix}. \tag{29}$$

Simplifying, we get $\tau(K_n \times K_2) = n^{n-2}(n+2)^{n-1}$. □

Corollary 1. *For all n, the complexity of the symmetric difference $K_n \ominus K_2$ is given as*

$$\tau(K_n \ominus K_2) = n^{n-2}(n+2)^{n-1}. \tag{30}$$

Proof. Since $K_n \times K_2 \cong K_n \ominus K_2$ (see Figure 6), $\tau(K_n \ominus K_2) = n^{n-2}(n+2)^{n-1} = \tau(K_n \times K_2)$. □

Theorem 6. *For all n, the complexity of the strong product $K_n \boxtimes K_2 \cong K_n + K_n$ is given as*

$$\tau(K_n \boxtimes K_2) = (2n)^{2n-2}. \tag{31}$$

Proof. Consider the network $K_n \boxtimes K_2$ with $|V(K_n \boxtimes K_2)| = 2n$ and $|E(K_n \boxtimes K_2)| = n(2n-1)$ (see Figure 7).

Applying Lemma 1, we have

$$\tau(K_n \boxtimes K_2) = \frac{1}{(2n)^2}\det\left((2n)I - \overline{D} + \overline{A}\right)$$

$$= \frac{1}{(2n)^2}\det\begin{pmatrix}
2n & 0 & 0 & \dots & 0 & 0 & 0 & 0 & 0 & 0 & \dots & 0 & 0 & 0 \\
0 & 2n & 0 & \dots & 0 & 0 & 0 & 0 & 0 & 0 & \dots & 0 & 0 & 0 \\
0 & 0 & 2n & \dots & 0 & 0 & 0 & 0 & 0 & 0 & \dots & 0 & 0 & 0 \\
\vdots & \vdots & \vdots & \ddots & \vdots & \vdots & \vdots & \vdots & \vdots & \vdots & \ddots & \vdots & \vdots & \vdots \\
0 & 0 & 0 & \dots & 2n & 0 & 0 & 0 & 0 & 0 & \dots & 0 & 0 & 0 \\
0 & 0 & 0 & \dots & 0 & 2n & 0 & 0 & 0 & 0 & \dots & 0 & 0 & 0 \\
0 & 0 & 0 & \dots & 0 & 0 & 2n & 0 & 0 & 0 & \dots & 0 & 0 & 0 \\
0 & 0 & 0 & \dots & 0 & 0 & 0 & 2n & 0 & 0 & \dots & 0 & 0 & 0 \\
0 & 0 & 0 & \dots & 0 & 0 & 0 & 0 & 2n & 0 & \dots & 0 & 0 & 0 \\
0 & 0 & 0 & \dots & 0 & 0 & 0 & 0 & 0 & 2n & \dots & 0 & 0 & 0 \\
\vdots & \vdots & \vdots & \ddots & \vdots & \vdots & \vdots & \vdots & \vdots & \vdots & \ddots & \vdots & \vdots & \vdots \\
0 & 0 & 0 & \dots & 0 & 0 & 0 & 0 & 0 & 0 & \dots & 2n & 0 & 0 \\
0 & 0 & 0 & \dots & 0 & 0 & 0 & 0 & 0 & 0 & \dots & 0 & 2n & 0 \\
0 & 0 & 0 & \dots & 0 & 0 & 0 & 0 & 0 & 0 & \dots & 0 & 0 & 2n
\end{pmatrix}_{2n \times 2n}, \tag{32}$$

$$\Rightarrow \tau(K_n \boxtimes K_2) = \frac{1}{(2n)^2}\det\begin{pmatrix} P_{n\times n} & O_{n\times n} \\ O_{n\times n} & S_{n\times n} \end{pmatrix}_{2n\times 2n},$$

$$\Rightarrow \tau(K_n \boxtimes K_2) = \frac{1}{(2n)^2}(2n)^{2n}.$$

Simplifying, we get $\tau(K_n \boxtimes K_2) = (2n)^{2n-2}$. □

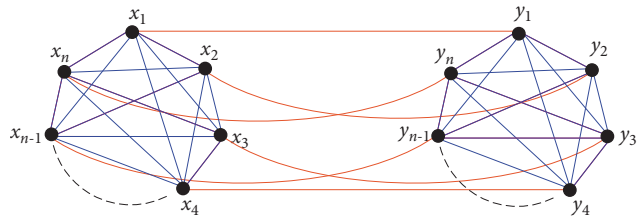

FIGURE 5: The Cartesian product $K_n \times K_2$.

Theorem 7. *For all n, the complexity of the symmetric difference $K_{2,n} \ominus K_2$ is given by*

$$\tau\left(K_{2,n} \ominus K_2\right) = (n+2)^{2n+2}. \tag{33}$$

Proof. Consider the network $K_{2,n} \ominus K_2$ with $|V(K_{2,n} \ominus K_2)| = 2n+4$ and $|E(K_{2,n} \ominus K_2)| = n^2 + 4n + 4$ (see the general formation in Figure 8).

Applying Lemma 1, we have

$$\begin{aligned}
\tau\left(K_{2,n} \ominus K_2\right) &= \frac{1}{(2n+4)^2} \det\left((2n+4)I - \overline{D} + \overline{A}\right) \\
&= \frac{1}{(2n)^2} \det \begin{pmatrix}
2n & 0 & 0 & \dots & 0 & 0 & 0 & 0 & 0 & 0 & \dots & 0 & 0 & 0 \\
0 & 2n & 0 & \dots & 0 & 0 & 0 & 0 & 0 & 0 & \dots & 0 & 0 & 0 \\
0 & 0 & 2n & \dots & 0 & 0 & 0 & 0 & 0 & 0 & \dots & 0 & 0 & 0 \\
\vdots & \vdots & \vdots & \ddots & \vdots & \vdots & \vdots & \vdots & \vdots & \vdots & \ddots & \vdots & \vdots & \vdots \\
0 & 0 & 0 & \dots & 2n & 0 & 0 & 0 & 0 & 0 & \dots & 0 & 0 & 0 \\
0 & 0 & 0 & \dots & 0 & 2n & 0 & 0 & 0 & 0 & \dots & 0 & 0 & 0 \\
0 & 0 & 0 & \dots & 0 & 0 & 2n & 0 & 0 & 0 & \dots & 0 & 0 & 0 \\
0 & 0 & 0 & \dots & 0 & 0 & 0 & 2n & 0 & 0 & \dots & 0 & 0 & 0 \\
0 & 0 & 0 & \dots & 0 & 0 & 0 & 0 & 2n & 0 & \dots & 0 & 0 & 0 \\
0 & 0 & 0 & \dots & 0 & 0 & 0 & 0 & 0 & 2n & \dots & 0 & 0 & 0 \\
\vdots & \vdots & \vdots & \ddots & \vdots & \vdots & \vdots & \vdots & \vdots & \vdots & \ddots & \vdots & \vdots & \vdots \\
0 & 0 & 0 & \dots & 0 & 0 & 0 & 0 & 0 & 0 & \dots & 2n & 0 & 0 \\
0 & 0 & 0 & \dots & 0 & 0 & 0 & 0 & 0 & 0 & \dots & 0 & 2n & 0 \\
0 & 0 & 0 & \dots & 0 & 0 & 0 & 0 & 0 & 0 & \dots & 0 & 0 & 2n
\end{pmatrix}_{2n \times 2n}, \\
\Rightarrow \tau\left(K_n \boxtimes K_2\right) &= \frac{1}{(2n)^2} \det \begin{pmatrix} P_{n\times n} & O_{n\times n} \\ O_{n\times n} & S_{n\times n} \end{pmatrix}_{2n\times 2n}, \\
\Rightarrow \tau\left(K_{2,n} \ominus K_2\right) &= \det \begin{pmatrix} P_{3\times 3} & Q_{3\times 2n} \\ R_{2n\times 3} & S_{2n\times 2n} \end{pmatrix}_{(2n+3)\times(2n+3)}.
\end{aligned} \tag{34}$$

By using Lemma 4, we get

$$\begin{aligned}
\tau\left(K_{2,n} \ominus K_2\right) &= \det(P).\det\left(S - RP^{-1}Q\right) \\
&= \frac{(n+2)^{2n+1}}{4\left(n^2+3n+2\right)} \times \frac{n+2}{4n+4} \det \begin{pmatrix} 3n+4 & -n-2 & -n-2 \\ -n-2 & 3n+4 & -n \\ -n-2 & -n & 3n+4 \end{pmatrix}.
\end{aligned} \tag{35}$$

Evaluating the determinant and simplifying, we obtain finally $\Rightarrow \tau(K_{2,n} \ominus K_2) = (n+2)^{2n+2}$. □

Theorem 8. *For all n, the complexity of the network $K_n + S_n$ is given by*

$$\tau\left(K_n + S_n\right) = (2n+1)^n (n+1)^{n-1}. \tag{36}$$

Proof. Consider the network $K_n + S_n$ with $|V(K_n + S_n)| = 2n + 1$ and $|E(K_n + S_n)| = 3n/2(n + 1)$. Applying Lemma 1, we have

$$\begin{aligned}
\tau(K_n + S_n) &= \frac{1}{(2n+1)^2}\det[(2n+1)I - \overline{D} + \overline{A}] \\
&= \frac{1}{(2n+1)^2} \\
&\det\begin{pmatrix}
2n+1 & 0 & 0 & 0 & \cdots & 0 & 0 & 0 & 0 & 0 & 0 & \cdots & 0 & 0 & 0 \\
0 & n+2 & 1 & 1 & \cdots & 1 & 1 & 1 & 0 & 0 & 0 & \cdots & 0 & 0 & 0 \\
0 & 1 & n+2 & 1 & \cdots & 1 & 1 & 1 & 0 & 0 & 0 & \cdots & 0 & 0 & 0 \\
0 & 1 & 1 & n+2 & \cdots & 1 & 1 & 1 & 0 & 0 & 0 & \cdots & 0 & 0 & 0 \\
\vdots & \vdots & \vdots & \vdots & \ddots & \vdots & \vdots & \vdots & \vdots & \vdots & \vdots & \ddots & \vdots & \vdots & \vdots \\
0 & 1 & 1 & 1 & \cdots & n+2 & 1 & 1 & 0 & 0 & 0 & \cdots & 0 & 0 & 0 \\
0 & 1 & 1 & 1 & \cdots & 1 & n+2 & 1 & 0 & 0 & 0 & \cdots & 0 & 0 & 0 \\
0 & 1 & 1 & 1 & \cdots & 1 & 1 & n+2 & 0 & 0 & 0 & \cdots & 0 & 0 & 0 \\
0 & 0 & 0 & 0 & \cdots & 0 & 0 & 0 & 2n+1 & 0 & 0 & \cdots & 0 & 0 & 0 \\
0 & 0 & 0 & 0 & \cdots & 0 & 0 & 0 & 0 & 2n+1 & 0 & \cdots & 0 & 0 & 0 \\
0 & 0 & 0 & 0 & \cdots & 0 & 0 & 0 & 0 & 0 & 2n+1 & \cdots & 0 & 0 & 0 \\
\vdots & \vdots & \vdots & \vdots & \ddots & \vdots & \vdots & \vdots & \vdots & \vdots & \vdots & \ddots & \vdots & \vdots & \vdots \\
0 & 0 & 0 & 0 & \cdots & 0 & 0 & 0 & 0 & 0 & 0 & \cdots & 2n+1 & 0 & 0 \\
0 & 0 & 0 & 0 & \cdots & 0 & 0 & 0 & 0 & 0 & 0 & \cdots & 0 & 2n+1 & 0 \\
0 & 0 & 0 & 0 & \cdots & 0 & 0 & 0 & 0 & 0 & 0 & \cdots & 0 & 0 & 2n+1
\end{pmatrix} \\
&= \det\begin{pmatrix}
n+1 & 0 & 0 & \cdots & 0 & 0 & 0 & -1 & -1 & -1 & \cdots & -1 & -1 & -1 \\
0 & n+1 & 0 & \cdots & 0 & 0 & 0 & -1 & -1 & -1 & \cdots & -1 & -1 & -1 \\
0 & 0 & n+1 & \cdots & 0 & 0 & 0 & -1 & -1 & -1 & \cdots & -1 & -1 & -1 \\
\vdots & \vdots & \vdots & \ddots & \vdots & \vdots & \vdots & \vdots & \vdots & \vdots & \ddots & \vdots & \vdots & \vdots \\
0 & 0 & 0 & \cdots & n+1 & 0 & 0 & -1 & -1 & -1 & \cdots & -1 & -1 & -1 \\
0 & 0 & 0 & \cdots & 0 & n+1 & 0 & -1 & -1 & -1 & \cdots & -1 & -1 & -1 \\
0 & 0 & 0 & \cdots & 0 & 0 & n+1 & -1 & -1 & -1 & \cdots & -1 & -1 & -1 \\
-1 & -1 & -1 & \cdots & -1 & -1 & -1 & 2n & 0 & 0 & \cdots & 0 & 0 & 0 \\
-1 & -1 & -1 & \cdots & -1 & -1 & -1 & 0 & 2n & 0 & \cdots & 0 & 0 & 0 \\
-1 & -1 & -1 & \cdots & -1 & -1 & -1 & 0 & 0 & 2n & \cdots & 0 & 0 & 0 \\
\vdots & \vdots & \vdots & \ddots & \vdots & \vdots & \vdots & \vdots & \vdots & \vdots & \ddots & \vdots & \vdots & \vdots \\
-1 & -1 & -1 & \cdots & -1 & -1 & -1 & 0 & 0 & 0 & \cdots & 2n & 0 & 0 \\
-1 & -1 & -1 & \cdots & -1 & -1 & -1 & 0 & 0 & 0 & \cdots & 0 & 2n & 0 \\
-1 & -1 & -1 & \cdots & -1 & -1 & -1 & 0 & 0 & 0 & \cdots & 0 & 0 & 2n
\end{pmatrix}_{2n\times 2n}, \\
\Rightarrow \tau(K_n + S_n) &= \det\begin{pmatrix} P_{n\times n} & Q_{n\times n} \\ R_{n\times n} & S_{n\times n} \end{pmatrix}_{2n\times 2n}.
\end{aligned} \tag{37}$$

By using Lemma 4, we obtain

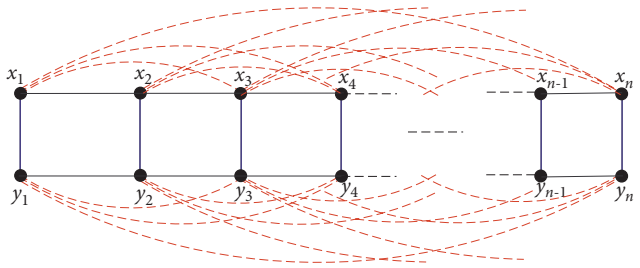

Figure 6: The symmetric difference $K_n \ominus K_2$.

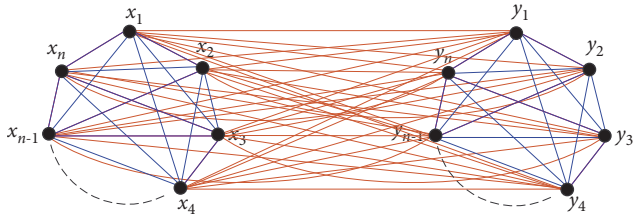

Figure 7: The strong product $K_n \boxtimes K_2$.

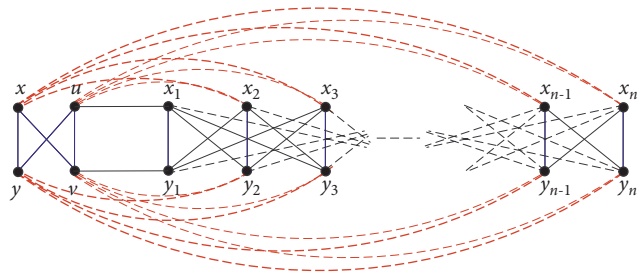

Figure 8: The symmetric difference $K_{2,n} \ominus K_2$.

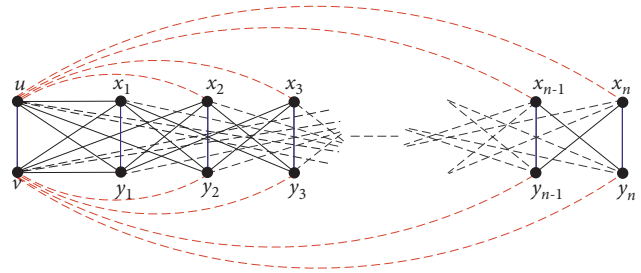

Figure 9: The disjunction network $S_n \wedge K_2$.

$$\tau(K_n + S_n) = \det(S).\det\left(P - QS^{-1}R\right)$$

$$= (n+1)^n \times \left(-\frac{2n+1}{n+1}\right)^n \det \begin{pmatrix} -n & 1 & 1 & 1 & \dots & 1 & 1 & 1 & \\ 1 & -n & 1 & 1 & \dots & 1 & 1 & 1 & 1 \\ 1 & 1 & -n & 1 & \dots & 1 & 1 & 1 & 1 \\ 1 & 1 & 1 & -n & \dots & 1 & 1 & 1 & 1 \\ \vdots & \vdots & \vdots & \vdots & \ddots & \vdots & \vdots & \vdots & \vdots \\ 1 & 1 & 1 & 1 & \dots & -n & 1 & 1 & 1 \\ 1 & 1 & 1 & 1 & \dots & 1 & -n & 1 & 1 \\ 1 & 1 & 1 & 1 & \dots & 1 & 1 & -n & 1 \\ 1 & 1 & 1 & 1 & \dots & 1 & 1 & 1 & -n \end{pmatrix}_{n \times n}. \tag{38}$$

Using Lemma 3 and simplifying, we get $\Rightarrow \tau(K_n + S_n) = (2n+1)^n (n+1)^{n-1}$. □

Theorem 9. *For all n, the complexity of the conjunction $S_n \wedge K_2$ is given as*

$$\tau(S_n \wedge K_2) = 4(n+1)^2 (n+2)^{2n-2}. \tag{39}$$

Proof. Consider the network $S_n \wedge K_2$ with $|V(S_n \wedge K_2)| = 2n + 2$ and $|E(S_n \wedge K_2)| = n^2 + 4n + 1$ (see Figure 9).

Applying Lemma 1, we have

$$\tau(S_n \wedge K_2) = \frac{1}{(2n+2)^2}\det[(2n+2)I - \overline{D} + \overline{A}]$$

$$= \frac{1}{(2n+2)^2}$$

$$\det\begin{pmatrix}
2n+2 & 0 & 0 & 0 & 0 & \cdots & 0 & 0 & 0 & 0 & 0 & 0 & \cdots & 0 & 0 & 0 \\
0 & 2n+2 & 0 & 0 & 0 & \cdots & 0 & 0 & 0 & 0 & 0 & 0 & \cdots & 0 & 0 & 0 \\
0 & 0 & n+3 & 1 & 1 & \cdots & 1 & 1 & 1 & 0 & 0 & 0 & \cdots & 0 & 0 & 0 \\
0 & 0 & 1 & n+3 & 1 & \cdots & 1 & 1 & 1 & 0 & 0 & 0 & \cdots & 0 & 0 & 0 \\
0 & 0 & 1 & 1 & n+3 & \cdots & 1 & 1 & 1 & 0 & 0 & 0 & \cdots & 0 & 0 & 0 \\
\vdots & \vdots & \vdots & \vdots & \vdots & \ddots & \vdots & \vdots & \vdots & \vdots & \vdots & \vdots & \ddots & \vdots & \vdots & \vdots \\
0 & 0 & 1 & 1 & 1 & \cdots & n+3 & 1 & 1 & 0 & 0 & 0 & \cdots & 0 & 0 & 0 \\
0 & 0 & 1 & 1 & 1 & \cdots & 1 & n+3 & 1 & 0 & 0 & 0 & \cdots & 0 & 0 & 0 \\
0 & 0 & 1 & 1 & 1 & \cdots & 1 & 1 & n+3 & 0 & 0 & 0 & \cdots & 0 & 0 & 0 \\
0 & 0 & 0 & 0 & 0 & \cdots & 0 & 0 & 0 & n+3 & 1 & 1 & \cdots & 1 & 1 & 1 \\
0 & 0 & 0 & 0 & 0 & \cdots & 0 & 0 & 0 & 1 & n+3 & 1 & \cdots & 1 & 1 & 1 \\
0 & 0 & 0 & 0 & 0 & \cdots & 0 & 0 & 0 & 1 & 1 & n+3 & \cdots & 1 & 1 & 1 \\
\vdots & \vdots & \vdots & \vdots & \vdots & \ddots & \vdots & \vdots & \vdots & \vdots & \vdots & \vdots & \ddots & \vdots & \vdots & \vdots \\
0 & 0 & 0 & 0 & 0 & \cdots & 0 & 0 & 0 & 1 & 1 & 1 & \cdots & n+3 & 1 & 1 \\
0 & 0 & 0 & 0 & 0 & \cdots & 0 & 0 & 0 & 1 & 1 & 1 & \cdots & 1 & n+3 & 1 \\
0 & 0 & 0 & 0 & 0 & \cdots & 0 & 0 & 0 & 1 & 1 & 1 & \cdots & 1 & 1 & n+3
\end{pmatrix} \tag{40}$$

$$= \det\begin{pmatrix}
2n+1 & -1 & -1 & -1 & \cdots & -1 & -1 & -1 & -1 & -1 & -1 & \cdots & -1 & -1 & -1 \\
-1 & n+2 & 0 & 0 & \cdots & 0 & 0 & 0 & -1 & -1 & -1 & \cdots & -1 & -1 & -1 \\
-1 & 0 & n+2 & 0 & \cdots & 0 & 0 & 0 & -1 & -1 & -1 & \cdots & -1 & -1 & -1 \\
-1 & 0 & 0 & n+2 & \cdots & 0 & 0 & 0 & -1 & -1 & -1 & \cdots & -1 & -1 & -1 \\
\vdots & \vdots & \vdots & \vdots & \ddots & \vdots & \vdots & \vdots & \vdots & \vdots & \vdots & \ddots & \vdots & \vdots & \vdots \\
-1 & 0 & 0 & 0 & \cdots & n+2 & 0 & 0 & -1 & -1 & -1 & \cdots & -1 & -1 & -1 \\
-1 & 0 & 0 & 0 & \cdots & 0 & n+2 & 0 & -1 & -1 & -1 & \cdots & -1 & -1 & -1 \\
-1 & 0 & 0 & 0 & \cdots & 0 & 0 & n+2 & -1 & -1 & -1 & \cdots & -1 & -1 & -1 \\
-1 & -1 & -1 & -1 & \cdots & -1 & -1 & -1 & n+2 & 0 & 0 & \cdots & 0 & 0 & 0 \\
-1 & -1 & -1 & -1 & \cdots & -1 & -1 & -1 & 0 & n+2 & 0 & \cdots & 0 & 0 & 0 \\
-1 & -1 & -1 & -1 & \cdots & -1 & -1 & -1 & 0 & 0 & n+2 & \cdots & 0 & 0 & 0 \\
\vdots & \vdots & \vdots & \vdots & \ddots & \vdots & \vdots & \vdots & \vdots & \vdots & \vdots & \ddots & \vdots & \vdots & \vdots \\
-1 & -1 & -1 & -1 & \cdots & -1 & -1 & -1 & 0 & 0 & 0 & \cdots & n+2 & 0 & 0 \\
-1 & -1 & -1 & -1 & \cdots & -1 & -1 & -1 & 0 & 0 & 0 & \cdots & 0 & n+2 & 0 \\
-1 & -1 & -1 & -1 & \cdots & -1 & -1 & -1 & 0 & 0 & 0 & \cdots & 0 & 0 & n+2
\end{pmatrix}_{(2n+1)\times(2n+1)},$$

$$\Rightarrow \tau(S_n \wedge K_2) = \det\begin{pmatrix} P_{1\times 1} & Q_{1\times 2n} \\ R_{2n\times 1} & S_{2n\times 2n} \end{pmatrix}_{(2n+1)\times(2n+1)}.$$

By using Lemma 4, we have

Table 1: Synopsis of the results.

Network	Parameters	Complexity	Planar ∨ non-planar
$K_{2,n}+W_3$	$\forall n \in \mathbb{N}$	$6^{n-1}(n+4)(n+6)^4$	Non-planar
$K_{2,n}\boxtimes K_2$	$\forall n \in \mathbb{N}$	$(24)^n(2(n^3+2n^2+n))$	Non-planar
$K_{2,n}\ltimes K_2$	$\forall n \in \mathbb{N}$	$8^{n-1}(n^3+6n^2+8n)$	Non-planar
$K_{2,n}+nK_1$	$\forall n \in \mathbb{N}$	$4n(n+1)(n+2)^{2n-2}$	Non-planar
$K_n \times K_2$	$\forall n \in \mathbb{N}$	$n^{n-2}(n+2)^{n-1}$	Non-planar
$K_n\boxtimes K_2$	$\forall n \in \mathbb{N}$	$(2n)^{2n-2}$	Non-planar
$K_{2,n}\ominus K_2$	$\forall n \in \mathbb{N}$	$(n+2)^{2n+2}$	Non-planar
K_n+S_n	$\forall n \in \mathbb{N}$	$(2n+1)^n(n+1)^{n-1}$	Non-planar
$S_n\wedge K_2$	$\forall n \in \mathbb{N}$	$4(n+1)^2(n+2)^{2n-2}$	Non-planar

$$\tau(S_n\wedge K_2) = \det(S).\det\left(P - QS^{-1}R\right)$$

$$= \frac{(-n)^n}{n+2} \times \det \begin{pmatrix} \frac{n^2+3n+4}{-n} & 1 & 1 & 1 & \dots & 1 & 1 & 1 & \\ 1 & \frac{n^2+3n+4}{-n} & 1 & 1 & \dots & 1 & 1 & 1 & 1 \\ 1 & 1 & \frac{n^2+3n+4}{-n} & 1 & \dots & 1 & 1 & 1 & 1 \\ 1 & 1 & 1 & \frac{n^2+3n+4}{-n} & \dots & 1 & 1 & 1 & 1 \\ \vdots & \vdots & \vdots & \vdots & \ddots & \vdots & \vdots & \vdots & \vdots \\ 1 & 1 & 1 & 1 & \dots & \frac{n^2+3n+4}{-n} & 1 & 1 & 1 \\ 1 & 1 & 1 & 1 & \dots & 1 & \frac{n^2+3n+4}{-n} & 1 & 1 \\ 1 & 1 & 1 & 1 & \dots & 1 & 1 & \frac{n^2+3n+4}{-n} & 1 \\ 1 & 1 & 1 & 1 & \dots & 1 & 1 & 1 & \frac{n^2+3n+4}{-n} \end{pmatrix}_{n\times n} \times \det([2n+1]-[n]). \tag{41}$$

Lemma 3 and simplification finally give

$$\tau(S_n\wedge K_2) = 4(n+1)^2(n+2)^{2n-2}. \tag{42}$$

□

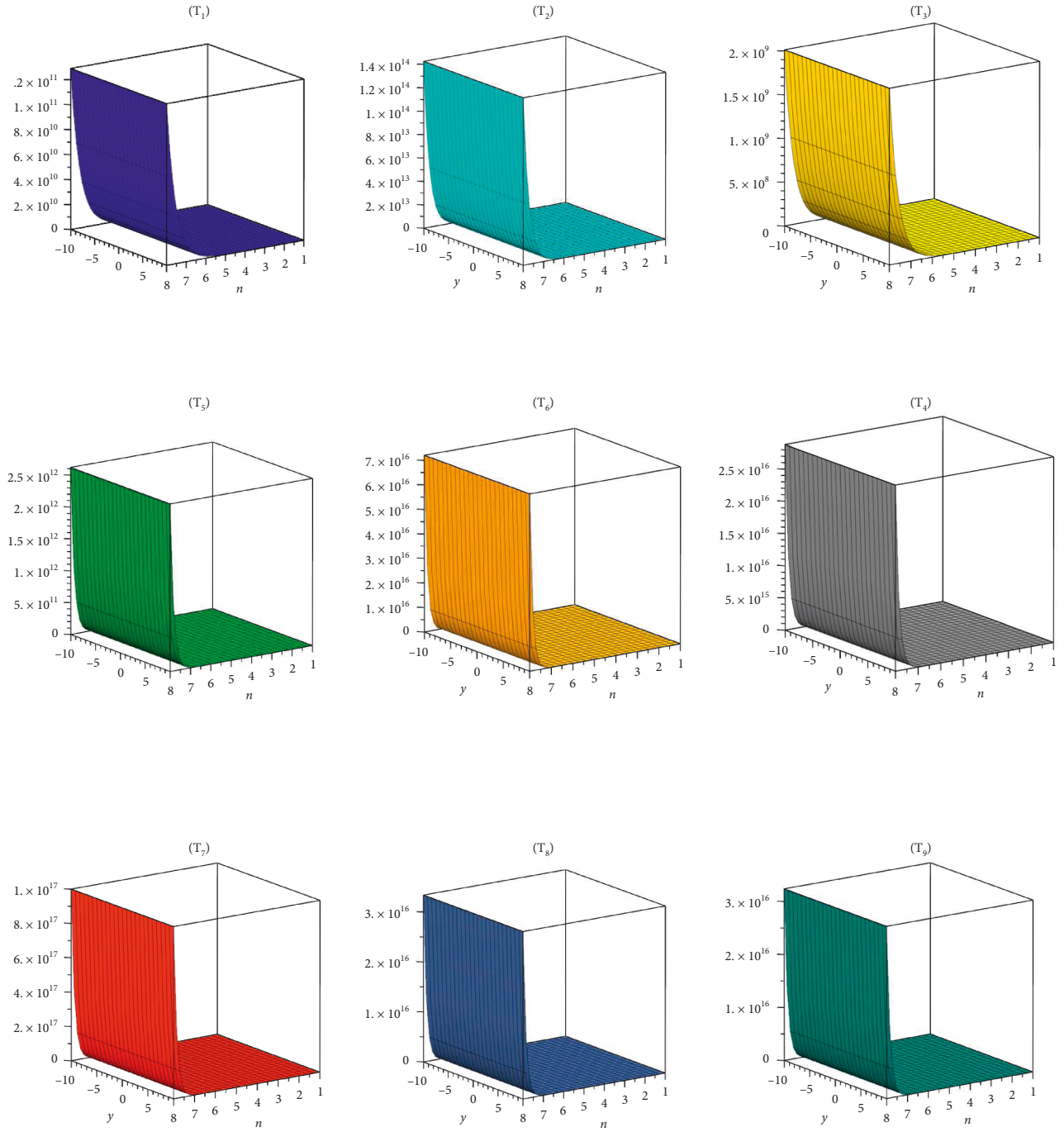

Figure 10: Trends of the enumerated complexities of $K_{2,n} + W_3 \longrightarrow (T_1)$, $K_{2,n} \boxtimes K_2 \longrightarrow (T_2)$, $K_{2,n} \ltimes K_2 \longrightarrow (T_3)$, $K_{2,n} + nK_1 \longrightarrow (T_4)$, $K_n \times K_2 \longrightarrow (T_5)$, $K_n \boxtimes K_2 \longrightarrow (T_6)$, $K_{2,n} \ominus K_2 \longrightarrow (T_7)$, $K_n + S_n \longrightarrow (T_8)$, and $S_n \wedge K_2 \longrightarrow (T_9)$.

4. Synopsis and the Diagrammatic Comparison of the Complexities of the Networks Obtained

This section consists of a briefing and graphical plots and juxtaposition of the values of complexities of the networks enumerated in this note.

Table 1 indicates a synopsis of our results in the shape of complexities of various networks and also categorically recognizes it being planar or not.

Figure 10 shows the discrete graphical shapes of the values of the complexity of networks obtained here, whereas Figure 11 addresses the relative comparison of the complexities of these networks, revealing the red one to be the dominating layer.

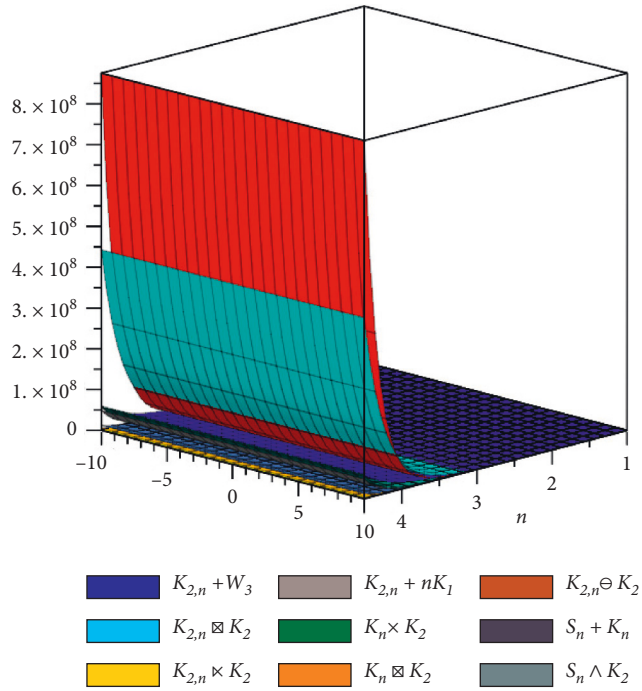

FIGURE 11: Comparison of the trends of the enumerated complexities.

5. Conclusion

One of the meaningful algebraic invariants in networking nowadays is complexity. This invariant provides us the information of the total number of acyclic networks present within the base network, which ultimately ensures the reliability and accuracy in the network. We have enumerated here the complexity of various operations on networks such as $K_{2,n} + W_3$, $K_{2,n} \boxtimes K_2$, $K_{2,n} \ltimes K_2$, $K_{2,n} + nK_1$, $K_n \times K_2$, $K_n \boxtimes K_2$, $K_{2,n} \ominus K_2$, $K_n + S_n$, and $S_n \wedge K_2$. The adopted methods are mainly algebraic and feature Chebyshev polynomials and the matrix theory in the calculations. As future work, we encourage the researchers to obtain the complexities of further generalized operations on networks such as corona product, zig zag product, homomorphic product, join, shadow, conjunction, and disjunction of various classes of networks.

Data Availability

The whole data are included within this article. However, the reader may contact the corresponding author for more details on the data.

Conflicts of Interest

The authors declare that they have no conflicts of interest.

References

[1] N. L. Biggs, *Algebraic Graph Theory*, Cambridge University Press, Cambridge, 1993.

[2] D. Cvetkovic, M. Doob, and H. Sachs, *Spectra of Graphs*, Academic, New York, 1978.

[3] H. N. V. Temperley and Combinatorics, *Proc. On Combinatorial Mathematics*, pp. 356-357, Mathematics Institute, Oxford, 1972.

[4] H. N. V. Temperley, *Graph Theory and Applications Ellis Horwood Series in Mathematics and its Applications*Ellis Horwood Ltd, New York, 1981.

[5] S. N. Daoud, "Some applications of number of spanning trees of complete and complete bipartite graphs," *Am. J. Appl. Sci. Sci. Publ.*, vol. 9, no. 4, pp. 584–592, 2012.

[6] J. C. Mason and D. C. Handscomb, *Chebyshev Polynomials*, Chapman and Hall/CRC, Boca Raton, Florida, 2003.

[7] S. N. Daoud, "Complexity of products of some complete and complete bipartite graphs," *Journal of Applied Mathematics*, vol. 2013, pp. 1–25, 2013.

[8] D. J. Gross, T. J. Saccoman, and L. C. Suffel, *Spanning Tree Results for Graphs and Multigraphs: A Matrix-Theoretic Approach*, World Scientific Publishing Company, Singapore, 2014.

[9] A. Bose and K. Saha, *Random Circulant Matrices*, CRC Press : Taylor and Francis Group, Boca Raton, Florida, USA, 2019.

[10] M. Marcus, *A Servy of Matrix Theory and Matrix Inequalities*, Unvi. Allyn and Bacon. Inc, Boston, 1964.

[11] M. R. Zeen El Deen and W. A. Aboamer, "Complexity of some duplicating networks," *IEEE Access*, vol. 9, pp. 56736–56756, 2021.

[12] R. Balakrishnan and K. Ranganathan, *A Textbook of Graph Theory*, Springer, New York, USA, 2000.

[13] D. B. West, *Introduction to Graph Theory*, Prentice- Hall of India, New Delhi, 2003.

[14] G. A. Cayley, "A theorm on trees," *The Quarterly Journal of Mathematics*, vol. 23, pp. 276–378, 1889.

[15] J. Sedlacek, "On the skeleton of a graph or digraph," in *Combinatorial Structures and Their Applications*, M. Guy, N. Saver Hanani, and J. Schonheim, Eds., pp. 387–391, Gordon & Breach, New York, 1970.

[16] G. G. Kirchhoff, "Uber die Auflosung der Gleichungen, auf welche man beider Untersuchung der Linearen Verteilung Galvanischer Strme gefhrt wird," *Ann. Phys. Chem.*, vol. 148, no. 12, pp. 497–508, 1847.

[17] S. N. Daoud, "The deletion-contraction method for counting the number of spanning trees of graphs," *European Physical Journal A: Hadrons and Nuclei*, vol. 130, no. 10, p. 217, 2015.

[18] W. Guo, N. Xiong, H. C. Chao, S. Hussain, and G. Chen, "Design and analysis of self-adapted task scheduling strategies in wireless sensor networks," *Sensors*, vol. 11, no. 7, pp. 6533–6554, 2011.

[19] X. Wang, Q. Li, N. Xiong, and Y. Pan, "Ant colony optimization-based location-aware routing for wireless sensor networks," in *Wireless Algorithms, Systems, and Applications, WASA, Lecture Notes in Computer Science*, Y. Li, D. T. Huynh, S. K. Das, and D. Z. Du, Eds., Vol. vol 5258, Springer, Berlin, Heidelberg, 2008.

[20] Y. Jiang, G. Tong, H. Yin, and N. Xiong, "A pedestrian detection method based on genetic algorithm for optimize XGBoost training parameters," *IEEE Access*, vol. 7, pp. 118310–118321, 2019.

[21] R. Wan, N. Xiong, and N. T. Loc, "An energy-efficient sleep scheduling mechanism with similarity measure for wireless sensor networks," *Human-centric Computing and Information Sciences*, vol. 8, no. 1, p. 18, 2018.

[22] Y. Lu, S. Wu, Z. Fang, N. Xiong, S. Yoon, and D. S. Park, "Exploring finger vein based personal authentication for secure IoT," *Future Generation Computer Systems*, vol. 77, pp. 149–160, 2017.

[23] S. N. Daoud, "Generating formulas of the number of spanning trees of some special graphs," *European Physical Journal A: Hadrons and Nuclei*, vol. 129, no. 7, p. 146, 2014.

[24] S. N. Daoud, "Number of spanning trees of different products of complete and complete bipartite graphs," *J. Math. Prob. Eng.*, vol. 2014, Article ID 965105, 2014.

Hindawi
Complexity
Volume 2022, Article ID 5800097, 14 pages
https://doi.org/10.1155/2022/5800097

WILEY | Hindawi

Research Article

Consensus of Time-Varying Interval Uncertain Multiagent Systems via Reduced-Order Neighborhood Interval Observer

Hui Luo, Jin Zhao, and Quan Yin

School of Artificial Intelligent and Automation, Huazhong University of Science and Technology, Wuhan, China

Correspondence should be addressed to Hui Luo; keyluo@hust.edu.cn

Received 12 April 2022; Accepted 14 June 2022; Published 28 August 2022

Academic Editor: Xiao Ling Wang

This work focuses on a multiagent system (MAS) with time-varying interval uncertainty in the system matrix, where multiple agents interact through an undirected topology graph and only the bounding matrices on the uncertainty in the system matrix are known. A reduced-order interval observer (IO), which is named the reduced-order neighborhood interval observer (NIO), is designed to estimate the relative state of each agent and those of its neighbors. It is shown that the reduced-order IO can guarantee the consensus of the uncertain multiagent system. Finally, simulation examples are proposed to verify the theoretical findings.

1. Introduction

With the discovery of the swarm intelligence and rapid development of the computer science [1–5], consensus of MASs has gained considerable attention [6–10], which means all the agents attain an agreement upon a common quantity of interest via distributed communications. Readers interested in consensus of MASs are referred to the great literature reviews on this topic, such as [11, 12].

Uncertainty exists widely in existing practical engineering, which can affect the stability of the control systems [13–15]. Most of the exisiting related works on MASs with uncertainties are carried out to eliminate the impact of uncertainties and achieve the consensus of the MASs [16, 17]. However, it is difficult or even impossible to get the specific information of the uncertainties. Thus, the acquirement of the bounding information on the uncertainties (BIU) is easier than that of the uncertainties. On the other hand, the states of the MASs cannot be achieved in some situations. Taking these two facts into consideration, IO is firstly proposed to single-agent systems [18, 19] to implement the state interval estimation and stabilization, where only the outputs and the BIU are related. An IO consists of two dynamical systems which are both in the form of Luenberger observer, where one is used to estimate the upper bound of the system state, while the other one aims at estimating the lower bound of the system state. Then, Wang et al. extended the IO to uncertain MASs and proposed some interesting results [20, 21]. According to the estimation objective, two kinds of IOs are defined for uncertain multiagent systems, the local IO [20–23] and the NIO [23, 24]. To be specific, the local IO is designed to do the estimation which relates only to the output information of the associated agent. Yet, the NIO is designed to estimate the relative states between agents and its neighbors, which relates to the sum of the relative outputs between each agent and its neighbors. In [20, 24], coordination control of MASs with uncertain disturbances is solved by introducing IO in MASs, including the local IO [20, 22] and the NIO [24]. In [21, 23], the IO-based consensus of MASs with time-varying interval uncertainties (TIUs) in the system dynamics is considered, by using only the outputs and the BIU, where the local full-order IO and neighborhood full-order IO are designed in [23], while local reduced-order IO is given in [21].

As stated above, the reduced-order NIO design problem of MASs with TIUs is not solved. This work pays attention to the reduced-order NIO design of MASs with TIUs and aims at estimating the sum of relative states between each agent and its neighbors and simultaneously achieving consensus. In this paper, the definition of reduced-order NIO is

proposed in detail. It shows that the consensus is a by-part of the reduced-order NIO.

The rest of this paper is organized as follows: Problem formulation and some useful preliminaries used in this paper are introduced in Section 2. The main results are given in Section 3, and numerical simulations are presented in Section 4. Finally, conclusion is presented in Section 5.

2. Preliminaries and Problem Statement

2.1. Notation. $\mathbb{R}, \mathbb{N}, \mathbb{R}^{m\times n}$, and $\mathbb{R}_+^{m\times n}$ are denoted as the sets of real numbers, natural numbers, $m\times n$ real matrices, and $m\times n$ real matrices in which each element is a matrix with nonnegative entries, respectively. A square matrix is called to be Metzler when all its off-diagonal elements are nonnegative. All vector inequalities are understood element-wise, for instance, $v_a < (\leq) v_b$ ($v_a = [\, v_{a1} \ \cdots \ v_{an} \,]$ and $v_b = [\, v_{b1} \ \cdots \ v_{bn} \,]$) if for all $i = 1, \ldots, n$, one has $v_{ai} < (\leq) v_{bi}$. For any symmetric$A \in \mathbb{R}^{n\times n}$, $\lambda_i(A)$ denotes its eigenvalues, which is arranged as $\lambda_1(A) \leq \lambda_2(A) \leq \ldots \leq \lambda_n(A)$. For any matrix $A = (a_{ij})$, $\|A\|$ denotes the 2-norm of A, $A^+ = (a_{ij}^+)$ (with $a_{ij}^+ = \max\{a_{ij}, 0\}$), $A^- = A^+ - A$ (similarly for vectors), and $|A| = (|a_{ij}|) = A^+ + A^-$. A^T denotes its transpose matrix. I_N and 1_N denote an N-dimensional identity matrix and an $N\times 1$ vector with all the entries being 1, respectively. 0 denotes the number zero (or the zero matrix with compatible dimensions). $\mathrm{diag}\{A1, \ldots, A_N\}$ denotes a block diagonal matrix, in which all the off-diagonal matrices are zeros and $A_i (i = 1, \ldots, N)$ is the i-th diagonal block.

2.2. Graph Theory. Let a triple $\mathcal{G} = (\mathcal{V}, \mathcal{E}, G)$ be an undirected network, where $\mathcal{V} = \{v_1, \ldots, v_N\}$ and $\mathcal{E} \subseteq \mathcal{V}\times\mathcal{V}$ are the node set and edge set, respectively, and $G = (g_{ij}) \in \mathbb{R}^{N\times N}$ is the adjacency matrix. If the information can be communicated between node v_i and node v_j, then $(v_i, v_j) \in \mathcal{E}$, that is, the edge (v_i, v_j) exists in $\mathcal{G} = (\mathcal{V}, \mathcal{E}, G)$. The neighbor set of node i is $\mathcal{N}_i = \{v_j | (v_i, v_j) \in \mathcal{E}\}$. A path is a sequence of edges in $\mathcal{G} = (\mathcal{V}, \mathcal{E}, G)$ of the form $(i_1, i_2) \ldots (i_2, i_3)$. If there exists a path from every node to every other node [9, 25, 26], it is said that $\mathcal{G} = (\mathcal{V}, \mathcal{E}, G)$ is connected.

The adjacency matrix $G = (g_{ij}) \in \mathbb{R}^{N\times N}$ is defined as $g_{ij} = 1$ when $(v_i, v_j) \in \mathcal{E}$ and $g_{ij} = 0$ otherwise. The Laplacian matrix is defined as $L = (l_{ij}) \in \mathbb{R}^{N\times N}$, where $l_{ij} = -g_{ij}$ for $j \neq i$ and $l_{ij} = \sum_{j\neq i} g_{ij}$ for $j = i$. For this symmetric matrix L, in [9, 25, 26], it has exactly one zero eigenvalue with an associated eigenvector 1_N, and all the other ones are positive, if and only if $\mathcal{G} = (\mathcal{V}, \mathcal{E}, G)$ is connected.

2.3. Problem Statement. Consider a continuous-time MAS with N agents and time-varying uncertainty in system matrix, where each agent moves in an n-dimensional Euclidean space and regulates itself based on the following dynamics:

$$\begin{cases} \dot{x}_i(t) = (A + \Delta A(t))x_i(t) + Bu_i(t), \\ y_i(t) = Cx_i(t), i = 1, 2, \ldots, N, \end{cases} \tag{1}$$

where $x_i(t) \in \mathbb{R}^{n\times 1}, u_i(t) \in \mathbb{R}^{m\times 1}$, and $y_i(t) \in \mathbb{R}^{p\times 1}$ are the state, control input, and output of agent i, respectively. The matrices A, B, C are with compatible dimensions, while $\Delta A(t)$ (the uncertainty in system matrix) is a matrix-valued function of the time variable t. Moreover, $\Delta A(t)$ is time-varying interval uncertainty, which satisfies Assumption 1.

Assumption 1. There exist $\overline{\Delta A} \in \mathbb{R}^{n\times n}$ and $\underline{\Delta A} \in \mathbb{R}^{n\times n}$ with $\underline{\Delta A} \leq \overline{\Delta A}$, such that $\Delta A(t) \in [\underline{\Delta A}, \overline{\Delta A}]$ for all $t \geq 0$.

Moreover, two technical assumptions are given.

Assumption 2. (A, B) is stabilizable.

Assumption 3. (C, A) is detectable.

Denote

$$w_i(t) = \sum_{j=1}^{N} l_{ij} x_j(t), \tag{2}$$

as the sum of relative state between the i-th agent and its neighbors. The main objective of this work is to realize the interval estimation on $w_i(t)$ on the basis of only the interval bound information of $\Delta A(t)$ given in Assumption 1, by using as few integrators as possible. Motivated by [27], a reduced-order NIO will be designed for system (1) to realize the interval estimation on $w_i(t)$. Again by [27], for C, there exists a matrix $D \in \mathbb{R}^{(n-p)\times n}$ to get a nonsingular matrix $P = [C/D] \in \mathbb{R}^{n\times n}$. Denote $P^{-1} = Q = [\, Q_1 \ Q_2 \,]$ with $Q_1 \in \mathbb{R}^{n\times p}$ and $Q_2 \in \mathbb{R}^{n\times(n-p)}$. With these matrices, one has $CQ_1 = I_p$ and $CQ_2 = 0$. For $i = 1, \ldots, N$, let $\widetilde{w}_i \triangleq Pw_i = [\widetilde{w}_{iy}/\widetilde{w}_{iu}] = [\sum_{j=1}^N l_{ij}\widetilde{x}_{jy}/\sum_{j=1}^N l_{ij}\widetilde{x}_{ju}]$ with $\widetilde{w}_{iy} \in \mathbb{R}^p$ and $\widetilde{w}_{iu} \in \mathbb{R}^{n-p}$. Intuitively, $\widetilde{w}_{iy} = \sum_{j=1}^N l_{ij}\widetilde{x}_{jy} = \sum_{j=1}^N l_{ij}y_j$, so that there is no need to estimate $\widetilde{w}_{iy}$ but we have to estimate $\widetilde{w}_{iu}$. For simplicity, denote $PAP^{-1} = \begin{bmatrix} \widetilde{A}_{11} & \widetilde{A}_{12} \\ \widetilde{A}_{21} & \widetilde{A}_{22} \end{bmatrix}$ and $PB = [\widetilde{B}_1/\widetilde{B}_2]$ with $\widetilde{A}_{11} \in \mathbb{R}^{p\times p}, \widetilde{A}_{12} \in \mathbb{R}^{p\times(n-p)}, \widetilde{A}_{21} \in \mathbb{R}^{(n-p)\times p}, \widetilde{A}_{22} \in \mathbb{R}^{(n-p)\times(n-p)}, \widetilde{B}_1 \in \mathbb{R}^{p\times m}$, and $\widetilde{B}_2 \in \mathbb{R}^{(n-p)\times m}$. If ΔA in (1) is known, under Assumption 3, motivated by [27] and the full-order NIO constructed in [23], a neighborhood reduced-order observer can be designed as

$$\begin{aligned} \dot{z}_{iu} = {} & \left(\widetilde{A}_{22} - K\widetilde{A}_{12}\right)z_{iu} + \left[\left(\widetilde{A}_{22} - K\widetilde{A}_{12}\right)K + \left(\widetilde{A}_{21} - K\widetilde{A}_{11}\right)\right]\sum_{j=1}^{N} l_{ij}y_j \\ & + \left(\widetilde{B}_2 - K\widetilde{B}_1\right)\sum_{j=1}^{N} l_{ij}u_j + D\Delta A w_i - KC\Delta A w_i, \end{aligned} \tag{3}$$

where $K \in \mathbb{R}^{(n-p)\times p}$ is chosen to make $\tilde{A}_{22} - K\tilde{A}_{12}$ Hurwitz. On the other hand, for $\tilde{w}_{iu}$ and $\tilde{w}_{iy}$ defined above, by (1), one can get that

$$z_{iu} = \tilde{w}_{iu} - K\tilde{w}_{iy} = \tilde{w}_{iu} - K\sum_{j=1}^{N} l_{ij} y_j. \tag{4}$$

However, in case that ΔA is unknown, the neighborhood reduced-order observer in (3) cannot be designed. Motivated by the local reduced-order IO given in [21], in this paper, we will solve the reduced-order NIO design for MASs steered by (1), where only the bounding information on ΔA is known. For better understanding, Definition 1 is given.

Definition 1. Consider two dynamical systems in the form of

$$\begin{aligned}
\dot{\overline{z}}_{iu} &= \overline{f}_1\left(A, B, C, \overline{\Delta A}, \underline{\Delta A}, \sum_{j=1}^{N} l_{ij} y_j, \sum_{j=1}^{N} l_{ij} u_j, \overline{z}_{iu}\right),\\
\dot{\underline{z}}_{i} &= \underline{f}_1\left(A, B, C, \overline{\Delta A}, \underline{\Delta A}, \sum_{j=1}^{N} l_{ij} y_j, \sum_{j=1}^{N} l_{ij} u_j, \underline{z}_{iu}\right),
\end{aligned} \tag{5}$$

$$\begin{aligned}
\overline{z}_{iu}(0) &= \overline{f}_2\left(\overline{w}_i(0), \underline{w}_i(0)\right),\\
\underline{z}_{iu}(0) &= \underline{f}_2\left(\overline{w}_i(0), \underline{w}_i(0)\right),
\end{aligned}$$

with

$$u_i = f\left(\overline{z}_{iu}, \underline{z}_{iu}, y_j\right), j \in \mathcal{N}_i, \tag{6}$$

where $\overline{f}_1, \underline{f}_1, \overline{f}_2, \underline{f}_2$, and f are some differentiable continuous functions. Define

$$\begin{aligned}
\overline{w}_i &= \overline{f}_3\left(\overline{z}_{iu}, \underline{z}_{iu}, y_j\right),\\
\underline{w}_i &= \underline{f}_3\left(\overline{z}_{iu}, \underline{z}_{iu}, y_j\right),
\end{aligned} \tag{7}$$

with $j \in \mathcal{N}_i$; if $\underline{w}_i \le w_i \le \overline{w}_i$ holds for $t \ge 0$, it is said that $\overline{z}_{iu}$ and $\underline{z}_{iu}$ in (4) constitute a neighborhood reduced framer for (1). Beyond the holding $\underline{w}_i \le w_i \le \overline{w}_i$ for $t \ge 0$, we also have

$$\begin{aligned}
\lim_{t\longrightarrow\infty}\left[\overline{w}_i - \sum_{j=1}^{N} l_{ij} x_j(t)\right] &= 0,\\
\lim_{t\longrightarrow\infty}\left[\underline{w}_i - \sum_{j=1}^{N} l_{ij} x_j(t)\right] &= 0, i = 1, \ldots, N.
\end{aligned} \tag{8}$$

It is said that $\overline{z}_{iu}$ and $\underline{z}_{iu}$ in (4) constitute a reduced NIO for (1).

2.4. The Theory of Positive Systems. In order to realize the main objective of this paper, two lemmas about the positive systems theory are introduced.

Lemma 1 (see [28]). *Given a nonautonomous system described by $\dot{x} = Ax + B$, where A is a Metzler matrix and $B \ge 0$ for $t \ge 0$. Then, $x \ge 0$ for $t > 0$, provided that $x(0) \ge 0$.*

Lemma 2 (see [29]). *Let $x \in \mathbb{R}^{n\times 1}$ be a vector variable, $\underline{x} \le x \le \overline{x}$ for some $\overline{x}, \underline{x} \in \mathbb{R}^{n\times 1}$. Then,*

(1) For $A \in \mathbb{R}^{m\times n}$, $A^+\underline{x} - A^-\overline{x} \le Ax \le A^+\overline{x} - A^-\underline{x}$

(2) For $A \in \mathbb{R}^{m\times n}$ satisfying $\underline{A} \le A \le \overline{A}$ for some $\underline{A}, \overline{A} \in \mathbb{R}^{m\times n}$ $\underline{A}^+\underline{x}^+ - \overline{A}^+\underline{x}^- - \underline{A}^-\overline{x}^+ + \overline{A}^-\overline{x}^- \le Ax \le \overline{A}^+\overline{x}^+ - \underline{A}^+\overline{x}^- - \overline{A}^-\underline{x}^+ + \underline{A}^-\underline{x}^-$

In the following, t will be omitted in all variables without confusion for notational simplicity. Similarly, we denote $x = \left[x_1^T \ \ldots \ x_N^T\right]^T$ and give similar manners for y, u as well as other variables.

3. Main Results

Define

$$\begin{aligned}
\dot{\overline{z}}_{iu} &= \left(\tilde{A}_{22} - K\tilde{A}_{12}\right)\overline{z}_{iu} + \left[\left(\tilde{A}_{22} - K\tilde{A}_{12}\right)K + \left(\tilde{A}_{21} - K\tilde{A}_{11}\right)\right]\sum_{j=1}^{N} l_{ij} y_j\\
&\quad + \left(\tilde{B}_2 - K\tilde{B}_1\right)\sum_{j=1}^{N} l_{ij} u_j + D^+\overline{h}_i - D^-\underline{h}_i + (-KC)^+\overline{h}_i - (-KC)^-\underline{h}_i,\\
\dot{\underline{z}}_{iu} &= \left(\tilde{A}_{22} - K\tilde{A}_{12}\right)\underline{z}_{iu} + \left[\left(\tilde{A}_{22} - K\tilde{A}_{12}\right)K + \left(\tilde{A}_{21} - K\tilde{A}_{11}\right)\right]\sum_{j=1}^{N} l_{ij} y_j\\
&\quad + \left(\tilde{B}_2 - K\tilde{B}_1\right)\sum_{j=1}^{N} l_{ij} u_j + D^+\underline{h}_i - D^-\overline{h}_i + (-KC)^+\underline{h}_i - (-KC)^-\overline{h}_i,
\end{aligned} \tag{9}$$

$$\begin{aligned}
\overline{z}_{iu}(0) &= D^+\overline{w}_i(0) - D^-\underline{w}_i(0) + (-KC)^+\overline{w}_i(0) - (-KC)^-\underline{w}_i(0),\\
\overline{z}_{iu}(0) &= D^+\underline{w}_i(0) - D^-\overline{w}_i(0) + (-KC)^+\underline{w}_i(0) - (-KC)^-\overline{w}_i(0),
\end{aligned}$$

where

$$\overline{h}_i \triangleq \overline{\Delta A}^{+}\overline{w}_i^{+} - \underline{\overset{+}{\Delta A}}\,\overline{w}_i^{-} - \overline{\Delta A}^{-}\underline{w}_i^{+} + \underline{\overset{-}{\Delta A}}\,\underline{w}_i^{-},$$

$$\underline{h}_i \triangleq \underline{\overset{+}{\Delta A}}\,\underline{w}_i^{+} - \overline{\Delta A}^{+}\underline{w}_i^{-} - \underline{\overset{-}{\Delta A}}\,\overline{w}_i^{+} + \overline{\Delta A}^{-}\overline{w}_i^{-}. \tag{10}$$

Then, one has Theorem 1.

Theorem 1. *Under Assumptions 1 and 3, if $\overline{w}_i(0)$ and $\underline{w}_i(0)$ in (8) are chosen to satisfy $\underline{w}_i(0) \le w_i(0) \le \overline{w}_i(0)$ and there exists an observer gain $K \in \mathbb{R}^{(n-p)\times p}$ to make $\widetilde{A}_{22} - K\widetilde{A}_{12}$ Metzler, then $\overline{z}_{iu}$ and $\underline{z}_{iu}$ given in (8) with this K are considered a neighborhood reduced-order framer for the uncertain MAS described by (1), where $\underline{w}_i \le w_i \le \overline{w}_i$ holds for $i = 1, \ldots, N$ with*

$$\begin{aligned}
\overline{w}_i &\triangleq Q^{+}\begin{bmatrix} \sum_{j=1}^{N} l_{ij}y_j \\ \overline{z}_{iu} + K\sum_{j=1}^{N} l_{ij}y_j \end{bmatrix} - Q^{-}\begin{bmatrix} \sum_{j=1}^{N} l_{ij}y_j \\ \underline{z}_{iu} + K\sum_{j=1}^{N} l_{ij}y_j \end{bmatrix}, \\
\underline{w}_i &\triangleq Q^{+}\begin{bmatrix} \sum_{j=1}^{N} l_{ij}y_j \\ \underline{z}_{iu} + K\sum_{j=1}^{N} l_{ij}y_j \end{bmatrix} - Q^{-}\begin{bmatrix} \sum_{j=1}^{N} l_{ij}y_j \\ \overline{z}_{iu} + K\sum_{j=1}^{N} l_{ij}y_j \end{bmatrix}.
\end{aligned} \tag{11}$$

Proof. 1 By Lemma 2 (1), if the following holds:

$$\begin{bmatrix} \sum_{j=1}^{N} l_{ij}y_j \\ \underline{z}_{iu} + K\sum_{j=1}^{N} l_{ij}y_j \end{bmatrix} \le \begin{bmatrix} \sum_{j=1}^{N} l_{ij}y_j \\ \widetilde{w}_{iu} \end{bmatrix} \le \begin{bmatrix} \sum_{j=1}^{N} l_{ij}y_j \\ \overline{z}_{iu} + K\sum_{j=1}^{N} l_{ij}y_j \end{bmatrix}, \tag{12}$$

for $t \ge 0$, then one can get $\underline{w}_i \le w_i \le \overline{w}_i$ for $t \ge 0$. Therefore, the proof of Theorem 1 will be completed if the inequality in (11) holds for $t \ge 0$, that is to prove the establishment of.

$$\underline{z}_{iu} \le \widetilde{w}_{iu} - K\sum_{j=1}^{N} l_{ij}y_j \le \overline{z}_{iu}. \tag{13}$$

By (3), (12), and (13) is equivalent to,

$$\underline{z}_{iu} \le z_{iu} \le \overline{z}_{iu}, \tag{14}$$

where z_{iu} is given in (2).

In order to prove the relationship in (13), let $\overline{e}_{iu} = \overline{z}_{iu} - z_{iu}$ and $\underline{e}_{iu} = z_{iu} - \underline{z}_{iu}$. By (2) and (8), one has

$$\begin{aligned}
\dot{\overline{e}}_{iu} &= \left(\widetilde{A}_{22} - K\widetilde{A}_{12}\right)\overline{e}_{iu} + D^{+}\overline{h}_i - D^{-}\underline{h}_i + (-KC)^{+}\overline{h}_i - (-KC)^{-}\underline{h}_i - D\Delta A w_i + KC\Delta A w_i \\
&= \left(\widetilde{A}_{22} - K\widetilde{A}_{12}\right)\overline{e}_{iu} + D^{+}\left(\overline{h}_i - \Delta A w_i\right) + D^{-}\left(\Delta A w_i - \underline{h}_i\right) \\
&\quad + (-KC)^{+}\left(\overline{h}_i - \Delta A w_i\right) + (-KC)^{-}\left(\Delta A w_i - \underline{h}_i\right), \\
\dot{\underline{e}}_{iu} &= \left(\widetilde{A}_{22} - K\widetilde{A}_{12}\right)\underline{e}_{iu} + D\Delta A w_i - KC\Delta A w_i - D^{+}\underline{h}_i + D^{-}\overline{h}_i - (-KC)^{+}\underline{h}_i + (-KC)^{-}\overline{h}_i \\
&= \left(\widetilde{A}_{22} - K\widetilde{A}_{12}\right)\underline{e}_{iu} + D^{+}\left(\Delta A w_i - \underline{h}_i\right) + D^{-}\left(\overline{h}_i - \Delta A w_i\right) \\
&\quad + (-KC)^{+}\left(\Delta A w_i - \underline{h}_i\right) + (-KC)^{-}\left(\overline{h}_i - \Delta A w_i\right).
\end{aligned} \tag{15}$$

Under Assumption 1, similar to the proof of Lemma 5 in [21], there hold $\overline{h}_i \geq \Delta A^+ \overline{w}_i - \Delta A^- \underline{w}_i$ and $\underline{h}_i \leq \Delta A^+ \underline{w}_i - \Delta A^- \overline{w}_i$, so that

$$\begin{aligned}
\dot{\overline{e}}_{iu} \geq & \left(\widetilde{A}_{22} - K\widetilde{A}_{12}\right)\overline{e}_{iu} + D^+\left[\Delta A^+ \overline{w}_i - \Delta A^- \underline{w}_i - \Delta A w_i\right] \\
& + D^-\left[\Delta A w_i - \left(\Delta A^+ \underline{w}_i - \Delta A^- \overline{w}_i\right)\right] \\
& + (-KC)^+\left[\Delta A^+ \overline{w}_i - \Delta A^- \underline{w}_i - \Delta A w_i\right] + (-KC)^-\left[\Delta A w_i - \left(\Delta A^+ \underline{w}_i - \Delta A^- \overline{w}_i\right)\right] \\
= & \left(\widetilde{A}_{22} - K\widetilde{A}_{12}\right)\overline{e}_{iu} \\
& + D^+\left[\Delta A^+\left(\overline{w}_i - w_i\right) + \Delta A^-\left(w_i - \underline{w}_i\right)\right] + D^-\left[\Delta A^+\left(w_i - \underline{w}_i\right) + \Delta A^-\left(\overline{w}_i - w_i\right)\right] \\
& + (-KC)^+\left[\Delta A^+\left(\overline{w}_i - w_i\right) + \Delta A^-\left(w_i - \underline{w}_i\right)\right] \\
& + (-KC)^-\left[\Delta A^+\left(w_i - \underline{w}_i\right) + \Delta A^-\left(\overline{w}_i - w_i\right)\right], \\
\dot{\underline{e}}_{iu} \geq & \left(\widetilde{A}_{22} - K\widetilde{A}_{12}\right)\underline{e}_{iu} + D^+\left[\Delta A w_i - \left(\Delta A^+ \underline{w}_i - \Delta A^- \overline{w}_i\right)\right] \\
& + D^-\left(\Delta A^+ \overline{w}_i - \Delta A^- \underline{w}_i - \Delta A w_i\right) \\
& + (-KC)^+\left[\Delta A w_i - \left(\Delta A^+ \underline{w}_i - \Delta A^- \overline{w}_i\right)\right] + (-KC)^-\left(\Delta A^+ \overline{w}_i - \Delta A^- \underline{w}_i - \Delta A w_i\right) \\
= & \left(\widetilde{A}_{22} - K\widetilde{A}_{12}\right)\underline{e}_{iu} \\
& + D^+\left[\Delta A^+\left(w_i - \underline{w}_i\right) + \Delta A^-\left(\overline{w}_i - w_i\right)\right] + D^-\left[\Delta A^+\left(\overline{w}_i - w_i\right) + \Delta A^-\left(w_i - \underline{w}_i\right)\right] \\
& + (-KC)^+\left[\Delta A^+\left(w_i - \underline{w}_i\right) + \Delta A^+\left(\overline{w}_i - w_i\right)\right] \\
& + (-KC)^-\left[\Delta A^+\left(\overline{w}_i - w_i\right) + \Delta A^-\left(w_i - \underline{w}_i\right)\right].
\end{aligned} \tag{16}$$

That is,

$$\begin{aligned}
\left[\dot{\overline{e}}_{iu}\ \dot{\underline{e}}_{iu}\right] = & \begin{bmatrix} \widetilde{A}_{22} - K\widetilde{A}_{12} & 0 \\ 0 & \widetilde{A}_{22} - K\widetilde{A}_{12} \end{bmatrix}\begin{bmatrix} \overline{e}_i \\ \underline{e}_i \end{bmatrix} \\
& + \begin{bmatrix} D^+\Delta A^+ + (-KC)^+\Delta A^+ & D^+\Delta A^- + (-KC)^+\Delta A^- \\ D^-\Delta A^- + (-KC)^-\Delta A^- & D^-\Delta A^+ + (-KC)^-\Delta A^+ \end{bmatrix}\begin{bmatrix} \overline{w}_i - w_i \\ w_i - \underline{w}_i \end{bmatrix}.
\end{aligned} \tag{17}$$

By (3) and (10), one has

$$\begin{aligned}
\overline{w}_i - w_i &= Q_2^+\left(\overline{z}_{iu} - z_{iu}\right) + Q_2^-\left(z_{iu} - \underline{z}_{iu}\right), \\
w_i - \underline{w}_i &= Q_2^-\left(\overline{z}_{iu} - z_{iu}\right) + Q_2^+\left(z_{iu} - \underline{z}_{iu}\right),
\end{aligned} \tag{18}$$

i.e.,

$$\begin{bmatrix} \overline{w}_i - w_i \\ w_i - \underline{w}_i \end{bmatrix} = \begin{bmatrix} Q_2^+ & Q_2^- \\ Q_2^- & Q_2^+ \end{bmatrix}\begin{bmatrix} \overline{e}_{iu} \\ \underline{e}_{iu} \end{bmatrix}. \tag{19}$$

Then, one has

$$\begin{aligned}
\left[\dot{\overline{e}}_{iu}\ \dot{\underline{e}}_{iu}\right] \geq & \begin{bmatrix} \widetilde{A}_{22} - K\widetilde{A}_{12} & 0 \\ 0 & \widetilde{A}_{22} - K\widetilde{A}_{12} \end{bmatrix}\begin{bmatrix} \overline{e}_i \\ \underline{e}_i \end{bmatrix} \\
& + \begin{bmatrix} D^+\Delta A^+ + (-KC)^+\Delta A^+ & D^+\Delta A^- + (-KC)^+\Delta A^- \\ D^-\Delta A^- + (-KC)^-\Delta A^- & D^-\Delta A^+ + (-KC)^-\Delta A^+ \end{bmatrix}\begin{bmatrix} Q_2^+ & Q_2^- \\ Q_2^- & Q_2^+ \end{bmatrix}\begin{bmatrix} \overline{e}_{iu} \\ \underline{e}_{iu} \end{bmatrix} \\
\triangleq & \begin{bmatrix} \widetilde{A}_{22} - K\widetilde{A}_{12} & 0 \\ 0 & \widetilde{A}_{22} - K\widetilde{A}_{12} \end{bmatrix}\begin{bmatrix} \overline{e}_i \\ \underline{e}_i \end{bmatrix} + \Pi\begin{bmatrix} \overline{e}_i \\ \underline{e}_i \end{bmatrix}.
\end{aligned} \tag{20}$$

It is apparent that $\Pi \geq 0$.

On the other hand, by (3), one has $w_i = (D - KC)w_i$, so that there hold

$$\begin{aligned}
\overline{e}_{iu}(0) &= \overline{z}_{iu}(0) - z_{iu}(0) \\
&= D^+\overline{w}_i(0) - D^-\underline{w}_i(0) + (-KC)^+\overline{w}_i(0) - (-KC)^-\underline{w}_i(0) - (D - KC)w_i(0) \\
&= D^+\left(\overline{w}_i(0) - w_i(0)\right) + (-KC)^+\left(\overline{w}_i(0) - w_i(0)\right) \\
&\quad + D^-\left(w_i(0) - \underline{w}_i(0)\right) + (-KC)^-\left(w_i(0) - \underline{w}_i(0)\right) \\
&= \left[D^+ + (-KC)^+ \quad D^- + (-KC)^-\right]\begin{bmatrix}\overline{w}_i(0) - w_i(0) \\ w_i(0) - \underline{w}_i(0)\end{bmatrix}, \\
\underline{e}_{iu}(0) &= z_{iu}(0) - \underline{z}_{iu}(0) \\
&= (D - KC)w_i(0) - D^+\underline{w}_i(0) + D^-\overline{w}_i(0) - (-KC)^+\underline{w}_i(0) + (-KC)^-\overline{w}_i(0) \\
&= D^+\left(w_i(0) - \underline{w}_i(0)\right) + D^-\left(\overline{w}_i(0) - w_i(0)\right) \\
&\quad + (-KC)^+\left(w_i(0) - \underline{w}_i(0)\right) + (-KC)^-\left(\overline{w}_i(0) - w_i(0)\right) \\
&= \left[D^- + (-KC)^- \quad D^+ + (-KC)^+\right]\begin{bmatrix}\overline{w}_i(0) - w_i(0) \\ w_i(0) - \underline{w}_i(0)\end{bmatrix},
\end{aligned} \tag{21}$$

which further result in

$$\left[\overline{e}_{iu}(0)\underline{e}_{iu}(0)\right] = \begin{bmatrix} D^+ + (-KC)^+ & D^- + (-KC)^- \\ D^- + (-KC)^- & D^+ + (-KC)^+ \end{bmatrix}\begin{bmatrix}\overline{w}_i(0) - w_i(0) \\ w_i(0) - \underline{w}_i(0)\end{bmatrix}. \tag{22}$$

Since $\underline{w}_i(0) \leq w_i(0) \leq \overline{w}_i(0)$, by (18), one has $\left[\overline{e}_{iu}(0)\underline{e}_{iu}(0)\right] \geq 0$.

Therefore, by Lemma 1, if $\widetilde{A}_{22} - K\widetilde{A}_{12}$ is a Metzler matrix, then $\overline{z}_{iu}$ and $\underline{z}_{iu}$ given in (8) are considered a neighborhood reduced-order framer for the uncertain MAS described by (1).

This completes the proof.

For $\overline{w}_i$ and $\underline{w}_i$ in (10), construct

$$u_i = -B^T P_1\left(\overline{w}_i + \underline{w}_i\right), \tag{23}$$

where $P_1 \succ 0$ is the solution of the algebraic Riccati equation

$$A^T P_1 + P_1 A - \lambda_0 P_1 B B^T P_1 + \epsilon I = 0, \tag{24}$$

with $\lambda_0 \geq 2\lambda_2(L)$ and $\epsilon > 0$.

Define

$$\begin{aligned}
\overline{E}_i &= \overline{w}_i - w_i, \\
\underline{E}_i &= w_i - \underline{w}_i.
\end{aligned} \tag{25}$$

By (16), one has

$$\begin{bmatrix}\overline{E}_i \\ \underline{E}_i\end{bmatrix} = \begin{bmatrix} Q_2^+ & Q_2^- \\ Q_2^- & Q_2^+ \end{bmatrix}\begin{bmatrix}\overline{e}_{iu} \\ \underline{e}_{iu}\end{bmatrix}. \tag{26}$$

For u_i in (19), by (1), (21), and (22), one has

$$\begin{aligned}
\dot{x}_i &= (A + \Delta A)x_i - BB^T P_1\left(\overline{w}_i + \underline{w}_i\right) \\
&= (A + \Delta A)x_i - BB^T P_1\left(2w_i + \overline{E}_i - \underline{E}_i\right) \\
&= (A + \Delta A)x_i - 2BB^T P\sum_{j=1}^{N} l_{ij}x_j \\
&\quad - BB^T P_1 Q_2\overline{e}_{iu} + BB^T P_1 Q_2\underline{e}_{iu}.
\end{aligned} \tag{27}$$

On the other hand, by (14), there hold

$$\begin{aligned}
\dot{\overline{e}}_{iu} &= \left(\widetilde{A}_{22} - K\widetilde{A}_{12}\right)\overline{e}_{iu} \\
&\quad + \left[D^+ + (-KC)^+ \quad D^- + (-KC)^-\right]\begin{bmatrix}\overline{h}_i - \Delta A w_i \\ \Delta A w_i - \underline{w}_i\end{bmatrix}, \\
\dot{\underline{e}}_{iu} &= \left(\widetilde{A}_{22} - K\widetilde{A}_{12}\right)\underline{e}_{iu} \\
&\quad + \left[D^- + (-KC)^- \quad D^+ + (-KC)^+\right]\begin{bmatrix}\overline{h}_i - \Delta A w_i \\ \Delta A w_i - \underline{w}_i\end{bmatrix}.
\end{aligned} \tag{28}$$

Since

$$\begin{aligned}\overline{h}_i - \Delta A w_i &= \begin{bmatrix}\overline{\Delta A}^+ & \overline{\Delta A}^-\end{bmatrix}\begin{bmatrix}\overline{E}_i\\ \underline{E}_i\end{bmatrix}^+ - \begin{bmatrix}\overset{+}{\underline{\Delta A}} & \overset{-}{\underline{\Delta A}}\end{bmatrix}\begin{bmatrix}\overline{E}_i\\ \underline{E}_i\end{bmatrix}^- \\ &\quad + (\overline{\Delta A} - \Delta A)w_i^+ + (\Delta A - \underline{\Delta A})w_i^-, \\ \Delta A w_i - \underline{h}_i &= \begin{bmatrix}\overset{-}{\underline{\Delta A}} & \overset{+}{\underline{\Delta A}}\end{bmatrix}\begin{bmatrix}\overline{E}_i\\ \underline{E}_i\end{bmatrix}^+ - \begin{bmatrix}\overline{\Delta A}^- & \overline{\Delta A}^+\end{bmatrix}\begin{bmatrix}\overline{E}_i\\ \underline{E}_i\end{bmatrix}^- \\ &\quad + (\Delta A - \underline{\Delta A})w_i^+ + (\overline{\Delta A} - \Delta A)w_i^-,\end{aligned} \tag{29}$$

that is,

$$\begin{aligned}\begin{bmatrix}\overline{h}_i - \Delta A w_i\\ \Delta A w_i - \underline{w}_i\end{bmatrix} &= \begin{bmatrix}\overline{\Delta A}^+ & \overline{\Delta A}^-\\ \overset{-}{\underline{\Delta A}} & \overset{+}{\underline{\Delta A}}\end{bmatrix}\begin{bmatrix}\overline{E}_i\\ \underline{E}_i\end{bmatrix}^+ - \begin{bmatrix}\overset{+}{\underline{\Delta A}} & \overset{-}{\underline{\Delta A}}\\ \overline{\Delta A}^- & \overline{\Delta A}^+\end{bmatrix}\begin{bmatrix}\overline{E}_i\\ \underline{E}_i\end{bmatrix}^- \\ &\quad + \begin{bmatrix}\overline{\Delta A} - \Delta A\\ \Delta A - \underline{\Delta A}\end{bmatrix}w_i^+ + \begin{bmatrix}\Delta A - \underline{\Delta A}\\ \overline{\Delta A} - \Delta A\end{bmatrix}w_i^-,\end{aligned} \tag{30}$$

with (22) and (24), one has

$$\begin{aligned}\begin{bmatrix}\dot{\overline{e}}_{iu}\\ \dot{\underline{e}}_{iu}\end{bmatrix} &= \begin{bmatrix}\widetilde{A}_{22} - K\widetilde{A}_{12} & 0\\ 0 & \widetilde{A}_{22} - K\widetilde{A}_{12}\end{bmatrix}\begin{bmatrix}\overline{e}_{iu}\\ \underline{e}_{iu}\end{bmatrix} \\ &\quad + \begin{bmatrix}D^+ + (-KC)^+ & D^- + (-KC)^-\\ D^- + (-KC)^- & D^+ + (-KC)^+\end{bmatrix} \\ &\quad \cdot \begin{bmatrix}\overline{\Delta A}^+ & \overline{\Delta A}^-\\ \overset{-}{\underline{\Delta A}} & \overset{+}{\underline{\Delta A}}\end{bmatrix}\left(\begin{bmatrix}Q_2^+ & Q_2^-\\ Q_2^- & Q_2^+\end{bmatrix}\begin{bmatrix}\overline{e}_{iu}\\ \underline{e}_{iu}\end{bmatrix}\right)^+ \\ &\quad - \begin{bmatrix}\overset{+}{\underline{\Delta A}} & \overset{-}{\underline{\Delta A}}\\ \overline{\Delta A}^- & \overline{\Delta A}^+\end{bmatrix}\left(\begin{bmatrix}Q_2^+ & Q_2^-\\ Q_2^- & Q_2^+\end{bmatrix}\begin{bmatrix}\overline{e}_{iu}\\ \underline{e}_{iu}\end{bmatrix}\right)^- \\ &\quad + \begin{bmatrix}\overline{\Delta A} - \Delta A\\ \Delta A - \underline{\Delta A}\end{bmatrix}w_i^+ + \begin{bmatrix}\Delta A - \underline{\Delta A}\\ \overline{\Delta A} - \Delta A\end{bmatrix}w_i^-.\end{aligned} \tag{31}$$

Let $\eta_i = \begin{bmatrix}x_i^T & \overline{e}_{iu}^T & \underline{e}_{iu}^T\end{bmatrix}^T$. It follows from (15) and (23) that

$$\begin{aligned}\dot{\eta}_i &= \begin{bmatrix}A & -BB^TP_1Q_2 & BB^TP_1Q_2\\ 0 & \widetilde{A}_{22} - K\widetilde{A}_{12} & 0\\ 0 & 0 & \widetilde{A}_{22} - K\widetilde{A}_{12}\end{bmatrix}\eta_i \\ &\quad - 2\begin{bmatrix}BB^TP_1 & 0 & 0\\ 0 & 0 & 0\\ 0 & 0 & 0\end{bmatrix}\sum_{j=1}^N l_{ij}\eta_j \\ &\quad + \Gamma_2\mathscr{M}_1(\Gamma_1\eta_i)^+ - \Gamma_2\mathscr{M}_2(\Gamma_1\eta_i)^- \\ &\quad + \Gamma_2\mathscr{M}_3\left(\sum_{j=1}^N l_{ij}\eta_j\right)^+ + \Gamma_2\Gamma_0\mathscr{M}_3\left(\sum_{j=1}^N l_{ij}\eta_j\right)^-,\end{aligned} \tag{32}$$

where

$$\begin{aligned}\Gamma_0 &= \begin{bmatrix}I_n & 0 & 0\\ 0 & 0 & I_n\\ 0 & I_n & 0\end{bmatrix}, \\ \Gamma_1 &= \begin{bmatrix}I_n & 0 & 0\\ 0 & Q_2^+ & Q_2^-\\ 0 & Q_2^- & Q_2^+\end{bmatrix}, \\ \Gamma_2 &= \begin{bmatrix}I_n & 0 & 0\\ 0 & D^+ + (-KC)^+ & D^- + (-KC)^-\\ 0 & D^- + (-KC)^- & D^+ + (-KC)^+\end{bmatrix}, \\ \mathscr{M}_1 &= \begin{bmatrix}\Delta A & 0 & 0\\ 0 & \overline{\Delta A}^+ & \overline{\Delta A}^-\\ 0 & \overset{-}{\underline{\Delta A}} & \overset{+}{\underline{\Delta A}}\end{bmatrix}, \\ \mathscr{M}_2 &= \begin{bmatrix}\Delta A & 0 & 0\\ 0 & \overset{+}{\underline{\Delta A}} & \overset{-}{\underline{\Delta A}}\\ 0 & \overline{\Delta A}^- & \overline{\Delta A}^+\end{bmatrix}, \\ \mathscr{M}_3 &= \begin{bmatrix}0 & 0 & 0\\ \overline{\Delta A} - \Delta A & 0 & 0\\ \Delta A - \underline{\Delta A} & 0 & 0\end{bmatrix},\end{aligned} \tag{33}$$

which induces

$$\begin{aligned}\dot{\eta} &= (I_N \otimes \mathscr{A} - L \otimes \mathscr{B})\eta \\ &\quad + (I_N \otimes \Gamma_2\mathscr{M}_1)((I_N \otimes \Gamma_1)\eta)^+ \\ &\quad - (I_N \otimes \Gamma_2\mathscr{M}_2)((I_N \otimes \Gamma_1)\eta)^- \\ &\quad + (I_N \otimes \Gamma_2\mathscr{M}_3)\left(\left(L \otimes I_{(3n-2p)}\right)\eta\right)^+ \\ &\quad + (I_N \otimes \Gamma_2\Gamma_0\mathscr{M}_3)\left(\left(L \otimes I_{(3n-2p)}\right)\eta\right)^-,\end{aligned} \tag{34}$$

where

$$\begin{aligned}\mathscr{A} &= \begin{bmatrix}A & -BB^TP_1Q_2 & BB^TP_1Q_2\\ 0 & \widetilde{A}_{22} - K\widetilde{A}_{12} & 0\\ 0 & 0 & \widetilde{A}_{22} - K\widetilde{A}_{12}\end{bmatrix}, \\ \mathscr{B} &= \begin{bmatrix}2BB^TP_1 & 0 & 0\\ 0 & 0 & 0\\ 0 & 0 & 0\end{bmatrix}.\end{aligned} \tag{35}$$

Since L is with an undirected graph, there is an orthogonal matrix $\mathscr{U} = \begin{bmatrix}1/\sqrt{N}\,1_N & \mathscr{U}_2\end{bmatrix}$ with $\mathscr{U}_2 \in \mathbb{R}^{N\times(N-1)}$ such that $\mathscr{U}^TL\mathscr{U} = \mathrm{diag}\{\lambda_1(L), \ldots, \lambda_N(L)\}$, where $\lambda_i(L) > 0$ for $i = 2, \ldots, N$, if $\mathscr{G} = (\mathscr{V}, \mathscr{E}, W)$ is connected. For better understanding, denote

$$\Lambda = \mathrm{diag}\{\lambda_2(L), \ldots, \lambda_N(L)\} = \mathscr{U}_2^TL\mathscr{U}_2. \tag{36}$$

Let $\eta_u = (\mathscr{U}^T \otimes I_{(3n-2p)})\eta$ and $\eta_{uu} = (\mathscr{U}_2^T \otimes I_{(3n-2p)})\eta = \begin{bmatrix}\eta_{u2}^T & \cdots & \eta_{uN}^T\end{bmatrix}^T$, and then one has

$$\begin{aligned}\dot{\eta}_{uu} &= \left(\mathcal{U}_2^T \otimes \mathcal{A} - \mathcal{U}_2^T L \otimes \mathcal{B}\right)\eta \\ &+ \left(\mathcal{U}_2^T \otimes \Gamma_2 \mathcal{M}_1\right)\left((I_N \otimes \Gamma_1)\eta\right)^+ - \left(\mathcal{U}_2^T \otimes \Gamma_2 \mathcal{M}_2\right)\left((I_N \otimes \Gamma_1)\eta\right)^- \\ &+ \left(\mathcal{U}_2^T \otimes \Gamma_2 \mathcal{M}_3\right)\left(\left(L \otimes I_{(3n-2p)}\right)\eta\right)^+ + \left(\mathcal{U}_2^T \otimes \Gamma_2\Gamma_0 \mathcal{M}_3\right)\left(\left(L \otimes I_{(3n-2p)}\right)\eta\right)^-.\end{aligned} \tag{37}$$

Since $\mathcal{U}_2^T\mathcal{U}_2 = I_{N-1}$, $\mathcal{U}_2\mathcal{U}_2^T = I_N - 1/N 1_N 1_N^T$ and $L1_N = 0$, one has

$$\begin{aligned}\dot{\eta}_{uu} &= (I_{N-1} \otimes \mathcal{A})\left(\mathcal{U}_2^T \otimes I_{(3n-2p)}\right)\eta - \left(\mathcal{U}_2^T L\left(\mathcal{U}_2\mathcal{U}_2^T + \frac{1}{N}1_N 1_N^T\right) \otimes \mathcal{B}\right)\eta \\ &+ \left(\mathcal{U}_2^T \otimes \Gamma_2 \mathcal{M}_1\right)\left((I_N \otimes \Gamma_1)\eta\right)^+ - \left(\mathcal{U}_2^T \otimes \Gamma_2 \mathcal{M}_2\right)\left((I_N \otimes \Gamma_1)\eta\right)^- \\ &+ \left(\mathcal{U}_2^T \otimes \Gamma_2 \mathcal{M}_3\right)\left(\left(L \otimes I_{(3n-2p)}\right)\eta\right)^+ + \left(\mathcal{U}_2^T \otimes \Gamma_2\Gamma_0 \mathcal{M}_3\right)\left(\left(L \otimes I_{(3n-2p)}\right)\eta\right)^- \\ &= (I_{N-1} \otimes \mathcal{A} - \Lambda \otimes \mathcal{B})\eta_{uu} \\ &+ \left(\mathcal{U}_2^T \otimes \Gamma_2 \mathcal{M}_1\right)\left((I_N \otimes \Gamma_1)\eta\right)^+ - \left(\mathcal{U}_2^T \otimes \Gamma_2 \mathcal{M}_2\right)\left((I_N \otimes \Gamma_1)\eta\right)^- \\ &+ \left(\mathcal{U}_2^T \otimes \Gamma_2 \mathcal{M}_3\right)\left(\left(L \otimes I_{(3n-2p)}\right)\eta\right)^+ + \left(\mathcal{U}_2^T \otimes \Gamma_2\Gamma_0 \mathcal{M}_3\right)\left(\left(L \otimes I_{(3n-2p)}\right)\eta\right)^-.\end{aligned} \tag{38}$$

Construct a Lyapunov function:

$$V = \eta_{uu}^T (I_{N-1} \otimes \mathcal{P})\eta_{uu}, \tag{39}$$

where $\mathcal{P} = \mathrm{diag}\{P_1, P_2, P_2\}$ with P_1 in (20), $P_2 \succ 0$ being the solution of the Lyapunov equation

$$\begin{aligned}&\left(\tilde{A}_{22} - K\tilde{A}_{12}\right)^T P_2 + P_2\left(\tilde{A}_{22} - K\tilde{A}_{12}\right) \\ &+ \epsilon I_{n-p} + Q_2^T P_1 B B^T P_1 Q_2 = 0.\end{aligned} \tag{40}$$

□

Theorem 2. *Consider an uncertain MAS (1) communicating through an undirected network $\mathcal{G} = (\mathcal{V}, \mathcal{E}, G)$ and suppose that Assumptions 1, 2, and 3 hold. If $K \in \mathbb{R}^{(n-p)\times p}$ is given to make $\tilde{A}_{22} - K\tilde{A}_{12}$ Hurwitz and Metzler, and*

$$\theta_1\theta_2 < \frac{\epsilon^2}{16}, \tag{41}$$

where

$$\begin{aligned}\theta_1 &= \|\Gamma_1\|^2 + \lambda_N(L), \\ \theta_2 &= \left(\gamma^2 + 2\left\|\overline{\Delta A} - \underline{\Delta A}\right\|^2\right)\|\Gamma_2\|^2 \max\left\{\lambda_n(P_1), \lambda_{3n-2p}(P_2)\right\},\end{aligned} \tag{42}$$

with $\gamma = \max\left\{\|\overline{\Delta A}\|, \|\underline{\Delta A}\|, \left\|\begin{bmatrix} \overline{\Delta A}^+ & \overline{\Delta A}^- \\ \underline{\Delta A}^- & \underline{\Delta A}^+ \end{bmatrix}\right\|\right\}$, then $\overline{z}_{iu}$ and $\underline{z}_{iu}$ given in (8) with the control algorithm (19) constitute a reduced-order NIO for (1), provided that $\underline{w}_i(0) \le w_i(0) \le \overline{w}_i(0)$.

Proof. 2 For the Lyapunov function given in (29), its derivative according to (28) yields

$$\begin{aligned}\dot{V} &= \sum_{i=2}^{N} \eta_{uu,i}^T \Phi_i \eta_{uu,i} \\ &+ \left[\left((I_N \otimes \Gamma_1)\eta\right)^+\right]^T \left(\mathcal{U}_2^T \otimes \Gamma_2 \mathcal{M}_1\right)^T (I_{N-1} \otimes \mathcal{P})\eta_{uu} \\ &+ \eta_{uu}^T (I_{N-1} \otimes \mathcal{P})\left(\mathcal{U}_2^T \otimes \Gamma_2 \mathcal{M}_1\right)\left((I_N \otimes \Gamma_1)\eta\right)^+ \\ &- \left[\left((I_{N-1} \otimes \Gamma_1)\eta\right)^-\right]^T \left(\mathcal{U}_2^T \otimes \Gamma_2 \mathcal{M}_2\right)^T (I_{N-1} \otimes \mathcal{P})\eta_{uu} \\ &- \eta_{uu}^T (I_{N-1} \otimes \mathcal{P})\left(\mathcal{U}_2^T \otimes \Gamma_2 \mathcal{M}_2\right)\left((I_N \otimes \Gamma_1)\eta\right)^- \\ &+ \left[\left(\left(L \otimes I_{(3n-2p)}\right)\eta\right)^+\right]^T \left(\mathcal{U}_2^T \otimes \Gamma_2 \mathcal{M}_3\right)^T (I_{N-1} \otimes \mathcal{P})\eta_{uu} \\ &+ \eta_{uu}^T (I_{N-1} \otimes \mathcal{P})\left(\mathcal{U}_2^T \otimes \Gamma_2 \mathcal{M}_3\right)\left(\left(L \otimes I_{(3n-2p)}\right)\eta\right)^+ \\ &+ \left[\left(\left(L \otimes I_{(3n-2p)}\right)\eta\right)^-\right]^T \left(\mathcal{U}_2^T \otimes \Gamma_2\Gamma_0 \mathcal{M}_3\right)^T (I_{N-1} \otimes \mathcal{P})\eta_{uu} \\ &+ \eta_{uu}^T (I_{N-1} \otimes \mathcal{P})\left(\mathcal{U}_2^T \otimes \Gamma_2\Gamma_0 \mathcal{M}_3\right)\left(\left(L \otimes I_{(3n-2p)}\right)\eta\right)^- \\ &\le \sum_{i=2}^{N} \eta_{uu,i}^T \Phi_i \eta_{uu,i} \\ &+ c\left[\left((I_N \otimes \Gamma_1)\eta\right)^+\right]^T \left(\mathcal{U}_2\mathcal{U}_2^T \otimes I_{(3n-2p)}\right)\left((I_N \otimes \Gamma_1)\eta\right)^+ \\ &+ \frac{\lambda_{3n-2p}(\mathcal{P})}{c}\|\Gamma_2\|^2\|\mathcal{M}_1\|^2 \eta_{uu}^T \eta_{uu} \\ &+ c\left[\left((I_N \otimes \Gamma_1)\eta\right)^-\right]^T \left(\mathcal{U}_2\mathcal{U}_2^T \otimes I_{(3n-2p)}\right)\left((I_N \otimes \Gamma_1)\eta\right)^- \\ &+ \frac{\lambda_{3n-2p}(\mathcal{P})}{c}\|\Gamma_2\|^2\|\mathcal{M}_2\|^2 \eta_{uu}^T \eta_{uu}\end{aligned}$$

$$
\begin{aligned}
&+ c\left[\left(\left(L\otimes I_{(3n-2p)}\right)\eta\right)^{+}\right]^{T}\left(\mathcal{U}_2\mathcal{U}_2^{T}\otimes I_{(3n-2p)}\right)\\
&\cdot\left(\left(L\otimes I_{(3n-2p)}\right)\eta\right)^{+}\\
&+\frac{\lambda_{3n-2p}\mathcal{P}}{c}\left\|\Gamma_2\right\|^{2}\left\|\mathcal{M}_3\right\|^{2}\eta_{uu}^{T}\eta_{uu}\\
&+ c\left[\left(\left(L\otimes I_{(3n-2p)}\right)\eta\right)^{-}\right]^{T}\\
&\cdot\left(\mathcal{U}_2\mathcal{U}_2^{T}\otimes I_{(3n-2p)}\right)\left(\left(L\otimes I_{(3n-2p)}\right)\eta\right)^{-}\\
&+\frac{\lambda_{3n-2p}\mathcal{P}}{c}\left\|\Gamma_2\right\|^{2}\left\|\Gamma_0\right\|^{2}\left\|\mathcal{M}_3\right\|^{2}\eta_{uu}^{T}\eta_{uu},
\end{aligned}
\tag{43}
$$

where $c>0$ is constant to be determined and

$$
\begin{aligned}
\Phi_i &= \left(\mathcal{A}-\lambda_i(L)\mathcal{B}\right)^{T}\mathcal{P}+\mathcal{P}\left(\mathcal{A}-\lambda_i(L)\mathcal{B}\right)\\
&=\begin{bmatrix}
A^{T}P_1+P_1A-4\lambda_i(L)P_1^{T}BB^{T}P_1 & -P_1^{T}BB^{T}P_1Q_2 & P_1^{T}BB^{T}P_1Q_2\\
-Q_2^{T}P_1^{T}BB^{T}P_1 & \begin{matrix}\left(\tilde{A}_{22}-K\tilde{A}_{12}\right)^{T}Q\\ +Q\left(\tilde{A}_{22}-K\tilde{A}_{12}\right)\end{matrix} & 0\\
Q_2P_1^{T}BB^{T}P_1 & 0 & \begin{matrix}\left(\tilde{A}_{22}-K\tilde{A}_{12}\right)^{T}Q\\ +Q\left(\tilde{A}_{22}-K\tilde{A}_{12}\right)\end{matrix}
\end{bmatrix},
\end{aligned}
\tag{44}
$$

with $i=2,3,\ldots,N$.

Since the eigenvalues of $\mathcal{U}_2\mathcal{U}_2^{T}$ are no less than 0, one has

$$
\begin{aligned}
\dot{V} &\le \sum_{i=2}^{N}\eta_{uu,i}^{T}\Phi_i\eta_{uu,i}\\
&+ c\left(\left(I_N\otimes\Gamma_1\right)\eta\right)^{T}\left(\mathcal{U}_2\mathcal{U}_2^{T}\otimes I_{(3n-2p)}\right)\left(I_N\otimes\Gamma_1\right)\eta\\
&+ c\left(\left(I_N\otimes\Gamma_1\right)\eta\right)^{T}\left(\mathcal{U}_2\mathcal{U}_2^{T}\otimes I_{(3n-2p)}\right)\left(I_N\otimes\Gamma_1\right)\eta\\
&+ c\left(\left(L\otimes I_{(3n-2p)}\right)\eta\right)^{T}\left(\mathcal{U}_2\mathcal{U}_2^{T}\otimes I_{(3n-2p)}\right)\left(L\otimes I_{(3n-2p)}\right)\eta\\
&+ c\left(\left(L\otimes I_{(3n-2p)}\right)\eta\right)^{T}\left(\mathcal{U}_2\mathcal{U}_2^{T}\otimes I_{(3n-2p)}\right)\left(L\otimes I_{(3n-2p)}\right)\eta\\
&+\frac{\lambda_{3n-2p}(\mathcal{P})}{c}\left\|\Gamma_2\right\|^{2}\left(\left\|\mathcal{M}_1\right\|^{2}+\left\|\mathcal{M}_2\right\|^{2}+\left\|\mathcal{M}_3\right\|^{2}+\left\|\Gamma_0\right\|^{2}\left\|\mathcal{M}_3\right\|^{2}\right)\eta_{uu}^{T}\eta_{uu}\\
&=\sum_{i=2}^{N}\eta_{uu,i}^{T}\Phi_i\eta_{uu,i}\\
&+ 2c\eta_{uu}^{T}\left(I_{N-1}\otimes\Gamma_1^{T}\Gamma_1\right)\eta_{uu}+2c\eta^{T}\left(L\mathcal{U}_2\mathcal{U}_2^{T}L\otimes I_{(3n-2p)}\right)\eta\\
&+\frac{\lambda_{3n-2p}(\mathcal{P})}{c}\left\|\Gamma_2\right\|^{2}\left(\left\|\mathcal{M}_1\right\|^{2}+\left\|\mathcal{M}_2\right\|^{2}+\left\|\mathcal{M}_3\right\|^{2}+\left\|\Gamma_0\right\|^{2}\left\|\mathcal{M}_3\right\|^{2}\right)\eta_{uu}^{T}\eta_{uu}.
\end{aligned}
\tag{45}
$$

Since

$$\begin{aligned}
&2c\eta^T\left(L\mathcal{U}_2\mathcal{U}_2^TL\otimes I_{(3n-2p)}\right)\eta\\
&=2c\eta^T\left(\mathcal{U}_2\mathcal{U}_2^T+\frac{1}{N}1_N1_N^T\right)\left(L\mathcal{U}_2\mathcal{U}_2^TL\otimes I_{(3n-2p)}\right)\left(\mathcal{U}_2\mathcal{U}_2^T+\frac{1}{N}1_N1_N^T\right)\eta\\
&=2c\eta_{uu}^T\Lambda^2\eta_{uu}\\
&\dot{V}\le\sum_{i=2}^{N}\eta_{uu,i}^T\Phi_i\eta_{uu,i}\\
&\quad+\left[2c\left(\|\Gamma_1\|^2+\lambda_N^2(L)\right)+\frac{\lambda_{3n-2p}(\mathscr{P})}{c}\|\Gamma_2\|^2\left(\|\mathscr{M}_1\|^2+\|\mathscr{M}_2\|^2+\|\mathscr{M}_3\|^2+\|\Gamma_0\|^2\|\mathscr{M}_3\|^2\right)\right]\eta_{uu}^T\eta_{uu}.
\end{aligned}\tag{46}$$

there holds

$$\Phi_i\le\begin{bmatrix}
A^TP_1+P_1A-2\lambda_i(L)P_1^TBB^TP_1 & 0 & 0\\
-0 & \begin{matrix}\left(\widetilde{A}_{22}-K\widetilde{A}_{12}\right)^TQ\\ +Q\left(\widetilde{A}_{22}-K\widetilde{A}_{12}\right)\\ +\frac{1}{\lambda_i(L)}Q_2^TP_1BB^TP_1Q_2\end{matrix} & 0\\
0 & 0 & \begin{matrix}\left(\widetilde{A}_{22}-K\widetilde{A}_{12}\right)^TQ\\ +Q\left(\widetilde{A}_{22}-K\widetilde{A}_{12}\right)\\ +\frac{1}{\lambda_i(L)}Q_2^TP_1BB^TP_1Q_2\end{matrix}
\end{bmatrix},\tag{47}$$

with $i=2,3,\ldots,N$. Therefore, one can get that

$$\begin{aligned}
\dot{V}\le&-\left\{\epsilon-\left[2c\left(\|\Gamma_1\|^2+\lambda_N^2(L)\right)\right]\right\}\eta_{uu}^T\eta_{uu}\\
&-\left\{\left[\frac{\lambda_{3n-2p}(\mathscr{P})}{c}\|\Gamma_2\|^2\left(\|\mathscr{M}_1\|^2+\|\mathscr{M}_2\|^2+\|\mathscr{M}_3\|^2+\|\Gamma_0\|^2\|\mathscr{M}_3\|^2\right)\right]\right\}\eta_{uu}^T\eta_{uu}.
\end{aligned}\tag{48}$$

Since $\Gamma_0^{-1} = \Gamma_0$ and $\|\Gamma_0\| = 1, \mathscr{M}_2 = \Gamma_0 \mathscr{M}_1 \Gamma_0$ and

$$\|\mathscr{M}_1\| = \max\left\{\|\overline{\Delta A}\|, \|\underline{\Delta A}\|, \left\|\begin{bmatrix} \overline{\Delta A}^{+} & \overline{\Delta A}^{-} \\ \underline{\Delta A}^{-} & \underline{\Delta A}^{+} \end{bmatrix}\right\|\right\} = \gamma, \tag{49}$$

$\|\mathscr{M}_3\|^2 \le 2\|\overline{\Delta A} - \underline{\Delta A}\|^2$, so that

$$\dot{V} \le -\left[\epsilon - 2\left(\theta_1 c + \frac{\theta_2}{c}\right)\right]\eta_{uu}^T \eta_{uu}. \tag{50}$$

Choose $c = \sqrt{\theta_2/\theta_1}$, and under (31), one has $\epsilon - 2(\theta_1 c + \theta_2/c) > 0$, which induces that $\dot{V} \le 0$, where the equality sign holds if and only if $\eta_{uu} = 0$. Thus, with u_i in (19), uncertain MAS (1) can achieve consensus. □

Remark 1. By Theorem 2, one has $\lim_{t\longrightarrow\infty} w_i^+ = 0$ and $\lim_{t\longrightarrow\infty} w_i^- = 0$ for $i = 1, \ldots, N$. Thus, by (25), as $t \longrightarrow \infty$, one can get that

$$\begin{bmatrix} \dot{\overline{e}}_{iu} & \dot{\underline{e}}_{iu} \end{bmatrix} = \mathsf{F}_1 \begin{bmatrix} \overline{e}_{iu} \\ \underline{e}_{iu} \end{bmatrix} + \mathsf{F}_2 \left\| \begin{bmatrix} Q_2^+ & Q_2^- \\ Q_2^- & Q_2^+ \end{bmatrix} \begin{bmatrix} \overline{e}_{iu} \\ \underline{e}_{iu} \end{bmatrix} \right\|, \tag{51}$$

where

$$\mathsf{F}_1 = \begin{bmatrix} \widetilde{A}_{22} - K\widetilde{A}_{12} & 0 \\ 0 & \widetilde{A}_{22} - K\widetilde{A}_{12} \end{bmatrix} + \frac{1}{2}\begin{bmatrix} D^+ + (-KC)^+ & D^- + (-KC)^- \\ D^- + (-KC)^- & D^+ + (-KC)^+ \end{bmatrix}\left(\begin{bmatrix} \overline{\Delta A}^{+} & \overline{\Delta A}^{-} \\ \underline{\Delta A}^{-} & \underline{\Delta A}^{+} \end{bmatrix} + \begin{bmatrix} \overline{\Delta A}^{+} & \overline{\Delta A}^{-} \\ \overline{\Delta A}^{-} & \overline{\Delta A}^{+} \end{bmatrix}\right)\begin{bmatrix} Q_2^+ & Q_2^- \\ Q_2^- & Q_2^+ \end{bmatrix},$$
$$\mathsf{F}_2 = \frac{1}{2}\begin{bmatrix} D^+ + (-KC)^+ & D^- + (-KC)^- \\ D^- + (-KC)^- & D^+ + (-KC)^+ \end{bmatrix}\left(\begin{bmatrix} \overline{\Delta A}^{+} & \overline{\Delta A}^{-} \\ \underline{\Delta A}^{-} & \underline{\Delta A}^{+} \end{bmatrix} - \begin{bmatrix} \overline{\Delta A}^{+} & \overline{\Delta A}^{-} \\ \overline{\Delta A}^{-} & \overline{\Delta A}^{+} \end{bmatrix}\right). \tag{52}$$

Consequently, by Lyapunov stability theory, $[\overline{e}_{iu}/\underline{e}_{iu}]$ may approach 0 as t goes to ∞. This result will be established, if F_1, F_2, and $[Q_2^+/Q_2^-Q_2^-/Q_2^+]$ in (33) meet some conditions. In this case, the interval on which the sum of the relative information of each agent is located can be estimated by $\overline{w}_i$ and $\underline{w}_i$ in (10).

Remark 2. The main results are provided under the premise that $\widetilde{A}_{22} - K\widetilde{A}_{12}$ is Hurwitz and Metzler. If there exists a K to make $\widetilde{A}_{22} - K\widetilde{A}_{12}$ Hurwitz and Metzler, it can be acquired according to Lemma 4 in [21]. However, if such K does not exist, the time-invariant transformation and time-varying transformation in [20, 21], respectively, can be introduced to carry out the problem of reduced-order NIO design.

4. Numerical Simulation

Some numerical simulations are proposed to verify the theoretical results in this section. Similar to [21], the system matrices are given as

$$A = \begin{bmatrix} -1 & 4 & 0 \\ 0 & 3 & -1 \\ 0 & 1 & -2 \end{bmatrix},$$
$$B = \begin{bmatrix} -5 \\ 1 \\ -1 \end{bmatrix}, \tag{53}$$
$$C = \begin{bmatrix} -1 & -2 & 1 \end{bmatrix}.$$

Obviously, (C, A) is observable, and (A, B) is stabilizable. The time-varying uncertainty is

$$\Delta A(t) = 10^{-2}\begin{bmatrix} \dfrac{\sin(t)}{10} & -\cos^2(t) & \dfrac{1}{11} \\ 0 & \dfrac{\sin(t/3)}{5} & 0 \\ \dfrac{1}{20} & 0 & \dfrac{\cos^2(2t)}{20} \end{bmatrix}, \tag{54}$$

which meets Assumption 1 and

$$\overline{\Delta A} = 10^{-2}\begin{bmatrix} \dfrac{1}{10} & 0 & \dfrac{1}{11} \\ 0 & \dfrac{1}{5} & 0 \\ \dfrac{1}{20} & 0 & \dfrac{1}{20} \end{bmatrix},$$
$$\underline{\Delta A} = 10^{-2}\begin{bmatrix} -\dfrac{1}{10} & -1 & 0 \\ 0 & -\dfrac{1}{5} & 0 \\ \dfrac{1}{20} & 0 & 0 \end{bmatrix}. \tag{55}$$

For $P = \begin{bmatrix} -1 & -2 & 1 \\ 0 & 1 & 0 \\ 0 & 0 & 1 \end{bmatrix}$, one has $\widetilde{A}_{21} = [0/0]$, $\widetilde{A}_{22} = \begin{bmatrix} 3 & -1 \\ 1 & -2 \end{bmatrix}$, $\widetilde{A}_{11} = [-1]$, and $\widetilde{A}_{12} = [-11 \quad 1]$. Here, we

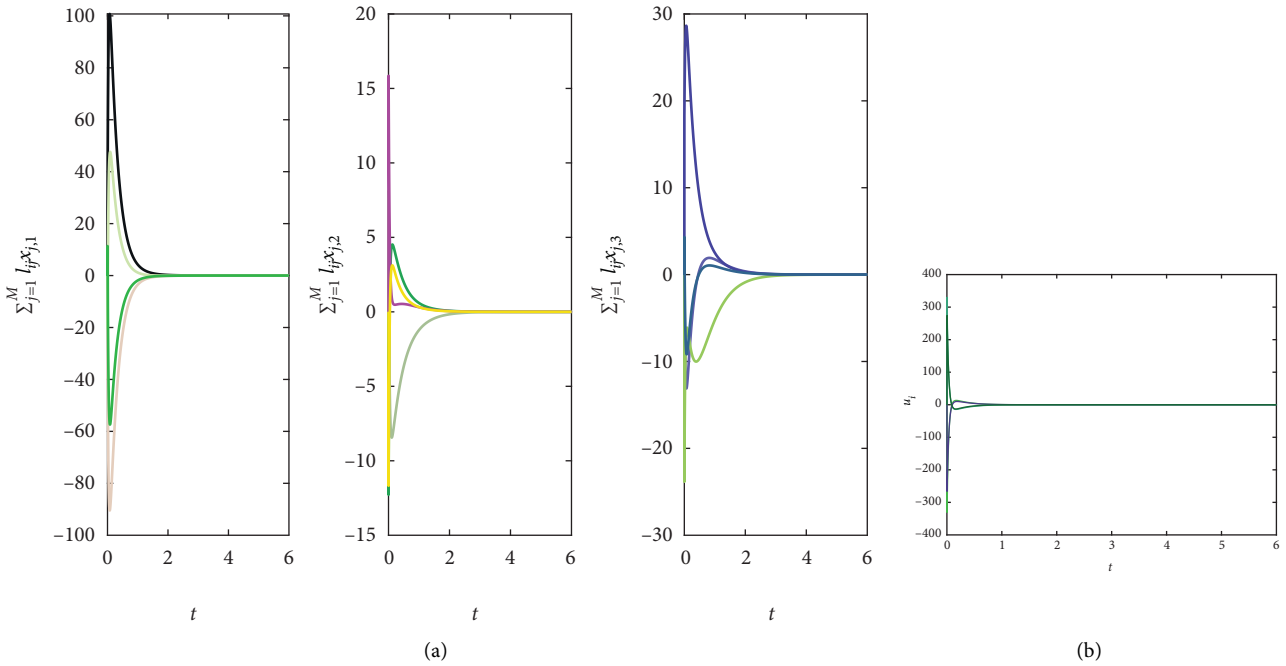

Figure 1: Reduced-order NIO-based consensus. (a) Convergence of $\sum_{i=10}^{N} l_{ij}x_j^t$. (b) Convergence of u_i.

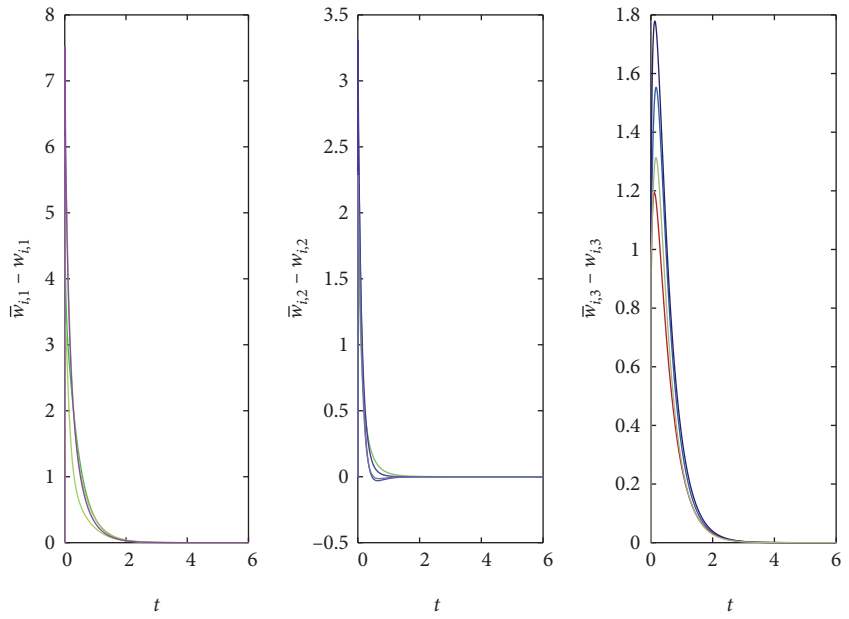

Figure 2: Continued.

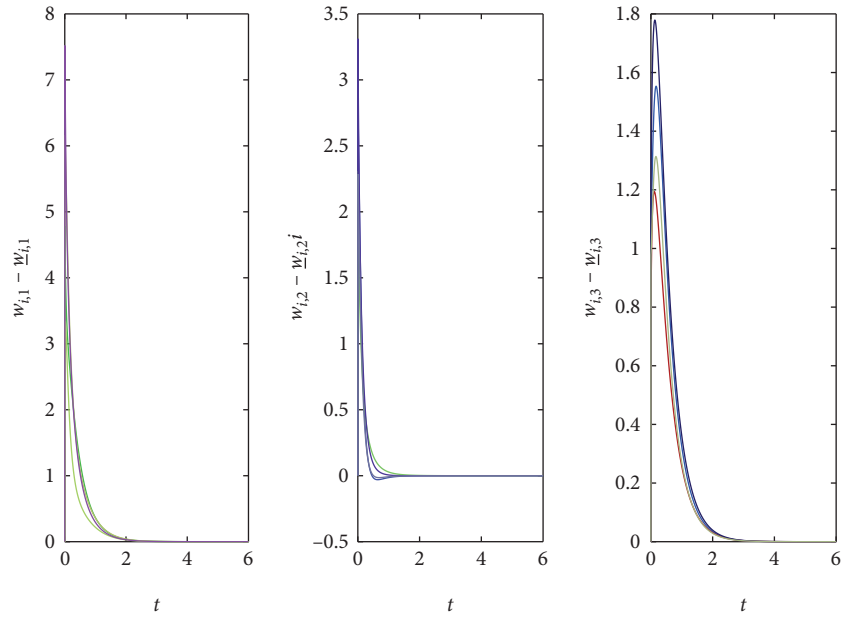

(b)

Figure 2: Reduced-order NIO-based consensus. (a) Trajectory of $\overline{w}_i - w_i$. (b) Trajectory of $\overline{w}_j - w_j$.

can choose $K = [-1/1/4]$, so that $\widetilde{A}_{22} - K\widetilde{A}_{12}$ is Hurwitz and Metzler. A multiagent system consists of $N = 4$ agents, which communicates through a connected graph with Laplacian matrix as follows:

$$L = \begin{bmatrix} 2 & -1 & 0 & -1 \\ -1 & 2 & -1 & 0 \\ 0 & -1 & 2 & -1 \\ -1 & 0 & -1 & 2 \end{bmatrix}. \tag{56}$$

The initial state of system is chosen randomly from $[-2020] \times [-2020] \times [-2020]$, $\overline{w}_i(0) = w_i(0) + \alpha$, and $\underline{w}_i(0) = w_i(0) - \alpha$, where α is a vector with each element choosing from [01]. Thus, the relationship $\underline{w}_i(0) \le w_i(0) \le \overline{w}_i(0)$ holds.

For multiagent system with above details, choose $\epsilon = 9$; then, (31) is satisfied. That is, the premises in Theorem 2 are satisfied.

Figure 1 is given to verify Theorem 2. As shown in Figure 1(a), $\sum_{j=1}^{N} l_{ij}x_j$ converges to 0 for $i = 1, \ldots, N$, and simultaneously, Figure 1(b) shows that the control input u_i can also converge to 0 for $i = 1, \ldots, N$. Both figures imply the consensus. Figures 2(a) and 2(b) display the trajectories of $\overline{w}_i - w_i$ and $w_i - \underline{w}_i$, respectively. As shown in these two figures, $\overline{w}_i - w_i$ and $w_i - \underline{w}_i$ are guaranteed to be nonnegative, provided that $\underline{w}_i(0) \le w_i(0) \le \overline{w}_i(0)$ holds. Therefore, Theorem 1 is established. Further, as shown in Figure 2, $\overline{w}_i - w_i$ and $w_i - \underline{w}_i$ approach 0 as time goes to ∞. That is, the interval on which the sum of the relative information of each agent associated with the uncertain multiagent system in this example is located can be estimated by the reduced-order NIO given in this paper. Consequently, Remark 1 holds.

5. Conclusions

In this paper, the reduced-order NIO is designed for MASs with TIUs in system matrix to implement the interval estimation, by using only the outputs and the bounding information of the uncertain system matrix. Consensus of this kind of uncertain multiagent systems can be achieved as a by-part of the reduced-order NIO design. This work is an important complement to the IO design for MASs with TIUs.

Data Availability

No data were used to support this study.

Conflicts of Interest

The authors declare that they have no conflicts of interest.

Acknowledgments

This study was supported by the National Natural Science Foundation of China under grant no. 61374049.

References

[1] T. Vicsek and A. Zafeiris, "Collective motion," *Physics Reports*, vol. 517, no. 3-4, pp. 71–140, 2012.

[2] H. Su, Y. Ye, X. Chen, and H. He, "Necessary and sufficient conditions for consensus in fractional-order multiagent systems via sampled data over directed graph," *IEEE Transactions on Systems, Man, and Cybernetics: Systems*, vol. 51, no. 4, pp. 2501–2511, 2021.

[3] B. Liu, L. Wu, R. Li, H. Su, and Y. Han, "On the group controllability of leader-based continuous-time multiagent

systems," *Complexity*, vol. 2020, Article ID 7892643, 11 pages, 2020.

[4] H. Su, Y. Liu, and Z. Zeng, "Second-order consensus for multiagent systems via intermittent sampled position data control," *IEEE Transactions on Cybernetics*, vol. 50, no. 5, pp. 2063–2072, 2020.

[5] B. Liu, Q. An, L. Wu, R. Li, H. Su, and Y. Han, "Group controllability of discrete-time time-delayed multiagent systems with multiple leaders," *Complexity*, vol. 2020, Article ID 5849532, 10 pages, 2020.

[6] R. Olfati-Saber, J. A. Fax, and R. M. Murray, "Consensus and cooperation in networked multi-agent systems," *Proceedings of the IEEE*, vol. 95, no. 1, pp. 215–233, 2007.

[7] H. Su, H. Wu, and J. Lam, "Positive edge-consensus for nodal networks via output feedback," *IEEE Transactions on Automatic Control*, vol. 64, no. 3, pp. 1244–1249, 2019.

[8] R. Olfati-Saber and R. M. Murray, "Consensus problems in networks of agents with switching topology and time-delays," *IEEE Transactions on Automatic Control*, vol. 49, no. 9, pp. 1520–1533, 2004.

[9] W. Ren and R. W. Beard, "Consensus seeking in multiagent systems under dynamically changing interaction topologies," *IEEE Transactions on Automatic Control*, vol. 50, no. 5, pp. 655–661, 2005.

[10] Z. Li and Z. Duan, *Cooperative Control of Multi-Agent Systems: A Consensus Region Approach*, CRC Press, Boca Raton, Florida, United Stat, 2017.

[11] Y. Cao, W. Yu, W. Ren, and G. Chen, "An overview of recent progress in the study of distributed multi-agent coordination," *IEEE Transactions on Industrial Informatics*, vol. 9, no. 1, pp. 427–438, 2013.

[12] J. Qin, Q. Ma, Y. Shi, and L. Wang, "Recent advances in consensus of multi-agent systems: a brief survey," *IEEE Transactions on Industrial Electronics*, vol. 64, no. 6, pp. 4972–4983, 2017.

[13] H. L. Trentelman, K. Takaba, and N. Monshizadeh, "Robust synchronization of uncertain linear multi-agent systems," *IEEE Transactions on Automatic Control*, vol. 58, no. 6, pp. 1511–1523, 2013.

[14] H.-X. Hu, G. Wen, and W. X. Zheng, "Collective behavior of heterogeneous agents in uncertain cooperation-competition networks: a nussbaum-type function based approach," *IEEE Transactions on Control of Network Systems*, vol. 7, no. 2, pp. 783–796, 2020.

[15] X. Li, Y. C. Soh, and L. Xie, "Robust consensus of uncertain linear multi-agent systems via dynamic output feedback," *Automatica*, vol. 98, pp. 114–123, 2018.

[16] Z. Zhang, S. Zhang, H. Li, and W. Yan, "Cooperative robust optimal control of uncertain multi-agent systems," *Journal of the Franklin Institute*, vol. 357, no. 14, pp. 9467–9483, 2020.

[17] X. Wang, G.-P. Jiang, H. Su, and X. Wang, "Robust global coordination of networked systems with input saturation and external disturbances," *IEEE Transactions on Systems, Man, and Cybernetics: Systems*, vol. 51, no. 12, pp. 7788–7800, 2021.

[18] D. Efimov, T. Raissi, and A. Zolghadri, "Control of nonlinear and lpv systems: interval observer-based framework," *IEEE Transactions on Automatic Control*, vol. 58, no. 3, pp. 773–778, 2013.

[19] J. Huang, H. Che, T. Raissi, and Z. Wang, "Functional interval observer for discrete-time switched descriptor systems," *IEEE Transactions on Automatic Control*, vol. 67, no. 5, pp. 2497–2504, 2022.

[20] X. Wang, X. Wang, H. Su, and J. Lam, "Coordination control for uncertain networked systems using interval observers," *IEEE Transactions on Cybernetics*, vol. 50, no. 9, pp. 4008–4019, 2020.

[21] X. Wang, X. Wang, H. Su, and J. Lam, "Reduced-order interval observer based consensus for mass with time-varying interval uncertainties," *Automatica*, vol. 135, Article ID 109989, 2022.

[22] X. Wang, H. Su, and G.-P. Jiang, "Interval observer-based robust coordination control of multi-agent systems over directed networks," *IEEE Transactions on Circuits and Systems I: Regular Papers*, vol. 68, no. 12, pp. 5145–5155, 2021.

[23] X. Wang, H. Su, F. Zhang, A. Zemouche, and G. Chen, "Interval observer design and consensus of multiagent systems with time-varying interval uncertainties," *SIAM Journal on Control and Optimization*, vol. 59, no. 5, pp. 3392–3417, 2021.

[24] X. Wang, G.-P. Jiang, W. Yang, H. Su, and X. Wang, "Neighborhood interval observer based coordination control for multi-agent systems with disturbances," *IFAC-PapersOnLine*, vol. 53, no. 2, pp. 994–10999, 2020.

[25] C. Godsil and G. F. Royle, *Algebraic Graph Theory*, Vol. 207, Springer Science & Business Media, , Berlin, Germany, 2013.

[26] W. Ren and R. W. Beard, *Distributed Consensus in Multi-Vehicle Cooperative Control*, Springer, Berlin, Germany, 2008.

[27] D. G. Luenberger, *Introduction to Dynamic Systems; Theory, Models, and Applications*, Wiley & Sons, New York, NY, USA, 1979.

[28] H. L. Smith, "Monotone dynamical systems," *Mathematical Surveys and Monographs*, vol. 41, 1995.

[29] S. Chebotarev, D. Efimov, T. Raïssi, and A. Zolghadri, "Interval observers for continuous-time LPV systems with L1/L2 performance," *Automatica*, vol. 58, no. 1, pp. 82–89, 2015.

Hindawi
Complexity
Volume 2022, Article ID 4112362, 25 pages
https://doi.org/10.1155/2022/4112362

WILEY | Hindawi

Research Article

On Topological Analysis of Niobium (II) Oxide Network via Curve Fitting and Entropy Measures

Muhammad Kamran Siddiqui,[1] Sana Javed,[1] Sadia Khalid,[1] Mazhar Hussain,[1] Muhammad Shahbaz,[1] and Samuel Asefa Fufa [2]

[1]*Department of Mathematics, COMSATS University Islamabad, Lahore Campus, Pakistan*
[2]*Department of Mathematics, Addis Ababa University, Addis Ababa, Ethiopia*

Correspondence should be addressed to Samuel Asefa Fufa; samuel.asefa@aau.edu.et

Received 24 April 2022; Revised 26 May 2022; Accepted 21 June 2022; Published 13 August 2022

Academic Editor: Yue Song

The remarkable optical features of metallic nanoparticles have extensively developed the interest of scientists and researchers. The generated heat overwhelms cancer tissue incident to nanoparticles with no damage to sound tissues. Niobium nanoparticles have the ability of easy ligands connection so they are very suitable in treating cancer optothermally. A modern field of applied chemistry is chemical graph theory. With the use of combinatorial methods, such as vertex and edge partitions, we explore the connection between atoms and bonds. Topological indices play a vital part in equipping directions to treat cancers or tumors. These indices might be derived experimentally or computed numerically. Although experimental results are worthful but they are expensive as well, so computational analysis provides an economical and rapid way. A topological index is a numerical value that is only determined by the graph. In this paper, we will discuss the chemical graph of niobium (II) oxide. Additionally, each topological index is related with thermodynamical properties of niobium (II) oxide, including entropy and enthalpy. This has been done in MATLAB software, using rational built-in method.

1. Introduction

All types of data quantitative, qualitative, processed, or unprocessed might be considered to gain information to address a simple or a complicated event or situation. If we consider the flow chart of the information, then on the top of the hierarchy we would find notion being the first qualitative obscure assessment of information. The central part of this flow chart comprises of the parameters and measurements while decision making extracted from inference is the final step. Different properties of a chemical compound like its nature, atoms, or chemical state provide us chemical information about the structure [1]. Different chemical reactions in a substance environment produce different physicochemical properties/activities that include boiling point, entropy, heat of formation, or density. In this way, the whole milieu of a substance becomes a promising root of information for the analysis of its chemistry [1]. Supplementary knowledge might be gained by *in silico* trials for the designing of new compounds for a specified study or objective. Stimulation in such approaches has been seen due to expensive experimental studies along with rigorous biotic and ecological regulations [2]. Such *in silico* studies are very progressive in medicine due to their cost effectiveness.

Different approaches including graphical quantitative/quantitative structure activity/property relationship (QSAR/QSPR) and modeling have become an essential part of *in silico* studies in drug development [3, 4]. This is due to the fact that biological variations can be explained in the form of chemical variations. Such analyses are performed continually to obtain profound results [5, 6]. Topological indices play a vital part in equipping directions to treat cancers or tumors. These indices might be derived experimentally or computed numerically [7, 8]. Although experimental results are worthful but they are expensive as well, so computational analysis provides an economical way Recently, several

studies are performed/reviewed using the concept of graph theoretical indices in drug research [9, 10]. There is a wide variety of such indices in the literature [11, 12].

A graph usually comprises of two sets, namely, vertex set, that contains the objects, and the edge set; this is based on the connections between the objects. Any chemical compound might be represented in the form of a graph where atoms make the vertex set and the bonding between atoms creates the edge set. Topological indices are based on the atomic connectivity table of the chemical compound [1]. Graphical descriptors, which are usually defined in the form of numerical numbers, can be used to appraise distinct immersed characteristics of a chemical compound from different point of view. Zagreb indices measure the compactness of a molecule so it can be correlated with the physicochemical properties of a compound which depend on the volume/surface ratio of the molecules.

The remarkable optical features of metallic nanoparticles have extensively developed the interest of scientists and researchers [13–15]. Researchers have analyzed that the thermoplasmonic features of nanoparticles might be utilized in treating cancers [16–18]. In optothermal cancer tissue therapy, the descendent laser light provokes the frequency of maximum response amplitude of external plasmon of metallic nanoparticles and consequently the immersed energy of descendent light preserves the heat in nanoparticles [19–21]. The generated heat overwhelms cancer tissue incident to nanoparticles with no damage to sound tissues [22, 23]. Niobium nanoparticles have the ability of easy ligands connection so they are very suitable in treating the cancer optothermally [24–26].

Niobium (Nb), a recalcitrant metal, is a suitable construction material for the first shell of nuclear fusion reactors [27]. It does, however, have a high affinity for oxygen and carbon, which are found in pyrotechnics and refrigerants such as liquid. Niobium is renowned to interact very efficiently with oxygen as a component for the first barrier. As a result, reliable thermodynamical data on niobium oxides, NbO, NbO_2, Nb_2O_5, and other intermediary phases, such as $Nb_{12}O_{29}$, are useful. Apart from that, niobium oxides have a variety of innovative uses. Niobium monoxide (NbO) is utilized as a gate electrode in transistors [28], and a (NbO/NbO_2) junction may be employed in robust switching devices [29]. NbO crystallises in the form of a face-centered cubic structure similar to sodium chloride crystal where every Nb atom in a square planar lattice is linked to four oxygen atoms [30]. Furthermore, the NbO crystal structure is unique in which it has 25 percent arranged voids in both the Nb and O sublattices as shown in Figure 1 [31].

Researchers have investigated the electrical and thermophysical properties of NbO. NbO has a density of around $7.3 g/cm^3$ and a melting temperature of 1940°C [31]. Niobium monoxide exhibits typical metallic behaviour and is usually recognised as a metal, with a resistivity of around $21l \times$ cm at 25°C that drops with temperature to $1.8l \times$ cm at 4.2 k. Researchers have measured X-ray fluorescence for several niobium oxides and correlated the findings of NbO to the conduction and valence band calculations of $Nb_{1.0}O_{\infty}$!, discovering substantial variances [32]. They

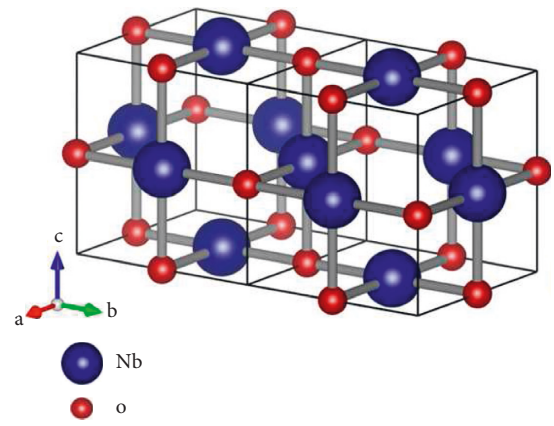

Figure 1: Cubic structure of NbO.

attempted to emulate the NbO structure by doing band structure calculations for $Nb_{0.75}O_{0.75}$ in order to account for the 25% vacancy (see Figure 1). However, the investigation pertaining to the thermodynamic data is very scarce. The laboratory work to study these characteristics is limited due to the analytical limitations. Therefore, computational techniques can be applied to estimate their thermodynamic characteristics. Topological study is useful in this regard [31].

Milan Randić presented the following index, namely, General Randić index [33–35] for a graph $G = (V, E)$, where $\mathfrak{L}(a)$ denotes the degree of a vertex a as the number of edges with a:

$$R_\alpha(G) = R_\alpha = \sum_{lm \in E(G)} (\mathfrak{L}(l) \times \mathfrak{L}(m))^\alpha, \quad \text{where } \alpha \in \left\{1, -1, \frac{1}{2}, -\frac{1}{2}\right\}, 2. \tag{1}$$

Estrada et al. [36, 37] established atom bond connectivity index as follows:

$$\mathrm{ABC}(G) = \mathrm{ABC} = \sum_{lm \in E(G)} \sqrt{\frac{\mathfrak{L}(l) + \mathfrak{L}(m) - 2}{\mathfrak{L}(l) \times \mathfrak{L}(m)}}. \tag{2}$$

Vukičević and Furtula [38] presented the geometric arithmetic index as follows:

$$GA(G) = GA = \sum_{lm \in E(G)} \frac{2\sqrt{\mathfrak{L}(l) \times \mathfrak{L}(m)}}{\mathfrak{L}(l) + \mathfrak{L}(m)}. \tag{3}$$

The Zagreb indices defined in [20, 39, 40] are as follows:

$$M_1(G) = M_1 = \sum_{lm \in E(G)} (\mathfrak{L}(l) + \mathfrak{L}(m)), \quad M_2(G) = M_2 = \sum_{lm \in E(G)} (\mathfrak{L}(l) \times \mathfrak{L}(m)). \tag{4}$$

The first and second Zagreb coindices defined in [41, 42] are as follows:

$$\overline{M}_1(G) = \overline{M}_1 = \sum_{lm \notin E(G)} (\mathfrak{L}(l) + \mathfrak{L}(m)), \quad \overline{M}_2(G) = \overline{M}_2 = \sum_{lm \notin E(G)} (\mathfrak{L}(l) \times \mathfrak{L}(m)). \tag{5}$$

Gutman and Trinajstić [40] and Furtula and Gutman [43] introduced forgotten index as follows:

$$F(G) = F = \sum_{lm\in E(G)} \left(\mathfrak{L}(l)^2 + \mathfrak{L}(m)^2\right). \tag{6}$$

Wang et al. [44] described the augmented Zagreb index as

$$\mathrm{AZI}(G) = \mathrm{AZI} = \sum_{lm\in E(G)} \left(\frac{\mathfrak{L}(l)\times\mathfrak{L}(m)}{\mathfrak{L}(l)+\mathfrak{L}(m)-2}\right)^3. \tag{7}$$

The Balaban index [45, 46] is presented as follows:

$$J(G) = J = \frac{l}{l-m}\sum_{lm\in E(G)} \frac{1}{\mathfrak{L}(l)\times\mathfrak{L}(m)}. \tag{8}$$

Ranjini et al. in [47] reformulated versions of Zagreb indices as follows:

$$\begin{aligned}
\mathrm{ReZG}_1(G) &= \mathrm{ReZG}_1 = \sum_{lm\in E(G)} \frac{\mathfrak{L}(l)+\mathfrak{L}(m)}{\mathfrak{L}(l)\times\mathfrak{L}(m)},\\
\mathrm{ReZG}_2(G) &= \mathrm{ReZG}_2 = \sum_{lm\in E(G)} \frac{\mathfrak{L}(l)\times\mathfrak{L}(m)}{\mathfrak{L}(l)+\mathfrak{L}(m)},\\
\mathrm{ReZG}_3(G) &= \mathrm{ReZG}_3\\
&= \sum_{lm\in E(G)} (\mathfrak{L}(l)\times\mathfrak{L}(m))(\mathfrak{L}(l)+\mathfrak{L}(m)).
\end{aligned} \tag{9}$$

2. Results for Niobium (II) Oxide

The number of vertices and edges of structure of Niobium (II) oxide denoted by NbO is $9lm + 5l + 5m + 2$ and $16lm + 6l + 6m$, respectively. In NbOthere are three types of vertices, namely, the vertices of degree 2,3, and 4, respectively. The vertex and edge partition of NbO is presented in Table 1 and Table 2, respectively.

Table 1: Vertex partition of NbO.

$\mathfrak{L}(v)$	Frequency	Set of vertices
2	8	V_1
3	$4lm + 8l + 8m - 8$	V_3
4	$5lm - 3l - 3m + 2$	V_4

Table 2: Edge partition of NbO.

$(\mathfrak{L}(l), \mathfrak{L}(m))$	Frequency	Set of edges
(2, 3)	16	E_1
(3, 3)	$16l + 16m - 24$	E_2
(3, 4)	$12lm - 8l - 8m + 8$	E_3
(4, 4)	$4lm - 2l - 2m$	E_4

Theorem 1. *Let $G \cong NbO[l, m]$ with $l, m \geq 1$. Then, Randić indices for $\alpha \in \{1, -1, (1/2), -(1/2)\}$ are as follows:*

$$\begin{aligned}
R_1 &= 208lm + 16l + 16m - 24,\\
R_{-1} &= 1.125lm + 1.1111l + 0.9861m + 0.6666,\\
R_{1/2} &= 49.5692lm + 20.2871l + 12.2871m - 5.0953,\\
R_{-(1/2)} &= 3.9641lm + 3.0239l + 2.5239m + 0.8413.
\end{aligned} \tag{10}$$

Proof. For $\alpha = 1$,

$$\begin{aligned}
R_1 &= \sum_{lm\in E(G)} \mathfrak{L}(l)\times\mathfrak{L}(m)\\
&= (16)(6) + (16l + 16m - 24)(9)\\
&\quad + (12lm - 8l - 8m + 8)(12) + (4lm - 2l - 2m)(16)\\
&= 208lm + 16l + 16m - 24.
\end{aligned} \tag{11}$$

For $\alpha = -1$,

$$\begin{aligned}
R_{-1} &= \sum_{lm\in E(G)} \frac{1}{\mathfrak{L}(l)\times\mathfrak{L}(m)}\\
&= (16)\left(\frac{1}{6}\right) + (16l + 16m - 24)\left(\frac{1}{9}\right)\\
&\quad + (12lm - 8l - 8m + 8)\left(\frac{1}{12}\right)\\
&\quad + (4lm - 2l - 2m)\left(\frac{1}{16}\right)\\
&= 1.125lm + 1.1111l + 0.9861m + 0.6666.
\end{aligned} \tag{12}$$

For $\alpha = 1/2$,

$$\begin{aligned}
R_{1/2} &= \sum_{lm\in E(G)} \sqrt{\mathfrak{L}(l)\times\mathfrak{L}(m)}\\
&= (16)(\sqrt{6}) + (16l + 16m - 24)(\sqrt{9})\\
&\quad + (12lm - 8l - 8m + 8)(\sqrt{12})\\
&\quad + (4lm - 2l - 2m)(\sqrt{16})\\
&= 49.5692lm + 20.2871l + 12.2871m - 5.0953.
\end{aligned} \tag{13}$$

For $\alpha = (-1/2)$,

$$\begin{aligned}
R_{-1/2} &= \sum_{lm\in E(G)} \frac{1}{\sqrt{\mathfrak{L}(l)\times\mathfrak{L}(m)}}\\
&= (16)\left(\frac{1}{\sqrt{6}}\right) + (16l + 16m - 24)\left(\frac{1}{\sqrt{9}}\right)\\
&\quad + (12lm - 8l - 8m + 8)\left(\frac{1}{\sqrt{12}}\right)\\
&\quad + (4lm - 2l - 2m)\left(\frac{1}{\sqrt{16}}\right)\\
&= 3.9641lm + 3.0239l + 2.5239m + 0.8413.
\end{aligned} \tag{14}$$

□

Theorem 2. *Let $G \cong NbO$, with $l, m \geq 1$. Then, the atom bond connectivity index corresponds to*

$$\mathrm{ABC} = 10.1954lm + 4.2779l + 4.2779m + 0.4776. \quad (15)$$

Proof

$$\begin{aligned}\mathrm{ABC} &= \sum_{lm\in E(G)} \sqrt{\frac{\mathfrak{L}(l)+\mathfrak{L}(m)-2}{\mathfrak{L}(l)\times\mathfrak{L}(m)}} \\ &= (16)\left(\sqrt{\frac{3}{6}}\right) + (16l+16m-24)\left(\sqrt{\frac{4}{9}}\right) \\ &\quad + (12lm-8l-8m+8)\left(\sqrt{\frac{5}{12}}\right) \\ &\quad + (4lm-2l-2m)\left(\sqrt{\frac{6}{16}}\right) \\ &= 10.1954lm + 4.2779l + 4.2779m + 0.4776.\end{aligned} \quad (16)$$

□

Theorem 3. *Consider the graph of $G \cong NbO$ which has $l, m \geq 1$ and geometric arithmetic index is corresponding to the following:*

$$\mathrm{GA} = 15.8769lm + 6.0820l + 6.0820m - 0.4053. \quad (17)$$

Proof

$$\begin{aligned}\mathrm{GA} &= \sum_{lm\in E(G)} \frac{2\sqrt{\mathfrak{L}(l)\times\mathfrak{L}(m)}}{\mathfrak{L}(l)+\mathfrak{L}(m)} \\ &= (16)\left(\frac{2\sqrt{6}}{5}\right) + (16l+16m-24)\left(\frac{2\sqrt{9}}{6}\right) \\ &\quad + (12lm-8l-8m+8)\left(\frac{2\sqrt{12}}{7}\right) \\ &\quad + (4lm-2l-2m)\left(\frac{2\sqrt{16}}{8}\right) \\ &= 15.8769lm + 6.0820l + 6.0820m - 0.4053.\end{aligned} \quad (18)$$

□

Theorem 4. *The forgotten index for the graph of $G \cong NbO[l, m]$ with $l, m \geq 1$ is corresponding to*

$$F = 428lm + 24l + 24m - 24. \quad (19)$$

Proof

$$\begin{aligned}F &= \sum_{lm\in E(G)} \left(\mathfrak{L}(l)^2 + \mathfrak{L}(m)^2\right) \\ &= (16)(13) + (16l+16m-24)(18) \\ &\quad + (12lm-8l-8m+8)(25) + (4lm-2l-2m)(32) \\ &= 428lm + 24l + 24m - 24.\end{aligned} \quad (20)$$

□

Theorem 5. *The augmented index for the graph of $G \cong NbO[l, m]$ with $l, m \geq 1$ is corresponding to*

$$\mathrm{AZI} = 241.7398lm + 33.7320l + 33.7320m - 34.783. \quad (21)$$

Proof

$$\begin{aligned}\mathrm{AZI} &= \sum_{lm\in E(G)} \left(\frac{\mathfrak{L}(l)\times\mathfrak{L}(m)}{\mathfrak{L}(l)+\mathfrak{L}(m)-2}\right)^3 \\ &= (16)\left(\frac{6}{3}\right)^3 + (16l+16m-24)\left(\frac{9}{4}\right)^3 \\ &\quad + (12lm-8l-8m+8)\left(\frac{12}{5}\right)^3 \\ &\quad + (4lm-2l-2m)\left(\frac{16}{6}\right)^3 \\ &= 241.7398lm + 33.7320l + 33.7320m - 34.783.\end{aligned} \quad (22)$$

□

Theorem 6. *Consider the graph of $G \cong NbO[l, m]$ such that $l, m \geq 1$ and the first and second Zagreb index is corresponding to*

$$\begin{aligned}M_1 &= 116lm + 24l + 24m - 8, \\ M_2 &= 208lm + 16l + 16m - 24.\end{aligned} \quad (23)$$

Proof

$$\begin{aligned}M_1 &= \sum_{lm\in E(G)} \mathfrak{L}(l) + \mathfrak{L}(m) \\ &= (16)(5) + (16l+16m-24)(6) \\ &\quad + (12lm-8l-8m+8)(7) + (4lm-2l-2m)(8) \\ &= 116lm + 24l + 24m - 8, \\ M_2 &= \sum_{lm\in E(G)} \mathfrak{L}(l)\times\mathfrak{L}(m) \\ &= (16)(6) + (16l+16m-24)(9) \\ &\quad + (12lm-8l-8m+8)(12) + (4lm-2l-2m)(16) \\ &= 208lm + 16l + 16m - 24.\end{aligned} \quad (24)$$

□

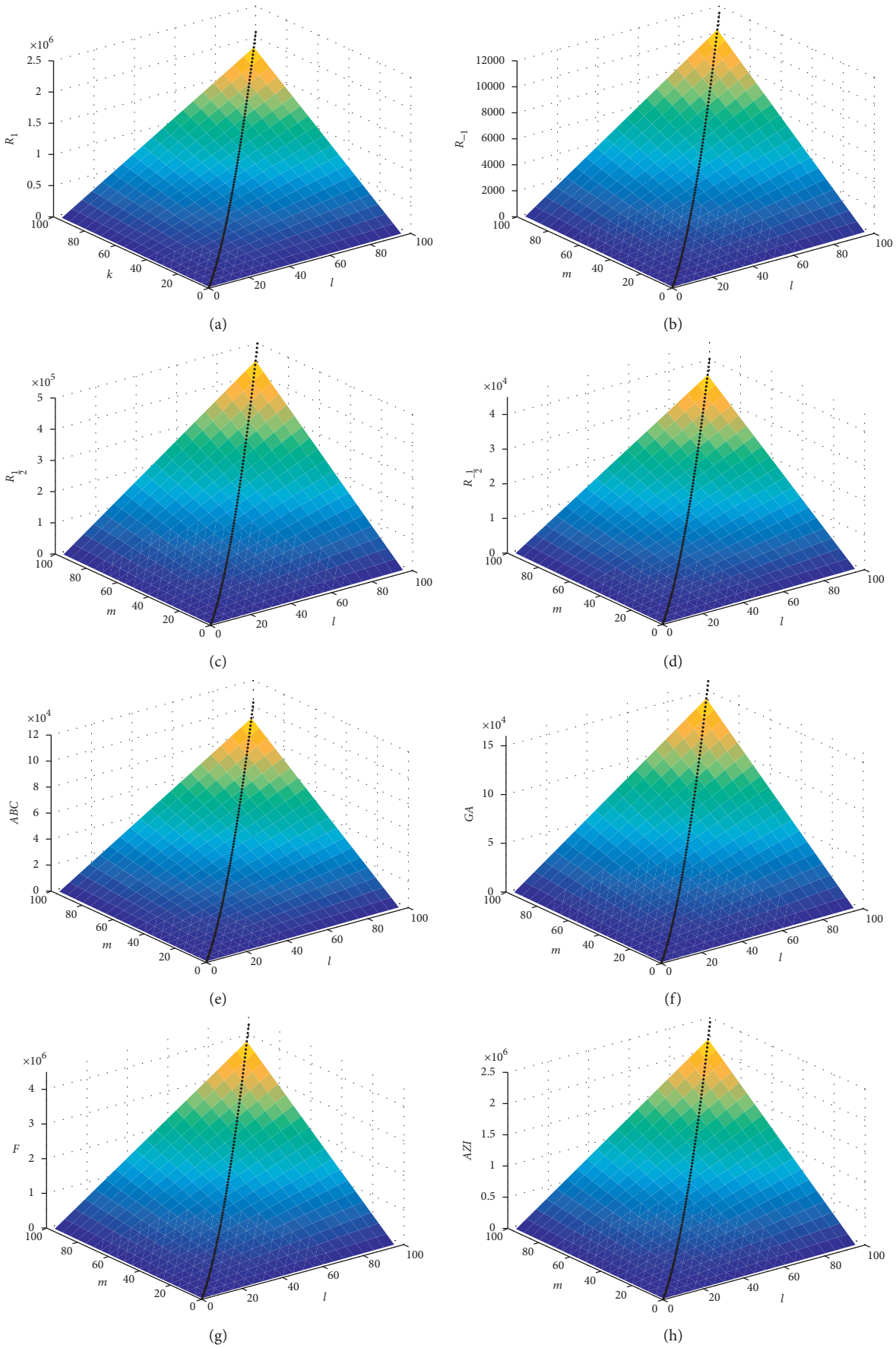

Figure 2: Continued.

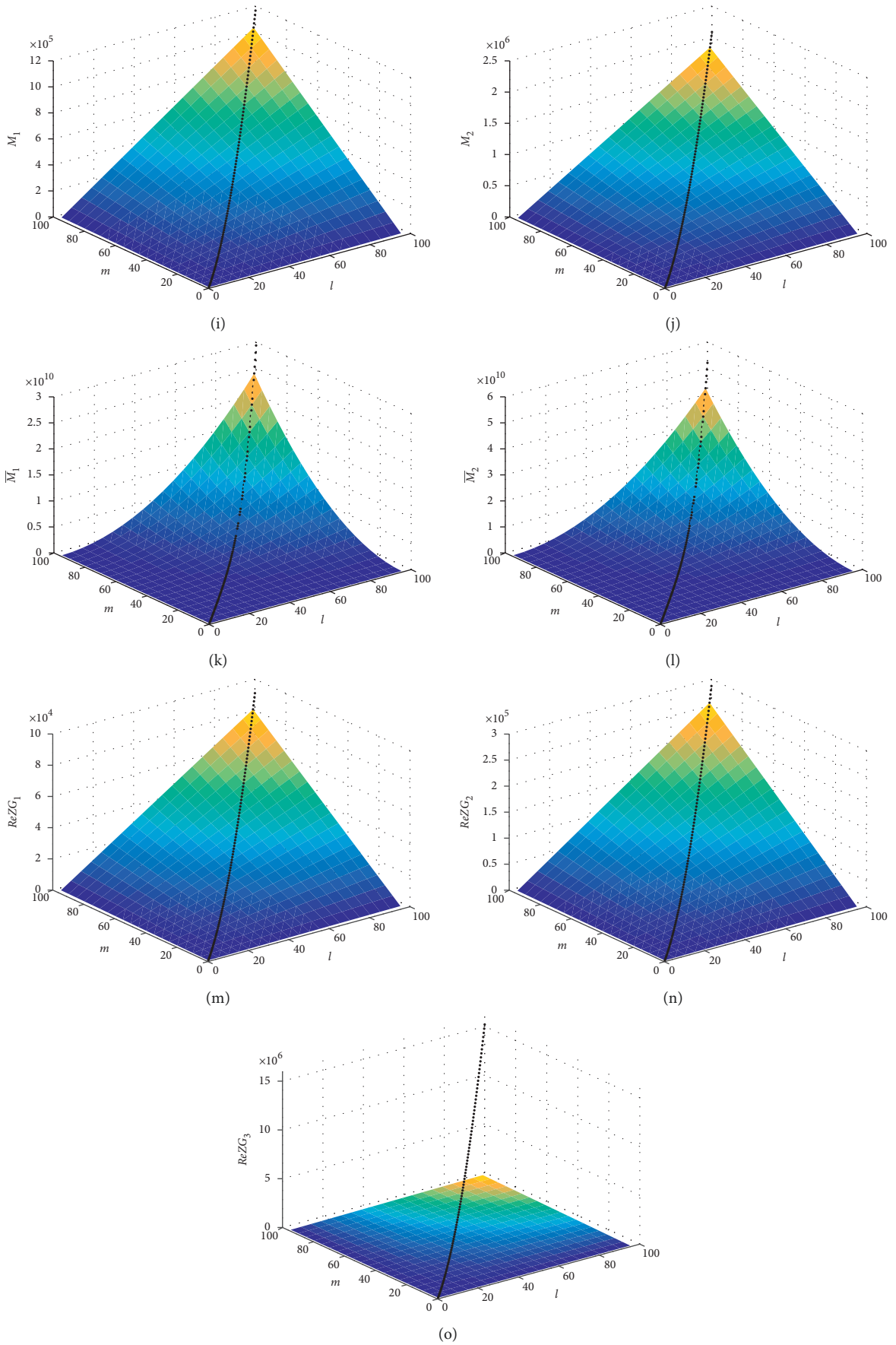

Figure 2: An interactive view of scattered plot together with surface plot of indices. (a) (m, n, R_1). (b) (m,n,R_{-1}). (c) $(m, n, R_{1/2})$. (d) $(m, n, R_{-1/2})$. (e) $(m, n,$ ABC). (f) $(m, n,$GA). (g) (m, n, F). (h) $(m, n,$ AZI). (i) (m, n, M_1). (j) (m, n, M_2). (k) $(m, n, \overline{M}_1)$. (l) $(m, n, \overline{M}_2)$. (m) $(m, n,$ ReZG$_1$). (n) $(m, n,$ ReZG$_2$). (o) $(m, n,$ ReZG$_3$).

Table 3: Values of HoF and Entropy for units of NbO.

$[m,n]$	Units of frequency	HoF $\times 10^{-22}$ kJ	Entropy $\times 10^{-22}$ Jmol^{-1}K^{-1}
[1, 1]	4	−26.9545	3.1949
[2, 2]	16	−107.8180	12.7798
[3, 3]	36	−242.5905	28.7545
[4, 4]	64	−431.2720	51.1192
[5, 5]	100	−673.8625	79.8737
[6, 6]	144	−970.3620	115.0182
[7, 7]	196	−1320.7705	156.5526

Theorem 7. *The first and second Zagreb coindices for the graph of* $(\mathcal{G}) \cong NbO[l,m]$ *with* $l,m \geq 1$ *are corresponding to*

$$\begin{aligned}\overline{M}_1 &= 288l^2m^2 + 268l^2m + 268lm^2 + 60l^2 \\ &\quad + 36lm + 60m^2 - 12l - 12m + 8, \\ \overline{M}_2 &= 512l^2m^2 + 384l^2m + 384lm^2 + 72l^2 \\ &\quad - 122lm + 72m^2 - 28l - 28m + 28.\end{aligned} \tag{25}$$

Proof

$$\begin{aligned}\overline{M}_1 &= \sum_{lm \notin E(G)} \mathfrak{L}(l) + \mathfrak{L}(m) \\ &= 2|E(G)|(|V(G)| - 1) - M_1 \\ &= 2(16lm + 6l + 6m)(9lm + 5l + 5m + 2 - 1) \\ &\quad - (116lm + 24l + 24m - 8) \\ &= 288l^2m^2 + 268l^2m + 268lm^2 + 60l^2 \\ &\quad + 36lm + 60m^2 - 12l - 12m + 8, \\ \overline{M}_2 &= \sum_{lm \notin E(G)} \mathfrak{L}(l) \times \mathfrak{L}(m) \\ &= 2|E(G)|^2 - \frac{1}{2}M_1 - M_2 \\ &= 2(16lm + 6l + 6m)^2 \\ &\quad - \frac{1}{2}(116lm + 24l + 24m - 8) \\ &\quad - (208lm + 16l + 16m - 24) \\ &= 512l^2m^2 + 384l^2m + 384lm^2 \\ &\quad + 72l^2 - 122lm + 72m^2 - 28l - 28m + 28.\end{aligned} \tag{26}$$

□

Theorem 8. *The redefined Zagreb indices for the graph of* $G \cong NbI[l,m]$ *with* $l,m \geq 1$ *correspond to*

$$\begin{aligned}\mathrm{ReZG}_1 &= 9lm + 5l + 5m + 2, \\ \mathrm{ReZG}_2 &= 28.5714lm + 6.2857l + 6.2857m - 3.0857, \\ \mathrm{ReZG}_3 &= 1520lm - 64l - 64m - 144.\end{aligned} \tag{27}$$

Proof

$$\begin{aligned}\mathrm{ReZG}_1 &= \sum_{lm \in E(G)} \frac{\mathfrak{L}(l) + \mathfrak{L}(m)}{\mathfrak{L}(l) \times \mathfrak{L}(m)} \\ &= (16)\left(\frac{5}{6}\right) + (16l + 16m - 24)\left(\frac{6}{9}\right) \\ &\quad + (12lm - 8l - 8m + 8)\left(\frac{7}{12}\right) \\ &\quad + (4lm - 2l - 2m)\left(\frac{8}{16}\right) \\ &= 9lm + 5l + 5m + 2, \\ \mathrm{ReZG}_2 &= \sum_{lm \in E(G)} \frac{\mathfrak{L}(l) \times \mathfrak{L}(m)}{\mathfrak{L}(l) + \mathfrak{L}(m)} \\ &= (16)\left(\frac{6}{5}\right) + (16l + 16m - 24)\left(\frac{9}{6}\right) \\ &\quad + (12lm - 8l - 8m + 8)\left(\frac{12}{7}\right) \\ &\quad + (4lm - 2l - 2m)\left(\frac{16}{8}\right) \\ &= 28.5714lm + 6.2857l + 6.2857m - 3.0857, \\ \mathrm{ReZG}_3 &= \sum_{lm \in E(G)} ((\mathfrak{L}(l) \times \mathfrak{L}(m))(\mathfrak{L}(l) + \mathfrak{L}(m))) \\ &= (16)(30) + (16l + 16m - 24)(54) \\ &\quad + (12lm - 8l - 8m + 8)(84) \\ &\quad + (4lm - 2l - 2m)(128) \\ &= 1520lm - 64l - 64m - 144.\end{aligned} \tag{28}$$

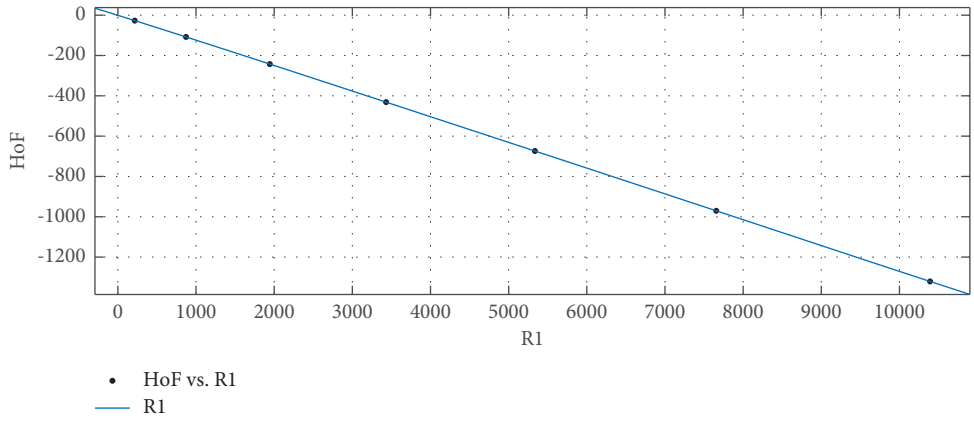

Figure 3: R_1 (x-axis) vs. HoF (y-axis).

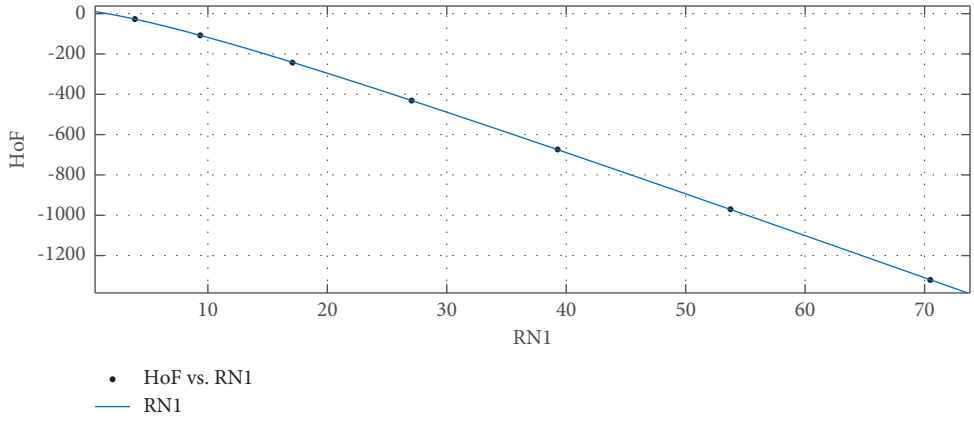

Figure 4: R_{-1} vs. HoF.

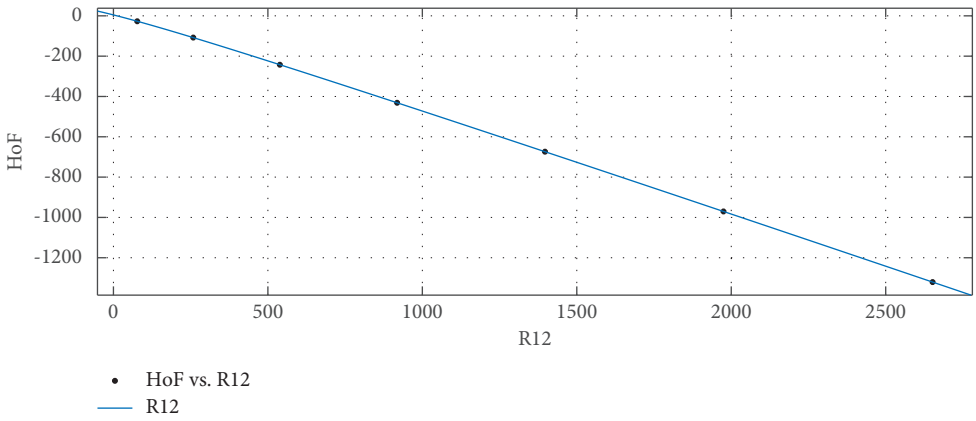

Figure 5: $R_{(1/2)}$ vs. HoF.

Graphical illustration for each index corresponding to $l = m = i; i = 1, 2, \ldots, 100$, computed above, is provided in Figure 2. □

2.1. Thermodynamical Properties (HoF and Entropy) of Niobium (II) Oxide. Many topological indices are derived for unit cell of NbO, including M_1; M_1; ABC; GA; and AZI.

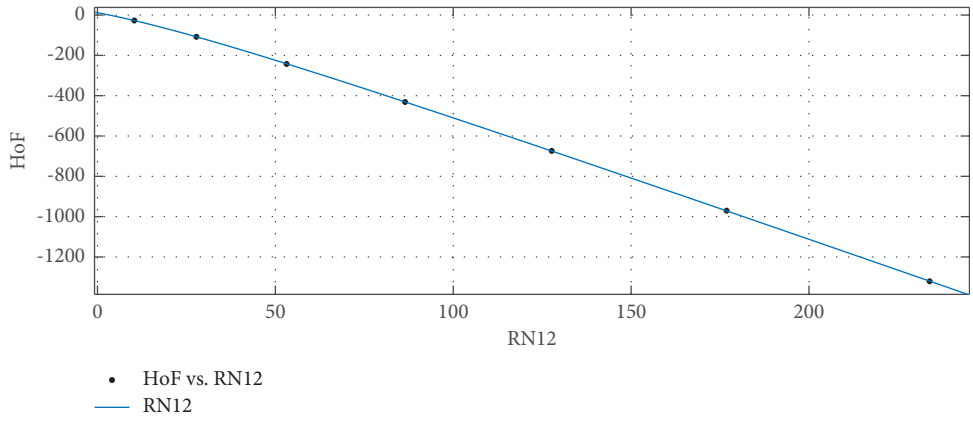

Figure 6: $R_{(-1/2)}$ vs. HoF.

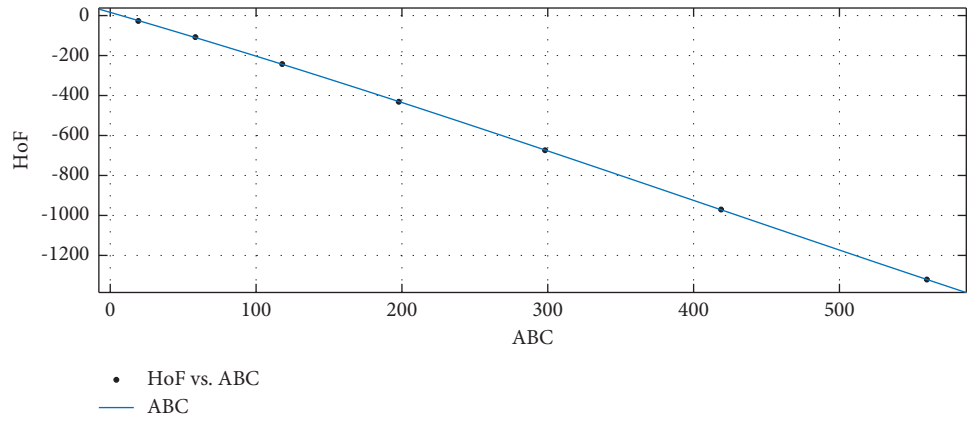

Figure 7: ABC vs. HoF.

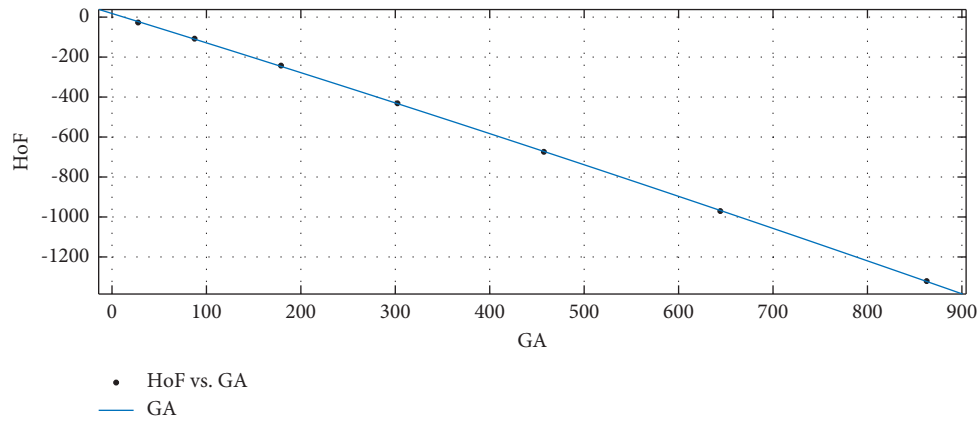

Figure 8: GA vs. HoF.

These indices are linked to thermodynamic properties of NbO, such as heat of formation (HoF) or enthalpy and entropy. The standard molar enthalpy and entropy of NbO is $-405.8\,\mathrm{kJmol}^{-1}$ and $48.1\mathrm{Jmol}^{-1}K^{-1}$, respectively. Table 3 represents the numerical values of HoF and Entropy.

2.2. Statistical Models for HoF and Topological Indices. In this section, mathematical frameworks are created for the topological index (computed in Section 2) and HoF (given in Section 2.1) of NbO. All fitted curves are shown in Figures 3–17 and also the constant quantity values of the

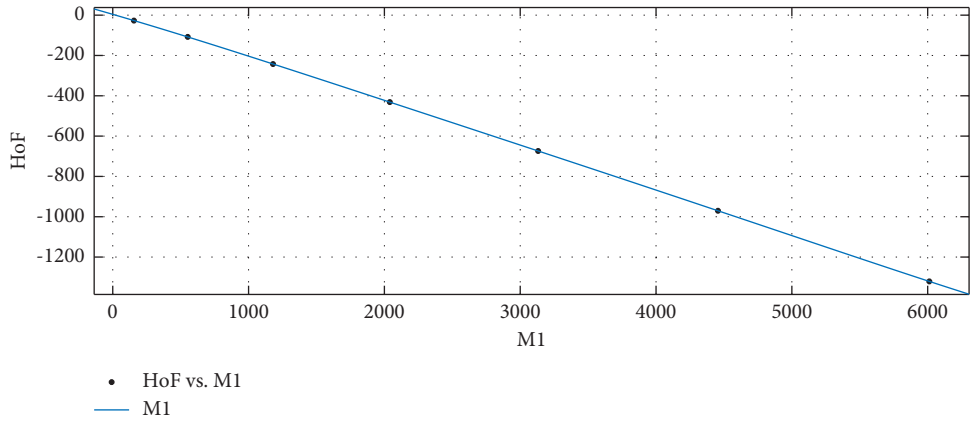

Figure 9: M_1 vs. HoF.

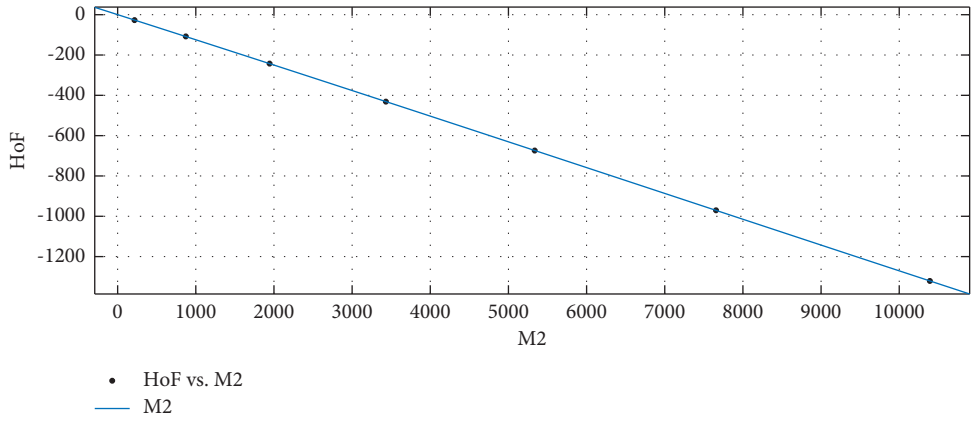

Figure 10: M_2 vs. HoF.

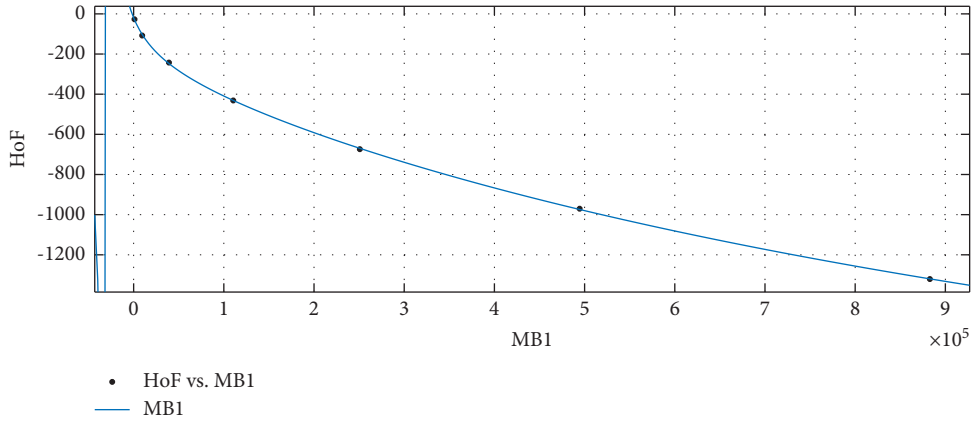

Figure 11: $\overline{M}_1$ vs. HoF.

fitted curves are depicted in Tables 4–18. Also, the goodness of fit for indices vs. HoF for NbO is depicted in Table 19. Let ε and γ denote the mean and standard deviation that is used to rescale the data.

(i) Estimation of rational polynomial for HoF vs. R_1 is

$$\mathrm{HoF}(x) = \frac{p_1 x + p_2}{x^4 + q_1 x^3 + q_2 x^2 + q_3 x + q_4}, \tag{29}$$

where $x = R_1$ is rescaled through $\varepsilon = 4264$ and $\gamma = 3746$.

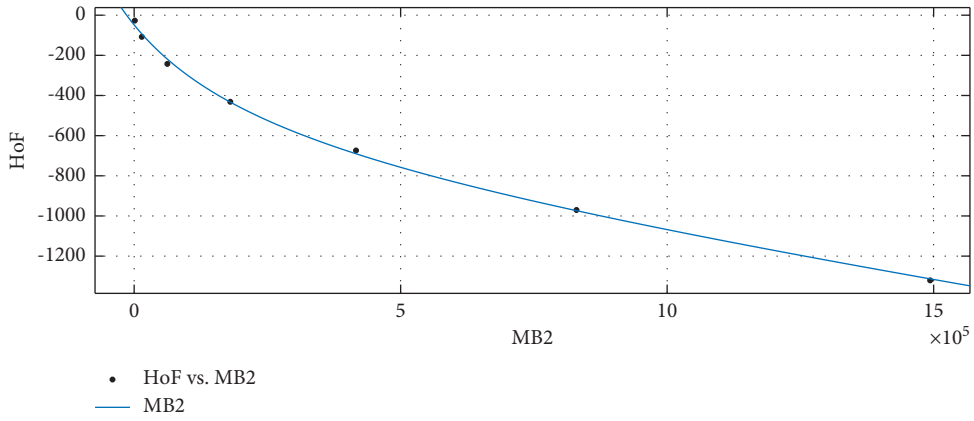

Figure 12: $\overline{M}_2$ vs. HoF.

(ii) Estimation of rational polynomial for HoF vs. R_{-1} is

$$\mathrm{HoF}(x) = \frac{p_1x^2 + p_2x + p_3}{x^2 + q_1x + q_2}, \tag{30}$$

where $x = R_{-1}$ is rescaled through $\varepsilon = 31.56$ and $\gamma = 24.34$.

(iii) Estimation of rational polynomial for HoF vs. $R_{1/2}$ is

$$\mathrm{HoF}(x) = \frac{p_1x^2 + p_2x + p_3}{x^3 + q_1x^2 + q_2x + q_3}, \tag{31}$$

where $x = R_{(1/2)}$ rescaled through $\varepsilon = 1117$ and $\gamma = 945.4$.

(iv) Estimation of rational polynomial for HoF vs. $R_{(-1/2)}$ is

$$\mathrm{HoF}(x) = \frac{p_1x^2 + p_2x + p_3}{x^2 + q_1x + q_2}, \tag{32}$$

where $x = R_{(-1/2)}$ is rescaled through $\varepsilon = 102.3$ and $\gamma = 81.85$.

(v) Estimation of rational polynomial for HoF vs. ABC is

$$\mathrm{HoF}(x) = \frac{p_1x + p_2}{x^2 + q_1x + q_2}, \tag{33}$$

where $x = \mathrm{ABC}$ is rescaled through $\varepsilon = 238.6$ and $\gamma = 198.4$.

(vi) Estimation of rational polynomial for HoF vs. GA is

$$\mathrm{HoF}(x) = \frac{p_1x^2 + p_2x + p_3}{x + q_1}, \tag{34}$$

where $x = \mathrm{GA}$ is rescaled through $\varepsilon = 365.8$ and $\gamma = 306.5$.

(vii) Estimation of rational polynomial for HoF vs. M_1 is

$$\mathrm{HoF}(x) = \frac{p_1x + p_2}{x^4 + q_1x^3 + q_2x^2 + q_3x + q_4}, \tag{35}$$

where $x = M_1$ is rescaled through $\varepsilon = 2504$ and $\gamma = 2153$.

(viii) Estimation of rational polynomial for HoF vs. M_2 is

$$\mathrm{HoF}(x) = \frac{p_1x + p_2}{x^3 + q_1x^2 + q_2x + q_3}, \tag{36}$$

where $x = M_2$ is rescaled through $\varepsilon = 4264$ and $\gamma = 3746$.

(ix) Estimation of rational polynomial for HoF vs. $\overline{M}_1$ is

$$\mathrm{HoF}(x) = \frac{p_1x^2 + p_2x + p_3}{x^2 + q_1x + q_2}, \tag{37}$$

where $x = \overline{M}_1$ is rescaled through $\varepsilon = 2.554e + 05$ and $\gamma = 3.276e + 05$.

(x) Estimation of rational polynomial for HoF vs. $\overline{M}_2$ is

$$\mathrm{HoF}(x) = \frac{p_1x^2 + p_2x + p_3}{x^2 + q_1x + q_2}, \tag{38}$$

where $x = \overline{M}_2$ is rescaled through $\varepsilon = 4.283e + 05$ and $\gamma = 5.545e + 05$.

(vi) Estimation of rational polynomial for HoF vs. AZI is

$$\mathrm{HoF}(x) = \frac{p_1x^2 + p_2x + p_3}{x + q_1}, \tag{39}$$

where $x = \mathrm{AZI}$ is rescaled through $\varepsilon = 1818$ and $\gamma = 1625$.

(vii) Estimation of rational polynomial for HoF vs. F is

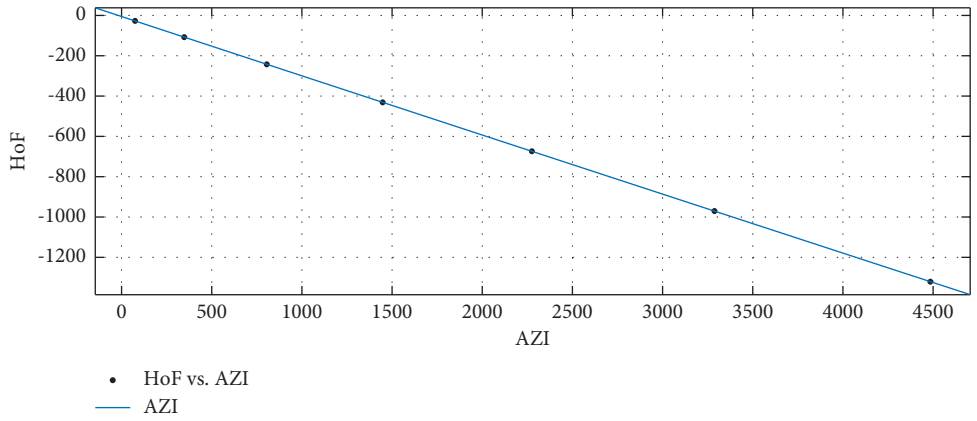

Figure 13: AZI vs. HoF.

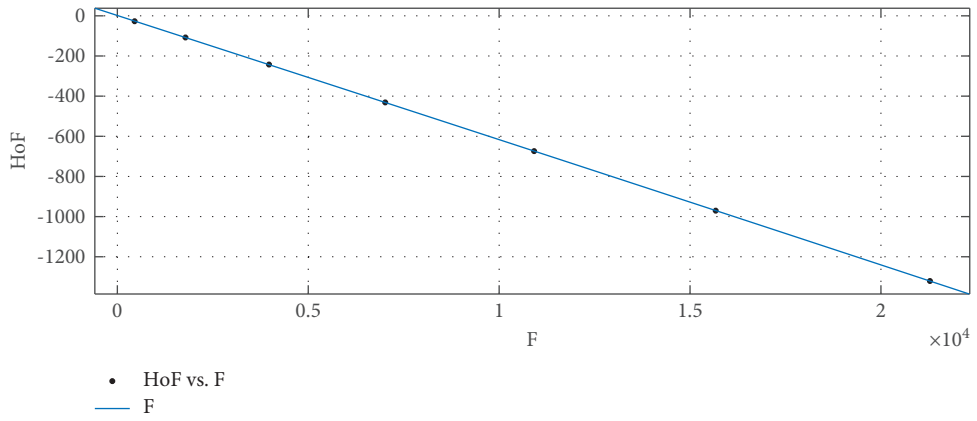

Figure 14: F vs. HoF.

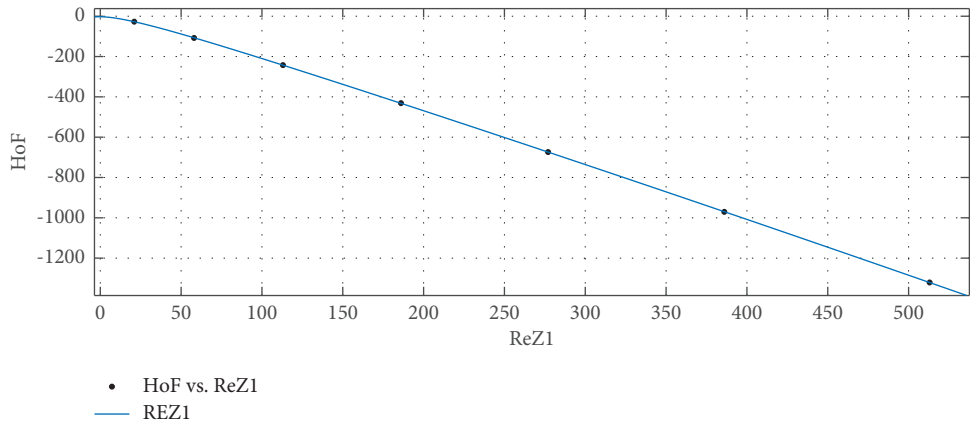

Figure 15: ReZG_1 vs. HoF.

$$\mathrm{HoF}(x) = \frac{p_1 x^2 + p_2 x + p_3}{x + q_1}, \tag{40}$$

where $x = F$ is rescaled through $\varepsilon = 8728$ and $\gamma = 7669$.

(viii) Estimation of rational polynomial for HoF vs. ReZG_1 is

$$\mathrm{HoF}(x) = \frac{p_1 x^2 + p_2 x + p_3}{x^3 + q_1 x^2 + q_2 x + q_3}, \tag{41}$$

where $x = \mathrm{ReZG}_1$ is rescaled through $\varepsilon = 222$ and $\gamma = 180.3$.

(ix) Estimation of rational polynomial for HoF vs. ReZG_2 is

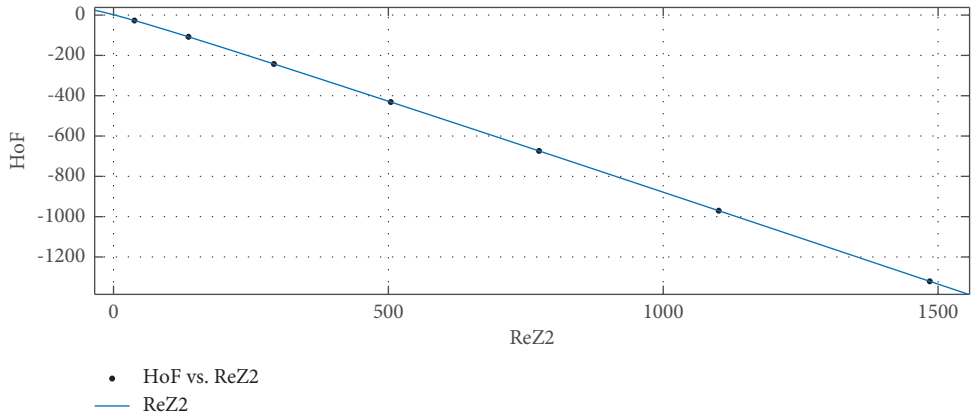

Figure 16: ReZG_2 vs. HoF.

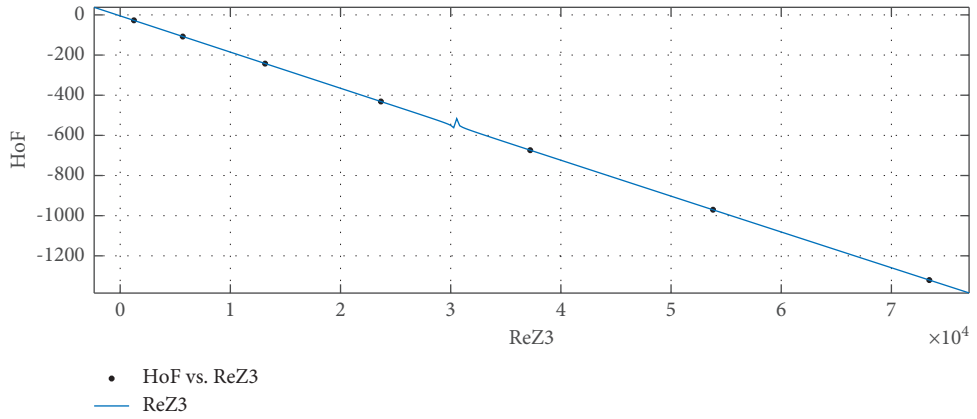

Figure 17: ReZG_3 vs. HoF.

Table 4: R_1 vs. HoF.

	p_i	Confidence interval (CI)	q_i	CI
$i = 1$	$-2.089e+05$	$(-1.39e+06, 9.72e+05)$	-3.028	$(-8.911, 2.856)$
$i = 2$	$-2.381e+05$	$(-1.583e+06, 1.107e+06)$	3.559	$(-15.22, 22.34)$
$i = 3$	—	—	-4.613	$(-33.85, 24.62)$
$i = 4$	—	—	443.2	$(-2061, 2947)$

Table 5: R_{-1} vs. HoF.

	p_i	CI	q_i	CI
$i = 1$	$-3.496e+07$	$(-1.177e+11, 1.176e+11)$	$6.704e+04$	$(-2.255e+08, 2.257e+08)$
$i = 2$	$-9.916e+07$	$(-3.337e+11, 3.335e+11)$	$1.33e+05$	$(-4.473e+08, 4.476e+08)$
$i = 3$	$-6.91e+07$	$(-2.325e+11, 2.324e+11)$	—	—

$$\text{HoF}(x) = \frac{p_1 x^2 + p_2 x + p_3}{x^3 + q_1 x^2 + q_2 x + q_3}, \tag{42}$$

where $x = \text{ReZG}_2$ is rescaled through $\varepsilon = 618.6$ and $\gamma = 531.8$.

(x) Estimation of rational polynomial for HoF vs. ReZG_3 is

$$\text{HoF}(x) = \frac{p_1 x^2 + p_2 x + p_3}{x^2 + q_1 x + q_2}, \tag{43}$$

Table 6: $R_{(1/2)}$ vs. HoF.

	p_i	CI	q_i	CI
$i = 1$	$3.108e+07$	$(-6.357e+10, 6.364e+10)$	229.4	$(-4.749e+05, 4.753e+05)$
$i = 2$	$8.362e+07$	$(-1.71e+11, 1.711e+11)$	$-6.361e+04$	$(-1.302e+08, 1.301e+08)$
$i = 3$	$5.528e+07$	$(-1.13e+11, 1.131e+11)$	$-1.04e+05$	$(-2.128e+08, 2.126e+08)$

Table 7: $R_{(-1/2)}$ vs. HoF.

	p_i	CI	q_i	CI
$i = 1$	$-3.55e+07$	$(-9.978e+10, 9.971e+10)$	$6.963e+04$	$(-1.956e+08, 1.957e+08)$
$i = 2$	$-9.948e+07$	$(-2.796e+11, 2.794e+11)$	$1.305e+05$	$(-3.666e+08, 3.668e+08)$
$i = 3$	$-6.838e+07$	$(-1.921e+11, 1.92e+11)$	—	—

Table 8: ABC vs. HoF.

	p_i	CI	q_i	CI
$i = 1$	$-3.504e+04$	$(-6.796e+04, -2111)$	-3.75	$(-5.523, -1.977)$
$i = 2$	$-4.081e+04$	$(-7.88e+04, -2822)$	77.34	(5.61, 149.1)

Table 9: *GA* vs. HoF.

	p_i	CI	q_i	CI
$i = 1$	$4.637e+05$	$(-2.16e+10, 2.16e+10)$	$-4.433e+04$	$(-2.063e+09, 2.063e+09)$
$i = 2$	$2.091e+07$	$(-9.735e+11, 9.736e+11)$	—	—
$i = 3$	$2.35e+07$	$(-1.094e+12, 1.094e+12)$	—	—

Table 10: M_1 vs. HoF.

	p_i	CI	q_i	CI
$i = 1$	$-8.239e+04$	$(-5.395e+05, 3.747e+05)$	-3.054	$(-8.908, 2.8)$
$i = 2$	$-9.506e+04$	$(-6.215e+05, 4.314e+05)$	3.673	$(-15.16, 22.51)$
$i = 3$	—	—	-4.831	$(-34.56, 24.9)$
$i = 4$	—	—	177.9	$(-807.8, 1164)$

where $x = \mathrm{ReZG}_3$ is rescaled through $\varepsilon = 2.974e+04$ and $\gamma = 2.661e+04$.

2.3. Statistical Models for Entropy and Topological Indices. In this section, mathematical frameworks for the topological index (computed in Section 2) and Entropy (given in Section 2.1) of NbO are shown. All fitted curves are shown in Figures 18–32, and the parametric values of the fitted curves are given in Tables 20–34. Also, the goodness of fit for indices vs. entropy for NbO is depicted in Table 35.

(i) Estimated rational polynomial of Entropy vs. R_1 is

$$\text{Entropy}(x) = \frac{p_1 x + p_2}{x^3 + q_1 x^2 + q_2 x + q_3}, \tag{44}$$

where $x = R_1$ is rescaled through $\varepsilon = 4264$ and $\gamma = 3746$.

(ii) Estimated rational polynomial of Entropy vs. R_{-1} is

$$\text{Entropy}(x) = \frac{p_1 x^2 + p_2 x + p_3}{x^3 + q_1 x^2 + q_2 x + q_3}, \tag{45}$$

where $x = R_{-1}$ is rescaled through $\varepsilon = 31.56$ and $\gamma = 24.34$.

(iii) Estimated rational polynomial of Entropy vs. $R_{1/2}$ is

Table 11: M_2 vs. HoF.

	p_i	CI	q_i	CI
$i = 1$	$-7.613e+07$	$(-9.059e+10, 9.044e+10)$	442.4	$(-5.281e+05, 5.29e+05)$
$i = 2$	$-8.664e+07$	$(-1.031e+11, 1.029e+11)$	−1634	$(-1.945e+06, 1.942e+06)$
$i = 3$	—	—	$1.614e+05$	$(-1.917e+08, 1.921e+08)$

Table 12: $\overline{M}_1$ vs. HoF.

	p_i	CI	q_i	CI
$i = 1$	−3053	(−4237, −1869)	6.184	(2.407, 9.962)
$i = 2$	−6405	(−1.054e+04, −2273)	4.651	(0.886, 8.417)
$i = 3$	−3146	(−5686, −606.9)	—	—

Table 13: $\overline{M}_2$ vs. HoF.

	p_i	CI	q_i	CI
$i = 1$	$1.765e+07$	$(-2.879e+12, 2.879e+12)$	$-7.947e+04$	$(-1.296e+10, 1.296e+10)$
$i = 2$	$1.026e+08$	$(-1.673e+13, 1.673e+13)$	$-1.008e+05$	$(-1.644e+10, 1.644e+10)$
$i = 3$	$7.063e+07$	$(-1.152e+13, 1.152e+13)$	—	—

Table 14: AZI vs. HoF.

	p_i	CI	q_i	CI
$i = 1$	−8568	$(-1.056e+08, 1.056e+08)$	$-1.092e+04$	$(-1.426e+08, 1.425e+08)$
$i = 2$	$5.208e+06$	$(-6.799e+10, 6.8e+10)$	—	—
$I = 3$	$5.894e+06$	$(-7.693e+10, 7.694e+10)$	—	—

Table 15: F vs. HoF.

	p_i	CI	q_i	CI
$i = 1$	$2.344e+04$	$(-4.068e+08, 4.069e+08)$	$-1.46e+04$	$(-2.484e+08, 2.484e+08)$
$i = 2$	$6.948e+06$	$(-1.182e+11, 1.182e+11)$	—	—
$i = 3$	$7.852e+06$	$(-1.336e+11, 1.336e+11)$	—	—

Table 16: ReZG_1 vs. HoF.

	p_i	CI	q_i	CI
$i = 1$	$4.092e+07$	$(-4.611e+11, 4.611e+11)$	1129	$(-1.274e+07, 1.275e+07)$
$i = 2$	$1.012e+08$	$(-1.14e+12, 1.14e+12)$	$-8.418e+04$	$(-9.487e+08, 9.485e+08)$
$i = 3$	$6.262e+07$	$(-7.054e+11, 7.056e+11)$	$-1.188e+05$	$(-1.339e+09, 1.338e+09)$

Table 17: ReZG_2 vs. HoF.

	p_i	CI	q_i	CI
$i = 1$	$-4.999e+05$	$(-1.692e+06, 6.922e+05)$	−5.973	(−14.18, 2.234)
$i = 2$	$-1.264e+06$	$(-4.372e+06, 1.845e+06)$	1037	(−1429, 3503)
$i = 3$	$-7.929e+05$	$(-2.795e+06, 1.209e+06)$	1486	(−2265, 5236)

Table 18: $ReZG_3$ vs. HoF.

	p_i	CI	q_i	CI
$i = 1$	$-1.746e+05$	$(-4.898e+05, 1.407e+05)$	364.5	(−298.9, 1028)
$i = 2$	$-1.921e+05$	$(-9.603e+05, 5.761e+05)$	−10.06	(−976, 955.8)
$i = 3$	5470	$(-5.163e+05, 5.272e+05)$	—	—

Table 19: Goodness of fit for nidices vs. HoF for NbO.

Index	Fit type	SSE	R^2	Adjusted R^2	RMSE
R_1	rat14	0.02675	1	1	0.1636
R_{-1}	rat22	4.062	1	1	1.425
$R_{1/2}$	rat23	0.0617	1	1	0.2484
$R_{-1/2}$	rat22	3.122	1	1	1.249
ABC	rat12	15.19	1	1	2.25
GA	rat21	61.11	1	0.9999	4.513
M_1	rat14	0.1551	1	1	0.3938
M_2	rat13	0.7451	1	1	0.6104
$\overline{M}_1$	rat22	92.31	0.9999	0.9998	6.794
$\overline{M}_2$	rat22	1769	0.9987	0.9961	29.74
HM	rat13	0.123	1	1	0.248
AZI	rat21	0.3795	1	1	0.3557
F	rat21	1.776	1	1	0.7695
$ReZG_1$	rat23	2.238	1	1	1.496
$ReZG_2$	rat23	0.0005708	1	1	0.02389
$ReZG_3$	rat22	0.8455	1	1	0.6502

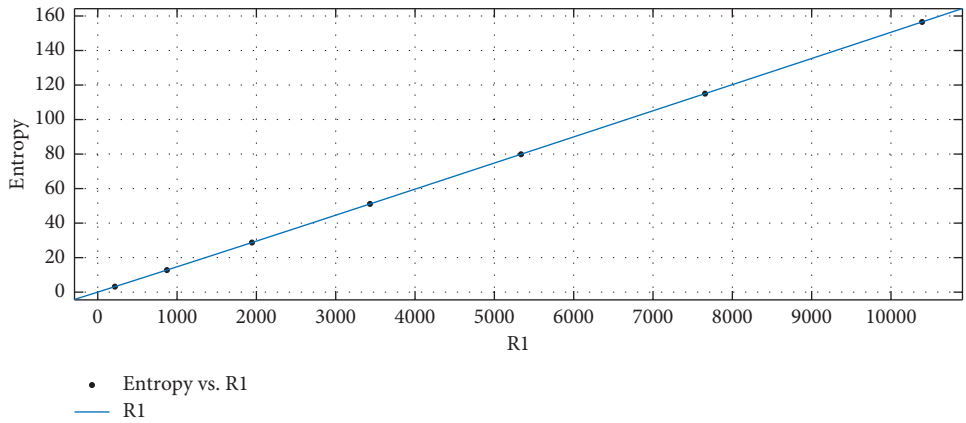

Figure 18: R_1 (x-axis) vs. Entropy (y-axis).

$$\text{Entropy}(x) = \frac{p_1x^2 + p_2x + p_3}{x^3 + q_1x^2 + q_2x + q_3}, \tag{46}$$

where $x = R_{1/2}$ is rescaled through $\varepsilon = 1117$ and $\gamma = 945.4$.

(iv) Estimated rational polynomial of Entropy vs. $R_{-1/2}$ is

$$\text{Entropy}(x) = \frac{p_1x^2 + p_2x + p_3}{x^3 + q_1x^2 + q_2x + q_3}, \tag{47}$$

where $x = R_{-1/2}$ is rescaled through $\varepsilon = 102.3$ and $\gamma = 81.85$.

(v) Estimated rational polynomial of Entropy vs. ABC is

$$\text{Entropy}(x) = \frac{p_1x^2 + p_2x + p_3}{x^3 + q_1x^2 + q_2x + q_3}, \tag{48}$$

where $x = \text{ABC}$ is rescaled through $\varepsilon = 238.6$ and $\gamma = 198.4$.

(vi) Estimated rational polynomial of Entropy vs. GA is

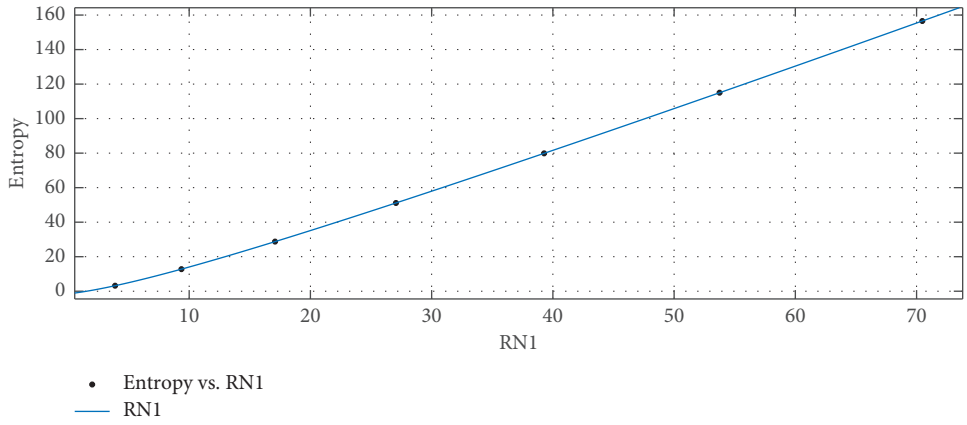

Figure 19: R_{-1} vs. Entropy.

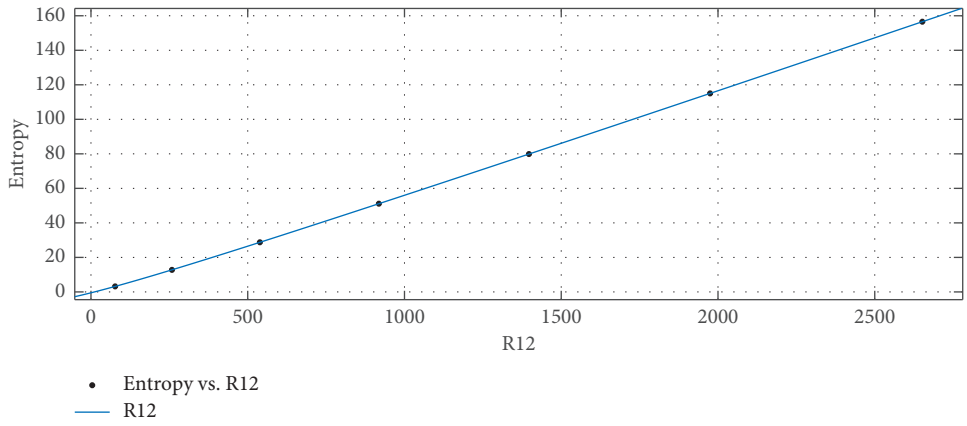

Figure 20: $R_{1/2}$ vs. Entropy.

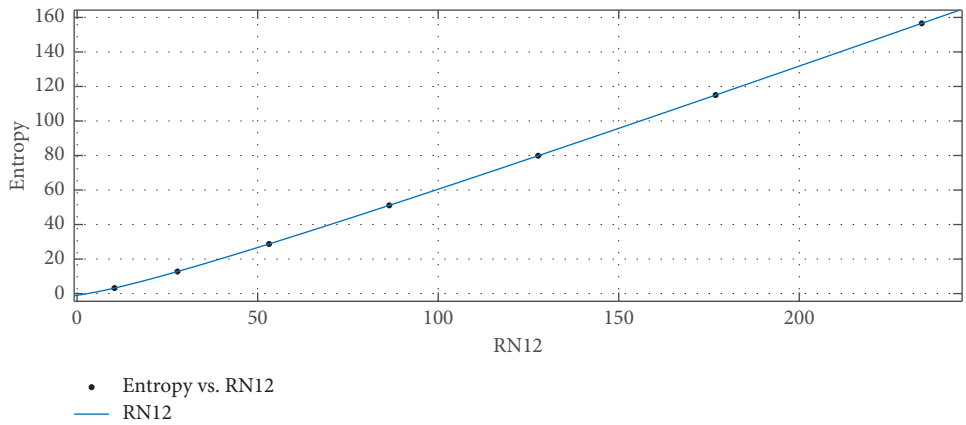

Figure 21: $R_{-1/2}$ vs. Entropy.

$$\text{Entropy}(x) = \frac{p_1 x + p_2}{x^3 + q_1 x^2 + q_2 x + q_3}, \tag{49}$$

where x = GA is rescaled through $\varepsilon = 365.8$ and $\gamma = 306.5$.

(vii) Estimated rational polynomial of Entropy vs. M_1 is

$$\text{Entropy}(x) = \frac{p_1 x + p_2}{x^4 + q_1 x^3 + q_2 x^2 + q_3 x + q_4}, \tag{50}$$

where $x = M_1$ is rescaled through $\varepsilon = 2504$ and $\gamma = 2153$.

(viii) Estimated rational polynomial of Entropy vs. M_2 is

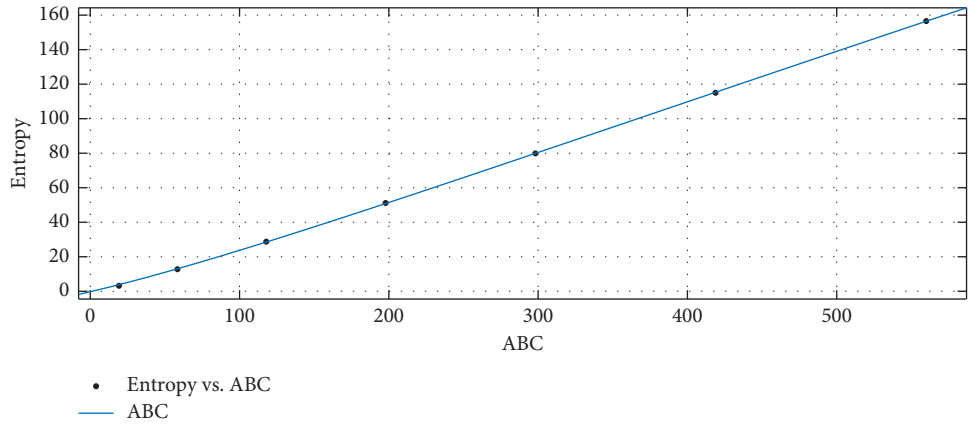

Figure 22: ABC vs. Entropy.

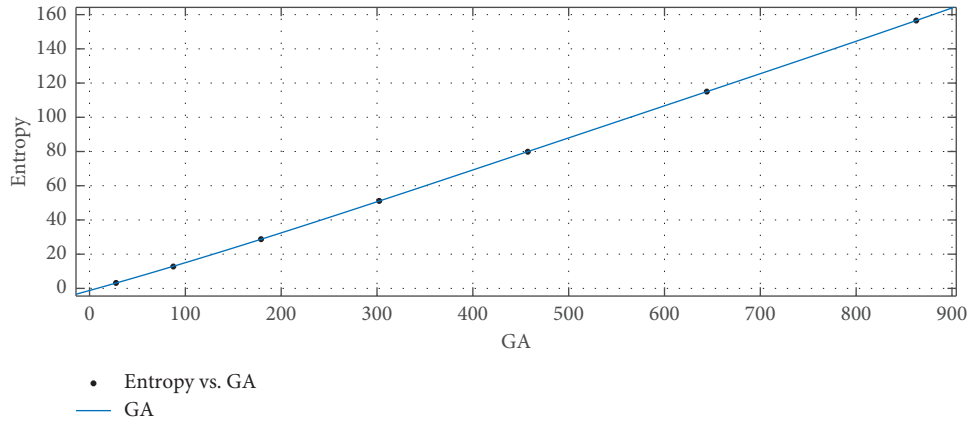

Figure 23: *GA* vs. Entropy.

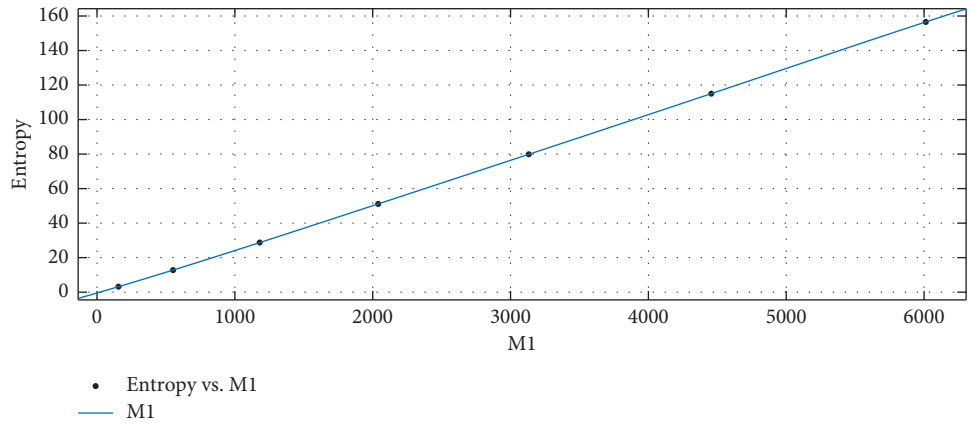

Figure 24: M_1 vs. Entropy.

$$\text{Entropy}(x) = \frac{p_1 x + p_2}{x^2 + q_1 x + q_2}, \tag{51}$$

where $x = M_2$ is rescaled through $\varepsilon = 4264$ and $\gamma = 3746$.

(ix) Estimated rational polynomial of Entropy vs. $\overline{M}_1$ is

$$\text{Entropy}(x) = \frac{p_1 x + p_2}{x^3 + q_1 x^2 + q_2 x + q_3}, \tag{52}$$

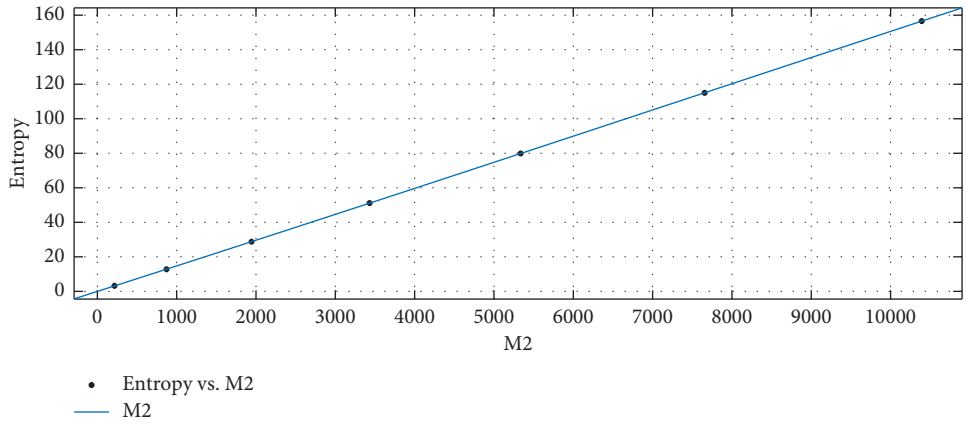

Figure 25: M_2 vs. Entropy.

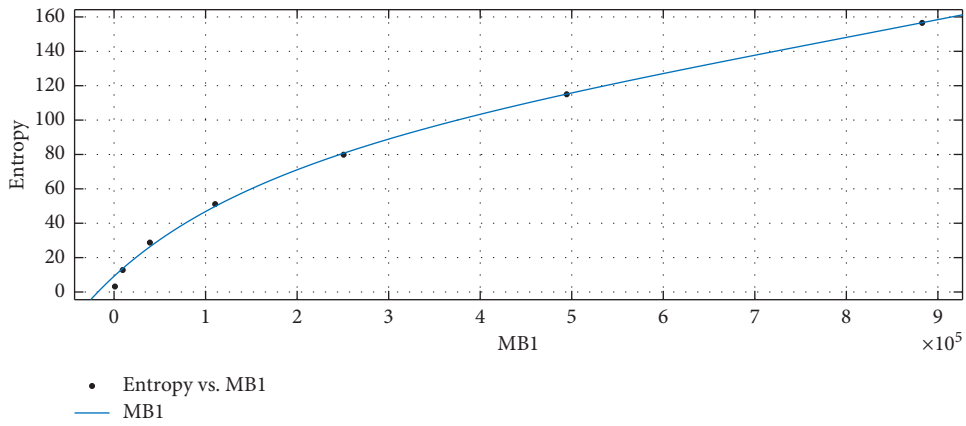

Figure 26: $\overline{M}_1$ vs. Entropy.

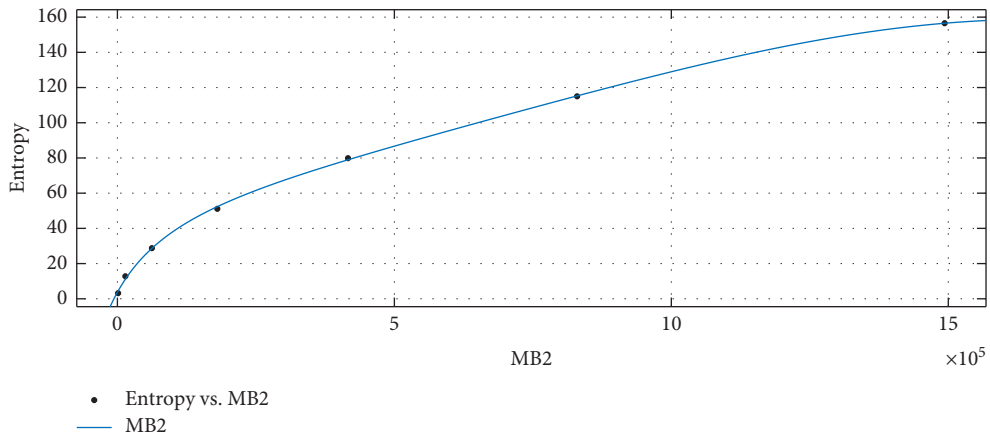

Figure 27: $\overline{M}_2$ vs. Entropy.

where $x = \overline{M}_1$ is rescaled through $\varepsilon = 2.554e + 05$ and $\gamma = 3.276e + 05$.

(x) Estimated rational polynomial of Entropy vs. $\overline{M}_2$ is

$$\text{Entropy}(x) = \frac{p_1 x + p_2}{x^4 + q_1 x^3 + q_2 x^2 + q_3 x + q_4}, \tag{53}$$

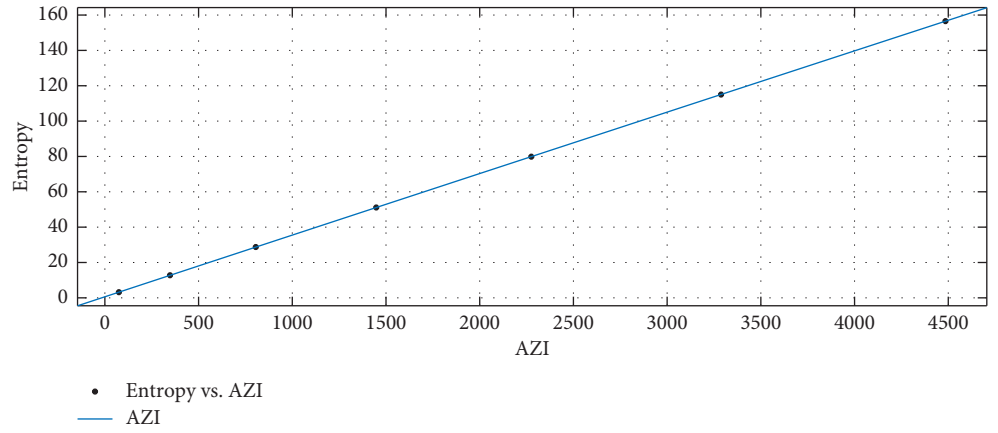

Figure 28: AZI vs. Entropy.

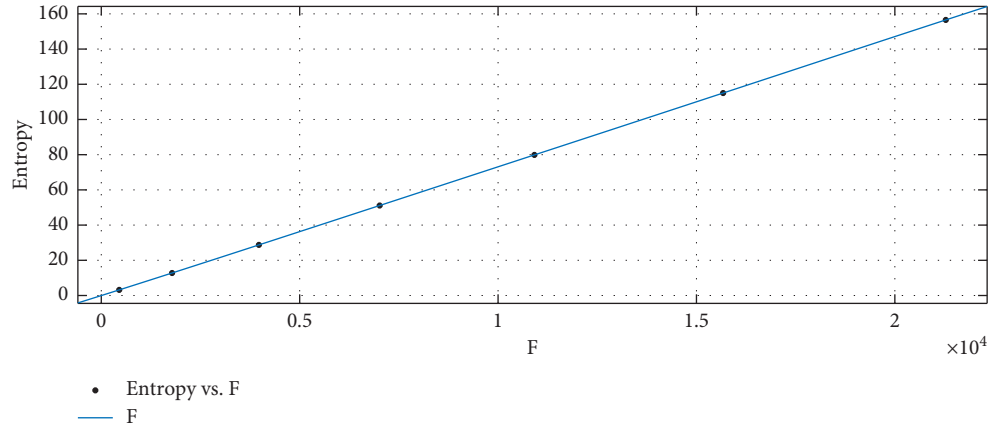

Figure 29: F vs. Entropy.

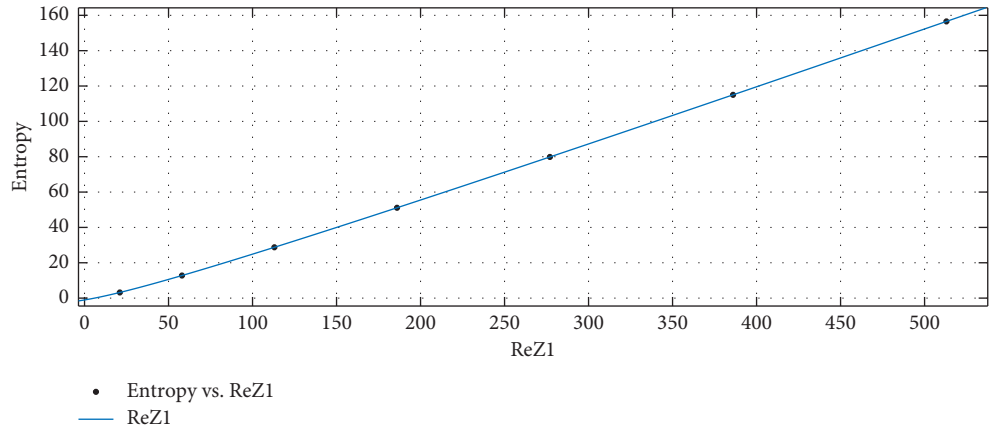

Figure 30: ReZG_1 vs. Entropy.

where $x = \overline{M}_2$ is rescaled through $\varepsilon = 4.283e + 05$ and $\gamma = 5.545e + 05$.

(xi) Estimated rational polynomial of Entropy vs. AZI is

$$\text{Entropy}(x) = \frac{p_1 x + p_2}{x^2 + q_1 x + q_2}, \tag{54}$$

where $x = \text{AZI}$ is rescaled through $\varepsilon = 1818$ and $\gamma = 1625$.

(xii) Estimated rational polynomial of Entropy vs. F is

$$\text{Entropy}(x) = \frac{p_1 x + p_2}{x^4 + q_1 x^3 + q_2 x^2 + q_3 x + q_4}, \tag{55}$$

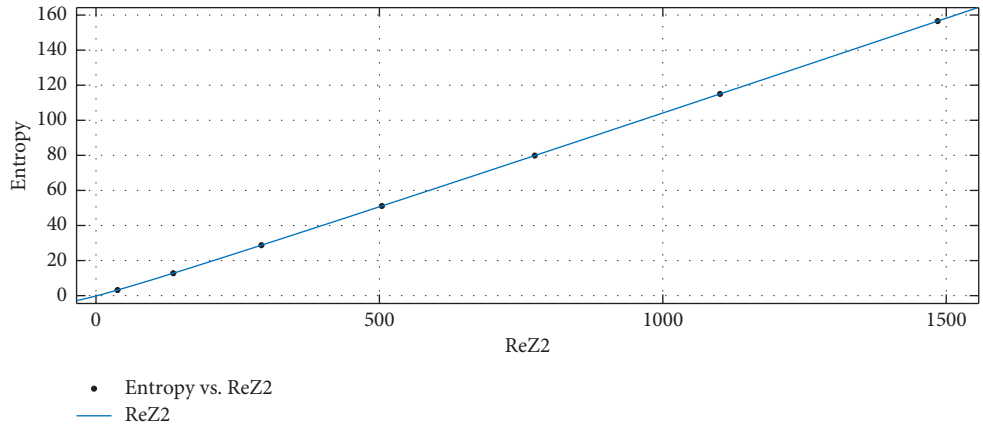

Figure 31: $ReZG_2$ vs. Entropy.

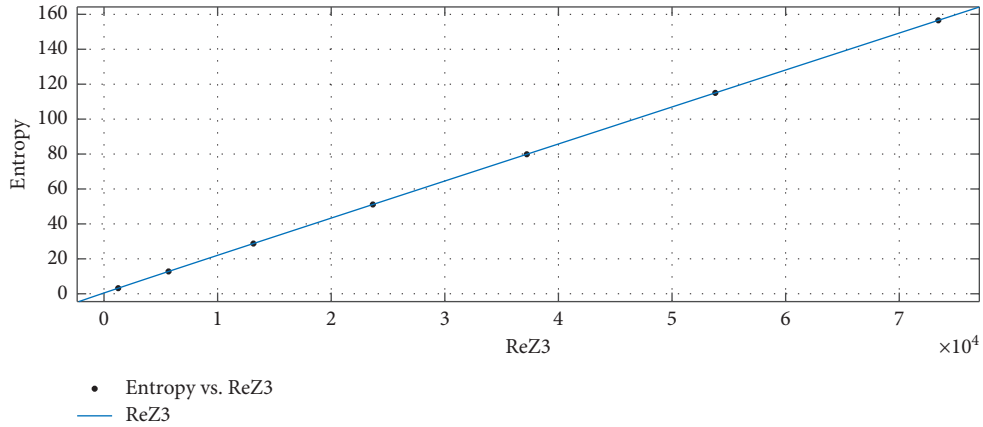

Figure 32: $ReZG_3$ vs. Entropy.

Table 20: R_1 vs. Entropy.

	p_i	CI	q_i	CI
$i = 1$	$-2.646e+04$	$(-6.984e+04,\ 1.691e+04)$	-3.384	$(-5.642,\ -1.127)$
$i = 2$	$-3.014e+04$	$(-7.949e+04,\ 1.921e+04)$	5.483	$(-2.395,\ 13.36)$
$i = 3$	—	—	-473.4	$(-1249,\ 302.2)$

Table 21: R_{-1} vs. Entropy.

	p_i	CI	q_i	CI
$i = 1$	$-7.6e+05$	$(-4.028e+08,\ 4.013e+08)$	135.2	$(-7.287e+04,\ 7.314e+04)$
$i = 2$	$-2.077e+06$	$(-1.1e+09,\ 1.096e+09)$	$-1.259e+04$	$(-6.675e+06,\ 6.65e+06)$
$i = 3$	$-1.406e+06$	$(-7.444e+08,\ 7.415e+08)$	$-2.283e+04$	$(-1.208e+07,\ 1.204e+07)$

Table 22: $R_{1/2}$ vs. Entropy.

	p_i	CI	q_i	CI
$i = 1$	$-1.575e+06$	$(-1.165e+09, 1.162e+09)$	102.9	$(-7.795e+04, 7.816e+04)$
$i = 2$	$-4.215e+06$	$(-3.115e+09, 3.106e+09)$	$-2.721e+04$	$(-2.013e+07, 2.008e+07)$
$i = 3$	$-2.775e+06$	$(-2.049e+09, 2.044e+09)$	$-4.406e+04$	$(-3.254e+07, 3.245e+07)$

Table 23: $R_{-1/2}$ vs. Entropy.

	p_i	CI	q_i	CI
$i = 1$	$2.454e+04$	$(-2.946e+04, 7.854e+04)$	−6.267	(−14.22, 1.686)
$i = 2$	$6.443e+04$	$(-8.139e+04, 2.102e+05)$	416.8	(−493.2, 1327)
$i = 3$	$4.205e+04$	$(-5.534e+04, 1.394e+05)$	677.3	(−891.1, 2246)

Table 24: ABC vs. Entropy.

	p_i	CI	q_i	CI
$i = 1$	$8.579e+05$	$(-2.287e+10, 2.287e+10)$	308	$(-8.305e+06, 8.306e+06)$
$i = 2$	$2.692e+06$	$(-7.184e+10, 7.185e+10)$	$1.379e+04$	$(-3.674e+08, 3.675e+08)$
$i = 3$	$1.993e+06$	$(-5.323e+10, 5.323e+10)$	$3.185e+04$	$(-8.508e+08, 8.508e+08)$

Table 25: *GA* vs. Entropy.

	p_i	CI	q_i	CI
$i = 1$	−5810	$(-1.493e+04, 3315)$	−3.43	(−5.625, −1.235)
$i = 2$	−6784	$(-1.739e+04, 3818)$	5.695	(−2.055, 13.45)
$i = 3$	—	—	−108	(−277.2, 61.22)

Table 26: M_1 vs. Entropy.

	p_i	CI	q_i	CI
$i = 1$	9765	$(-4.435e+04, 6.388e+04)$	−3.054	(−8.9, 2.792)
$i = 2$	$1.127e+04$	$(-5.105e+04, 7.358e+04)$	3.672	(−15.14, 22.48)
$i = 3$	—	—	−4.83	(−34.52, 24.86)
$i = 4$	—	—	177.9	(−806.6, 1162)

Table 27: M_2 vs. Entropy.

	p_i	CI	q_i	CI
$i = 1$	$2.117e+04$	$(421.2, 4.192e+04)$	−3.726	(−5.577, −1.875)
$i = 2$	$2.408e+04$	$(522.6, 4.765e+04)$	378.5	(8.47, 748.6)

Table 28: $\overline{M}_1$ vs. Entropy.

	p_i	CI	q_i	CI
$i = 1$	$-6.943e+06$	$(-2.572e+11, 2.572e+11)$	4530	$(-1.679e+08, 1.679e+08)$
$i = 2$	$-5.788e+06$	$(-2.144e+11, 2.144e+11)$	$-3.523e+04$	$(-1.305e+09, 1.305e+09)$
$i = 3$	—	—	$-7.099e+04$	$(-2.63e+09, 2.63e+09)$

Table 29: $\overline{M}_2$ vs. Entropy.

	p_i	CI	q_i	CI
$i = 1$	$4.171e+06$	$(-3.796e+11, 3.796e+11)$	3482	$(-3.171e+08, 3.171e+08)$
$i = 2$	$3.268e+06$	$(-2.975e+11, 2.975e+11)$	$-1.149e+04$	$(-1.045e+09, 1.045e+09)$
$i = 3$	—	—	$2.548e+04$	$(-2.319e+09, 2.319e+09)$
$i = 4$	—	—	$4.081e+04$	$(-3.714e+09, 3.715e+09)$

Table 30: AZI vs. Entropy.

	p_i	CI	q_i	CI
$i = 1$	$5.214e+06$	$(-1.034e+09, 1.044e+09)$	166.1	$(-3.334e+04, 3.367e+04)$
$i = 2$	$5.886e+06$	$(-1.167e+09, 1.179e+09)$	$9.2e+04$	$(-1.825e+07, 1.843e+07)$

Table 31: F vs. Entropy.

	p_i	CI	q_i	CI
$i = 1$	$3.363e+04$	$(-1.563e+05, 2.236e+05)$	−3.023	(−8.886, 2.84)
$i = 2$	$3.825e+04$	$(-1.777e+05, 2.542e+05)$	3.538	(−15.15, 22.22)
$i = 3$	—	—	−4.576	(−33.6, 24.45)
$i = 4$	—	—	600.1	(−2788, 3988)

Table 32: ReZG_1 vs. Entropy.

	p_i	CI	q_i	CI
$i = 1$	$2.858e+04$	$(-3.576e+04, 9.292e+04)$	−6.187	(−14.22, 1.843)
$i = 2$	$7.425e+04$	$(-9.781e+04, 2.463e+05)$	490.1	(−606, 1586)
$i = 3$	$4.793e+04$	$(-6.582e+04, 1.617e+05)$	768.1	(−1054, 2590)

Table 33: ReZG_2 vs. Entropy.

	p_i	CI	q_i	CI
$i = 1$	$5.915e+04$	$(-7.923e+04, 1.975e+05)$	−5.968	(−14.01, 2.073)
$i = 2$	$1.495e+05$	$(-2.114e+05, 5.104e+05)$	1035	(−1380, 3450)
$i = 3$	$9.381e+04$	$(-1.386e+05, 3.262e+05)$	1483	(−2190, 5155)

Table 34: ReZG_3 vs. Entropy.

	p_i	CI	q_i	CI
$i = 1$	$8.157e+04$	$(3.2e+04, 1.311e+05)$	1448	(566.3, 2329)
$i = 2$	$2.083e+05$	$(7.129e+04, 3.454e+05)$	2048	(618.7, 3478)
$i = 3$	$1.311e+05$	$(3.961e+04, 2.227e+05)$	—	—

where $x = F$ is rescaled through $\varepsilon = 8728$ and $\gamma = 7669$.

(xiii) Estimated rational polynomial of Entropy vs. ReZG_1 is

$$\mathrm{Entropy}(x) = \frac{p_1 x^2 + p_2 x + p_3}{x^3 + q_1 x^2 + q_2 x + q_3}, \tag{56}$$

where $x = \mathrm{ReZG}_1$ is rescaled through $\varepsilon = 222$ and $\gamma = 180.3$.

(xiv) Estimated rational polynomial of Entropy vs. ReZG_2 is

$$\mathrm{Entropy}(x) = \frac{p_1 x^2 + p_2 x + p_3}{x^3 + q_1 x^2 + q_2 x + q_3}, \tag{57}$$

where $x = \mathrm{ReZG}_2$ is rescaled through $\varepsilon = 618.6$ and $\gamma = 531.8$.

(xv) Estimated rational polynomial of Entropy vs. ReZG_3 is

Table 35: Goodness of fit for indices vs. entropy for $Nb0$.

Index	Fit type	SSE	R^2	Adjusted R^2	RMSE
R_1	rat13	0.002287	1	1	0.03382
R_{-1}	rat23	0.001106	1	1	0.03325
$R_{1/2}$	rat23	0.0006468	1	1	0.02543
$R_{-1/2}$	rat23	2.69e−05	1	1	0.005187
ABC	rat23	0.7225	1	0.9998	0.85
GA	rat13	0.0376	1	1	0.1371
M_1	rat14	0.002174	1	1	0.04663
M_2	rat12	0.01024	1	1	0.05843
$\overline{M}_1$	rat13	50.83	0.9973	0.992	5.041
$\overline{M}_2$	rat14	6.75	0.9996	0.9979	2.598
HM	rat23	9.678e−07	1	1	0.0009838
AZI	rat12	0.007279	1	1	0.04926
F	rat14	0.0002058	1	1	0.01434
ReZG_1	rat23	2.314e−05	1	1	0.00481
ReZG_2	rat23	7.752e−06	1	1	0.002784
ReZG_3	rat22	1.334e−05	1	1	0.002582

$$\mathrm{Entropy}(x) = \frac{p_1 x^2 + p_2 x + p_3}{x^2 + q_1 x + q_2}, \tag{58}$$

where $x = \mathrm{ReZG}_3$ is rescaled through $\varepsilon = 2.974e + 04$ and $\gamma = 2.661e + 04$.

3. Conclusion

After determining the topological degree-based indices, the thermodynamical parameters of niobium (II) oxide are derived. Fitting curves and building mathematical models are used to create a relationship between each index and each thermodynamical property. In MATLAB software, the rational fitting method is utilized as it gives the least mean squared error of all the built-in methods.

Data Availability

The data used to support the findings of this study are cited at relevant places within the text as references.

Conflicts of Interest

The authors declare that they have no conflicts of interest.

Authors' Contributions

This work was equally contributed by all authors.

References

[1] Y. S. Prabhakar and M. K. Gupta, "Chemical structure indices in in silico molecular design," *Scientia Pharmaceutica*, vol. 76, no. 2, pp. 101–132, 2008.

[2] W. L. Jorgensen, "The many roles of computation in drug discovery," *Science*, vol. 303, no. 5665, pp. 1813–1818, 2004.

[3] H. Kubinyi, "QSAR and 3D QSAR in drug design Part 2: applications and problems," *Drug Discovery Today*, vol. 2, no. 12, pp. 538–546, 1997.

[4] R. Perkins, H. Fang, W. Tong, and W. J. Welsh, "Quantitative structure-activity relationship methods: perspectives on drug discovery and toxicology," *Environmental Toxicology and Chemistry*, vol. 22, no. 8, p. 1666, 2003.

[5] X. Zhang, M. K. Siddiqui, S. Javed, L. Sherin, F. Kausar, and M. H. Muhammad, "Physical analysis of heat for formation and entropy of ceria oxide using topological indices," *Combinatorial Chemistry & High Throughput Screening*, vol. 25, no. 3, pp. 441–450, 2022.

[6] Q. N. Hu, Y. Z. Liang, and K. T. Yi-Zeng, "The matrix expression, topological index and atomic attribute of molecular topological structure," *Journal of Data Science*, vol. 1, no. 4, pp. 361–389, 2021.

[7] F. Yamashita and M. Hashida, "In silico approaches for predicting ADME properties of drugs," *Drug Metabolism and Pharmacokinetics*, vol. 19, no. 5, pp. 327–338, 2004.

[8] J. C. Dearden, "In silico prediction of drug toxicity," *Journal of Computer-Aided Molecular Design*, vol. 17, no. 2, pp. 119–127, 2003.

[9] S. Ekins and S. A. Wrighton, "Application of in silico approaches to predicting drug-drug interactions," *Journal of Pharmacological and Toxicological Methods*, vol. 45, no. 1, pp. 65–69, 2001.

[10] I. Muegge, "Selection criteria for drug-like compounds," *Medicinal Research Reviews*, vol. 23, no. 3, pp. 302–321, 2003.

[11] X. Zhang, H. M. Awais, M. Javaid, and M. K. Siddiqui, "Multiplicative Zagreb indices of molecular graphs," *Journal of Chemistry*, vol. 2019, Article ID 5294198, 19 pages, 2019.

[12] W. P. Walters and B. B. Goldman, "Feature selection in quantitative structure-activity relationships," *Current opinion in drug discovery & development*, vol. 8, no. 3, pp. 329–333, 2005.

[13] P. Yu, J. Wu, S. Liu, J. Xiong, C. Jagadish, and Z. M. Wang, "Design and fabrication of silicon nanowires towards efficient solar cells," *Nano Today*, vol. 11, no. 6, pp. 704–737, 2016.

[14] M. K. Siddiqui, S. Javed, L. Sherin et al., "On analysis of topological properties for terbium IV oxide via enthalpy and entropy measurements," *Journal of Chemistry*, vol. 202116 pages, Article ID 5351776, 2021.

[15] X. Zhang, X. Wu, S. Akhter, M. K. Jamil, J. B. Liu, and M. R. Farahani, "Edge-version atom-bond connectivity and geometric arithmetic indices of generalized bridge molecular graphs," *Symmetry*, vol. 10, no. 12, p. 751, 2018.

[16] S. A. Razek, M. A. Swillam, and N. K. Allam, "Vertically aligned crystalline silicon nanowires with controlled

diameters for energy conversion applications: experimental and theoretical insights," *Journal of Applied Physics*, vol. 115, no. 19, Article ID 194305, 2014.

[17] N. Dhindsa, J. Walia, and S. S. Saini, "A platform for colorful solar cells with enhanced absorption," *Nanotechnology*, vol. 27, no. 49, Article ID 495203, 2016.

[18] M. K. Siddiqui, M. Naeem, N. A. Rahman, and M. Imran, "Computing topological indices of certain networks," *Journal of Optoelectronics and Advanced Materials*, vol. 18, pp. 884–892, 2016.

[19] D. Adikaari and S. R. P. Silva, "Thickness dependence of properties of excimer laser crystallized nano-polycrystalline silicon," *Journal of Applied Physics*, vol. 97, no. 11, Article ID 114305, 2005.

[20] X. Zhang, H. Jiang, J. B. Liu, and Z. Shao, "The cartesian product and join graphs on edge-version atom-bond connectivity and geometric arithmetic indices," *Molecules*, vol. 23, no. 7, p. 1731, 2018.

[21] Z. Shao, M. K. Siddiqui, and M. H. Muhammad, "Computing zagreb indices and zagreb polynomials for symmetrical nanotubes," *Symmetry*, vol. 10, no. 7, p. 244, 2018.

[22] Y. F. Tang, S. R. P. Silva, B. O. Boskovic, J. M. Shannon, and M. J. Rose, "Electron field emission from excimer laser crystallized amorphous silicon," *Applied Physics Letters*, vol. 80, no. 22, pp. 4154–4156, 2002.

[23] S. Jin, S. Hong, M. Mativenga et al., "Low temperature polycrystalline silicon with single orientation on glass by blue laser annealing," *Thin Solid Films*, vol. 616, pp. 838–841, 2016.

[24] X. Zhang, A. Rauf, M. Ishtiaq, M. K. Siddiqui, and M. H. Muhammad, "On degree based topological properties of two carbon nanotubes," *Polycyclic Aromatic Compounds*, vol. 42, no. 3, pp. 866–884, 2020.

[25] C. Wu, C. H. Crouch, L. Zhao et al., "Near-unity below-band-gap absorption by microstructured silicon," *Applied Physics Letters*, vol. 78, no. 13, pp. 1850–1852, 2001.

[26] A. J. Pedraza, J. D. Fowlkes, and D. H. Lowndes, "Silicon microcolumn arrays grown by nanosecond pulsed-excimer laser irradiation," *Applied Physics Letters*, vol. 74, no. 16, pp. 2322–2324, 1999.

[27] M. R. Gilbert, K. Arakawa, Z. Bergstrom et al., "Perspectives on multiscale modelling and experiments to accelerate materials development for fusion," *Journal of Nuclear Materials*, vol. 554, Article ID 153113, 2021.

[28] W. Gao, J. F. Conley, and Y. Ono, "NbO as gate electrode for n-channel metal-oxide-semiconductor field-effect-transistors," *Applied Physics Letters*, vol. 84, no. 23, pp. 4666–4668, 2004.

[29] S. H. Shin, T. Halpern, and P. M. Raccah, "High-speed high-current field switching of NbO2," *Journal of Applied Physics*, vol. 48, no. 7, pp. 3150–3153, 1977.

[30] A. L. Bowman, T. C. Wallace, J. L. Yarnell, and R. G. Wenzel, "The crystal structure of niobium monoxide," *Acta Crystallographica*, vol. 21, no. 5, p. 843, 1966.

[31] C. Nico, T. Monteiro, and M. P. F. Graça, "Niobium oxides and niobates physical properties: review and prospects," *Progress in Materials Science*, vol. 80, pp. 1–37, 2016.

[32] J. K. Hulm, C. K. Jones, R. A. Hein, and J. W. Gibson, "Superconductivity in the TiO and NbO systems," *Journal of Low Temperature Physics*, vol. 7, no. 3, pp. 291–307, 1972.

[33] M. A. Rashid, S. Ahmad, M. K. Siddiqui, and M. K. Kaabar, "On computation and analysis of topological index-based invariants for complex coronoid systems," *Complexity*, vol. 2021, Article ID 4646501, 12 pages, 2021.

[34] D. Amić, D. Bešlo, B. Lučić, S. Nikolić, and N. Trinajstić, "The vertex-connectivity index revisited," *Journal of Chemical Information and Computer Sciences*, vol. 38, no. 5, pp. 819–822, 1998.

[35] B. Bollobás and P. Erdos, "Graphs of extremal weights," *Ars Combinatoria*, vol. 50, pp. 225–233, 1998.

[36] E. Estrada, L. Torres, L. Rodriguez, and I. Gutman, "An atom-bond connectivity index: modelling the enthalpy of formation of alkanes," *Indian Journal of Chemistry*, vol. 37A, pp. 849–855, 1998.

[37] W. Gao, W. F. Wang, M. K. Jamil, R. Farooq, and M. R. Farahani, "Generalized atom-bond connectivity analysis of several chemical molecular graphs," *Bulgarian Chemical Communications*, vol. 48, no. 3, pp. 543–549, 2016.

[38] D. Vukičević and B. Furtula, "Topological index based on the ratios of geometrical and arithmetical means of end-vertex degrees of edges," *Journal of Mathematical Chemistry*, vol. 46, no. 4, pp. 1369–1376, 2009.

[39] K. C. Das and I. Gutman, "Some properties of the second Zagreb index," *MATCH Commun. Math. Comput. Chem*, vol. 52, no. 1, pp. 13–21, 2004.

[40] I. Gutman and N. Trinajstić, "Graph theory and molecular orbitals. Total φ-electron energy of alternant hydrocarbons," *Chemical Physics Letters*, vol. 17, no. 4, pp. 535–538, 1972.

[41] I. Gutman, B. Furtula, Z. K. Vukicevic, and G. Popivoda, "On Zagreb indices and coindices," *MATCH Commun. Math. Comput. Chem*, vol. 74, no. 1, pp. 5–16, 2015.

[42] I. Gutman and K. C. Das, "The first Zagreb index 30 years after," *MATCH Commun. Math. Comput. Chem*, vol. 50, no. 1, pp. 83–92, 2004.

[43] B. Furtula and I. Gutman, "A forgotten topological index," *Journal of Mathematical Chemistry*, vol. 53, no. 4, pp. 1184–1190, 2015.

[44] D. Wang, Y. Huang, and B. Liu, "Bounds on augmented zagreb index," *MATCH Commun. Math. Comput. Chem.*vol. 68, pp. 209–216, 2011.

[45] A. T. Balaban, "Highly discriminating distance-based topological index," *Chemical Physics Letters*, vol. 89, no. 5, pp. 399–404, 1982.

[46] A. T. Balaban and L. V. Quintas, "The smallest graphs, trees, and 4-trees with degenerate topological index," *Journal of Mathematical Chemistry*, vol. 14, pp. 213–233, 1983.

[47] P. S. Ranjini, V. Lokesha, and A. Usha, "Relation between phenylene and hexagonal squeeze using harmonic index," *Int. J. Graph Theory*, vol. 1, no. 4, pp. 116–121, 2013.

Hindawi
Complexity
Volume 2022, Article ID 1337959, 9 pages
https://doi.org/10.1155/2022/1337959

Research Article

Mean Square Consensus of General Linear Multiagent Systems with Communication Noises under Switching Topologies

Kairui Chen,[1,2] **Chuance Yan**,[1] **Qijun Ren**,[3] **Xianxian Zeng**,[4] **and Junwei Wang**[3]

[1]*School of Mechanical and Electrical Engineering, Guangzhou University, Guangzhou 510006, China*
[2]*School of Computer & Information, Qiannan Normal University for Nationalities, Guizhou 558000, China*
[3]*School of Mathematics and Statistics, Guangdong University of Foreign Studies, Guangzhou 510006, China*
[4]*School of Computer Science, Guangdong Polytechnic Normal University, Guangzhou 510000, China*

Correspondence should be addressed to Junwei Wang; wangjwlj@gmail.com

Received 22 February 2022; Revised 17 May 2022; Accepted 27 June 2022; Published 13 August 2022

Academic Editor: Xiao Ling Wang

This paper investigates the distributed consensus problem of general linear multiagent systems (MASs) with communication noises under fixed and Markovian switching topologies, respectively. Each agent can obtain full state of itself and receive its neighbors' state with noises, where intensities of noises are vector functions of relative states of agents. Bearing in mind the above constrains, a consensus protocol is proposed, where the gain matrix is obtained by the algebraic Riccati equation and the coupling strength is restricted in a given interval. By using the stochastic stability theorem, we show that mean square consensus is achieved in fixed topology case and switching topologies case, respectively. Furthermore, an estimation of the exponential convergence rate of consensus is given explicitly. Finally, simulation examples are given to show the correctness of the proposed results.

1. Introduction

In system and control community, the coordination problem of MASs is one of the most concerned hotspots in the past decade, which has shown its potential in real-world applications, such as distributed sensor networks, smart grids, and multirobot formation [1–4]. Consensus is a fundamental issue in the control problem of MASs, which refers to designing a protocol such that all agents converge to a common value. Research results on the consensus problem can be extended to solve many coordination problems of MASs, including flocking, swarming, and rendezvous formation [5–7].

In real world, agents and their connections are often affected by noises, which could sometimes affect the performance or even destroy the stability of systems [8, 9]. Generally, noises can be divided into two categories: additive noise and multiplicative noise, and both kinds of noises have been considered in the study of MASs [10]. For additive noise, which destroys the signal in the form of superposition, its intensity is determined by external factors, such as lightning, and pulse. In 2009, Huang and Manton introduced the stochastic approximation technique to design a decreasing nonnegative gain function $c(t)$, which could attenuate the impact of additive noise while letting the MASs achieve consensus [11]. The idea of nonnegative gain function was then utilized by some scholars to investigate MASs with additive noise. For example, Li et al. proposed sufficient and necessary conditions for the decreasing nonnegative gain function to achieve asymptotic unbiased mean square average consensus [12]. Based on these results, leader-following consensus problem was solved in [13], containment control problem was studied in [14], and bipartite consensus problem was concerned in [15]. For multiplicative noise, its intensity depends on states of the system, e.g., measuring relative states through analog fading channels [16]. In [17], by using the small gain theorem, Zhang et al. developed necessary and sufficient conditions for mean square consensus and almost sure consensus for MASs. By using the stochastic stability theorem, heterogeneous MASs were studied in [18], and MASs with nonidentical channel fading were analyzed in [19]. In practical

applications, the two kinds of noise may coexist in MASs [20]. Motivated by this phenomenon, MASs with both additive and multiplicative noises were considered in [10] for the consensus problem, and in [21], for the containment control problem. However, in the above studies, the concerned MASs were in first- or second-order dynamics under fixed topology.

Typically, agents are connected through a network, which is not only affected by noises, but also has problems of link failure or abrupt change, etc. [22–25]. Many significant results on MASs under switching topologies have been addressed [26–29]. It can be found that the switching signals in many existing results were subject to deterministic time sequences [30–32]. However, due to unpredictable changes in the communication networks, it is more significant to study the case that topologies switch randomly [33]. In [34], consensus problem of double-integrator MASs was studied under Markovian switching topologies. In [35, 36], consensus problems were investigated for MASs with semi-Markovian switching topologies. In addition, there are reports involving Markovian switching topologies and communication noises at the same time. For example, in [13], Wang et al. considered the mean square and almost sure consensus problem for MASs with Markovian switching topologies and additive noises. The results in [13] were then extended in [37], where sufficient and necessary conditions were obtained for single-integrator MASs with Markovian switching topologies and additive noises.

Inspired by the above discussions, mean square consensus of general linear MASs with communication noises under Markovian switching topologies is investigated in this paper. Consensus protocol will be designed by combining the stochastic stability theory, the Riccati equation, and some theories on matrix. The contributions of this paper are summarized as follows:

(i) Consensus problem of general linear MASs with communication noises is studied. The considered noises are induced by the communication among agents, which is a distinct feature of networked systems. Moreover, the general linear MASs include some results concerned with first-order MASs as special cases [37].

(ii) To capture the time-varying communication among agents in real, we extend the consensus problem by studying the switching topologies case. We assume that the switching signals are subject to a Markovian process, under which we merely require the combined topology rather than each underlying topology being connected.

We organize the rest of the paper in the following way. Section 2 contains some useful preliminaries and a formulation of the problem. In Sections 3 and 4, consensus results for fixed and Markovian switching topologies under communication noises are provided. Section 5 is devoted to simulation examples. Finally, a conclusion of the paper is given in Section 6.

The following notations will be used. We define a column vector that is all ones as 1, the N-dimensional column vector with the i th element being 1 and others being zero as $\eta_{N,i}$, the matrix $(1/N)11^T$ as J_N, and the N-dimensional identity matrix as I_N. For any given square matrix $\mathbf{A} \in \mathbb{R}^{N\times N}$, define $\lambda_{\min}(A) = \min_{1\le i\le N}\{|\lambda_i(A)|\}$. Denote $\mathbf{I}_a^b = \{a, a+1, \ldots, b\}$ for $a < b$. $\mathbb{E}[\cdot]$ denotes the mathematical expectation.

2. Problem Formulation

2.1. Graph Theory. Let $\mathcal{G} = (\mathcal{V}, \mathcal{E}, \mathcal{A})$ be an undirected graph, where $\mathcal{V} = \{1, 2, \ldots, N\}$ is the set of nodes; $\mathcal{E} \subseteq \mathcal{V} \times \mathcal{V}$ is the set of edges. Node i means agent i. An edge of $\mathcal{G}$ is denoted by (i, j), and it implies that the information can be exchanged between node j and node i. The adjacency matrix $\mathcal{A} = [a_{ij}] \in \mathbb{R}^{N\times N}$ represents the structure of the graph, where $a_{ij} = 1$ if $(i, j) \in \mathcal{E}$, otherwise, $a_{ij} = 0$. Assume that there are no self-loops, i.e., $a_{ii} = 0$ for all $i \in \mathcal{V}$. The set of neighbors of agent i is denoted as $N_i = \{j | (i, j) \in \mathcal{E}\}$. Let $\mathcal{D} = \mathrm{diag}\{d_1, d_2, \ldots, d_N\}$, where $d_i = \sum_{j\in N_i} a_{ij}$ is the degree of agent i. The Laplacian matrix $L = [l_{ij}] \in \mathbb{R}^{N\times N}$ of $\mathcal{G}$ is defined to be $L = \mathcal{D} - \mathcal{A}$.

For a positive integer m, the union of m graphs $\mathcal{G}^1 = (\mathcal{V}, \mathcal{E}^1, \mathcal{A}^1), \ldots, \mathcal{G}^m = (\mathcal{V}, \mathcal{E}^m, \mathcal{A}^m)$ is denoted by $\cup_{\mathbf{r}=1}^{\mathbf{m}} \mathbf{G}^{\mathbf{r}} = (\mathbf{V}, \cup_{\mathbf{r}=1}^{\mathbf{m}} \mathbf{E}^{\mathbf{r}}, \cup_{\mathbf{r}=1}^{\mathbf{m}} \mathbf{A}^{\mathbf{r}})$. Let $\mathcal{G}(\sigma(t)) = (\mathcal{V}, \mathcal{E}(\sigma(t)), \mathcal{A}(\sigma(t)))$ be the interaction topology of agents at time t, where the edge set $\mathcal{E}(\sigma(t))$ and the adjacency matrix $\mathcal{A}(\sigma(t))$ are time varying.

Lemma 1 (see [26]). *If $\mathcal{G}$ is a connected graph that is undirected, $L \in \mathbb{R}^{N\times N}$ is the corresponding Laplacian matrix, and its eigenvalues can be ordered in ascending order as*

$$0 = \lambda_1(L) < \lambda_2(L) \le \cdots \le \lambda_N(L), \tag{1}$$

and

$$\min_{1^T x = 0, x \ne 0} \frac{x^T L x}{\|x\|^2} = \lambda_2(L), \tag{2}$$

where $\lambda_2(L)$ is called the algebraic connectivity of $\mathcal{G}$.

2.2. Problem Formulation. In this section, we consider MASs with the following dynamics:

$$\dot{x}_i(t) = Ax_i(t) + Bu_i(t), \mathrm{i} \in \mathbf{I}_1^{\mathrm{N}}, \tag{3}$$

where $x_i(t) \in \mathbb{R}^n$ is the state of the i th agent and $u_i(t) \in \mathbb{R}^n$ is the control input. A and B are given constant matrices with appropriate dimensions satisfying that (A, B) is controllable.

Remark 1. Comparing with first-order systems, states in general linear system (3) are coupled through matrix A and the control u_i is not placed on the state x_i directly. It can be found that the general linear MASs (3) include the first-order MASs in [37] as special cases. Therefore, in this paper, we require (A, B) to be controllable and employ the Riccati equation to obtain a feasible gain matrix. Then, a kind of

Lyapunov function, which differs from that in integrator cases, will be designed to prove the stability of the consensus error.

In real MASs, each agent receives information from its neighbors with random perturbations. Hence, when agent i communicates with its neighbor agent j, agent i receives the state of agent j in the following form:

$$y_{ji}(t) = x_j(t) + g_{ij}\big(x_i(t) - x_j(t)\big)\xi_{ij}(t), \tag{4}$$

where $y_{ji}(t) \in \mathbb{R}^n$ denotes the measurement of $x_j(t)$ by agent i and $\xi_{ij}(t) \in \mathbb{R}$ denotes the communication noises. The noise intensity function $g_{ij}(\cdot)$ is a mapping from $\mathbb{R}^n$ to $\mathbb{R}^n$. There exists a constant $\varepsilon > 0$, such that $\|g_{ij}(x)\| \le \varepsilon\|x\|$, $i = 1, \ldots, N$, and $j \in N_i$, for any $x \in \mathbb{R}^n$. The noise process $\xi_{ij}(t), i, j = 1, \ldots, N$ satisfies $\int_0^t \xi_{ij}(s)ds = w_{ij}(t), \quad t \ge 0$, where $w_{ij}(t), i, j = 1, \ldots, N$ is an independent Brownian motion.

Due to the existence of communication noises, the consensus protocol is designed as

$$u_i(t) = cK\sum_{j=1}^{N} a_{ij}\big(y_{ji}(t) - x_i(t)\big), \tag{5}$$

where c is the coupling strength and K is the gain matrix to be designed later.

In this work, we also consider the consensus of MASs (3) over randomly switching topologies and the consensus protocol is modified as follows:

$$u_i(t) = cK\sum_{j=1}^{N} a_{ij}(\sigma(t))\big(y_{ji}(t) - x_i(t)\big), \tag{6}$$

where $a_{ij}(\sigma(t))$ is the element of $\mathscr{A}(\sigma(t))$ and $\mathscr{G}(\sigma(t)) = \mathscr{V}, \mathscr{E}(\sigma(t)), \mathscr{A}(\sigma(t))$ will randomly switch among m distinct topologies $\mathscr{G}(\sigma(t)) \in \{\mathscr{G}^1, \ldots, \mathscr{G}^m\}$, and $\mathscr{G}(\sigma(t)) = \mathscr{G}_r$, if and only if the random variable $\sigma(t) = r \in \mathbb{M} = \{1, \ldots, m\}$. The switching process $\{\sigma(t), t \ge 0\}$ is governed by a time-homogeneous Markov process, whose state space corresponds to all possible topologies.

For MASs (3) and distributed control protocols (5) or (6), the following questions need to be addressed. (i) Under what conditions can the mean square consensus be achieved? (ii) How to design the control gain matrix K and coupling strength c?

In this paper, the common probability space for all random variables is denoted by $(\Omega, \mathbb{F}, \mathbb{P})$, where Ω is the sample space of elementary events. $\mathbb{F}$ is the σ-field of subsets of the sample space and $\mathbb{P}$ is the probability measure on $\mathbb{F}$. Let the infinitesimal generator of the continuous-time Markov process $\{\sigma(t), t \ge 0\}$ be $\Xi = [q_{rs}]_{m\times m}$, which is given by

$$\mathbb{P}\{\sigma(t+h) = s | \sigma(t) = r\} = \begin{cases} q_{rs}h + o(h), & \text{if } \sigma(t) \text{jumps from } r \text{ to } s, \\ 1 + q_{rr}h + o(h), & \text{otherwise,} \end{cases} \tag{7}$$

where q_{rs} is the transition rate from state r to state s with $q_{rs} \ge 0$, if $r \ne s$, $q_{rr} = -\sum_{s\ne r} q_{rs}$, and $o(h)$ denote an infinitesimal of a higher order than h, that is, $\lim_{h\longrightarrow 0}(o(h)/h) = 0$. Note that Ξ is a transition rate matrix, whose row summation is zero and all off-diagonal elements are non-negative.

Definition 1. The MASs (3) with proper designed consensus protocol are said to achieve mean square consensus if for any given $x_i(0)$

$$\lim_{t\longrightarrow\infty} \mathbb{E}\left\|x_i - x_j\right\|^2 = 0, \quad \forall i, j. \tag{8}$$

Remark 2. Mean square stable is generally used to reflect the stability of a stochastic system. Due to the existence of noises, the overall MASs become stochastic systems. Therefore, the mean square consensus defined above is suitable to describe the consensus of the concerned MASs with noises.

3. Consensus on Fixed Topology

Substituting consensus protocol (5) into (3), we get

$$dx(t) = \big((I_N \otimes A) - (cL \otimes BK)\big)x(t)dt + c\sum_{i,j=1}^{N} a_{ij} \times \Big(\eta_{N,i} \otimes \big(BKg_{ij}\big(x_i(t) - x_j(t)\big)\big)\Big)dw_{ij}(t). \tag{9}$$

As (A, B) is controllable and let matrices $Q \in \mathbb{R}^{n\times n}$ be positive definite. The control gain matrix K is designed as

$$K = \frac{1}{2}B^T P, \tag{10}$$

where P is the unique positive definite solution to the following algebraic Riccati equation (ARE)

$$0 = A^T P + PA + Q - PBB^T P. \tag{11}$$

Theorem 1. *For the undirected connected graph, the MASs (3) with communication noises achieve mean square consensus under consensus protocol (3), if K is designed as (10) and c satisfies*

$$\frac{1}{\lambda_2^2(L)} \le c^2 < \frac{N\lambda_{\min}(Q)}{2(N-1)\varepsilon^2\lambda_{\max}(L)\lambda_{\max}\big(K^T B^T PBK\big)}. \tag{12}$$

Proof. Denote $e(t) = ((I_N - J_N) \otimes I_n)x(t)$; we have

$$de(t) = \big((I_N \otimes A) - (cL \otimes BK)\big)e(t)dt + c\sum_{i,j=1}^{N} a_{ij}\Big(\big(I_N - J_N\big)\eta_{N,i} \otimes \big(BKg_{ij}\big(e_i(t) - e_j(t)\big)\big)\Big)dw_{ij}(t). \tag{13}$$

According to the definition of $\eta_{N,i}$ and J_N, we can get $\eta_{N,i}^T(I_N - J_N)\eta_{N,i} = (N-1)/N$. Let $V(t) = e^T(t)(I_N \otimes P)e(t)$. Using It $\hat{o}$'s formula [38], we have

$$\begin{aligned} dV(t) &= e^T(t)\Big(\big((I_N \otimes A) - (cL \otimes BK)\big)^T (I_N \otimes P) \\ &\quad + (I_N \otimes P)\big((I_N \otimes A) - (cL \otimes BK)\big)\Big)e(t)dt \\ &\quad + M_1(t) + \frac{N-1}{N}c^2 \sum_{i,j=1}^{N} a_{ij}^2 g_{ij}^T\big(e_i(t) - e_j(t)\big) \\ &\quad \times K^T B^T PBK g_{ij}\big(e_i(t) - e_j(t)\big)dt \\ &\le e^T(t)\Big(\big((I_N \otimes A) - (cL \otimes BK)\big)^T (I_N \otimes P) \\ &\quad + (I_N \otimes P)\big((I_N \otimes A) - (cL \otimes BK)\big)\Big)e(t)dt \\ &\quad + M_1(t) + \frac{N-1}{N}c^2\lambda_{\max}\big(K^T B^T PBK\big) \\ &\quad \times \sum_{i,j=1}^{N} a_{ij}^2 g_{ij}^T\big(e_i(t) - e_j(t)\big)g_{ij}\big(e_i(t) - e_j(t)\big)dt, \end{aligned} \tag{14}$$

where $M_1(t) = 2e^T(t)c\sum_{i=1}^{N}\sum_{j=1}^{N} a_{ij}((I_N - J_N)\eta_{N,i} \otimes PBKg_{ij}(e_i(t) - e_j(t)))dw_{ij}(t)$.

By using K in (10) and the inequality in (12), we have

$$\begin{aligned} &e^T(t)\Big(\big((I_N \otimes A) - (cL \otimes BK)\big)^T (I_N \otimes P) \\ &\quad + (I_N \otimes P)\big((I_N \otimes A) - (cL \otimes BK)\big)\Big)e(t)dt \\ &= e^T(t)\Big(I_N \otimes \big(A^T P + PA\big) - cL \otimes \big(PBB^T P\big)\Big)e(t)dt \\ &\le e^T(t)\Big(I_N \otimes \big(A^T P + PA\big) - c\lambda_2 I_N \otimes PBB^T P\Big)e(t)dt \\ &\le e^T(t)\Big(I_N \otimes \big(A^T P + PA - PBB^T P\big)\Big)e(t)dt \\ &= -e^T(t)(I_N \otimes Q)e(t)dt. \end{aligned} \tag{15}$$

Combining (14) and (15), we have

$$\begin{aligned} dV(t) &= -e^T(t)(I_N \otimes Q)e(t)dt + M_1(t) \\ &\quad + \frac{N-1}{N}c^2\lambda_{\max}\big(K^T B^T PBK\big) \\ &\quad \times \sum_{i,j=1}^{N} a_{ij}^2 g_{ij}^T\big(e_i(t) - e_j(t)\big)g_{ij}\big(e_i(t) - e_j(t)\big)dt \\ &\le -\lambda_{\min}(Q)\|e(t)\|^2 dt + M_1(t) \\ &\quad + 2\frac{N-1}{N}c^2\varepsilon^2\lambda_{\max}(L)\lambda_{\max}\big(K^T B^T PBK\big)\|e(t)\|^2 dt \\ &= -\rho\|e(t)\|^2 dt + M_1(t), \end{aligned} \tag{16}$$

where

$$\rho = \lambda_{\min}(Q) - 2\frac{N-1}{N}c^2\varepsilon^2\lambda_{\max}(L)\lambda_{\max}\big(K^T B^T PBK\big) > 0. \tag{17}$$

Finally, we have

$$\frac{d\|\mathbb{E}e(t)\|^2}{dt} \le \frac{-\rho}{\lambda_{\min}(P)}\|\mathbb{E}e(t)\|^2. \tag{18}$$

Then by the comparison theorem [39], we get

$$\mathbb{E}\|e(t)\|^2 \le \|e(0)\|^2 \exp\left\{\frac{-\rho}{\lambda_{\min}(P)}t\right\}, \tag{19}$$

leading to $\lim_{t\longrightarrow\infty}\mathbb{E}\|x_i(t) - x_j(t)\|^2 = 0$. This completes the proof. □

Remark 3. Comparing with existing works concerning with noises, general linear MASs with communication noises are considered in this paper. For MASs with additive noises, stochastic approximation technique was widely adopted, which resulted in time-varying coupling strengths [12, 21]. In this paper, by employing Riccati equation and It $\hat{o}$'s formula, the coupling strength in the consensus protocol is time-invariant, but restricted in a given interval. For some works dealt with communication noises, the concerned MASs were in first-order dynamics, which were special cases of this paper [37].

4. Consensus on Markovian Switching Topologies

In this section, we will analyze consensus of MASs (3) on Markovian switching topologies.

Theorem 2. *Assume that the union graph of $\{\mathcal{G}^r, 1 \le r \le m\}$ is connected, the MASs (3) achieve mean square consensus under consensus protocol (6), if K is designed as (9) and c satisfies*

$$\frac{1}{\lambda_2^2(L_{un})} \le c^2 < \frac{N\lambda_{\min}(Q)}{2(N-1)\varepsilon^2\lambda_{\max}(L_{un})\lambda_{\max}\big(K^T B^T PBK\big)}. \tag{20}$$

Proof. The dynamics of error system in switching topologies case is

$$\begin{aligned} \frac{de(t)}{dt} &= \big[(I_N \otimes A) - (cL(\sigma(t)) \otimes BK)\big]e(t) \\ &\quad + c\sum_{i,j=1}^{N} a_{ij}(\sigma(t))\Big[(I_N - J_N)\eta_{N,i} \\ &\quad \otimes \big(BKg_{ij}\big(e_i(t) - e_j(t)\big)\big)\Big]\xi_{ij}(t). \end{aligned} \tag{21}$$

In this case, we choose a Lyapunov function for $\sigma(t) = r$ as

$$V_r(t) = \mathbb{E}\Big[e^T(t)(I_N \otimes P)e(t)1_{\{\sigma(t)=r\}}\Big], \quad \forall r \in \mathbb{M}, \tag{22}$$

where $\sigma(t)$ admits a unique stationary distribution $\pi = [\pi_1, \ldots, \pi_m]^T$. Then the Lyapunov function $V(t)$ for the overall system can be expressed as $V(t) = \sum_{r=1}^{m} V_r(t)$.

By using the stationary distribution π, the expectation of $V(e(t), \sigma(r))$ becomes

$$\mathbb{E}[V(e(t), \sigma(r))] = \sum_{r=1}^{m} \mathbb{E}[V_r(e(t), \sigma(r))]\pi_r. \tag{23}$$

By employing the It $\widehat{o}$'s formula, we have

$$\begin{aligned}
\frac{dV(t)}{dt} &= \sum_{r=1}^{m} \pi_r \frac{dV_r(t)}{dt} = \sum_{r=1}^{m} \mathbb{E}\left[e^T(t)\left(I_N \otimes \left(A^T P + PA\right)\right)e(t)\right]\pi_r - 2c\sum_{r=1}^{m} \mathbb{E}\left[e^T(t)\left(L_r \otimes PBK\right)e(t)\right]\pi_r \\
&+ c^2 \frac{N-1}{N} \sum_{r=1}^{m} \mathbb{E}\left[\sum_{i,j=1}^{N} a_{ij}^2(\sigma(r)) g_{ij}^T\left(e_i(t) - e_j(t)\right) \times K^T B^T PBK g_{ij}\left(e_i(t) - e_j(t)\right)\right]\pi_r \\
&+ \sum_{r,s=1}^{m} \pi_s q_{rs} V_s(t) \le \mathbb{E}\left[e^T(t)\left(I_N \otimes \left(A^T P + PA\right)\right)e(t)\right] - 2c\mathbb{E}\left[e^T(t)\left(L_{un} \otimes PBK\right)e(t)\right] \\
&+ 2c^2 \frac{N-1}{N} \lambda_{\max}\left(K^T B^T PBK\right)\varepsilon^2 \\
&\times \mathbb{E}\left[e^T(t)\left(L_{un} \otimes I_n\right)e(t)\right],
\end{aligned} \tag{24}$$

where $L_{un} = \sum_{r=1}^{m} \pi_r L_r$. Similar to (10), we have

$$\begin{aligned}
&e^T(t)\left[\left(I_N \otimes \left(A^T P + PA\right)\right) - 2c\left(L_{un} \otimes PBK\right)\right]e(t) \\
&\le e^T(t)\left[\left(I_N \otimes \left(A^T P + PA\right)\right) - 2c\lambda_2\left(L_{un}\right)\left(I_N \otimes PBK\right)\right]e(t) \\
&\le e^T(t)\left[\left(I_N \otimes \left(A^T P + PA\right)\right) - 2\left(I_N \otimes PBK\right)\right]e(t) \\
&= e^T(t) I_N \otimes \left(A^T P + PA - PBB^T P\right)e(t) \\
&= -e^T(t)\left(I_N \otimes Q\right)e(t).
\end{aligned} \tag{25}$$

By (24) and (25), it yields

$$\begin{aligned}
\frac{dV(t)}{dt} &= -\mathbb{E}\left[e^T(t)\left(I_N \otimes Q\right)e(t)\right] + 2c^2\varepsilon^2 \frac{N-1}{N} \\
&\times \lambda_{\max}\left(K^T B^T PBK\right)\mathbb{E}\left[e^T(t)\left(L_{un} \otimes I_n\right)e(t)\right] \\
&\le \left[-\lambda_{\min}(Q) + 2c^2\varepsilon^2 \frac{N-1}{N}\lambda_{\max}\left(L_{un}\right)\right. \\
&\left.\times \lambda_{\max}\left(K^T B^T PBK\right)\right]\mathbb{E}\|e(t)\|^2 \\
&= -\varrho\mathbb{E}\|e(t)\|^2,
\end{aligned} \tag{26}$$

where $\varrho = \lambda_{\min}(Q) - 2c^2\varepsilon^2 N - 1/N\lambda_{\max}(L_{un})\lambda_{\max}(K^T B^T PBK) > 0$.

Similar to (16), we get

$$\mathbb{E}\|e(t)\|^2 \le \|e(0)\|^2 \exp\left\{\frac{-\varrho}{\lambda_{\min}(P)}t\right\}. \tag{27}$$

This completes the proof. □

Remark 4. In light of the assumption on the vector function g_{ij}, the intensity of noises gets weaker while achieving consensus. Specifically, when the norm of relative state between two agents decreases, the intensity of noise in their communication channel becomes smaller. Therefore, compared with additive noises, the multiplicative noises with intensities depending on relative states can better describe noises in the analog fading communication channel. If all of the communication noises $g_{ij}(\cdot) \equiv 0\,(i, j = 1, \ldots, N)$, our result can be degenerated into the noise-free case [22].

Remark 5. Compared with existing studies, we consider Markovian switching topologies and communication noises for general linear MASs. In this case, the impact of noises on the MASs is changing while the underlying topology is switching, which brings challenges for the analysis of the consensus problem. Compared with the fixed topology case, we only require the combined topology to be connected, which relax the assumption on the topology at each instant.

5. Simulation Example

In this section, we present two numerical examples to verify our theoretical results. We consider a MAS of 6 agents under

fixed topology and under switching topology in Examples 1 and 2, respectively.

Example 1. Considering a MAS with the following dynamics:

$$\dot{x}_i(t) = Ax_i(t) + Bu_i(t),$$
$$A = \begin{bmatrix} -1 & 0 & -1 \\ 0 & 0 & -1 \\ 0 & 1 & 0 \end{bmatrix}, B = \begin{bmatrix} 1 & 1 & 0 \\ 0 & 1 & 1 \\ 0 & 1 & 0 \end{bmatrix}. \quad (28)$$

The underlying communication topology is depicted in Figure 1. The corresponding Laplacian matrix is

$$L = \begin{bmatrix} 2 & -1 & -1 & 0 & 0 & 0 \\ -1 & 1 & 0 & 0 & 0 & 0 \\ -1 & 0 & 3 & -1 & 0 & -1 \\ 0 & 0 & -1 & 2 & -1 & 0 \\ 0 & 0 & 0 & -1 & 2 & -1 \\ 0 & 0 & -1 & 0 & -1 & 2 \end{bmatrix}. \quad (29)$$

We choose

$$Q = \begin{bmatrix} 1 & 0 & 1 \\ 1 & 1 & 0 \\ 0 & 1 & 0 \end{bmatrix}. \quad (30)$$

According to ARE (10), we have

$$K = \begin{bmatrix} 0.2061 & -0.07046 & 0.1090 \\ 0.0342 & 0.5317 & 0.3632 \\ 0.0992 & 0.3666 & -0.2323 \end{bmatrix}. \quad (31)$$

Let $g_{ij}(x_i(t) - x_j(t)) = \varepsilon(x_i(t) - x_j(t))$, $\varepsilon = 0.2$, and by simple calculation, we have $c = 2.3$, which ensures the sufficient condition (9) in Theorem 1. The noises here are subject to Brownian process and the simulation is conducted by the Euler–Maruyama method. Under these settings, the MASs achieve consensus as shown in Figure 2. According to Figure 2, we find that the process of achieving consensus is chartering due to the existence of communication noises. We generate 100 sample paths to simulate the mean square average, and Figure 3 shows the system achieves mean square consensus.

Example 2. Consider a MAS of 6 agents with the interaction topology randomly switches among $\mathcal{G}^1$, $\mathcal{G}^2$, and $\mathcal{G}^3$ in Figure 4. The Laplacian of the combined graph is $L_{un} = \pm \sum_{r=1}^{m} \pi_r L_r$. The transition rate matrix is chosen as

$$\Xi = \begin{bmatrix} -6 & 2 & 4 \\ 3 & -4 & 1 \\ 2 & 1 & -3 \end{bmatrix}. \quad (32)$$

Let $g_{ij}(x_i(t) - x_j(t)) = \varepsilon(x_i(t) - x_j(t))$, $\varepsilon = 0.3$, and by simple calculation, we have $c = 2$, which ensures the sufficient condition (19) in Theorem 2. Figure 5 shows the sample paths of 6 agents under a known generator matrix. After a realization of randomly switching topologies, the consensus is reached. Figure 6 shows the switching signals, which are subject to a Markovian process. Compared with Example 1,

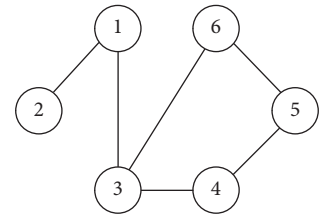

Figure 1: The fixed topology of Example 1.

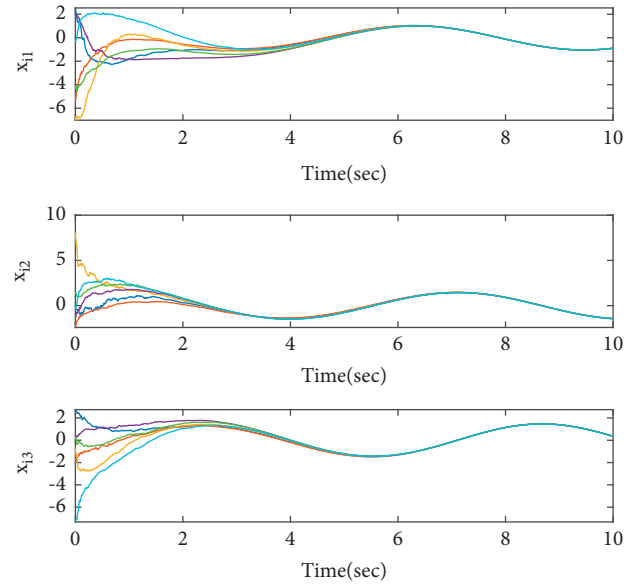

Figure 2: States of 6 agents of Example 1.

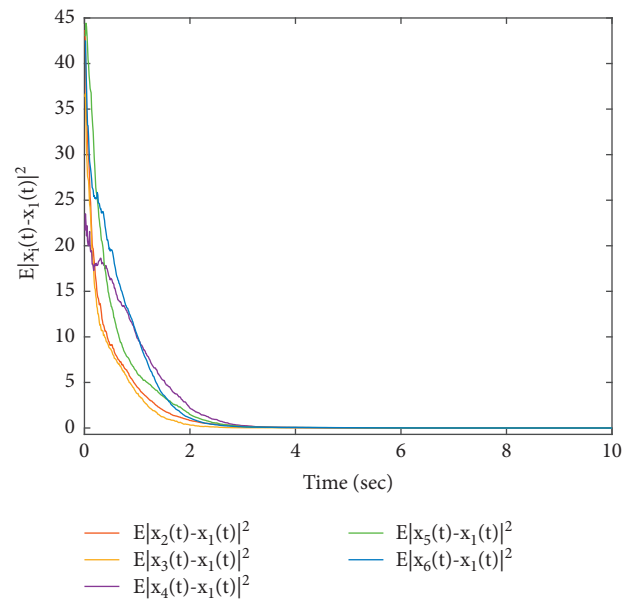

Figure 3: Mean square errors $\mathbb{E}|x_i(t) - x_1(t)|^2$ of Example 1.

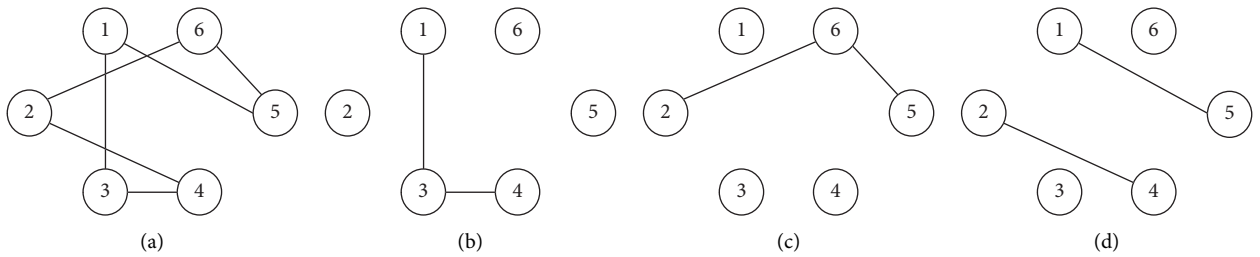

Figure 4: The switching topologies of Example 2. (a) $\mathcal{G}$. (b) $\mathcal{G}^1$. (c) $\mathcal{G}^2$. (d) $\mathcal{G}^3$.

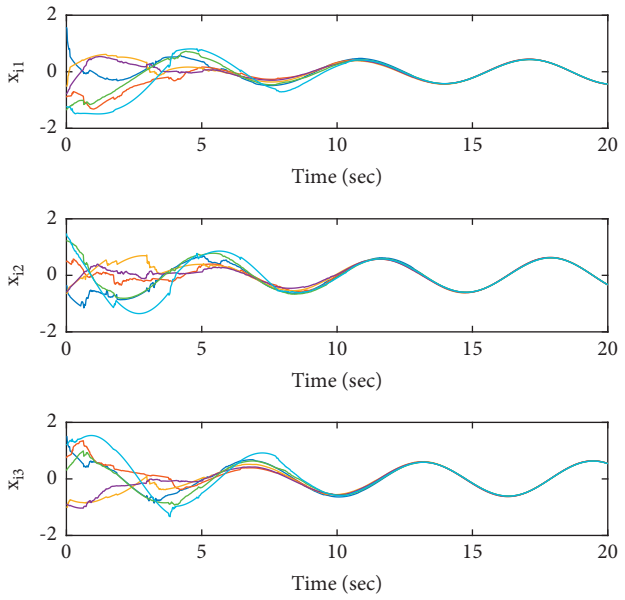

Figure 5: States of the 6 agents in Example 2.

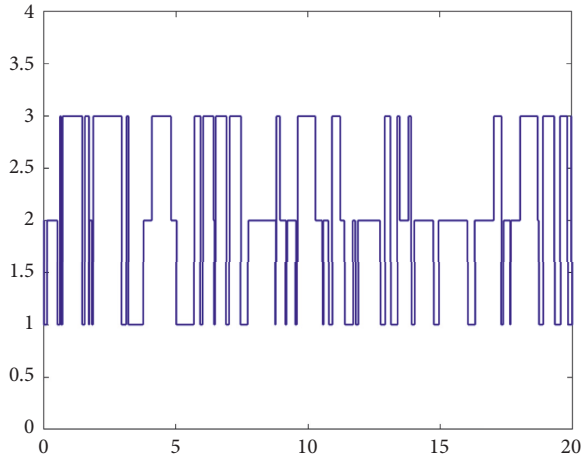

Figure 6: The Markovian switching signals.

it takes much longer for the switching topologies case to achieve consensus. We generate 100 sample paths to simulate the mean square average, and Figure 7 shows the MAS achieves mean square consensus.

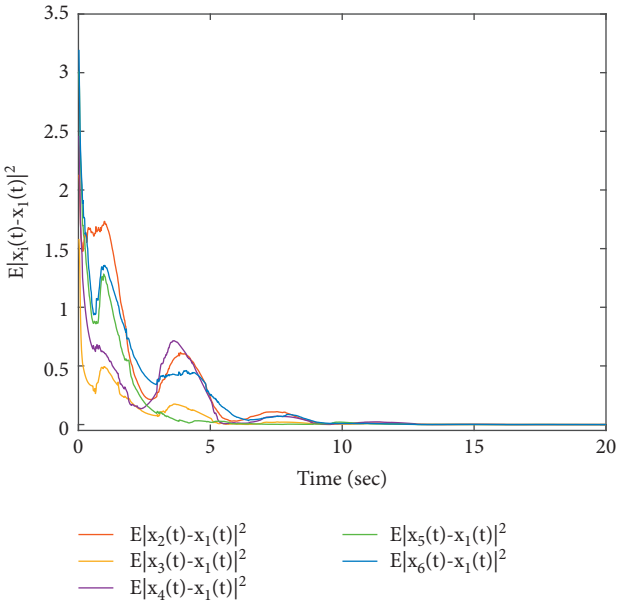

Figure 7: Mean square errors $\mathbb{E}|x_i(t) - x_1(t)|^2$ of Example 2.

6. Conclusions

Motivated by the uncertainties in real communication networks, in this article, we study the consensus problem of the general linear continuous-time MASs with communication noises. Each agent can obtain full state of itself and receive its neighbors' state information with noises, whose intensity is a vector function of agents' relative states. Research is conducted on both fixed topology and switching topologies, respectively. Mean square consensus is proved by using stochastic analysis and algebraic graph theory, and an estimation of the exponential convergence rate of consensus is given. For future research on this topic, the case of finite time consensus will be taken into account.

Data Availability

No data were used to support this study.

Conflicts of Interest

The authors declare that they have no conflicts of interest.

Acknowledgments

This work was supported in part by the National Natural Science Foundation of China (62103115 and 11771102), in part by the Natural Science Foundation of Guangdong Province (2021A1515011636), in part by the Science and Technology Research Program of Guangzhou (202102020975), in part by the Special Projects in Key Fields of Colleges and Universities in Guangdong Province (2021ZDZX1109), in part by the Characteristic Innovation Projects of Colleges and Universities in Guangdong Province, China (2019GKTSCX081), and in part by the Yangcheng Scholars Scientific Research Project of Colleges and Universities in Guangzhou City (202235364).

References

[1] K. Shen, C. Zhang, P. Dong, Z. Jing, and H. Leung, "Consensus-based labeled multi-Bernoulli filter with event-triggered communication," *IEEE Transactions on Signal Processing*, vol. 70, pp. 1185–1196, 2022.

[2] O. Mahela, M. Khosravy, N. Gupta et al., "Comprehensive overview of multi-agent systems for controlling smart grids," *CSEE Journal of Power and Energy Systems*, vol. 8, no. 1, pp. 115–131, 2022.

[3] Y. Zhou, J. Xiao, Y. Zhou, and G. Loianno, "Multi-robot collaborative perception with graph neural networks," *IEEE Robotics and Automation Letters*, vol. 7, no. 2, pp. 2289–2296, 2022.

[4] K. Chen, J. Wang, Y. Zhang, and Z. Liu, "Leader-following consensus for a class of nonlinear strick-feedback multiagent systems with state time-delays," *IEEE Transactions on Systems, Man, and Cybernetics: Systems*, vol. 50, no. 7, pp. 2351–2361, 2020.

[5] Y. Xu and S. Xu, "A novel connectivity-preserving control design for rendezvous problem of networked uncertain nonlinear systems," *IEEE Transactions on Neural Networks and Learning Systems*, vol. 31, no. 12, pp. 5127–5137, 2020.

[6] S. Su and H. Su, "A fully distributed protocol for flocking of time-varying linear systems with dynamic leader and external disturbance," *IEEE Transactions on Systems, Man, and Cybernetics: Systems*, vol. 52, no. 2, pp. 1234–1242, 2022.

[7] M. H. Qasem, N. Obeid, A. Hudaib, M. A. Almaiah, A. Al-Zahrani, and A. Al-Khasawneh, "Multi-agent system combined with distributed data mining for mutual collaboration classification," *IEEE Access*, vol. 9, 2021.

[8] T. Zhang and J. F. Zhang, "Consensus conditions of multi-agent systems with time-varying topologies and stochastic communication noises," *IEEE Transactions on Automatic Control*, vol. 55, no. 9, pp. 2043–2057, 2010.

[9] J. Wang, Y. Yan, C. Ma, Z. Liu, K. Ma, and C. Philip Chen, "Fuzzy adaptive event-triggered finite-time constraint control for output-feedback uncertain nonlinear systems," *Fuzzy Sets and Systems*, vol. 443, pp. 236–257, 2022.

[10] X. Zong, T. Li, and J. F. Zhang, "Consensus conditions of continuous-time multi-agent systems with additive and multiplicative measurement noises," *SIAM Journal on Control and Optimization*, vol. 56, no. 1, pp. 19–52, 2018.

[11] M. Manton and J. H. Manton, "Coordination and consensus of networked agents with noisy measurements: stochastic algorithms and asymptotic behavior," *SIAM Journal on Control and Optimization*, vol. 48, no. 1, pp. 134–161, 2009.

[12] T. Li, J. F. Zhang, and J. Zhang, "Mean square average-consensus under measurement noises and fixed topologies: necessary and sufficient conditions," *Automatica*, vol. 45, no. 8, pp. 1929–1936, 2009.

[13] Y. Wang, L. Cheng, W. Ren, Z. G. Hou, and M. Tan, "Seeking consensus in networks of linear agents: communication noises and Markovian switching topologies," *IEEE Transactions on Automatic Control*, vol. 60, no. 5, pp. 1374–1379, 2015.

[14] W. Li, L. Xie, and J. F. Zhang, "Containment control of leader-following multi-agent systems with Markovian switching network topologies and measurement noises," *Automatica*, vol. 51, pp. 263–267, 2015.

[15] Y. Du, Y. Wang, and Z. Zuo, "Mean square bipartite consensus for multiagent systems with antagonistic information and time-varying topologies," *IEEE Transactions on Systems, Man, and Cybernetics: Systems*, vol. 52, no. 3, pp. 1744–1754, 2022.

[16] R. Zong and X. Zong, "Time-varying formation control of linear multiagent systems with time delays and multiplicative noises," *International Journal of Robust and Nonlinear Control*, vol. 31, no. 18, pp. 9008–9025, 2021.

[17] T. Li, F. Wu, and J. F. Zhang, "Multi-agent consensus with relative-state-dependent measurement noises," *IEEE Transactions on Automatic Control*, vol. 59, no. 9, pp. 2463–2468, 2014.

[18] K. Zhang, Y. Zhang, X. Zong, and R. Li, "Mean square and almost sure consensus of heterogeneous multi-agent systems with multiplicative noise," *International Journal of Robust and Nonlinear Control*, vol. 32, no. 4, pp. 2399–2419, 2022.

[19] J. Xu, Z. Zhang, and W. Wang, "Mean-square consentability of multiagent systems with nonidential channel fading," *IEEE Transactions on Automatic Control*, vol. 66, no. 4, pp. 1887–1894, 2021.

[20] Y. Du, Y. Wang, and Z. Zuo, "Bipartite consensus for multi-agent systems with noises over Markovian switching topologies," *Neurocomputing*, vol. 419, pp. 295–305, 2021.

[21] Y. Du, Y. Wang, Z. Zuo, and W. Zhang, "Containment control for distributed networks subject to multiplicative and additive noises with stochastic approximation-type protocols," *International Journal of Robust and Nonlinear Control*, vol. 30, no. 2, pp. 665–684, 2019.

[22] K. You, Z. Li, and L. Xie, "Consensus condition for linear multi-agent systems over randomly switching topologies," *Automatica*, vol. 49, no. 10, pp. 3125–3132, 2013.

[23] J. Wang, H. Zhang, K. Ma, Z. Liu, C. L. P. Chen, and J. Liu, "Neural adaptive self-triggered control for uncertain nonlinear systems with input hysteresis," *IEEE Transactions on Neural Networks and Learning Systems*, 2021.

[24] J. Wang, Z. Liu, Y. Zhang, and C. P. Chen, "A novel fuzzy control with filter-based event-triggered mechanism for nonlinear uncertain stochastic systems suffered input hysteresis," *Fuzzy Sets and Systems*, vol. 432, pp. 68–88, 2022.

[25] J. Wang, W. Chen, K. Ma, Z. Liu, and C. L. Philip Chen, "Adaptive neural event-triggered control for nonlinear uncertain system with input constraint based on auxiliary system," *International Journal of Robust and Nonlinear Control*, vol. 31, no. 15, pp. 7528–7545, 2021.

[26] R. Olfati-Saber and R. Murray, "Consensus problems in networks of agents with switching topology and time-delays," *IEEE Transactions on Automatic Control*, vol. 49, no. 9, pp. 1520–1533, 2004.

[27] W. Cheng and D. Cheng, "Leader-following consensus of multi-agent systems under fixed and switching topologies," *Systems & Control Letters*, vol. 59, no. 3-4, pp. 209–217, 2010.

[28] Y. Wang and L. Wang, "Distributed consensus of heterogeneous multi-agent systems with fixed and switching topologies," *International Journal of Control*, vol. 85, no. 12, pp. 1967–1976, 2012.

[29] S. A. Ajwad, E. Moulay, M. Defoort, T. Menard, and P. Coirault, "Leader-following consensus of second-order multi-agent systems with switching topology and partial aperiodic sampled data," *IEEE Control Systems Letters*, vol. 5, no. 5, pp. 1567–1572, 2021.

[30] S. Li, G. Feng, J. Wang, X. Luo, and X. Guan, "Adaptive control for cooperative linear output regulation of heterogeneous multi-agent systems with periodic switching topology," *IET Control Theory & Applications*, vol. 9, no. 1, pp. 34–41, 2015.

[31] Z. Li, M. Z. Chen, and Z. Ding, "Distributed adaptive controllers for cooperative output regulation of heterogeneous agents over directed graphs," *Automatica*, vol. 68, pp. 179–183, 2016.

[32] X. Li, M. Z. Q. Chen, H. Su, and C. Li, "Distributed bounds on the algebraic connectivity of graphs with application to agent networks," *IEEE Transactions on Cybernetics*, vol. 47, no. 8, pp. 2121–2131, 2017.

[33] M. Meng, L. Liu, and G. Feng, "Adaptive output regulation of heterogeneous multiagent systems under Markovian switching topologies," *IEEE Transactions on Cybernetics*, vol. 48, no. 10, pp. 2962–2971, 2018.

[34] Y. Tian and Y. P. Tian, "Consentability and protocol design of multi-agent systems with stochastic switching topology," *Automatica*, vol. 45, no. 5, pp. 1195–1201, 2009.

[35] X. He and M. He, "H ∞ consensus of multi-agent systems with semi-Markovian switching topologies and mode-dependent delays," *International Journal of Systems Science*, vol. 52, no. 1, pp. 173–184, 2020.

[36] X. Mu and X. Mu, "Output feedback containment control of multi-agent systems with semi-markovian switching topologies and input-bounded leaders," *International Journal of Systems Science*, vol. 51, no. 16, pp. 3299–3319, 2020.

[37] M. Deng and F. Deng, "Necessary and sufficient conditions for consensus of continuous-time multiagent systems with Markovian switching topologies and communication noises," *IEEE Transactions on Cybernetics*, vol. 50, no. 7, pp. 3264–3270, 2020.

[38] X. Mao, *Stochastic Differential Equations and Applications*, Horwood Publishing, Chichester, U.K, Second Edition, 2007.

[39] A. Michel, R. Miller, and M. Vidyasagar, *Qualitative Analysis of Large Scale Dynamical Systems*, Academic, New York, NY, USA, 1980.

Hindawi
Complexity
Volume 2022, Article ID 3458094, 14 pages
https://doi.org/10.1155/2022/3458094

Research Article

Topological Aspects of Molecular Networks: Crystal Cubic Carbons

Muhammad Javaid,[1] **Aqsa Sattar**,[1] **and Ebenezer Bonyah**[2]

[1]*Department of Mathematics, School of Science, University of Management and Technology, Lahore 54770, Pakistan*
[2]*Department of Mathematics Education, Akenten Appiah-Menka University of Skills Training and Enterpreneurial Development, Kumasi 00233, Ghana*

Correspondence should be addressed to Ebenezer Bonyah; ebbonya@gmail.com

Received 31 March 2022; Revised 13 May 2022; Accepted 3 June 2022; Published 21 July 2022

Academic Editor: Yue Song

Theory of networks serves as a mathematical foundation for the construction and modeling of chemical structures and complicated networks. In particular, chemical networking theory has a wide range of utilizations in the study of chemical structures, where examination and manipulation of chemical structural information are made feasible by utilizing the numerical graph invariants. A network invariant or a topological index (TI) is a numerical measure of a chemical compound which is capable to describe the chemical structural properties such as melting point, freezing point, density, pressure, tension, and temperature of chemical compounds. Wiener initiated the first distance-based TI which is considered to be the most important TI to preserve the chemical and physical properties of chemical structures. Later on, degree-based TI was introduced to find the π-electron energy of molecules. Recently, connection number-based TIs are studied which are more efficient than degree and distance-based TIs. In this paper, we compute the connection number-based TIs of the structure of crystal cubic carbons which are one of the most significant and interesting composites in modern resources of science due to the involvement of carbon atoms.

1. Introduction

Mathematical chemistry, the field of theoretical chemistry, utilizes the mathematical tools to explain and predict chemical structures and complicated networks. Chemical network theory (NT) is a field of mathematical chemistry in which we use methods of network theory to mathematically represent the chemical phenomena of molecular chemical structures. NT is used to describe, develop, analyze, and comprehend the molecular structures and their characteristics. In chemical NT, chemical structures are incorporated by vertices and edges, where the vertices (nodes) speak to the atoms while the edges speak to the bonds between the atoms. This theory plays an important function in the realm of chemical sciences.

Chemical NT uses network theoretic invariants to restrict the molecular structure into a unique number that reveals the electronic structures, structural sections, and energy of atoms. Interpreting the molecular structural information with the help of these TIs is gaining popularity among the researchers over the years. The research work in the area of chemical NT regarding the topological utilizations nanostructures, polyphenylene dendrimer nanostars, tree like polyphenylene, carbon nanocones, extremal pentagonal chains, spiro hexagonal systems, and polyomino chains can be seen in [1–3]. These chemical applications inspired us to investigate TIs of some novel chemical networks. A huge number of early medication studies indicate that substantial internal linkages exist between the pharmacology and biomedical properties of drugs and their subatomic compositions. The topological descriptors such as

Zagreb indices (ZIs) and modified ZIs were defined to be used in the investigation of medication subatomic structures, which are very helpful for medicinal and pharmaceutical research.

There are many chemical substances that are beneficial for the survival of living things. The basic components that help in the formation of cells in living beings are oxygen, nitrogen, hydrogen, and carbon. The essential component for the human life is carbon. It is important for the production of proteins, carbohydrates, and nucleic acids. It is also essential for plant development in the form of carbon dioxide. It is found in the form of carbonates and bicarbonates in oceans, as a good conductor of electricity, and in the form of limestone in rocks. The particles of carbon may connect in distinct ways, which are referred to as allotropes of carbon. Carbon atom is well recognized in the shape of diamond, graphite, bucky balls, etc. The structure of distinct carbon allotropes is represented in Figure 1. In the structure of crystal cubic carbon, the carbon atoms are piled tightly together which make it a very strong material. There are wide ranging utilizations of carbon allotropes (for details, we refer the readers to [4–6]).

The Wiener index initiated by Wiener in 1947 while researching the boiling point of paraffin was the fundamental TI [7]. Gutman [8] initiated degree-based TIs. Following that, researchers investigated a variety of distance-based descriptors in chemical fields which helped them to interpret the chemical molecular information of chemical structures such as freezing and melting point, flammability, stability, and density. For more information, see [9, 10].

Gutman and Trinajstic [11] examined the new notion of the first ZI in 1975. Gutman et al. [12] then pioneered the unique concept of second ZI in 1975. Due to the vast span of their applications, these classical ZIs are very important in the study of chemical NT. Later on, Furtula and Gutman [13] proposed the notion of third ZI, which is also known as the forgotten index since it was discovered after a lengthy period of time. Nikolic et al. [14] investigated modified ZI in 2003. In 2018, Yang et al. [15] found some degree-based ZIs of the crystal cubic carbon structures. Gao et al. [16] and Zahid et al. [17] computed the ZIs of crystal cubic carbon structures. Further, Zhang and Naeem [18] found the metric dimension of these structures of carbon atom. Moreover, Yang et al. [19] computed the vertex Szeged index of the structure of cubic crystals. Furthermore, Arockiaraj et al. [20] and Abraham et al. [21] explored the topological properties of other types of three-dimensional structures. Recently, Ali and Trinajstić [22] initiated a novel conception of connection number (CN) which is the cardinality of those nodes having length two from a certain vertex. They computed all the ZIs on connection bases instead of degrees of the vertices and reported that the connection-based Zagreb indices (CBZIs) have larger ability to forecast the physical and chemical properties of molecular structures of chemistry than that of degree-based indices. After the initiation of CBZIs, all the researchers started working on measuring the properties of chemical structure with the help of these CBZIs. Cao et al. [23] computed ZCIs of molecular graphs. Sattar et al. [24–26] just discovered the CBZIs of dendrimer nanostars. Further, Ali et al. [27] estimated modified CBZIs for T-sum graphs in 2020. Haoer et al. [28] introduced the multiplicative leap ZIs. Javaid et al. [29] computed connection-based multiplicative ZIs (CBMZI) for various wheel networks. Du et al. [30] computed modified CBZIs for alkanes. Yang et al. [31] investigated the molecular characteristics of cubic carbon crystal formations. The motivation to this article is as follows.

(1) TIs, the numerical measure of a chemical compound, can describe the properties of chemical structure such as melting point, freezing point, density, pressure, tension, and temperature of chemical compounds. These TIs have much importance due to their wide range of applicability in reticular chemistry. They are efficient enough to characterize the topology of molecular compounds.

(2) Crystal cubic carbon structures are one of the important chemical structures due to the involvement of primary carbon element in it.

(3) Connection-based ZIs are more appropriate to anticipate the chemical and physical properties of chemical compounds than all the other introduced ZIs found in literature.

In this paper, we calculate the CBMZIs of crystal cubic carbon structure which is the most important allotrope of carbon. We find first CBMZI, second CBMZI, third CBMZI, and fourth CBMZI. We also compute the modified CBMZI, namely, modified first CBMZI, modified second CBMZI, and modified third CBMZI. This paper is organized as follows. Section 2 defines the basic definitions which are compulsory to understand and are helpful for the computation of main results. Section 3 consists of general expressions to compute the CBMZIs of structure of crystal cubic carbon. Section 4 draws the conclusions of this article.

2. Primary Definitions

This section involves the basic definitions which are helpful for the further calculations.

Definition 1 (see [11]). Let $G = (\mathscr{H}(G), \mathscr{T}(G))$ be a network, where $\mathscr{H}(G)$ denotes the set of vertices and $\mathscr{T}(G)$ denotes the set of edges, respectively. Then, the degree-based ZIs are defined as

(1) $\widehat{\mathfrak{Z}}_1(G) = \sum_{h\in\mathscr{H}(G)}(d_G(h))^2 = \sum_{ht\in\mathscr{T}(G)}(d_G(h) + d_G(t))$,

(2) $\widehat{\mathfrak{Z}}_2(G) = \sum_{ht\in\mathscr{T}(G)}(d_G(h) \times d_G(t))$,

where $d_G(h)$ and $d_G(t)$ show the degree of vertices h and t, respectively.

Definition 2 (see [22]). For a network G, connection-based Zagreb indices (CBZIs) are given as

(1) $\mathfrak{Z}_1\mathbb{C}\widetilde{I}(G) = \sum_{h\in\mathscr{H}(G)}(\tau_G(h))^2$,

(2) $\mathfrak{Z}_2\mathbb{C}\widetilde{I}(G) = \sum_{ht\in\mathscr{T}(G)}(\tau_G(h) \times \tau_G(t))$,

where $\tau_G(h)$ and $\tau_G(t)$ indicate the connection number (CN) of vertices h and t, respectively. These

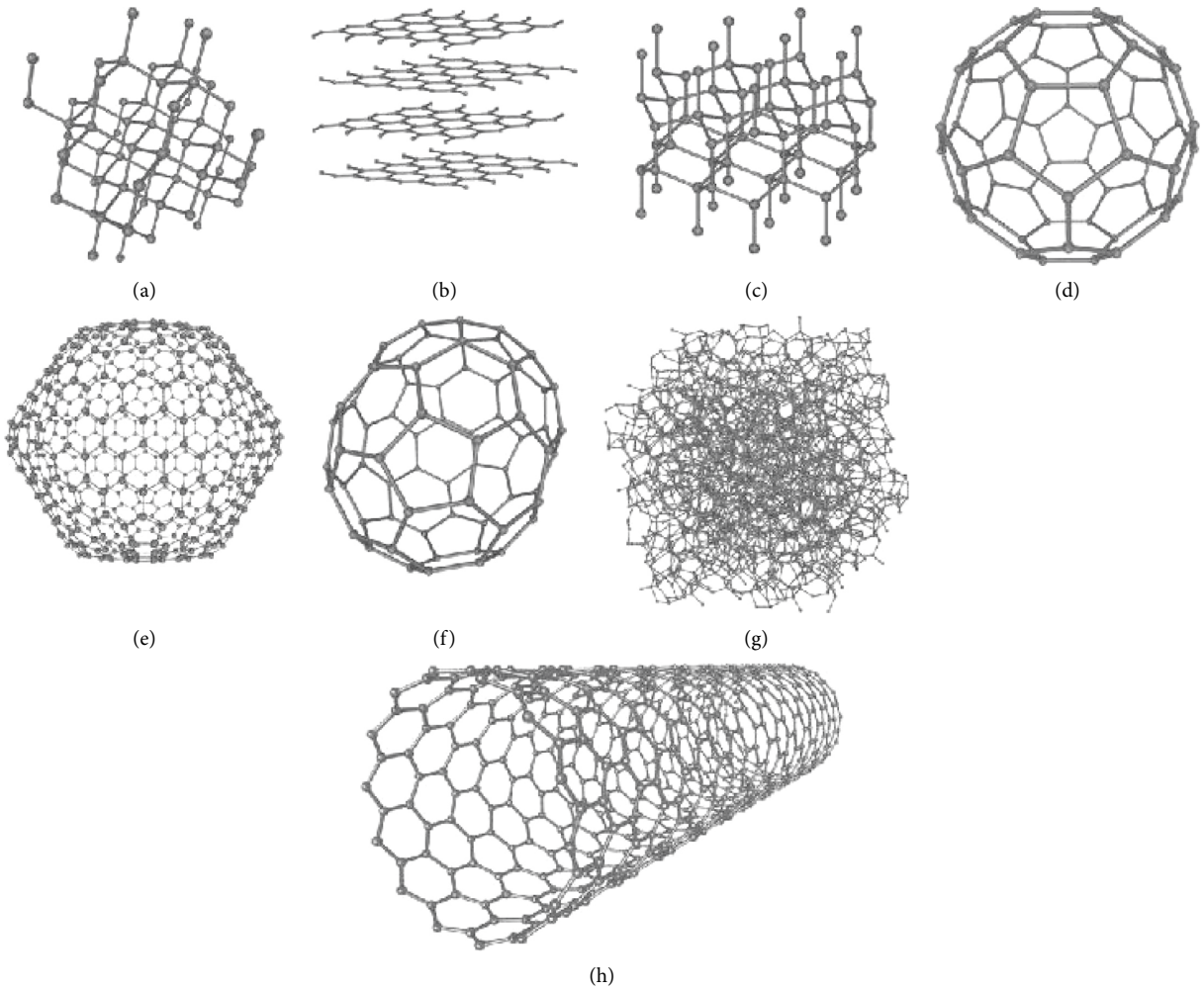

Figure 1: (a) Diamond. (b) Graphite. (c) Lonsdaleite. (d) C_{60}. (e) Fullerite. (f) C_{70}. (g) Amorphous carbon. (h) Carbon nanotube with single wall.

CBZIs are known as first CBZI and second CBZI, respectively.

Definition 3 (see [22, 27]). For a network G, the modified CBZIs can be given as

(1) $\mathfrak{Z}_1\mathbb{C}^*\widetilde{I}(G) = \sum_{ht\in\mathscr{T}(G)}(\tau_G(h) + \tau_G(t)) = \sum_{h\in\mathscr{H}(G)}(d_G(h)\ \tau_G(t))$,

(2) $\mathfrak{Z}_2\mathbb{C}^*\widetilde{I}(G) = \sum_{ht\in\mathscr{T}(G)}[d_G(h)\tau_G(t) + d_G(t)\tau_G(h)]$,

(3) $\mathfrak{Z}_3\mathbb{C}^*\widetilde{I}(G) = \sum_{ht\in\mathscr{T}(G)}[d_G(h)\tau_G(h) + d_G(t)\tau_G(t)]$.

These modified CBZIs are known as the modified first CBZI, modified second CBZI, and modified third CBZI, respectively.

Definition 4 (see [29]). For a network G, first CBMZI, second CBMZI, third CBMZI, and fourth CBMZI can be defined as

$$M\mathfrak{Z}_1\mathbb{C}\widetilde{I}(G) = \prod_{h\in\mathscr{H}(G)}(\tau_G(h))^2, \tag{1}$$

$$M\mathfrak{Z}_2\mathbb{C}\widetilde{I}(G) = \prod_{ht\in\mathscr{T}(G)}(\tau_G(h)\times\tau_G(t)), \tag{2}$$

$$M\mathfrak{Z}_3\mathbb{C}\widetilde{I}(G) = \prod_{h\in\mathscr{H}(G)}(d_G(h)\tau_G(h)), \tag{3}$$

$$M\mathfrak{Z}_4\mathbb{C}\widetilde{I}(G) = \prod_{ht\in\mathscr{T}(G)}(\tau_G(h) + \tau_G(t)). \tag{4}$$

Definition 5 (see [29]). For a network G, modified first CBMZI, modified second CBMZI, and modified third CBMZI can be defined as

$$M\mathfrak{Z}_1\mathscr{C}^*\tilde{I}(G) = \prod_{ht\in\mathscr{T}(G)} [d_G(h)\tau_G(t) + d_G(t)\tau_G(h)], \tag{5}$$

$$M\mathfrak{Z}_2\mathscr{C}^*\tilde{I}(G) = \prod_{ht\in\mathscr{T}(G)} [d_G(h)\tau_G(h) + d_G(t)\tau_G(t)], \tag{6}$$

$$M\mathfrak{Z}_3\mathscr{C}^*\tilde{I}(G) = \prod_{ht\in\mathscr{T}(G)} [d_G(h)\tau_G(h) \times d_G(t)\tau_G(t)]. \tag{7}$$

3. Connection-Based Multiplicative Zagreb Indices of Crystal Cubic Carbon Structure

The carbon's valency allows it to form a wide range of allotropes. Carbon is well recognized in the forms of graphite, bucky balls, diamond, etc. Graphite is the smooth, dark-colored substance found in lead of pencil. Diamonds, on the other hand, are extremely hard, typically clear, colorless, and extremely valuable jewels. Both of these structures are made up of carbon atom. In both of these structures, the carbon atom is piled differently and that is why both of these structures are very different to each other. Diamond is a tremendously strong substance made up of carbon atoms stacked densely together in a cubic crystal form. The strong bonds between the carbon atom make this structure very strong. There are many utilizations of these allotropes of carbon (for details, see [32]).

In this section, we deal with the computation of CBMZIs of this significant allotrope of carbon, namely, crystal cubic carbon structure ($CCC(j)$), where $j \geq 1$ is the level of the structure. Figure 2 depicts the molecular structure of rare stone cubic carbon structure $CCC(j)$ for the first level. For the next level, new 3D squares are linked at every terminal vertex of degree 3 of the previous first layer. Figure 3 depicts the second level of $CCC(j)$. Furthermore, the same technique is repeated to obtain the next level, and so on. Let $G = CCC(j)$ be a molecular network of $CCC(j)$ for $j \geq 2$. Molecular networks of $CCC(j)$ for $j = 2$ and $j = 3$ are shown in Figures 3 and 4, where we label the nodes (vertices) with their CNs. In Figures 5–7, we label the vertices with their degrees. The cardinality of vertices and edges in $CCC(j)$ is presented separately below.

$$\begin{aligned} |\mathscr{H}(CCC(j))| &= 8 + (8)^2 \sum_{k=2}^{j} \left(2^3 - 1\right)^{k-2}, \\ |\mathscr{T}(CCC(j))| &= 4\left[3 + 2\sum_{k=0}^{j-2} \left(2^3 - 1\right)^{k} + 24\left(2^3 - 1\right)^{j-2} + 24\sum_{k=3}^{j} \left(2^3 - 1\right)^{k-3}\right]. \end{aligned} \tag{8}$$

For our convenience, we divide the structure of G into three categories as given below.

(1) Basic cube: the cube which lies in the center of the molecular network of $CCC(j)$ is considered to be basic cube.

(2) Outer layer of cubes: the layer of cubes in which every cube has seven vertices with CN 6 is considered to be the outer layer of cubes.

(3) Central layer of cubes: the layer of cubes which is not the outer layer of cubes is said to be central layer of cube.

Theorem 1. *Consider a network $G = CCC(j)$ for $j \geq 2$. Then, the first CBMZI is equal to*

$$M\mathfrak{Z}_1\mathbb{C}\tilde{I}(G) = [36]^{8\left(2^3-1\right)^{j-1}} \times [81]^{8\left(2^3-1\right)^{j-2}} \times [144]^{\left(8+(8)^2\sum_{k=2}^{j}\left(2^3-1\right)^{k-2} - 8^2\left(2^3-1\right)^{j-2}\right)}. \tag{9}$$

Proof. In order to find the first CBMZI, we classify the collection of vertices based on their CNs into three classes. We have

$$\begin{aligned} \mathscr{H}_1 &= \{h \in \mathscr{H}\colon \tau_G(h) = 6\}, \\ \mathscr{H}_2 &= \{h \in \mathscr{H}\colon \tau_G(h) = 9\}, \\ \mathscr{H}_3 &= \{h \in \mathscr{H}\colon \tau_G(h) = 12\}. \end{aligned} \tag{10}$$

The cardinalities of $\mathscr{H}_1$, $\mathscr{H}_2$, and $\mathscr{H}_3$ are

$$\begin{aligned} |\mathscr{H}_1(G)| &= 8 \times \left(2^3 - 1\right)^{j-1}, \\ |\mathscr{H}_2(G)| &= 8 \times \left(2^3 - 1\right)^{j-2}, \\ |\mathscr{H}_3(G)| &= 8 + (8)^2 \sum_{k=2}^{j} \left(2^3 - 1\right)^{k-2} - 8^2\left(2^3 - 1\right)^{j-2}. \end{aligned} \tag{11}$$

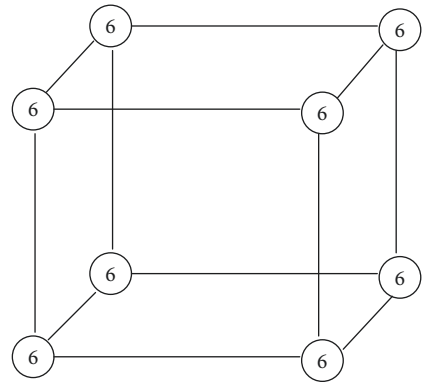

Figure 2: CCC(1) along with the labeling of CN 6 on the vertices of all the cubes.

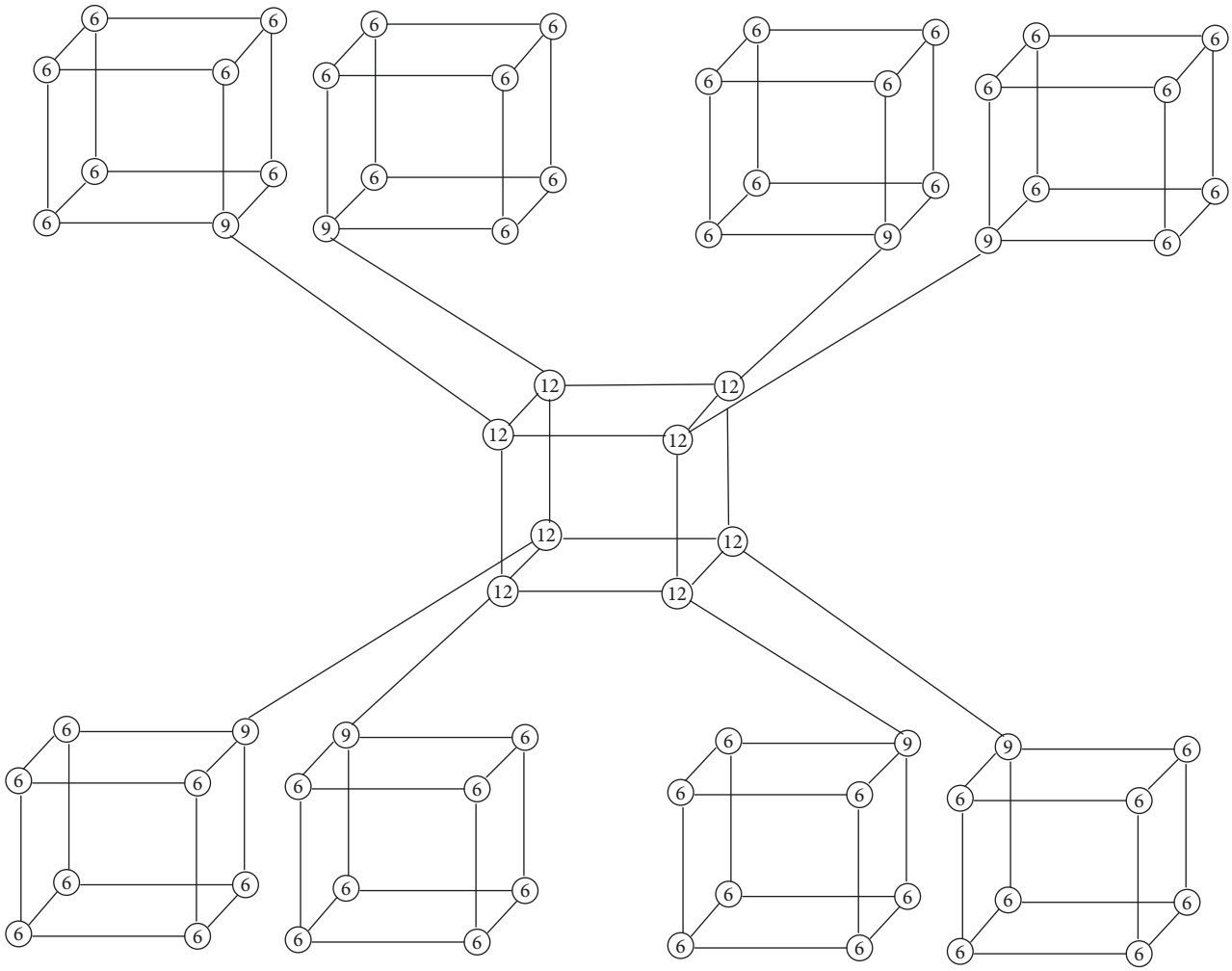

Figure 3: CCC(2) along with the labeling of CNs 6, 9, and 12 on the vertices of all the cubes.

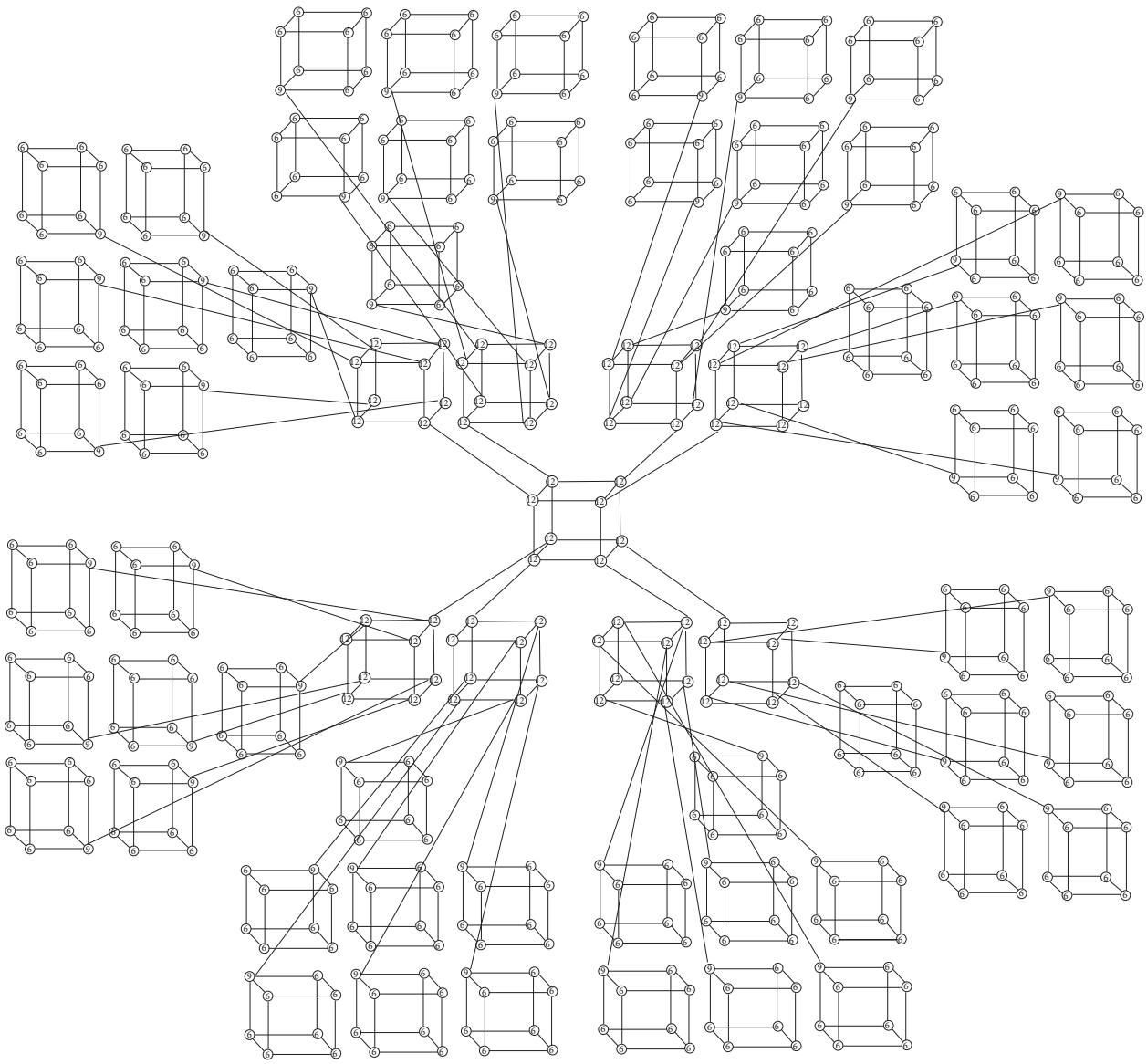

Figure 4: CCC(3) along with the labeling of CNs 6, 9, and 12 on the vertices of all the cubes.

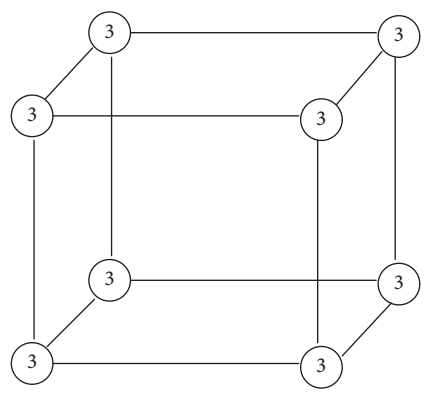

Figure 5: CCC(1) along with the labeling of degree 3 on the vertices of all the cubes.

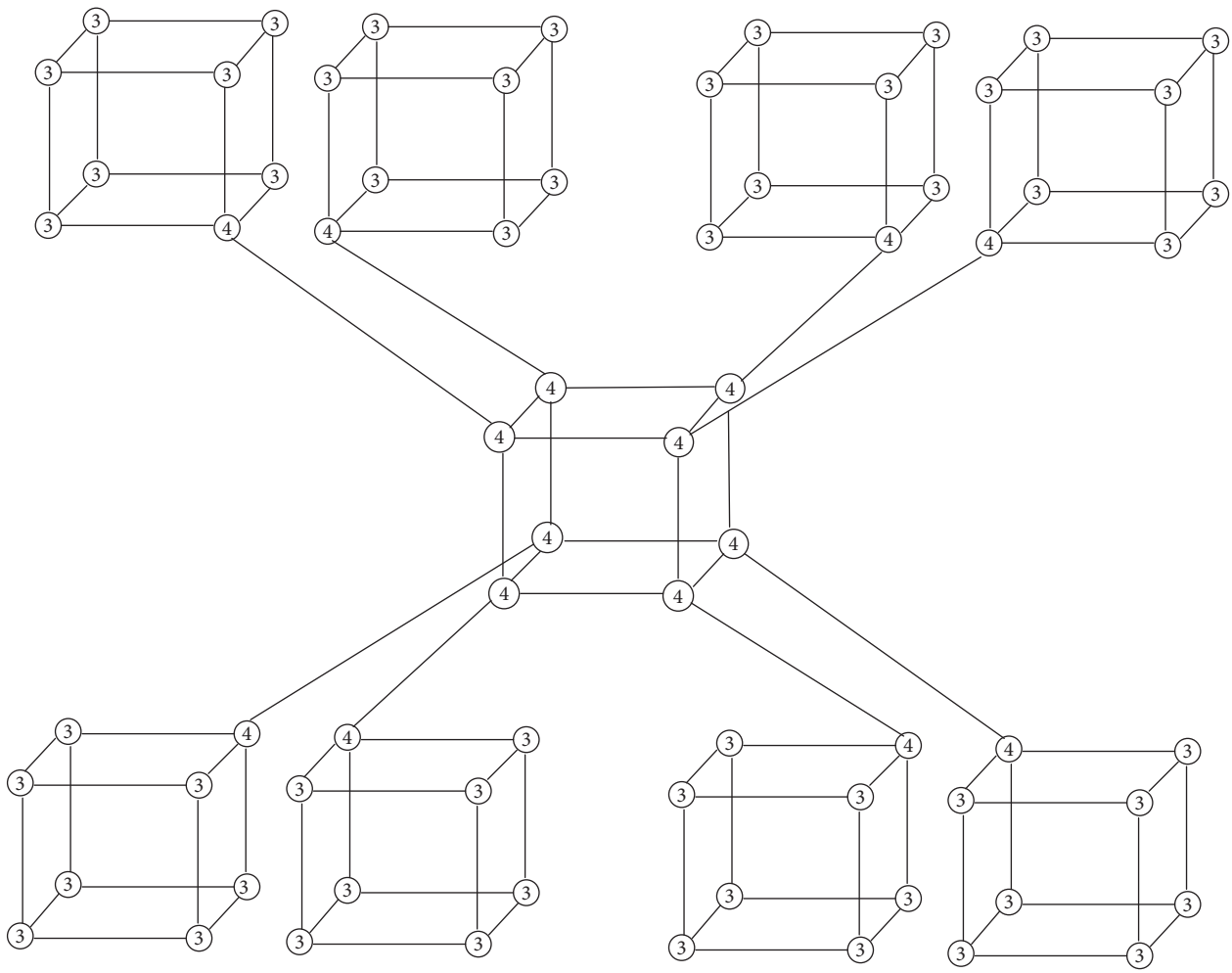

Figure 6: CCC(2) along with the labeling of degrees 3 and 4 on the vertices of all the cubes.

Now, by using equation (1), we get

$$
\begin{aligned}
M\mathfrak{Z}_1\mathbb{C}\tilde{I}(G) &= \prod_{h\in\mathscr{H}(G)} (\tau_G(h))^2, \\
&= \left[6^2\right]^{|\mathscr{H}_1(G)|} \times \left[9^2\right]^{|\mathscr{H}_2(G)|} \times \left[12^2\right]^{|\mathscr{H}_3(G)|}, \\
&= \left[6^2\right]^{\left(8\left(2^3-1\right)^{j-1}\right)} \times \left[9^2\right]^{\left(8\left(2^3-1\right)^{j-2}\right)} \\
&\quad \times \left[12^2\right]^{\left(8+(8)^2\sum_{k=2}^{j}\left(2^3-1\right)^{k-2}-8^2\left(2^3-1\right)^{j-2}\right)}, \\
&= [36]^{\left(8\left(2^3-1\right)^{j-1}\right)} \times [81]^{\left(8\left(2^3-1\right)^{j-2}\right)} \\
&\quad \times [144]^{\left(8+(8)^2\sum_{k=2}^{j}\left(2^3-1\right)^{k-2}-8^2\left(2^3-1\right)^{j-2}\right)}, \\
&= [36]^{8\left(2^3-1\right)^{j-1}} \times [81]^{8\left(2^3-1\right)^{j-2}} \times [144]^{\left(8+(8)^2\sum_{k=2}^{j}\left(2^3-1\right)^{k-2}-8^2\left(2^3-1\right)^{j-2}\right)}.
\end{aligned}
\tag{12}
$$

□

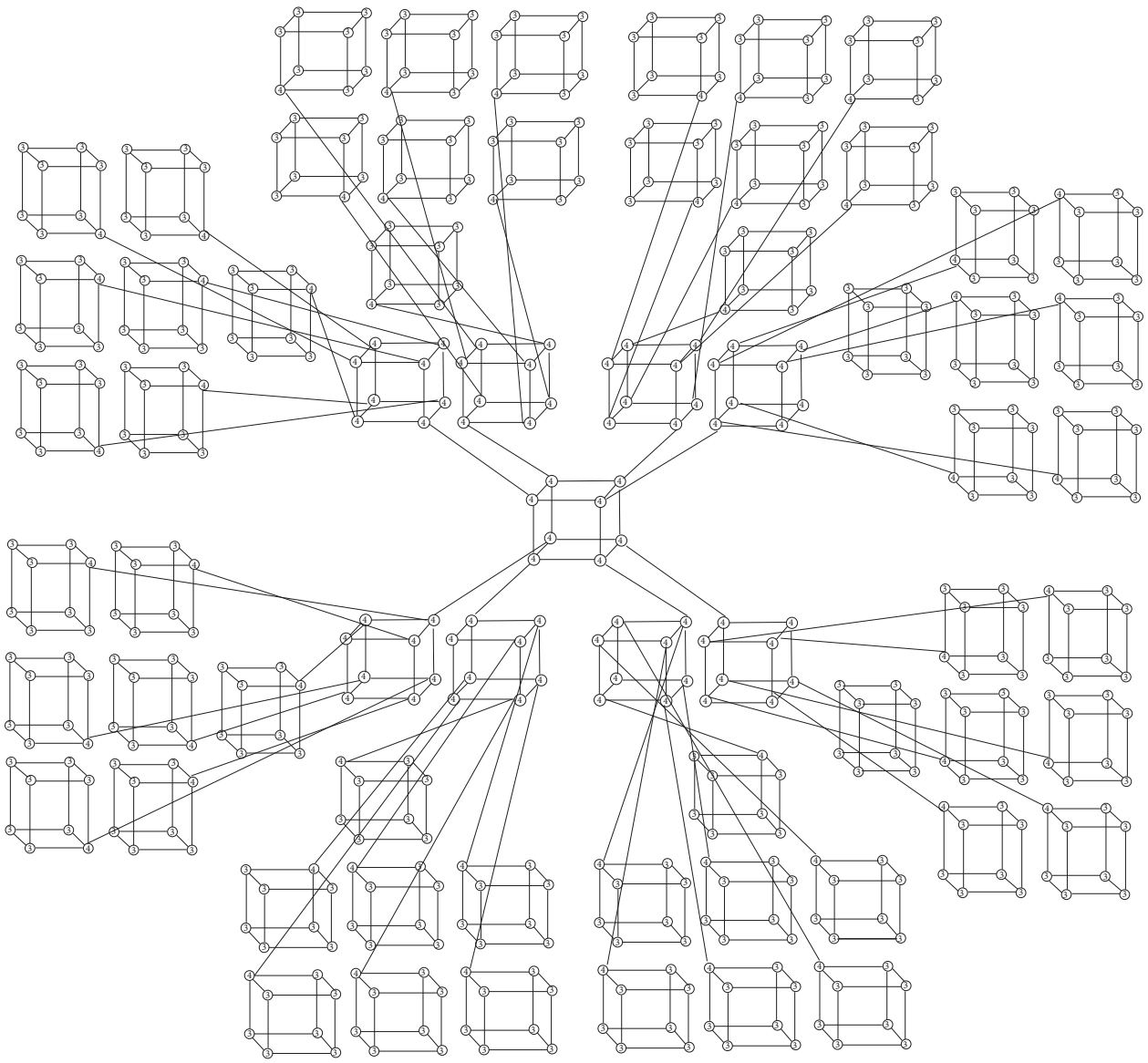

Figure 7: CCC(3) along with the labeling of degrees 3 and 4 on the vertices of all the cubes.

Theorem 2. *Consider a network $G = CCC(j)$ for $j \geq 2$. Then, the second CBMZI is equal to*

$$M\mathfrak{Z}_2\mathbb{C}\tilde{I}(G) = [36]^{72(2^3-1)^{j-2}} \times [54]^{24(2^3-1)^{j-2}} \times [108]^{\left(8\sum_{k=0}^{j-2}(2^3-1)^k\right)} \times [144]^{\left(12+96\sum_{k=3}^{j}(2^3-1)^{k-3}\right)}. \tag{13}$$

Proof. Firstly, we divide the edges into four classes with respect to their CNs. We have

$$\begin{aligned}
\mathscr{C}_1 &= \mathscr{T}_{(6,6)}(G) = \{ht \in \mathscr{T}\colon \tau_G(h) = 6, \tau_G(t) = 6\},\\
\mathscr{C}_2 &= \mathscr{T}_{(6,9)}(G) = \{ht \in \mathscr{T}\colon \tau_G(h) = 6, \tau_G(t) = 9\},\\
\mathscr{C}_3 &= \mathscr{T}_{(9,12)}(G) = \{ht \in \mathscr{T}\colon \tau_G(h) = 9, \tau_G(t) = 12\},\\
\mathscr{C}_4 &= \mathscr{T}_{(12,12)}(G) = \{ht \in \mathscr{T}\colon \tau_G(h) = 12, \tau_G(t) = 12\}.
\end{aligned} \tag{14}$$

To find second CBMZI, we find the cardinalities of above partitioned edges. For this, we first find the number of edges in basic cube, outer layer of the vertices, and central layer of the cubes. After some simple calculation, we have

$$\begin{aligned}&\text{total edges in basic cube} = 12,\\ &\text{total edges in outer layer} = 96\left(2^3-1\right)^{j-2},\\ &\text{total edges in central layer} = 96\sum_{k=3}^{j}\left(2^3-1\right)^{k-3}.\end{aligned} \tag{15}$$

The edges which are not the part of any cube are considered to be free edges. The total number of free edges is $8\sum_{k=0}^{j-2}(2^3-1)^k$. Now, we compute $|\mathscr{T}_{(6,6)}(G)|$. As from the network of G, we can observe that $(6,6)$–type edges only exist in the outer layer of the cubes. After some easy calculation, we get

$$|\mathscr{T}_{(6,6)}(G)| = 72\times\left(2^3-1\right)^{j-2}. \tag{16}$$

Now, we compute $|\mathscr{T}_{(6,9)}(G)|$. Similar to $(6,6)$–type edges, $(6,9)$–type edges also lie only in outer layer of the cubes. Thus, we have

$$\begin{aligned}|\mathscr{T}_{(6,9)}(G)| &= 96\left(2^3-1\right)^{j-2}-72\left(2^3-1\right)^{j-2},\\ &= 24\left(2^3-1\right)^{j-2}.\end{aligned} \tag{17}$$

Next, we find the number of edges with CNs $(9,12)$. We can see that only the free edges have CNs (9,12). The total number of free edges is $8\sum_{k=0}^{j-2}(2^3-1)^k$. Thus, we have

$$|\mathscr{T}_{(9,12)}(G)| = 8\sum_{k=0}^{j-2}\left(2^3-1\right)^k. \tag{18}$$

Lastly, we compute $|\mathscr{T}_{(12,12)}(G)|$. It can be easily observed from the network of G that basic cube and central layer of cubes contain all those edges which have CNs (12,12). Thus, the total number of $(12,12)$ edges must be the sum of edges of basic cube and the edges of central layer of the cubes. Hence, we have

$$|\mathscr{T}_{(12,12)}(G)| = 12+96\sum_{k=3}^{j}\left(2^3-1\right)^{k-3}. \tag{19}$$

Adding all types of edges gives the cardinality of edges of G. Now, by using equation (2), we have

$$\begin{aligned}M\mathfrak{Z}_2\mathbb{C}\tilde{I}(G) &= \prod_{ht\in\mathscr{T}(G)}\left(\tau_G(h)\times\tau_G(t)\right)\\ &= [6\times6]^{|\mathscr{T}_{(6,6)}(G)|}\times[6\times9]^{|\mathscr{T}_{(6,9)}(G)|}\times[9\times12]^{|\mathscr{T}_{(9,12)}(G)|}\times[12\times12]^{|\mathscr{T}_{(12,12)}(G)|}\\ &= [6\times6]^{\left(72\left(2^3-1\right)^{j-2}\right)}\times[6\times9]^{\left(24\left(2^3-1\right)\right)^{j-2}}\times[9\times12]^{\left(8\sum_{k=0}^{j-2}\left(2^3-1\right)^k\right)}\times[12\times12]^{\left(12+96\sum_{k=3}^{j}\left(2^3-1\right)^{k-3}\right)}\\ &= [36]^{72\left(2^3-1\right)^{j-2}}\times[54]^{24\left(2^3-1\right)^{j-2}}\times[108]^{\left(8\sum_{k=0}^{j-2}\left(2^3-1\right)^k\right)}\times[144]^{\left(12+96\sum_{k=3}^{j}\left(2^3-1\right)^{k-3}\right)}.\end{aligned} \tag{20}$$

□

Theorem 3. *Consider a network $G = CCC(j)$ for $j \geq 2$. Then, the third CBMZI is equal to*

$$M\mathfrak{Z}_3\mathbb{C}\tilde{I}(G) = [18]^{8\times\left(2^3-1\right)^{j-1}}\times[36]^{8\times\left(2^3-1\right)^{j-2}}\times[48]^{8+(8)^2\sum_{k=2}^{j}\left(2^3-1\right)^{k-2}-8^2\left(2^3-1\right)^{j-2}}. \tag{21}$$

Proof. Before computing third CBMZI, we make the classes of vertices on the bases of their degrees. We have only two classes of vertices on the basis of degrees of vertices.

$$\begin{aligned}\mathscr{H}_1^d(G) &= \{h\in\mathscr{H}\colon d_G(h)=3\},\\ \mathscr{H}_2^d(G) &= \{h\in\mathscr{H}\colon d_G(h)=4\}.\end{aligned} \tag{22}$$

Now, we make the partitions of vertices with respect to the degrees and CNs of the vertices. We have

$$\begin{aligned}\mathscr{H}_1'(G) &= \{h\in\mathscr{H}\colon d_G(h)=3,\tau_G(h)=3\},\\ \mathscr{H}_2'(G) &= \{h\in\mathscr{H}\colon d_G(h)=4,\tau_G(h)=9\},\\ \mathscr{H}_3'(G) &= \{h\in\mathscr{H}\colon d_G(h)=4,\tau_G(h)=12\}.\end{aligned} \tag{23}$$

The cardinalities of these vertices are given in the following:

$$\begin{aligned}
\left|\mathscr{H}_1'(G)\right| &= 8\times\left(2^3-1\right)^{j-1},\\
\left|\mathscr{H}_2'(G)\right| &= 8\times\left(2^3-1\right)^{j-2},\\
\left|\mathscr{H}_3'(G)\right| &= 8+(8)^2\sum_{k=2}^{j}\left(2^3-1\right)^{k-2}-8^2\left(2^3-1\right)^{j-2}.
\end{aligned} \tag{24}$$

By using equation (3), we get

$$\begin{aligned}
M\mathfrak{Z}_3\mathbb{C}\tilde{I}(G) &= \prod_{h\in\mathscr{H}(G)}\left(d_G(h)\tau_G(h)\right)\\
&= [3\times 6]^{\left|\mathscr{H}_1'(G)\right|}\times[4\times 9]^{\left|\mathscr{H}_2'(G)\right|}\times[4\times 12]^{\left|\mathscr{H}_3'(G)\right|}\\
&= [3\times 6]^{8\times\left(2^3-1\right)^{j-1}|}\times[4\times 9]^{8\times\left(2^3-1\right)^{j-2}|}\times[4\times 12]^{\left(8+(8)^2\sum_{k=2}^{j}\left(2^3-1\right)^{k-2}-8^2\left(2^3-1\right)^{j-2}\right)}\\
&= [18]^{8\times\left(2^3-1\right)^{j-1}}\times[36]^{8\times\left(2^3-1\right)^{j-2}}\times[48]^{\left(8+(8)^2\sum_{k=2}^{j}\left(2^3-1\right)^{k-2}-8^2\left(2^3-1\right)^{j-2}\right)}.
\end{aligned} \tag{25}$$

□

Theorem 4. *Consider a network $G = CCC(j)$ for $j \geq 2$. Then, the fourth CBMZI is equal to*

$$M\mathfrak{Z}_4\mathbb{C}\tilde{I}(G) = [12]^{72\left(2^3-1\right)^{j-2}}\times[15]^{24\left(2^3-1\right)^{j-2}}\times[21]^{\left(8\sum_{k=0}^{j-2}\left(2^3-1\right)^{k}\right)}\times[36]^{\left(12+96\sum_{k=3}^{j}\left(2^3-1\right)^{k-3}\right)}. \tag{26}$$

Proof. By placing the values of $\mathscr{T}_{(\tau_G(h),\tau_G(t))}$ in equation (4), we have

$$\begin{aligned}
M\mathfrak{Z}_4\mathbb{C}\tilde{I}(G) &= \prod_{ht\in\mathscr{T}(G)}\left(\tau_G(h)+\tau_G(t)\right), = [6+6]^{\left|\mathscr{T}_{(6,6)}(G)\right|}+[6+9]^{\left|\mathscr{T}_{(6,9)}(G)\right|}\times[9+12]^{\left|\mathscr{T}_{(9,12)}(G)\right|}\times[12+12]^{\left|\mathscr{T}_{(12,12)}(G)\right|}\\
&= [6+6]^{\left(72\left(2^3-1\right)^{j-2}\right)}\times[6+9]^{\left(24\left(2^3-1\right)\right)^{j-2}}\times[9+12]^{\left(8+\sum_{k=0}^{j-2}\left(2^3-1\right)^{k}\right)}\times[12+12]^{\left(12+96\sum_{k=3}^{j}\left(2^3-1\right)^{k-3}\right)}\\
&= [12]^{72\left(2^3-1\right)^{j-2}}\times[15]^{24\left(2^3-1\right)^{j-2}}\times[21]^{\left(8\sum_{k=0}^{j-2}\left(2^3-1\right)^{k}\right)}\times[36]^{\left(12+96\sum_{k=3}^{j}\left(2^3-1\right)^{k-3}\right)}.
\end{aligned} \tag{27}$$

□

Theorem 5. *Consider a network $G = CCC(j)$ for $j \geq 2$. Then, the modified first CBMZI is equal to*

$$M\mathfrak{Z}_1\mathbb{C}^*\tilde{I}(G) = [36]^{72\left(2^3-1\right)^{j-2}}\times[51]^{24\left(2^3-1\right)^{j-2}}\times[84]^{\left(8\sum_{k=0}^{j-2}\left(2^3-1\right)^{k}\right)}\times[96]^{\left(12+96\sum_{k=3}^{j}\left(2^3-1\right)^{k-3}\right)}. \tag{28}$$

Proof. Firstly, we divide the edges into three classes with respect to their degrees. We have

$$\begin{aligned}\mathscr{C}_1 &= \mathscr{T}^d_{(3,3)}(G) = \{ht \in \mathscr{M}:\ d_G(h) = 3,\ d_G(t) = 3\},\\ \mathscr{C}_2 &= \mathscr{T}^d_{(3,4)}(G) = \{ht \in \mathscr{M}:\ d_G(h) = 3,\ d_G(t) = 4\},\\ \mathscr{C}_3 &= \mathscr{T}^d_{(4,4)}(G) = \{ht \in \mathscr{M}:\ d_G(h) = 4,\ d_G(t) = 4\}.\end{aligned} \tag{29}$$

In order to calculate the modified first CBMZI, first we need to calculate the number of edges on the basis of their degrees of incident vertices. Initially, we calculate $|\mathscr{T}^d_{(3,3)}(G)|$. It can be observed that (3,3)-type edges only lie in the cubes of the outer layer. For simple calculations, we have

$$\left|\mathscr{T}^d_{(3,3)}(G)\right| = 72\left(2^3 - 1\right)^{j-2}. \tag{30}$$

Now, we compute $|\mathscr{T}^d_{(3,4)}(G)|$. Similar to (3,3)-type edges of G, (3,4)-type edges also exist only in the cubes of the outer layer of G. The number of $(3,4)-$type edges must be equal to the total number of edges in the cubes of outer layer minus the (3,3)-type edges present in the cubes of outer layer of G. Thus, we have

$$\begin{aligned}\left|\mathscr{T}^d_{(3,4)}(\text{ outer layer of the cubes})\right| &= 96\left(2^3 - 1\right)^{j-2},\\ \left|\mathscr{T}^d_{(3,3)}(\text{ outer layer of the cubes})\right| &= 72\left(2^3 - 1\right)^{j-2},\\ \left|\mathscr{T}^d_{(3,4)}(G)\right| &= 96\left(2^3 - 1\right)^{j-2} - 72\left(2^3 - 1\right)^{j-2},\\ &= 24\left(2^3 - 1\right)^{j-2}.\end{aligned} \tag{31}$$

Lastly, we compute $|\mathscr{T}^d_{(4,4)}(G)|$. One can see from the network of G that the basic cube and central layer of cubes have all those edges which have CNs (4,4). Also, all the free edges are (4,4)-type edges. Thus, the total number of $(4,4)-$type edges must be the sum of edges of basic cube and the edges of central layer of the cubes plus all the free edges. Hence, we have

$$\begin{aligned}\text{Total edges in basic cube} &= 12,\\ \text{Number of edges in central layer} &= 96\sum_{k=3}^{j}\left(2^3 - 1\right)^{k-3},\\ \text{Total free edges} &= 8\sum_{k=0}^{j-2}\left(2^3 - 1\right)^{k},\\ \left|\mathscr{T}^d_{(4,4)}(G)\right| &= 12 + 96\sum_{k=3}^{j}\left(2^3 - 1\right)^{k-3} + 8\sum_{k=0}^{j-2}\left(2^3 - 1\right)^{k}.\end{aligned} \tag{32}$$

To compute the modified first CBMZI, we split the classified number of edges on degree bases with respect to the number of edges on connection bases. The partitioning of degree-based edges with respect to connection-based edges is shown in Table 1.

To compute the modified first CBZI, we are not concerning with degrees or CNs of edges separately, instead we are dealing with both degrees and CNs of the edges . From Figures 4 and 7, we can see that there are total four such partitions of edges as given below.

$$\begin{aligned}\mathscr{T}_{(3,3)(6,6)}(G) &= \{ht \in \mathscr{T}:\ d_G(h) = 3, \tau_G(h) = 6, d_G(t) = 3, \tau_G(t) = 6\},\\ \mathscr{T}_{(3,4)(6,9)}(G) &= \{ht \in \mathscr{T}:\ d_G(h) = 3, \tau_G(h) = 6, d_G(h) = 4, \tau_G(t) = 9\},\\ \mathscr{T}_{(4,4)(9,12)}(G) &= \{ht \in \mathscr{T}:\ d_G(h) = 4, \tau_G(h) = 9, d_G(h) = 4, \tau_G(t) = 12\},\\ \mathscr{T}_{(4,4)(12,12)}(G) &= \{ht \in \mathscr{T}:\ d_G(h) = 4, \tau_G(h) = 12, d_G(h) = 4, \tau_G(t) = 12\}.\end{aligned} \tag{33}$$

Table 1: Partitioning of degree-based edges with respect to connection-based edges.

$\lvert\mathcal{T}^{d}_{(d_G(h),d_G(t))}(G)\rvert$ (degree based)	$\lvert\mathcal{T}_{(\tau_G(h),\tau_G(t))}(G)\rvert$ (connection based)
$\lvert\mathcal{T}^{d}_{(3,3)}(G)\rvert = 72(2^3-1)^{j-2}$	$\lvert\mathcal{T}_{(6,6)}(G)\rvert = 72(2^3-1)^{j-2}$
$\lvert\mathcal{T}^{d}_{(3,4)}(G)\rvert = 24(2^3-1)^{j-2}$	$\lvert\mathcal{T}_{(6,9)}(G)\rvert = 24(2^3-1)^{j-2}$
$\lvert\mathcal{T}^{d}_{(4,4)}(G)\rvert = 8\sum_{k=0}^{j-2}(2^3-1)^{k}$	$\lvert\mathcal{T}_{(9,12)}(G)\rvert = 8\sum_{k=0}^{j-2}(2^3-1)^{k}$
$\lvert\mathcal{T}^{d}_{(4,4)}(G)\rvert = 12 + 96\sum_{k=3}^{j}(2^3-1)^{k-3}$	$\lvert\mathcal{T}_{(12,12)}(G)\rvert = 12 + 96\sum_{k=3}^{j}(2^3-1)^{k-3}$

Table 2: Cardinalities of partitioned edges on degree and connection bases.

$\mathcal{T}_{(d(h),d(t))(\tau(h),\tau(t))}(G)$	$\lvert\mathcal{T}_{(d(h),d(t))(\tau(h),\tau(t))}(G)\rvert$
$\lvert\mathcal{T}_{(3,3)(6,6)}(G)\rvert$	$72(2^3-1)^{j-2}$
$\lvert\mathcal{T}_{(3,4)(6,9)}(G)\rvert$	$24(2^3-1)^{j-2}$
$\lvert\mathcal{T}_{(4,4)(9,12)}(G)\rvert$	$8\sum_{k=0}^{j-2}(2^3-1)^{k}$
$\lvert\mathcal{T}_{(4,4)(12,12)}(G)\rvert$	$12 + 96\sum_{k=3}^{j}(2^3-1)^{k-3}$

By using Table 1, the cardinalities of these partitioned vertices are displayed in Table 2.

By using equation (5), we get

$$\begin{aligned}
M\mathfrak{Z}_1\mathbb{C}^{*}\tilde{I}(G) &= \prod_{ht\in\mathcal{T}(G)}\left[d_G(h)\tau_G(t)+d_G(t)\tau_G(h)\right]\left[(4)(12)+(4)(9)\right]^{\lvert\mathcal{T}_{(4,4)(9,12)}(G)\rvert}\times\left[(4)(12)+(4)(12)\right]^{\lvert\mathcal{T}_{(4,4)(12,12)}(G)\rvert}\\
&= \left[(3)(6)+(3)(6)\right]^{72(2^3-1)^{j-2}}\times\left[(3)(9)+(4)(6)\right]^{24(2^3-1)^{j-2}}+\left[(4)(12)+(4)(9)\right]^{\left(8\sum_{k=0}^{j-2}(2^3-1)^{k}\right)}\\
&\quad\times\left[(4)(12)+(4)(12)\right]^{\left(12+96\sum_{k=3}^{j}(2^3-1)^{k-3}\right)}\\
&= \left[(3)(6)+(3)(6)\right]^{\lvert\mathcal{T}_{(3,3)(6,6)}(G)\rvert}\times\left[(3)(9)+(4)(6)\right]^{\lvert\mathcal{T}_{(3,4)(6,9)}(G)\rvert}+\\
&= \left[18+18\right]^{72(2^3-1)^{j-2}}\times\left[27+24\right]^{24(2^3-1)^{j-2}}+\left[48+36\right]^{\left(8\sum_{k=0}^{j-2}(2^3-1)^{k}\right)}\times\left[48+48\right]^{\left(12+96\sum_{k=3}^{j}(2^3-1)^{k-3}\right)}\\
&= \left[36\right]^{72(2^3-1)^{j-2}}\times\left[51\right]^{24(2^3-1)^{j-2}}\times\left[84\right]^{\left(8\sum_{k=0}^{j-2}(2^3-1)^{k}\right)}\times\left[96\right]^{\left(12+96\sum_{k=3}^{j}(2^3-1)^{k-3}\right)}.
\end{aligned}\tag{34}$$

□

Theorem 6. *Consider a network $G = CCC(j)$ for $j \geq 2$. Then, the modified second CBMZI is*

$$M\mathfrak{Z}_2\mathbb{C}^{*}\tilde{I}(G) = \left[36\right]^{\left(72(2^3-1)^{j-2}\right)}\times\left[54\right]^{\left(24(2^3-1)^{j-2}\right)}\times\left[84\right]^{\left(8\sum_{k=0}^{j-2}(2^3-1)^{k}\right)}\times\left[96\right]^{\left(12+96\sum_{k=3}^{j}(2^3-1)^{k-3}\right)}.\tag{35}$$

Proof. By using equation (6), we get

$$\begin{aligned}
M\mathfrak{Z}_2\mathbb{C}^{*}\tilde{I}(G) &= \prod_{ht\in\mathcal{T}(G)}\left[d_G(h)\tau_G(h)+d_G(t)\tau_G(t)\right]\\
&= \left[(3)(6)+(3)(6)\right]^{\lvert\mathcal{T}_{(3,3)(6,6)}(G)\rvert}\times\left[(3)(6)+(4)(9)\right]^{\lvert\mathcal{T}_{(3,4)(6,9)}(G)\rvert}\times\left[(4)(9)+(4)(12)\right]^{\lvert\mathcal{T}_{(4,4)(9,12)}(G)\rvert}\times\left[(4)(12)+(4)(12)\right]^{\lvert\mathcal{T}_{(4,4)(12,12)}(G)\rvert}\\
&= \left[(3)(6)+(3)(6)\right]^{\left(72(2^3-1)^{j-2}\right)}\times\left[(3)(6)+(4)(9)\right]^{\left(24(2^3-1)^{j-2}\right)}\times\left[(4)(9)+(4)(12)\right]^{\left(8\sum_{k=0}^{j-2}(2^3-1)^{k}\right)}\\
&\quad\times\left[(4)(12)+(4)(12)\right]^{\left(12+96\sum_{k=3}^{j}(2^3-1)^{k-3}\right)}\\
&= \left[18+18\right]^{\left(72(2^3-1)^{j-2}\right)}\times\left[18+36\right]^{\left(24(2^3-1)^{j-2}\right)}\times\left[36+48\right]^{\left(8\sum_{k=0}^{j-2}(2^3-1)^{k}\right)}\times\left[48+48\right]^{\left(12+96\sum_{k=3}^{j}(2^3-1)^{k-3}\right)}\\
&= \left[36\right]^{\left(72(2^3-1)^{j-2}\right)}\times\left[54\right]^{\left(24(2^3-1)^{j-2}\right)}\times\left[84\right]^{\left(8\sum_{k=0}^{j-2}(2^3-1)^{k}\right)}\times\left[96\right]^{\left(12+96\sum_{k=3}^{j}(2^3-1)^{k-3}\right)}.
\end{aligned}\tag{36}$$

□

Theorem 7. *Consider a network $G = CCC(j)$ for $j \geq 2$. Then, the modified third CBMZI is equal to*

$$M\mathfrak{Z}_3\mathbb{C}^*\tilde{I}(G) = [324]^{\left(72(2^3-1)^{j-2}\right)} \times [648]^{\left(24(2^3-1)^{j-2}\right)} \times [1728]^{\left(8\sum_{k=0}^{j-2}(2^3-1)^k\right)} \times [2304]^{\left(12+96\sum_{k=3}^{j}(2^3-1)^{k-3}\right)}. \tag{37}$$

Proof. By using equation (7), we get

$$\begin{aligned}
M\mathfrak{Z}_3\mathbb{C}^*\tilde{I}(G) &= \prod_{ht\in\mathcal{T}(G)} [d_G(h)\tau_G(h) \times d_G(t)\tau_G(t)] \\
&= [(3)(6)\times(3)(6)]^{|\mathcal{T}_{(3,3)(6,6)}(G)|} \times [(3)(6)\times(4)(9)]^{|\mathcal{T}_{(3,4)(6,9)}(G)|} \times [(4)(9)\times(4)(12)]^{|\mathcal{T}_{(4,4)(9,12)}(G)|} \\
&\quad \times [(4)(12)\times(4)(12)]^{|\mathcal{T}_{(4,4)(12,12)}(G)|} \\
&= [(3)(6)\times(3)(6)]^{\left(72(2^3-1)^{j-2}\right)} \times [(3)(6)\times(4)(9)]^{\left(24(2^3-1)^{j-2}\right)} \times [(4)(9)\times(4)(12)]^{\left(8\sum_{k=0}^{j-2}(2^3-1)^k\right)} \\
&\quad \times [(4)(12)\times(4)(12)]^{\left(12+96\sum_{k=3}^{j}(2^3-1)^{k-3}\right)} \\
&= [18\times18]^{\left(72(2^3-1)^{j-2}\right)} \times [18\times36]^{\left(24(2^3-1)^{j-2}\right)} \times [36\times48]^{\left(8\sum_{k=0}^{j-2}(2^3-1)^k\right)} \times [48\times48]^{\left(12+96\sum_{k=3}^{j}(2^3-1)^{k-3}\right)} \\
&= [324]^{\left(72(2^3-1)^{j-2}\right)} \times [648]^{\left(24(2^3-1)^{j-2}\right)} \times [1728]^{\left(8\sum_{k=0}^{j-2}(2^3-1)^k\right)} \times [2304]^{\left(12+96\sum_{k=3}^{j}(2^3-1)^{k-3}\right)}.
\end{aligned} \tag{38}$$

□

4. Conclusion

In this study, we have found the general expressions to compute the TIs of the allotrope of carbon, namely, crystal structure of carbon. TIs help the researchers for the examination and manipulation of chemical structural information. Here, we have calculated various TIs, named as first CBMZI and second CBMZI. We have also computed modified first CBMZI, modified second CBMZI, and modified third CBMZI. This computational study will make it easier for the researchers to understand the selected structure and will encourage others to concentrate on the organic networks. The mathematical method considered here is efficient to examine the physical and chemical properties of the considered network.

Future Directions. In future, we are interested in computing the connection-based Zagreb indices for other types of chemical structures.

Data Availability

The data used to support the findings of this study are included within this article. However, the reader may contact the corresponding author for more details on the data.

Conflicts of Interest

The authors declare that they have no conflicts of interest.

References

[1] A. Q. Baig, M. Imran, and H. Ali, "On topological indices of poly oxide, poly silicate, DOX, and DSL networks," *Canadian Journal of Chemistry*, vol. 93, no. 7, pp. 730–739, 2015.

[2] M. Bača, J. Horváthová, M. Mokrišová, A. Semaničová-Feňovčíková, and A. Suhányiová, "On topological indices of a carbon nanotube network," *Canadian Journal of Chemistry*, vol. 93, no. 10, pp. 1157–1160, 2015.

[3] M. V. Diudea and G. Katona, "Molecular topology of dendrimers," *ChemInform*, vol. 30, no. 50, 1999.

[4] J. Asadpour and L. Safikhani, "A study of CNC_7[n] carbon nanocone by M-eccentric connectivity polynomial," *Australian Journal of Basic and Applied Sciences*, vol. 7, no. 7, pp. 883–887, 2013.

[5] N. De, S. M. A. Nayeem, and A. Pal, "On eccentric connectivity index and polynomial of thorn graph," *Applied Mathematics*, vol. 03, no. 08, pp. 931–934, 2012.

[6] Y. Huo, J.-B. Liu, A. Q. Baig, W. Sajjad, and M. R. Farahani, "Connective eccentric index of NAnm nanotube," *Journal of Computational and Theoretical Nanoscience*, vol. 14, no. 4, pp. 1832–1836, 2017.

[7] H. Wiener, "Structural determination of paraffin boiling points," *Journal of the American Chemical Society*, vol. 69, no. 1, pp. 17–20, 1947.

[8] I. Gutman, "Degree-based topological indices," *Croatica Chemica Acta*, vol. 86, no. 4, pp. 351–361, 2013.

[9] M. Hu, H. Ali, M. A. Binyamin, B. Ali, J.-B. Liu, and C. Fan, "On distance-based topological descriptors of chemical interconnection networks," *Journal of Mathematics*, vol. 2021, pp. 1–10, 2021.

[10] K. Xu, M. Liu, K. C. Das, I. Gutman, and B. Furtula, "A survey on graphs extremal with respect to distance-based topological indices," *MATCH Communications in Mathematical and in Computer Chemistry*, vol. 71, no. 3, pp. 461–508, 2014.

[11] I. Gutman and N. Trinajstić, "Graph theory and molecular orbitals. Total φ-electron energy of alternant hydrocarbons," *Chemical Physics Letters*, vol. 17, no. 4, pp. 535–538, 1972.
[12] I. Gutman, B. Ruscic, N. Trinajstic, and C. F. Wilcox, "Graph theory and molecular orbitals. XII. Acyclic polyenes," *The Journal of Chemical Physics*, vol. 62, no. 9, p. 3399, 1975.
[13] B. Furtula and I. Gutman, "A forgotten topological index," *Journal of Mathematical Chemistry*, vol. 53, no. 4, pp. 1184–1190, 2015.
[14] S. Nikolic, G. Kovacevic, A. Milicevic, and N. Trinajstic, "The Zagreb indices 30 years after," *Croatica Chemica Acta*, vol. 76, no. 2, pp. 113–124, 2003.
[15] H. Yang, M. Siddiqui, M. Arshad, and M. Naeem, "Degree-distance based topological indices of crystal cubic carbon structure," *Atoms*, vol. 6, no. 4, p. 62, 2018.
[16] W. Gao, M. Siddiqui, M. Naeem, and N. Rehman, "Topological characterization of carbon graphite and crystal cubic carbon structures," *Molecules*, vol. 22, no. 9, p. 1496, 2017.
[17] M. A. Zahid, M. Naeem, A. Q. Baig, and W. Gao, "General fifth M-Zagreb indices and fifth M-Zagreb polynomials of crystal cubic carbon," *Utilitas Mathematica*, vol. 109, pp. 263–270, 2018.
[18] X. Zhang and M. Naeem, "Metric dimension of crystal cubic carbon structure," *Journal of Mathematics*, vol. 2021, pp. 1–8, Article ID 3438611, 2021.
[19] H. Yang, M. Naeem, A. Q. Baig, H. Shaker, and M. K. Siddiqui, "Vertex Szeged index of crystal cubic carbon structure," *Journal of Discrete Mathematical Sciences and Cryptography*, vol. 22, no. 7, pp. 1177–1187, 2019.
[20] M. Arockiaraj, J. Clement, D. Paul, and K. Balasubramanian, "Relativistic distance-based topological descriptors of Linde type A zeolites and their doped structures with very heavy elements," *Molecular Physics*, vol. 119, no. 3, Article ID e1798529, 2021.
[21] J. Abraham, M. Arockiaraj, J. Jency, S. R. J. Kavitha, and K. Balasubramanian, "Graph entropies, enumeration of circuits, walks and topological properties of three classes of isoreticular metal organic frameworks," *Journal of Mathematical Chemistry*, vol. 60, no. 4, pp. 695–732, 2022.
[22] A. Ali and N. Trinajstić, "A novel/old modification of the first Zagreb index," *Molecular informatics*, vol. 37, no. 6-7, Article ID 1800008, 2018.
[23] J. Cao, U. Ali, M. Javaid, and C. Huang, "Zagreb connection indices of molecular graphs based on operations," *Complexity*, vol. 2020, Article ID 7385682, 2020.
[24] A. Sattar, M. Javaid, and E. Bonyah, "Connection-based multiplicative Zagreb indices of dendrimer nanostars," *Journal of Mathematics*, vol. 2021, pp. 1–14, Article ID 2107623, 2021.
[25] A. Sattar, M. Javaid, and M. N. Alam, "On the studies of dendrimers via connection-based molecular descriptors," *Mathematical Problems in Engineering*, vol. 2022, no. 2022, pp. 1–13, Article ID 1053484, 2022.
[26] A. Sattar, M. Javaid, and E. Bonyah, "Computing connection-based topological indices of dendrimers," *Journal of Chemistry*, vol. 2022, no. 2022, pp. 1–15, Article ID 7204641, 2022.
[27] U. Ali, M. Javaid, and A. Kashif, "Modified Zagreb connection indices of the T-sum graphs," *Main Group Metal Chemistry*, vol. 43, no. 1, pp. 43–55, 2020.
[28] R. S. Haoer, M. A. Mohammed, T. Selvarasan, N. Chidambaram, and N. Devadoss, "Multiplicative leap Zagreb indices of T-thorny graphs," *Eurasian Chemical Communications*, vol. 2, no. 8, pp. 841–846, 2020.
[29] M. Javaid, M. K. Siddiqui, and U. Ali, "Novel connection based Zagreb indices of several wheel-related graphs," *Computational Journal of Combinatorial Mathematics*, vol. 2, pp. 31–58, 2021.
[30] Z. Du, A. Ali, and N. Trinajstić, "Alkanes with the first three maximal/minimal modified first Zagreb connection indices," *Molecular informatics*, vol. 38, no. 4, Article ID 1800116, 2019.
[31] H. Yang, M. Kamran Siddiqui, M. Naeem, and N. Abdul Rehman, "Molecular properties of carbon crystal cubic structures," *Open Chemistry*, vol. 18, no. 1, pp. 339–346, 2020.
[32] H. O. Pierson, *Handbook of Carbon, Graphite, Diamonds and Fullerenes: Processing, Properties and Applications*, Nayos Publications, Mill Road, Park Ridge, NJ, USA, 2012.

Hindawi
Complexity
Volume 2022, Article ID 6673618, 11 pages
https://doi.org/10.1155/2022/6673618

WILEY | Hindawi

Research Article

Potential Effects of Delay on the Stability of a Class of Impulsive Neural Networks

Nan Zhan[1] **and Ailong Wu**[1,2]

[1]*College of Mathematics and Statistics, Hubei Normal University, Huangshi 435002, China*
[2]*Institute for Information and System Science, Xi'an Jiaotong University, Xi'an 710049, China*

Correspondence should be addressed to Ailong Wu; hbnuwu@yeah.net

Received 16 March 2022; Accepted 7 June 2022; Published 15 July 2022

Academic Editor: Miaomiao Wang

Aiming at the interference of the delay term in continuous dynamics to the impulsive systems, we study the potential effects of time delay on the stability of a class of impulsive neural networks (INNs) in this paper. Two cases of delay are considered. For the case of small delay, a sufficient condition for the stability of delayed INNs is obtained by virtue of the average impulsive interval (AII) method. The derived results illustrate that within limits, the convergence rate of the system becomes larger with the increase of time delay. For another case, a strict comparison principle is proposed to prove that the impulsive system still maintains the original stability for any large but bounded delay under certain conditions. In particular, as an extension, the stability of delayed INNs for hybrid impulses containing both stabilizing and destabilizing impulses is also discussed. Finally, three examples are simulated to demonstrate the validity of the theoretical results.

1. Introduction

As a mathematical model of information processing, neural network (NN) is one of the most active branches of computational intelligence and machine learning. There are many kinds of NNs, and as a special kind of NNs, impulsive neural networks (INNs) have unique research value. INN was first proposed by Alan Lloyd Hodgkin and Andrew Huxley in 1952. The simulation of its neurons is closer to reality because it characterizes the transient state mutation of neurons in neural networks at a certain moment. The impulsive system is a mixture of continuous dynamic system and discrete-time system, which is different from the pure continuous-time dynamic system and pure discrete-time system. It is suitable for studying a class of dynamic systems affected by sudden change or instantaneous disturbance [1]. Furthermore, impulsive phenomena exist in various fields such as secure communication, automatic control, and mechanical system. With the help of impulsive control, we can reduce a lot of application costs. So far, many interesting results have been obtained on INNs (see [2, 3] and their references).

Time delay is known to exist in many complex networks and control systems due to the influence of some practical situations. Over the past decades, time-delay systems have been vigorously studied because of their wide applications in NNs, sampling data control, biological modeling, and other fields. Meanwhile, various types of delays are discussed in NNs, such as distributed delay [4], time-varying delay [5], and state-dependent delay [6]. However, in previous studies, time delay is generally considered to be an important source of poor system performance and system instability. Few researchers have noticed that time delay may be beneficial to system stability. This is because our impression of time delay is so rigid that we ignore the stabilizing effects of time delay. Actually, we can also extract the stabilizing information of time delay through some analysis methods. For instance, in [7], the authors make a point that the increase of time delay has a dual effect on the stability of the system, that is, it may stabilize a previously unstable system or destabilize a previously stable system.

Combining the two points of time delay and impulsive effects, many scholars have done a lot of work on INNs with

delay [8–12]. For example, in [8], Chen et al. utilized an auxiliary state variable to transform the impulsive delayed system into an equivalent augmented model. On the basis of this model, the stability criterion of the system was derived. In [9], Zhang et al. firstly designed an impulsive controller for the time-delay discrete system to guarantee that the system can achieve stability. In [11], Jiang et al. investigated the impacts of time delay in impulses on system stability through average impulsive delay and average impulsive interval (AII) methods. In [12], Li and Song focused on the stabilization of time-delay systems under impulsive control, and the results show that the delay term in impulses may be conducive to the stabilization of the system. Obviously, studying a system with both time delay and impulsive effects is challenging because we need to consider the interaction of the two on the system.

Furthermore, it can be observed that both references [11, 12] have investigated the impacts of the delay term in impulses on stability of the system, but few papers have studied the latent effects of the delay term in continuous dynamics on stability of the impulsive system. Knowing that an impulsive system is a combination of continuous and discrete subsystems, it is interesting to think about the overall effects of the delay term in the continuous subsystem and the impulsive effect in the discrete subsystem on the system stability. In addition, looking back at the fact that time delays may facilitate the stability of systems, a natural problem emerges: under what conditions does the delay term in continuous dynamics play a positive role in the stability of systems?

In view of the above discussion, this paper mainly studies the potential effects of delay term in continuous dynamics on the stability of a class of INNs. Compared with some existing results, this paper fully captures the information that time delay can enhance stability. With regard to small delay and large delay, the stability of INNs with delay is investigated by using AII condition, and the hidden role that delay plays in the stability of system is revealed. With regard to hybrid impulses, the AII condition is replaced by the dwell-time condition so as to deal with the impulsive parameters as a whole, and the stability criterion of INNs is also derived. On the whole, the main features of this paper can be generalized as follows:

(1) The time delay in two cases is considered. When the delay is small, we capture the stabilizing information of time delay by means of the impulsive delay inequality and then integrate it into the Lyapunov-based function. Finally, with the help of the AII condition, the stability criterion of a kind of general INNs is derived. The results show that in a certain range, the system converges more quickly when the delay value is larger.

(2) In order to handle the case of large delay, we adopt a strict comparison principle which is different from the comparison-like principle, and it is proved that these kinds of INNs are robust to any large but bounded delay.

(3) Considering the dual effects of impulses, we extend the ideas of the first two points to the hybrid INNs containing stabilizing and destabilizing impulses.

This paper is organized as follows. In Section 2, a kind of general INNs with delay is introduced, and some requisite definitions and assumptions are presented. In Section 3, the main theorem results of this paper are derived, which fully illustrate the latent effects of delay term in continuous dynamics on stability of a kind of INNs. In Section 4, three numerical examples are simulated to indicate the validity of the derived results. Finally, Sections 5 gives a brief conclusion and prospects of the feasibility of the future research.

2. Preliminaries

2.1. Notations. Let $\mathbb{R}$, $\mathbb{R}_+$, and $\mathbb{R}^n$ stand for the set of real numbers, the set of nonnegative real numbers, and the set of n−dimensional real-valued vectors, respectively. Denote $\mathbb{Z}_+$ and $\mathbb{Z}_+^0$ as the set of positive integer numbers and nonnegative integer numbers, respectively. For vector $x = (x_1, x_2, \ldots, x_n)^T \in \mathbb{R}^n$, let $\|x\| = \sum_{i=1}^n |x_i|$. Denote $PC([-\tau, 0], \mathbb{R}^n)$ as the set of piecewise right continuous function ϕ: $[-\tau, 0] \longrightarrow \mathbb{R}^n$, where $\|\phi\|_\tau \triangleq \sup_{-\tau\le\theta\le 0}\|\phi(\theta)\|$. Denote the upper right-hand Dini derivative of function V as $D^+V(t) = \lim_{h\longrightarrow 0^+} \sup V(t+h) - V(t)/h$.

2.2. Model. In this paper, based on relevant work in reference [13], we consider a class of INNs, the main form of which is as follows:

$$\left\{\begin{array}{c} \dot{x}_i(t) = -a_i x_i(t) + \sum_{j=1}^n b_{ij} f_j\left(x_j(t)\right) + \sum_{j=1}^n c_{ij} g_j\left(x_j(t-\tau)\right), t \ne t_k, t \ge t_0 \ge 0, \\ \Delta x_i(t_k) = U\left(k, x_i(t_k^-)\right), k \in \mathbb{Z}_+, \\ x_i(t_0 + \theta) = \phi_i(\theta), \theta \in [-\tau, 0], \end{array}\right\} \tag{1}$$

where $a_i > 0, i = 1, 2, \ldots, n$ are constants, n is the number of neurons, $x_i(t)$ represents the state variable of the ith neuron at time t, $\dot{x}_i(t)$ represents the derivative of $x_i(t)$, τ is the transmission delay, $f_j(x_j(t))$ and $g_j(x_j(t-\tau))$ are the neuron activation functions at time t and $t-\tau$, respectively, b_{ij} and c_{ij} are real constants representing the connection weight, $\{t_k\}$ is the impulse sequence satisfying $0 \le t_0 < t_1 < \cdots < t_k < \cdots$ and $\lim_{k\longrightarrow+\infty} t_k = +\infty$, and

$\Delta x_i(t_k) \triangleq x_i(t_k^+) - x_i(t_k^-)$, where $x_i(t^+) = \lim_{t \longrightarrow t^+} x_i(t)$ and $x_i(t^-) = \lim_{t \longrightarrow t_k^-} x_i(t)$. Generally, we suppose that the solution of network (1) is right continuous, that is, $x_i(t_k^+) = x_i(t_k)$, and the sequence $\{t_k, U(k, x_i(t_k^-))\}$ is called the impulsive control rule. As a matter of convenience, we let $h_k(x_i(t_k^-)) \triangleq x_i(t_k^-) + U(k, x_i(t_k^-))$, which means $x_i(t_k^+) = h_k(x_i(t_k^-)), k \in \mathbb{Z}_+$. Define the solution of network (1) through (t_0, ϕ) as $x(t) = x(t, t_0, \phi)$, where $\phi \in PC([-\tau, 0], \mathbb{R}^n)$ represents the initial state.

For subsequent needs, we give some requisite definitions and assumptions as follows.

Definition 1 (see [14]). Suppose that there exist positive constants N_0 and T_a such that

$$N(t_2, t_1) \geq \frac{t_2 - t_1}{T_a} - N_0, \forall t_2 \geq t_1 \geq t_0, \tag{2}$$

where $N(t_2, t_1)$ represents the number of impulses in the interval $(t_1, t_2]$. Then, N_0 is called the elasticity number, and T_a denotes the AII constants.

Remark 1. The concept of AII is proposed to handle various types of impulses. In fact, AII condition (2) allows an upper bound, that is, $N(t_2, t_1) \leq t_2 - t_1/T_a + N_0$. Particularly, at least one impulse is required for each interval of length T_a in the case of $N_0 = 1$. For AII constant T_a, it can be observed that it contains more impulsive instant sequences when the elasticity number N_0 is larger.

Definition 2. For any given initial value $\phi \in PC([-\tau, 0], \mathbb{R}^n)$, if there exist positive numbers M and λ such that

$$\|x(t, t_0, \phi)\| \leq M\|\phi\|_\tau e^{-\lambda(t - t_0)}, \forall t \geq t_0, \tag{3}$$

holds for every sequence $\{t_k\} \in \mathcal{J}^*(T_a, N_0)$, then we can say that the network (1) is globally uniformly exponentially stable (GUES) over the class $\mathcal{J}^*(T_a, N_0)$.

Remark 2. $\mathcal{J}^*(T_a, N_0)$ mentioned in the above definition represents a collection of impulsive instant sequences $\{t_k\}$ that satisfy AII condition (2).

Assumption 1. The functions $f(\cdot), g(\cdot) \in \mathbb{R}^n$ satisfy $f(0) = 0$, $g(0) = 0$, and function $h_k: \mathbb{R} \longrightarrow \mathbb{R}$ satisfies $h_k(0) = 0$.

Remark 3. Clearly, Assumption 1 guarantees that $x = 0$ is an equilibrium point to network (1).

Assumption 2. The functions $f(\cdot), g(\cdot)$ are all Lipschitz continuous and meet

$$\begin{aligned} |f_j(\theta_1) - f_j(\theta_2)| &\leq \gamma_j|\theta_1 - \theta_2|, \\ |g_j(\theta_1) - g_j(\theta_2)| &\leq \overline{\gamma}_j|\theta_1 - \theta_2|, \end{aligned} \tag{4}$$

for all $\theta_1, \theta_2 \in \mathbb{R}, j = 1, 2, \ldots, n$, where $\gamma_j, \overline{\gamma}_j > 0$ are constants.

Assumption 3. The impulsive operator h_k meets

$$|h_k(\theta_1) - h_k(\theta_2)| \leq q|\theta_1 - \theta_2|, \tag{5}$$

for all $\theta_1, \theta_2 \in \mathbb{R}, k \in \mathbb{Z}_+$, where $q > 0$ is Lipschitz constant.

In order to facilitate the subsequent expression, we make

$$\begin{aligned} \alpha_1 &= \max_{1 \leq i \leq n}\left(-a_i + \sum_{j=1}^{n} |b_{ji}|\gamma_i\right), \\ \alpha_2 &= \max_{1 \leq i \leq n}\left(\sum_{j=1}^{n} |c_{ji}|\overline{\gamma}_i\right). \end{aligned} \tag{6}$$

3. Main Results

We will discuss the stability of INNs from the following three aspects in current section. Firstly, we consider the stability of a kind of INNs with small delay (the delay does not exceed any two consecutive impulsive time intervals, i.e., $\tau \leq t_k - t_{k-1}$). Besides, the latent effects of time delay are also explored. Secondly, the stability of INNs with arbitrarily finite delay is considered. Compared with small delay, we use large delay (which implies that the delay may be greater than a certain impulsive time interval, namely, $\tau \leq t_k - t_{k-1}$ may not be true) to represent relatively larger delay (which is collectively referred to as arbitrarily finite delay here). For arbitrarily finite delay, we analyze the robustness of the stability of INNs with delay and verify that the system can remain stable for any large but bounded delay under certain conditions. Finally, in view of the fact that the impulsive effects may promote or suppress system stability, we extend the ideas of the first two points to delayed INNs with hybrid impulses.

3.1. INNs with Small Delay. In what follows, we will discuss the case where the delay is small. We capture the stabilizing information of time delay with the help of the impulsive delay inequality and then integrate it into the Lyapunov-based function. Finally, through the AII method, we can derive the stability criterion of INNs.

Theorem 1. *If there exist constants $q \in (0, 1)$, $\eta^* = \max\{\alpha_1 + \alpha_2, \eta_0\}$ and the following conditions hold:*

$$\begin{aligned} \alpha_1 + \alpha_2 &> 0, \\ \frac{\ln q}{T_a} + \eta^* &< 0, \end{aligned} \tag{7}$$

where

$$\alpha_1 + \frac{\alpha_2}{q} e^{-\eta_0 \tau} - \eta_0 = 0, \tag{8}$$

then under Assumptions 1–3, network (1) is GUES over the class $\mathcal{J}^*(T_a, N_0)$.

Proof. Construct a function $V(t) \triangleq V(t, x(t)) = \|x(t)\| = \sum_{i=1}^{n} |x_i(t)|$ and make $\overline{V}(t_0) = \sup_{t_0 - \tau \leq s \leq t_0} V(s)$. For any $\varepsilon > 0$, let $\eta = \eta^* + \varepsilon$, and design an auxiliary function

$$L(t)=\left\{\begin{array}{c} V(t)e^{-\eta(t-t_k)}, t\in[t_k,t_{k+1}), \\ V(t), t_0-\tau\le t\le t_0. \end{array}\right\} \tag{9}$$

To start with, let $\Omega_k = q^k\overline{V}(t_0)$, and then we will confirm that

$$V(t)\le\Omega_k e^{\eta(t-t_0)}, t\in[t_k,t_{k+1}], k\in\mathbb{Z}_+^0. \tag{10}$$

Together with (7) and (8),

$$L(t)\le\Omega_k e^{\eta(t_k-t_0)}, t\in[t_k,t_{k+1}]. \tag{11}$$

Firstly, we demonstrate that (9) is true for $k=0$, namely, $L(t)\le\Omega_0=\overline{V}(t_0), t\in[t_0,t_1]$. Note that $L(t_0)=V(t_0)\le\overline{V}(t_0)=\Omega_0$. If the above statement is incorrect, then there is an instant $t^*\in[t_0,t_1]$ such that

$$L(t^*)=\Omega_0, L(t)\le\Omega_0, t\in[t_0,t^*) \text{and} D^+L(t^*)\ge 0. \tag{12}$$

When $s\in[t_0-\tau,t_0]$, it is apparent that $L(s)=V(s)\le\overline{V}(t_0)=\Omega_0$, and in combination with (10), we derive $L(s)\le\Omega_0, t\in[t_0-\tau,t^*]$. For $t\in[t_k,t_{k+1}], k\in\mathbb{Z}_+^0$, we can calculate that

$$\begin{aligned} D^+V(t) &= \sum_{i=1}^n \operatorname{sgn}(x_i(t))\left[-a_i x_i(t)+\sum_{j=1}^n b_{ij}f_j(x_j(t))+\sum_{j=1}^n c_{ij}g_j(x_j(t-\tau))\right] \\ &\le \sum_{i=1}^n(-a_i|x_i(t)|)+\sum_{i=1}^n\sum_{j=1}^n|b_{ij}|\gamma_j|x_j(t)|+\sum_{i=1}^n\sum_{j=1}^n|c_{ij}|\overline{\gamma}_j|x_j(t-\tau)| \\ &\le \max_{1\le i\le n}\left(-a_i+\sum_{j=1}^n|b_{ji}|\gamma_i\right)\|x(t)\|+\max_{1\le i\le n}\left(\sum_{j=1}^n|c_{ji}|\overline{\gamma}_i\right)\|x(t-\tau)\| \\ &= \alpha_1V(t)+\alpha_2V(t-\tau). \end{aligned} \tag{13}$$

When $t^*-\tau\in[t_0-\tau,t^*]$, combining the definition of $L(t)$ and conditions (6), (10), and (11), one has

$$\begin{aligned} D^+L(t)|_{t=t^*} &= e^{-\eta(t^*-t_0)}D^+V(t)|_{t=t^*}-\eta e^{-\eta(t^*-t_0)}V(t^*) \\ &\le e^{-\eta(t^*-t_0)}[\alpha_1V(t^*)+\alpha_2V(t^*-\tau)] \\ &\quad -\eta e^{-\eta(t^*-t_0)}V(t^*) \\ &= \alpha_1L(t^*)+\alpha_2L(t^*-\tau)e^{-\eta\tau}-\eta L(t^*) \\ &\le (\alpha_1+\alpha_2e^{-\eta\tau}-\eta)\Omega_0<0. \end{aligned} \tag{14}$$

Obviously, it could be observed that it contradicts $D^+L(t^*)\ge 0$, namely, (9) holds for $k=0$.

Next, through mathematical induction method, we assume that (9) is true for $k\le p, p\in\mathbb{Z}_+^0$, i.e.,

$$L(t)\le\Omega_k e^{\eta(t_K-t_0)}, t\in[t_k,t_{k+1}), k\le p, \tag{15}$$

which means

$$L(t)\le\Omega_p e^{\eta(t_p-t_0)}, t\in[t_p,t_{p+1}). \tag{16}$$

Subsequently, we demonstrate that

$$L(t)\le\Omega_{p+1}e^{\eta(t_{p+1}-t_0)}, t\in[t_{p+1},t_{p+2}). \tag{17}$$

Recall (7) and (14), and we obtain

$$\begin{aligned} L(t_{p+1}) &= V(t_{p+1})=\|x(t_{p+1})\| \\ &= \|h_{p+1}(x(t_{p+1}^-))-h_{p+1}(0)\| \\ &\le qL(t_{p+1}^-)e^{\eta(t_{p+1}-t_p)} \\ &= \Omega_{p+1}e^{\eta(t_{p+1}-t_0)}. \end{aligned} \tag{18}$$

Thus, (15) holds for $t=t_{p+1}$. On the contrary, it is assumed that there is an instant $t^*\in[t_{p+1},t_{p+2}]$ which makes

$$\begin{aligned} &L(t^*)=\Omega_{p+1}e^{\eta(t_{p+1}-t_0)}, L(t)\le\Omega_{p+1}e^{\eta(t_{p+1}-t_0)}, t\in \\ &\cdot[t_{p+1},t^*] \text{and} D^+L(t^*)\ge 0. \end{aligned} \tag{19}$$

If $t^*-\tau\ge t_{p+1}$, referring to (12), we derive that

$$\begin{aligned} &D^+L(t)|_{t=t^*}\le\alpha_1L(t^*)+\alpha_2L(t^*-\tau)e^{-\eta\tau}-\eta L(t^*)\le \\ &\cdot(\alpha_1+\alpha_2e^{-\eta\tau}-\eta)\Omega_{p+1}e^{\eta(t_{p+1}-t_0)}<0. \end{aligned} \tag{20}$$

Similarly, what calls for special attention is that when $s\in[t_p,t_{p+1}]$, it follows from (14) that

$$\begin{aligned} L(s) &\le \Omega_p e^{\eta(t_p-t_0)}=\frac{\Omega_{p+1}}{q}e^{\eta(t_{p+1}-t_0)}e^{-\eta(t_{p+1}-t_p)} \\ &= \frac{L(t^*)}{q}e^{-\eta(t_{p+1}-t_p)}\le\frac{L(t^*)}{q}e^{-\eta\tau}. \end{aligned} \tag{21}$$

At this time, if $t^* - \tau < t_{p+1}$, on account of $t_p \le t_{p+1} - \tau \le t^* - \tau < t_{p+1}$, and together with (6), (16), and (17), we could compute that

$$\begin{aligned} D^+L(t)|_{t=t^*} &\le \alpha_1 L(t^*) + \alpha_2 L(t^* - \tau)e^{-\eta\tau} - \eta L(t^*) \\ &\le \alpha_1 L(t^*) + \alpha_2 \frac{L(t^*)}{q} e^{-\eta\tau} - \eta L(t^*) \\ &= \left(\alpha_1 + \frac{\alpha_2}{q}e^{-\eta\tau} - \eta\right)\Omega_{p+1}e^{\eta(t_{p+1}-t_0)} < 0, \end{aligned} \tag{22}$$

which contradicts $D^+L(t^*) \ge 0$, namely, (15) holds.

Hence, we can get

$$L(t) \le \Omega_k e^{\eta(t_k - t_0)}, \forall t \in [t_k, t_{k+1}), k \in \mathbb{Z}_+^0, \tag{23}$$

which means (8) is true, namely, $V(t) \le \Omega_k e^{\eta(t-t_0)} = \Omega_k e^{(\eta^*+\varepsilon)(t-t_0)}, t \in [t_k, t_{k+1})$.

Let $\varepsilon \longrightarrow 0^+$, and then we obtain

$$V(t) \le \Omega_k e^{\eta^*(t-t_0)}, \forall t \in [t_k, t_{k+1}), k \in \mathbb{Z}_+^0. \tag{24}$$

Since $\{t_k\} \in \mathcal{J}^*(T_a, N_0)$, the AII method further yields that

$$\begin{aligned} V(t) &\le q^{N(t,t_0)} e^{\eta^*(t-t_0)} \overline{V}(t_0) \\ &\le q^{t-t_0/T_a - N_0} e^{\eta^*(t-t_0)} \overline{V}(t_0) \\ &\le q^{-N_0} e^{(\ln q/T_a + \eta^*)(t-t_0)} \overline{V}(t_0), \forall t \ge t_0, \end{aligned} \tag{25}$$

where $N(t, t_0)$ represents the number of impulses in the interval $(t_0, t]$.

According to (18) and the definition of $V(t)$, we have

$$\|x(t)\| \le Me^{-\lambda(t-t_0)}\|\phi\|_\tau, \forall t \ge t_0, \tag{26}$$

where $M = q^{-N_0}, \lambda = -(\ln q/T_a + \eta^*) > 0$. Until now, we have done the proof. □

Remark 4. From (6) and (8) in Theorem 1, we can notice the latent impacts of time delay τ on the decay rate of Lyapunov function $V(t)$. In particular, if $\eta_0 > \alpha_1 + \alpha_2$, then we have $\eta^* = \eta_0$. Meanwhile, the implicit function $\eta^*(\tau)$ is determined by $\alpha_1 + \alpha_2/qe^{-\eta^*\tau} - \eta^* = 0$, which decreases as τ increases. Obviously, the result derived from the above theorem shows that the convergence rate λ is related to parameter η^*, and in view of the relationship between η^* and delay τ, it can be concluded that the convergence rate of the system will become larger with the increase of delay, which means that we have captured the stabilizing effects of time delay. In addition, what needs special attention is that in the majority of the available literature about the stability of delayed INNs, we can see that the stability of the system tends to be destroyed as delay increases, but different results are obtained in this paper.

Remark 5. It should be noted that the conclusion of the relationship between time delay and system stability derived from Remark 4 is based on $\eta^* = \eta_0$, so the results may be conservative to some extent. Furthermore, the conclusion of Theorem 1 is a sufficient condition rather than a necessary condition; then, it is possible for the system to be stable when τ is small and does not meet the conditions of Theorem 1.

3.2. INNs with Arbitrarily Finite Delay. For the case of arbitrarily finite delay, based on strict comparison principle and the concept of AII, a stability criterion of INNs is also derived.

Lemma 1 (see [13]). *Let $\alpha_1 \in \mathbb{R}, \alpha_2 \ge 0$ and $q > 0$. Suppose that $a(t), b(t) \in C([t_{k-1}, t_k], \mathbb{R}_+)$ meet*

$$\left\{\begin{array}{c} D^+a(t) \le \alpha_1 a(t) + \alpha_2 a(t-\tau), t \ge t_0, t \ne t_k, \\ a(t) \le qa(t^-), t = t_k, \end{array}\right\}, \tag{27}$$

$$\left\{\begin{array}{c} D^+b(t) = \alpha_1 b(t) + \alpha_2 b(t-\tau), t \ge t_0, t \ne t_k, \\ v(t) = qb(t^-), t = t_k, \end{array}\right\}, \tag{28}$$

for all $k \in \mathbb{Z}_+$. Then, $a(t) \le b(t), \forall t_0 - \tau \le t \le t_0$ implies that $a(t) \le b(t), \forall t \ge t_0$.

Theorem 2. *If there exists constant $q \in (0, 1)$ such that*

$$\alpha_1 + \frac{\alpha_2}{q^{N_0}} + \frac{\ln q}{T_a} < 0, \tag{29}$$

then under Assumptions 1–3, network (1) is GUES over the class $\mathcal{J}^*(T_a, N_0)$ for arbitrarily finite delay τ.

Proof. Construct a function $V(t) = \|x(t)\| = \sum_{i=1}^n |x_i(t)|$, and let $\overline{V}(t_0) = \sup_{t_0-\tau \le s \le t_0} V(s)$.

Next, similar to (11), we have

$$D^+V(t) \le \alpha_1 V(t) + \alpha_2 V((t-\tau)), \forall t \in [t_{k-1}, t_k), k \in \mathbb{Z}_+. \tag{30}$$

When $t = t_k$, according to Assumptions 1–3, we could get

$$\begin{aligned} V(t_k) &= \|x(t_k)\| = \|h_k(x(t_k^-))\| = \|h_k(x(t_k^-)) - h_k(0)\| \\ &\le q\|x(t_k^-)\| = qV(t_k^-). \end{aligned} \tag{31}$$

Introduce an impulsive delayed system with $u(t)$ as its unique solution:

$$\left\{\begin{array}{c} D^+u(t) = \alpha_1 u(t) + \alpha_2 u(t-\tau), t \ge t_0, t \ne t_k, \\ u(t) = qu(t^-), t = t_k, \\ u(t) = \overline{V}(t_0), t \in [t_0 - \tau, t_0]. \end{array}\right\} \tag{32}$$

Apparently, $V(t) \le \overline{V}(t_0) = u(t)$ when $t \in [t_0 - \tau, t_0]$. In accordance with Lemma 1, we have

$$0 \le V(t) \le u(t), \forall t \ge t_0. \tag{33}$$

From the variable parameter formula, we obtain

$$u(t) = K(t, t_0)u(t_0) + \int_{t_0}^t K(t, s)\alpha_2 u(s-\tau)\mathrm{d}s, t \ge t_0, \tag{34}$$

where $K(t,s)$ denotes the Cauchy matrix of the following system:

$$\left\{\begin{array}{l} D^{+}u(t)=\alpha_1 u(t), t\geq t_0, t\neq t_k, \\ u(t)=qu(t^{-}), t=t_k, k\in\mathbb{Z}_{+}. \end{array}\right\} \tag{35}$$

According to the properties of the Cauchy matrix, combining $0<q<1$ and $\{t_k\}\in\mathcal{J}^{*}(T_a,N_0)$, we can obtain

$$\begin{aligned} K(t,s) &= e^{\alpha_1(t-s)}\Pi_{s<t_k\leq t}q\leq e^{\alpha_1(t-s)}q^{t-s/T_a-N_0} \\ &= q^{-N_0}e^{(\alpha_1+\ln q/T_a)(t-s)}=q^{-N_0}e^{-c(t-s)}, \end{aligned} \tag{36}$$

where $c=-(\alpha_1+\ln q/T_a)$, and it is evident that $c>0$ by using condition (21).

Reviewing (26) and (28), we have

$$\begin{aligned} u(t)&\leq q^{-N_0}e^{-c(t-t_0)}u(t_0) \\ &\quad+\int_{t_0}^{t}q^{-N_0}e^{-c(t-s)}\alpha_2 u(s-\tau)\mathrm{d}s, \forall t\geq t_0. \end{aligned} \tag{37}$$

Since $c>0, N_0>0$, and $0<q<1$, this implies

$$\begin{aligned} u(t)=\overline{V}(t_0)&=u(t_0)\leq u(t_0)e^{-c(t-t_0)} \\ &<q^{-N_0}u(t_0)e^{-\lambda(t-t_0)}, t\in[t_0-\tau,t_0], \end{aligned} \tag{38}$$

where $\lambda=c-q^{-N_0}\alpha_2 e^{\lambda\tau}$. In fact, by using (21), we can obtain $\lambda>0$. Then, we shall confirm that

$$u(t)<q^{-N_0}u(t_0)e^{-\lambda(t-t_0)}, t\geq t_0. \tag{39}$$

On the contrary, suppose (31) is untenable; then, there exists an instant $t^{*}>t_0$ which makes

$$u(t^{*})\geq q^{-N_0}u(t_0)e^{-\lambda(t^{*}-t_0)}, \tag{40}$$

$$u(t)<q^{-N_0}u(t_0)e^{-\lambda(t-t_0)}, t<t^{*}. \tag{41}$$

Subsequently, from (29) and (33), one has

$$\begin{aligned} u(t^{*})&\leq q^{-N_0}e^{-c(t^{*}-t_0)}u(t_0)+\int_{t_0}^{t^{*}}q^{-N_0}e^{-c(t^{*}-s)}\alpha_2 u(s-\tau)\mathrm{d}s \\ &<q^{-N_0}e^{-c(t^{*}-t_0)}u(t_0)+\int_{t_0}^{t^{*}}q^{-N_0}e^{-c(t^{*}-s)}\alpha_2 q^{-N_0}u(t_0)e^{-\lambda(s-\tau-t_0)}\mathrm{d}s \\ &=q^{-N_0}u(t_0)\left[e^{-c(t^{*}-t_0)}+q^{-N_0}\alpha_2 e^{\lambda\tau}e^{-ct^{*}+\lambda t_0}\int_{t_0}^{t^{*}}e^{(c-\lambda)s}\mathrm{d}s\right] \\ &=q^{-N_0}u(t_0)e^{-\lambda(t^{*}-t_0)}, \end{aligned} \tag{42}$$

which is in contradiction with (32). Thus, we can derive that (31) holds. Finally, combining (25), we have

$$V(t)\leq u(t)<q^{-N_0}u(t_0)e^{-\lambda(t-t_0)}, \forall t\geq t_0, \tag{43}$$

i.e.,

$$\|x(t)\|\leq q^{-N_0}e^{-\lambda(t-t_0)}\|\phi\|_{\tau}, \forall t\geq t_0. \tag{44}$$

So far, we have done the proof. □

Remark 6. It can be observed from Theorems 1 and 2 that the AII constant T_a should be small enough to meet conditions (5) and (21) in the case of $0<q<1$. The AII constant means the frequency of impulsive control. The smaller T_a is, the higher the impulsive frequency will be. In addition, it should be noted that the result derived from Theorem 2 involves elasticity number N_0, and equation (21) may not hold when N_0 is sufficiently large. However, for delay-free system (see [14]), the derived result does not involve N_0, so we cannot obtain such a conclusion. Moreover, we can obverse that the elasticity number N_0 is not involved in the result of Theorem 1, which is the difference between Theorems 1 and 2. Therefore, under the condition of AII, Theorem 2 further illustrates the internal relationship between large delay and system stability.

Remark 7. Although Theorems 1 and 2 are proposed for small and large delays, respectively, this does not mean that Theorem 2 and Theorem 1 are mutually exclusive. Actually, Theorem 2 is a supplement to Theorem 1 because the so-called large delay in Theorem 2 just means that $\tau\leq t_k-t_{k-1}$ may not be true, in which case it covers the case of small delay. Therefore, Theorem 2 is also applicable to the case of small delay.

3.3. Extension to INNs with Hybrid Impulses. In recent years, hybrid impulse as an important topic has attracted wide attention, and numerous meaningful results have emerged. Particularly, in [15], considering the influence of hybrid impulses on the synchronization process, the authors designed an effective hybrid impulsive controller so as to achieve the quasi-synchronization of NNs. In this case, a sufficient delay-dependent criterion for quasi-synchronization is obtained. Meanwhile, in [15, 16], the authors adopted AII and average impulsive gain methods to deal with the hybrid impulses. In this paper, an improved dwell-time condition is introduced to treat the hybrid impulses. In view

of the above discussion, we extend the results of the first two theorems in this section.

First of all, in order to extend Theorem 1, we put forward Theorem 3 by referring to the processing procedure of the small delay case.

Theorem 3. *If Assumption 3 is replaced by the following condition:*

$$\left|h_k(\theta_1) - h_k(\theta_2)\right| \le e^{-\rho_k}\left|\theta_1 - \theta_2\right|, \tag{45}$$

where $\rho_k \in \mathbb{R}$, then under Assumptions 1 and 2 and (35), for given constants $\overline{\rho} > 0, \rho^* > 0, c > 0, \delta > 0$, the following conditions are satisfied:

$$\begin{aligned} &(A_1)\alpha_1 + \alpha_2 > 0\\ &(A_2)\sum_{k=1}^{N(t,t_0)} \rho_k > \overline{\rho}N(t,t_0) - \rho^*\\ &(A_3)\overline{\rho}N(t,t_0) \ge c(t-t_0) - \delta\\ &(A_4)\eta^* - c < 0, \end{aligned} \tag{46}$$

where $\eta^* = \max\{\alpha_1 + \alpha_2, \eta_1\}$, and η_1 satisfies $\alpha_1 + \alpha_2 e^{\rho_{sup}} e^{-\eta_1\tau} - \eta_1 = 0$ with $\rho_{sup} = \sup_{k\in\mathbb{Z}_+}\{\rho_k\} < \infty$; then, network (1) is GES.

Proof. The same analysis method as Theorem 1 is used here, except that the impulsive parameters are changed, so we shall take advantage of (A_1) and (A_4) to acquire the following statement:

$$V(t) \le \Pi_{k=1}^{N(t,t_0)}\left(e^{-\rho_k}\right)e^{\eta^*(t-t_0)}\overline{V}(t_0), \forall t \ge t_0. \tag{47}$$

Then, by using (A_2) and (A_3), one has

$$\begin{aligned} V(t) &\le e^{\left(-\sum_{k=1}^{N(t,t_0)} e^{-\rho_k}\right)} e^{\eta^*(t-t_0)}\overline{V}(t_0)\\ &\le e^{-\overline{\rho}N(t,t_0)+\rho^*} e^{\eta^*(t-t_0)}\overline{V}(t_0)\\ &\le e^{-c(t-t_0)+\delta+\rho^*} e^{\eta^*(t-t_0)}\overline{V}(t_0)\\ &\le e^{\delta+\rho^*} e^{-(c-\eta^*)(t-t_0)}\overline{V}(t_0), \forall t \ge t_0. \end{aligned} \tag{48}$$

That is,

$$\|x(t)\| \le e^{\delta+\rho^*} e^{-(c-\eta^*)(t-t_0)}\|\phi\|_\tau, \forall t \ge t_0. \tag{49}$$

The proof is completed.

Next, referring to the analysis method of arbitrarily finite delay case, we obtain Theorem 4 as an extension of Theorem 2. □

Theorem 4. *Suppose that the parameter q in Assumption 3 is replaced by $e^{-\rho_k}$, then under Assumptions 1 and 2 and modified Assumption 3, for given constants $\overline{\rho} > 0, \rho^* > 0, c > 0, \delta > 0$, the following conditions are fulfilled:*

$$\begin{aligned} &(\widehat{A}_1)\sum_{k=1}^{N(t,t_0)} \rho_k > \overline{\rho}N(t,t_0) - \rho^*\\ &(\widehat{A}_2)\overline{\rho}N(t,t_0) \ge (\alpha_1 + c)(t-t_0) - \delta\\ &(\widehat{A}_3)\alpha_2 e^{\delta+\rho^*} - c < 0. \end{aligned} \tag{50}$$

Then, network (1) is GES.

Proof. It is easy to prove this theorem by combining the analytical methods of Theorems 2 and 3, so we leave out it for brevity. □

Remark 8. The parameter $e^{-\rho_k}$ in Theorems 3 and 4 is used to describe the variable of hybrid impulses in impulsive control systems. As you can see, q in Theorems 1 and 2 is required to be $0 < q < 1$, but $e^{-\rho_k}$ in Theorem 3 and 4 satisfies $\rho_k \in \mathbb{R}$, that is, $e^{-\rho_k} < 1$ if $\rho_k > 0$ and $e^{-\rho_k} > 1$ if $\rho_k < 0$. It implies that stabilizing impulses and destabilizing impulses may exist at the same time. Furthermore, in order to handle these parameters overall, we propose conditions (A_2) and $(\widehat{A}_1)$, and in a sense, the parameter $\overline{\rho}$ may be approximately regarded as the "average value" of ρ_k. In fact, condition (A_2) combined with (A_3) or $(\widehat{A}_1)$ combined with $(\widehat{A}_2)$ can be considered as an improvement of dwell-time condition.

Remark 9. Compared with reference [11], this paper studies the effects of time delay in continuous dynamics on system stability. Bear in mind that the relationship between time delay in continuous dynamics and the stability of impulsive systems is not easy to find, and the derived results based on AII method contain both time delay and the AII constant T_a, which is not obtained in previous results. Furthermore, we extend the results to systems with hybrid impulses. In addition, when discussing the delay effects in reference [12], the authors limit the time delay to be less than any two consecutive impulsive time intervals. However, we loosen the condition of time delay in this paper, that is, the time delay can be smaller than any two consecutive impulsive intervals, or it can be greater than any two consecutive impulsive time intervals.

Remark 10. On the basis of this paper, we could also investigate the case of neural network models with time-varying delays. Actually, the results of this paper are still valid after the constant delay is replaced by time-varying delay in the model. We will continue to explore this question in depth in future studies.

4. Illustrative Examples

Finally, for the purpose of verifying the above achievements, we put forward the following three examples in current section.

Example 1. Consider a 2-dimensional INN with small delay:

$$\begin{aligned}\begin{bmatrix}\dot{x}_1(t)\\ \dot{x}_2(t)\end{bmatrix} &= -\begin{bmatrix}0.2 & 0\\ 0 & 0.3\end{bmatrix}\begin{bmatrix}x_1(t)\\ x_2(t)\end{bmatrix}\\ &+\begin{bmatrix}0.2 & 0.4\\ 0.03 & 0.01\end{bmatrix}\begin{bmatrix}\tanh(x_1(t))\\ \tanh(x_2(t))\end{bmatrix}\\ &+\begin{bmatrix}0.25 & 0.25\\ 0.05 & 0.02\end{bmatrix}\begin{bmatrix}\tanh(x_1(t-\tau))\\ \tanh(x_2(t-\tau))\end{bmatrix},\end{aligned} \tag{51}$$

under impulsive control

$$\begin{bmatrix}x_1(t_k)\\ x_2(t_k)\end{bmatrix} = \begin{bmatrix}0.01 & 0\\ 0 & 0.01\end{bmatrix}\begin{bmatrix}x_1(t_k^-)\\ x_2(t_k^-)\end{bmatrix}, \tag{52}$$

where $t \geq 0, k \in \mathbb{Z}_+, t_k - t_{k-1} \geq \tau > 0$.

Obviously, $\gamma_1 = \gamma_2 = 1, \overline{\gamma}_1 = \overline{\gamma}_2 = 1, q = 0.01$. By calculating,

$$\begin{aligned}\alpha_1 &= \max_{1\leq i\leq n}\left(-a_i + \sum_{j=1}^{n}|b_{ji}|\gamma_i\right) = 0.11,\\ \alpha_2 &= \max_{1\leq i\leq n}\left(\sum_{j=1}^{n}|c_{ji}|\overline{\gamma}_i\right) = 0.3.\end{aligned} \tag{53}$$

Here, we set the initial value $\phi = [3, -0.4]^T$ and choose impulsive instants $t_k = 5k, k \in \mathbb{Z}_+$, which means $T_a = 5$. When $\tau \in [4, 5]$, we can figure out $\eta^* \leq 0.91$ and $\ln q/T_a + \eta^* < 0$, and it can be tested that all conditions in Theorem 1 hold. Therefore, we can derive that systems (39) and (40) are GUES when $\tau \in [4, 5]$. In addition, according to Remark 4, it can be seen that the system may converge faster with the increase of delay, which corresponds to the simulation results in Figures 1–3. Moreover, we calculate its corresponding parameter η^* and estimate its convergence rate for different time delays $\tau = 4, 4.5, 5$, which are shown in Table 1. More importantly, it also reveals the potential stabilizing effect of time delay.

Example 2. Consider another 2-dimensional INN with large delay:

$$\begin{aligned}\begin{bmatrix}\dot{x}_1(t)\\ \dot{x}_2(t)\end{bmatrix} &= -\begin{bmatrix}0.1 & 0\\ 0 & 0.1\end{bmatrix}\begin{bmatrix}x_1(t)\\ x_2(t)\end{bmatrix}\\ &+\begin{bmatrix}0.08 & 0.5\\ 0.2 & 0.35\end{bmatrix}\begin{bmatrix}\tanh\left(\frac{x_1(t)}{2}\right)\\ \tanh\left(\frac{x_2(t)}{2}\right)\end{bmatrix}\\ &+\begin{bmatrix}0.03 & 0.1\\ 0.1 & 0.07\end{bmatrix}\begin{bmatrix}\tanh\left(\frac{x_1(t-\tau)}{8}\right)\\ \tanh\left(\frac{x_2(t-\tau)}{2}\right)\end{bmatrix},\end{aligned} \tag{54}$$

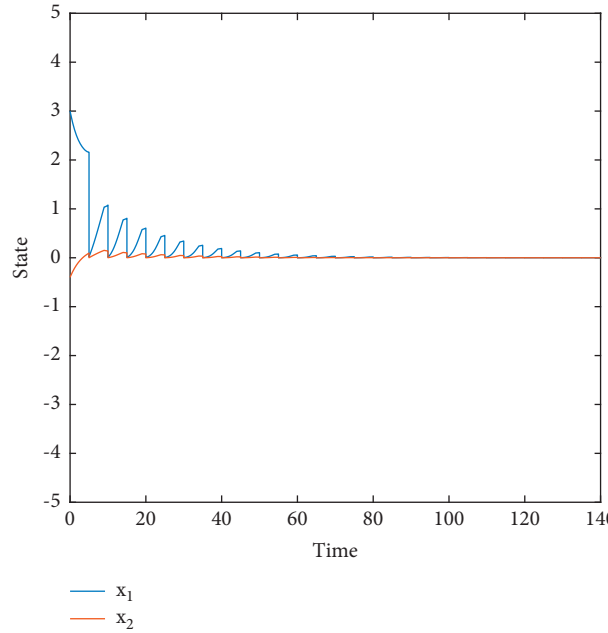

Figure 1: The state of (39) and (40) with $\tau = 4$.

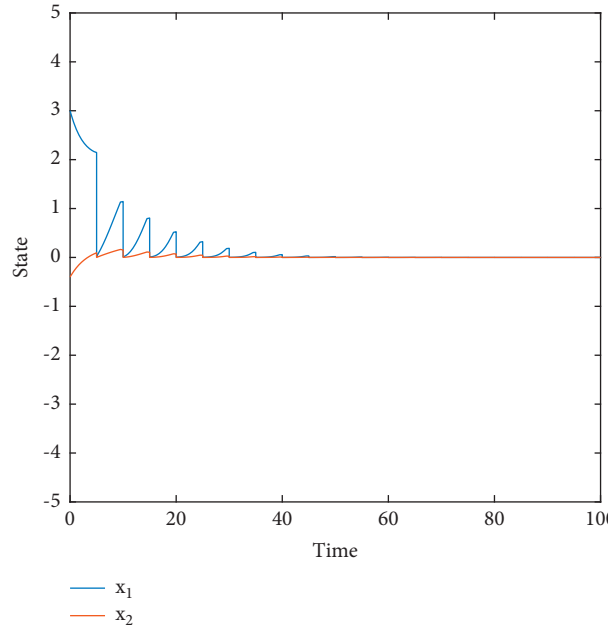

Figure 2: The state of (39) and (40) with $\tau = 4.5$.

under impulsive control

$$\begin{bmatrix}x_1(t_k)\\ x_2(t_k)\end{bmatrix} = \begin{bmatrix}\sin\left(\frac{x_1(t_k^-)}{5}\right)\\ \sin\left(\frac{x_2(t_k^-)}{5}\right)\end{bmatrix}, \tag{55}$$

where $t \geq 0, k \in \mathbb{Z}_+$ and $\tau = 25, t_k = 2k$. Here, we set the initial value $\phi = [0.4, 3]^T$. As shown in Figure 4, the impulse-free system is unstable.

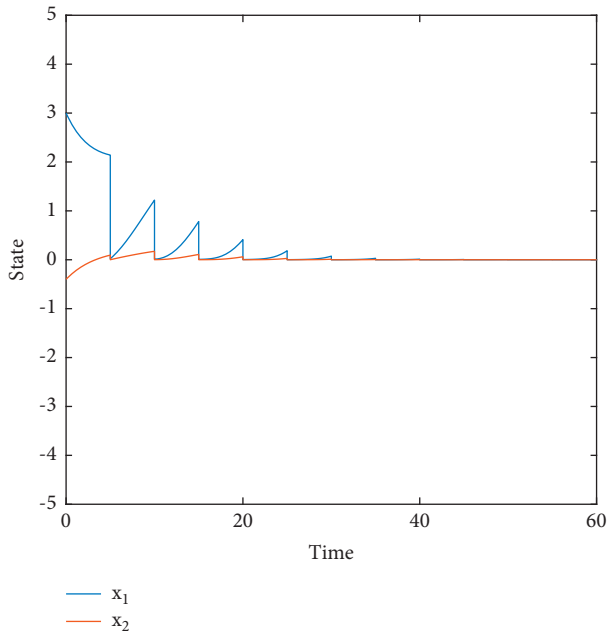

Figure 3: The state of (39) and (40) with $\tau = 5$.

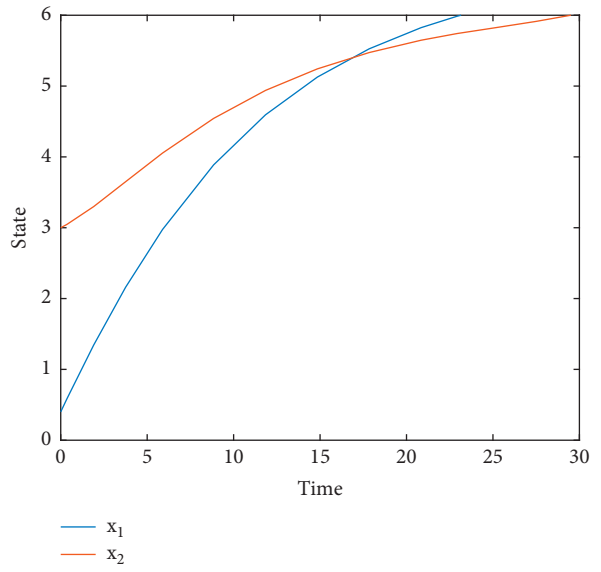

Figure 4: The state of (41) without impulse.

Table 1: The convergence rate λ for different time delays.

Time delay τ	Parameter η^*	Convergence rate λ
4	0.9070	0.0140
4.5	0.8291	0.0919
5	0.7649	0.1561

In addition, it is apparent that $\gamma_1 = \gamma_2 = 1/2, \overline{\gamma}_1 = 1/8, \overline{\gamma}_2 = 1/2, q = 1/5, T_a = 2, N_0 = 1$. By calculating,

$$\begin{aligned} \alpha_1 &= \max_{1\le i\le n}\left(-a_i + \sum_{j=1}^{n}\left|b_{ji}\right|\gamma_i\right) = 0.325, \\ \alpha_2 &= \max_{1\le i\le n}\left(\sum_{j=1}^{n}\left|c_{ji}\right|\overline{\gamma}_i\right) = 0.085. \end{aligned} \tag{56}$$

Therefore, we can conclude that $\alpha_1 + \alpha_2/q^{N_0} + \ln q/T_a \approx -0.05 < 0$. That is to say, the conditions in Theorem 2 are fulfilled, and it is deduced that systems (43) and (44) are GUES, which is well reflected in Figure 5. By the way, the time delay could be much larger and the system would still be stable. In what follows, we calculate the corresponding convergence rate for different time delays $\tau = 25, 60, 100$, which are shown in Table 2. Actually, the delay is not limited to 100, and it can even be greater than 100. As long as the delay is bounded under certain conditions, the initial stability of impulsive system can be guaranteed. Here we only calculate the convergence rate of the system when the delay increases to 100.

Example 3. Consider a 3-dimensional INN:

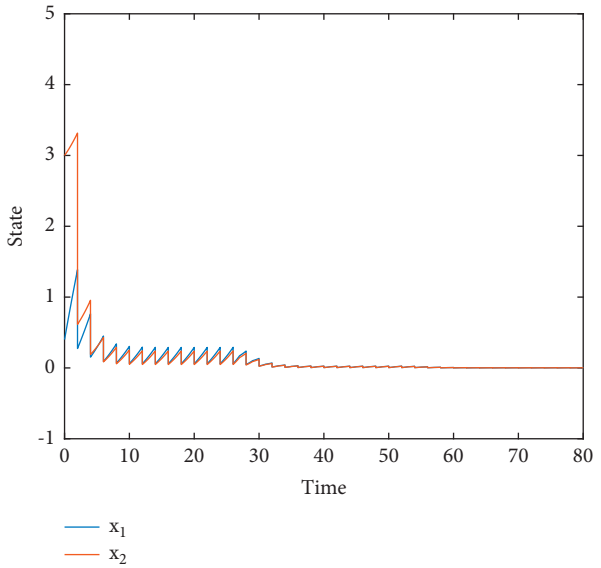

Figure 5: The state of (41) with impulsive effects (42).

Table 2: Stability of systems with different time delays.

Time delay τ	Stable or not	Convergence rate λ
25	✓	0.0045
60	✓	0.0019
100	✓	0.0012

$$\dot{x}(t) = -Ax(t) + Bf(x(t)) + Cg(x(t-\tau)), \tag{57}$$

under hybrid impulsive control

$$x(t_k) = e^{-\rho_k}x(t_k^-), t_k = 8k, k \in \mathbb{Z}_+, \tag{58}$$

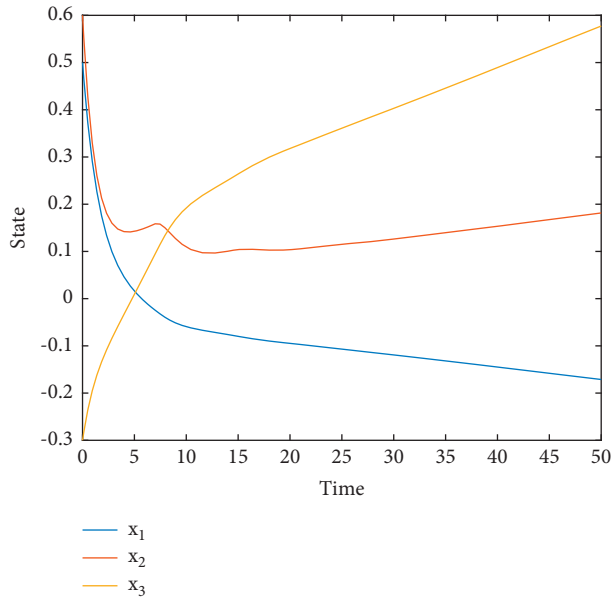

Figure 6: The state of (43) without impulse.

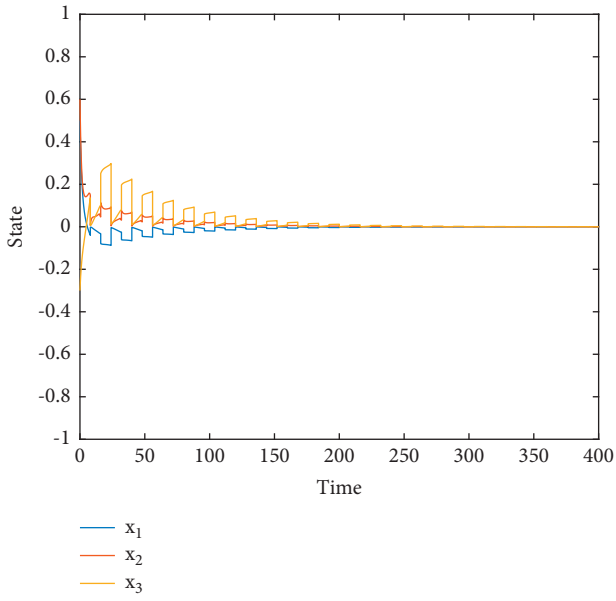

Figure 7: The state of (43) under hybrid impulsive control (44).

where

$$A = \begin{bmatrix} 0.6 & 0 & 0 \\ 0 & 0.6 & 0 \\ 0 & 0 & 0.6 \end{bmatrix}, B = \begin{bmatrix} 0.24 & -0.3 & -0.2 \\ -0.2 & -0.24 & 0.3 \\ -0.4 & 0.7 & 0.9 \end{bmatrix}, C = \begin{bmatrix} 0.01 & 0 & 0 \\ 0 & 0.2 & 0 \\ 0 & 0 & 0.01 \end{bmatrix}, \tag{59}$$

$$\rho_k = \left\{ \begin{array}{c} 3.1, k = 2l-1 \\ -0.9, k = 2l \end{array} \right\}, l \in \mathbb{Z}_+. \tag{60}$$

Suppose that $f(x) = (f_1(x_1), f_2(x_2), f_3(x_3))^T$, $g(x) = (g_1(x_1), g_2(x_2), g_3(x_3))^T$ and $f_i(x_i) = \tanh(x_i(t)/2)$, $g_i(x_i) = \tanh(x_i(t))$, $i = 1, 2, 3$. We give the initial value $\phi = [0.5, 0.6, -0.3]^T$ and take time delay $\tau = 7$. As shown in Figure 6, the impulse-free system is unstable.

Additionally, it is evident that $\gamma_1 = \gamma_2 = \gamma_3 = 1/2, \overline{\gamma}_1 = \overline{\gamma}_2 = \overline{\gamma_3} = 1, \rho_{\sup} = 3.1, \overline{\rho} = 1.1 > 0$. By calculating,

$$\begin{aligned} \alpha_1 &= \max_{1 \le i \le n} \left(-a_i + \sum_{j=1}^{n} |b_{ji}| \gamma_i \right) = 0.1, \\ \alpha_2 &= \max_{1 \le i \le n} \left(\sum_{j=1}^{n} |c_{ji}| \overline{\gamma}_i \right) = 0.2. \end{aligned} \tag{61}$$

Furthermore, we can figure out $\eta_1 \approx 0.3899$ by Matlab. That is, $\eta^* = \max\{\alpha_1 + \alpha_2, \eta_1\} \approx 0.39$ and $c = 0.4$ in conditions $(A_1) - (A_4)$ of Theorem 3 are fulfilled. At the same time, a series of conditions in Theorem 3 are completely true. Therefore, systems (43) and (44) are GES, which is well illustrated in Figure 7. From the simulation results, the impulsive effects indeed have both stabilizing and destabilizing effects.

5. Conclusion

In this paper, we have discussed the stability of a kind of INNs with delay. Particularly, the internal relation between time delay and system stability has been revealed. Firstly, we have investigated the case where the delay is small. By constructing Lyapunov function, combining the impulsive delay inequality and AII condition, we have obtained a sufficient condition to assure the exponential stability of INNs. The results have shown that within limits, the system converges more quickly with the increase of time delay. Secondly, we have explored the case where the delay is arbitrarily large but bounded and derived a Lyapunov-based stability criterion by virtue of the strict comparison principle. Finally, as an extension, we have considered the case where INN is a system with hybrid impulses. In future studies, we may discuss the delay effects of a kind of INN with state-dependent delay.

Data Availability

No data were used to support this study.

Conflicts of Interest

The authors declare that there are no conflicts of interest regarding the publication of this paper.

Acknowledgments

This study was supported by the Natural Science Foundation of China under grant no. 61976084, the Natural Science Foundation of Hubei Province of China under grant no. 2021CFA080, and the Young Top-Notch Talent Cultivation Program of Hubei Province of China.

References

[1] G. Mu, L. Li, and X. Li, "Quasi-bipartite synchronization of signed delayed neural networks under impulsive effects," *Neural Networks*, vol. 129, pp. 31–42, 2020.

[2] Z. Daoyi Xu and D. Xu, "Stability analysis of delay neural networks with impulsive effects," *IEEE Transactions on Circuits and Systems II: Express Briefs*, vol. 52, no. 8, pp. 517–521, 2005.

[3] J. Yu, C. Hu, H. Jiang, and Z. Teng, "Stabilization of nonlinear systems with time-varying delays via impulsive control," *Neurocomputing*, vol. 125, pp. 68–71, 2014.

[4] Z. Y. Zhou, Y. W. Wang, W. Yang, and M. J. Hu, "Exponential stability of switched positive systems with unstable modes and distributed delays," *Journal of the Franklin Institute*, vol. 359, no. 1, pp. 66–83, 2022.

[5] Y. He, M. Wu, G.-P. Liu, and J.-H. She, "Output feedback stabilization for a discrete-time system with a time-varying delay," *IEEE Transactions on Automatic Control*, vol. 53, no. 10, pp. 2372–2377, 2008.

[6] F. Hartung, "Linearized stability in periodic functional differential equations with state-dependent delays," *Journal of Computational and Applied Mathematics*, vol. 174, no. 2, pp. 201–211, 2005.

[7] K. Gu, J. Chen, and V. L. Kharitonov, *Stability of Time-Delay Systems*, Springer Science and Business Media, Berlin, Germany, 2003.

[8] W.-H. Chen, J. Wen, X. Lu, and S. Niu, "New stability criteria for linear impulsive systems with interval impulse-delay," *Journal of the Franklin Institute*, vol. 358, no. 13, pp. 6775–6797, 2021.

[9] Y. Zhang, J. Jitao Sun, and G. Gang Feng, "Impulsive control of discrete systems with time delay," *IEEE Transactions on Automatic Control*, vol. 54, no. 4, pp. 830–834, 2009.

[10] A. Weng and J. Sun, "Globally exponential stability of periodic solutions for nonlinear impulsive delay systems," *Nonlinear Analysis: Theory, Methods & Applications*, vol. 67, no. 6, pp. 1938–1946, 2007.

[11] B. Jiang, J. Lu, and Y. Liu, "Exponential stability of delayed systems with average-delay impulses," *SIAM Journal on Control and Optimization*, vol. 58, no. 6, pp. 3763–3784, 2020.

[12] X. Li and S. Song, "Stabilization of delay systems: delay-dependent impulsive control," *IEEE Transactions on Automatic Control*, vol. 62, no. 1, pp. 406–411, 2017.

[13] J. Lu, B. Jiang, and W. X. Zheng, "Potential impacts of delay on stability of impulsive control systems," *IEEE Transactions on Automatic Control*, p. 1, 2021.

[14] J. Lu, D. W. C. Ho, and J. Cao, "A unified synchronization criterion for impulsive dynamical networks," *Automatica*, vol. 46, no. 7, pp. 1215–1221, 2010.

[15] R. Kumar, S. Das, and Y. Cao, "Effects of infinite occurrence of hybrid impulses with quasi-synchronization of parameter mismatched neural networks," *Neural Networks*, vol. 122, pp. 106–116, 2020.

[16] S. Li, J. Sun, and X. Ding, "Improved almost sure stability criteria of stochastic complex-valued dynamical networks with hybrid impulses," *Neurocomputing*, vol. 465, pp. 525–539, 2021.

Hindawi
Complexity
Volume 2022, Article ID 6122921, 11 pages
https://doi.org/10.1155/2022/6122921

Research Article

Event-Based State Estimation for Networked Singularly Perturbed Complex Networks

Zerong Ren

School of Mathematics, Zunyi Normal College, Zunyi 563006, China

Correspondence should be addressed to Zerong Ren; zerongren@163.com

Received 2 March 2022; Revised 22 June 2022; Accepted 27 June 2022; Published 14 July 2022

Academic Editor: Yue Song

This paper deals with the multievent-triggering-based state estimation for a class of discrete-time networked singularly perturbed complex networks (SPCNs). A small singularly perturbed scalar is adopted to establish a discrete-time SPCNs model. To reduce the communication burdens, the data transmission between the sensor and the estimator is managed by a multievent generator function. Depending on the singularly-perturbed-based Lyapunov theory, a sufficient condition is constructed to guarantee that the estimation error is exponentially ultimately bounded in the mean square. Finally, the validity of the developed result is demonstrated by a simulation example.

1. Introduction

A complex network is a set of interconnected nodes coupled by certain network topology, each node of which can be considered as a class of dynamic subsystems. Owing to its complex inherent structure, most systems in real life can be regarded simply as complex networks, including, but not limited to social networks, biological networks, power grid networks, and Internet [1–3]. Consequently, considerable research interest has been stirred over the past few decades and there has been a host of meaningful published achievements of complex networks [4–9].

As far as we know, however, the complex networks with two-time scales receive little attention. However, the two-time scale case of many real-life complex networks [10–12] is continually encountered. For instance, the circuit state variables become faster than the mechanical state variables in electronic power grids, due to the difference in the time scalars on the circuit and the mechanical systems [10]. This can result in the appearance of diverse time-scale subsystems in hosts of electromechanical systems, named fast and slow dynamics. In most of the existing literature [13–15], a singularly perturbed approach is adopted to deal with the two-time scale phenomenon of these real-life systems. In other words, the fast-slow subsystem is distinguished by introducing a small singularly perturbed scalar. Hence, such complex networks can be regarded as SPCNs [16–23].

What is worth mentioning is that a host of the reporting efforts [16–20] merely focuses on the synchronization phenomenon of the SPCNs. However, in some real-world scenarios, the exact state of the SPCNs on account of various factors, like the high number of nodes, disturbances in all directions, and high dimensions, is unavailable [7]. Thus, what we should pay attention to is the state estimation of the SPCNs. On the other hand, we noticed that besides [22, 23], the discrete-time SPCNs get little research concerns. The two important reasons for considering the discrete-time SPCNs are that computational simulation and network communication. Therefore, it is very necessary to investigate the state estimation of the discrete-time SPCNs.

In addition, increasing attention is devoted to the event-triggered protocol (ETP), in which the current packet is released if the ETP-based triggering condition is satisfied [24–26]. Past years have witnessed an increasing interest in ETPs, including static ETPs, dynamic ETPs, and memory ETPs [27–34]. It is noted that in the above-referred ETPs, the triggering parameter is assumed to be the same for all dynamic outputs/states. Nevertheless, such an assumption is difficult to be satisfied, especially in multisensor networks, which contributes to the varying triggering parameters. In

light of above-discussed phenomenon, in this work, in order to save resource consumption and solve the communication congestion, a multi-ETP is employed to deal with the large information communication among nodes of the discrete-time SPCNs, which, to some extent, promotes the current research. As such, a natural and interesting question is how to design a proper multi-ETP for discrete-time SPCNs.

Based on the aforementioned observations, we try our best to develop the multi-ETP-based estimator design issue for the discrete-time SPCNs. Then, the mean square exponential bounded and state estimations are studied by using the Lyapunov function dependent on a singular perturbed parameter. In the end, a numerical example is presented to prove the effectiveness of the state estimator design method. It is worth emphasizing that even though the discrete-time SPCNs are unstable, the result of this work is still efficient. The highlights of our contributions are outlined as follows: (1) A nonlinear discrete-time SPCNs model is developed, which includes nonlinearities of complex networks and multitime scales. (2) As the study progress, the multi-ETP-based state estimation problem for the discrete-time SPCNs with nonlinearities is considered.

Notation: $\mathbb{N}$ refers to a set of all nonnegative integers. $\mathscr{Z}^\top$ represents the transpose of the matrix $\mathscr{Z}$. diag$\{\cdot\}$ symbolizes the diagonal matrix. $\mathbf{He}\{\mathscr{Z}\} = \mathscr{Z}^\top + \mathscr{Z}$. I_m denotes the m-dimensional unit matrix. $\lambda_{\min}(\cdot)/\lambda_{\max}(\cdot)$ denotes the minimal/maximal eigenvalue. $\|\cdot\|$ means Euclidean vector norm. $\mathscr{E}\{\cdot\}$ signifies the mathematical expectation.

2. Problem Formulations

Consider a type of SPCNs composed of N coupled nodes described by

$$\begin{cases} x_i(k+1) = g_\epsilon(x_i(k)) + \sum_{j=1}^{N} \omega_{ij}\Gamma_\epsilon x_j(k) + C_{i,\epsilon}\nu(k), \\ y_i(k) = D_i x_i(k) + E_i\nu(k), \ (i = 1, 2, \ldots, N), \end{cases} \tag{1}$$

where $x_i(k) = [x_{is}^\top(k)x_{if}^\top(k)]^\top \in \mathbb{R}^{n_x}$, $y_i(k) = [y_{is}^\top(k)y_{if}^\top(k)]^\top \in \mathbb{R}^{n_y}$, $g_\epsilon(x_i(k)) = \begin{bmatrix} f(x_{is}(k)) + Ax_{if}(k) \\ \epsilon(h(x_{is}(k)) + Bx_{if}(k)) \end{bmatrix}$, $\Gamma_\epsilon = \begin{bmatrix} \Gamma_{11} & \Gamma_{12} \\ \epsilon\Gamma_{21} & \epsilon\Gamma_{22} \end{bmatrix}$, $C_{i,\epsilon} = \begin{bmatrix} C_{is} \\ \epsilon C_{if} \end{bmatrix}$, $D_i = \mathrm{diag}\{D_{is}, D_{if}\}$, $E_i = \begin{bmatrix} E_{is} \\ E_{if} \end{bmatrix}$, $x_{is}(k) \in \mathbb{R}^{n_{x_s}}$, and $x_{if}(k) \in \mathbb{R}^{n_{x_f}}$ ($n_x = n_{x_s} + n_{x_f}$) refer to the slow state and the fast state of node i, respectively. $y_{is}(k) \in \mathbb{R}^{n_{y_s}}$ and $y_{if}(k) \in \mathbb{R}^{n_{y_f}}$ ($n_y = n_{y_s} + n_{y_f}$) mean the measurement outputs of node i, ϵ is a singular perturbation parameter, and $\nu(k) \in \mathbb{R}^{n_\nu}$ signifies the bound disturbance input belonging to $l_2[0, \infty)$, which meets $\|\nu(k)\|^2 \le \overline{\nu}$. Γ_ϵ refers to an inner-coupling matrix with given dimensions. A, B, $C_{i,\epsilon}$, D_i, and E_i are known matrices with suitable dimensions.

The network topology $\mathfrak{W} = \{\mathscr{N}, \mathscr{X}, \mathscr{W}\}$ is devoted to reflect the outer coupling phenomenon of the SPCNs. $\mathscr{N} = \{1, 2, \ldots, N\}$ and $\mathscr{X} \subseteq \mathscr{N} \times \mathscr{N}$ symbolize the sets of nodes and edges. For any $(i, j \in \mathscr{N})$, the out-coupled configuration matrix $\mathscr{W} = \{\omega_{ij}\}$ is symmetric if $\omega_{ij} = \omega_{ji} > 0$, which satisfies

$$\omega_{ii} = -\sum_{j=1, j\neq i}^{N} \omega_{ij}, \tag{2}$$

where $\omega_{ij} > 0 (\forall i \neq j)$ implies a connection between nodes j and i; otherwise, $\omega_{ij} = 0$.

Assumption 1 (see [23]). The nonlinear sector-valued functions $f(\cdot)$: $\mathbb{R}^{n_{x_s}} \longrightarrow \mathbb{R}^{n_{x_s}}$ and $h(\cdot)$: $\mathbb{R}^{n_{x_s}} \longrightarrow \mathbb{R}^{n_{x_f}}$ of SPCNs (1) satisfy the following assumption:

$$\begin{aligned} &\left[f(x_{is}(k)) - f(x_{js}(k)) - \Lambda_1(x_{is}(k) - x_{js}(k))\right]^\top \left[f(x_{is}(k)) - f(x_{js}(k)) - \Lambda_2(x_{is}(k) - x_{js}(k))\right] \le 0, \\ &\left[h(x_{is}(k)) - h(x_{js}(k)) - \Upsilon_1(x_{is}(k) - x_{js}(k))\right]^\top \left[h(x_{is}(k)) - h(x_{js}(k)) - \Upsilon_2(x_{is}(k) - x_{js}(k))\right] \le 0, \end{aligned} \tag{3}$$

where $x_{is}(k)$, $x_{js}(k) \in \mathbb{R}^{n_{x_s}}$, $f(0) = 0$, $h(0) = 0$, Λ_ℓ, and $\Upsilon_\ell (\ell = 1, 2)$ are constant matrices.

In this paper, for the sake of saving the communication resources between the sensors and estimators, a multievent-triggered approach is presented to reduce transmission energy. The triggering instant series of node i can be assumed as $0 \le k_0^i < k_1^i < \ldots < k_t^i < \ldots, (i = 1, 2, \ldots, N)$ where the new transmitted instant k_{t+1}^i can be formulated as

$$k_{t+1}^i = \min\{k \in [0, \mathbb{N}] | k > k_t^i, \theta_i - \varepsilon_i^\top(k)\Phi_i\varepsilon_i(k) < 0\}. \tag{4}$$

With $k_0^i = 0$, $\theta_i \in [0, 1]$ is the given parameter of the i-th node, $\Phi_i = \mathrm{diag}\{\Phi_{is}, \Phi_{if}\} > 0$ is a weighting matrix of the i-th node to be determined, and $\varepsilon_i(k) \triangleq y_i(k) - y_i(k_t^i) \triangleq [\varepsilon_{is}^\top(k)\varepsilon_{if}^\top(k)]^\top$ with $y_i(k_t^i)$ referring to the latest transmitted measurement of node i. Hence, for $k \in [k_t^i, k_{t+1}^i)$,

$$\theta_i - \varepsilon_i^\top(k)\Phi_i\varepsilon_i(k) \ge 0. \tag{5}$$

Remark 1. Note that different from the existing static ETP, the multievent-triggered protocol is studied in (2). The proposed triggering protocol can be seen as a generalized framework of ETP, which cover the existing static ETP as a special case (i.e., $i = 1$).

Subsequently, based on the multievent-triggered approach, a state estimator is constructed as

$$\hat{x}_i(k+1) = g_\epsilon(\hat{x}_i(k)) + \sum_{j=1}^{N} \omega_{ij}\Gamma_\epsilon \hat{x}_j(k) + K_i\left(y_i\left(k_t^i\right) - D_i\hat{x}_i(k)\right), (i = 1, 2, \ldots, N), \tag{6}$$

where $\hat{x}_i(k) = [\hat{x}_{is}^\top(k)\hat{x}_{if}^\top(k)]^\top$ with $\hat{x}_{is}(k)$ and $\hat{x}_{if}(k)$ representing the state estimations of $x_{is}(k)$ and $x_{if}(k)$, respectively. $K_i = \mathrm{diag}\{K_{is}, K_{if}\}$ means the estimator gain of the i-th node to be judged.

Let

$$\begin{aligned}
\tilde{e}_i(k) &= \left[\tilde{e}_{is}^\top(k)\tilde{e}_{if}^\top(k)\right]^\top,\\
\tilde{e}_{is}(k) &= x_{is}(k) - \hat{x}_{is}(k),\\
\tilde{e}_{if}(k) &= x_{if}(k) - \hat{x}_{if}(k),\\
\mathfrak{A}(k) &= \left[\mathfrak{A}_1^\top(k)\mathfrak{A}_2^\top(k)\ldots\mathfrak{A}_N^\top(k)\right]^\top(\tilde{e}, \varepsilon,),\\
\tilde{\mathfrak{B}}(\tilde{e}_{is}(k)) &= \mathfrak{B}(x_{is}(k)) - \mathfrak{B}(\hat{x}_{is}(k))(\mathfrak{B} = f, h),\\
\tilde{g}_\epsilon^\top(\tilde{e}_{is}(k)) &= \left[\tilde{f}^\top(\tilde{e}_{is}(k))\epsilon\tilde{h}^\top(\tilde{e}_{is}(k))\right],\\
\overrightarrow{g}_\epsilon(\tilde{e}_s(k)) &= \left[\tilde{g}_\epsilon^\top(\tilde{e}_{1s}(k))\tilde{g}_\epsilon^\top(\tilde{e}_{2s}(k))\ldots\tilde{g}_\epsilon^\top(\tilde{e}_{Ns}(k))\right]^\top.
\end{aligned} \tag{7}$$

Combining (1) and (4), the dynamics of the estimation error can be built as

$$\tilde{e}(k+1) = \overrightarrow{g}_\epsilon(\tilde{e}_s(k)) + (\mathscr{W}\otimes\Gamma_\epsilon + I_N\otimes G_\epsilon - KD)\tilde{e}(k) + (C_\epsilon - KE)\nu(k) + K\varepsilon(k), \tag{8}$$

where

$$\begin{aligned}
C_\epsilon &= \left[C_{1,\epsilon}^\top C_{2,\epsilon}^\top\ldots C_{N,\epsilon}^\top\right]^\top,\\
\mathfrak{K} &= \mathrm{diag}\{\mathfrak{K}_1, \mathfrak{K}_2, \ldots, \mathfrak{K}_N\}(\mathfrak{K} = K, D),\\
E &= \left[E_1^\top E_2^\top\ldots E_N^\top\right]^\top,\\
G_\epsilon &= \begin{bmatrix} 0 & A \\ 0 & \epsilon B \end{bmatrix}.
\end{aligned} \tag{9}$$

In the sequel, one reschedules the order of dynamic estimation errors (8). Denote $\mathscr{T} = \mathscr{T}_1 \times \mathscr{T}_2 \times \cdots \times \mathscr{T}_N$, with $\mathscr{T}_\ell \in \mathbb{R}^{Nn_x\otimes Nn_x}(\ell = 1, 2, \ldots, N)$ being row-switching elementary matrices and $\mathscr{T}$ being invertible. Then, one has

$$\mathscr{T}\tilde{e}(k+1) = \mathscr{T}\overrightarrow{g}_\epsilon(\tilde{e}_s(k)) + \mathscr{T}(\mathscr{W}\otimes\Gamma_\epsilon + I_N\otimes G_\epsilon - KD)\mathscr{T}^{-1}\mathscr{T}\tilde{e}(k) + \mathscr{T}(C_\epsilon - KE)\nu(k) + \mathscr{T}K\varepsilon(k), \tag{10}$$

which yields

$$e(k+1) = \mathscr{A}_\epsilon e(k) + \mathscr{J}_1\mathbf{f}(e_s(k)) + \epsilon\mathscr{J}_2\mathbf{h}(e_s(k)) + \mathscr{C}_\epsilon\nu(k) + \mathscr{K}\bar{\varepsilon}(k), \tag{11}$$

where

$$
\begin{aligned}
e(k) &= \left[\widetilde{e}_{1s}^{\top}(k)\widetilde{e}_{2s}^{\top}(k)\ldots\widetilde{e}_{Ns}^{\top}(k)\widetilde{e}_{1f}^{\top}(k)\widetilde{e}_{2f}^{\top}(k)\ldots\widetilde{e}_{Nf}^{\top}(k)\right]^{\top},\\
\mathfrak{D}(e_s(k)) &= \left[\widetilde{\mathfrak{D}}^{\top}(\widetilde{e}_{1s}(k))\widetilde{\mathfrak{D}}^{\top}(\widetilde{e}_{2s}(k))\ldots\widetilde{\mathfrak{D}}^{\top}(\widetilde{e}_{Ns}(k))\right]^{\top}(\mathfrak{D}=f,h),\\
\overline{\varepsilon}(k) &= \left[\varepsilon_{1s}^{\top}(k)\varepsilon_{2s}^{\top}(k)\ldots\varepsilon_{Ns}^{\top}(k)\varepsilon_{1f}^{\top}(k)\varepsilon_{2f}^{\top}(k)\ldots\varepsilon_{Nf}^{\top}(k)\right]^{\top},\\
\mathscr{A}_{\epsilon} &= \begin{bmatrix} -K_sD_s+\mathscr{W}\otimes\Gamma_{11} & I_N\otimes A+\mathscr{W}\otimes\Gamma_{12}\\ \epsilon(\mathscr{W}\otimes\Gamma_{21}) & \epsilon(I_N\otimes B+\mathscr{W}\otimes\Gamma_{22})-K_fD_f\end{bmatrix},\\
\mathscr{I}_1 &= \begin{bmatrix} I_{Nn_{x_s}}\\ 0_{Nn_{x_f}\times Nn_{x_s}}\end{bmatrix},\\
\mathscr{I}_2 &= \begin{bmatrix} 0_{Nn_{x_s}\times Nn_{x_f}}\\ I_{Nn_{x_f}}\end{bmatrix},\\
\mathscr{C}_{\epsilon} &= \begin{bmatrix} C_s-K_sE_s\\ \epsilon C_f-K_fE_f\end{bmatrix},\\
\mathscr{K} &= \operatorname{diag}\{K_s,K_f\},\\
\mathfrak{E}_{\ell} &= \operatorname{diag}\{\mathfrak{E}_{1\ell},\mathfrak{E}_{2\ell},\ldots,\mathfrak{E}_{N\ell}\}(\mathfrak{E}=K,D,\ell=s,f),\\
\mathfrak{F}_{\ell} &= \left[\mathfrak{F}_{1\ell}^{\top}\mathfrak{F}_{2\ell}^{\top}\ldots\mathfrak{F}_{N\ell}^{\top}\right]^{\top}(\mathfrak{F}=C,E,\ell=s,f).
\end{aligned}
\tag{12}
$$

To facilitate the derivation of the main results, the following definition and lemma are introduced.

Definition 1 (see [35]). Estimation error dynamics (7) is exponentially ultimately bounded in mean square (EUBMS), if for any solution $e(k)$ with initial state $e(0)$,

$$
\mathscr{E}\left\{\|e(k)\|^2\right\}\le\alpha\|e(0)\|^2\beta^k+\gamma(k),\lim_{k\longrightarrow\infty}\gamma(k)=\overline{\gamma},\tag{13}
$$

holds, where $\alpha>0$, $\beta\in[0,1)$, and $\overline{\gamma}>0$ imply the mean square asymptotic upper bound of (11).

Lemma 1 (see [23]). *Combined with Assumption 1, the nonlinear functions* $\mathbf{f}(e_s(k))$ *and* $\mathbf{h}(e_s(k))$ *of estimation error dynamics (7) satisfy the conditions as follows:*

$$
\begin{aligned}
&\begin{bmatrix} e^{\top}(k) & \mathbf{f}^{\top}(e_s(k))\end{bmatrix}\begin{bmatrix} F_1 & *\\ F_2 & I_{Nn_{x_s}}\end{bmatrix}\begin{bmatrix} e(k)\\ \mathbf{f}(e_s(k))\end{bmatrix}\le 0,\\
&\begin{bmatrix} e^{\top}(k) & \mathbf{h}^{\top}(e_s(k))\end{bmatrix}\begin{bmatrix} H_1 & *\\ H_2 & I_{Nn_{x_f}}\end{bmatrix}\begin{bmatrix} e(k)\\ \mathbf{h}(e_s(k))\end{bmatrix}\le 0,
\end{aligned}
\tag{14}
$$

where

$$
\begin{aligned}
F_1 &= \operatorname{diag}\left\{I_N\otimes\left(\frac{\Lambda_1^{\top}\Lambda_2+\Lambda_2^{\top}\Lambda_1}{2}\right),0_{Nn_{x_f}}\right\},\\
F_2 &= \begin{bmatrix} -I_N\otimes\left(\frac{\Lambda_1+\Lambda_2}{2}\right) & 0_{Nn_{x_s}}\end{bmatrix},\\
H_1 &= \operatorname{diag}\left\{I_N\otimes\left(\frac{\Upsilon_1^{\top}\Upsilon_2+\Upsilon_2^{\top}\Upsilon_1}{2}\right),0_{Nn_{x_f}}\right\},\\
H_2 &= \begin{bmatrix} -I_N\otimes\left(\frac{\Upsilon_1+\Upsilon_2}{2}\right) & 0_{Nn_{x_f}}\end{bmatrix}.
\end{aligned}
\tag{15}
$$

Lemma 2 (see [23]). *For any matrices* $\mathscr{H}$ *and* $\mathscr{G}$ *and a scalar* $\epsilon_0>0$, $\forall\epsilon\in(0,\epsilon_0]$, *if* $\mathscr{H}\le 0$ *and* $\mathscr{H}+\epsilon_0\mathscr{G}<0$ *hold, it yields* $\mathscr{H}+\epsilon<0$.

3. Main Results

In this section, a sufficient condition is presented to guarantee that the estimation error dynamics (7) is exponentially ultimately bounded in mean square and the desired state estimator will be designed.

Theorem 1. *For given $\epsilon > 0$ and $c \in [0, 1)$, estimation error dynamics (7) is EUBMS, if there exist scalars $\lambda_\varsigma > 0\,(\varsigma = 1, 2, 3)$ and $\kappa > 0$ and matrices $P_\epsilon > 0$, such that*

$$\begin{bmatrix} -(1-c)P_\epsilon - \lambda_1 F_1 - \lambda_2 H_1 & * & * & * & * \\ -\lambda_1 F_2 & -\lambda_1 I_{Nn_{x_s}} & * & * & * \\ -\lambda_2 H_2 & 0 & -\lambda_2 I_{Nn_{x_f}} & * & * \\ 0 & 0 & 0 & -\lambda_3 \Phi & * \\ \sqrt{1+\kappa}\,\mathscr{A}_\epsilon & \sqrt{1+\kappa}\,\mathscr{J}_1 & \sqrt{1+\kappa}\,\epsilon\mathscr{J}_2 & \sqrt{1+\kappa}\,\mathscr{K} & -P_\epsilon^{-1} \end{bmatrix} < 0, \tag{16}$$

where

$$\Phi = \operatorname{diag}\left\{\Phi_{1s}, \Phi_{2s}, \ldots, \Phi_{Ns}, \Phi_{1f}, \Phi_{2f}, \ldots, \Phi_{Nf}\right\}. \tag{17}$$

Proof. Firstly, construct the following Lyapunov functional candidate:

$$V(k) = e^\top(k) P_\epsilon e(k). \tag{18}$$

According to (5), another equivalent form of the event-triggering condition is as follows:

$$\sum_{i=1}^{N} \theta_i - \bar{\varepsilon}^\top(k)\Phi\bar{\varepsilon}(k) \geq 0. \tag{19}$$

Along the trajectory of (11), calculating the mathematical expectation of the difference of $V(k)$, one gains that

$$\begin{aligned}
\mathscr{E}\{\Delta V(k)\} &= \mathscr{E}\{V(k+1) - (1-c)V(k) - cV(k)\} \\
&= \mathscr{E}\{e^\top(k+1)P_\epsilon e(k+1) - (1-c)e^\top(k)P_\epsilon e(k) - cV(k)\} \\
&\leq \mathscr{E}\{e^\top(k+1)P_\epsilon e(k+1) - (1-c)e^\top(k)P_\epsilon e(k) - cV(k)\} \\
&= \mathscr{E}\Big\{\big(\mathscr{A}_\epsilon e(k) + \mathscr{J}_1\mathbf{f}(e_s(k)) + \epsilon\mathscr{J}_2\mathbf{h}(e_s(k)) + \mathscr{C}_\epsilon\nu(k) + \mathscr{K}\bar{\varepsilon}(k)\big)^\top P_\epsilon\big(\mathscr{A}_\epsilon e(k) + \mathscr{J}_1\mathbf{f}(e_s(k)) \\
&\quad + \epsilon\mathscr{J}_2\mathbf{h}(e_s(k)) + \mathscr{C}_\epsilon\nu(k) + \mathscr{K}\bar{\varepsilon}(k)\big) - (1-c)e^\top(k)P_\epsilon e(k) - cV(k)\Big\} \\
&\leq \mathscr{E}\Big\{\big(\mathscr{A}_\epsilon e(k) + \mathscr{J}_1\mathbf{f}(e_s(k)) + \epsilon\mathscr{J}_2\mathbf{h}(e_s(k)) + \mathscr{K}\bar{\varepsilon}(k)\big)^\top P_\epsilon\big(\mathscr{A}_\epsilon e(k) + \mathscr{J}_1\mathbf{f}(e_s(k))\big) + \epsilon\mathscr{J}_2\mathbf{h}(e_s(k))\big) \\
&\quad + \mathscr{K}\bar{\varepsilon}(k)\big) + \nu^\top(k)\mathscr{C}_\epsilon^\top P_\epsilon\mathscr{C}_\epsilon\nu(k) + 2\big(\mathscr{A}_\epsilon e(k) + \mathscr{J}_1\mathbf{f}(e_s(k))\big) + \epsilon\mathscr{J}_2\mathbf{h}(e_s(k)) + \mathscr{K}\bar{\varepsilon}(k)\big)^\top P_\epsilon\mathscr{C}_\epsilon\nu(k) \\
&\quad - (1-c)e^\top(k)P_\epsilon e(k) - cV(k)\Big\}.
\end{aligned} \tag{20}$$

Depending on Young's inequality, the following inequality holds:

$$\begin{aligned}
&2\big(\mathscr{A}_\epsilon e(k) + \mathscr{J}_1\mathbf{f}(e_s(k)) + \epsilon\mathscr{J}_2\mathbf{h}(e_s(k)) + \mathscr{K}\bar{\varepsilon}(k)\big)^\top P_\epsilon\mathscr{C}_\epsilon\nu(k) \\
&\quad \leq \kappa\big(\mathscr{A}_\epsilon e(k) + \mathscr{J}_1\mathbf{f}(e_s(k)) + \epsilon\mathscr{J}_2\mathbf{h}(e_s(k)) + \mathscr{K}\bar{\varepsilon}(k)\big)^\top P_\epsilon\big(\mathscr{A}_\epsilon e(k) + \mathscr{J}_1\mathbf{f}(e_s(k)) + \epsilon\mathscr{J}_2\mathbf{h}(e_s(k)) + \mathscr{K}\bar{\varepsilon}(k)\big)\big) \\
&\qquad + \frac{1}{\kappa}\big(\nu^\top(k)\mathscr{C}_\epsilon^\top P_\epsilon\mathscr{C}_\epsilon\nu(k)\big).
\end{aligned} \tag{21}$$

Combining (19) and (21) and Lemma 1, we obtain that

$$\mathscr{E}\{\Delta V(k)\} \le \mathscr{E}\left\{\begin{array}{l}(1+\kappa)\left(\mathscr{A}_\epsilon e(k)+\mathscr{J}_1\mathbf{f}(e_s(k))+\epsilon\mathscr{J}_2\mathbf{h}(e_s(k))+\mathscr{K}\bar{\varepsilon}(k)\right)^\top P_\epsilon\left(\mathscr{A}_\epsilon e(k)+\mathscr{J}_1\mathbf{f}(e_s(k))+\epsilon\mathscr{J}_2\mathbf{h}(e_s(k))+\mathscr{K}\bar{\varepsilon}(k)\right)\\ +\left(1+\dfrac{1}{\kappa}\right)\nu^\top(k)\mathscr{C}_\epsilon^\top P_\epsilon\mathscr{C}_\epsilon\nu(k)-(1-c)e^\top(k)P_\epsilon e(k)-cV(k)-\lambda_1\left(\begin{bmatrix}e^\top(k) & \mathbf{f}^\top(e_s(k))\end{bmatrix}\begin{bmatrix}F_1 & * \\ F_2 & I_{Nn_{x_s}}\end{bmatrix}\begin{bmatrix}e(k)\\ \mathbf{f}(e_s(k))\end{bmatrix}\right)\\ -\lambda_2\left(\begin{bmatrix}e^\top(k) & \mathbf{h}^\top(e_s(k))\end{bmatrix}\begin{bmatrix}H_1 & * \\ H_2 & I_{Nn_{x_f}}\end{bmatrix}\begin{bmatrix}e(k)\\ \mathbf{h}(e_s(k))\end{bmatrix}\right)+\lambda_3\left(\sum_{i=1}^{N}\theta_i-\bar{\varepsilon}^\top(k)\Phi\bar{\varepsilon}(k)\right)\end{array}\right\} \tag{22}$$

$$= \aleph^\top(k)\Xi_\epsilon\aleph(k)-cV(k)+\varrho,$$

where

$$\aleph(k)=\left[e^\top(k)\mathbf{f}^\top(e_s(k))\mathbf{h}^\top(e_s(k))\bar{\varepsilon}^\top(k)\right]^\top,$$

$$\varrho=\lambda_3\sum_{i=1}^{N}\theta_i+\left(1+\frac{1}{\kappa}\right)\lambda_{\max}\{\mathscr{C}_\epsilon^\top P_\epsilon\mathscr{C}_\epsilon\}\overline{\nu},$$

$$\Xi_\epsilon=\begin{bmatrix}\Xi_\epsilon^{11} & * & * & * \\ (1+\kappa)\mathscr{J}_1^\top P_\epsilon\mathscr{A}_\epsilon-\lambda_1F_2 & (1+\kappa)\mathscr{J}_1^\top P_\epsilon\mathscr{J}_1-\lambda_1I_{Nn_{x_s}} & * & * \\ (1+\kappa)\epsilon\mathscr{J}_2^\top P_\epsilon\mathscr{A}_\epsilon-\lambda_2H_2 & (1+\kappa)\epsilon\mathscr{J}_2^\top P_\epsilon\mathscr{J}_1 & (1+\kappa)\epsilon^2\mathscr{J}_2^\top P_\epsilon\mathscr{J}_2-\lambda_2I_{Nn_{x_f}} & * \\ (1+\kappa)\mathscr{K}^\top P_\epsilon\mathscr{A}_\epsilon & (1+\kappa)\mathscr{K}^\top P_\epsilon\mathscr{J}_1 & (1+\kappa)\mathscr{K}^\top P_\epsilon\epsilon\mathscr{J}_2 & (1+\kappa)\mathscr{K}^\top P_\epsilon\mathscr{K}-\lambda_3\Phi\end{bmatrix}, \tag{23}$$

$$\Xi_\epsilon^{11}=(1+\kappa)\mathscr{A}_\epsilon^\top P_\epsilon\mathscr{A}_\epsilon-(1-c)P_\epsilon-\lambda_1F_1-\lambda_2H_1.$$

Applying the Schur complement lemma to (16), it is clear that $\Xi_\epsilon<0$. Consequently, one has

$$\mathscr{E}\{\Delta V(k)\} \le -cV(k)+\varrho, \tag{24}$$

which yields

$$\mathscr{E}\{V(k+1)\} \le (1-c)V(k)+\varrho. \tag{25}$$

Then, it follows from (25) that

$$\mathscr{E}\{V(k)\} \le (1-c)^kV(0)+\frac{1-(1-c)^k}{c}\varrho. \tag{26}$$

Moreover, it is easy to obtain that $V(k)\ge\lambda_{\min}\{P_\epsilon\}e^\top(k)e(k)$ and $V(0)\le\lambda_{\max}\{P_\epsilon\}e^\top(0)e(0)$; combining (26), it yields that

$$\mathscr{E}\left\{\|e(k)\|^2\right\} \le \frac{(1-c)^k\lambda_{\max}\{P_\epsilon\}}{\lambda_{\min}\{P_\epsilon\}}\|e(0)\|^2+\frac{1-(1-c)^k}{c\lambda_{\min}\{P_\epsilon\}}\varrho. \tag{27}$$

Consequently, estimation error dynamics (7) is EUBMS, and $\overline{\gamma}=1/c\lambda_{\min}\{P_\epsilon\}\varrho$ is the mean square asymptotic upper bound of (7), which completes the proof. □

Theorem 2. *For $\forall\epsilon\in(0,\epsilon_0]$ with the upper bound $\epsilon_0>0$ and $c\in[0,1)$, estimation error dynamics (7) is EUBMS, if there exist scalars $\lambda_\varsigma(\varsigma=1,2,3)$ and $\kappa>0$ and matrices $\breve{P}=\begin{bmatrix}\breve{P}_{11} & * \\ \breve{P}_{21} & \breve{P}_{22}\end{bmatrix}$, $\widehat{P}=\begin{bmatrix}\widehat{P}_{11} & * \\ \widehat{P}_{21} & \widehat{P}_{22}\end{bmatrix}$, $X_\ell=diag\{X_{\ell1},X_{\ell2},\ldots,X_{\ell N}\}$ $(\ell=1,2)$, and $\overline{K}_{i\wp}(i=1,2,\ldots,N,\wp=s,f)$, such that*

$$\breve{P} \geq 0, \breve{P} + \epsilon_0 \widehat{P} > 0, \tag{28}$$

$$\begin{bmatrix} -(1-c)\breve{P} - \lambda_1 F_1 - \lambda_2 H_1 & * & * & * & * \\ -\lambda_1 F_2 & -\lambda_1 I_{Nn_{x_s}} & * & * & * \\ -\lambda_2 H_2 & 0 & -\lambda_2 I_{Nn_{x_f}} & * & * \\ 0 & 0 & 0 & -\lambda_3 \Phi & * \\ \sqrt{1+\kappa}\,\breve{\mathscr{A}} & \sqrt{1+\kappa}\, X\mathscr{J}_1 & 0 & \sqrt{1+\kappa}\,\widetilde{\mathscr{K}} & \breve{P} - X - X^\top \end{bmatrix} \leq 0, \tag{29}$$

$$\begin{bmatrix} -(1-c)\left(\breve{P} + \epsilon_0 \widehat{P}\right) - \lambda_1 F_1 - \lambda_2 H_1 & * & * & * & * \\ -\lambda_1 F_2 & -\lambda_1 I_{Nn_{x_s}} & * & * & * \\ -\lambda_2 H_2 & 0 & -\lambda_2 I_{Nn_{x_f}} & * & * \\ 0 & 0 & 0 & -\lambda_3 \Phi & * \\ \sqrt{1+\kappa}\left(\breve{\mathscr{A}} + \epsilon_0 \widehat{\mathscr{A}}\right) & \sqrt{1+\kappa}\, X\mathscr{J}_1 & \sqrt{1+\kappa}\,\epsilon_0 X\mathscr{J}_2 & \sqrt{1+\kappa}\,\widetilde{\mathscr{K}} & \breve{P} + \epsilon_0 \widehat{P} - X - X^\top \end{bmatrix} < 0, \tag{30}$$

where

$$\begin{aligned} X &= \operatorname{diag}\{X_1, X_2\}, \\ \overline{K}_\wp &= \operatorname{diag}\left\{\overline{K}_{1\wp}, \overline{K}_{2\wp}, \ldots, \overline{K}_{N\wp}\right\}, (\wp = s, f), \\ \breve{\mathscr{A}} &= \begin{bmatrix} -\overline{K}_s D_s + X_1(\mathscr{W} \otimes \Gamma_{11}) & X_1(I_N \otimes A + \mathscr{W} \otimes \Gamma_{12}) \\ 0 & -\overline{K}_f D_f \end{bmatrix}, \\ \widehat{\mathscr{A}} &= \begin{bmatrix} 0 & 0 \\ X_2(\mathscr{W} \otimes \Gamma_{21}) & X_2(I_N \otimes B + \mathscr{W} \otimes \Gamma_{22}) \end{bmatrix}, \\ \widetilde{\mathscr{K}} &= \operatorname{diag}\left\{\overline{K}_s, \overline{K}_f\right\}. \end{aligned} \tag{31}$$

Moreover, the estimator gain matrices are calculated as

$$\begin{aligned} K_{is} &= X_{1i}^{-1} \overline{K}_{is}, \\ K_{if} &= X_{2i}^{-1} \overline{K}_{if}, \\ &(i = 1, 2, \ldots, N). \end{aligned} \tag{32}$$

Proof. From (28)–(30) and Lemma 2, it follows that for $\forall \epsilon \in (0, \epsilon_0]$, the following conditions hold:

$$\begin{aligned} &P_\epsilon = \breve{P} + \epsilon \widehat{P} > 0 \\ &\cdot \begin{bmatrix} -(1-c)(\breve{P} + \epsilon \widehat{P}) - \lambda_1 F_1 - \lambda_2 H_1 & * & * & * & * \\ -\lambda_1 F_2 & -\lambda_1 I_{Nn_{x_s}} & * & * & * \\ -\lambda_2 H_2 & 0 & -\lambda_2 I_{Nn_{x_f}} & * & * \\ 0 & 0 & 0 & -\lambda_3 \Phi & * \\ \sqrt{1+\kappa}\,(\breve{\mathscr{A}} + \epsilon \widehat{\mathscr{A}}) & \sqrt{1+\kappa}\, X\mathscr{J}_1 & \sqrt{1+\kappa}\,\epsilon X\mathscr{J}_2 & \sqrt{1+\kappa}\,\widetilde{\mathscr{K}} & \breve{P} + \epsilon \widehat{P} - X - X^\top \end{bmatrix} < 0. \end{aligned} \tag{33}$$

Substituting (32) into (33) and noticing that $-XP_\epsilon^{-1}X^\top \leq P_\epsilon - \mathbf{He}\{X\}$, one has

$$\begin{bmatrix} -(1-c)P_\epsilon - \lambda_1 F_1 - \lambda_2 H_1 & * & * & * & * \\ -\lambda_1 F_2 & -\lambda_1 I_{Nn_{x_s}} & * & * & * \\ -\lambda_2 H_2 & 0 & -\lambda_2 I_{Nn_{x_f}} & * & * \\ 0 & 0 & 0 & -\lambda_3 \Phi & * \\ \sqrt{1+\kappa}\, X\mathscr{A}_\epsilon & \sqrt{1+\kappa}\, X\mathscr{J}_1 & \sqrt{1+\kappa}\,\epsilon X\mathscr{J}_2 & \sqrt{1+\kappa}\, X\mathscr{K} & -XP_\epsilon^{-1}X^\top \end{bmatrix} < 0. \tag{34}$$

Recalling (29), it is clear that $\breve{P} - X - X^{\top} < 0$ with $\breve{P} \geq 0$. Then, X is invertible.

Premultiplying and postmultiplying (34) by $\mathrm{diag}\left\{I_{Nn_x}, I_{Nn_{x_s}}, I_{2Nn_{x_f}}, I_{Nn_y}, X^{-1}\right\}$, its transposes yields (16). Therefore, inequality (16) can be guaranteed if (28)–(30) hold. This completes the proof. □

4. Numerical Example

Similar to [23], consider SPCNs (1) with three nodes and the following parameters:

$$
\begin{aligned}
A &= \begin{bmatrix} 1.2 & 0.45 \end{bmatrix}, \\
B &= \begin{bmatrix} 1.3 & 0.6 \\ 2.3 & 0.9 \end{bmatrix}, \\
C_{1s} &= 0.2, \\
C_{2s} &= 0.1, \\
C_{3s} &= 0.4, \\
C_{1f} &= \begin{bmatrix} 0.86 \\ 1.15 \end{bmatrix}, \\
C_{2f} &= \begin{bmatrix} 0.5 \\ 1.75 \end{bmatrix}, \\
C_{3f} &= \begin{bmatrix} 0.02 \\ 0.05 \end{bmatrix}, \\
D_{1s} &= \begin{bmatrix} 2 \\ 1.2 \end{bmatrix}, \\
D_{2s} &= \begin{bmatrix} 0.9 \\ 2.1 \end{bmatrix}, \\
D_{3s} &= \begin{bmatrix} 1.6 \\ 1.62 \end{bmatrix}, \\
D_{1f} &= \begin{bmatrix} 2.4 & 1 \end{bmatrix}, \\
D_{2f} &= \begin{bmatrix} -1.4 & 0.6 \end{bmatrix}, \\
D_{3f} &= \begin{bmatrix} 2.3 & 2 \end{bmatrix}, \\
E_{1s} &= \begin{bmatrix} 0.8 \\ 1 \end{bmatrix}, \\
E_{2s} &= \begin{bmatrix} 0.5 \\ 0.1 \end{bmatrix}, \\
E_{3s} &= \begin{bmatrix} 0.4 \\ -1 \end{bmatrix}, \\
E_{1f} &= 0.2, \\
E_{1f} &= 0.4, \\
E_{1f} &= 0.25.
\end{aligned} \tag{35}
$$

The out-coupled configuration matrix $\mathscr{W}$ of SPCNs (1) and its inner-coupling matrix, respectively, are selected as follows:

$$
\begin{aligned}
\Gamma_{11} &= 0.45, \\
\Gamma_{12} &= \begin{bmatrix} 0.2 & 0.6 \end{bmatrix}, \\
\Gamma_{21} &= \begin{bmatrix} 0.1 \\ 0.5 \end{bmatrix}, \\
\Gamma_{22} &= \begin{bmatrix} 0.6 & 0.2 \\ 0.4 & 0.25 \end{bmatrix}, \\
\mathscr{W} &= \begin{bmatrix} -0.2 & 0.1 & 0.1 \\ 0.1 & -0.2 & 0.1 \\ 0.1 & 0.1 & -0.2 \end{bmatrix}.
\end{aligned} \tag{36}
$$

In light of Assumption 1, the nonlinear vector-valued functions are chosen as

$$
\begin{aligned}
f\left(x_{is}(k)\right) &= 0.8x_{is}(k) - \tanh\left(0.4x_{is}(k)\right), \\
h\left(x_{is}(k)\right) &= \begin{bmatrix} 0.3x_{is}(k) - \tanh\left(0.1x_{is}(k)\right) \\ 0.4x_{is}(k) - \tanh\left(0.2x_{is}(k)\right) \end{bmatrix}, \quad (i = 1, 2, \ldots, N),
\end{aligned} \tag{37}
$$

and $\Lambda_1 = 0.5, \Lambda_2 = 0.58, \Upsilon_1 = \begin{bmatrix} 0.2 & 0.2 \end{bmatrix}^{\top}$, and $\Upsilon_2 = \begin{bmatrix} 0.5 & 0.41 \end{bmatrix}^{\top}$. The event-triggered thresholds are set as $\theta_1 = 0.17$, $\theta_2 = 0.104$, and $\theta_3 = 0.5$, and the weighting matrices are calculated as $\Phi_i = \mathrm{diag}\{44.1124, 44.1124, 44.1124\}\,(i = 1, 2, 3)$. Other parameters are given as follows: $\epsilon_0 = 0.0193$ and $c = 0.1$.

According to Theorem 2, the gain matrices of state estimator (6) can be obtained as

$$
\begin{aligned}
K_s &= \begin{bmatrix} 0.1755 & 0.1053 & 0 & 0 & 0 & 0 \\ 0 & 0 & 0.0824 & 0.1924 & 0 & 0 \\ 0 & 0 & 0 & 0 & 0.1473 & 0.1491 \end{bmatrix}, \\
K_f &= \begin{bmatrix} 0.0107 & 0 & 0 \\ 0.0290 & 0 & 0 \\ 0 & -0.0179 & 0 \\ 0 & -0.1104 & 0 \\ 0 & 0 & 0.0102 \\ 0 & 0 & 0.0222 \end{bmatrix}.
\end{aligned} \tag{38}
$$

The bound disturbance input is considered as $\nu(k) = 0.05\cos(2k)$, and the initial conditions of (1) and (6) are given as $x_1(0) = \begin{bmatrix} 0.04 & 0.01 & 0.02 \end{bmatrix}^{\top}$, $x_2(0) = \begin{bmatrix} 0.03 & 0.015 & 0.02 \end{bmatrix}^{\top}$, $x_3(0) = \begin{bmatrix} 0.1 & 0.004 & 0.004 \end{bmatrix}^{\top}$, and $\hat{x}_1(0) = \hat{x}_2(0) = \hat{x}_3(0) = \begin{bmatrix} 0 & 0 & 0 \end{bmatrix}^{\top}$.

The simulation results are presented in Figures 1–5. Figures 1–3 display the state trajectories and their estimations of three nodes, respectively. The event-based release instants and release intervals of three nodes are shown in Figure 4. Figure 5 plots the evolutions of the estimation error dynamics. It can be discovered from Figure 5 that estimation error dynamics (7) is EUBMS.

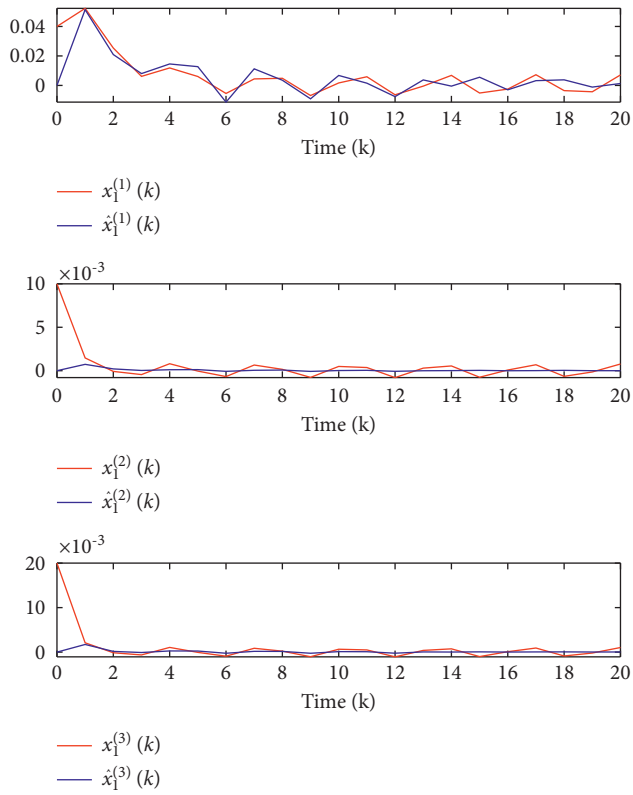

Figure 1: The state trajectories and estimations of node 1.

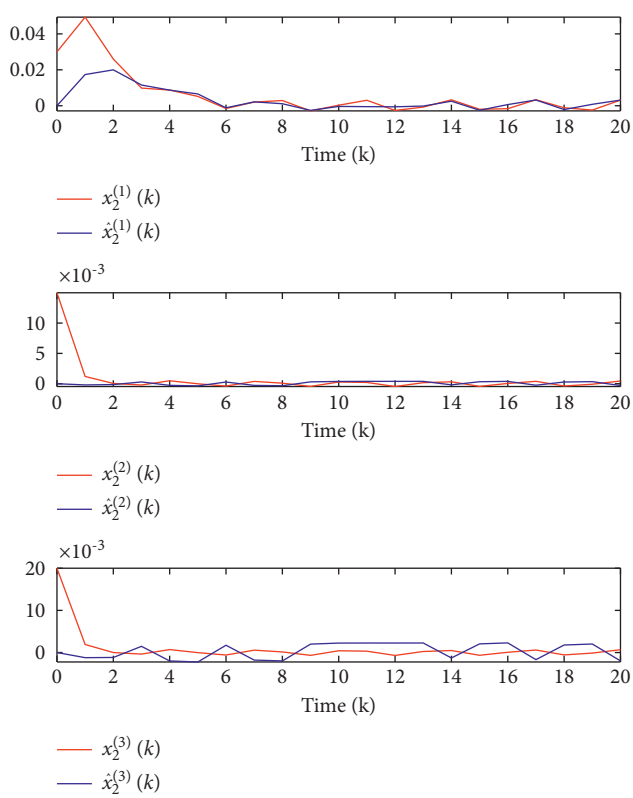

Figure 2: The state trajectories and estimations of node 2.

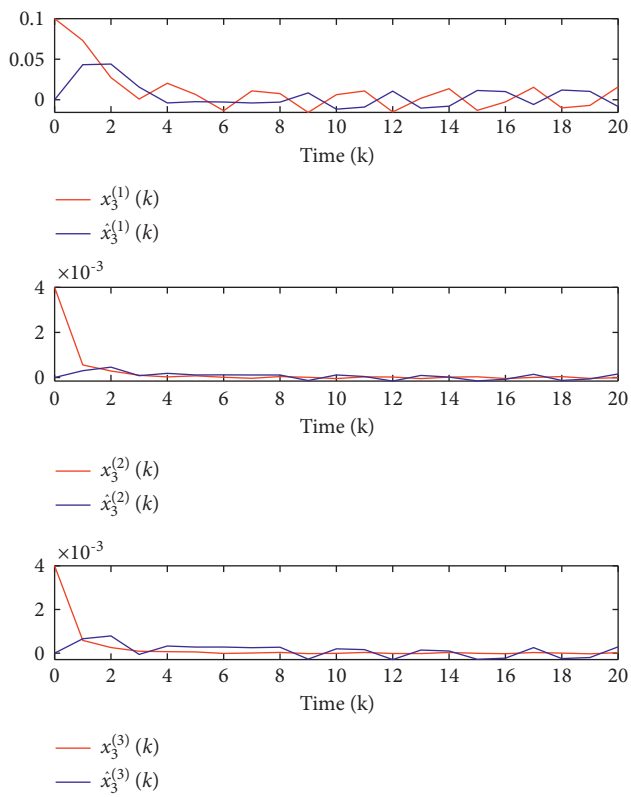

Figure 3: The state trajectories and estimations of node 3.

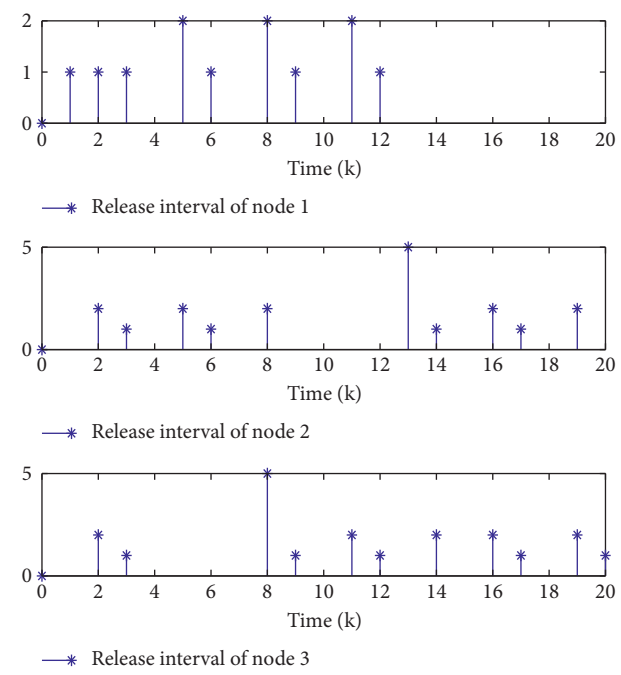

Figure 4: The event-based release instants and release intervals of three nodes.

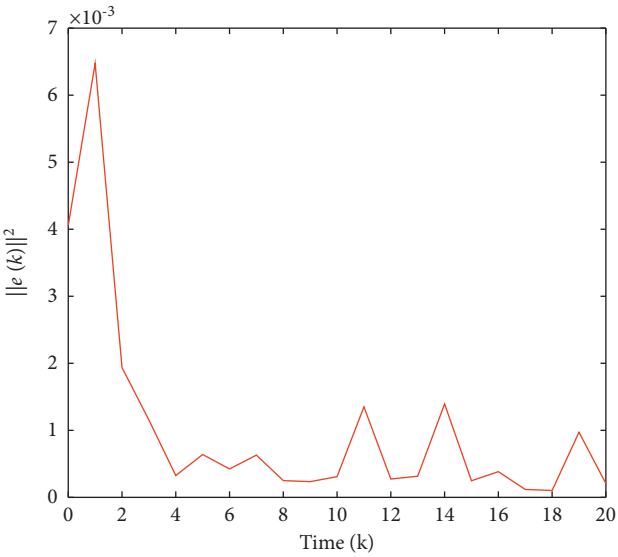

Figure 5: Dynamics of the estimation error $e(k)$.

5. Conclusions

This paper has investigated the issue of the multievent-triggered state estimation for a novel class of discrete-time nonlinear SPCNs. A discrete-time SPCN model with nonlinearities has been modeled. To alleviate energy consumption, a multievent triggered protocol is applied to regulate the communication among nodes of the SPCNs. Finally, a simulation has demonstrated the rationality, superiority, and effectiveness of the proposed method.

Data Availability

The data used to support the findings of this study are available from the author upon request.

Conflicts of Interest

The author declares no conflicts of interest.

Acknowledgments

This work was supported by the Project of Youth Science and Technology Talents of Guizhou Province (Grant Number: Qian Jiao He KY Zi[2020]095).

References

[1] J. M. Carrasco, L. G. Franquelo, J. T. Bialasiewicz et al., "Power-electronic systems for the grid integration of renewable energy sources: a survey," *IEEE Transactions on Industrial Electronics*, vol. 53, no. 4, pp. 1002–1016, 2006.

[2] G. Feng, J. Cao, and J. Lu, "Impulsive synchronization of nonlinearly coupled complex networks," *Mathematical Problems in Engineering*, vol. 2012, Article ID 969402, 11 pages, 2012.

[3] Y. Chen, D. Zhang, H. Zhang, and Q.-G. Wang, "Dual-path mixed domain residual threshold networks for bearing fault diagnosis," *IEEE Transactions on Industrial Electronics*, p. 1, 2022.

[4] K. Musial, P. Bródka, and P. De Meo, "Analysis and Applications of Complex Social Networks," *Complexity*, vol. 2017, Article ID 3014163, 17 pages, 2017.

[5] X. Wu, J. Feng, and Z. Nie, "Outer synchronization of drive-response complex-valued complex networks via intermittent pinning control," *Complexity*, vol. 2021, Article ID 6649519, 10 pages, 2021.

[6] Z.-G. Wu, Z. Xu, P. Shi, M. Z. Chen, and H. Su, "Nonfragile state estimation of quantized complex networks with switching topologies," *IEEE Transactions on Neural Networks and Learning Systems*, vol. 29, no. 10, pp. 5111–5121, 2018.

[7] W. Qi, G. Zong, and C. K. Ahn, "Input-output finite-time asynchronous smc for nonlinear semi-markov switching systems with application," *IEEE Transactions on Systems, Man, and Cybernetics: Systems*, pp. 1–10, 2021.

[8] S. Fan, H. Yan, H. Zhang, H. Shen, and K. Shi, "Dynamic event-based non-fragile dissipative state estimation for quantized complex networks with fading measurements and its application," *IEEE Transactions on Circuits and Systems I: Regular Papers*, vol. 68, no. 2, pp. 856–867, 2020.

[9] S. Wang, Z. Wang, H. Dong, and Y. Chen, "A dynamic event-triggered approach to recursive nonfragile filtering for complex networks with sensor saturations and switching topologies," *IEEE Transactions on Cybernetics*, pp. 1–14, 2021.

[10] P. Kokotović, H. K. Khalil, and J. O'reilly, *Singular Perturbation Methods in Control: Analysis and Design*, Academic Press Inc, Cambridge, MA, USA, 1999.

[11] J. R. Winkelman, J. H. Chow, J. J. Allemong, and P. V. Kokotovic, "Multi-time-scale analysis of a power system," *Automatica*, vol. 16, no. 1, pp. 35–43, 1980.

[12] R. Wang, T. Chen, Z. Zhou, and L. Jing, "Modelling periodic oscillation of biological systems with multiple timescale networks," *Systematic Biology*, vol. 1, no. 1, pp. 71–84, 2004.

[13] J. Cheng, J. H. Park, Z.-G. Wu, and H. Yan, "Ultimate boundedness control for networked singularly perturbed systems with deception attacks: a Markovian communication protocol approach," *IEEE Transactions on Network Science and Engineering*, vol. 9, no. 2, pp. 445–456, 2021.

[14] J. Cheng, W. Huang, H.-K. Lam, J. Cao, and Y. Zhang, "Fuzzy-model-based control for singularly perturbed systems with nonhomogeneous Markov switching: a dropout compensation strategy," *IEEE Transactions on Fuzzy Systems*, vol. 30, no. 2, pp. 530–541, 2022.

[15] J. Cheng, Y. Wang, J. H. Park, J. Cao, and K. Shi, "Static output feedback quantized control for fuzzy Markovian switching singularly perturbed systems with deception attacks," *IEEE Transactions on Fuzzy Systems*, vol. 30, no. 4, pp. 1036–1047, 2022.

[16] P. Zeng and Z. Zeng, "Synchronization of delayed complex networks on time scales via aperiodically intermittent control using matrix-based convex combination method," *IEEE Transactions on Neural Networks and Learning Systems*, pp. 1–13, 2021.

[17] K. Sivaranjani, R. Rakkiyappan, J. Cao, and A. Alsaedi, "Synchronization of nonlinear singularly perturbed complex networks with uncertain inner coupling via event triggered control," *Applied Mathematics and Computation*, vol. 311, pp. 283–299, 2017.

[18] W.-H. Chen, Y. Liu, and W. X. Zheng, "Synchronization analysis of two-time-scale nonlinear complex networks with time-scale-dependent coupling," *IEEE Transactions on Cybernetics*, vol. 49, no. 9, pp. 3255–3267, 2018.

[19] K. Liang, W. He, J. Xu, and F. Qian, "Impulsive effects on synchronization of singularly perturbed complex networks with semi-markov jump topologies," *IEEE Transactions on Systems, Man, and Cybernetics: Systems*, vol. 52, no. 5, pp. 3163–3173, 2022.

[20] S. Yang and X.-S. Yang, "Bounded synchronisation of singularly perturbed complex network with an application to power systems," *IET Control Theory & Applications*, vol. 8, no. 1, pp. 61–66, 2014.

[21] C. Cai, Z. Wang, J. Xu, X. Liu, and F. E. Alsaadi, "An integrated approach to global synchronization and state estimation for nonlinear singularly perturbed complex networks," *IEEE Transactions on Cybernetics*, vol. 45, no. 8, pp. 1597–1609, 2014.

[22] X. Wan, Z. Wang, M. Wu, and X. Liu, "State estimation for discrete-time nonlinear singularly perturbed complex networks under the round-robin protocol," *IEEE Transactions on Neural Networks and Learning Systems*, vol. 30, no. 2, pp. 415–426, 2018.

[23] X. Wan, Y. Li, Y. Li, and M. Wu, "Finite-time H ∞ state estimation for two-time-scale complex networks under stochastic communication protocol," *IEEE Transactions on Neural Networks and Learning Systems*, vol. 33, no. 1, pp. 25–36, 2022.

[24] N. Hou, H. Dong, W. Zhang, Y. Liu, and F. E. Alsaadi, "Event-triggered state estimation for time-delayed complex networks with gain variations based on partial nodes," *International Journal of General Systems*, vol. 47, no. 5, pp. 477–490, 2018.

[25] L. Wang, Z. Wang, T. Huang, and G. Wei, "An event-triggered approach to state estimation for a class of complex networks with mixed time delays and nonlinearities," *IEEE Transactions on Cybernetics*, vol. 46, no. 11, pp. 2497–2508, 2015.

[26] Y. Liu, Z. Wang, Y. Yuan, and W. Liu, "Event-triggered partial-nodes-based state estimation for delayed complex networks with bounded distributed delays," *IEEE Transactions on Systems, Man, and Cybernetics: Systems*, vol. 49, no. 6, pp. 1088–1098, 2017.

[27] Z. Yan, X. Huang, Y. Fan, J. Xia, and H. Shen, "Threshold-function-dependent quasi-synchronization of delayed memristive neural networks via hybrid event-triggered control," *IEEE Transactions on Systems, Man, and Cybernetics: Systems*, vol. 51, no. 11, pp. 6712–6722, 2020.

[28] J. Cheng, L. Liang, J. H. Park, H. Yan, and K. Li, "A dynamic event-triggered approach to state estimation for switched memristive neural networks with nonhomogeneous sojourn probabilities," *IEEE Transactions on Circuits and Systems I: Regular Papers*, vol. 68, no. 12, pp. 4924–4934, 2021.

[29] Y. Fan, X. Huang, Z. Wang, J. Xia, and H. Shen, "Discontinuous event-triggered control for local stabilization of memristive neural networks with actuator saturation: discrete- and continuous-time lyapunov methods," *IEEE Transactions on Neural Networks and Learning Systems*, pp. 1–13, 2021.

[30] Z. Ye, D. Zhang, Z.-G. Wu, and H. Yan, "A3C-based intelligent event-triggering control of networked nonlinear unmanned marine vehicles subject to hybrid attacks," *IEEE Transactions on Intelligent Transportation Systems*, pp. 1–14, 2021.

[31] L. Xie, J. Cheng, H. Wang, J. Wang, M. Hu, and Z. Zhou, "Memory-based event-triggered asynchronous control for semi-markov switching systems," *Applied Mathematics and Computation*, vol. 415, Article ID 126694, 2022.

[32] S. Zhu, E. Tian, D. Xu, and J. Liu, "An adaptive torus-event-based controller design for networked T-S fuzzy systems under deception attacks," *International Journal of Robust and Nonlinear Control*, vol. 32, no. 6, pp. 3425–3441, 2022.

[33] F. Qu, X. Zhao, X. Wang, and E. Tian, "Probabilistic-constrained distributed fusion filtering for a class of time-varying systems over sensor networks: a torus-event-triggering mechanism," *International Journal of Systems Science*, vol. 53, no. 6, pp. 1288–1297, 2022.

[34] J. Cheng, Y. Wu, H. Yan, Z.-G. Wu, and K. Shi, "Protocol-based filtering for fuzzy Markov affine systems with switching chain," *Automatica*, vol. 141, Article ID 110321, 2022.

[35] D. Zhao, Z. Wang, D. W. Ho, and G. Wei, "Observer-based pid security control for discrete time-delay systems under cyber-attacks," *IEEE Transactions on Systems, Man, and Cybernetics: Systems*, vol. 51, no. 6, pp. 3926–3938, 2019.

Hindawi
Complexity
Volume 2022, Article ID 6784886, 13 pages
https://doi.org/10.1155/2022/6784886

Research Article

A Study on the 3D Hopfield Neural Network Model via Nonlocal Atangana–Baleanu Operators

Shahram Rezapour,[1,2] **Pushpendra Kumar**,[3] **Vedat Suat Erturk**,[4] **and Sina Etemad**[1]

[1]*Department of Mathematics, Azarbaijan Shahid Madani University, Tabriz, Iran*
[2]*Department of Medical Research, China Medical University Hospital, China Medical University, Taichung, Taiwan*
[3]*Department of Mathematics and Statistics, School of Basic and Applied Sciences, Central University of Punjab, Bathinda, Punjab 151001, India*
[4]*Department of Mathematics, Faculty of Arts and Sciences, Ondokuz Mayis University, Atakum-55200, Samsun, Turkey*

Correspondence should be addressed to Sina Etemad; sina.etemad@azaruniv.ac.ir

Received 2 April 2022; Revised 6 May 2022; Accepted 15 June 2022; Published 7 July 2022

Academic Editor: Xiao Ling Wang

Hopfield neural network (HNN) is considered as an artificial model derived from the brain structures and it is an important model that admits an adequate performance in neurocomputing. In this article, we solve a dynamical model of 3D HNNs via Atangana–Baleanu (AB) fractional derivatives. To find the numerical solution of the considered dynamical model, the well-known Predictor-Corrector (PC) method is used. A number of cases are taken by using two different sets of values of the activation gradient of the neurons as well as six different initial conditions. The given results have been perfectly established using the different fractional-order values on the given derivative operator. The objective of this research is to investigate the dynamics of the proposed HNN model at various values of fractional orders. Nonlocal characteristic of the AB derivative contains the memory in the system which is the main motivation behind the proposal of this research.

1. Introduction

Neural networks (NNs) are a part of machine learning that are at the centre of deep learning techniques. Their identity and dynamics are taken from the human brain, and they dovetail the path real neurons transfuse to each other. In some branches of artificial intelligence (AI), deep learning, and machine learning, NNs are mimetic to the function of the human brain, helping computer algorithms to locate patterns and estimate general problems. As a result of their widespread use in a variety of sectors, NNs have elicited a great deal of anxiety [1–3]. Practice data is utilized by neural networks to swot and improve their performance over time. However, when these learning tactics have been improved for precision, they get as the knotty features in computer science and AI, helping us to hastily classify and hoard data. In comparison to manual recognition by human experts, actions in speech or picture identification can take minutes rather than hours. Various types of NNs are present, each of which is used for a specific target.

For the first time in 1984, Hopfield introduced the Hopfield neural network (HNN) [4]. Since then, a greater learning of the Hopfield neural network's dynamical behaviour has been crucial in the study of applications of engineering and information processing, such as pattern identification [5], signal processing, and associative memory [6]. Moreover, there have been several studies published in the literature on the dynamical characteristics of a range of complex-valued neural network models. HNN, as previously said, is an artificial model derived from brain dynamics, and it is an important model in neurocomputing [7]. A neural model like this is capable of accumulating information or material in an identical fashion to a human brain. Njitacke et al. in [8] discussed the space magnetization, hysteretic dynamics, and offset boosting in a third-order memristive system. In [9], the authors analyzed the complex structure of

a 3D autonomous system without linear terms having line of equilibria. A study on the control of multistability with selection of chaotic attractor along with an application to image encryption is given in [10]. In [11], a dynamical analysis on a simple autonomous jerk system with multiple attractors is proposed.

Nowadays, fractional-order operators are highly useful to solve varieties of real-world problems [12–14]. The main feature of fractional derivatives is their nonlocal properties which help to capture memory effects in the systems. These operators are an advanced version of the integer-order operators. To date, fractional operators have been used in various scientific and engineering fields by using different kinds of mathematical modelings. Recently, fractional derivatives have been used in disease dynamics [15, 16], mechanics [17], psychology [18], engineering [19], advanced modeling via fractal-fractional operators [20], etc. For the sake of the various advantages of fractional operators for memory effects, modeling dynamic systems using fractional calculus has been met with scepticism [21, 22]. In [23], the explicit stability dependency on a variable time delay was presented and delay-dependent stability switches of linear systems of the fractional type were examined. This theory has recently been included into NNs, resulting in fractional-order neural networks (FONNs). So such a medication can strengthen the ability of neurons to process information. Fortunately, owing to the unwavering tenacity of researchers, various worldwide applications of FONNs have been discovered, including network approximation [24], state estimation [25], system identification [26], robotic manipulators [27], and formation control [28]. For neurons, fractional-order elements have two clear benefits. On the one hand, fractional calculus, as compared to ordinary calculus, has a far better depiction of memory and hereditary features [29]. Fractional-order parameters, on the other hand, can improve system performance by adding one degree of freedom [30]. By combining memory peculiarity into NNs, there is clearly an enormous improvement. FONNs have produced some astonishing effects [31, 32].

In this article, we perform some novel mathematical simulations on the dynamical model of 3D HNNs which was investigated in ref. [33] given as follows:

$$\begin{cases} \dot{x}_1 = -x_1 + 2\tanh(\beta_1 x_1) - 1.2\tanh(\beta_2 x_2) + 0.48\tanh(\beta_3 x_3), \\ \dot{x}_2 = -x_2 + 3.6\tanh(\beta_1 x_1) + 1.7\tanh(\beta_2 x_2) + 1.776\tanh(\beta_3 x_3), \\ \dot{x}_3 = -x_3 - 9\tanh(\beta_1 x_1), \end{cases} \tag{1}$$

where terms x_1, x_2, x_3 are state variables and $\beta_1, \beta_2, \beta_3$ stand for the variable gradient in relation to the activation function. Firstly, we give some preliminaries related to the fractional calculus in Section 2. Then, to solve the above given dynamical model (1), we generalise the model into Atangana–Baleanu (AB) fractional derivative under the Mittag–Leffler kernel in Section 3. For investigating the numerical solution of the fractional-order model, we apply Predictor-Corrector (PC) method. In Section 4, a number of graphs are plotted to check the correctness of the derived solution. Lastly, we give the supporting conclusion.

2. Preliminaries

Several important notions are recalled here.

Definition 1 (see [34]). For the function $X \in \mathcal{H}^1(a,b)$, where $b > a$ and $0 \le \gamma \le 1$, the γ^{th}-AB derivative is

$${}_a^{AB}D_t^{\gamma}(X(t)) = \frac{AB[\gamma]}{1-\gamma}\int_a^t X'(\eta)E_{\gamma}\left[\gamma\frac{(t-\eta)^{\gamma}}{\gamma-1}\right]d\eta, \tag{2}$$

where $\mathrm{AB}[\gamma]$ with $\mathrm{AB}[1] = \mathrm{AB}[0] = 1$ is the normalization function.

Definition 2 (see [34]). The AB fractional integral is given by

$${}_a^{AB}I_t^{\gamma}(X(t)) = \frac{1-\gamma}{AB[\gamma]}X(t) + \frac{\gamma}{\Gamma(\gamma)AB[\gamma]} \cdot \int_a^t X(\eta)(t-\eta)^{\gamma-1}d\eta. \tag{3}$$

Lemma 1 (see [34]). *For $0 < \gamma < 1$, the solution of the system*

$$\begin{aligned} {}^{\mathscr{B}}\mathbf{D}_0^{\gamma}x(t) &= z(t), t \in [0,T], \\ x(0) &= x_0, \end{aligned} \tag{4}$$

is derived by

$$x(t) = x_0 + \frac{(1-\gamma)}{AB(\gamma)}z(t) + \frac{\gamma}{AB(\gamma)\Gamma(r)}\int_0^t (t-\omega)^{\gamma-1}z(\omega)d\omega\ . \tag{5}$$

Lemma 2 (see [35]). *Let a_1 is a nonnegative integer and $0 < \gamma < 1$, then there exist two constants $C_{\gamma,1} > 0$ and $C_{\gamma,2} > 0$ in terms of γ, such that*

$$(a_1+1)^{\gamma} - a_1^{\gamma} \le C_{\gamma,1}(a_1+1)^{\gamma-1}, \tag{6}$$

and $(a_1+2)^{\gamma+1} - 2(a_1+1)^{\gamma+1} + a_1^{\gamma+1} \le C_{\gamma,2}(a_1+1)^{\gamma-1}$.

Lemma 3 (see [35]). *Let us suppose $\nu_{s,r} = (r-s)^{\gamma-1}(s = 1, 2, \ldots, r-1)$ and $\nu_{s,r} = 0$ for $s \ge r, \gamma, M, h, T > 0, a_1 h \le T$ and a_1 is a positive integer. Let*

$\sum_{s=a_1}^{s=r} \nu_{s,r}|e_s| = 0$ *for* $k > r \geq 1$. *If* $|e_r| \leq Mh^{\gamma}\sum_{s=1}^{r-1}\nu_{s,r}|e_s| + |\eta_0|, \quad r = 1, 2, \ldots, a_1,$ *then* $|e_{a_1}| \leq C|\eta_0|, \quad a_1 = 1, 2, \ldots$ *in which* $C > 0$ *is independent of both* a_1 *and* h.

3. The Structure of the Model

Here we generalise the aforementioned integer-order model (1) into the fractional-order sense by using a nonsingular type fractional derivative called Atangana–Baleanu fractional derivative. Nonlocal characteristic of the AB derivative contains the memory in the system which is the main motivation behind this generalization. So, the fractional form of the given system (1) in the AB-operator sense is given by

$$\begin{cases} {}^{AB}D_t^{\gamma}x_1 = -x_1 + 2\tanh(\beta_1 x_1) - 1.2\tanh(\beta_2 x_2) + 0.48\tanh(\beta_3 x_3), \\ {}^{AB}D_t^{\gamma}x_2 = -x_2 + 3.6\tanh(\beta_1 x_1) + 1.7\tanh(\beta_2 x_2) + 1.776\tanh(\beta_3 x_3), \\ {}^{AB}D_t^{\gamma}x_3 = -x_3 - 9\tanh(\beta_1 x_1), \end{cases} \tag{7}$$

where ${}^{AB}D_t^{\gamma}$ is the AB fractional derivative of order γ.

3.1. Derivation of the Numerical Solution. In the current literature, there are many computational methods available to solve different types of fractional-order systems. Some very recent works on the proposal of numerical methods in the sense of fractional derivatives can be seen from ref. [36, 37]. Here we implement the Predictor-Corrector method for solving the given dynamical model (7). The complete methodology of the proposed method has been defined in ref. [38]. Firstly, we consider the initial value problem (IVP)

$$\begin{aligned} {}^{AB}\mathbf{D}_t^{\gamma}\mathscr{B}(t) &= \Phi(t, \mathscr{B}(t)), \quad t \in [0, \tau],\ 0 < \gamma \leq 1, \\ \mathscr{B}(0) &= \mathscr{B}_0. \end{aligned} \tag{8}$$

From ref. [38], the equivalent Volterra integral equation is written by

$$\mathscr{B}_{r+1} = \mathscr{B}_0 + (1-\gamma)\Phi(t_{r+1}, \mathscr{B}_{r+1}) + \frac{\gamma}{\Gamma(\gamma)}\int_0^{t_{r+1}} (t_{r+1} - s)^{\gamma-1}\Phi(s, \mathscr{B}(s))\mathrm{d}s. \tag{9}$$

According to the derivation of the method proposed in [38] for the fractional-order $\gamma \in [0, 1]$, $0 \leq t \leq T$ and considering $h = (T/N)$ and $t_n = nh$, for $n = 0, 1, \ldots, N \in \mathbb{Z}^+$, the corrector term for the IVP (8) is derived by

$$\mathscr{B}_{r+1} = \mathscr{B}_0 + \frac{\gamma h^{\zeta}}{\Gamma(\gamma+2)}\left(a_{r+1,r+1}\Phi\left(t_{r+1}, \mathscr{B}_{r+1}^{P}\right) \cdot + \sum_{w=0}^{r} a_{r+1,w}\Phi(t_w, \mathscr{B}_w)\right), \tag{10}$$

where

$$a_{r+1,w} = \begin{cases} r^{\gamma+1} - (r-\gamma)(r+1)^{\gamma}, & \text{if } w = 0, \\ (r-w+2)^{\gamma+1} + (r-w)^{\gamma+1} - 2(r-w+1)^{\gamma+1}, & \text{if } 1 \leq w \leq r, \\ 1, & w = r+1, \end{cases} \tag{11}$$

and $a_{r+1,r+1} = 1 + ((1-\gamma)\Gamma(\gamma+2)/\gamma h^{\gamma})$. The predictor term is given by

where

$$\mathscr{B}_{r+1}^{P} = \mathscr{B}_0 + \frac{h^{\gamma}}{\Gamma(\gamma)}\sum_{w=0}^{r} b_{r+1,w}\Phi(t_w, \mathscr{B}_w), \tag{12}$$

$$b_{r+1,w} = \begin{cases} -(r-w)^{\gamma} + (r-w+1)^{\gamma}, & w = 0, \ldots, r-1, \\ 1 + \dfrac{(1-\gamma)\Gamma(\gamma)}{h^{\gamma}}, & w = r. \end{cases} \tag{13}$$

We can see that our proposed model (7) is just a generalized form of the considered IVP (8). Hence the corrector formulae in relation to the proposed model (7) are given by

$$x_{1_{r+1}} = x_{10} + \frac{\gamma h^{\gamma}}{\Gamma(\gamma+2)}\left(\begin{array}{l}\left(a_{r+1,r+1}\right)\left(-x^{P}_{1_{r+1}} + 2\tanh\left(\beta_1 x^{P}_{1_{r+1}}\right) - 1.2\tanh\left(\beta_2 x^{P}_{2_{r+1}}\right) + 0.48\tanh\left(\beta_3 x^{P}_{3_{r+1}}\right)\right)\\ + \sum_{w=0}^{r}\left(a_{r+1,w}\right)\left(-x_{1_w} + 2\tanh\left(\beta_1 x_{1_w}\right) - 1.2\tanh\left(\beta_2 x_{2_w}\right) + 0.48\tanh\left(\beta_3 x_{3_w}\right)\right)\end{array}\right),$$

$$x_{2_{r+1}} = x_{20} + \frac{\gamma h^{\gamma}}{\Gamma(\gamma+2)}\left(\begin{array}{l}\left(a_{r+1,r+1}\right)\left(-x^{P}_{2_{r+1}} + 3.6\tanh\left(\beta_1 x^{P}_{1_{r+1}}\right) + 1.7\tanh\left(\beta_2 x^{P}_{2_{r+1}}\right) + 1.776\tanh\left(\beta_3 x^{P}_{3_{r+1}}\right)\right)\\ + \sum_{w=0}^{r}\left(a_{r+1,w}\right)\left(-x_{2_w} + 3.6\tanh\left(\beta_1 x_{1_w}\right) + 1.7\tanh\left(\beta_2 x_{2_w}\right) + 1.776\tanh\left(\beta_3 x_{3_w}\right)\right)\end{array}\right), \tag{14}$$

$$x_{3_{r+1}} = x_{30} + \frac{\gamma h^{\gamma}}{\Gamma(\gamma+2)}\left(\begin{array}{l}\left(a_{r+1,r+1}\right)\left(-x^{P}_{3_{r+1}} - 9\tanh\left(\beta_1 x^{P}_{1_{r+1}}\right)\right)\\ + \sum_{w=0}^{r}\left(a_{r+1,w}\right)\left(-x_{3_w} - 9\tanh\left(\beta_1 x_{1_w}\right)\right)\end{array}\right),$$

where

$$\begin{aligned} x^{P}_{1_{r+1}} &= x_{10} + \frac{h^{\gamma}}{\Gamma(\gamma)}\sum_{w=0}^{r} b_{r+1,w}\left(-x_{1_w} + 2\tanh\left(\beta_1 x_{1_w}\right) - 1.2\tanh\left(\beta_2 x_{2_w}\right) + 0.48\tanh\left(\beta_3 x_{3_w}\right)\right),\\ x^{P}_{2_{r+1}} &= x_{20} + \frac{h^{\gamma}}{\Gamma(\gamma)}\sum_{w=0}^{r} b_{r+1,w}\left(-x_{2_w} + 3.6\tanh\left(\beta_1 x_{1_w}\right) + 1.7\tanh\left(\beta_2 x_{2_w}\right) + 1.776\tanh\left(\beta_3 x_{3_w}\right)\right),\\ x^{P}_{3_{r+1}} &= x_{30} + \frac{h^{\gamma}}{\Gamma(\gamma)}\sum_{w=0}^{r} b_{r+1,w}\left(-x_{3_w} - 9\tanh\left(\beta_1 x_{1_w}\right)\right). \end{aligned} \tag{15}$$

3.1.1. Stability of the Scheme

Theorem 1. *The derived scheme (14) and (15) is conditionally stable.*

Proof. Consider $\widetilde{\mathscr{B}_0}, \widetilde{\mathscr{B}_w}\,(w = 0, \ldots, r+1)$ and $\widetilde{\mathscr{B}}^{P}_{r+1}\,(r = 0, \ldots, N-1)$ be perturbations of $\mathscr{B}_0, \mathscr{B}_w$ and $\mathscr{B}^{P}_{r+1}$, respectively. Then the perturbations given from (14) and (15) are

$$\begin{aligned} \widetilde{\mathscr{B}}^{P}_{r+1} &= \widetilde{\mathscr{B}_0} + \frac{h^{\gamma}}{\Gamma(\gamma)}\sum_{w=0}^{r} b_{r+1,w}\left(\Phi\left(t_w, \mathscr{B}_w + \widetilde{\mathscr{B}_w}\right) - \Phi\left(t_w, \mathscr{B}_w\right)\right),\\ \widetilde{\mathscr{B}}_{r+1} &= \widetilde{\mathscr{B}_0} + \frac{\gamma h^{\gamma}}{\Gamma(\gamma+2)}\left(\begin{array}{l} a_{r+1,r+1}\left(\Phi\left(t_{r+1}, \mathscr{B}^{P}_{r+1} + \widetilde{\mathscr{B}}^{P}_{r+1}\right) - \Phi\left(t_{r+1}, \mathscr{B}^{P}_{r+1}\right)\right)\\ + \sum_{w=0}^{r} a_{r+1,w}\left(\Phi\left(t_w, \mathscr{B}_w + \widetilde{\mathscr{B}}_w\right) - \Phi\left(t_w, \mathscr{B}_w\right)\right)\end{array}\right). \end{aligned} \tag{16}$$

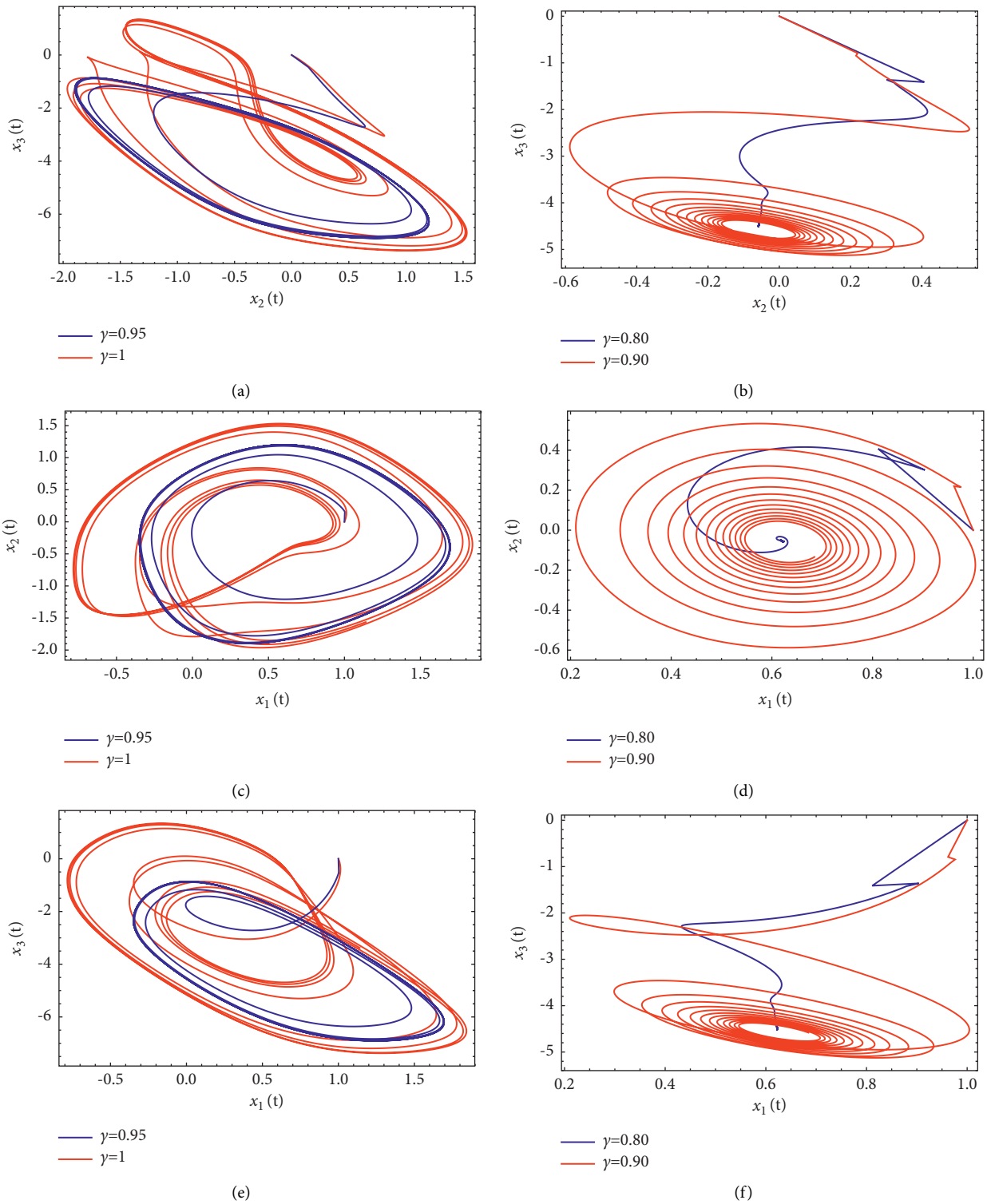

FIGURE 1: Dynamics of coexisting multiple attractors' for gradient $\beta_2 = 1.15$ and $x_1(0) = 1, x_2(0) = x_3(0) = 0$ at different fractional orders. (a) State variables x_2 versus x_3; (b) state variables x_2 versus x_3; (c) state variables x_1 versus x_2; (d) state variables x_1 versus x_3; (e) state variables x_1 versus x_2; (f) state variables x_1 versus x_3.

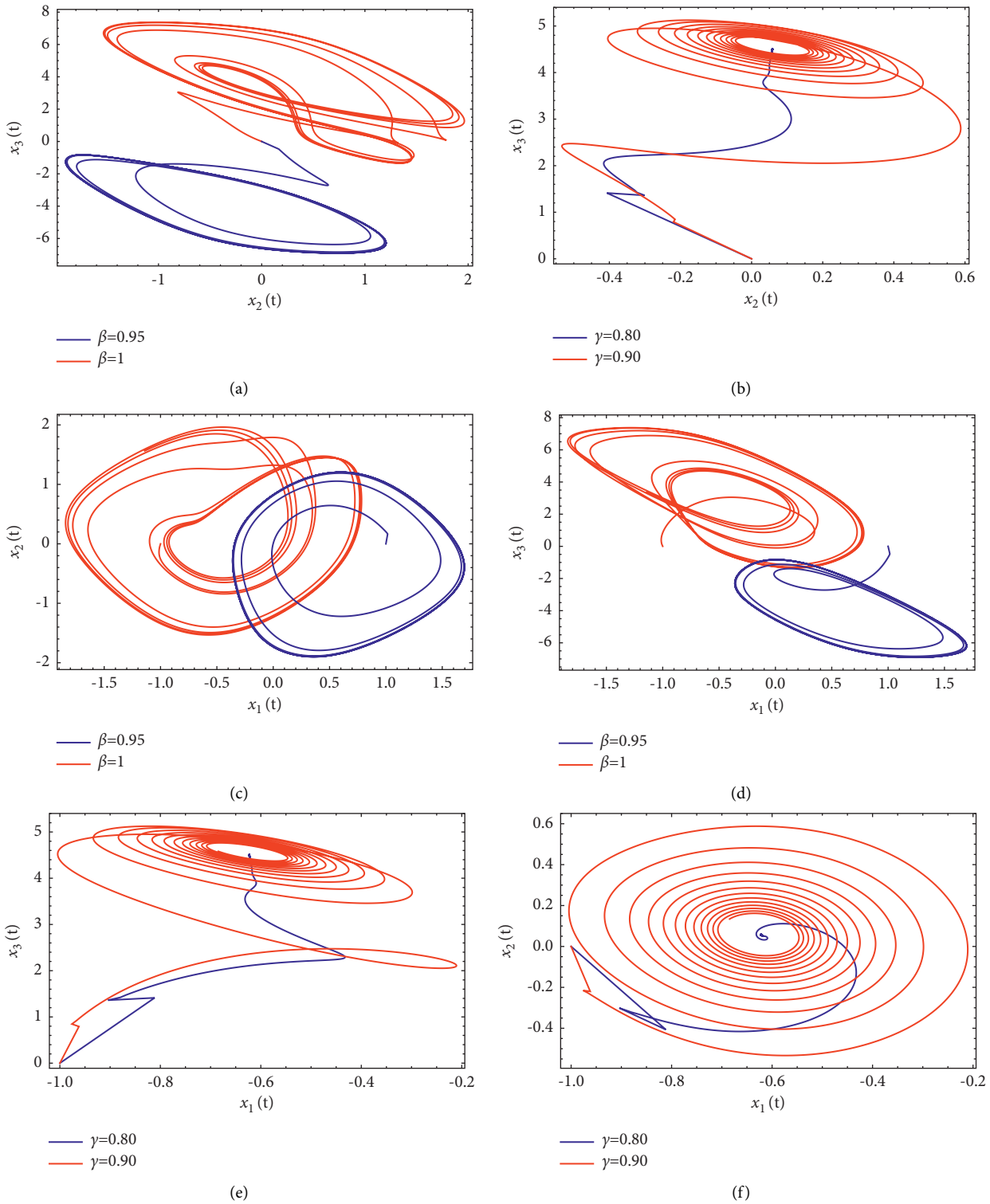

FIGURE 2: Dynamics of coexisting multiple attractors' for gradient $\beta_2 = 1.15$ and $x_1(0) = -1, x_2(0) = x_3(0) = 0$ at different fractional orders. (a) State variables x_2 versus x_3; (b) state variables x_2 versus x_3; (c) state variables x_1 versus x_2; (d) state variables x_1 versus x_3; (e) state variables x_1 versus x_2; (f) state variables x_1 versus x_3.

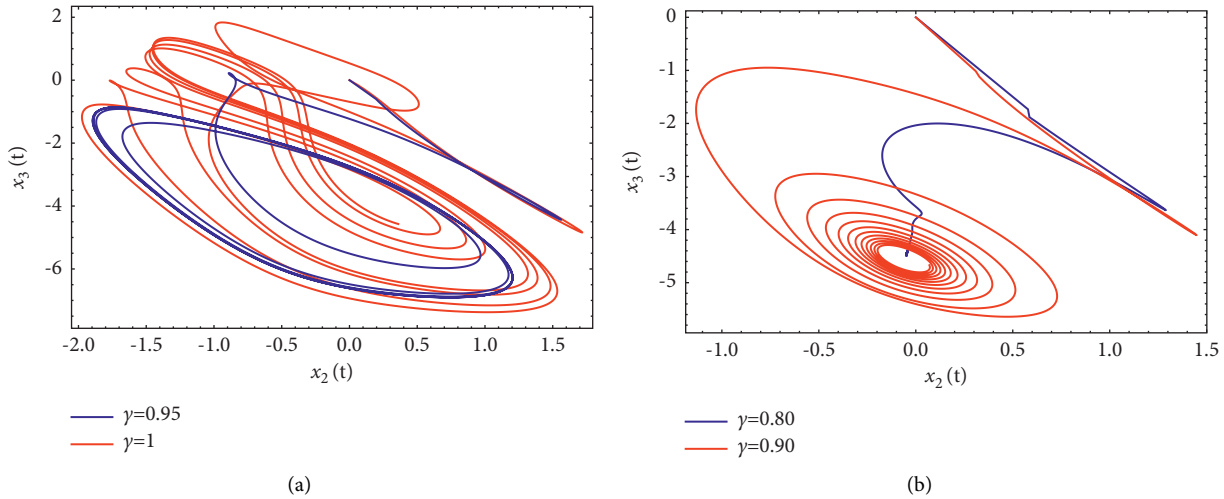

FIGURE 3: Dynamics of coexisting multiple attractors' for gradient $\beta_2 = 1.15$ and $x_1(0) = 2, x_2(0) = x_3(0) = 0$ at different fractional orders. (a) State variables x_2 versus x_3; (b) state variables x_2 versus x_3.

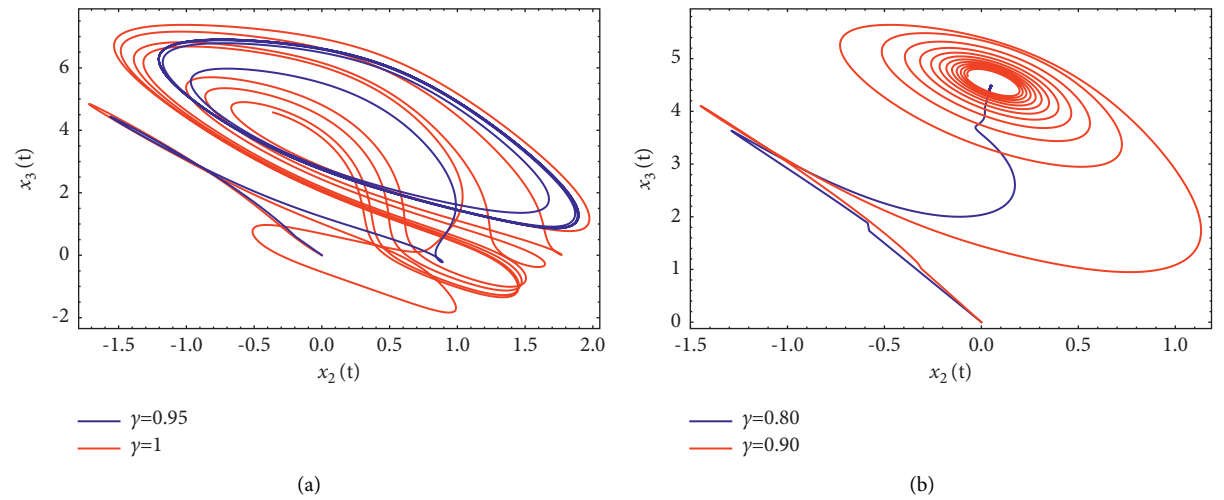

FIGURE 4: Dynamics of coexisting multiple attractors' for gradient $\beta_2 = 1.15$ and $x_1(0) = -2, x_2(0) = x_3(0) = 0$ at different fractional orders. (a) State variables x_2 versus x_3; (b) state variables x_2 versus x_3.

According to the Lipschitz condition, we get

$$\left|\widetilde{\mathscr{B}}_{r+1}\right| \le \gamma_0 + \frac{\gamma h^\gamma M}{\Gamma(\gamma+2)}\left(a_{r+1,r+1}\left|\widetilde{\mathscr{B}}^P_{r+1}\right| + \sum_{w=1}^{r} a_{w,r+1}\left|\widetilde{\mathscr{B}}_w\right|\right), \quad (17)$$

where $\gamma_0 = \max_{0\le r\le N}\left\{\left|\widetilde{\mathscr{B}}_0\right| + (\gamma h^\gamma M a_{r,0}/\Gamma(\gamma+2))\left|\widetilde{\mathscr{B}}_0\right|\right\}$. Also, from Eq.(3.18) in [35] we write

$$\left|\widetilde{\mathscr{B}}^P_{r+1}\right| \le \eta_0 + \frac{h^\gamma M}{\Gamma(\gamma)}\sum_{w=1}^{r} b_{w,r+1}\left|\widetilde{\mathscr{B}}_w\right|, \quad (18)$$

where $\eta_0 = \max_{0\le r\le N}\left\{\left|\widetilde{\mathscr{B}}_0\right| + (h^\gamma M b_{n,0}/\Gamma(\gamma))\left|\widetilde{\mathscr{B}}_0\right|\right\}$. Substituting $\left|\widetilde{\mathscr{B}}^P_{r+1}\right|$ from (18) into (17) reads as follows:

$$\begin{aligned}\left|\widetilde{\mathscr{B}}_{r+1}\right| &\le \gamma_0 + \frac{\gamma h^\gamma M}{\Gamma(\gamma+2)}\sum_{w=1}^{r}\left(a_{r+1,w} + \frac{h^\gamma M a_{r+1,r+1} b_{r+1,w}}{\Gamma(\gamma)}\right)\left|\widetilde{\mathscr{B}}_w\right| \\ &\le \gamma_0 + \frac{\gamma h^\gamma M C_{\gamma,2}}{\Gamma(\gamma+2)}\sum_{w=1}^{r}(r+1-w)^{\gamma-1}\left|\widetilde{\mathscr{B}}_w\right|\end{aligned} \quad (19)$$

where $\gamma_0 = \max\left\{\gamma_0 + (\gamma h^\gamma M a_{r+1,r+1}/\Gamma(\gamma+2))\eta_0\right\}$. $C_{\gamma,2} > 0$ is a constant dependent on γ (from Lemma 2) and h is supposed to be very small. From Lemma 3, it is obtained that $\left|\widetilde{\mathscr{B}}_{r+1}\right| \le C\gamma_0$, which is the desired result. □

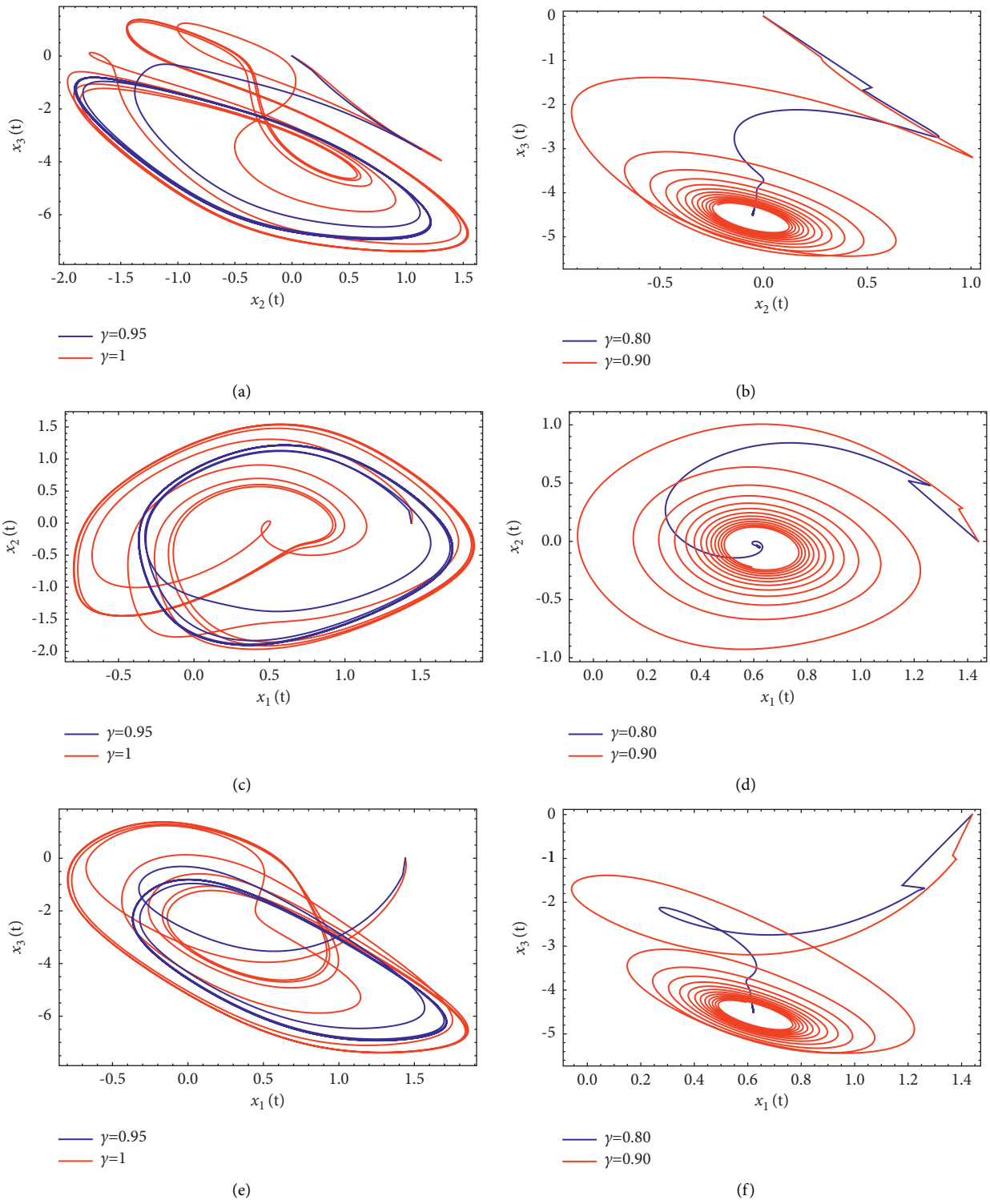

FIGURE 5: Dynamics of coexisting multiple attractors' for gradient $\beta_2 = 1.18$ and $x_1(0) = 1.44, x_2(0) = x_3(0) = 0$ at different fractional orders. (a) State variables x_2 versus x_3; (b) state variables x_2 versus x_3; (c) state variables x_1 versus x_2; (d) state variables x_1 versus x_3; (e) state variables x_1 versus x_2; (f) state variables x_1 versus x_3.

4. Graphical Observations

Now to check the role of the proposed Atangana–Baleanu fractional derivative, we plot a number of graphs with the help of the above mentioned numerical method. The values of the parameters β_1 and β_3 are fixed and equal to $\beta_1 = 0.9, \beta_3 = 1.4$. For the activation gradient of the second neuron $\beta_2 = 1.15$, we plotted the coexistence of four distinct stable states in the group of Figures 1–4. In the frame of Figure 1, the initial values are taken as

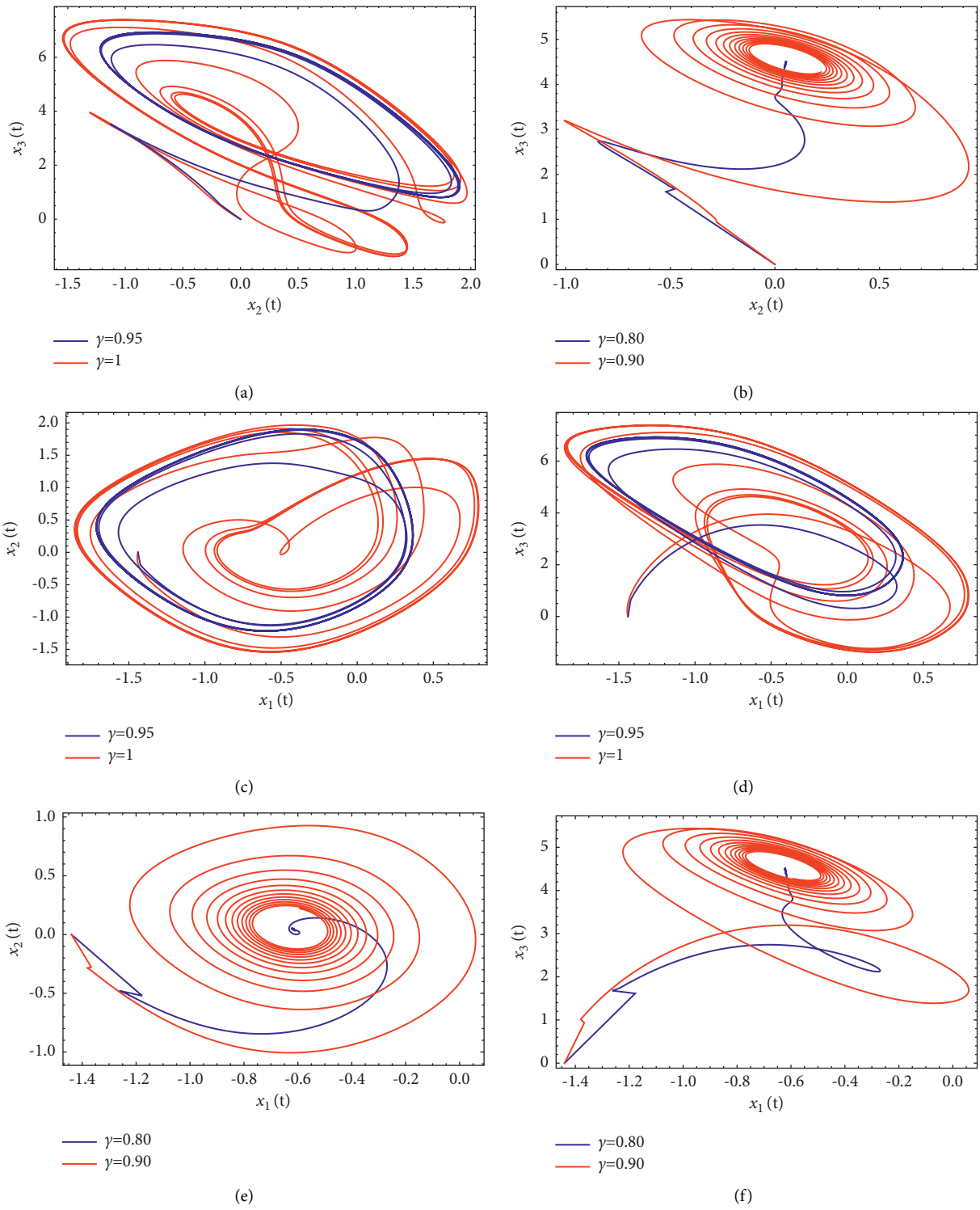

FIGURE 6: Dynamics of coexisting multiple attractors' for gradient $\beta_2 = 1.18$ and $x_1(0) = -1.44, x_2(0) = x_3(0) = 0$ at different fractional orders. (a) State variables x_2 versus x_3; (b) state variables x_2 versus x_3; (c) state variables x_1 versus x_2; (d) state variables x_1 versus x_3; (e) state variables x_1 versus x_2; (f) state variables x_1 versus x_3.

$x_1(0) = 1, x_2(0) = x_3(0) = 0$. Here Figures 1(a) and 1(b) represent the dynamics of x_2 versus x_3 at $\gamma = 1, 0.95, 0.90, 0.80$.

Figures 1(c) and 1(e) show the dynamics of x_1 versus x_2, and Figures 1(d) and 1(f) justify the variations of x_1 versus x_3 at the given values of order γ. Similarly, we perform some other cases of different initial values. In the frame of Figure 2, the initial values are taken as $x_1(0) = -1, x_2(0) = x_3(0) = 0$. In the case of Figure 3, these values are $x_1(0) = 2, x_2(0) = x_3(0) = 0$ and for Figure 4 are fixed as

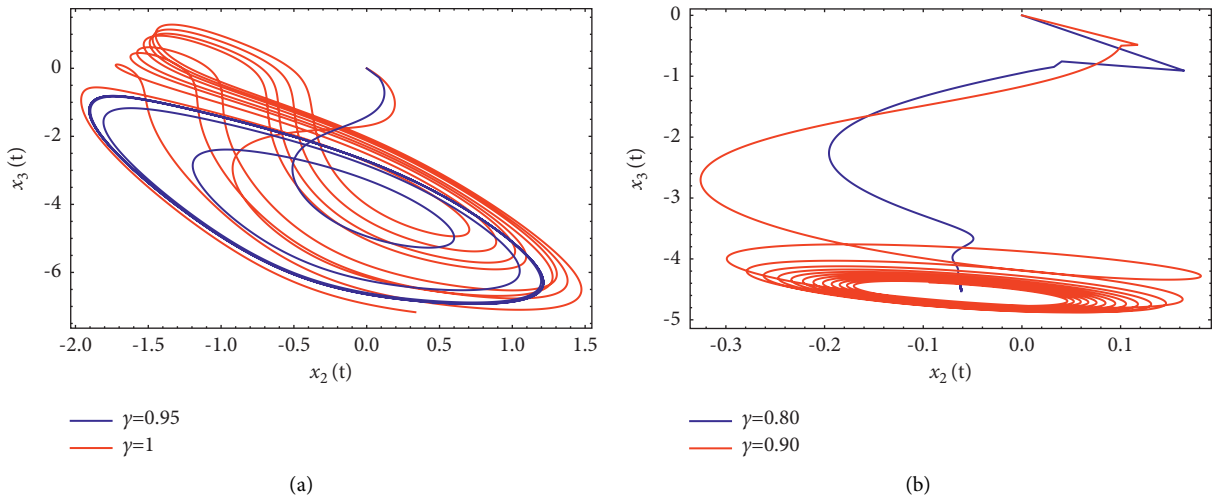

FIGURE 7: Dynamics of coexisting multiple attractors' for gradient $\beta_2 = 1.18$ and $x_1(0) = 0.5, x_2(0) = x_3(0) = 0$ at different fractional orders. (a) State variables x_2 versus x_3; (b) state variables x_2 versus x_3.

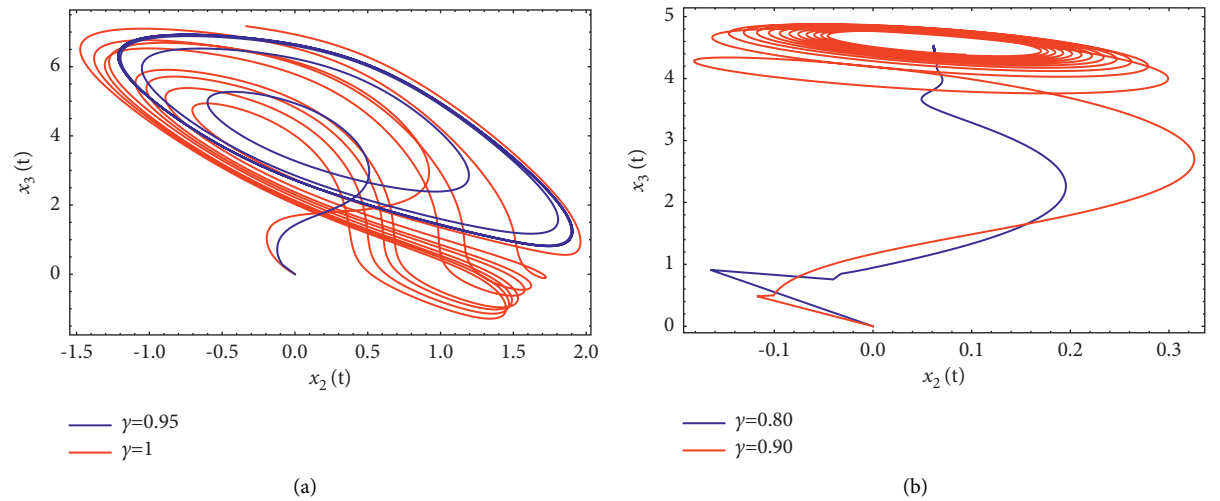

FIGURE 8: Dynamics of coexisting multiple attractors' for gradient $\beta_2 = 1.18$ and $x_1(0) = -0.5, x_2(0) = x_3(0) = 0$ at different fractional orders. (a) State variables x_2 versus x_3; (b) state variables x_2 versus x_3.

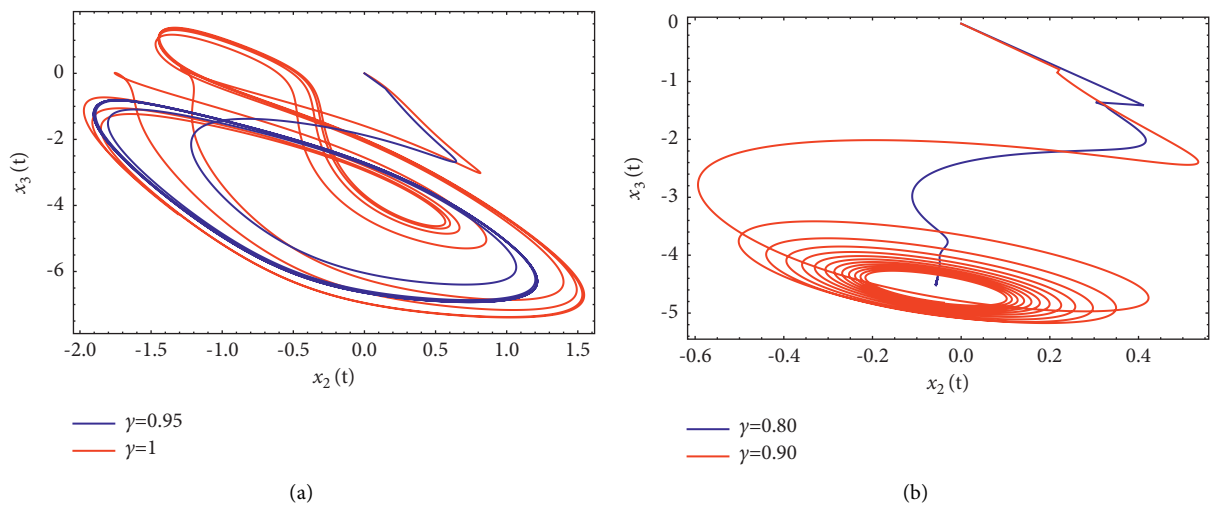

FIGURE 9: Dynamics of coexisting multiple attractors' for gradient $\beta_2 = 1.18$ and $x_1(0) = 1, x_2(0) = x_3(0) = 0$ at different fractional orders. (a) State variables x_2 versus x_3; (b) state variables x_2 versus x_3.

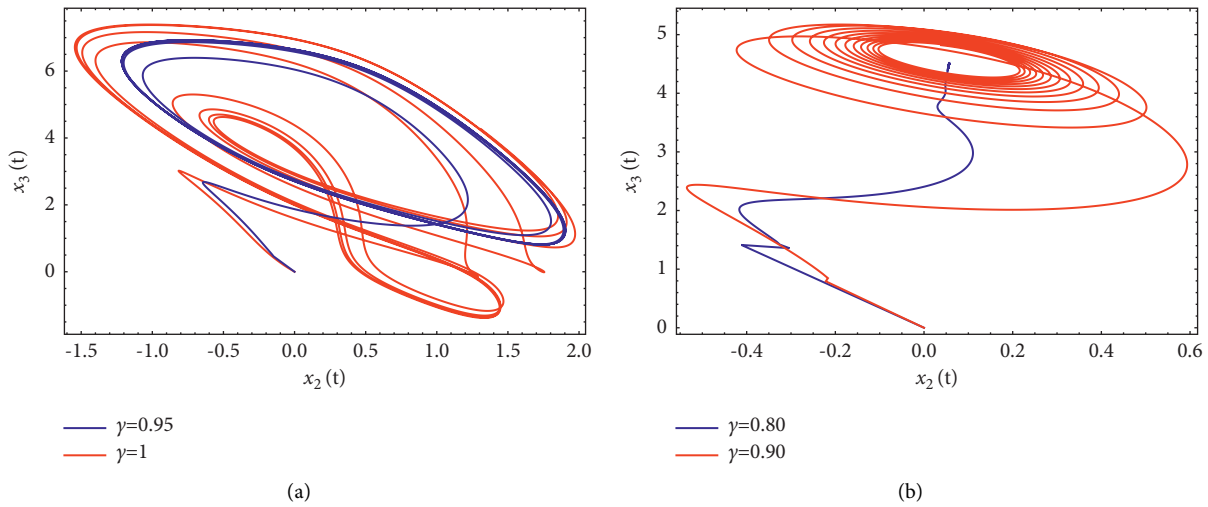

FIGURE 10: Dynamics of coexisting multiple attractors' for gradient $\beta_2 = 1.18$ and $x_1(0) = -1, x_2(0) = x_3(0) = 0$ at different fractional orders. (a) State variables x_2 versus x_3; (b) state variables x_2 versus x_3.

$x_1(0) = -2, x_2(0) = x_3(0) = 0$. Here we can see that the proposed results are slightly different to the previously given results of ref. [33]. When we change the values of γ, the nature of the assumed multiple attractors also changes. One of the main differences in the proposed fractional-order analysis and the previously performed results of [33] is that there is no existence of any perfect periodic attractors at any fractional-order values, but the chaotic attractors are achieved in much better form. All simulations are performed by using *Mathematica* software.

In the same line when $\beta_2 = 1.18$, we consider the coexistence of six different stable states in the group of Figures 5–10. In the frame of Figure 5, we assume $x_1(0) = 1.44, x_2(0) = x_3(0) = 0$. Here Figures 5(a) and 5(b) represent the dynamics of x_2 versus x_3 at $\gamma = 1, 0.95, 0.90, 0.80$.

Figures 5(c) and 5(e) show the dynamics of x_1 versus x_2, and Figures 5(d) and 5(f) justify the variations of x_1 versus x_3 at the given values of order γ. In Figure 6, we take $x_1(0) = 1, x_2(0) = x_3(0) = 0$. In the case of Figure 7, these are $x_1(0) = 0.5, x_2(0) = x_3(0) = 0$ and for Figure 8 are fixed as $x_1(0) = -0.5, x_2(0) = x_3(0) = 0$. Then for Figure 9, values are $x_1(0) = 1, x_2(0) = x_3(0) = 0$ and for Figure 10 are $x_1(0) = -1, x_2(0) = x_3(0) = 0$. Here again we notice that the proposed results are different to the previously given results of ref. [33]. Again, the main difference in the proposed fractional-order analysis and the previously performed results of [33] is that there is no existence of any periodic attractors at any fractional-order values, but the chaotic attractors are achieved in much better form.

5. Conclusions

In this paper, we simulated a dynamical model of 3D HNNs in terms of Atangana–Baleanu fractional derivative. The numerical solution of the suggested dynamical model has derived via the Predictor-Corrector method. A number of cases for initial values are considered for the better understanding of the role of initial changes. By using the two different values of the second activation gradient of the neuron, the behaviour of the proposed model is investigated at four different fractional orders. From the given graphical simulations, we conclude that in the case of fractional-order values there is no clear existence of any periodic attractors, but the chaotic attractors are achieved in much better form. In the future, the proposed dynamical model can be further solved by using any other fractional operators.

Data Availability

Data sharing is not applicable to this article as no datasets were generated or analyzed during the current study.

Conflicts of Interest

The authors declare that they have no competing interests.

Authors' Contributions

The authors declare that the study was realized in collaboration with equal responsibility. All authors read and approved the final manuscript.

Acknowledgments

The first and fourth authors would like to thank Azarbaijan Shahid Madani University.

References

[1] Y. Cao, R. Samidurai, and R. Sriraman, "Robust passivity analysis for uncertain neural networks with leakage delay and additive time-varying delays by using general activation function," *Mathematics and Computers in Simulation*, vol. 155, pp. 57–77, 2019.

[2] Y. Fan, X. Huang, Y. Li, J. Xia, and G. Chen, "Aperiodically intermittent control for quasi-synchronization of delayed memristive neural networks: an interval matrix and matrix

measure combined method," *IEEE Transactions on Systems, Man, and Cybernetics: Systems*, vol. 49, no. 11, pp. 2254–2265, 2019.

[3] Y. Liu, Y. Zheng, J. Lu, J. Cao, and L. Rutkowski, "Constrained quaternion-variable convex optimization: a quaternion-valued recurrent neural network approach," *IEEE Transactions on Neural Networks and Learning Systems*, vol. 31, no. 3, pp. 1022–1035, 2020.

[4] J. J. Hopfield, "Neurons with graded response have collective computational properties like those of two-state neurons," *Proceedings of the National Academy of Sciences*, vol. 81, no. 10, pp. 3088–3092, 1984.

[5] H. Qiu, X. Chen, W. Liu, G. Zhou, Y. Wang, and J. Lai, "A fast-solver and its applications to robust face recognition," *Journal of Industrial and Management Optimization*, vol. 8, pp. 163–178, 2012.

[6] Y. Wang, G. Zhou, L. Caccetta, and W. Liu, "An alternative Lagrange-dual based algorithm for sparse signal reconstruction," *IEEE Transactions on Signal Processing*, vol. 59, no. 4, pp. 1895–1901, 2011.

[7] X. S. Yang and Q. Yuan, "Chaos and transient chaos in simple Hopfield neural networks," *Neurocomputing*, vol. 69, no. 1-3, pp. 232–241, 2005.

[8] Z. T. Njitacke, R. L. T. Mogue, J. Kengne, M. Kountchou, and H. B. Fotsin, "Hysteretic dynamics, space magnetization and offset boosting in a third-order memristive system," *Iranian Journal of Science and Technology, Transactions of Electrical Engineering*, vol. 44, no. 1, pp. 413–429, 2020.

[9] R. W. Tapche, Z. T. Njitacke, J. Kengne, and F. B. Pelap, "Complex dynamics of a novel 3D autonomous system without linear terms having line of equilibria: coexisting bifurcations and circuit design," *Analog Integrated Circuits and Signal Processing*, vol. 103, no. 1, pp. 57–71, 2020.

[10] Z. T. Njitacke, M. E. Sone, T. F. Fozin, N. Tsafack, G. D. Leutcho, and C. T. Tchapga, "Control of multistability with selection of chaotic attractor: application to image encryption," *The European Physical Journal - Special Topics*, vol. 230, no. 7-8, pp. 1839–1854, 2021.

[11] J. Kengne, Z. T. Njitacke, and H. B. Fotsin, "Dynamical analysis of a simple autonomous jerk system with multiple attractors," *Nonlinear Dynamics*, vol. 83, no. 1-2, pp. 751–765, 2015.

[12] A. Kilbas, H. M. Srivastava, and J. J. Trujillo, *Theory and Applications of Fractional Differential Equations*, Elsevier, Amsterdam, Netherlands, 2006.

[13] I. Podlubny, *Fractional Differential Equations: An Introduction to Fractional Derivatives, Fractional Differential Equations, to Methods of Their Solution and Some of Their Applications*, Elsevier, Amsterdam, Netherlands, 1998.

[14] M. Caputo and M. Fabrizio, "A new definition of fractional derivative without singular kernel," *Progr Fract Differ Appl*, vol. 1, no. 2, pp. 73–85, 2015.

[15] H. Mohammadi, S. Kumar, S. Rezapour, and S. Etemad, "A theoretical study of the Caputo-Fabrizio fractional modeling for hearing loss due to Mumps virus with optimal control," *Chaos, Solitons & Fractals*, vol. 144, Article ID 110668, 2021.

[16] S. Rezapour, S. Etemad, and H. Mohammadi, "A mathematical analysis of a system of Caputo-Fabrizio fractional differential equationsfor the anthrax disease model in animals," *Advances in Differential Equations*, vol. 2020, no. 1, p. 481, 2020.

[17] V. S. Erturk, E. Godwe, D. Baleanu, P. Kumar, J. Asad, and A. Jajarmi, "Novel fractional-order Lagrangian to describe motion of beam on nanowire," *Acta Physica Polonica A*, vol. 140, no. 3, pp. 265–272, 2021.

[18] P. Kumar, V. S. Erturk, and M. Murillo-Arcila, "A complex fractional mathematical modeling for the love story of Layla and Majnun," *Chaos, Solitons & Fractals*, vol. 150, Article ID 111091, 2021.

[19] C. T. Deressa, S. Etemad, and S. Rezapour, "On a new four-dimensional model of memristor-based chaotic circuit in the context of nonsingular Atangana-Baleanu-Caputo operators," *Advances in Differential Equations*, vol. 2021, no. 1, pp. 1–24, 2021.

[20] H. Najafi, S. Etemad, N. Patanarapeelert, J. K. K. Asamoah, S. Rezapour, and T. Sitthiwirattham, "A study on dynamics of CD4+ T-cells under the effect of HIV-1 infection based on a mathematical fractal-fractional model via the Adams-Bashforth scheme and Newton polynomials," *Mathematics*, vol. 10, no. 9, p. 1366, 2022.

[21] Y. Fan, X. Huang, Z. Wang, and Y. Li, "Global dissipativity and quasi-synchronization of asynchronous updating fractional-order memristor-based neural networks via interval matrix method," *Journal of the Franklin Institute*, vol. 355, no. 13, pp. 5998–6025, 2018.

[22] L. Yao, Z. Wang, X. Huang, Y. Li, H. Shen, and G. Chen, "Aperiodic sampled-data control for exponential stabilization of delayed neural networks: a refined two-sided looped-functional approach," *IEEE Transactions on Circuits and Systems II: Express Briefs*, vol. 67, no. 12, pp. 3217–3221, 2020.

[23] J. Cermak and T. Kisela, "Delay-dependent stability switches in fractional differential equations," *Communications in Nonlinear Science and Numerical Simulation*, vol. 79, Article ID 104888, 2019.

[24] V. A. Vyawahare, G. Espinosa-Paredes, G. Datkhile, and P. Kadam, "Artificial neural network approximations of linear fractional neutron models," *Annals of Nuclear Energy*, vol. 113, pp. 75–88, 2018.

[25] G. Nagamani, M. Shafiya, G. Soundararajan, and M. Prakash, "Robust state estimation for fractional-order delayed BAM neural networks via LMI approach," *Journal of the Franklin Institute*, vol. 357, no. 8, pp. 4964–4982, 2020.

[26] Z. Aslipour and A. Yazdizadeh, "Identification of nonlinear systems using adaptive variable-order fractional neural networks (Case study: a wind turbine with practical results," *Engineering Applications of Artificial Intelligence*, vol. 85, pp. 462–473, 2019.

[27] R. Sharma, S. Bhasin, P. Gaur, and D. Joshi, "A switching-based collaborative fractional order fuzzy logic controllers for robotic manipulators," *Applied Mathematical Modelling*, vol. 73, pp. 228–246, 2019.

[28] J. Liu, P. Li, W. Chen, K. Qin, and L. Qi, "Distributed formation control of fractional-order multi-agent systems with relative damping and nonuniform time-delays," *ISA Transactions*, vol. 93, pp. 189–198, 2019.

[29] M. Syed Ali, G. Narayanan, S. Sevgen, V. Shekher, and S. Arik, "Global stability analysis of fractional-order fuzzy BAM neural networks with time delay and impulsive effects," *Communications in Nonlinear Science and Numerical Simulation*, vol. 78, Article ID 104853, 2019.

[30] L. Chen, T. Huang, J. T. Machado et al., "Delay-dependent criterion for asymptotic stability of a class of fractional-order memristive neural networks with time-varying delays," *Neural Networks*, vol. 118, pp. 289–299, 2019.

[31] B. N. Lundstrom, M. H. Higgs, W. J. Spain, and A. L. Fairhall, "Fractional differentiation by neocortical pyramidal neurons,"

Nature Neuroscience, vol. 11, no. 11, pp. 1335–1342, Article ID 18931665, 2008.

[32] J. Jia, X. Huang, Y. Li, J. Cao, and A. Alsaedi, "Global stabilization of fractional-order memristor-based neural networks with time delay," *IEEE Transactions on Neural Networks and Learning Systems*, vol. 31, no. 3, pp. 997–1009, 2020.

[33] Z. T. Njitacke, S. D. Isaac, T. Nestor, and J. Kengne, "Window of multistability and its control in a simple 3D Hopfield neural network: application to biomedical image encryption," *Neural Computing & Applications*, vol. 33, no. 12, pp. 6733–6752, 2021.

[34] A. Atangana and D. Baleanu, "T-cells under the effect of HIV-1 infection based on a mathematical fractal-fractional model via the Adams-Bashforth scheme and Newton polynomials," *New fractional derivatives with nonlocal and non-singular kernel: theory and application to heat transfer model*, https://arxiv.org/abs/1602.03408, 2016.

[35] C. Li and F. Zeng, "The finite difference methods for fractional ordinary differential equations," *Numerical Functional Analysis and Optimization*, vol. 34, no. 2, pp. 149–179, 2013.

[36] Z. Odibat and D. Baleanu, "Numerical simulation of initial value problems with generalized caputo-type fractional derivatives," *Applied Numerical Mathematics*, vol. 156, pp. 94–105, 2020.

[37] P. Kumar, V. S. Erturk, and A. Kumar, "A new technique to solve generalized Caputo type fractional differential equations with the example of computer virus model," *Journal of Mathematical Extension*, vol. 15, 2021.

[38] D. Baleanu, A. Jajarmi, and M. Hajipour, "On the nonlinear dynamical systems within the generalized fractional derivatives with Mittag-Leffler kernel," *Nonlinear Dynamics*, vol. 94, no. 1, pp. 397–414, 2018.

Hindawi
Complexity
Volume 2022, Article ID 2665925, 16 pages
https://doi.org/10.1155/2022/2665925

WILEY | Hindawi

Research Article

Consensus of Second-Order Heterogeneous Hybrid Multiagent Systems via Event-Triggered Protocols

Hong Zhang, Yanhan Li, and Ying Zheng

China-Belt and Road Joint Laboratory on Measurement and Control Technology, School of Artificial Intelligence and Automation, Huazhong University of Science and Technology, Wuhan, Hubei 430074, China

Correspondence should be addressed to Hong Zhang; sunracer@hust.edu.cn

Received 12 January 2022; Revised 3 March 2022; Accepted 14 March 2022; Published 30 April 2022

Academic Editor: Ning Cai

This paper investigates the event-based consensus problem for the heterogeneous hybrid multiagent system (MAS). First, the heterogeneous hybrid MAS is proposed which contains continuous and discrete-time subsystems with second-order and first-order heterogeneous dynamics. Second, the event-triggered protocols are proposed, which mainly include the event-based control laws and event-triggered conditions for different kinds of agents. Then, the consensus conclusions of fixed topology and switching topologies are obtained based on graph theory and nonnegative matrix theory, which include the constraints on control parameters, coupling gains, and sampling interval to guarantee consensus. Finally, a simulation example is given to verify the efficiency of the proposed protocols.

1. Introduction

With the popularity of distributed artificial intelligence, multiagent system (MAS) has been widely researched and applied to engineering, military, and other fields. It can accomplish huge and complex tasks in the real world through the mutual communication and coordination among individuals. It can also explain some complex phenomena in nature and human society, such as fish schools, bird flocks [1, 2], and the dynamics of opinion forming in human society [3]. At present, the research on multiagent system is mainly about consensus [4–8], flocking [9–11], formation [12–15], and so on.

Consensus, as one of the most fundamental cooperative behaviors of MASs, has attracted extensive interest. It means that the agents can reach the same states from any initial states by a suitable consensus algorithm or control law. Up to now, researchers have proposed many consensus algorithms for MASs through different analysis methods, such as the analysis based on nonnegative matrix theory [16–19], Lyapunov function analysis [20, 21], and frequency domain analysis [22–24]. In 2006, Xiao et al. studied the consensus problem for discrete-time first-order MASs with fixed topology and considered the structural decomposition of the leader-follower model [25]. Then, Xie et al. and Ren et al. gave some sufficient conditions for solving the consensus problem for second-order MASs with fixed and switching topologies [26, 27]. Shi et al. further considered the weighted-average consensus problem for second-order MASs and obtained necessary and sufficient conditions [28]. In recent years, the multiagent networks studied have become more and more complicated with the wide application of MASs. The heterogeneous MASs composed of agents with different dynamics are more suitable for real systems. Taking the multirobots systems into account, heterogeneous systems composed of robots with different perceptual capabilities can complete tasks faster [29]. A number of results about the consensus of heterogeneous MASs have been obtained, including low-order linear systems [30–32] and high-order linear systems [33–35]. In addition, the hybrid MASs including continuous and discrete-time subsystems have also attracted attention. Examples include the refrigeration and heating system. The heat-loss dynamics and the control of air conditioners belong to continuous-time systems, whereas the thermostat is controlled by a discrete-time system [36]. Since 2018, Zheng et al. have studied the

consensus problems of first-order and second-order hybrid systems and have proposed a game-theoretic approach to analyze the hybrid systems [37–39]. Su et al. designed an event-triggered consensus strategy for the second-order hybrid system [40] in 2019. Other researchers obtained more results about the hybrid MAS [41, 42].

In addition, interest in the event-based consensus problem for MASs has grown in the past decade. Compared with traditional methods, the event-triggered method has certain advantages in studying practical problems, such as minimizing the number of control actions and saving energy by updating the controller only at the trigger time and avoiding continuous communications. However, it also brings new theoretical and practical problems. The main task is the design of distributed event-triggered protocols, including event-triggered control laws and trigger conditions. In 2012, Dimarogonas et al. proposed effective event-triggered consensus algorithms for the first-order agents under undirected connected communication topologies [43]. Then, Fan et al. designed a fully distributed event-triggered strategy for solving the consensus problem of general linear MASs [44]. In recent years, several event-triggered consensus problems based on state feedback, output feedback, and leader-follower models were considered in [45–50].

In this paper, we consider the heterogeneous multiagent systems with continuous-time and discrete-time individuals (the heterogeneous hybrid MASs). For example, in the complex system of nature and human interaction, the biological signals are continuous signals, whereas the automated instruments with different functions are mostly discrete-time systems. Compared with the MASs in [42], the consensus problem for the heterogeneous hybrid MASs with a more general form is investigated, and the event-triggered protocols are proposed. First-order and second-order dynamic agents coexist in a system. Some of them belong to the continuous-time system, whereas the other agents are controlled by the discrete-time system. The main contributions of this paper are as follows. First, for the different dynamic characteristics of first-order and second-order agents, two kinds of event-triggered control laws are proposed. The event-triggered conditions are designed, which contain the position of all agents and the velocity of only second-order agents. Second, the sampled-data approach is used to solve the consensus problem for the heterogeneous hybrid MASs. On the one hand, the continuous-time subsystem and discrete-time subsystem can be better analyzed by the overall analysis method. On the other hand, this approach shows that the trigger time interval exists in a lower bound. Hence, the Zeno behavior is avoided. Finally, under the assumption that the fixed topology or the union of switching topologies contains a spanning tree, several results for solving the consensus problem are obtained by using graph theory and nonnegative matrix theory. Some selection conditions of control parameters, as well as the constraints of coupling gains and sampling interval, are given to guarantee consensus.

Throughout this paper, assume $0 < M < N$, $I_M = \{1, 2, \ldots, M\}$ and $I_N/I_M = \{M+1, M+2, \ldots, N\}$. $\mathcal{N}^+$ represents the set of positive integers. Consider a vector or a matrix A, $A \in R^n$ means A is a real column vector of length N. Similarly, A is an $n \times p$-dimensional real matrix, which is defined by $A \in R^{n\times p}$. The symbol A^T and $\|A\|$ represent the transpose and Euclidean norm of A, respectively. The calculational symbols $\otimes$ represent the Kronecker product of matrices.

2. Preliminaries and Problem Formulation

2.1. Preliminaries. The communication topology is described by a weighted directed graph $\mathcal{G}(\mathcal{V}, \mathcal{E}, \mathcal{A})$, where $\mathcal{V} = \{v_1, \ldots, v_N\}$ represents the nodes set and $\mathcal{E} \subseteq \mathcal{V} \times \mathcal{V}$ represents the set of edges between nodes. $\mathcal{A} = [a_{ij}] \in R^{N\times N}$ denotes the related adjacency matrix. If there is a directed path $\epsilon_{ji} \in \mathcal{E}$, indicating that the j th agent can transmit data to the i th agent, then $a_{ij} > 0$; otherwise, $a_{ij} = 0$. A diagonal matrix $\mathcal{D} = \mathrm{diag}(d_1, d_2, \ldots, d_N)$ is defined as the degree matrix of the directed graph $\mathcal{G}$, where $d_i = \sum_{j=1}^{N} a_{ij}$. The Laplacian matrix is expressed as $\mathcal{L} = \mathcal{D} - \mathcal{A}$. For a weighted directed graph $\mathcal{G}$, it is said to contain a directed spanning tree, indicating that there is a node, which has directed paths that can lead to all other nodes.

A nonnegative matrix $\mathcal{C} \in R^{n\times r}$ is also called a row stochastic matrix if the sum of its each row is equal to 1. Furthermore, if it also satisfies $\lim_{k\longrightarrow\infty} \mathcal{C}^k = 1_n \times v^T$, where $v \in R^n$, then it is indecomposable and aperiodic (SIA).

2.2. Problem Formulation. Considering the position and velocity states of the second-order agents and the position states of the first-order agents, the dynamic models are proposed, respectively. Suppose the number of agents in the entire system is N, where the first $M(M < N)$ agents are second-order agents, the remaining $(N - M)$ agents are first-order. The second-order dynamic agents are expressed as follows:

$$\begin{cases} \dot{x}_i^c(t) = v_i^c(t), & i \in I_M, \\ \dot{v}_i^c(t) = u_i^c(t), & i \in I_M, \\ x_i^d(kh+h) = x_i^d(kh) + hv_i^d(kh) + \dfrac{h^2}{2}u_i^d(kh), & i \in I_M, \\ v_i^d(kh+h) = v_i^d(kh) + hu_i^d(kh), & i \in I_M, \end{cases} \tag{1}$$

where $x_i \in R$, $v_i \in R$, and $u_i \in R$ represent the position, velocity, and control input of the second-order agent i, respectively. The superscripts c and d denote that the agent belongs to continuous and discrete-time subsystems. $h > 0$ is the sampling interval of the discrete-time subsystem. The dynamic model of first-order agents is given by

$$\begin{cases} \dot{x}_l^c(t) = u_l^c(t)\, l \in \dfrac{I_N}{I_M}, \\ x_l^d(kh+h) = x_l^d(kh) + hu_l^d(kh),\ l \in \dfrac{I_N}{I_M}. \end{cases} \tag{2}$$

Definition 1. The heterogeneous hybrid MAS is said to reach consensus if the position of all agents satisfies the following conditions from any initial state.

$$\begin{aligned} \lim_{t\longrightarrow\infty} x_i^c(t) &= \lim_{kh\longrightarrow\infty} x_i^d(kh) \\ &= C,\ i \in I_N, \end{aligned} \tag{3}$$

where C is a constant. To ensure that all agents can keep the same position state, (3) also indicates that the velocity of the second-order agents will tend to zero when $t \longrightarrow \infty$ or $kh \longrightarrow \infty$.

In order to propose the event-triggered protocols to solve this consensus problem, we first design the following event-triggered control laws for second-order agents:

$$\begin{cases} u_i^c(t) = -\beta v_i^c\left(t_\xi^i\right) + \alpha \sum_{j=1}^{N} a_{ij}\left[x_j^{c,d}\left(t_\xi^i\right) - x_i^c\left(t_\xi^i\right)\right],\ i \in I_N,\ t \in \left(t_\xi^i, t_{\xi+1}^i\right], \\ u_i^d(kh) = -\beta v_i^d\left(k_\xi^i h\right) + \alpha \sum_{j=1}^{N} a_{ij}\left[x_j^{c,d}\left(k_\xi^i h\right) - x_i^d\left(k_\xi^i h\right)\right],\ i \in I_N,\ kh \in \left(k_\xi^i h, k_{\xi+1}^i h\right], \end{cases} \tag{4}$$

where $\alpha, \beta > 0$ are control parameters, and $(t_0^i, \ldots, t_\xi^i, \cdots)$ and $(k_0^i h, \ldots, k_\xi^i h, \cdots)$ are the trigger time series. The event-triggered control laws of the first-order agents are designed as follows:

$$\begin{cases} u_i^c(t) = \alpha \sum_{j=1}^{N} a_{ij}\left[x_j^{c,d}\left(t_\xi^i\right) - x_i^c\left(t_\xi^i\right)\right],\ i \in \dfrac{I_N}{I_M},\ t \in \left(t_\xi^i, t_{\xi+1}^i\right], \\ u_i^d(kh) = \alpha \sum_{j=1}^{N} a_{ij}\left[x_j^{c,d}\left(k_\xi^i h\right) - x_i^d\left(k_\xi^i h\right)\right],\ i \in \dfrac{I_N}{I_M},\ kh \in \left(k_\xi^i h, k_{\xi+1}^i h\right]. \end{cases} \tag{5}$$

Before proposing the event-triggered conditions, the following definitions of the combined measurement and combined measurement error are given. The combined measurement is defined as

$$\begin{cases} q_i^c(t) &= \sum_{j=1}^{N} a_{ij}\left[x_j^{c,d}(t) - x_i^c(t)\right],\ i \in I_N, \\ q_i^d(kh) &= \sum_{j=1}^{N} a_{ij}\left[x_j^{c,d}(kh) - x_i^d(kh)\right],\ i \in I_N. \end{cases} \tag{6}$$

The combined measurement error is defined as

$$\begin{cases} e_{xi}^c(t) &= q_i^c\left(t_\xi^i\right) - q_i^c(t), i \in I_N, \\ e_{xi}^d(kh) &= q_i^d\left(k_\xi^i h\right) - q_i^d(kh),\ i \in I_N, \\ e_{vi}^c(t) &= v_i^c\left(t_\xi^i\right) - v_i^c(t),\ i \in I_M, \\ e_{vi}^d(kh) &= v_i^d\left(k_\xi^i h\right) - v_i^d(kh),\ i \in I_M. \end{cases} \tag{7}$$

In this paper, the event-triggered conditions are presented as follows:

$$\begin{aligned} t_{\xi+1}^i &= t_\xi^i + \min\{l_i h\},\ i \in I_N,\ l_i \in \mathcal{N}^+, \\ k_{\xi+1}^i h &= k_\xi^i h + \min\{l_i h\},\ i \in I_N,\ l_i \in \mathcal{N}^+, \end{aligned} \tag{8}$$

where $\min\{l_i h\}$ is the time interval between two adjacent trigger times, which $l_i h$ satisfies the following inequalities for the continuous and discrete-time agents:

$$\begin{cases} \left\|e_{xi}^c\left(t_\xi^i + l_i h\right)\right\| \geq \gamma_1 \left\|q_i^c\left(t_\xi^i\right)\right\| + \gamma_2 \delta^{t_\xi^i + l_i h}, & i \in I_N, \\ \left\|e_{vi}^c\left(t_\xi^i + l_i h\right)\right\| \geq \gamma_1 \left\|z_i^c\left(t_\xi^i\right)\right\| + \gamma_2 \delta^{t_\xi^i + l_i h}, & i \in I_M, \\ \left\|e_{xi}^d\left(k_\xi^i ht + nl_i qh\right)\right\| \geq \gamma_1 \left\|q_i^d\left(k_\xi^i h\right)\right\| + \gamma_2 \delta^{k_\xi^i h + l_i h}, & i \in I_N, \\ \left\|e_{vi}^d\left(k_\xi^i h + l_i h\right)\right\| \geq \gamma_1 \left\|z_i^d\left(k_\xi^i h\right)\right\| + \gamma_2 \delta^{k_\xi^i h + l_i h}, & i \in I_M, \end{cases} \tag{9}$$

where $\gamma_1, \gamma_2 > 0$ are the threshold parameters, $\delta > 0$ is the exponential component. And z_i is a new definition of hybrid state quantity for the second-order agent, which is defined as

$$z_i = x_i + hv_i,\ i = 1, 2, \ldots, M \tag{10}$$

According to the event-triggered conditions proposed above, the Zeno behavior is avoided because there is a lower bound $h > 0$ for the event-trigger interval $l_i h$, which ensures that the agent does not trigger infinitely for a limited time. Then, based on the definitions of (6) and (7), the event-triggered control laws (4) and (5) can be written as follows:

$$\begin{cases} u_i^c(t) = -\beta\left[v_i^c(t)t + ne_{vi}^c q(t)\right] \\ \quad + \alpha\left[q_i^c(t)t + ne_{xi}^c q(t)\right], & i \in I_M, t \in \left(t_\xi^i, t_{\xi+1}^i\right], \\ u_i^d(kh) = -\beta\left[v_i^d(kh)t + ne_{vi}^d q(kh)\right] \\ \quad + \alpha\left[q_i^d(kh)t + ne_{xi}^d q(kh)\right], & i \in I_M, kh \in \left(k_\xi^i h, k_{\xi+1}^i h\right], \\ u_l^c(t) = \alpha\left[q_l^c(t)t + ne_{xl}^c q(t)\right], & l \in I_N/I_M, t \in \left(t_\xi^l, t_{\xi+1}^l\right], \\ u_l^d(kh) = \alpha\left[q_l^d(kh)t + ne_{xl}^d q(kh)\right], & l \in I_N/I_M, kh \in \left(k_\xi^l h, k_{\xi+1}^l h\right]. \end{cases} \tag{11}$$

Each controller updates only at its own trigger time, so the energy can be saved. For any $t \in (t_\xi^i, t_{\xi+1}^i]$, $u_i(t) = u_i(t_\xi^i)$ does not change, and the continuous-time dynamics in (1) and (2) can be described as

$$\begin{cases} x_i^c(t) = x_i^c\left(t_\xi^i\right) + \int_{t_\xi^i}^t v_i^c(\tau)d\tau \\ \qquad = x_i^c\left(t_\xi^i\right) + \left(t - t_\xi^i\right)v_i^c\left(t_\xi^i\right) + \dfrac{\left(t - t_\xi^i\right)^2}{2}u_i^c\left(t_\xi^i\right), \; i \in I_M, \\ v_i^c(t) = v_i^c\left(t_\xi^i\right) + \int_{t_\xi^i}^t u_i^c(\tau)d\tau = v_i^c\left(t_\xi^i\right) + \left(t - t_\xi^i\right)u_i^c\left(t_\xi^i\right), i \in I_M, \\ x_l^c(t) = x_l^c\left(t_\xi^l\right) + \int_{t_\xi^l}^t u_l^c(\tau)d\tau = x_l^c\left(t_\xi^l\right) + \left(t - t_\xi^l\right)u_l^c\left(t_\xi^l\right), \; l \in I_N/I_M. \end{cases} \tag{12}$$

To analyze the entire MAS with continuous and discrete-time subsystems by the overall analysis method, the sampled-data method is applied in this paper. Considering the continuous subsystem in the discrete-time scale, a new discrete-time scale $\kappa h = l_i' h$ is defined to describe the entire MASs. $\kappa_\xi^i h$ represents the trigger time t_ξ^i and $k_\xi^i h$. The unified form of the entire MASs can be described as the following expression:

$$\begin{cases} x_i^{c,d}(\kappa h + h) = x_i^{c,d}(\kappa h) + h v_i^{c,d}(\kappa h) + \dfrac{h^2}{2}\left[-\beta v_i^{c,d}\left(\kappa_\xi^i h\right) + \alpha q_i^{c,d}\left(\kappa_\xi^i h\right)\right], \; i \in I_M, \\ v_i^{c,d}(\kappa h + h) = v_i^{c,d}(\kappa h) + h\left[-\beta v_i^{c,d}\left(\kappa_\xi^i h\right) + \alpha q_i^{c,d}\left(\kappa_\xi^i h\right)\right], \; i \in I_M, \\ x_l^{c,d}(\kappa h + h) = x_l^{c,d}(\kappa h) + h\alpha q_l^{c,d}\left(\kappa_\xi^i h\right), \; l \in I_N/I_M. \end{cases} \tag{13}$$

Substituting (7) into (13), we get the following expression:

$$\begin{cases} x_i^{c,d}(\kappa h + h) = x_i^{c,d}(\kappa h) + h v_i^{c,d}(\kappa h) - \dfrac{h^2\beta}{2}\left[v_i^{c,d}(\kappa h) + e_{vi}^{c,d}(\kappa h)\right] \\ +\dfrac{h^2\alpha}{2}\left[q_i^{c,d}(\kappa h) + e_{xi}^{c,d}(\kappa h)\right],\ i \in I_M, \\ v_i^{c,d}(\kappa h + h) = v_i^{c,d}(\kappa h)\left[-h\beta v_i^{c,d}(\kappa h) + e_{vi}^{c,d}(\kappa h)\right] \\ +h\alpha\left[q_i^{c,d}(\kappa h) + e_{xi}^{c,d}(\kappa h)\right],\ i \in I_M, \\ x_l^{c,d}(\kappa h + h) = x_l^{c,d}(\kappa h) + h\alpha\left[q_l^{c,d}(\kappa h) + e_{xl}^{c,d}(\kappa h)\right],\ l \in I_N/I_M. \end{cases} \tag{14}$$

In order to obtain the relationship between consensus achievement and system parameters, the following definitions are given:

$$\begin{aligned} x_s(kh) &= \left[x_1^T(kh), x_2^T(kh), \ldots, x_M^T(kh)\right]^T, \\ x_f(kh) &= \left[x_{M+1}^T(kh), x_{M+2}^T(kh), \ldots, x_N^T(kh)\right]^T, \\ v_s(kh) &= \left[v_1^T(kh), v_2^T(kh), \ldots, v_M^T(kh)\right]^T, \\ z_s(kh) &= \left[z_1^T(kh), z_2^T(kh), \ldots, z_M^T(kh)\right]^T, \\ Q_s(kh) &= \left[q_1^T(kh), q_2^T(kh), \ldots, q_M^T(kh)\right]^T, \\ Q_f(kh) &= \left[q_{M+1}^T(kh), q_{M+2}^T(kh), \ldots, q_N^T(kh)\right]^T, \\ E_{xs}(kh) &= \left[e_{x,1}^T(kh), e_{x,2}^T(kh), \ldots, e_{x,M}^T(kh)\right]^T, \\ E_{xf}(kh) &= \left[e_{x,M+1}^T(kh), e_{x,M+2}^T(kh), \ldots, e_{x,N}^T(kh)\right]^T, \\ E_v(kh) &= \left[e_{v,1}^T(kh), e_{v,2}^T(kh), \ldots, e_{v,M}^T(kh)\right]^T. \end{aligned} \tag{15}$$

Then, (14) can be written as

$$\begin{cases} x_s(\kappa h + h) = \dfrac{h\beta}{2}x_s(\kappa h) + \dfrac{2 - h\beta}{2}z_s(\kappa h) + \dfrac{h^2\alpha}{2}Q_s(\kappa h) \\ -\dfrac{h^2\beta}{2}E_v(\kappa h) + \dfrac{h^2\alpha}{2}E_{xs}(\kappa h), \\ z_s(\kappa h + h) = \dfrac{3h\beta - 2}{2}x_s(\kappa h) + \dfrac{4 - 3h\beta}{2}z_s(\kappa h) + \dfrac{3h^2\alpha}{2}Q_s(\kappa h) \\ -\dfrac{3h^2\beta}{2}E_v(\kappa h) + \dfrac{3h^2\alpha}{2}E_{xs}(\kappa h), \\ x_f(\kappa h + h) = x_f(\kappa h) + h\alpha Q_f(\kappa h) + h\alpha E_{xf}(\kappa h). \end{cases} \tag{16}$$

Considering the communication between different dynamics, the Laplacian matrix representing the communication topology is divided into four parts.

$$\mathscr{L}(kh) = \begin{bmatrix} \mathscr{L}_1(kh)\mathscr{L}_2(kh) \\ \mathscr{L}_3(kh)\mathscr{L}_4(kh) \end{bmatrix}, \tag{17}$$

where $\mathscr{L}_1$ represents the directed communication from second-order agents to second-order agents; $\mathscr{L}_2$, $\mathscr{L}_3$, and $\mathscr{L}_4$ represent the directed communication from first-order agents to second-order agents, from first-order agents to first-order agents, and from second-order agents to first-order agents, respectively. (16) can be converted into the following expression:

$$\begin{cases} x_s(\kappa h + h) = \left[\dfrac{h\beta}{2} I_M - \dfrac{h^2\alpha}{2}\mathscr{L}_1(\kappa h)\right] x_s(\kappa h) + \dfrac{2 - h\beta}{2} z_s(\kappa h) \\ -\dfrac{h^2\alpha}{2}\mathscr{L}_2(\kappa h) x_f(\kappa h) + \dfrac{h^2\alpha}{2} E_{xs}(\kappa h) \dfrac{h^2\beta}{2} E_v(\kappa h), \\ z_s(\kappa h + h) = \left[\dfrac{3h\beta - 2}{2} I_M - \dfrac{3h^2\alpha}{2}\mathscr{L}_1(\kappa h)\right] x_s(\kappa h) + \dfrac{4 - 3h\beta}{2} z_s(\kappa h) \\ -\dfrac{3h^2\alpha}{2}\mathscr{L}_2(\kappa h) x_f(\kappa h) + \dfrac{3h^2\alpha}{2} E_{xs}(\kappa h) - \dfrac{3h^2\beta}{2} E_v(\kappa h), \\ x_f(\kappa h + h) = -h\alpha\mathscr{L}_3(\kappa h) x_s(\kappa h) + \left[I_{N-M} - h\alpha\mathscr{L}_4(\kappa h)\right] x_f(\kappa h) \\ +h\alpha E_{xf}(\kappa h). \end{cases} \tag{18}$$

Then, two large matrices

$$\begin{aligned} Y(kh) &= \left[x_s^T(kh), z_s^T(kh), x_f^T(kh)\right]^T, \\ E(kh) &= \left[E_{xs}^T(kh), E_v^T(kh), E_{xf}^T(kh)\right]^T. \end{aligned} \tag{19}$$

are defined. We can get

$$Y(\kappa h + h) = H(\kappa h) Y(\kappa h) + PE(\kappa h), \tag{20}$$

where

$$\begin{aligned} H(\kappa h) &= \begin{bmatrix} \dfrac{h\beta}{2} I_M - \dfrac{h^2\alpha}{2}\mathscr{L}_1(\kappa h) & \dfrac{2 - h\beta}{2} I_M & -\dfrac{h^2\alpha}{2}\mathscr{L}_2(\kappa h) \\ \dfrac{3h\beta - 2}{2} I_M - \dfrac{3h^2\alpha}{2}\mathscr{L}_1(\kappa h) & \dfrac{4 - 3h\beta}{2} I_M & -\dfrac{3h^2\alpha}{2}\mathscr{L}_2(\kappa h) \\ -h\alpha\mathscr{L}_3(\kappa h) & 0 & I_{N-M} - h\alpha\mathscr{L}_4(\kappa h) \end{bmatrix} \otimes I_n, \\ P &= \begin{bmatrix} \dfrac{h^2\alpha}{2} I_M & -\dfrac{h^2\beta}{2} I_M & 0 \\ \dfrac{3h^2\alpha}{2} I_M & -\dfrac{3h^2\beta}{2} I_M & 0 \\ 0 & 0 & h\alpha I_{N-M} \end{bmatrix} \otimes I_n. \end{aligned} \tag{21}$$

Based on the analysis method in [40], the error system is further constructed. Define

$$\begin{aligned}
\phi_s(kh) &= \left[x_2^T(kh) - x_1^T(kh), \ldots, x_M^T(kh) - x_1^T(kh)\right]^T,\\
\psi_s(kh) &= \left[z_2^T(kh) - z_1^T(kh), \ldots, z_M^T(kh) - z_1^T(kh)\right]^T,\\
\phi_f(kh) &= \left[x_{M+1}^T(kh) - x_1^T(kh), \ldots, x_N^T(kh) - x_1^T(kh)\right]^T,\\
\mathscr{L} &= \begin{bmatrix} l_{2,2} - l_{1,2} & l_{2,3} - l_{1,3} & \cdots & l_{2,N} - l_{1,N} \\ l_{3,2} - l_{1,2} & l_{3,3} - l_{1,3} & \cdots & l_{3,N} - l_{1,N} \\ \vdots & \vdots & \ddots & \vdots \\ l_{N,2} - l_{1,2} & l_{N,3} - l_{1,3} & \cdots & l_{N,N} - l_{1,N} \end{bmatrix}\\
&= \begin{bmatrix} \overline{\mathscr{L}}_1 \overline{\mathscr{L}}_2 \\ \overline{\mathscr{L}}_3 \overline{\mathscr{L}}_4 \end{bmatrix},\\
\overline{Y}(kh) &= \left[\, \phi_s^T(kh)\psi_s^T(kh)\phi_f^T(kh) \,\right]^T.
\end{aligned} \tag{22}$$

Then, (18) can be rewritten as

$$\overline{Y}(\kappa h + h) = \overline{H}(\kappa h)\overline{Y}(\kappa h) + \overline{P}E(\kappa h), \tag{23}$$

where

$$\begin{aligned}
\overline{H}(\kappa h) &= \begin{bmatrix} \frac{h\beta}{2} I_M - \frac{h^2\alpha}{2}\overline{\mathscr{L}}_1(\kappa h) & \frac{2 - h\beta}{2} I_M & -\frac{h^2\alpha}{2}\overline{\mathscr{L}}_2(\kappa h) \\ \frac{3h\beta - 2}{2} I_M - \frac{3h^2\alpha}{2}\overline{\mathscr{L}}_1(\kappa h) & \frac{4 - 3h\beta}{2} I_M & -\frac{3h^2\alpha}{2}\overline{\mathscr{L}}_2(\kappa h) \\ -h\alpha\overline{\mathscr{L}}_3(\kappa h) & 0 & I_{N-M} - h\alpha\overline{\mathscr{L}}_4(\kappa h) \end{bmatrix} \otimes I_n,\\
\overline{P} &= \begin{bmatrix} \frac{h^2\alpha}{2} I_M & -\frac{h^2\beta}{2} I_M & 0 \\ \frac{3h^2\alpha}{2} I_M & -\frac{3h^2\beta}{2} I_M & 0 \\ 0 & 0 & h\alpha I_{N-M} \end{bmatrix} \times \begin{bmatrix} -1_{M-1} & I_{M-1} & 0 & 0 & 0 \\ 0 & 0 & -1_{M-1} & I_{M-1} & 0 \\ -1_{N-M} & 0 & 0 & 0 & I_{N-M} \end{bmatrix} \otimes I_n.
\end{aligned} \tag{24}$$

3. Main Result

3.1. Fixed Communication Topology. Consider the consensus problem of fixed communication topology, which means the directed graph $\mathscr{G}(\mathscr{V}, \mathscr{E}, \mathscr{A})$ does not change over time and $a_{ij}(t) = a_{ij}(kh) = a_{ij}$.

Lemma 1. *[8] If the sum of each row of nonnegative matrix $H = [h_{ij}] \in R^{(M+N)\times(M+N)}$ is a positive constant $\mu > 0$, then μ is an eigenvalue of H corresponding to the eigenvector 1_{N+M}. Furthermore, if the algebraic multiplicity of the eigenvalue μ of H is 1 and $h_{ii} > 0, i = 1, 2, \ldots, M + N$, then, for each eigenvalue $\lambda \neq \mu$, $|\lambda| < \mu$ is satisfied.*

Remark 1. In practical applications, the movement of the agents should be multidimensional. This article only considers motion in a single dimension; in other words, $I_n = 1$, because motion in a certain direction can be decomposed into motion in several independent directions. Therefore, the conclusion under a single dimension can also be extended to a multidimensional scale.

Theorem 1. *The matrix H defined in (18) contains eigenvalue 1, and the remaining eigenvalues satisfy $|\lambda| < 1$, and all the eigenvalues of $\overline{H}$ defined in (20) satisfy $|\overline{\lambda}| < 1$, if and only if the fixed communication topology contains a directed spanning tree and coupling gains, and sampling interval and control parameters satisfy as follows:*

$$\begin{cases} \dfrac{4}{3} > h\beta > \dfrac{2}{3} + h^2\alpha \max\limits_{i\in I_M}\left(\sum\limits_{j=1}^{N} a_{ij}\right), \\ 1 > h\alpha \max\limits_{i\in I_N/I_M}\left(\sum\limits_{j=1}^{N} a_{ij}\right). \end{cases} \tag{25}$$

Proof. Under condition (21), H is a row stochastic matrix with positive diagonal elements, and $\lambda = 1$ is one of the eigenvalues of H corresponding to eigenvector 1_{N+M}. The column and row transformations of $H - I_{N+M}$ are performed as follows:

$$H - I_{N+M} = \begin{bmatrix} \frac{h\beta-2}{2}I_M - \frac{h^2\alpha}{2}\mathscr{L}_1 & \frac{2-h\beta}{2}I_M & -\frac{h^2\alpha}{2}\mathscr{L}_2 \\ \frac{3h\beta-2}{2}I_M - \frac{3h^2\alpha}{2}\mathscr{L}_1 & \frac{2-3h\beta}{2}I_M & -\frac{3h^2\alpha}{2}\mathscr{L}_2 \\ -h\alpha\mathscr{L}_3 & 0 & -h\alpha\mathscr{L}_4 \end{bmatrix} \longrightarrow \begin{bmatrix} \mathscr{L}_1 & 0 & \mathscr{L}_2 \\ I_M & -I_M & 0 \\ \mathscr{L}_3 & 0 & \mathscr{L}_4 \end{bmatrix} \longrightarrow \begin{bmatrix} I_M & 0 & 0 \\ 0 & \mathscr{L}_1 & \mathscr{L}_2 \\ 0 & \mathscr{L}_3 & \mathscr{L}_4 \end{bmatrix}. \tag{26}$$

We obtain $\operatorname{rank}(H - I_{M+N}) = M + \operatorname{rank}(\mathscr{L})$. H has one eigenvalue $\lambda = 1$ with algebraic multiplicity 1, if and only if $\operatorname{rank}(L) = N - 1$, which is equivalent to the topology containing a directed spanning tree [8]. Based on Lemma 1, we can obtain that all the other eigenvalues of H satisfy $|\lambda| < 1$.

Next, it can be proved that all the nonzero eigenvalues of $\mathscr{L}$ are also the eigenvalues of $\overline{\mathscr{L}}$. By observing (18) and (20), the mapping of the eigenvalues of H and $\mathscr{L}$ is the same as the mapping of the eigenvalues of $\overline{H}$ and $\overline{\mathscr{L}}$. Thus, the eigenvalues of H and $\overline{H}$ are equal if $\mathscr{L}$ and $\overline{\mathscr{L}}$ have the same eigenvalues. Additionally, the eigenvalue of H corresponding to the zero eigenvalue of $\mathscr{L}$ is one. Therefore, all eigenvalues of H are also eigenvalues of $\overline{H}$ except for eigenvalue 1. In other words, all the eigenvalues of $\overline{H}$ satisfy $|\bar{\lambda}| < 1$. □

Lemma 2. *[40] If a matrix $\overline{H}$ satisfies that all its eigenvalues are inside the unit circle, then the following inequality is satisfied:*

$$\|\overline{H}\|^k \le a \cdot b^k, \tag{27}$$

where a and b are positive constants that satisfy $a \ge 1$ and $0 < b < 1$.

Theorem 2. *Consider the consensus of the heterogeneous hybrid MASs (1) and (2) with fixed communication topology under the event-triggered control laws (4) and (5) and event-triggered conditions (8), (9), and (10) with $\gamma_1 \in (0, 1)$, $\gamma_2 \in (0, \infty)$, and $\delta \in (b, 1)$. If the fixed communication topology $\mathcal{G}$ has a directed spanning tree and conditions (21) in Theorem 1 are satisfied, the heterogeneous hybrid MASs can reach the consensus condition (3).*

Proof. Firstly, (20) is written in the following form by iteration.

$$\overline{Y}(\kappa h) = \overline{H}^{\kappa}\overline{Y}(0) + \overline{P}\sum_{s=0}^{\kappa-1}\overline{H}^{\kappa-1-s}E(sh). \tag{28}$$

By Theorem 1 and Lemma 2, we have

$$\|\overline{Y}(\kappa h)\| \le ab^{\kappa}\|\overline{Y}(0)\| + \|\overline{P}\|\sum_{s=0}^{\kappa-1}ab^{\kappa-1-s}\|E(sh)\|, \tag{29}$$

where $a \ge 1$ and $0 < b < 1$. According to the designed event-trigger conditions (9) and (10), $\|E(\kappa h)\|$ can be expressed as

$$\|E(\kappa h)\| \le \gamma_1\left\|\begin{bmatrix} Q_s(\kappa h) \\ Q_f(\kappa h) \\ z_s(\kappa h) \end{bmatrix}\right\| + \gamma_2\sqrt{N+M}\delta^{\kappa}. \tag{30}$$

Two positive constants C_1 and C_2 are defined, and then

$$\left\|\begin{bmatrix} Q_s(\kappa h) \\ Q_f(\kappa h) \end{bmatrix}\right\| \le \|\mathscr{L}\| \cdot \left\|\begin{bmatrix} \phi_s(\kappa h) \\ \phi_f(\kappa h) \end{bmatrix}\right\| = C_1\left\|\begin{bmatrix} \phi_s(\kappa h) \\ \phi_f(\kappa h) \end{bmatrix}\right\|,$$

$$\begin{aligned}\left\|z_s(\kappa h)\right\| &\le \left\| \begin{bmatrix} 1 & 0_{1\times(M-1)} \\ -1_{(M-1)\times 1} & I_{M-1} \end{bmatrix} \right\| \cdot \left\| \begin{bmatrix} z_1(\kappa h) \\ \psi_s(\kappa h) \end{bmatrix} \right\| \\ &\le \left\| \begin{bmatrix} 1 & 0_{1\times(M-1)} \\ -1_{(M-1)\times 1} & I_{M-1} \end{bmatrix} \right\| \left\{ \left\|z_s(\kappa h)\right\| + \left\|\psi_s(\kappa h)\right\| \right\}. \end{aligned} \tag{31}$$

Through (28), we further obtain

$$\left\|z_s(\kappa h)\right\| \le \frac{\left\| \begin{bmatrix} 1 & 0_{1\times(M-1)} \\ -1_{(M-1)\times 1} & I_{M-1} \end{bmatrix} \right\|}{1 - \left\| \begin{bmatrix} 1 & 0_{1\times(M-1)} \\ -1_{(M-1)\times 1} & I_{M-1} \end{bmatrix} \right\|} \cdot \left\|\psi_s(\kappa h)\right\| = C_2 \cdot \left\|\psi_s(\kappa h)\right\|. \tag{32}$$

From (27) and (29), (30) can be converted as follows:

$$\|E(\kappa h)\| \le \gamma_1 \|C\overline{Y}(\kappa h)\| + \gamma_2 \sqrt{N+M}\,\delta^{\kappa}, \tag{33}$$

where C is a bounded positive constant only related to communication topology. Letting $\rho = \|\overline{P}\|$ and $\mathcal{Z} = \max\{\rho a\gamma_2\sqrt{N+M}/(\delta - b - \rho a\gamma_1 C), a\|\overline{Y}(0)\|\}$, ρ and $\mathcal{Z}$ are also bounded positive constants related to communication topology. Then, the following inequality will be proved by contradiction:

$$\|\overline{Y}(\kappa h)\| \le \mathcal{Z}\delta^{\kappa}. \tag{34}$$

Consider that there is a constant $k^* > \kappa > 0$ that makes inequality (31) invalid. Thus,

$$\left\|\overline{Y}(k^* h)\right\| > \mathcal{Z}\delta^{k^*}. \tag{35}$$

According to (25) and (30), one has

$$\begin{aligned} \mathcal{Z}\delta^{k^*} &< \left\|\overline{Y}(k^* h)\right\| \\ &\le ab^{k^*}\|\overline{Y}(0)\| + \rho \sum_{s=0}^{k^*-1} ab^{k^*-1-s}\left(\gamma_1 C\mathcal{Z} + \gamma_2\sqrt{N+M}\right)\delta^{s} \\ &\le ab^{k^*}\|\overline{Y}(0)\| + \rho a\left(\gamma_1 C\mathcal{Z} + \gamma_2\sqrt{N+M}\right)\frac{b^{k^*} - \delta^{k^*}}{b-\delta} \\ &= \left[a\|\overline{Y}(0)\| + \frac{\rho a\left(\gamma_1 C\mathcal{Z} + \gamma_2\sqrt{N+M}\right)}{b-\delta}\right]b^{k^*} \\ &\quad + \frac{\rho a\left(\gamma_1 C\mathcal{Z} + \gamma_2\sqrt{N+M}\right)}{\delta - b}\delta^{k^*}. \end{aligned} \tag{36}$$

Next, (31) can be proved in three cases. □

Case 1.

$$\mathcal{Z} = \rho a\gamma_2 \frac{\sqrt{N+M}}{(\delta - b - \rho a\gamma_1 C)}, \tag{37}$$

which indicates that

$$\frac{\rho a\left(\gamma_1 C\mathcal{Z} + \gamma_2\sqrt{N+M}\right)}{(\delta - b)} = \mathcal{Z} \tag{38}$$

$$\frac{\rho a\left(\gamma_1 C\mathcal{Z} + \gamma_2\sqrt{N+M}\right)}{(\delta - b)} > a\|\overline{Y}(0)\|. \tag{39}$$

According to (33), we have

$$\begin{aligned} \mathcal{Z}\delta^{k^*} &< \left[a\|\overline{Y}(0)\| + \frac{\rho a\left(\gamma_1 C\mathcal{Z} + \gamma_2\sqrt{N+M}\right)}{b-\delta}\right]b^{k^*} \\ &\quad + \frac{\rho a\left(\gamma_1 C\mathcal{Z} + \gamma_2\sqrt{N+M}\right)}{\delta - b}\delta^{k^*} \\ &< \frac{\rho a\left(\gamma_1 C\mathcal{Z} + \gamma_2\sqrt{N+M}\right)}{\delta - b}\delta^{k^*} = \mathcal{Z}\delta^{k^*}. \end{aligned} \tag{40}$$

Case 2. $\mathcal{Z} = a\|\overline{Y}(0)\|$ and $\rho a\gamma_2\sqrt{N+M}/(\delta - b - \rho a\gamma_1 C) > 0$, which indicates $\delta > b$. According to (33), we can obtain that

$$\begin{aligned} \mathcal{Z}\delta^{k^*} &< \left[a\|\overline{Y}(0)\| + \frac{\rho a\left(\gamma_1 C\mathcal{Z} + \gamma_2\sqrt{N+M}\right)}{b-\delta}\right]\delta^{k^*} \\ &\quad + \frac{\rho a\left(\gamma_1 C\mathcal{Z} + \gamma_2\sqrt{N+M}\right)}{\delta - b}\delta^{k^*} \\ &= a\|\overline{Y}(0)\|\delta^{k^*} = \mathcal{Z}\delta^{k^*}. \end{aligned} \tag{41}$$

Case 3. $\mathcal{Z} = a\|\overline{Y}(0)\|$ and $\rho a\gamma_2\sqrt{N+M}/(\delta - b - \rho a\gamma_1 C) > 0$, which indicates $a\|\overline{Y}(0)\| < \rho a(\gamma_1 C\mathcal{Z} + \gamma_2\sqrt{N+M})/(\delta - b)$. The proof is similar to case 1 that

$$\mathcal{Z}\delta^{k^*} < \frac{\rho a\left(\gamma_1 C\mathcal{Z} + \gamma_2\sqrt{N+M}\right)}{\delta - b}\delta^{k^*} < \mathcal{Z}\delta^{k^*}. \tag{42}$$

Combining the three cases, the inequality (31) holds, from which we can obtain that

$$\lim_{\kappa h \longrightarrow \infty} \left\| \begin{bmatrix} \phi_s(kh) \\ \psi_s(kh) \\ \phi_f(kh) \end{bmatrix} \right\| = 0. \tag{43}$$

Then, we further consider the consensus of the continuous-time agents in real time. The following inequality is established:

$$\begin{aligned} \left\| v_i^c(t) - v_j^c(t) \right\| &\le \left\| v_i^c(t) - v_i^c(kh) \right\| + \left\| v_i^c(kh) - v_j^c(kh) \right\| \\ &\quad + \left\| v_j^c(kh) - v_j^c(t) \right\|, i \in I_M, \\ \left\| x_i^c(t) - x_j^c(t) \right\| &\le \left\| x_i^c(t) - x_i^c(kh) \right\| + \left\| x_i^c(kh) - x_j^c(kh) \right\| \\ &\quad + \left\| x_i^c(kh) - x_j^c(t) \right\|, i \in I_N. \end{aligned} \tag{44}$$

When $\kappa h \longrightarrow \infty$, we can get $v_i^{c,d}(k_\xi^i h) \longrightarrow 0, q_i^{c,d}(k_\xi^i h) \longrightarrow 0$. Combined with (4), (5), (6), and (12), when $t \in (kh, kh + h]$, the following inequalities are obtained:

$$\begin{aligned} \lim_{t,kh \longrightarrow \infty} \left\| v_i^c(t) - v_i^c(kh) \right\| &\le \lim_{t,kh \longrightarrow \infty} h\left\{ -\beta v_i^{c,d}\left(k_\xi^i h\right) + \alpha q_i^{c,d}\left(k_\xi^i h\right) \right\}, i \in I_M, \\ \lim_{t,kh \longrightarrow \infty} = \left\| x_i^c(t) - x_i^c(kh) \right\| &\le \lim_{t,kh \longrightarrow \infty} h v_i^{c,d}\left(k_\xi^i h\right) \\ &\quad + \frac{\left(t - k_\xi^i h\right)^2 - \left(kh - k_\xi^i h\right)^2}{2} \left\{ -\beta v_i^{c,d}\left(k_\xi^i h\right) + \alpha q_i^{c,d}\left(k_\xi^i h\right) \right\}, i \in I_M, \\ \lim_{t,kh \longrightarrow \infty} \|\theta\| &\le \lim_{t,kh \longrightarrow \infty} h\alpha q_l^{c,d}\left(k_\xi^l h\right), l \in I_N / I_M. \end{aligned} \tag{45}$$

Then,

$$\begin{aligned} \lim_{t,kh \longrightarrow \infty} \left\| x_i^c(t) - x_i^c(kh) \right\| &= 0, i \in I_M, \\ \lim_{t,kh \longrightarrow \infty} \left\| x_i^c(t) - x_i^c(kh) \right\| &= 0, l \in \frac{I_N}{I_M}. \end{aligned} \tag{46}$$

From (44) and (46), continuous-time individuals can also achieve consensus on continuous-time scales. Combined with (43), the consensus conditions (3) are satisfied.

3.2. Switching Communication Topologies. According to the above conclusions with the fixed topology, the consensus of the heterogeneous hybrid MASs with switching communication topologies is considered. The system description (18) is rewritten as

$$Y\left(k_{p+1} h\right) = \Omega\left(k_p\right)\left(k_p h\right) + Q_E\left(k_p\right), \; p = 1, 2, \ldots, \infty, \tag{47}$$

where $k_p \in \kappa$ is the p th event-triggering instant of an agent from its initial state, $\Omega(k_p) = \prod_{s=k_p}^{k_{p+1}-1} H(sh)$ is the matrix product of H, corresponding to all switching communication topologies during each interval $[k_p h, k_{p+1} h)$, and

$$Q_E\left(k_p\right) = \mathrm{PE}\left[\left(k_{p+1} - 1\right)h\right] + P \sum_{s=k_p}^{k_{p+1}-2} E(sh) \cdot \prod_{d=s+1}^{k_{p+1}-1} H(dh) \tag{48}$$

is the accumulation of errors. Similarly, the error system description (20) can also be rewritten as

$$\overline{Y}\left(k_{p+1} h\right) = \overline{\Omega}\left(k_p\right)\overline{Y}\left(k_p h\right) + \overline{Q}_E\left(k_p\right), p = 1, 2, \ldots, \infty, \tag{49}$$

where

$$\overline{\Omega}\left(k_p\right) = \prod_{s=k_p}^{k_{p+1}-1} \overline{H}(sh), \tag{50}$$

$$\overline{Q}_E\left(k_p\right) = \overline{P} E\left[\left(k_{p+1} - 1\right)h\right] + \overline{P} \sum_{s=k_p}^{k_{p+1}-2} E(sh) \cdot \prod_{d=s+1}^{k_{p+1}-1} \overline{H}(dh). \tag{51}$$

Remark 2. To simplify subsequent proofs, it is assumed that $k_{p+1} - k_p > 1$ in the subsection on switching communication topologies, which means there are at least two different

communication topologies in the period $[k_p, k_{p+1})$. Otherwise, it can be regarded as a fixed communication topology in a short period of time, and the convergence will not be destroyed according to the existing conclusions.

Theorem 3. *The matrix product $\Omega(k_p)$ is SIA, and all the eigenvalues of $\overline{\Omega}(k_p)$ satisfy $|\lambda_\Omega| < 1$ if the union of communication topologies $\{G[k_p h], G[(k_p+1)h], \ldots, G[(k_{p+1}-1)h]\}$ of each interval $[k_p h, k_{p+1} h)$ contains a spanning tree and the coupling gains, and sampling interval and control parameters satisfy conditions (21) in Theorem 1.*

Proof. Define $\widetilde{\mathscr{L}} = \sum_{s=k_p}^{k_{p+1}-1} \mathscr{L}(sh)/(k_{p+1}-k_p)$ as the Laplacian matrix of the union of directed graphs during time interval $[k_p h, k_{p+1} h)$, and $\widetilde{\overline{\mathscr{L}}}$ is the matrix obtained by $\widetilde{\mathscr{L}}$ through the same transformation as $\overline{\mathscr{L}}$ in (19).

$$\widetilde{H} = \sum_{s=k_p}^{k_{p+1}-1} \frac{H(sh)}{(k_{p+1}-k_p)} \tag{52}$$

still satisfies the sum of each row is 1. Then, we can get $\operatorname{rank}(\widetilde{H} - I_{N+M}) = M + \operatorname{rank}(\widetilde{\mathscr{L}})$ by taking the elements column and row transforms as follows:

$$\widetilde{H} - I_{N+M} = \begin{bmatrix} \frac{h\beta-2}{2} I_M - \frac{h^2\alpha}{2}\widetilde{\overline{\mathscr{L}}}_1 & \frac{2-h\beta}{2} I_M & -\frac{h^2\alpha}{2}\widetilde{\overline{\mathscr{L}}}_2 \\ \frac{3h\beta-2}{2} I_M - \frac{3h^2\alpha}{2}\widetilde{\overline{\mathscr{L}}}_1 & \frac{2-3h\beta}{2} I_M & -\frac{3h^2\alpha}{2}\widetilde{\overline{\mathscr{L}}}_2 \\ -h\alpha\widetilde{\overline{\mathscr{L}}}_3 & 0 & -h\alpha\widetilde{\overline{\mathscr{L}}}_4 \end{bmatrix} \longrightarrow \begin{bmatrix} I_M & 0 \\ 0 & \widetilde{\mathscr{L}} \end{bmatrix}. \tag{53}$$

Thus, $\widetilde{H}$ has eigenvalue $\tilde{\lambda} = 1$ with algebraic multiplicity 1, if and only if $\operatorname{rank}(\widetilde{\mathscr{L}}) = N - 1$, which means that the union of topologies contains a spanning tree. According to Lemma 3.1 in [18], we can get that

$$\prod_{s=k_p}^{k_{p+1}-1} H(sh) > \sum_{s=k_p}^{k_{p+1}-1} H(sh)/\left(k_{p+1}-k_p\right), \tag{54}$$

which indicates that the graph of the matrix product $\Omega(k_p)$ also contains a spanning tree. Besides, $\Omega(k_p)$ is a stochastic matrix with positive diagonal elements if conditions (21) are satisfied, because the matrix multiplication among stochastic matrixes with positive diagonal elements is closed. In other words, $\Omega(k_p)$ is SIA.

Similar to the proof of Theorem 1, for the error system, it can be proved that all eigenvalues of $\Omega(k_p)$ except eigenvalue 1 are also eigenvalues of $\overline{\Omega}(k_p)$. □

Theorem 4. *Consider the consensus of the heterogeneous hybrid MASs (1) and (2) with switching communication topologies under the event-triggered control laws (4) and (5) and event-triggered conditions (8), (9), and (10) with $\gamma_1 \in (0,1)$, $\gamma_2 \in (0,\infty)$, and $\delta \in (b,1)$. If the union of switching topologies $\{G[k_p h], G[(k_p+1)h], \ldots, G[(k_{p+1}-1)h]\}$ of each interval $[k_p h, k_{p+1} h)$ has a directed spanning tree and conditions (21) in Theorem 1 are satisfied, the heterogeneous hybrid MASs can reach the consensus condition (3).*

Proof. Through iteration, the error system description (39) with switching communication topologies can be expressed as

$$\begin{aligned} \overline{Y}\left(k_p h\right) = {} & \overline{\Omega}(k_0)\overline{\Omega}(k_1)\cdots\overline{\Omega}\left(k_{p-1}\right)\overline{Y}(0) \\ & + \overline{\Omega}(k_1)\Omega(k_2)\cdots\overline{\Omega}\left(k_{p-1}\right)\overline{Q}_E(k_0) \\ & + \cdots \\ & + \overline{\Omega}\left(k_{p-1}\right)\overline{Q}_E\left(k_{p-2}\right) \\ & + \overline{Q}_E\left(k_{p-1}\right). \end{aligned} \tag{55}$$

Let

$$\Omega^* = \max\left\{\left\|\overline{\Omega}(k_0)\right\|, \left\|\overline{\Omega}(k_1)\right\|, \ldots, \left\|\overline{\Omega}\left(k_{p-1}\right)\right\|\right\}. \tag{56}$$

Combined with Lemma 2, we have

$$\begin{aligned} \left\|\overline{Y}\left(k_p h\right)\right\| &\le \Omega^{*p}\left\|\overline{Y}(0)\right\| + \sum_{s=0}^{p-1} \Omega^{*p-1-s}\left\|\overline{Q}_E(k_s)\right\| \\ &\le a' B^p \left\|\overline{Y}(0)\right\| + \sum_{s=0}^{p-1} a' B^{p-1-s}\left\|\overline{Q}_E(k_s)\right\|, \end{aligned} \tag{57}$$

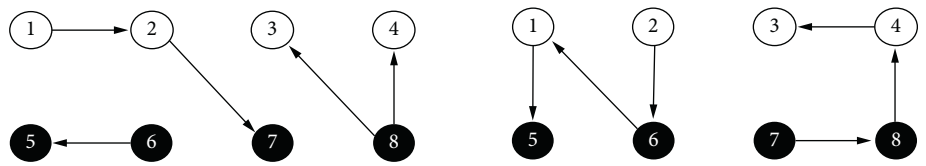

(a) Topology 1 (b) Topology 2

①②: CTS0; ③④: DTS0; ❺❻: CTF0; ❼❽: DTF0;

Figure 1: Switching topologies.

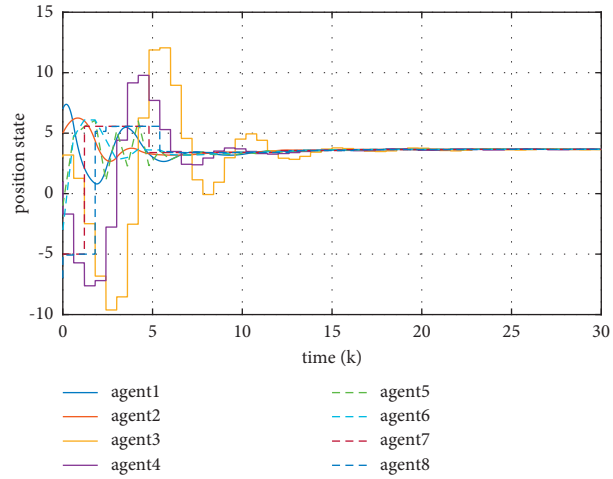

Figure 2: Position of the dynamic agents.

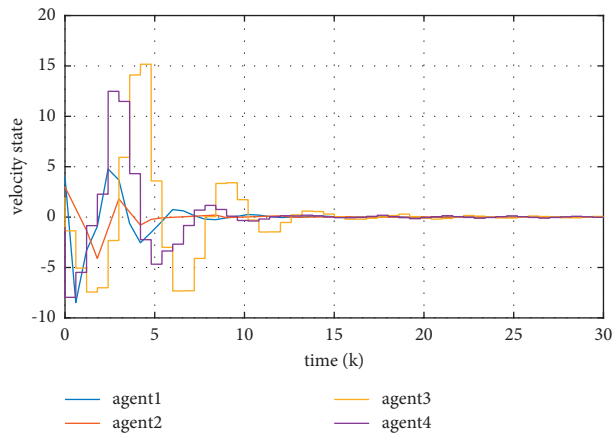

Figure 3: Velocity of the second-order dynamic agents.

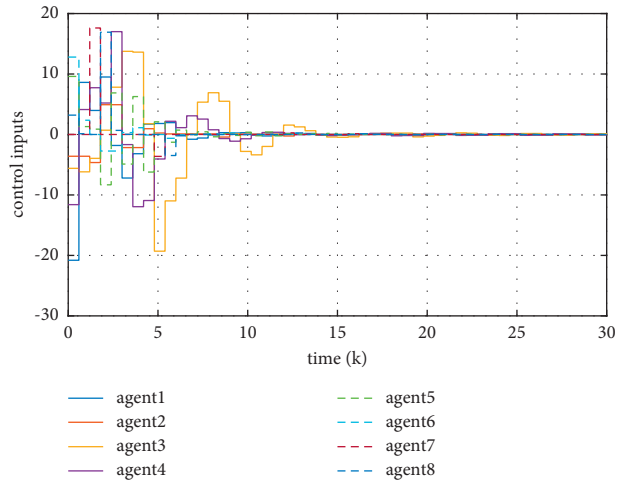

Figure 4: Control inputs of the dynamic agents.

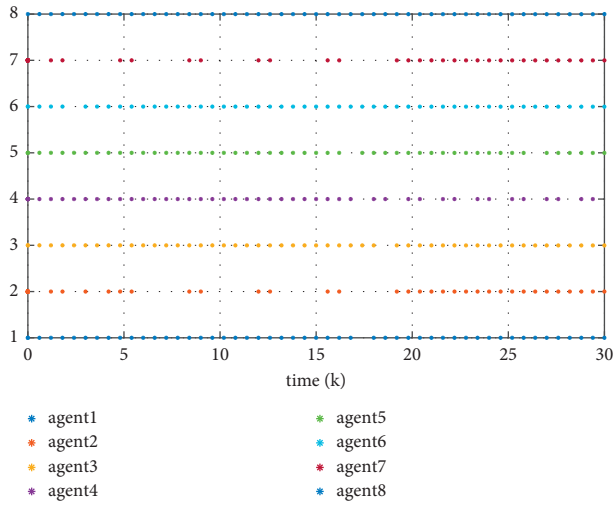

Figure 5: Event-triggered instants of the agents.

where $0 < B < 1$ and $a' > 1$ are positive constants. Next, the norm of $\overline{Q}_E(k_s)$ is considered as follows:

$$\begin{aligned}\left\|\overline{Q}_E(k_s)\right\| \le{}& \rho\left\|\overline{H}[(k_s+1)h]\right\|\left\|\overline{H}[(k_s+2)h]\right\|\cdots\left\|\overline{H}[(k_{s+1}-1)h]\right\|\left\|E(k_s h)\right\| \\ &+\cdots \\ &+\rho\left\|\overline{H}[(k_{s+1}-1)h]\right\|\left\|\overline{H}[(k_{s+1}-2)h]\right\| \\ &+\rho\left\|\overline{H}[(k_{s+1}-1)h]\right\| \\ <{}& \rho\eta_s\sum_{\tau=k_s}^{k_{s+1}-1}\|E(\tau h)\|,\end{aligned} \tag{58}$$

where

$$\eta_s = \max\left\{\left\|\overline{H}[(k_s+1)h]\cdots\left\|H[(k_s+1)h]\right\|,\ldots,\left\|\overline{H}[(k_s+1)h]\right\|,1\right\},\tag{59}$$

is a positive constant. In addition, there are b_p and b_p' that satisfy $b_p^{k_{p+1}-k_p} = B$ and $b_p'^{k_{p+1}-k_p-1} = B$ for each interval $[k_p h, k_{p+1}h)$. Letting $\eta = \max\{\eta_s\}$, $b' = \max\{b_p, b_p'\}$, we can get $b' < 1$ and (42) can be converted into

$$\begin{aligned}B\left\|\overline{Y}(k_p h)\right\| &< a' b'^{k_p} B\|\overline{Y}(0)\| \\ &\quad + a'\rho\eta b'^{k_p-1}\left[\left\|E(k_0)\right\| + \left\|E(k_0+1)\right\| + \cdots + \left\|E(k_1-1)\right\|\right] + \cdots \\ &\quad + a'\rho\eta b'^{k_0-1}\left[\left\|E(k_{p-1})\right\| + \left\|E(k_{p-1}+1)\right\| + \cdots + \left\|E(k_p-1)\right\|\right] \\ &< a' b'^{k_p} B\|\overline{Y}(0)\| + a'\rho\eta\sum_{s=0}^{k_p-1} b'^{k_p-1-s}\|E(sh)\|.\end{aligned}\tag{60}$$

Thus, let

$$\rho' = \frac{a' p\eta}{B},\tag{61}$$

$$\left\|\overline{Y}(k_p h)\right\| < a' b'^{k_p}\|\overline{Y}(0)\| + \rho'\sum_{s=0}^{k_p-1} b'^{k_p-1-s}\|E(sh)\|,\tag{62}$$

which has a similar form to (25). The subsequent proof of this theorem is the same as Theorem 2. □

Remark 3. The parameters of switching communication topologies, such as the switching rate and the dwell time, have certain impacts on the convergence rate. It mainly depends on the structure of each switching communication topology. In a period of time, more different agents communicating can improve the convergence efficiency. If there are different edges in the switching topologies, increasing the switching rate can reduce the time for the system to reach consensus.

4. Simulation Examples

A heterogeneous hybrid MAS is assumed to consist of four second-order (SO) agents and four first-order (FO) agents. They both contain two continuous-time (CT) individuals and two discrete-time (DT) individuals, respectively. Let $[x_s(0), x_f(0)]^T = [7,5,3,1,-1,-3,-5,-7]^T$ and $v(0)^T = [4,3,2,-1]^T$.

Consider the consensus of heterogeneous hybrid MASs with switching topologies. The communication topology can be switched between topology 1 and topology 2 in Figure 1 every step. The union of topology 1 and topology 2 has a spanning tree. Suppose the coupling gains of each edge in topology 1 and topology 2 are 1 and $\alpha = 1.6$, $\beta = 1.2$. By calculating, we choose $h = 0.6 < 0.625$ to satisfy conditions (21) in Theorem 1. Then, choosing $\gamma_1 = 0.2$ and $\gamma_2 = 0.01$, we can obtain the simulation graphics as follows. The position and velocity are shown in Figures 2 and 3. The control inputs are shown in Figure 4. And the triggered instants of each agent are shown in Figure 5.

All agents can achieve consensus, and the controllers are triggered a limited number of times within a finite time, which indicates that the event-triggered protocols algorithm is effective.

5. Conclusion

In this paper, the event-triggered consensus was studied for the heterogeneous hybrid MASs, consisting of continuous and discrete-time subsystems with second-order and first-order heterogeneous dynamics. We designed the effective event-triggered protocols, including the event-triggered control laws for the first-order and second-order agents, respectively, and the event-triggered conditions, which can make the controllers only update at their own trigger time and ensure all agents meet consensus. Some criteria were obtained for solving the consensus problems of the heterogeneous hybrid MASs with fixed topology and switching topologies. The main results showed that the MASs can reach consensus if the control parameter, coupling gains, and sampling interval meet certain conditions, and the fixed topology or the union of switching topologies contain a directed spanning tree. Future work may consider the consensus of the heterogeneous hybrid MASs with time delay or communication noise.

Data Availability

No other data were used in this study.

Conflicts of Interest

The authors declare that they have no conflicts of interest.

Acknowledgments

The authors sincerely thank the Natural Science Foundation of Hubei Province under Grant no. 2019CFb423 for the financial support of this research.

References

[1] C. W. Reynolds, "Flocks, herds and schools: a distributed behavioral model," *ACM SIGGRAPikH Computer Graphics*, vol. 21, no. 4, pp. 25–34, 1987.

[2] D. J. Low, "Following the crowd," *Nature*, vol. 407, no. 6803, pp. 465-466, 2000.

[3] C. Altafini and G. Lini, "Predictable dynamics of opinion forming for networks with antagonistic interactions," *IEEE Transactions on Automatic Control*, vol. 60, pp. 342–357, 2014.

[4] X. Lin and Y. Zheng, "Finite-time consensus of switched multiagent systems," *IEEE Transactions on Systems, Man, and Cybernetics: Systems*, vol. 47, pp. 1535–1545, 2016.

[5] X. H. Chang, R. Huang, H. Wang, and L. Liu, "Robust design strategy of quantized feedback control," *IEEE Transactions on Circuits and Systems II: Express Briefs*, vol. 67, pp. 730–734, 2019.

[6] H. Su, H. Wu, X. Chen, and M. Z. Chen, "Positive edge consensus of complex networks," *IEEE Transactions on Systems, Man, and Cybernetics: Systems*, vol. 48, pp. 2242–2250, 2017.

[7] X. Wang and H. Su, "Self-triggered leader-following consensus of multi-agent systems with input time delay," *Neurocomputing*, vol. 330, pp. 70–77, 2019.

[8] W. Ren and R. W. Beard, *Distributed consensus in multi-vehicle cooperative control*, Vol. 27, Springer, , Berlin, Germany, 2008.

[9] R. Olfati-Saber, "Flocking for multi-agent dynamic systems: algorithms and theory," *IEEE Transactions on Automatic Control*, vol. 51, no. 3, pp. 401–420, 2006.

[10] S. Chen, H. Pei, Q. Lai, and H. Yan, "Multitarget tracking control for coupled heterogeneous inertial agents systems based on flocking behavior," *IEEE Transactions on Systems, Man, and Cybernetics: Systems*, vol. 49, pp. 2605–2611, 2018.

[11] H. Su, X. Wang, and Z. Lin, "Flocking of multi-agents with a virtual leader," *IEEE Transactions on Automatic Control*, vol. 54, no. 2, pp. 293–307, 2009.

[12] B. Wang, J. Wang, B. Zhang, and X. Li, "Global cooperative control framework for multiagent systems subject to actuator saturation with industrial applications," *IEEE Transactions on Systems, Man, and Cybernetics: Systems*, vol. 47, pp. 1270–1283, 2016.

[13] H. Su, J. Zhang, and X. Chen, "A stochastic sampling mechanism for time-varying formation of multiagent systems with multiple leaders and communication delays," *IEEE Transactions on Neural Networks and Learning Systems*, vol. 30, no. 12, pp. 3699–3707, 2019.

[14] J. Xi, L. Wang, J. Zheng, and X. Yang, "Energy-constraint formation for multiagent systems with switching interaction topologies," *IEEE Transactions on Circuits and Systems I: Regular Papers*, vol. 67, no. 7, pp. 2442–2454, 2020.

[15] X. Yang, L. Liao, Q. Yang, B. Sun, and J. Xi, "Limited-energy output formation for multiagent systems with intermittent interactions," *Journal of the Franklin Institute*, vol. 358, no. 13, pp. 6462–6489, 2021.

[16] A. Jadbabaie, J. Jie Lin, and A. S. Morse, "Coordination of groups of mobile autonomous agents using nearest neighbor rules," *IEEE Transactions on Automatic Control*, vol. 48, no. 6, pp. 988–1001, 2003.

[17] P. Lin and Y. Jia, "Consensus of second-order discrete-time multi-agent systems with nonuniform time-delays and dynamically changing topologies," *Automatica*, vol. 45, no. 9, pp. 2154–2158, 2009.

[18] W. Wei Ren and R. W. Beard, "Consensus seeking in multiagent systems under dynamically changing interaction topologies," *IEEE Transactions on Automatic Control*, vol. 50, no. 5, pp. 655–661, 2005.

[19] F. Xiao and L. Wang, "State consensus for multi-agent systems with switching topologies and time-varying delays," *International Journal of Control*, vol. 79, no. 10, pp. 1277–1284, 2006.

[20] Y. Hong, L. Gao, D. Cheng, and J. Hu, "Lyapunov-based approach to multiagent systems with switching jointly connected interconnection," *IEEE Transactions on Automatic Control*, vol. 52, no. 5, pp. 943–948, 2007.

[21] W. Ni and D. Cheng, "Leader-following consensus of multi-agent systems under fixed and switching topologies," *Systems & Control Letters*, vol. 59, no. 3-4, pp. 209–217, 2010.

[22] D. Lee and M. W. Spong, "Agreement with Non-uniform Information delays," in *Proceedings of the 2006 American Control Conference*, p. 6, IEEE, MN, USA, June 2006.

[23] Y.-P. Tian and C.-L. Liu, "Consensus of multi-agent systems with diverse input and communication delays," *IEEE Transactions on Automatic Control*, vol. 53, no. 9, pp. 2122–2128, 2008.

[24] W. Yang, A. L. Bertozzi, and X. Wang, "Stability of a second order consensus algorithm with time delay," in *Proceedings of the 2008 47th IEEE Conference on Decision and Control*, pp. 2926–2931, IEEE, Cancun, December 2008.

[25] F. Xiao, L. Wang, and A. Wang, "Consensus problems in discrete-time multiagent systems with fixed topology," *Journal of Mathematical Analysis and Applications*, vol. 322, no. 2, pp. 587–598, 2006.

[26] G. Xie and L. Wang, "Consensus control for a class of networks of dynamic agents," *International Journal of Robust and Nonlinear Control*, vol. 17, no. 10-11, pp. 941–959, 2007.

[27] W. Ren and E. Atkins, "Distributed multi-vehicle coordinated controlvia local information exchange," *International Journal of Robust and Nonlinear Control*, vol. 17, no. 10-11, pp. 1002–1033, 2007.

[28] Y. Shi, J. Zhu, and T. Chen, "On the general weighted-average consensus protocol of multi-agent systems with double-integrator dynamics," in *Proceedings of the 2009 Chinese Control and Decision Conference*, pp. 4860–4865, IEEE, Guilin, China, June 2009.

[29] Q. Wang, M. Wu, Y. Huang, and L. Wang, "Formation control of heterogeneous multi-robot systems," *IFAC Proceedings Volumes*, vol. 41, no. 2, pp. 6596–6601, 2008.

[30] C.-L. Liu and F. Liu, "Stationary consensus of heterogeneous multi-agent systems with bounded communication delays," *Automatica*, vol. 47, no. 9, pp. 2130–2133, 2011.

[31] Y. Zheng, L. Wang, and Y. Zhu, "Consensus of heterogeneous multi-agent systems," *IET Control Theory & Applications*, vol. 5, no. 16, pp. 1881–1888, 2011.

[32] Z. Li, Z. Duan, and F. L. Lewis, "Distributed robust consensus control of multi-agent systems with heterogeneous matching uncertainties," *Automatica*, vol. 50, no. 3, pp. 883–889, 2014.

[33] H. Kim, H. Shim, and J. H. Seo, "Output consensus of heterogeneous uncertain linear multi-agent systems," *IEEE Transactions on Automatic Control*, vol. 56, pp. 200–206, 2010.

[34] G. S. Seyboth, D. V. Dimarogonas, K. H. Johansson, P. Frasca, and F. Allgöwer, "On robust synchronization of heterogeneous linear multi-agent systems with static couplings," *Automatica*, vol. 53, pp. 392–399, 2015.

[35] Y.-P. Tian and Y. Zhang, "High-order consensus of heterogeneous multi-agent systems with unknown communication delays," *Automatica*, vol. 48, no. 6, pp. 1205–1212, 2012.

[36] P. J. Antsaklis, J. A. Stiver, and M. Lemmon, "Hybrid system modeling and autonomous control systems," in *Hybrid Systems*, pp. 366–392, Springer, Berlin, Germany, 1992.

[37] Y. Zheng, J. Ma, and L. Wang, "Consensus of hybrid multi-agent systems," *IEEE Transactions on Neural Networks and Learning Systems*, vol. 29, pp. 1359–1365, 2017.
[38] Y. Zheng, Q. Zhao, J. Ma, and L. Wang, "Second-order consensus of hybrid multi-agent systems," *Systems & Control Letters*, vol. 125, pp. 51–58, 2019.
[39] J. Ma, M. Ye, Y. Zheng, and Y. Zhu, "Consensus analysis of hybrid multiagent systems: a game-theoretic approach," *International Journal of Robust and Nonlinear Control*, vol. 29, no. 6, pp. 1840–1853, 2019.
[40] H. Su, X. Wang, and Z. Zeng, "Consensus of second-order hybrid multiagent systems by event-triggered strategy," *IEEE Transactions on Cybernetics*, vol. 50, pp. 4648–4657, 2019.
[41] Y. Shang, "Consensus of hybrid multi-agent systems with malicious nodes," *IEEE Transactions on Circuits and Systems II: Express Briefs*, vol. 67, pp. 685–689, 2019.
[42] Q. Zhao, Y. Zheng, and Y. Zhu, "Consensus of hybrid multi-agent systems with heterogeneous dynamics," *International Journal of Control*, vol. 93, no. 12, pp. 2848–2858, 2020.
[43] D. V. Dimarogonas, E. Frazzoli, and K. Johansson, "Distributed event-triggered control for multi-agent systems," *IEEE Transactions on Automatic Control*, vol. 57, pp. 1291–1297, 2011.
[44] Y. Fan, G. Feng, Y. Wang, and C. Song, "Distributed event-triggered control of multi-agent systems with combinational measurements," *Automatica*, vol. 49, no. 2, pp. 671–675, 2013.
[45] D. Yang, W. Ren, X. Liu, and W. Chen, "Decentralized event-triggered consensus for linear multi-agent systems under general directed graphs," *Automatica*, vol. 69, pp. 242–249, 2016.
[46] H. Zhang, G. Feng, H. Yan, and Q. Chen, "Observer-based output feedback event-triggered control for consensus of multi-agent systems," *IEEE Transactions on Industrial Electronics*, vol. 61, pp. 4885–4894, 2013.
[47] W. Zhu, Z.-P. Jiang, and G. Feng, "Event-based consensus of multi-agent systems with general linear models," *Automatica*, vol. 50, no. 2, pp. 552–558, 2014.
[48] G. Guo, L. Ding, and Q.-L. Han, "A distributed event-triggered transmission strategy for sampled-data consensus of multi-agent systems," *Automatica*, vol. 50, no. 5, pp. 1489–1496, 2014.
[49] Y. Cheng and V. Ugrinovskii, "Event-triggered leader-following tracking control for multivariable multi-agent systems," *Automatica*, vol. 70, pp. 204–210, 2016.
[50] T.-H. Cheng, Z. Kan, J. R. Klotz, J. M. Shea, and W. E. Dixon, "Event-triggered control of multiagent systems for fixed and time-varying network topologies," *IEEE Transactions on Automatic Control*, vol. 62, no. 10, pp. 5365–5371, 2017.

Hindawi
Complexity
Volume 2022, Article ID 8344699, 11 pages
https://doi.org/10.1155/2022/8344699

Research Article

Analysis of Topological Aspects for Metal-Insulator Transition Superlattice Network

Rongbing Huang,[1] M.H. Muhammad,[2] M.K. Siddiqui,[3] S. Khalid,[3] S. Manzoor,[3] and E. Bashier[4]

[1]*School of Computer Science, Chengdu University, Chengdu, China*
[2]*College of Chemistry, School of Chemical Engineering and Energy, Zhengzhou University, Zhengzhou 450001, China*
[3]*Department of Mathematics, COMSATS University Islamabad, Lahore Campus, Pakistan*
[4]*Department of Applied Mathematics, Faculty of Mathematical Sciences, University of Khartoum, Sudan*

Correspondence should be addressed to E. Bashier; eihabbashier@gmail.com

Received 15 January 2022; Revised 17 February 2022; Accepted 28 February 2022; Published 25 March 2022

Academic Editor: Yue Song

In this research work, we have explored the physical and topological properties of the crystal structure of metal-insulator transition superlattice (GST-SL). In recent times, two-dimensional substantial have enamored comprehensive considerations owing to their novel ophthalmic and mechanical properties for anticipated employment. Recently, some researchers put their interest in modifying this material into useful forms in human life. Also, Metal-Insulator Transition Superlattice (GST–SL) is useful in form of a thin film to utilize as two-dimensional (2D) transition metal dichalcogenides (TMDs). Moreover, we have defined the computed-based bond properties such as the degree constructed topological indices and their heat of formation for single crystal and monolayered structure of Ge-Sb-Te. Also, this structure is one of the most interesting composites in modern resources of science.

1. Introduction

The germanium (Ge), Antimony (Sb), Tellurium (Te) (GST), and some other elements are present as metalloids. These metalloids lead to heat, electricity intermediates, metals, and they form large structure oxides. Metalloids are normal elements that have divided properties among metal and nonmetals, present in the Earth's outside layer [1], which occurred in an environment with a combination of organic and inorganic mixtures and other normal synthetics. The unpredictable modern abuse of these elements and possible dangers to humans are restricted in free use [2].

Some researchers put their interest in modification this material into useful forms in human life for different fields such as the GST alloy in form of a thin film is utilized as then the two-dimensional (2D) transition metal dichalcogenides (TMD) were discovered comparable applications in numerous fields [3]. These are made of cationic elements such as transition metals, group IIIA (In, Ga), and group IVA (Sn, Pb) [4]. Moreover, the anionic elements of chalcogenides (*O*, *S*, Se, Te) are essential in numerous fields. Moreover, to improve the bandgap energy of Ge–Sb–Te (GST), the physico-chemical properties are useful for sensing, in nonvolatile RAM, thermoelectric, and face change properties [5, 6]. The 2D TMDs are mainly dissimilar to pure transition bulk compounds and show new properties [7, 8]. Phase change material (PCM) properties of Ge – Sb – Te (GST) complex with a group of chalcogenides are promising technology and well known for so many years [9, 10].

A chemical graph $S = S(S_V, S_E)$ is an ordered pair of two finite sets S_V and S_E, where S_V is the set of vertices (atoms) and S_E is the set of edges (bonds) in chemical graph S [11]. The valence of molecules is usually portrayed by the vertex degrees [7, 12].

The number of edges affiliated with a vertex is identified as the degree of the vertex [13]. In this study, it is indicated by τ. Among different categories of topological indices, we will deliberate about degree-based topological indices depending on degree of end vertices of a graph, (see Table 1). For detailed study and application of these indices, see [24–27], respectively. In current circumstances, the basic aim of graph theory is the elaboration and enforcement of many contemporary scientific theories in assorted branches of chemistry. The QSPR/QSAR study is one of the essential reasons for broadening graph theory to chemistry [28].

2. Structure of GST – SL$[n]$

Another kind of PCM material named Ge – Sb – Te superlattice (GST-SL) has attracted large attention because of its ultralow power utilization. This superb exhibition has been ascribed to a special information storage system such as crystalline to crystalline stage change as compared to previous references [10, 29]. 1D semiconductor nano stares, attributable to their low dimensionality, display novel properties that discover application in numerous gadget fields [30]. The working rule of ordinary PCM gadgets depends on the changes between the metastable and amorphous crystalline stages set off either by optical. The thin film is deposited by femtosecond, picosecond, and nanosecond laser ablation [31, 32].

To this point, numerous investigations have been distributed over the most recent couple of years, proposing various distinctive atomic arrangements either for the amorphous and glasslike structure of the conceivable GST compounds or highlight by three unique stoichiometries, specifically $Ge_2Sb_2Te_5$ (most common for PMC s) [33], $Ge_1Sb_2Te_4$, and $Ge_1Sb_4Te_7$. The bulk GST intensifies two distinctive glasslike polymorphs: a metastable stage with rock salt design and a stable ground state structure at marginally low energy having a hexagonal/rhombohedral structure [34].

It is shown that the imperfection is restricted into two atomic layers of Ga, Sb, Te and shows confirmed stacking flaws. In-situ analysis demonstrated that the GeSb and Te bilayers can be effectively reconfigured into such bilayer stacking shortcomings with ensuring the arrangement of another van der Waals hole, showing a component of underlying reconfiguration of the building block in layered Ge – Sb – Te compounds [35]. The enormous distinction of dielectric capacities between the amorphous and glass-like structure of Ge – Sb – Te-based stage change materials (PCM s) utilized in-memory storage gadgets likewise influences their Schottky barrier heights (SBHs) and consequently their electric gadget properties. Here, the SBHs of each structure of $Ge_2Sb_2Te_5$, GeSb, GeSe, and SnTe are found by thickness of useful supercell computations [2].

The worldwide substance stoichiometry of the material and the local substance stoichiometry of individual layer blocks are needed to have a protecting band hole as per the electron checking model examination. The electron property can be changed by changing the local stoichiometry, for example, creating flaws around van der Waals holes (Figure 1) [10]. Moreover, the unite cell and generalized structure of GST – SL$[n]$ are depicted in Figure 2.

After some basic computation, we can see that $|V(\text{GST} - \text{SL}[n])| = 9n + 3$ and $|E(\text{GST} - \text{SL}[n])| = 13n$. The principle strategy utilized here is the way to deal with edge partitioning and vertice degree calculating (see Table 2).

2.1. Computations of Results for GST – SL$[n]$

(i) The general Randi $\acute{c}$ index of GST – SL$[n]$.

$$R_\alpha(S) = (n+2)(1\times 3)^\alpha + (2n+6)(2\times 3)^\alpha + (2n)(3\times 3) + (8n-8)(3\times 4). \tag{1}$$

For $\alpha = 1, -1, 1/2, -1/2$, we have

$$\begin{aligned} R_1(\text{GST}-\text{SL}) &= 3(43n-18),\\ R_{-1}(\text{GST}-\text{SL}) &= \frac{14n}{9}+1,\\ R_{1/2}(\text{GST}-\text{SL}) &= 6\sqrt{6}-14\sqrt{3}+(6+17\sqrt{3}+2\sqrt{6})n,\\ R_{-1/2}(\text{GST}-\text{SL}) &= \sqrt{6}-\frac{2}{\sqrt{3}}+\left(\frac{2}{3}+\frac{5}{\sqrt{3}}+\sqrt{\frac{2}{3}}\right)n. \end{aligned} \tag{2}$$

(ii) The atom bond connectivity index of GST – SL$[n]$.

The ABC index with the help of Tables 1 and 2 is

$$\begin{aligned} \text{ABC}(G) &= \sqrt{\frac{2}{3}}(n+2)++\frac{1}{\sqrt{2}}(2n+6)+\frac{2}{3}(2n)+\frac{\sqrt{5}}{2\sqrt{3}}(8n-8)\\ &= \left(\frac{4\sqrt{5}}{\sqrt{3}}+\frac{4}{3}+\sqrt{2}+\sqrt{\frac{2}{3}}\right)n+3\sqrt{2}+\frac{2\sqrt{2}}{\sqrt{3}}-\frac{4\sqrt{5}}{\sqrt{3}}. \end{aligned} \tag{3}$$

(iii) The geometric arithmetic index of GST – SL$[n]$.

The GA index with the help of Tables 1 and 2 is

Table 1: Topological descriptors.

Topological descriptors	Expression
The Randi´c index R_α with $\alpha = 1, -1, 1/2, -1/2$	$(\tau(a) \times \tau(s))^\alpha$
The atom bond connectivity index ABC(S) [14–17]	$\sqrt{\tau(a) + \tau(s) - 2/\tau(a) \times \tau(s)}$
The geometric arithmetic index GA(S) [14–17]	$2\sqrt{\tau(a) \times \tau(s)}/\tau(a) + \tau(s)$
The first Zagreb index $M_1(S)$ [14–17]	$\tau(a) + \tau(s)$
The second Zagreb index $M_2(S)$ [14, 15, 17]	$\tau(a) + \tau(s)$
The hyper Zagreb index HM(S) [18]	$[\tau(a) + \tau(s)]^2$
The forgotten index $F(S)$ [19]	$(\tau(a))^2 + (\tau(s))^2$
The augmented Zagreb index AZI(S) [20]	$(\tau(a)\tau(s)/\tau(a) + \tau(s) - 2)^3$
The Balaban index $J(S)$ [21, 22]	$(m/m - n + 2)1/\sqrt{\tau(a)\tau(s)}$
The redefined first Zagreb index $\mathrm{ReZG}_1(S)$ [23]	$\tau(a) + \tau(s)/\tau(a)\tau(s)$
The redefined second Zagreb index $\mathrm{ReZG}_2(S)$ [23]	$\tau(a)\tau(s)/\tau(a) + \tau(s)$
The redefined third Zagreb index $\mathrm{ReZG}_3(S)$ [23]	$(\tau(a)\tau(s))(\tau(a) + \tau(s))$

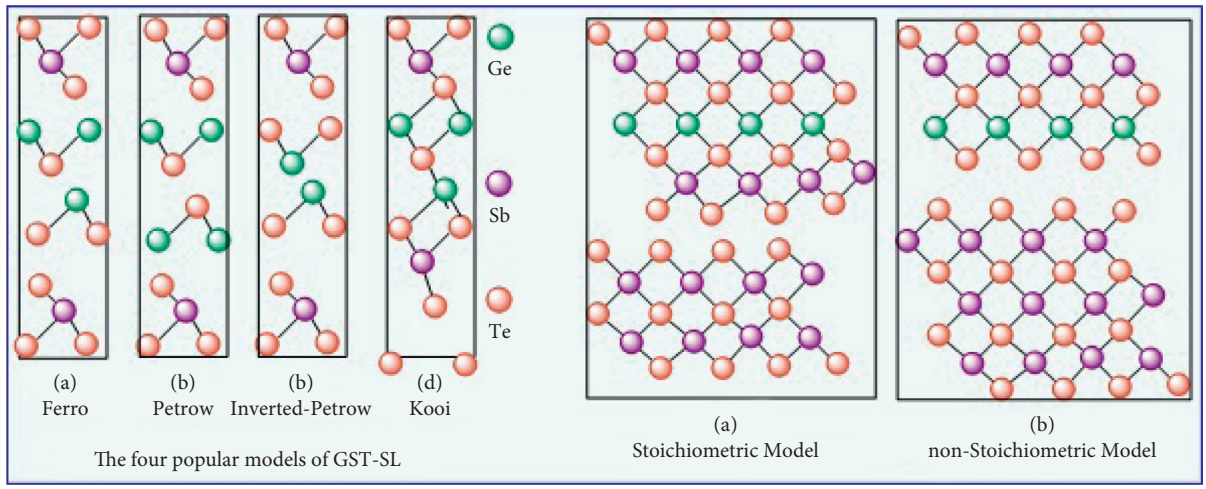

Figure 1: The general structure of (GST − SL).

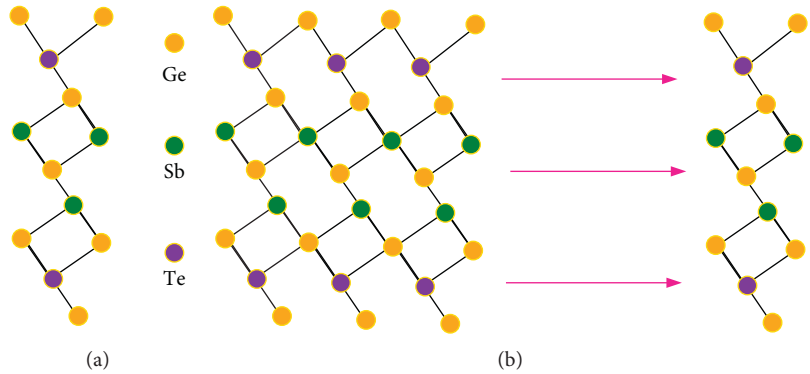

Figure 2: (a) Unit cell. (b) Generalized structure of GST − SL$[n]$.

Table 2: Edge partition of GST − SL$[n]$.

$(\tau(y), \tau(z))$	Number of repetitions	Types of edges
$(1, 3)$	$n + 2$	S_{E_1}
$(2, 3)$	$2n + 6$	S_{E_2}
$(3, 3)$	$2n$	S_{E_3}
$(3, 4)$	$8n - 8$	S_{E_4}

$$\begin{aligned}\mathrm{GA}(S) &= \frac{\sqrt{3}}{2}(n+2) + \frac{2\sqrt{6}}{5}(2n+6) + \frac{2\sqrt{9}}{6}(2n) \\ &\quad + \frac{2\sqrt{12}}{7}(8n-8) \\ &= \left(2 + \frac{4\sqrt{6}}{5} + \frac{71\sqrt{3}}{14}\right)n + \frac{12\sqrt{6}}{5} - \frac{25\sqrt{3}}{7}.\end{aligned} \tag{4}$$

(iv) The first Zagreb index of GST − SL[n].

The first Zagreb index by using Tables 1 and 2 is

$$M_1(\mathrm{GST}-SL) = 4(n+2) + 5(2n+6) + 6(2n) + 7(8n-8) = 82n - 18. \tag{5}$$

(v) The second Zagreb index of GST − SL[n].

The second Zagreb index by using Tables 1 and 2 is

$$M_2(\mathrm{GST}-SL) = 3(n+2) + 6(2n+6) + 9(2n) + 12(8n-8) = 129n - 54. \tag{6}$$

(vi) The hyper Zagreb index of GST − SL[n].

The hyper Zagreb index by using Tables 1 and 2 is

$$\mathrm{HM}(\mathrm{GST}-\mathrm{SL}) = 16(n+2) + 25(2n+6) + 36(2n) + 49(8n-8) = 530n - 210. \tag{7}$$

(vii) The forgotten index of GST − SL[n].

The forgotten index calculated by using Tables 1 and 2 is

$$F(\mathrm{GST}-\mathrm{SL}) = 10(n+2) + 13(2n+6) + 18(2n) + 25(8n-8) = 272n - 102. \tag{8}$$

(viii) The augmented Zagreb index of GST − SL[n].

The augmented Zagreb index with the help of Tables 1 and 2 is

$$\begin{aligned}\mathrm{AZI}(\mathrm{GST}-\mathrm{SL}) &= \left(\frac{3}{2}\right)^3(n+2) + 8(2n+6) + \left(\frac{9}{4}\right)^3(2n) + \left(\frac{12}{5}\right)^3(8n-8) \\ &= \frac{610993}{4000}n - \frac{27921}{500}.\end{aligned} \tag{9}$$

(xi) The Balaban index of GST − SL[n].

It is easy to see that the Balaban index by using Tables 1 and 2 is

$$\begin{aligned}J(\mathrm{GST}-\mathrm{SL}) &= \frac{13n}{13n-9n-3+2}\left[\frac{1}{\sqrt{3}}(n+2) + \frac{1}{\sqrt{6}}(2n+6) + \frac{1}{3}(2n) + \frac{1}{\sqrt{12}}(8n-8)\right] \\ &= \frac{13n}{4n-1}\left[\left(\frac{5}{\sqrt{3}} + \sqrt{\frac{2}{3}} + \frac{2}{3}\right)n - \frac{2}{\sqrt{3}} + \sqrt{6}\right].\end{aligned} \tag{10}$$

(x) The redefined first Zagreb index of GST − SL[n].

The redefined first Zagreb index with the help of Tables 1 and 2 is

$$\begin{aligned}\mathrm{ReZG}_1(\mathrm{GST}-\mathrm{SL}) &= \frac{4}{3}(n+2)+\frac{5}{6}(2n+6)+\frac{6}{9}(2n)+\frac{7}{12}(8n-8)\\ &= 3(3n+1).\end{aligned} \tag{11}$$

(xi) The redefined second Zagreb index of GST − SL[n].

The redefined second Zagreb index by using Tables 1 and 2 is

$$\begin{aligned}\mathrm{ReZG}_2(\mathrm{GST}-\mathrm{SL}) &= \frac{3}{4}(n+2)+\frac{6}{5}(2n+6)+\frac{9}{6}(2n)+\frac{12}{7}(8n-8)\\ &= \frac{2781n}{140}-\frac{351}{70}.\end{aligned} \tag{12}$$

(xii) The redefined third Zagreb index of GST − SL[n]. The Redefined third Zagreb index by using Tables 1 and 2 is:

$$\begin{aligned}\mathrm{ReZG}_3(\mathrm{GST}-\mathrm{SL}) &= 12(n+2)+30(2n+6)+54(2n)+84(8n-8)\\ &= 852n-468.\end{aligned} \tag{13}$$

3. Applications and Discussion of Computed Results

The geometric arithmetic index gives improved prediction as compared to other descriptors. We can easily see that the heat formation of GST − SL[n] is lower as the values of n increases. The first and the second Zagreb indices are established to appear within specific estimated expressions for the total π-electron energy [7, 20]. The augmented Zagreb index gives better correlation for measuring the strain energy of molecules.

The computed numerical results of Randi $\acute{c}$ indices are portrayed in Tables 3 and 4. The graphical illustration of $R_\alpha(S)$ for $\alpha = 1, -1, 1/2, -1/2$ is characterized in Figures 3 and 4.

We can use equation (14) for the transformation of Randi c indices into the approximate heat of formation for GST − SL[n].

$$\begin{aligned}H_{R_1(S)} &= 1030\cdot\left(-0.0094\cdot R_1(S)+3.0145\right),\\ H_{R_{-1}(S)} &= 1030\cdot\left(-0.6133\cdot R_{-1}(S)+4.7743\right),\\ H_{R_{1/2}(S)} &= 1030\cdot\left(-0.0810\cdot R_{1/2}(S)+3.9374\right),\\ H_{R_{-1/2}(S)} &= 1030\cdot\left(-0.2913\cdot R_{-1/2}(S)+4.1071\right).\end{aligned} \tag{14}$$

The computed numerical results of ABC index and GA index are portrayed in Table 5. The graphical illustration of these indices is characterized in Figure 5. The transformation of ABC index and GA index into the approximate heat of formation of GST − SL[n] at any level can be estimated with the help of the following equation:

$$\begin{aligned}H_{\mathrm{ABC}} &= 1040\cdot(-0.0045\cdot\mathrm{ABC}-3.4699),\\ H_{\mathrm{GA}} &= 1030\cdot(-0.0917\cdot\mathrm{GA}+2.0126).\end{aligned} \tag{15}$$

The computed numerical results for the first and the second Zagreb indices are shown in Table 6, while their graphical illustration is shown in Figure 6. The transformation of the first and the second Zagreb indices into the approximate heat of formation of GST − SL[n] at any level can be exercised with the help of the equation as follows:

$$\begin{aligned}H_{M_1} &= 1030\cdot\left(-0.045\cdot M_1+4.3142\right),\\ H_{M_2} &= 1030\cdot\left(-0.0094\cdot M_2+3.0145\right).\end{aligned} \tag{16}$$

Numerical comparison of hyper Zagreb index and forgotten index is shown in Table 7, while graphically, their comparison is shown in Figure 7 Equation (17) can be employed for the transformation of hyper and forgotten indices into the approximate heat of formation of GST − SL[n] at any cubic level.

$$\begin{aligned}H_{\mathrm{HM}}(S) &= 1020\cdot(-0.0238\cdot\mathrm{HM}(S)+3.4663),\\ H_F(S) &= 1030\cdot(-0.008\cdot F(S)+3.6558).\end{aligned} \tag{17}$$

Table 3: Comparison of R_1 and R_{-1} with their respective heat of formation for GST – SL[n].

[n]	R_1	H_{R_1}	R_{-1}	$H_{R_{-1}}$
[21]	75	2378.785	2.555 6	3303.159 0
[22]	204	1129.807	4.111 1	2320.551 2
[14]	333	−119.171	5.666 7	1337.943 4
[3]	462	−1368.149	7.222 2	355.272 5
[9]	591	−2617.127	8.777 8	−627.3985
[12]	720	−3866.105	10.333 3	−1610.0063
[31]	849	−5115.083	11.888 9	−2592.6709

Table 4: Comparison of $R_{1/2}$ and $R_{-1/2}$ with their respective heat formation for GST – SL[n].

[n]	$R_{1/2}$	$H_{R_{1/2}}$	$R_{-1/2}$	$H_{R_{-1/2}}$
[21]	30.792 1	2755.171 6	5.664 7	2530.682 1
[22]	71.135 9	1051.452 9	10.034 6	1219.541 7
[14]	111.479 8	−652.2699	14.404 5	−91.5988
[3]	151.823 6	−2355.9886	18.774 4	−1402.7392
[9]	192.167 4	−4059.7073	23.144 3	−2713.8796
[12]	232.511 2	−5763.4260	27.514 3	−4025.0501
[31]	272.855 1	−7467.1489	31.884 2	−5336.1905

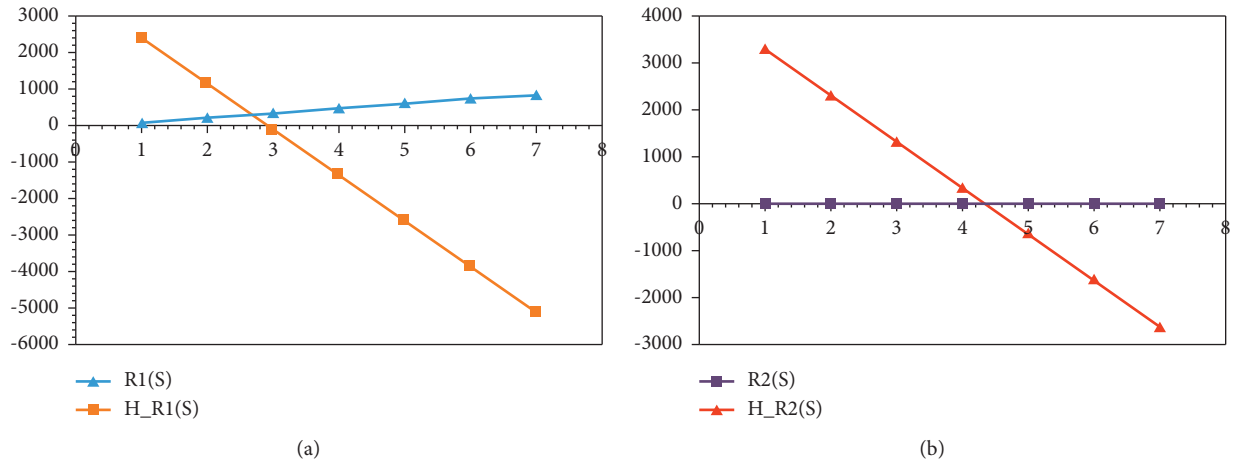

Figure 3: (a) Comparison of Randi c index for $\alpha = 1$ with heat of formation. (b) Comparison of Randi c index for $\alpha = -1$ with heat of formation.

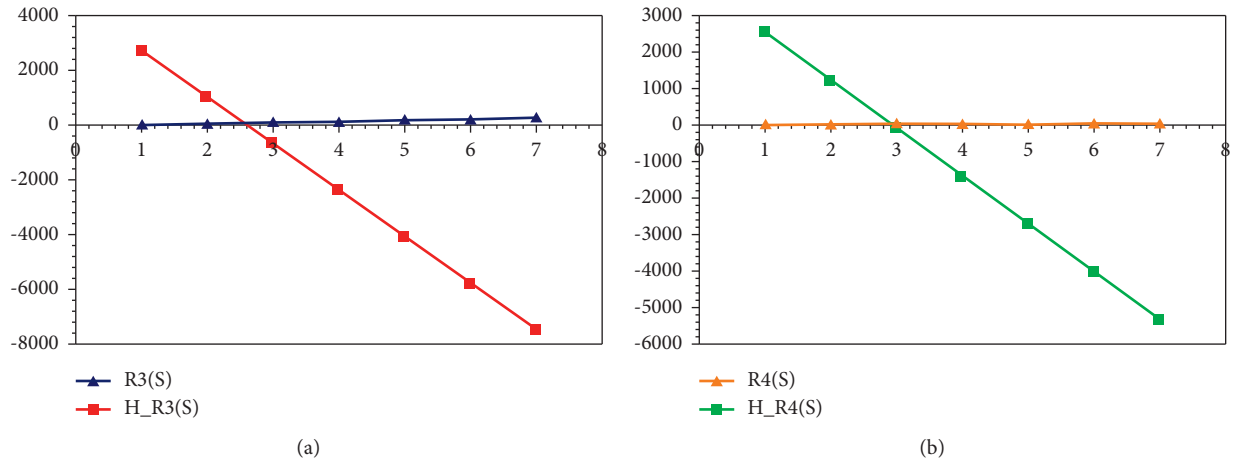

Figure 4: (a) Randi c index for $\alpha = 1/2$ with heat of formation, (b) Randi c index for $\alpha = -1/2$ with heat of formation.

Table 5: Comparison of ABC index and GA index with their respective heat of formation for GST – SL[n].

[n]	ABC	H_{ABC}	GA	H_{GA}
[21]	9.439 7	−3652.8738	12.436 4	898.3476
[22]	18.167 7	−3693.7208	25.18	−305.2982
[14]	26.895 7	−3734.569	37.923 6	−1508.9439
[3]	35.623 7	−3775.4149	50.667 1	−2712.5803
[9]	44.351 8	−3816.2624	63.410 7	−3916.2260
[12]	53.079 8	−3857.1095	76.154 3	−5119.8718
[31]	61.807 8	−3897.9565	88.897 8	−6323.5081

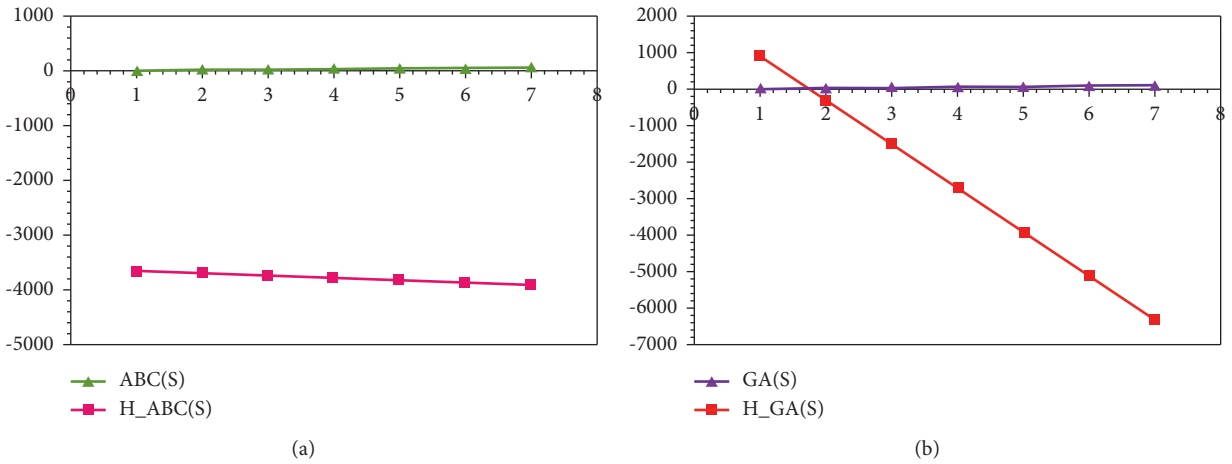

Figure 5: (a) The ABC index with heat of formation (b) The GA index with heat of formation.

Table 6: Comparison of Zagreb indices with their respective heat of formations for GST – SL[n].

[n]	M_1	H_{M_1}	M_2	H_{M_2}
[21]	64	2424.826 0	75	2378.785
[22]	146	1157.926 0	204	1129.807 0
[14]	228	−108.9740	333	−119.1710
[3]	310	−1375.8740	462	−1368.1490
[9]	392	−2642.7740	591	−2617.1270
[12]	474	−3909.6740	720	−3866.1050
[31]	556	−5176.5740	849	−5115.0830

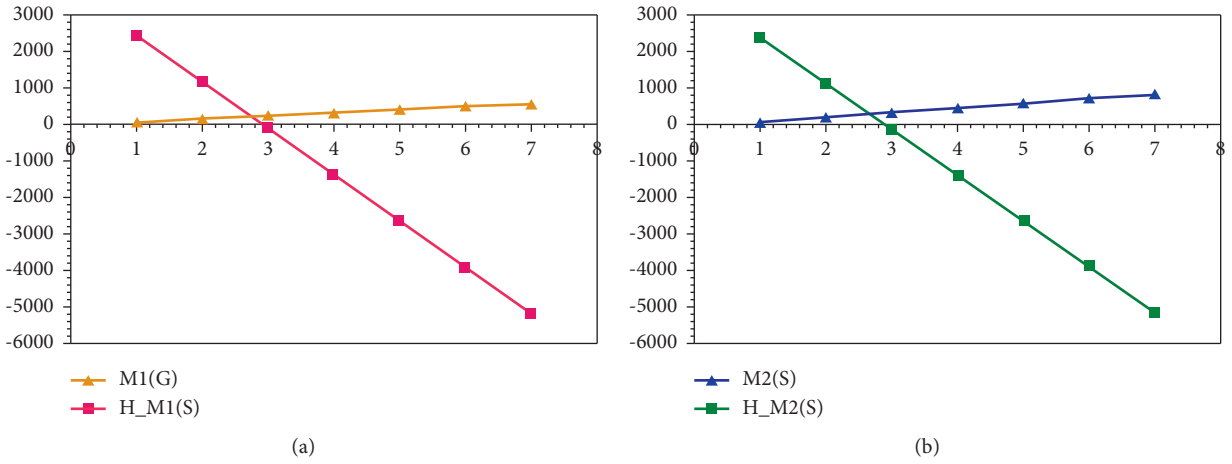

Figure 6: (a) The rirst Zagreb index with heat of formation. (b) The second Zagreb index with heat of formation.

Table 7: Comparison of HM and F indices with their respective heat of formation for GST – SL[n].

[n]	HM	H_{HM}	F	H_F
[21]	320	−5252.6940	170	2364.6740
[22]	850	−18118.9740	442	123.3940
[14]	1380	−30985.2540	714	−2117.8860
[3]	1910	−43851.5340	986	−4359.1660
[9]	2440	−56717.8140	1258	−6600.4460
[12]	2970	−69584.0940	1530	−8841.7260
[31]	3500	−82450.3740	1802	−11083.006

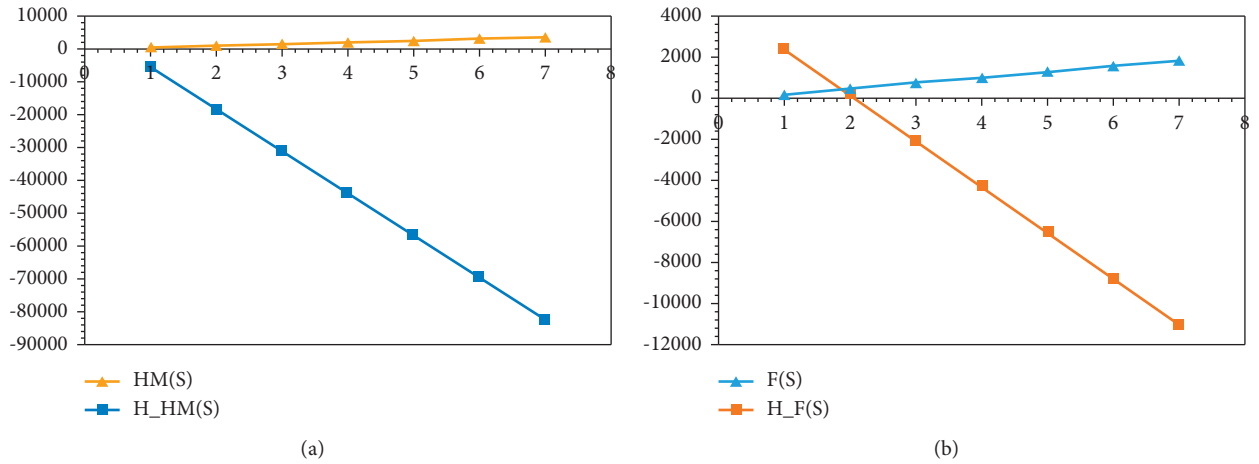

Figure 7: (a) The hyper Zagreb index with heat of formation. (b) The forgotten index with heat of formation.

Table 8: Comparison of AZI and J indices with their respective heat of formation for GST – SL[n].

[n]	AZI	H_{AZI}	J	H_J
[21]	96.906 3	1711.769 2	24.547	−6023.6551
[22]	249.654 5	−490.8599	37.271 4	−8256.9399
[14]	402.402 8	−2693.4904	51.070 6	−10678.8652
[3]	555.151	−4896.1194	65.084 8	−13138.5254
[9]	707.899 3	−7098.7499	79.178 1	−15612.0687
[12]	860.647 5	−9301.3790	93.309 3	1486.552 8
[31]	1013.396	−11504.0123	107.461 5	361.706 6

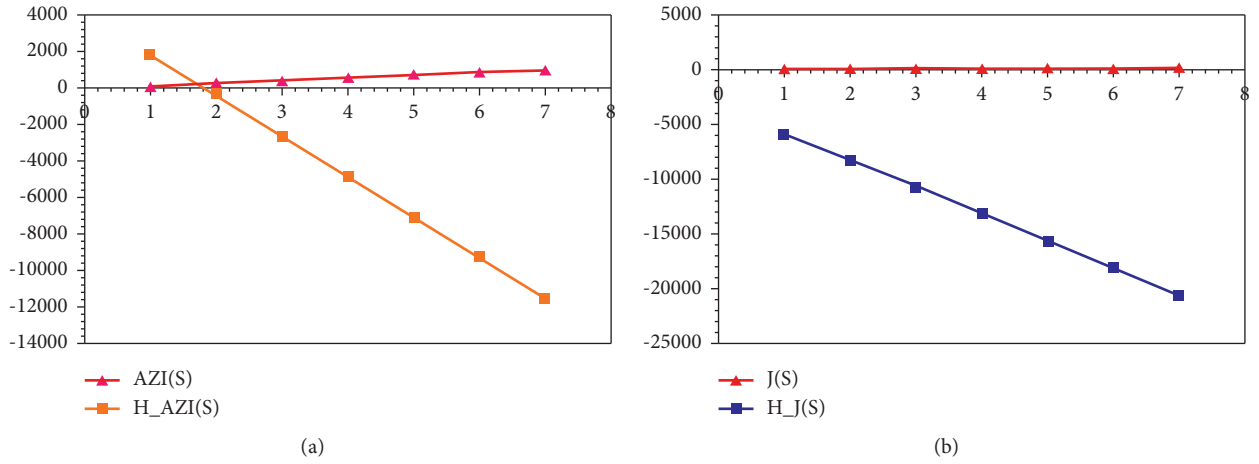

Figure 8: (a) The augmented Zagreb index with heat of formation. (b) The Balaban index with heat of formation.

Table 9: Comparison of the redefined Zagreb rntropies with their respective heat of formations for GST − SL[n].

[n]	$ReZG_1$	H_{ReZG_2}	$ReZG_2$	H_{ReZG_2}	$ReZG_3$	H_{ReZG_3}
[21]	2	2371.060	14.85	172.782 5	384	1548.090
[22]	21	−5691.780	34.714 3	−2793.9507	1236	−2839.710
[14]	30	−9511.020	54.578 6	−5760.6839	2088	−7227.51
[3]	39	−13330.260	74.442 9	−8727.4171	2940	−11615.31
[9]	48	−17149.5	94.307 1	−11694.1354	3792	−16003.11
[12]	57	−20968.74	114.171 4	−14660.8686	4644	−20390.91
[31]	66	−24787.98	134.035 7	−17627.6018	5496	−24778.71

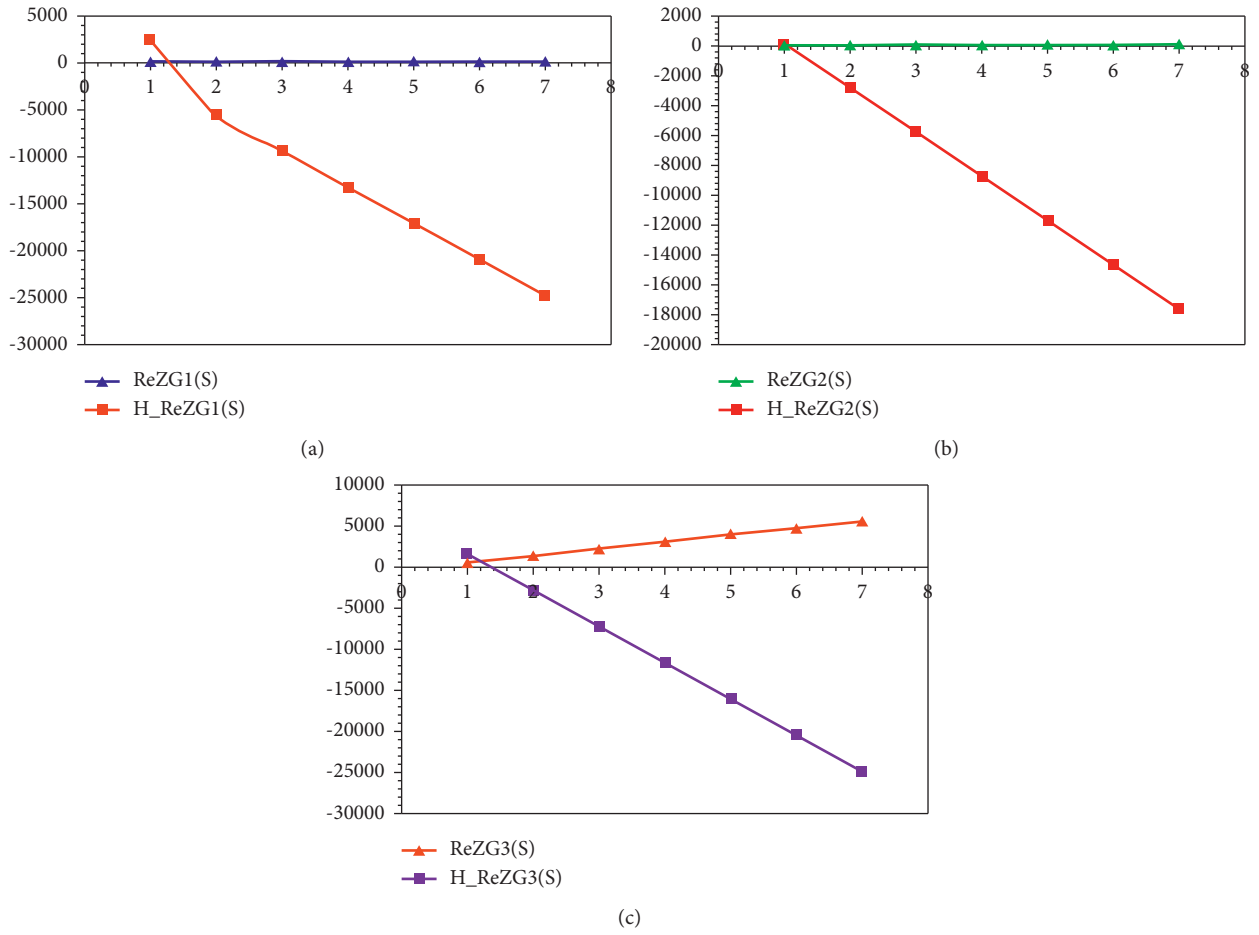

Figure 9: (a) The redefined first Zagreb index, (b) the redefined second Zagreb entropy, and (c) the Redefined third Zagreb index, with respective heat of formation for GST − SL[n].

Numerical results for AZI and J indices are shown in Table 8, while Figure 8 illustrates the results graphically. For the transformation of augmented Zagreb index and Balaban index into the approximate heat of formation of GST − SL[n] at any level can be exercised with the help of the equation as follows:

$$\begin{aligned} H_{AZI} &= 1030 \cdot (-0.014 \cdot AZI + 3.0186), \\ H_J &= 1030 \cdot (-0.1704 \cdot J + 1.6654). \end{aligned} \tag{18}$$

Numerical results of redefined Zagreb indices are shown in Table 9, while Figure 9 illustrates these indices graphically. The transformation of redefined Zagreb entropies into the approximate heat of formation of GST − SL[n] at any cubic level can be employed by using the equation as follows:

$$\begin{aligned} H_{ReG_1}(S) &= 1030 \cdot (-0.412 \cdot ReG_1 + 3.126), \\ H_{ReG_2} &= 1030 \cdot (-0.145 \cdot ReG_2 + 2.321), \\ H_{ReG_3} &= 1030 \cdot (-0.0050 \cdot ReG_3 - 3.2173). \end{aligned} \tag{19}$$

4. Conclusion

In this paper, some degree constructed topological indices are computed which can be used to find out different physicochemical properties. More preciously, we have computed the Randić index, the atom bond connectivity index, the geometric arithmetic index, the first and second Zagreb indices, and the Balaban index. We also determined a relation between the degree constructed topological indices with heat of formation, and then, we discussed the crystal structure of Ge – Sb – Te (GST) and also its applications in different fields. The heat of formation and the entropy measure are computed in this study, which is useful to analyze the thermodynamic properties of the metal-insulator transition. We illustrated the comparison between the degree constructed topological indices and heat of formation, which leads us to know the physicochemical properties of this two-dimensional material GST.

Data Availability

The data used to support the findings of this study are cited at relevant places within the text as references.

Conflicts of Interest

The authors declare that they have no conflicts of interest.

Authors' Contributions

This work was equally contributed by all writers.

References

[1] R. E. Simpson, P. Fons, A. V. Kolobov et al., "Interfacial phase-change memory," *Nature Nanotechnology*, vol. 6, no. 8, pp. 501–505, 2011.

[2] N. Parveen, R. Berni, S. Sudhakaran et al., "Metalloids in plants: a systematic discussion beyond description," *Annals of Applied Biology*, vol. 180, no. 1, pp. 7–25, 2021.

[3] B. Balasubramaniam, N. Singh, P. Kar, A. Tyagi, J. Prakash, and R. K. Gupta, "Engineering of transition metal dichalcogenide-based 2*D* nanomaterials through doping for environmental applications," *Molecular Systems Design & Engineering*, vol. 4, no. 4, pp. 804–827, 2019.

[4] X. B. Li, N. K. Chen, X. P. Wang, and H. B. Sun, "Phase-change superlattice materials toward low power consumption and high density data storage: microscopic picture, working principles, and optimization," *Advanced Functional Materials*, vol. 28, no. 44, pp. 45–55, Article ID 1803380, 2018.

[5] D. P. Wong, M. Aminzare, T.-L. Chou et al., "Origin of band modulation in GeTe-Rich Ge-Sb-Te thin film," *ACS Applied Electronic Materials*, vol. 1, no. 12, pp. 2619–2625, 2019.

[6] J. Feng, A. Lotnyk, H. Bryja et al., "'Stickier'-surface Sb2Te3 templates enable fast memory switching of phase change material GeSb2Te4 with growth-dominated crystallization," *ACS Applied Materials & Interfaces*, vol. 12, no. 29, pp. 33397–33407, 2020.

[7] D. Vukicevic and B. Furtula, "Topological index based on the ratios of geometrical and arithmetical means of end-vertex degrees of edges," *Journal of Mathematical Chemistry*, vol. 46, no. 4, pp. 1369–1376, 2009.

[8] T. Siegrist, P. Jost, H. Volker et al., "Disorder-induced localization in crystalline phase-change materials," *Nature Materials*, vol. 10, no. 3, pp. 202–208, 2011 March.

[9] G. Bianconi, "The entropy of randomized network ensembles," *Europhysics Letters*, vol. 81, no. 2, pp. 28–35, 2008.

[10] N. K. Chen, X. B. Li, X. P. Wang et al., "Metal–insulator transition of Ge–Sb–Te superlattice: an electron counting model study," *IEEE Transactions on Nanotechnology*, vol. 17, no. 1, pp. 140–146, 2017.

[11] Y. M. Chu, M. K. Siddiqui, S. Javed, L. Sherin, and F. Kausar, "On zagreb type molecular descriptors of ceria oxide and their applications," *Journal of Cluster Science*, vol. 11, pp. 1–10, 2021.

[12] D. Bonchev, *Complexity in Chemistry, Introduction and Fundamentals*, Taylor & Francis, Boca Raton, FL, USA, 2003.

[13] S. Manzoor, M. K. Siddiqui, and S. Ahmad, "On entropy measures of molecular graphs using topological indices," *Arabian Journal of Chemistry*, vol. 13, no. 8, pp. 6285–6298, 2020.

[14] A. Balaban, I. Motoc, D. Bonchev, and O. Mekenyan, "Topological indices for structure-activity correlations," *Steric Effects in Drug Design*, Springer, Berlin, Heidelberg, pp. 21–56, 1983.

[15] I. Gutman, B. Ruscic, N. Trinajstić, and C. F. Wilcox Jr, "Graph theory and molecular orbitals. XII. acyclic polyenes," *The Journal of Chemical Physics*, vol. 62, no. 9, pp. 3399–3405, 1975.

[16] I. Gutman and K. C. Das, "The first zagreb index 30 years after," *MATCH Commun. Math. Comput. Chem,* vol. 50, pp. 83–92, 2004.

[17] R. Todeschini and V. Consonni, *Handbook of Molecular Descriptors*, John Wiley & Sons, USA, 2008.

[18] G. H. Shirdel, H. RezaPour, and A. M. Sayadi, "The hyper zagreb index of graph operations," *Iranian Journal of Mathematical Chemistry*, vol. 4, no. 2, pp. 213–220, 2013.

[19] B. Furtula and I. Gutman, "A forgotten topological index," *Journal of Mathematical Chemistry*, vol. 53, no. 4, pp. 1184–1190, 2015.

[20] B. Furtula, A. Graovac, and D. Vukičević, "Augmented zagreb index," *Journal of Mathematical Chemistry*, vol. 48, no. 2, pp. 370–380, 2010.

[21] A. T. Balaban, "Highly discriminating distance-based topological index," *Chemical Physics Letters*, vol. 89, no. 5, pp. 399–404, 1982.

[22] A. T. Balaban and L. V. Quintas, "The smallest graphs, trees, and 4-trees with degenerate topological index," *Journal of Mathematical Chemistry*, vol. 14, pp. 213–233, 1983.

[23] P. S. Ranjini, V. Lokesha, and A. Usha, "Relation between phenylene and hexagonal squeez using harmonic index," *Int J Graph Theory*, vol. 1, pp. 116–121, 2013.

[24] M. K. Siddiqui, M. Naeem, N. A. Rahman, and M. Imran, "Computing topological indicesof certain networks," *Journal of Optoelectronics and Advanced Materials*, vol. 18, no. No. 9-10, pp. 884–892, 2016.

[25] W. Gao and M. R. Farahani, "Degree-based indices computation for special chemical molecular structures using edge dividing method," *Applied Mathematics and Nonlinear Sciences*, vol. 1, no. 1, pp. 94–117, 2015.

[26] W. Gao, M. Siddiqui, M. Naeem, and N. Rehman, "Topological characterization of carbon graphite and crystal cubic carbon structures," *Molecules*, vol. 22, no. 9, pp. 1496–1507, 2017.

[27] M. Imran, M. K. Siddiqui, M. Naeem, and M. A. Iqbal, "On topological properties of symmetric chemical structures," *Symmetry*, vol. 10, no. 173, pp. 1–21, 2018.
[28] M. K. Siddiqui, M. Imran, and A. Ahmad, "On zagreb indices, zagreb polynomials of some nanostar dendrimers," *Applied Mathematics and Computation*, vol. 280, pp. 132–139, 2016.
[29] R. Shayduk and W. Braun, "Epitaxial films for Ge-Sb-Te phase change memory," *Journal of Crystal Growth*, vol. 311, no. 7, pp. 2215–2219, 2009.
[30] A. Lotnyk, U. Ross, T. Dankwort, I. Hilmi, L. Kienle, and B. Rauschenbach, "Atomic structure and dynamic reconfiguration of layered defects in van der waals layered Ge-Sb-Te based materials," *Acta Materialia*, vol. 141, pp. 92–96, 2017.
[31] G. Bulai, O. Pompilian, S. Gurlui et al., "*Ge-Sb-Te* chalcogenide thin films deposited by nanosecond, picosecond, and femtosecond laser ablation," *Nanomaterials*, vol. 9, no. 5, pp. 676–687, 2019.
[32] J.-Y. Lee, J.-H. Kim, D.-J. Jeon, J. Han, and J.-S. Yeo, "Atomic migration induced crystal structure transformation and core-centered phase transition in single crystal Ge2Sb2Te5 nanowires," *Nano Letters*, vol. 16, no. 10, pp. 6078–6085, 2016.
[33] A. Hirata, T. Ichitsubo, P. F. Guan, T. Fujita, and M. W. Chen, "Distortion of local atomic structures in amorphous *Ge-Sb-Te* phase change materials," *Physical Review Letters*, vol. 120, no. 20, pp. 205502–206212, 2018.
[34] M. N. Schneider and O. Oeckler, "Unusual solid solutions in the System Ge-Sb-Te: the crystal structure of 33R-Ge4–xSb2–yTe7(x, y ≈ 0.1) is isostructural to that of Ge3Sb2Te6," *Zeitschrift fur Anorganische und Allgemeine Chemie*, vol. 634, no. 14, pp. 2557–2561, 2008.
[35] U. Ross, A. Lotnyk, E. Thelander, and B. Rauschenbach, "Microstructure evolution in pulsed laser deposited epitaxial Ge-Sb-Te chalcogenide thin films," *Journal of Alloys and Compounds*, vol. 676, pp. 582–590, 2016.